Positron Emission Tomography Radiochemistry: Improved Methodology and a Novel PET Imaging Agent for the Dopamine D_3 Receptor

By

Megan N. Stewart

A dissertation submitted in partial fulfillment
of the requirements for the degree of
Doctor of Philosophy
(Medicinal Chemistry)
In the University of Michigan
2018

Doctoral Committee:

Associate Professor Peter J.H. Scott, Chair
Professor Robert A. Koeppe
Research Professor Scott D. Larsen
Professor Henry I. Mosberg

Megan N. Stewart

mestewar@umich.edu

ORCID iD: 0000-0002-6938-4781

Dedicated to my mom, Sally

My Sunshine

Acknowledgements

First and foremost, I want to express my deep appreciation to Professor Peter J.H. Scott for accepting me as a part of his group as a naïve graduate student with minimal chemistry skills over five years ago. Pete pushed me to be a better scientist, speaker, and writer. I am grateful for his mentorship, guidance and support. He always had a little faith in me when I didn't have much in myself. As his first graduate student, I think we both learned a lot along the way and I'm grateful for the lessons, both successes and opportunities for growth, shared along the way. I am thankful for Pete's dedication to the science and to the group he leads. The sacrifices and behind-the-scenes work are not unnoticed and are most appreciated.

I am extremely grateful to Dr. Xia (Shannon) Shao, carbon-11 chemistry goddess. Her creativity and resilience are second to none, and her willingness to mentor graduate students is more than I could have ever asked for. Brian Hockley, my "big brother", took me under his wing, taught me ^{18}F chemistry (and how not to irradiate myself), and was always there for coffee-based support. Tim (sunshine cyclist) Desmond, for his invaluable contributions and advice regarding all things biology-related. The contributions made by Shannon, Brian, and Tim to this work, and my PhD studies, are numerous and deserve a most sincere thank you.

To current and former Scott lab members: Dr. Andrew V. Mossine and Dr. Stephen Thompson –my go-to postdocs to talk everything chemistry. Their excitement and passion to talk science, troubleshoot, and provide support got me through many tough days. Dr. Allen F. Brooks and Dr. So Jeong Lee, for always being there to offer guidance. Allie Sowa, I could not have had a better cubicle mate or fume hood buddy (Kaw Kaw!). To my other science siblings, and the rest of the Scott lab, a sincere thanks for making the lab a pleasurable place to work.

I owe a special thanks to my committee members, Dr. Scott Larsen, Dr. Henry Mosberg, and Dr. Robert Koeppe for their continued support and encouragement. A genuine thanks to Dr. George Garcia and Sarah Loyd for their guidance and support as well. Dr. Kenneth P. Mitton (my “science dad”): a deepest thanks for his heartfelt mentorship from my time as an undergrad student in his lab to now, and in the future.

To my run family/best friends: Fritz Kramp, Ellen Rowe, Melissa “Mountain Giraffe” Ruse, Tony Hanks, and Dr. Lee Connor. They are sources of endless support and smiles, and constantly pushing me to do better in running and in life. With special thanks to Ellen and Fritz: for sticking with me at my absolute best and absolute worst and having been unwavering in friendship and love. A heartfelt thanks to Melissa for many shared “we can do this!”, and how to survive the “dark cloud days” conversations. There are no other people I’d rather traverse up and down mountains, and over 100s of miles with.

Loving thanks to my family. Angie Ransdell, for always being a strong, positive role model and friend. Thanks to Cory “Thumper” Bachor for his lightheartedness, support, and endless source of comic relief. To the family we were blessed to pick: Pat and Andy, Matt and Katelyn, and the lovely Aubrey Gauthier. Their love and support are priceless.

Dr. Jung Hwan Kim, thank you for your tough love in mentoring me as a scientist when I needed it (even though you encouraged me to pursue medical school), and helping me navigate through many hard days. For your patience, levelheadedness, your love and friendship – I'm lucky to have you as my best friend. To my companions for their unspoken love and source of endless smiles: my sweet bay mare, Danci, and Siberian Husky, Helios.

Finally, a very special thank you to my mom, Sally K. Stewart. Thank you for loving me when I wasn't very lovable, and when I didn't deserve it. For always encouraging and seeing the best in me, and for showing me there's a life worth living. I'm blessed to have you as my mom, and as my very best friend to share in so many wonderful adventures with. None of this would have been possible without you. I love you more than the sky is blue.

Table of Contents

List of Figures

Figures

List of Schemes

Schemes

List of Tables

Tables

Abstract

Positron Emission Tomography (PET) imaging is a powerful non-invasive imaging modality used to quantify biochemical processes *in vivo*. The work described in this thesis encompasses two aspects of PET radiochemistry: (1) the development of new chemical methodology applying the principles of green chemistry to late-stage ^{18}F-fluorination, and (2) developing a PET radioligand for the dopamine D_3 receptor.

(1) As a way to simplify FDA mandated quality control and residual solvent analysis prior to the release of PET radiopharmaceuticals we sought to apply the principles of green chemistry to ^{18}F-radiochemistry. Green radiochemistry in late-stage stage ^{18}F-fluorination with [^{18}F]KF employs ethanol and ethanol/water mixtures as the only solvents used throughout the entire radiopharmaceutical production: azeotropic drying, nucleophilic fluorination, purification and formulation. This work developed a method in which using ethanol in place of acetonitrile is a viable option for azeotroptic drying of [^{18}F]fluoride. Furthermore, it demonstrated that aliphatic ^{18}F-fluorination reactions can proceed in an optimized 15% water, 85% ethanol mixture. Proof of concept was demonstrated through the synthesis of clinically relevant PET radiopharmaceuticals. The new methodology described challenges the long held belief that nucleophilic fluorination reactions cannot proceed in protic solvents or aqueous media, and encourages further exploration into the utility of green fluorine chemistry.

(2) Dopamine is a monoamine neurotransmitter in the Central Nervous System (CNS), and its signaling is mediated by pre-synaptic and post-synaptic dopamine receptors. These are D_1-like (D_1 and D_5) and D_2-like (D_2, D_3, D_4) receptors, which are G protein-coupled receptors (GPCRs) and are classified based on these two subfamilies due to sequence homology and pharmacological similarities. The D_3 receptor is implicated in many neurological and neurodegenerative diseases and disorders, including substance abuse, depression and schizophrenia. Significant efforts have gone into developing ligands as therapeutics, and as positron emission tomography (PET) diagnostics at this receptor. Significant challenges to this pursuit include the high sequence homology between the D_2 and D_3 receptors, and the physicochemical properties associated with BBB permeability and *in vivo* stability, while maintaining selectivity at this receptor.

The synthesis and initial evaluation of a series of new carbon-11 and fluorine-18 PET radioligands for the D_3 receptor is described. These radioligands are based on known ligands with good selectivity for the D_3 receptor (pramipexole and BP897). Due to stability issues when using pramipexole-containing scaffolds, BP897 derivatives containing a naphthamide moiety were developed and evaluated *in vitro* using rad brain autoradiography, and *in vivo* using rodent microPET imaging. A carbon-11 D_3-selective compound was synthesized and identified as a promising candidate, owing to its high affinity for D_3 receptors, selectivity for D_3 over D_2 receptors, and good blood-brain barrier (BBB) penetration. Further evaluation and optimization of the scaffold is merited prior to clinical translation in the future.

Chapter 1

Introduction: Positron Emission Tomography: From Bench to Bedside

Medical imaging encompasses several techniques used to diagnose and treat diseases and disorders within the body. These include X-rays, discovered in 1895 by Wilhelm Röntgen, [1] which ultimately paved the way for radiology and diagnostic imaging. From here, other more modern techniques emerged such as computed tomography (CT), magnetic resonance imaging (MRI), and ultrasound (US). All of these techniques provide valuable structural/anatomical information, but provide little functional information about the physiological and biochemical processes ongoing within a complex biological system.

Visualizing a specific biological target or process in this context is routinely performed through the use of radioactive probes, otherwise known as radiopharmaceuticals, for use in positron (β^+) emission tomography (PET) and single-photon emission computed tomography (SPECT) – and are the pillars of diagnostic medical imaging in modern Nuclear Medicine (NM). Interventional nuclear medicine includes radiotherapy with alpha and beta emitters. Although they will be discussed briefly, a detailed discussion of radiotherapeutics is outside the scope of this thesis which is focused upon diagnostic radiopharmaceuticals, but radiotherpy has been recently reviewed.[2] These scanning techniques can be superimposed, *via* hybrid cameras or software, on other anatomical imaging modalities such as MRI or CT to provide a more

complete picture about the function and anatomy of interest (SPECT/CT, PET/CT, PET/MR). The work described herein will focus on positron emission tomography, and radiopharmaceutical development: including the development of novel radiolabeling method(s) of small, drug-like molecules (Chapter 3), and the synthesis and (initial) pre-clinical evaluation of PET probes for CNS diseases and disorders (Chapter 4). Multi-disciplined, this encompasses the fields of medicinal chemistry, organic chemistry, radiochemistry, and chemical methodology development.

a. Beginnings: Radioactivity

The diagnostic radiology story began with the discovery of x-rays by WC Röntgen in 1895.[1] Röntgen's experiments with an electron beam tube and photographic plate lead to the imaging of his wife Anna Bertha's hand with her wedding ring, when, upon seeing the image, exclaimed "I have seen my death!" (Figure 1-1).[3,4] This work was followed closely by the discovery of the electron by JJ Thomson in 1897[5] – both of these discoveries resulting in an individual Nobel Prize in Physics in 1901 and 1906, respectively. In 1896, Henri Becquerel discovered naturally occurring radioemissions.[6] Becquerel, after unsuccessful attempts at observing X-rays (known as Röntgen rays at the time) emitted from minerals post-light absorption, later observed these rays from uranium salts. The unusual aspect of this experiment was that these rays could be observed in the absence of initial light absorption (or energy input). Becquerel had just discovered radiation, and those rays emitted were, for a time, called "Becquerel Rays", and were later identified as the result of radioactive decay from the uranium salts

themselves. Rumored to have little interest in the results, Becquerel passed this work on to his graduate student looking for a topic for her PhD dissertation, Marie Sklodowska (Figure 1-2).

Figure 1-1 First Medical X-Ray of Anna Bertha's hand by Wilhelm Röntgen (public domain)[7]

As Sklodowska began looking at other elements, compounds or minerals, to observe the emission of these rays, she became intrigued by different chemicals emitting different radiation and decided to isolate and purify them. With this, she requested the assistance of her husband, Pierre Curie, whose focus would be on the physical

measurements. This collaboration, between Marie and Pierre Curie, would later be known as one of the most famous scientific partnerships in history. Together, they extracted two new elements, polonium (Po) and radium (Ra), and found them both to be more radioactive than uranium (U). Thus, with the 1896 discovery of radioactivity by Henri Becquerel and the inspired research by Marie and Pierre Curie, they would share the 1903 Nobel Prize in Physics. Also, in 1903, the University of Paris awarded Marie her Ph.D. in physics.[6]

The field of radiochemistry, or chemistry of radioactive elements, was born with M. Curie. It wasn't until later that the term "radiochemistry" was introduced by Frederick Soddy, and much of the terminology used today coined by Ernest Rutherford. The radiation as a result of the decay of atoms, although assumed by M. Curie, was demonstrated by Rutherford and Soddy in 1902 by the discovery of α and β emissions (Rutherford won the Nobel Prize in Chemistry in 1908 for this work).[6,8,9] It is worth noting that M. Curie continued her work and was later awarded the 1911 Nobel Prize in Chemistry for characterization of polonium and radium, as well as the isolation of pure metal radium. With two Nobel Prizes, Marie Sklodowska-Curie was the first person to win/share two Nobel's, and is one of four people to have been awarded two Nobel Prizes in distinct fields. The Curie's daughter, Irène Joliot-Curie, in collaboration with her husband Frédéric, later won the 1935 Nobel Prize in Chemistry for the synthesis of new radioactive elements.[6] A testament to their impact on the field, the units of radioactivity are denoted as Becquerels (Bq) or Curies (Ci).

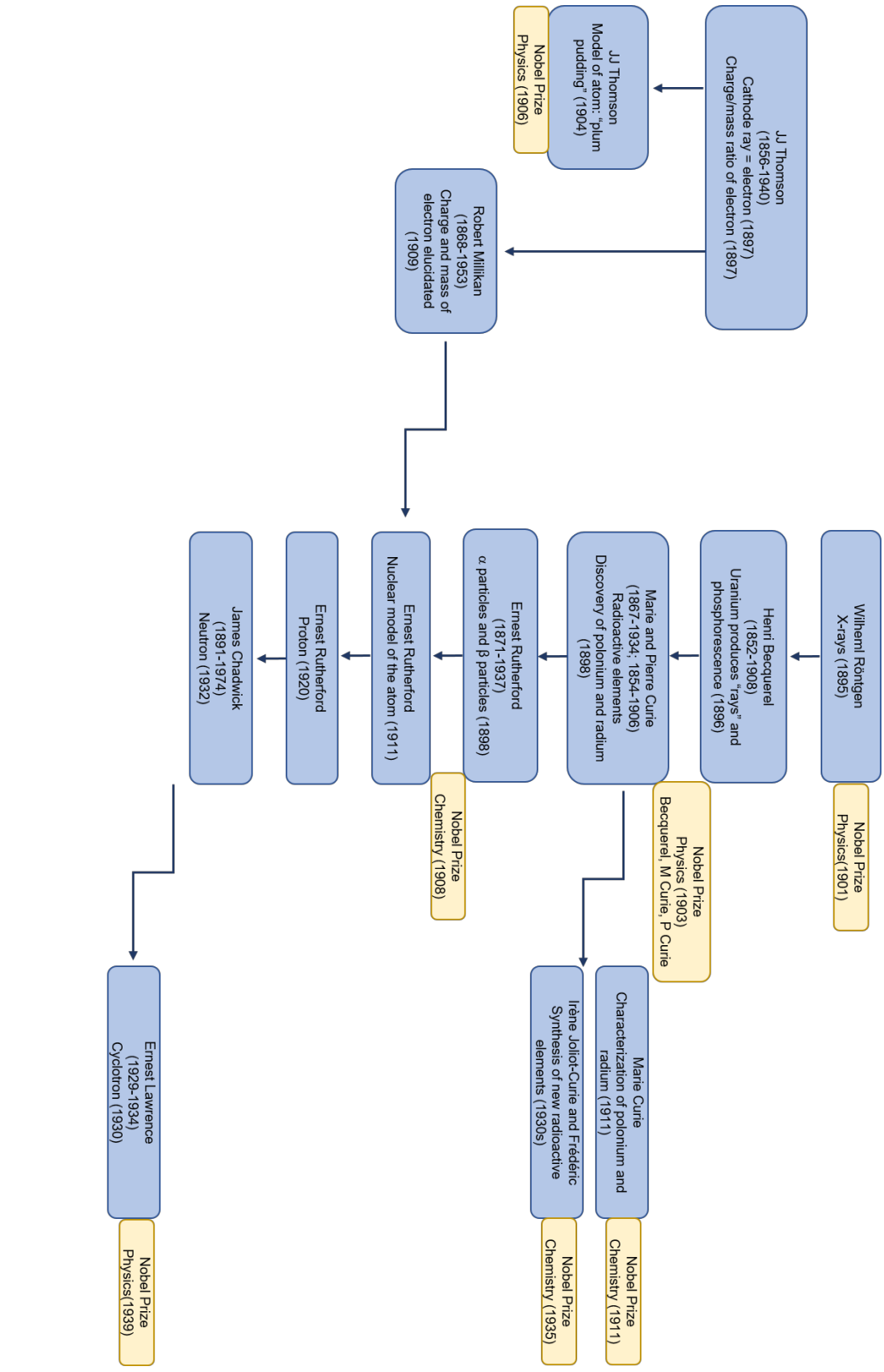

Figure 1-2 Brief Historical Summary of the Atom and Radioactivity

With this budding, new field and speculation about the applications to science and medicine, researchers were searching for new radioisotopes. Irène Curie and Frederic Joliot's work demonstrated the production of artificially produced radioactivity through the bombardment of aluminum, boron and magnesium with α particles to isotopes such as phosphorus, nitrogen and aluminum (1930s).[10] Specifically, and one of the first artificially made radionuclides, nitrogen-13, *via* $^{10}B(\alpha,n)^{13}N$.[11] In 1934, Oliphant, Rutherford and Harteck produced tritium through the collision of deuterium atoms.[12] Interestingly, as ^{3}H (low β emitter used frequently to label proteins, nucleic acids and organic drug-like molecules) and ^{14}C (labeling for use in absorption, distribution, metabolism, and excretion, ADME, studies in drug discovery) are the most commonly used isotopes in the laboratory today[13,14], carbon-14 was not the first carbon isotope to be discovered. The positron emitting isotope (used in PET imaging), ^{11}C was discovered by Kamen and used to demonstrate that the source of molecular oxygen in photosynthesis was water and not CO_2.[15] Shortly after, the existence of a long-lived carbon isotope, ^{14}C, was predicted before it was discovered in 1940 by Kamen and Ruben while working with Earnest O. Lawrence, a Nobel Laureate for the development of the cyclotron, at the Berkeley Radiation Laboratory (currently known as the Lawrence Berkeley National Laboratory).[16] Other organic, or physiological, isotopes ^{13}N and ^{15}O were utilized for biological studies, but diminished in popularity due to their impractically short half-lives, 10 min and 120 sec respectively.[11]

b. Production of Radionuclides

Particle accelerators were invented to investigate the structure of the atomic nucleus. Their principle job is to take a beam of particles, speed them up and increase their energy through an electric field (acceleration) and magnetic field (steering). It is interesting to note that the cyclotron was established with the goal of transmutation of elements, not the production of artificial radioactivity. It was not until Irène Curie and Frederic Joliot's synthesis of new radioactive elements in the 1930s that the Berkeley group noted the extended utility of their new instrument.[11]

With the incorporation of radioisotopes in biochemically significant pathways and molecules, the natural progression of the field spread into several branches of science. Indeed, the modern day nuclear medicine program requires a diverse group of specialists, with individuals often possessing more than one area of expertise. This ranges from physicists, engineers, biomathematicians, medical physicists, nuclear medicine physicians, kinetic modelers, organic chemists, medicinal chemists, radiochemists, and biochemists, etc. This exodus from traditional academic boundaries of departmental sciences to multidisciplinary national laboratories was launched by the father of the cyclotron, Ernest Lawrence – at the age of 27, as a new Professor at the University of California, Berkeley. Lawrence's need for space lead to the acquisition of an entire building in August 1931, called the "Radiation Laboratory", to house the research, design, construction, and operation of his cyclotron, as well as the increasing number of physicists, engineers and chemists critical to the research. The university later recognized his departure from traditional academic divisions, and established the Radiation

Laboratory as a free standing entity for the pursuit of nuclear science (broader than the customary “nuclear physics”, “nuclear chemistry” or “accelerator physics” terms often used).[17]

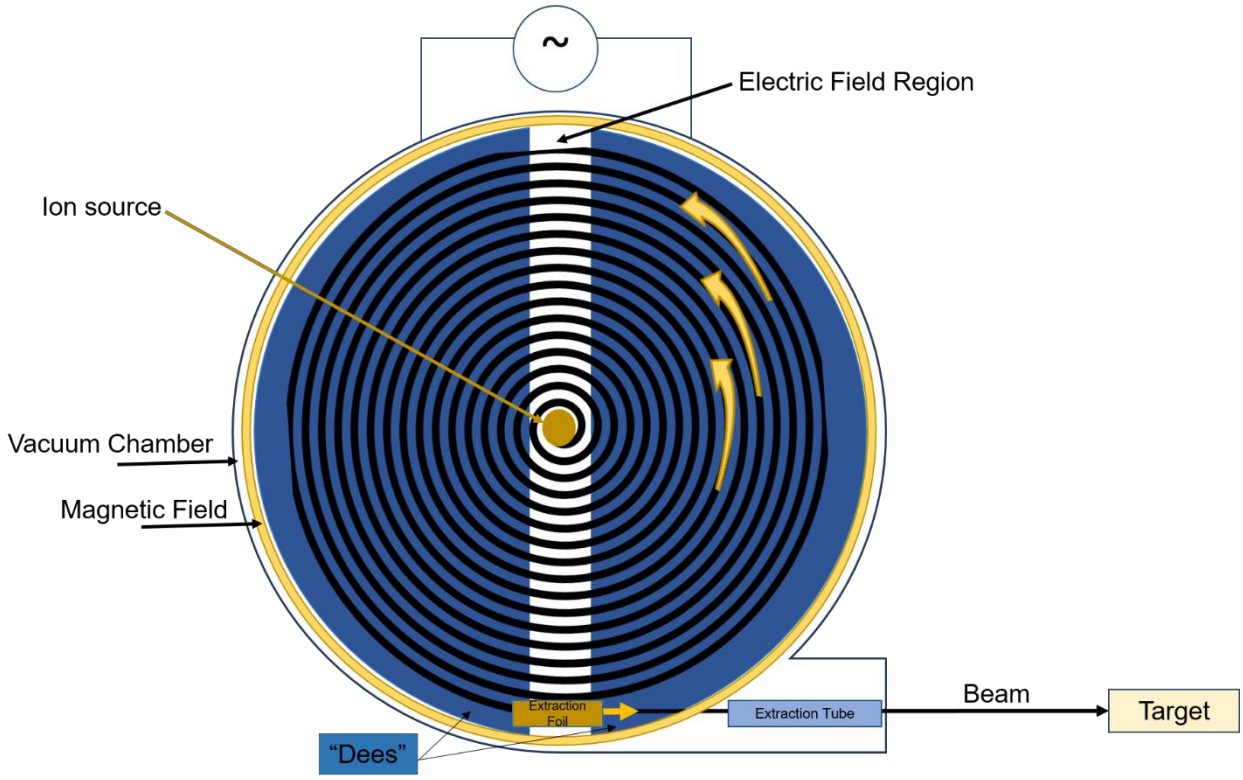

Figure 1-3 Simple Cyclotron

While the idea of the cyclotron was conceived years prior, Ernest O. Lawrence finalized its creation in 1932 and patented it in 1934.[17–20] Lawrence was awarded the 1939 Nobel Prize in Physics, in the field of accelerator physics and instrumentation. In consideration of the scope of this work, the workings of the modern cyclotron as it applies to the production of PET radionuclides will only be discussed. A cyclotron (Figure 1-3) is

composed of two D-shaped metal electrodes (often called “Dees”), between the poles of a large electromagnet, all contained in a vacuum chamber. In the center is either H_2 or D_2 gas, which is the source of the particles accelerated, in the form of H^- or D^- anions. In the presence of a strong magnetic field and alternating voltage of the electrodes, the anions are accelerated in a circular path. As they gain energy, the radius of the anion’s path increases until it passes through a stripping foil to remove the electrons, thus producing H^+ or D^+. These particles, now positively charged, are deflected out of the acceleration chamber to irradiate the target of choice. Once the high-energy particle hits the stable isotope target, the desired radionuclide is produced and subsequently delivered to appropriate containment for utilization.

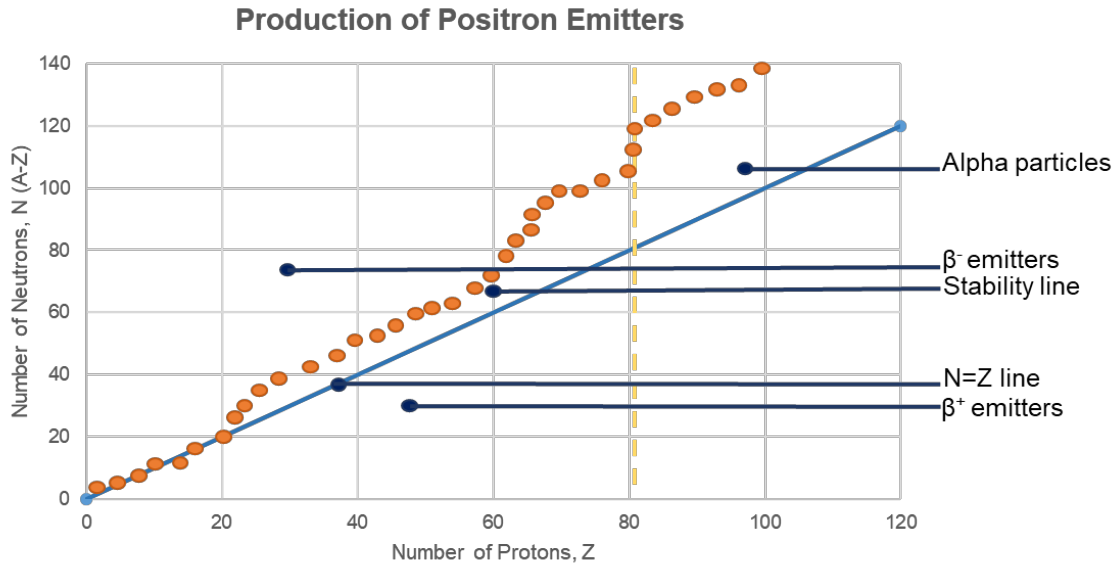

Figure 1-4 Nuclear Stability

Nuclear stability (Figure 1-4 Nuclear Stability) is often determined by proton to neutron ratio; above the stability line are the radionuclides that decay *via* alpha decay (α or He nucleus emission to decrease the mass number), below is positron (β^+) emission or electron capture (whereby the isotope gains more neutrons to become stable). Elements with Z>82 have no fully stable isotopes. Radioactive decay modes of interest for therapy are α and β, and for imaging β^+ (positron) or γ (gamma) emission (Scheme 1-1).

Radiation therapy utilizes ionizing radiation largely in oncology to kill cancer cells, shrink tumors, etc. External radiation therapy exposes a specific area of the patient's body to radiation, via high-energy x-rays. On the other hand, targeted radionuclide therapy is systemic (like chemotherapy). This employs a drug-like molecule labeled with a radionuclide to deliver a (toxic) dose of radiation to a diseased site (tumor). The three available radionuclides are, α (alpha) emitters, β (beta) emitters, and Auger electrons, which offer a variety of radionuclides that can be chosen for half-life, tissue range, and chemistries to tailor the therapeutic (personalized medicine).[21]

For targeted radiotherapy, α emitters travel a shorter distance in tissue but can deliver 5MeV of energy over several microns, whereas β emitters typically deliver a few hundred KeV over a distance magnitudes larger (millimeters).[22] Alpha emitting radionuclides include ^{213}Bismuth, ^{211}Astatine, and ^{223}Radium, and have been demonstrated in monoclonal antibodies, and gold nanoparticles. Beta emitting radionuclides FDA approved for human use include ^{90}Yttrium, ^{131}Iodine, ^{153}Samarium, and ^{89}Strontium; other β emitters include ^{177}Lutetium, ^{166}Holmium, ^{185}Rhenium, ^{188}Rhenium, ^{67}Copper, ^{149}Promethium, ^{199}Gold, and ^{105}Rhodium.[21,22] Auger therapy, on the other hand,

relies on the Auger electron. The Auger electron is the result of an inner shell electron vacancy (as the result of radionuclide decay by electron capture, for example); the vacancy is filled by electron transitions from shells or subshells of higher energy, and that energy difference can be emitted as a photon, or transferred to other orbital electrons that are released (this is the Auger electron). Some Auger-emitting radionuclides include: ^{111}Indium, ^{123}Iodine, and ^{77}Bromine; this therapy relies on large quantities of these electrons at low energy to target and kill tumors/cancer cells in a short range.[21,23]

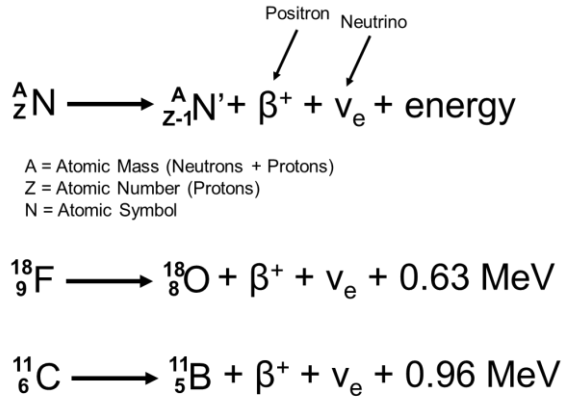

Scheme 1- 1 Selected PET Radionuclides and Positron Decay

With regard to for imaging β^{+} (positron) or γ (gamma) emission as the result of positron PET isotopes are proton rich, typically short lived (minutes to hours), and are produced by proton reactions, such as (p,n) and (p,α). Most of the radionuclides utilized in PET are produced in a cyclotron, while others are produced as daughter products in generators. Common PET radionuclides include carbon-11, nitrogen-13, oxygen-15, fluorine-18, copper-62 (generator), gallium-68 (generator or cyclotron), rubidium-82 (generator), iodine-122, iodine-124 and zirconium-89.[24]

Table 1-1 Common PET radionuclides

Entry	Name	Half-life	Nuclear Reaction	Final Product	Decay Product Z-1; N+1
1	Carbon-11 (^{11}C)	20 min	$^{14}N(p,\alpha)^{11}C$	$[^{11}C]CO_2$	$^{11}C \rightarrow {}^{11}B + \beta^+ + \nu_e$ $^{11}C + e^- \rightarrow {}^{11}B + \nu_e$
2	Nitrogen-13 (^{13}N)	10 min	$^{16}O(p,\alpha)^{13}N$	$[^{13}N]NH_3$	$^{13}N \rightarrow {}^{13}C + \beta^+ + \nu_e$
3	Fluorine-18 (^{18}F)	110 min	$^{18}O(p,n)\,^{18}F$	$[^{18}F^-]$ in $[^{18}O]H_2O$	$^{18}F \rightarrow {}^{18}O + \beta^+ + \nu_e$
4	Oxygen-15 (^{15}O)	2 min	$^{15}N(p,n)\,^{15}O$		$^{15}O \rightarrow {}^{15}N + \beta^+ + \nu_e$
Key: p (proton), α (alpha-particle), β^+ (positron), ν_e (electron neutrino)					

A common list of PET radionuclides (Table 1-1 Common PET radionuclides) and non-conventional positron emitters for imaging (Table 1-2 Non-standard PET Radionuclides[26]) are listed as such. The choice of radionuclide depends on a number of factors including the ability to incorporate it into a given bioactive molecule and the intended application (e.g. commercial distribution). Generally, it is good practice to match the physical half-life of the radionuclide with the biological half-life of the labeled molecule. Thus, carbon-11 and fluorine-18 are most commonly used to labeling small, drug-like molecules, while longer lived isotopes such as zirconium-89 find utility labeling biologics, including antibodies.[25]

While the most common F-18 fluorination method for the production of radiopharmaceuticals is nucleophilic fluorination, certain compounds are still optimally prepared by using electrophilic techniques. Fluorine gas, $[^{18}F]F_2$, is the most simple fluorination reagent to handle, but is highly reactive and end products suffer with reduced radiochemical yields, selectivity, and low specific activity due to carrier-added production. Electrophilic fluorine can be produced *via* $^{20}Ne(d,\alpha)^{18}F$ to encourage F-18/F-19 exchange

for a carrier added production of $[^{18}F]F_2$; on the other hand, another method is through $^{18}O(p,n)^{18}F$ followed by secondary irradiation in ^{19}F (gas) to provide $[^{18}F]F_2$.[27–30] Other electrophilic reagents have been derived and used extensively.[31] Nucleophilic F-18 fluorinations are the most widely used and perhaps the most classical method to radiolabel with fluorine-18.

Table 1-2 Non-standard PET Radionuclides[26]

Entry	Isotope	Half-life	Decay Modes/%	Max β^+ energy (MeV)	Reaction	Natural Abundance of Target Isotope
1	^{76}Br	16.2 h	β^+/58.2 EC/41.8	3.98	^{76}Se(p,n)	9.1%
2	^{124}I	4.18 d	β^+/22.0 EC/78.0	2.15	^{124}Te(p,n)	4.8%
3	^{86}Y	14.74 h	β^+/34.0 EC/66.0	3.15	^{86}Sr(p,n)	9.9%
4	^{94m}Tc	52 min	β^+/72.0 EC/28.0	2.47	^{94}Mo(p,n)	9.3%
5	^{68}Ga	68 min	β^+/88	1.9	^{68}Ge/^{68}Ga generator	n/a
6	^{66}Ga	9.49 h	β^+/56.5 EC/43.5	4.15	^{66}Zn(p,n)	27.8%
7	^{60}Cu	23.7 min	β^+/93.0 EC/7.0	3.92	^{60}Ni(p,n)	26.1%
8	^{64}Cu	12.7 h	β^+/17.8 EC/43.8 β^-/38.4	0.66	^{64}Ni(p,n)	1.16%
9	^{89}Zr	78.5 h	β^+/22.8 EC/77.2	0.40	^{89}Y(p,n)	100%

c. Positron Emission Tomography

PET is a non-invasive multidimensional imaging modality for investigating *in vivo* physiological and biochemical processes (*in vivo* defined here as imaging these processes in living creatures); it has applications in many different disciplines including neurology, psychiatry, oncology, and cardiology. PET utilizes a positron emitting (β^+)

radionuclide such as ^{11}C, ^{13}N, ^{18}F and ^{15}O. As the radionuclides decay, a positron (β^+) and electron neutrino (ν_e) are released. Essentially a core proton is transformed into a neutron and a positron (basically a positively charged electron) and a neutrino.[32] ^{18}F decays by emitting a positron with an energy (max) of 635 MeV, ^{11}C with a (max) energy of 0.96 MeV(Scheme 1- 1).[33,34]

The positron travels in tissue (up to 1mm) until it meets its antiparticle, the electron (e^-) and an annihilation event occurs. This event produces two 511 KeV gamma ray photons (γ) that project 180° from the event location to detectors on the PET scanner; here the photon pair is simultaneously detected as a coincident event. Localization of the radiopharmaceutical is then determined by reconstruction of all the annihilation events that occurred during a PET scan into a 2D or 3D image (Figure 1-5 General PET Workflow).[32]

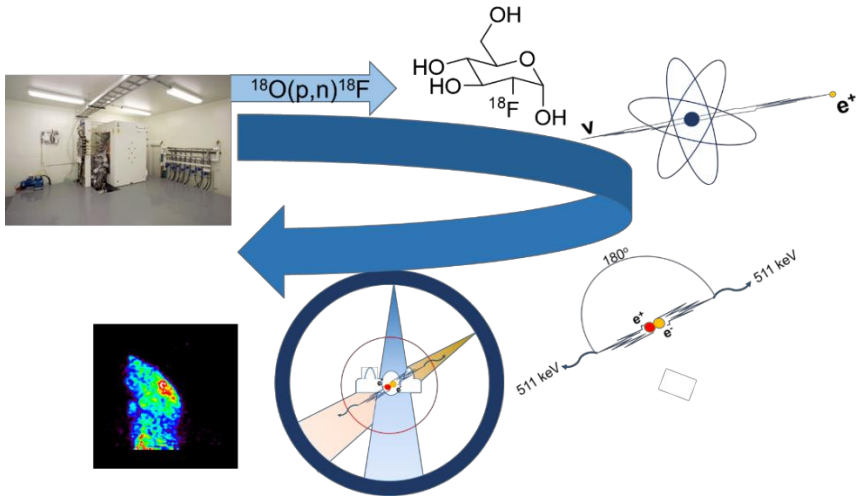

Figure 1-5 General PET Workflow

Radiopharmaceutical doses are reformulated in ≤10% EtOH/saline doses, and undergo stringent quality control (QC) in a timely manner before being released to a nuclear pharmacist and nuclear medicine physician for clinical use. These are completed in accordance with 21CFR212 – Current Good Manufacturing Practice for Positron Emission Tomography Drugs or the U.S. Pharmacopeia Chapter 823 [USP-32, NF-27, 2009] – Standards for PET Drugs. As such, the doses are analyzed as follows: visual inspection (clear, colorless, free of particulate matter), pH (pH paper, typically 4.5-8), chemical and radiochemical purity (HPLC or TLC), radionuclidic identity (half-life), radionuclidic purity (multi-channel analyzer), sterile filter integrity (bubble-point or filter integrity), bacterial endotoxins, sterility, and residual solvent analysis (GC). Chemical purity if often calculated by normalizing to specific activity of 2 Ci/μmol. As mentioned before, radioactivity is given the SI unit Becquerel (Bq), or the non-SI, but commonly used unit, Curie (Ci) (1 Ci = 37 GBq). Specific activity is a measure of “hot” to “cold” in the final radiopharmaceutical: carbon-11 (hot) to carbon-12 (cold), or fluorine-18 (hot) to fluorine-19 (cold); this is of more concern when the radiosynthesis involves a cold carrier and would yield a higher injected cold mass. Optimally, radiopharmaceuticals are prepared no-carrier-added (N.C.A.).

Strategies to quickly and efficiently radiolabel drug-like molecules have developed vastly over the years. Indeed, advancements in carbon-11 and fluorine-18 chemistry in the last decade have enabled the radiosynthesis of novel PET radiotracer otherwise inaccessible for PET.

d. Fluorine in Medicinal Chemistry

Fluorine is the most electronegative element on the periodic table and has the smallest atomic radius of the Period 2 elements ($1s^2 2s^2 2p^5$). It was discovered in 1886 by chemist Henri Moissan (who was later awarded the Nobel Prize for these efforts in 1906). In organic chemistry, the C-F bond is the strongest bond at 105.4 kcal/mol. The strength of this bond is largely attributed to the significant electrostatic attraction between $F^{\delta-}$ and $C^{\delta+}$ as opposed to the traditional covalent bond sharing of electrons.[34,35]

In medicinal chemistry, fluorine is a common bioisostere for hydrogen. Thus, a C-H to C-F substitution is common and approximately 15% of approved pharmaceuticals contain at least one (or more) fluorine atoms.[36] Given steric considerations (F and H share similar van der Waal's radii, F =1.47 Å, H = 1.2 Å), this substitution is conservative and is often a substitute to hinder metabolism at a labile site. Another common bioisostere is the F for O substitution, which matches size for electronegative atoms (van der Waal's radii: F =1.47 Å, O =1.52 Å), as well as geometry. C-F for C-OH is another common substitution, which can also provide excellent insight into the H-bonding properties and requirements in biological systems.[34–38] Fluorine also improves other physicochemical property considerations, such as pK_a (not including inductive changes to neighboring functional groups), solubility, logD and binding affinities (selectivity and potency), and can additionally improve brain penetration (for CNS drugs) by hindering susceptibility to P-glycoprotein (Pgp)-mediated efflux.[34,36–38]

A major concern in drug discovery, oxidative metabolism by liver enzymes such as cytochrome P450 prior to drug elimination can be evaded by substitution of a fluorine.[34,37] Fluorine's ability to block oxidative metabolism in saturated aliphatic systems is, in part, due to the high heat of formation and bond energy of the C-O and O-H bond relative to the F-O bond, which excludes oxidative attack on fluorine. Moreover, this is also seen in steric and conformation effects through the use of a $-CF_3$ group next to a C-H, which retards metabolism and aids in stability.[37,39] Para-fluoro substitution is a common substitution to block or retard oxidation in aromatic systems (e.g. to prevent oxidation to a phenol), in addition to aromatic/ aliphatic methyl oxidation and dealkylation.[37,39] One such clinical example of fluorine being used to modify drug metabolism is on the optimization of lead SH48461 (ED_{50} (hamster) = 2.2 mg/kg/day) to SCH58235 (Ezetimib) (ED_{50} = 0.04 mg/kg/day), the oral cholesterol absorption inhibitor (Figure 1-6 Part of Ezetimib Optimization: Blocking Metabolically Labile Sites With Fluorine Substitution[40]). As is a common substitution, the *para*-phenyl position was blocked by inclusion of a fluorine, as well as complete replacement of the 4-methoxy group with an additional fluorine to prevent oxidation to the phenol.[36–40]

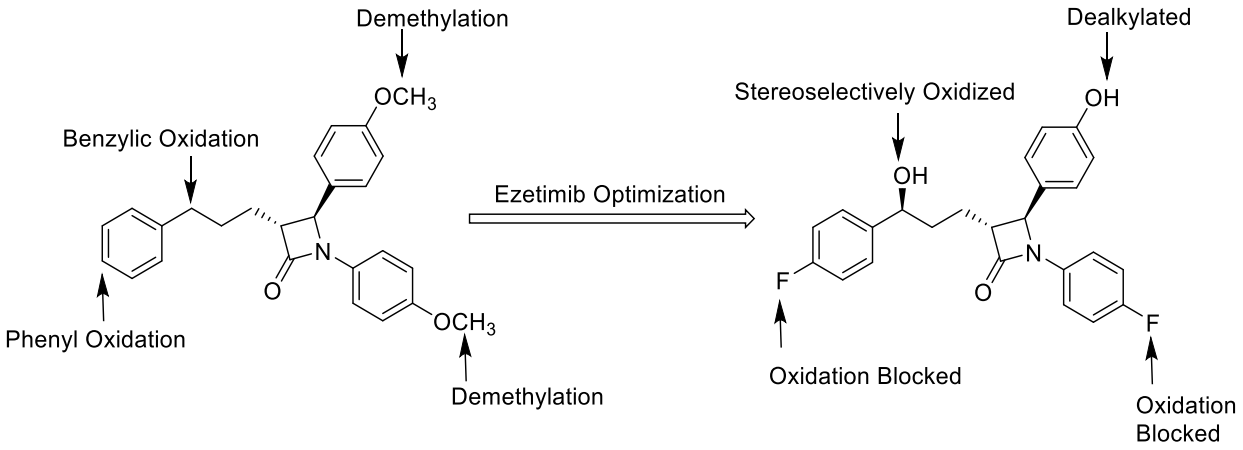

Figure 1-6 Part of Ezetimib Optimization: Blocking Metabolically Labile Sites With Fluorine Substitution[40]

e. Late-Stage ^{18}F Fluorination PET Radiochemistry

Radiochemical limitations currently limit the potential impact of PET imaging on personalized medicine and drug discovery. The development of new radiopharmaceuticals is largely represented by the compounds that can be readily radiolabeled but do not necessarily represent the best compound regarding selectivity, or fit the desired pharmacology or pharmacokinetic profile of a PET imaging agent.[41,42] The development of fluorine-18-labeling strategies to access any radiopharmaceutical scaffold remains a unique challenge to the field. Fluorinations alone are challenging reactions, but these challenges are exacerbated when working with fluorine-18. It is important to note that standard (cold) F-19 fluorinations largely proceed with excess fluorinating agent (e.g. fluoride), whereas this system necessitates the use of F-18 as the limiting reagent, thus posing a unique challenge. Consequently, these reactions need to have stoichiometry compatible with small amounts of radionuclide (typically nanomolar

quantities). Moreover, radiofluorination reaction times must be short, typically 3 to 30 minutes due to the short half-life of ^{18}F (110 min), and be able to produce clinically usable amounts (> 50 mCi) in high specific activity (>1 Ci/μmol).

Nucleophilic [^{18}F]fluoride is produced by the $^{18}O(p,n)^{18}F$ nuclear reaction from [^{18}O]H_2O. Typically the $^{18}F^-$ anion is delivered in a bolus of [^{18}O]H_2O from where it is loaded on to an ion-exchange column, typically a quaternary methyl ammonium (QMA) anion exchange cartridge, and eluted to a cryptand, K_{222} (Kryptofix), an aminopolyether, which also acts as a phase transfer catalyst and used in conjunction with potassium carbonate to activate the [^{18}F]fluoride. While the most common way to produce ^{18}F tracers in the clinic is through [^{18}F]KF·K_{222}, other options include [^{18}F]cesium fluoride, [^{18}F]tetrabutylammonium fluoride ([^{18}F]TBAF), and [^{18}F]tetraethylammonium fluoride; this is done *via* elution with cesium carbonate, tetrabutylammonium bicarbonate, and tetraethylammonium bicarbonate.[31,43,44] From here, the fluorine-18 (complex) is azeotropically dried (typically in water/MeCN) to remove residual water from the target, leaving an activated ^{18}F nucleophile. The ^{18}F nucleophile is then reacted with the precursor in aprotic, anhydrous solvents, such as MeCN and DMF.

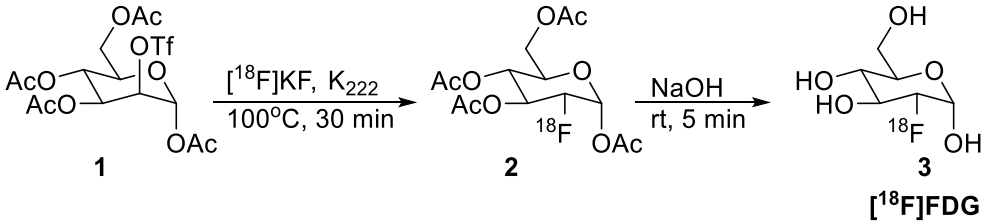

Scheme 1- 2 [^{18}F]FDG

Radiochemical considerations include incorporation of the fluorine label at the end of synthesis due to the short half-life of the radionuclide and lends itself to the recently coined term “late stage” fluorination. These “late-stage” fluorination reactions can be divided into nucleophilic aromatic substitution, S_NAr, direct nucleophilic fluorinations, S_N2, and special cases such as prosthetic groups (an auxiliary that can labeled and attached to a precursor otherwise unsuitable for direct nucleophilic fluorination)[45] and unactivated arenes (this is not an exhaustive list). Direct nucleophilic fluorinations traditionally utilize a leaving group such as a tosylate, mesylate, or triflate, then any deprotection following the ^{18}F fluorination, making this labeling strategy often a two-step procedure. [^{18}F]Fludeoxyglucose, aka 2-[^{18}F]fluoro-2-deoxy-D-glucose ([^{18}F]FDG, **3**) is the most widely used F-18 PET radiopharmaceutical and it synthesized from the mannose-triflate precursor **1** and later deprotected (Scheme 1- 2 [^{18F}]FDG). Other clinically relevant tracers of a direct fluorine-18 labeling strategy include [^{18}F]FEOBV (**5**) ([^{18}F]fluoroethoxybenzovesamicol) with a tosyl precursor (**4**) and [^{18}F]FLT (**8**) (3’deoxy-3’-[^{18}F]fluorothymidine) with a nosyl precursor (**6**)(Scheme 1- 3). As with the [^{18}F]FLT precursor, the Boc-Boc-Nosyl precursor (**7**) provides higher yields compared to the cyclic precursor.[46] [^{18}F]fluoroethyl tyrosine ([^{18}F]FET) is accessed through direct labeling of a prosthetic group, and 2-nitroimidazoles such as [^{18}F]fluoroazomycin arabinoside ([^{18}F]FAZA) and [^{18}F]fluoromisonidazole ([^{18}F]FMISO) through simple S_N2 displacement of a tosylate.[47,48]

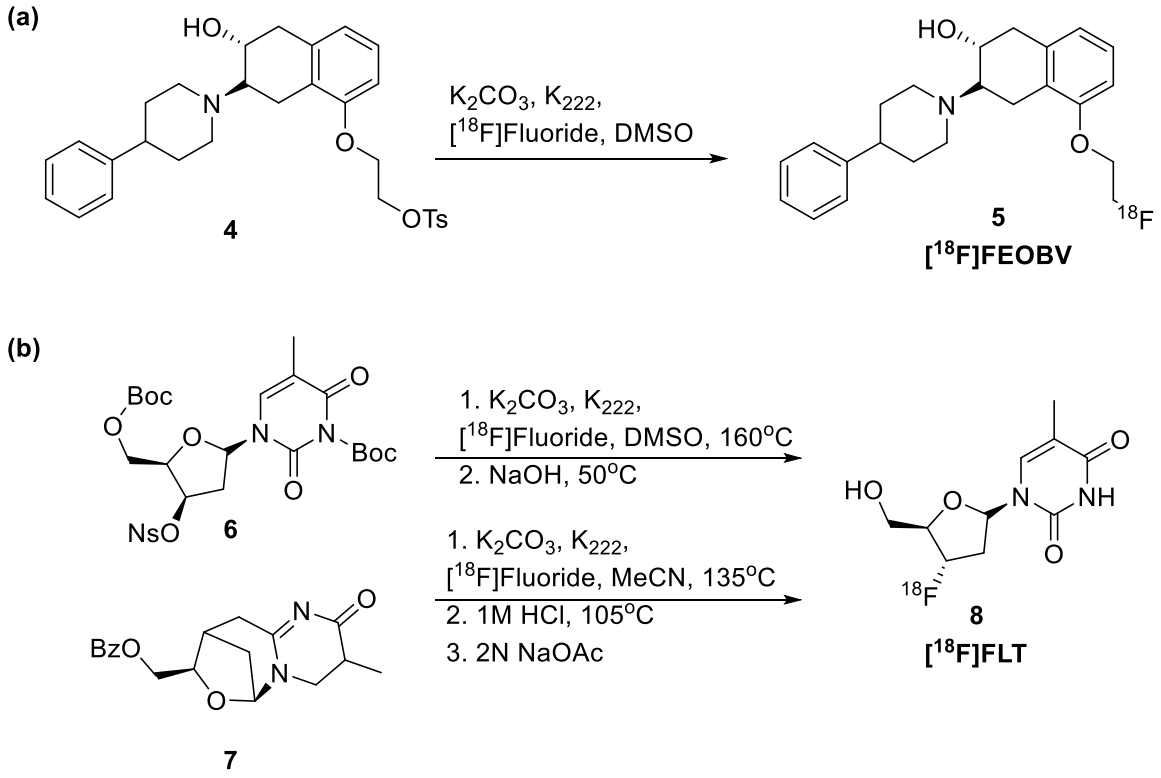

Scheme 1- 3 Direct F-18 fluorination of [^{18}F]FEOBV and [^{18}F]FLT

Other non-classical reactions include palladium-catalyzed allylic ^{18}F fluorination reactions. Allyl 4-nitrophenyl carbonate and cinnamyl methyl carbonate (**9**), with [^{18}F]TBAF (*t*BuOH)$_4$ and catalytic (Pd(dba)$_2$ (dibenzylidenacetone = dba), were converted to the cinnamyl fluoride (**10**) (R = $C_6H_4NO_2$ in 5-7% RCY and R = Me 10-52% RCY). Cinnamyl bromide under similar conditions provided (**10**) in 40-42 % RCY from the chloro- and bromo-precursors (**11**) (Scheme 1- 4).[49] Other work to access these substrates included iridium-catalyzed allyl fluorination of trichloroacetimidates, and allylic carbonates.[49–51]

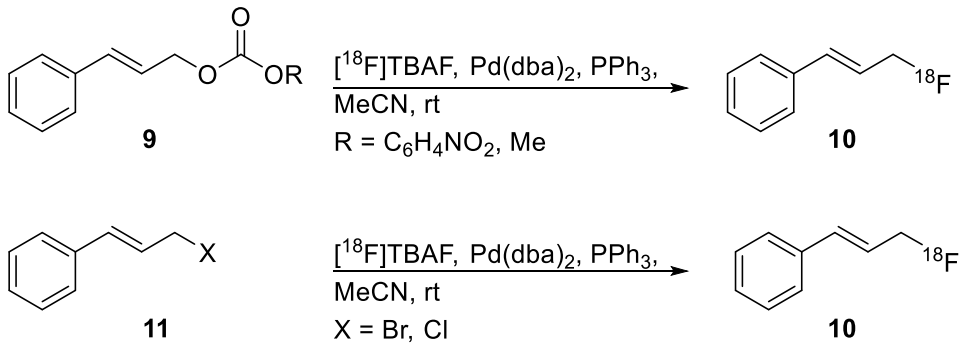

Scheme 1- 4 Palladium-catalyzed allylic [^{18}F]fluorination reactions

Nucleophilic aromatic substitution, S_NAr, reactions with [^{18}F]fluoride is another strategy, even though these reactions require an appropriately activated arene, and often requires harsh reaction conditions (such as longer reaction times and high temperatures). Isotopic exchange with ^{19}F, while it is an attractive option and has been applied in

syntheses of [^{18}F]flumazenil, suffers from poor specific activity and the inability to separate the two F-19/F-18 products.[52]

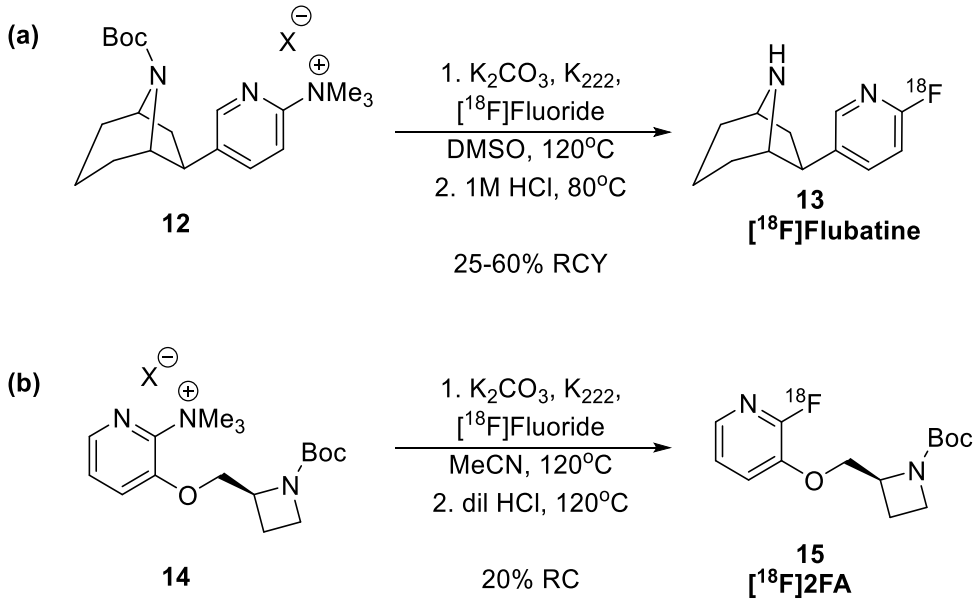

Scheme 1- 5 Trimethylammonium salt precursors for [^{18}F]Flubatine and [^{18}F]2FA

Traditionally, direct [^{18}F]fluorination of activated arenes with electron-withdrawing groups, contain -NMe^+, -NO_2, -Cl, -SAr_2^+, etc, leaving groups and makes these substrates amenable to S_NAr conditions.[31,53] One such example is with the purpose of imaging the $\alpha4\beta2$ subtype of the nichotinic acetylcholine receptor (NaChR); this is accessed *via* S_NAr of the the Boc-protected trimethyl ammonium salt (**12**) to provide [^{18}F]Flubatine (**13**) (an epibatidine derivative) or [^{18}F]2FA (**15**) (Scheme 1- 5).[54–56]

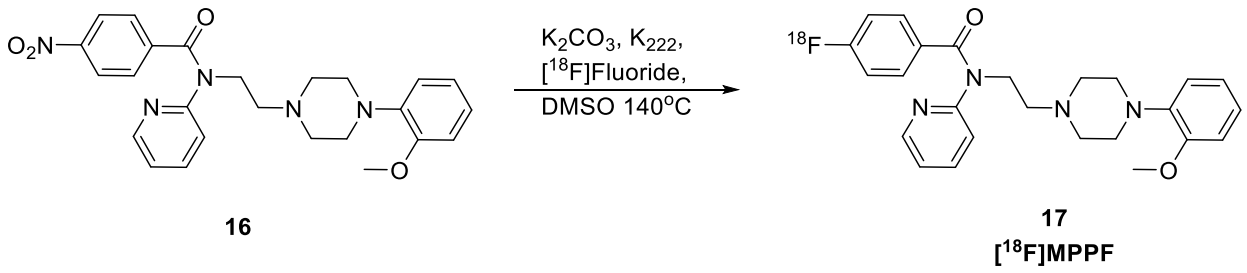

16 **17**
[^{18}F]MPPF

Scheme 1- 6 Direct S_NAr for production of [^{18}F]MPPF

Another radiopharmaceutical that utilizes a nitro-precursor (**16**) is [^{18}F]MPPF (**17**), or 4-(2'-methoxyphenyl)-1-[2'(*N*-2''pyridinyl)-*p*-[^{18}F]fluorobenzoamido]ethylpiperazine, and is used to image serotonin-1A (5HT1A) receptors. This radiolabling utilizes direct S_NAr of the nitro- precursor (**16**) and [^{18}F]fluoride with no secondary deprotection step (Scheme 1- 6 Direct S_NAr for production of [^{18}F]MPPF).[31,46,57]

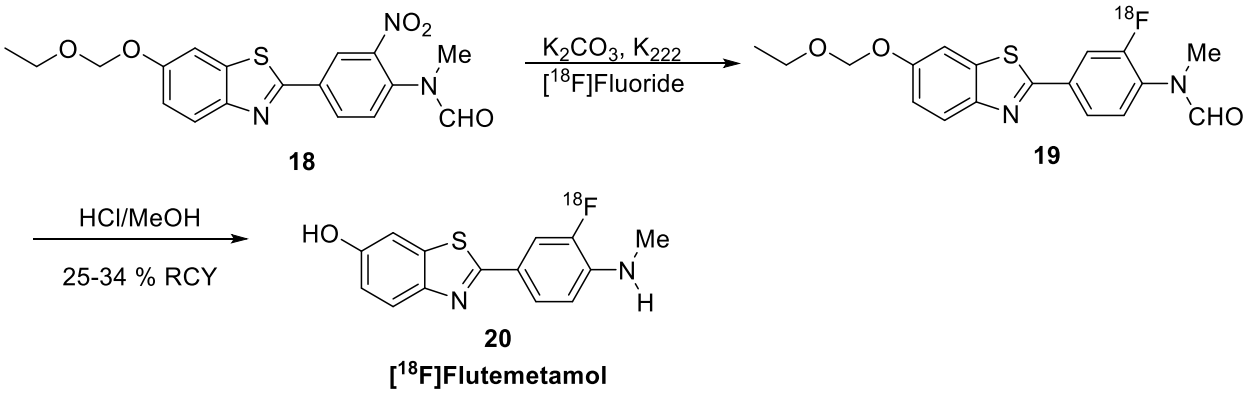

18 **19**
20
[^{18}F]Flutemetamol

Scheme 1- 7 Radiosynthesis of [^{18}F]Flutemetamol

Accessing scaffolds with electron rich, unactivated or electron neutral arenes pose a unique challenge to ^{18}F nucleophilic fluorination. Protecting group manipulation through

alteration of the electron donating/withdrawing characteristics is such a solution for direct fluorination. Such is the case of [^{18}F]flumetamol (**20**), which demonstrates direct labeling of the *ortho*-nitroaniline (**18**) through the use of a formamide protecting group to enable displacement of the nitro with ^{18}F, followed by deprotection of the phenol (**19**) (Scheme 1- 7 Radiosynthesis of [^{18}F]Flutemetamol).[58]

Another ingenious method to radiolabel a phenol is fluorination of the aldehyde (**21** to **22**) or ketone followed by Baeyer-Villiger oxidation (**23**), then saponification with NaOH to generate the desired phenol (**24**) (Scheme 1- 8 Radiolabeling phenols utilizing Baeyer-Villiger Chemistry).[59] While these approaches are a testament to the creative and rather resourceful steps radiochemists are willing to take to access these radiopharmaceuticals, these reactions are limited in that they are lengthy, often messy, and difficult to automate. In an attempt to simplify the ease with which one radiolabels a phenol, Gouverneur reported a metal-free oxidative ^{18}F fluorination with phenyliodine diacetate (PIDA) as the oxidant and [^{18}F]TBAF as the fluorine source. This proceeded in one step, with excellent yields and good substrate tolerance.[60]

The Balz-Schiemann and Wallach reaction is another established method(s) to incorporate ^{18}F into arenes. The Balz-Schiemann reaction involves an aryl diazonium salt (diazonium fluoroborate), followed by thermal decomposition with a fluoride source to produce fluoroarenes. The Wallach reaction, on the other hand, prepares fluoroarenes through decomposition of an aryl triazene precursor. This reaction is thought to proceed through a diazonium salt, *via* triflic acid promoted protonation of the triazene. Due to low RCYs and emerging techniques, however, these reactions are rarely used.[61–63]

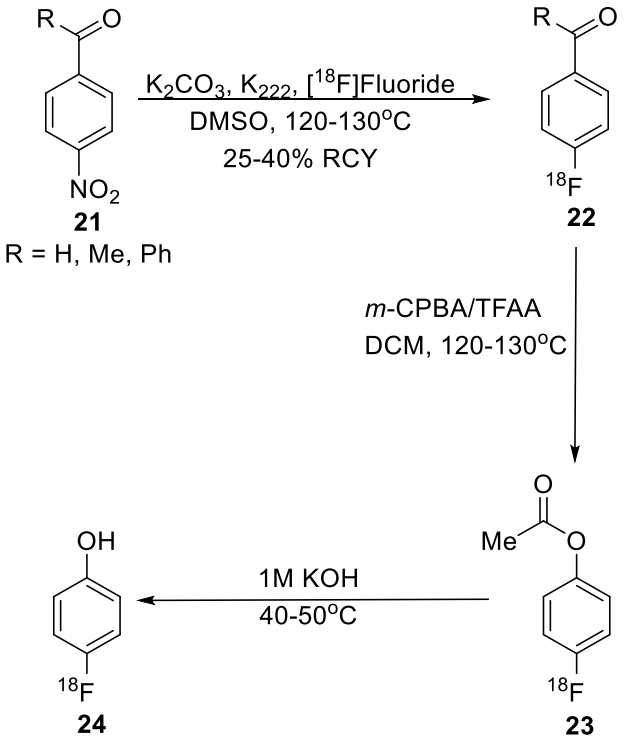

Scheme 1- 8 Radiolabeling phenols utilizing Baeyer-Villiger Chemistry

The introduction of diaryliodonium salt precursors (Scheme 1- 9 Diaryliodonium salt precursors for the synthesis of [^{18}F]fluoroarenes) allowed moderately electron-rich arene systems to be accessed. Independently, aryl(2-thienyl)iodonium salts (**25**) were developed as suitable substrates for ^{18}F S_NAr (Scheme 1- 9a).[64,65] Pike's group used a similar strategy with diaryliodonium tosylates (**27**) to synthesize PET ligands selective for the metabotropic glutamate receptor 5 (mGluR5) (Scheme 1- 9b).[66] A challenge to this chemistry, however, is extreme reaction conditions (high temperatures, over 150°C), limited functional group tolerance, and less than optimum radiochemical yields. To improve upon this chemistry, iodonium ylides, later expanded to spirocyclic iodonium ylides to improve precursor stability, were demonstrated to be suitable precursors for

labeling arenes with electron donating, neutral, and withdrawing characteristics and was applied to existing PET radiopharmaceuticals in good radiochemical yield (**29, 31**) (Scheme 1- 9c, d).[67,68]

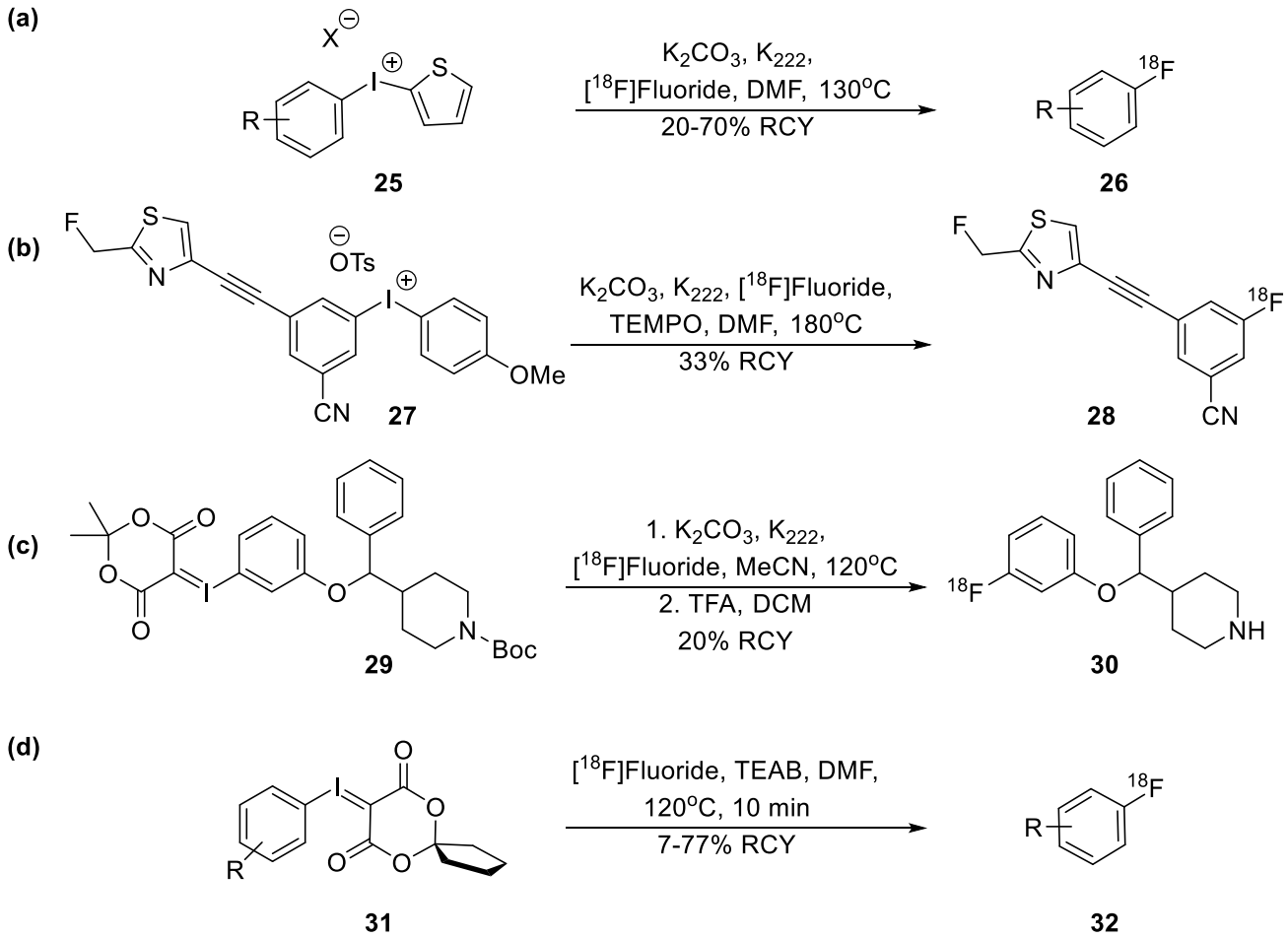

Scheme 1- 9 Diaryliodonium salt precursors for the synthesis of [^{18}F]fluoroarenes

Another approach reported by Ametamey *et al.* utilizes triarylsulfonium salts (**33, 34**) for fluorine-18 labeling *via* SNAr, utilizing [^{18}F]KF and [^{18}F]CsF as the nucleophilic ^{18}F

source on a variety of model substrates (Scheme 1- 10 Triarylsulfonium salt precursors for the synthesis of [^{18}F]fluoroarenes).[69,70]

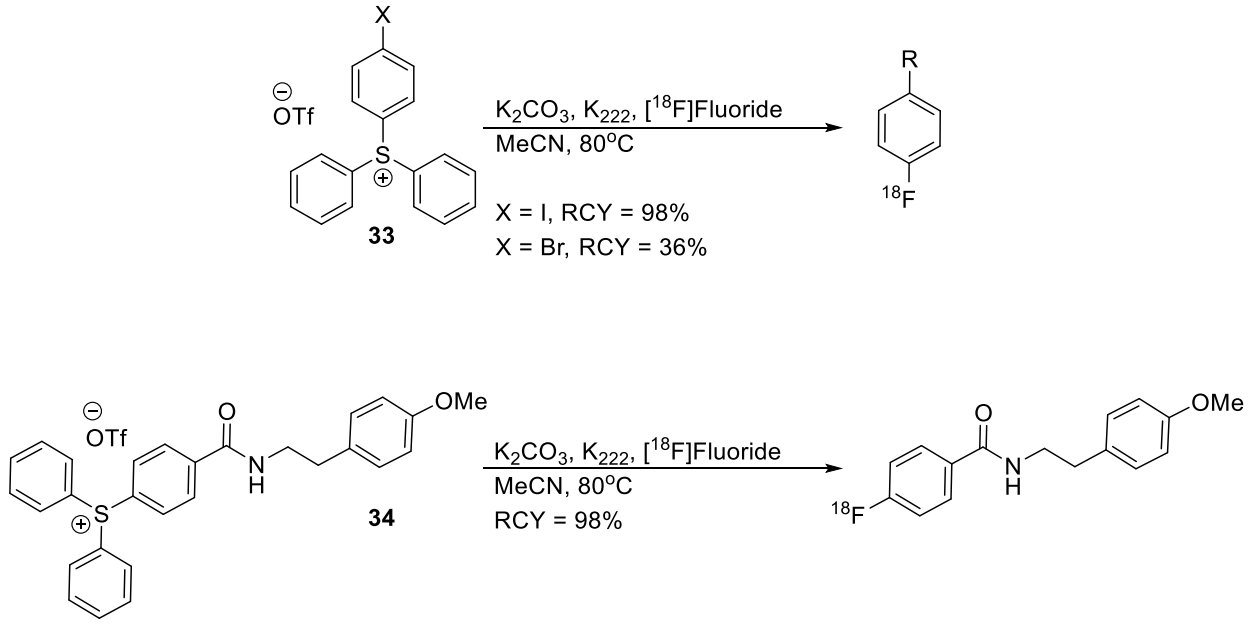

Scheme 1- 10 Triarylsulfonium salt precursors for the synthesis of [^{18}F]fluoroarenes

Diarylsulfoxide precursors were also described by Pike and coworkers, and proceeded in moderate to good yields, within only a few minutes, with symmetrical and asymmetrical substrates (Scheme 1- 11 Diarylsulfoxide precursors for the preparation of p-[^{18}F]fluoroarenes).[71,72]

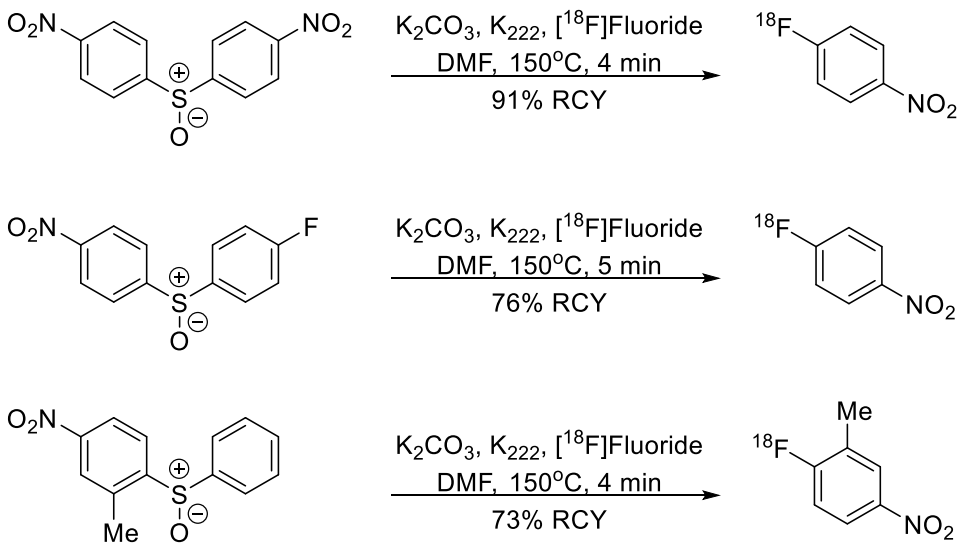

Scheme 1- 11 Diarylsulfoxide precursors for the preparation of p-[^{18}F]fluoroarenes

A recent advancement from the Murphy group that doesn't require the use of transition metal catalysts, or special handling includes the nucleophilic ^{18}F fluorination of aniline-derived N-arylsydnones (**35**) (Scheme 1- 12). This uses simple air stable reagents for direct radiofluorination, but is unusable for electron rich or unactivated arenes (no F-18 fluorinated product was detected). The group produced 18 examples of this chemistry (**36**), fully automatable, and one labeled peptide to demonstrate utility in PET.[73]

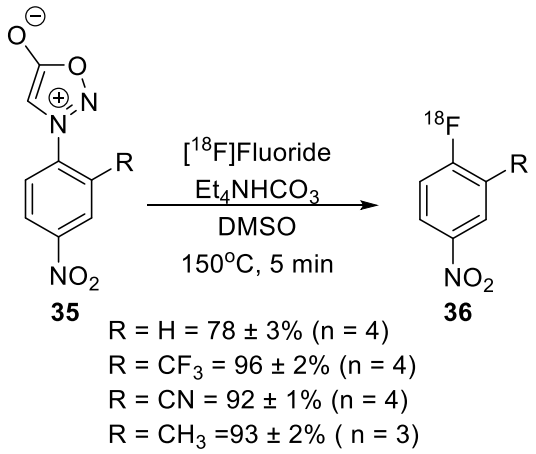

Scheme 1- 12 F-18 Nucleophilic Radiofluorination of N -Arylsydnones

A more recent development in ^{18}F fluorination of electron-rich arenes is with transition metal catalysts. Radiofluorination of arenes using palladium complexes (**37/38)** was demonstrated by Hooker and Ritter as a two-step labeling procedure (**37** to **40**) with reasonable yields, and on a variety of substrates (**41**, **42**, **43**) (Scheme 1- 13).[74–76] Though useful, air and water sensitivity (including azeotropic drying of the ^{18}F fluoride) hindered the translation of this approach to automated synthesis modules. A nickel-mediated oxidative fluorination method was subsequently developed to address some of these limitations.

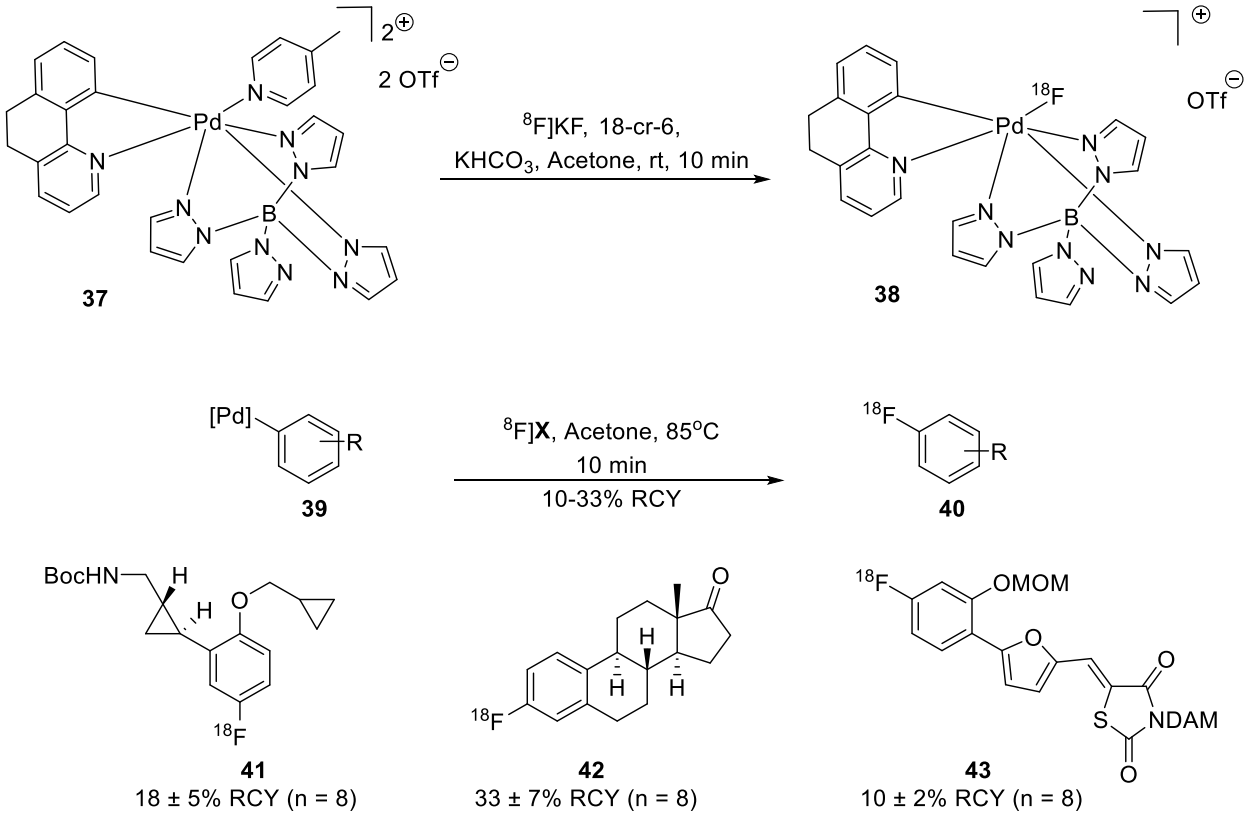

Scheme 1- 13 Palladium catalyzed F-18 Fluorination

Hooker and Ritter demonstrated utility of a nickel-mediated oxidative fluorination (**44**, **45**) over their previously mentioned palladium complexes, this time utilizing aqueous F-18 fluoride and an oxidant (Scheme 1- 14a).[77,78] While this helped counter the water sensitivity of the palladium complexes, this method is limited in degradation of the Ni complex and oxidant due to the volume of aq. ^{18}F fluoride volume ratio, and azeotropic drying resulting in solutions too alkaline, and causing low radiochemical yields. Moreover, the application of this method to the $5HT_{2A}$ receptor, [^{18}F]MDL100907 (**46**), showed moderate yields, but was too complicated and difficult to reproduce to merit this an ideal labeling strategy (Scheme 1- 14b).[78]

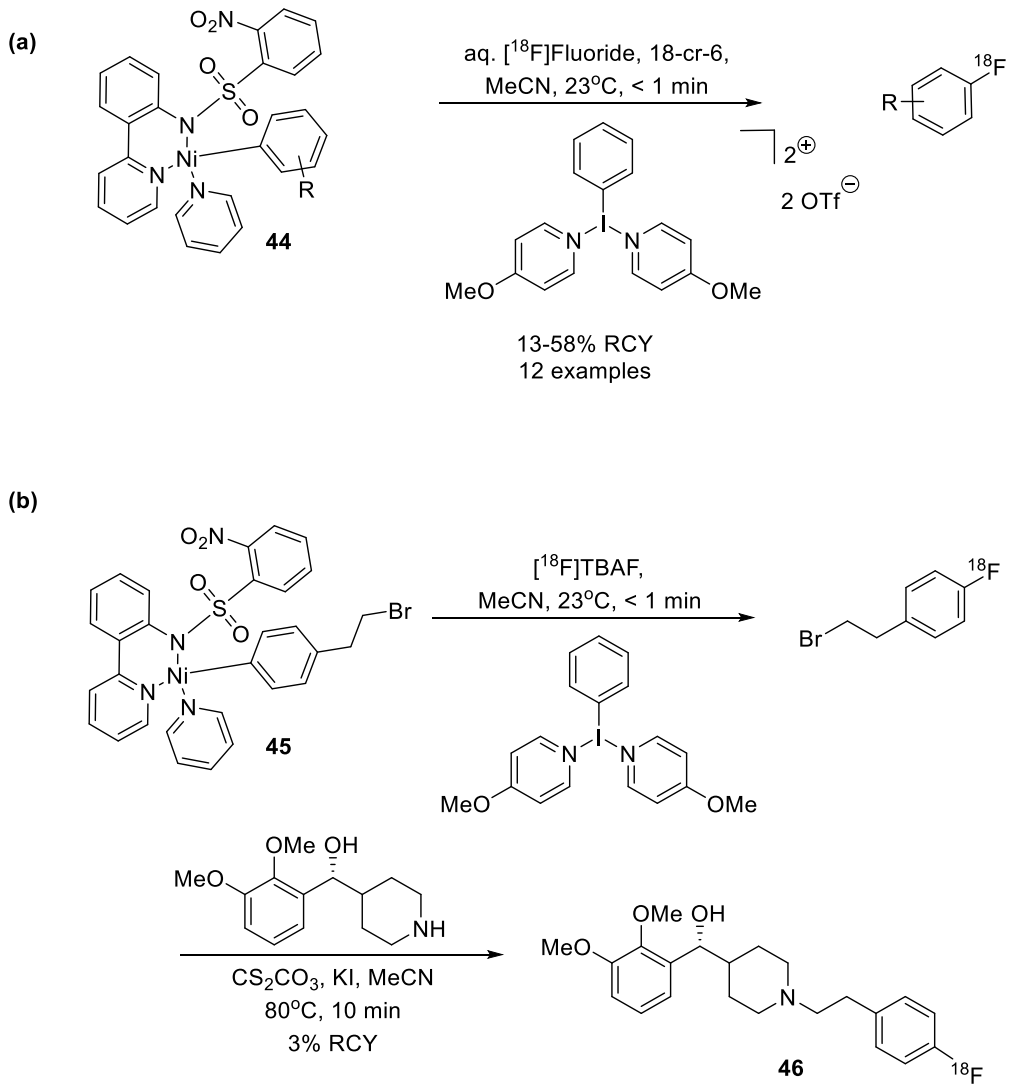

Scheme 1- 14 Nickel-mediated oxidative F-18 Fluorination

Hooker and Ritter also demonstrated C-F bond formation through deoxyfluorination of phenols and alcohols. This was shown in ^{18}F and ^{19}F with their PhenoFluor and AlkylFluor reagents. PhenoFluor and AlkylFluor were later made commercially available through Sigma Aldrich and Strem Chemicals Inc.[79–85]

Another foray into the fluorination space was by the Sanford group demonstrating that copper salts catalyzed the nucleophilic fluorination of mesityl-substituted diaryliodonium salts (**47**) with high chemoselectivity and with good functional group tolerance.[86] This work with copper(II) catalysts and KF, in collaboration with the Scott group, was later translated to K^{18}F, even though catalysts were rescreened and copper(I) catalysts were found to provide higher yields of the desired ^{18}F labeled arenes. This mild method was demonstrated on electron rich, neutral and deficient arenes, as well as clinically relevant PET tracers (4-[^{18}F]fluorophenylalanine (**48**) and 6-[^{18}F]fluorodopa (**49**)) in promising yields. However, the diaryliodonium precursors are challenging to prepare, and automated synthesis requires optimization to improve yields (Scheme 1- 15).[87]

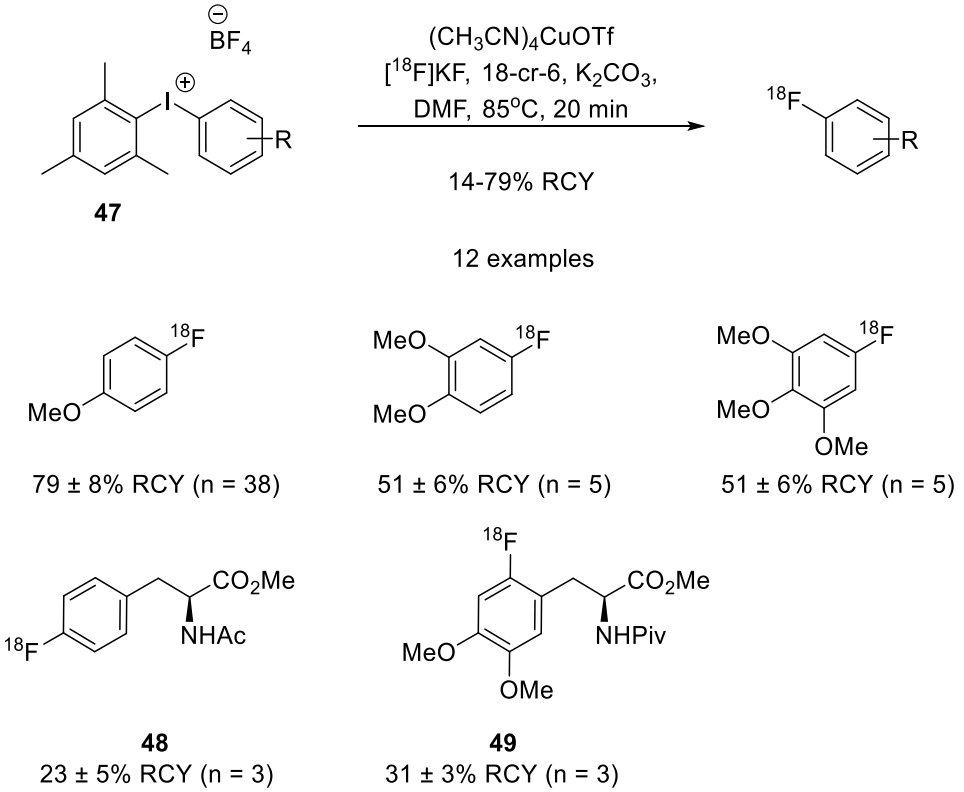

Scheme 1- 15 Copper-catalyzed F-18 Fluorination of (mesityl)(aryl)iodonium salts

The Sanford group also showed that aryl fluorides can be produced from aryl boron reagents, such as potassium aryl- and heteroaryltrifluoroborates, aryl boronic acids, and aryl pinacol boronate esters, in the presence of copper catalysts.[88] This work was extended to ^{18}F radiochemistry by Gouverneur as well as Sanford and Scott (Scheme 1-16a).[89,90] Gouverneur showed that pinacol-derived aryl (**50a**) and heteroacyl-boronic ester (**50b**), using $[Cu(OTf)_2(py)_4]$, could be fluorinated in good yield. This work also included successful labeling of PET tracers, 6-[^{18}F]fluorodopa (**51**) and [^{18}F]DAA1106 (**52**).[89] Scott and Sanford reported a mild synthetic procedure compatible with aryl, heteroaryl, and vinyl boronic acids utilizing $Cu(OTf)_2$ and [^{18}F]KF. This procedure was also automated and demonstrated in the production of [^{18}F]FPEB (**53**) (Scheme 1- 16b).[90]

Another attractive precursor for copper-mediated late-stage nucleophilic radiofluorination are aryl and vinyl stannanes. An ^{19}F method for oxidative fluorination of aryl stannanes *via* tetrabutylammonium triphenyldifluorosilcate (TBAT) and copper (II) triflate was described, under mild conditions and good functional group tolerance by the Murphy group in 2016.[91] Scott and Sanford reported a Cu-mediated ^{18}F fluorination of aryl stannanes. The latter provided high specific activity, good radiochemical yields, and was also compatible with electron-deficient and electron-rich substrates, as well as clinically relevant PET tracers (**54**-**58**) (Scheme 1- 17).[92] While Cu-mediated fluorination reactions are desired due to commercial availability and air stable catalysts, the iodonium, boronic ester, and stannane precursors can be synthetically challenging to prepare and not necessarily accessible to chemists often staffing PET Centers around the world.

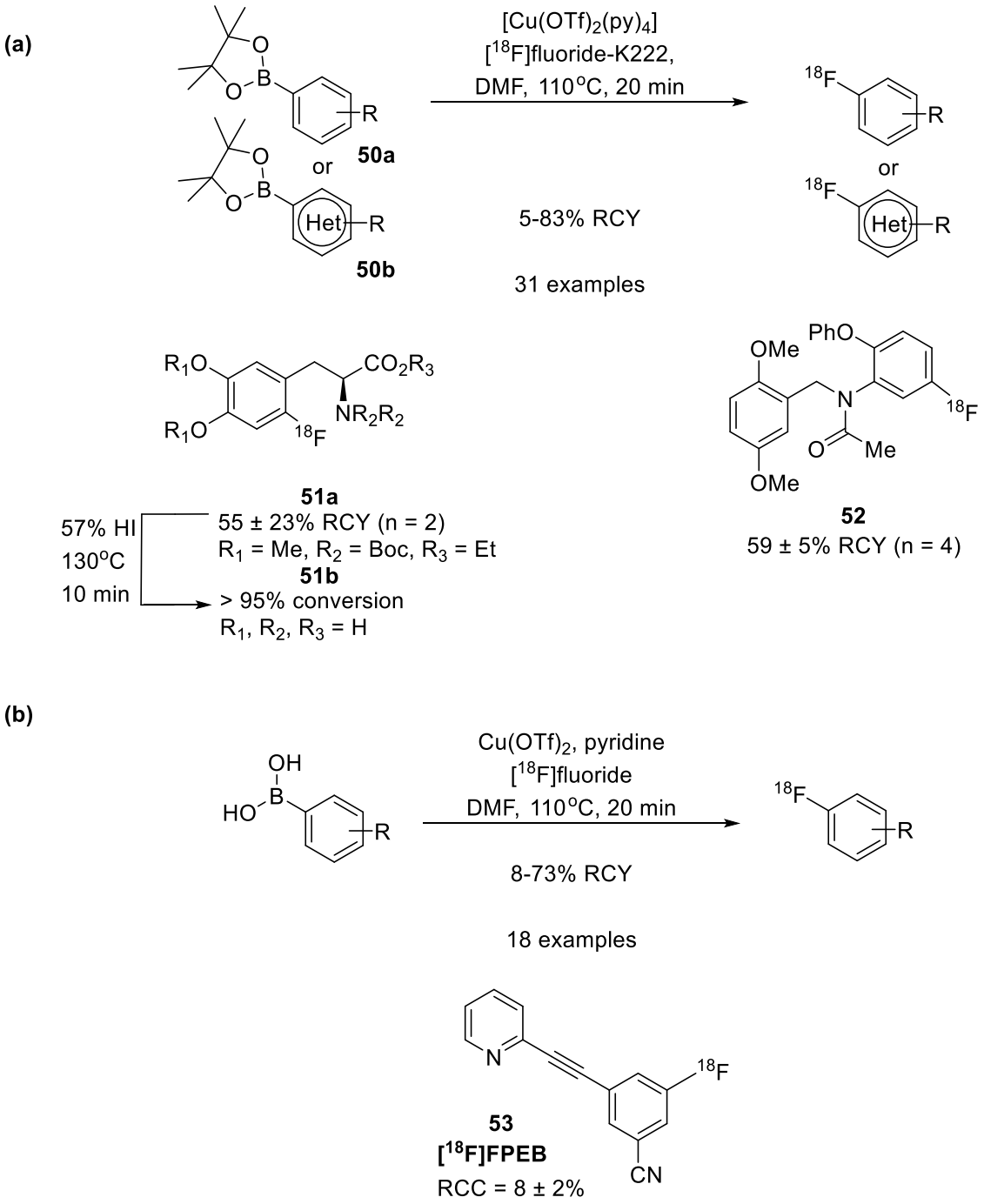

Scheme 1- 16 Copper-mediated F-18 Fluorination of aryl boronic acids

These transition-metal mediated radiofluorination methods are expanding the range of scaffolds available for PET imaging and the way in which chemists view ^{18}F

fluorination (reactivity of the $^{18}F^-$ nucleophile). The methods are also beginning to be used for production of clinical PET radiotracers,[93] demonstrated through the synthesis of Hooker and Ritter's Ni-mediated synthesis of T [^{18}F]5-FU to provide a cGMP compliant human-injectable dose free of residual metals.[94]

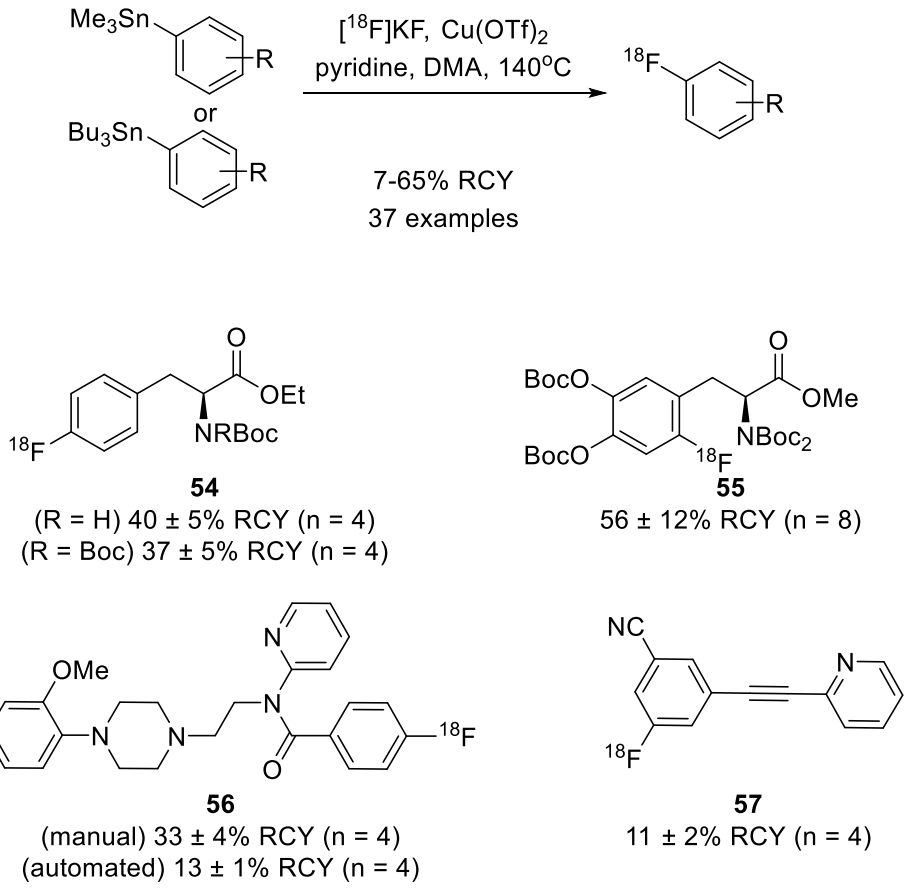

Scheme 1- 17 Copper-mediated F-18 Fluorination of aryl stannanes

Another straightforward radiolabeling strategy is to prepare a radiolabeled alkylating agent (or prosthetic group). This is used in the preparation of [^{18}F]fluoroethyl tosylate (**64**), [^{18}F]SFB, and can be found in ^{18}F-click chemistry; moreover, it is routine in

carbon-11 chemistry (such is *O*-, *S*-, or *N*-alkylation at a heteroatom *via* [^{11}C]methyl iodide or [^{11}C]methyl triflate). Starting from dibromomethane (**58**), or 2-bromoethyl trifluoromethanesulfonate (**61**), ^{18}F fluorination *via* standard procedure, then subsequent S_N2 reactions for the production of the desired tracer. This is a common strategy for the production of several PET tracers, including [^{18}F]fluorocholine ([^{18}F]FCH) (**60**) and *O*-(2-[^{18}F]fluoroethyl)-L-tyrosine ([^{18}F]FET) (**64**) (Scheme 1- 18).[31,47,48]

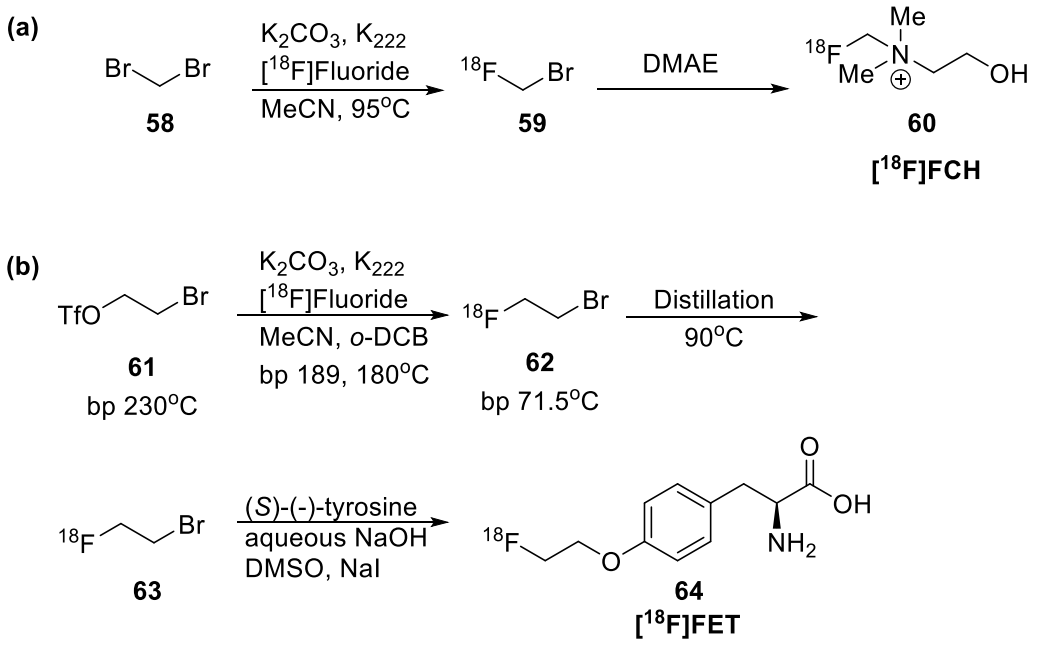

Scheme 1- 18 Radiolabeled Alkylating Agents

C-H radiofluorination is another labeling strategy for quick incorporation of the F-18 label, bypassing the oftentimes lengthy synthetic steps to prepare sophisticated precursors. This was first reported by Hooker and Groves, utilizing Mn(salen)OTs as a catalyst in the presence of PhIO, K_2CO_3, and [^{18}F]fluoride.[95] The [^{18}F]fluoride could be directly eluted from the ion exchange cartridge and used directly, thus shortening the synthesis time and negating the need for the azeotropic drying of the fluoride. This method

was demonstrated in a variety of substrates, including drug-like bioactive molecules (**65** and **66**) (Scheme 1- 19).

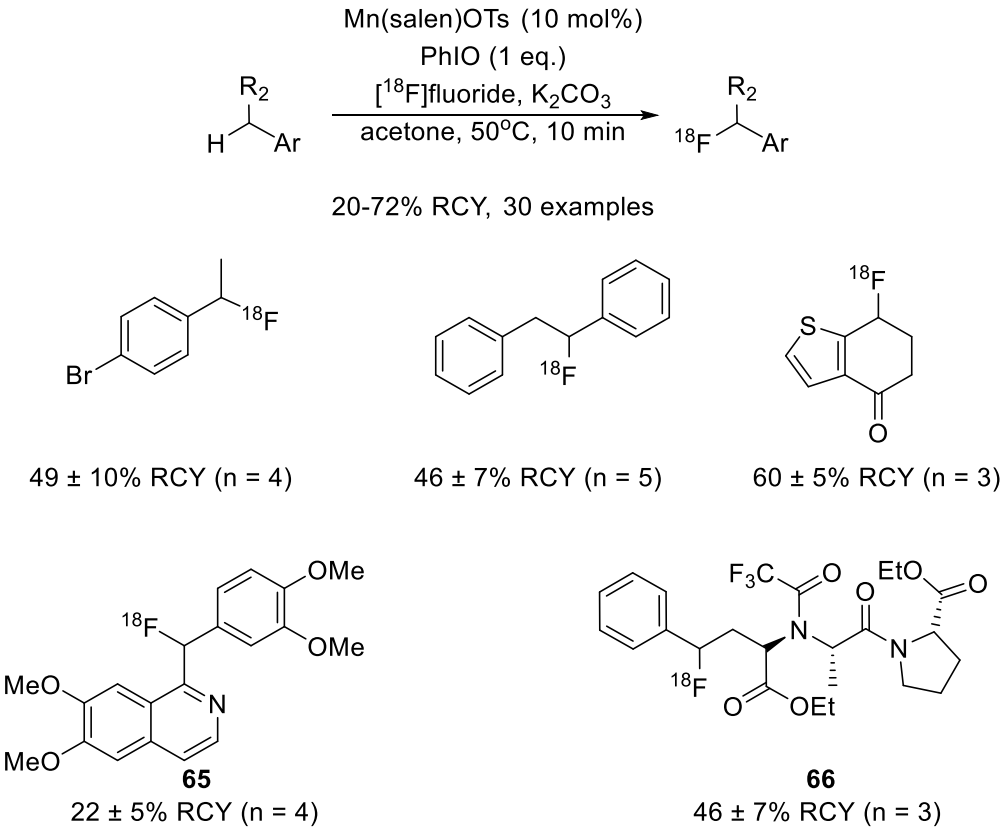

Scheme 1- 19 Benzylic C-H Fluorination

An sp^2 C-H [^{18}F]fluorination was developed by Scott and Sanford that utilizes MesI(OH)OTs to form a (mesityl)(aryl)iodonium salt *in situ* that is then used for Cu-mediated ^{18}F fluorination. This was demonstrated on 18 electron rich or neutral (hetero)arenes, and eliminates the requirement to prepare, isolate, and store otherwise bench instable starting materials (Scheme 1- 20).[96]

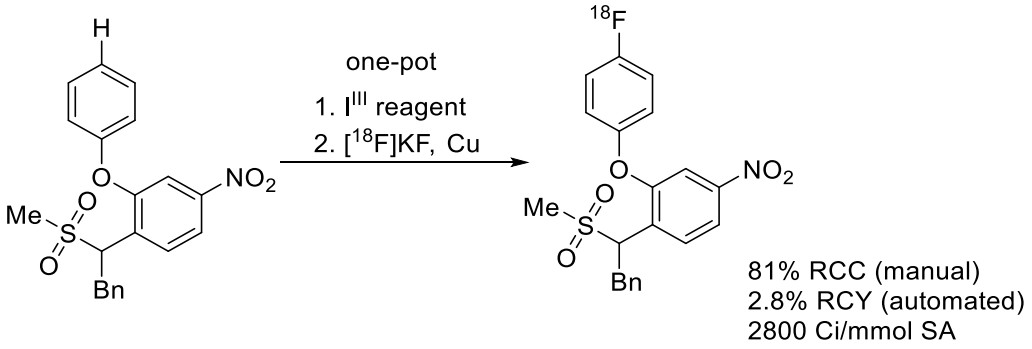

Scheme 1- 20 Cu-Mediated C-H ^{18}F-Fluorination

Approaches to [^{18}F]trifluoromethylation is another attractive target, as it is a privileged motif in small molecule drugs, found widely in an array of pharmaceuticals and prevalent in potential radiotracers. Historically, [^{18}F]trifluoromethyl is typically prepared from the -CF_2Br precursors. As one would expect, separation of the radiolabeled product from the precursor can be a challenging endeavor, often leading to low specific activity radiotracers. A common theme here, the development of a method to increase the specific activity and ease of labeling was desired. Approaches include [^{18}F]alkyl and [^{18}F]aryl-CF_3.[97–99] An efficient preparation from difluorovinylsulfonate (**67**) to the 2-[^{18}F]fluoro-2,2,-difluoroethyltosylate (**68**); the resultant [^{18}F]fluoroethylating agent (**69**) was used in the preparation of couple bioactive molecules, including the neurofibrillary tangle imaging agent [^{18}F]lansoprazole (**71**) from commercially available **70** (Scheme 1-21b).[99]

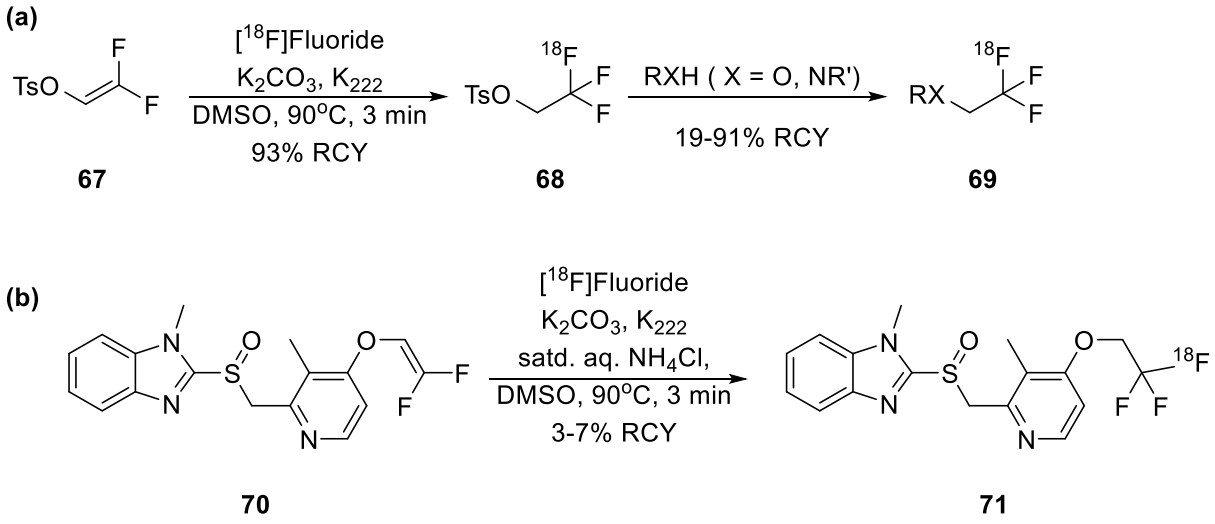

Scheme 1- 21 Strategies for alkyl [^{18}F] trifluoromethylation

While alkyl [^{18}F]trifluoromethylation has good utility, [^{18}F]trifluoromethyl arenes are a money maker and of sincere interest to the fluorine-18 community. Copper-mediated [^{18}F]trifluoromethylation from CuI or CuCl to produce [^{18}F]$CuCF_3$ as a reagent has been the driving force of this chemistry.[100–103] Gouverneur reported the preparation of [^{18}F]$CuCF_3$ from methyl chlorodifluoroacetate,CuI, *N,N,N',N'*-tetramethylethylenediamine (TMEDA) and [^{18}F]fluoride-K222 in DMF; this could then we cross-coupled in moderate to high RCY with a range of aryl and heteroaryl iodides (**72-74**), and 31 examples (Scheme 1- 22a).[100] This methodology was also utilized with direct C-H oxidative [^{18}F]trifluoromethylation of drug-like molecules, include indole **75** to form **76** (Scheme 1-22b).[95] By combining difluoroiodomethane, potassium bicarbonate, DIPEA and [^{18}F]fluoride-K222 in DMF the [^{18}F]$CuCF_3$ reagent was as produced and demonstrated by the Riss group. Similarly, this could be coupled to a range of aryl iodides to produce the desired F-18 labeled trifluoromethyl arenes (**77-79**), 15 examples, in good yields (Scheme

1- 22c). It is exciting to note that this transformation was tolerant of a free phenol functionality, even though the desired ^{18}F-product was formed in lower radiochemical yield.[98]

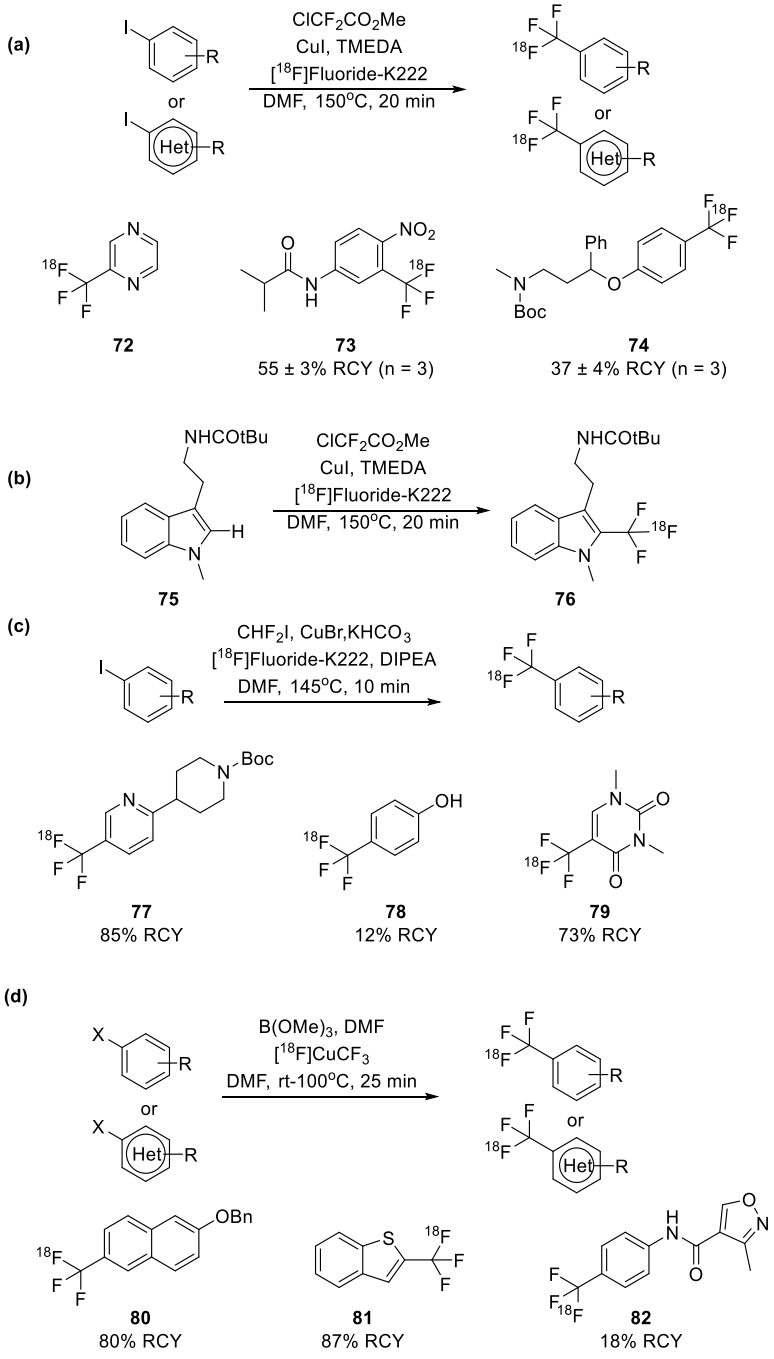

Scheme 1- 22 Strategies for [18F]trifluoromethylation of arenes

Finally, [^{18}F]fluoroform, from difluorocarbene from the initial difluoromethylsulfonium salt, with a coppyer catalyst (CuI or CuCl) and potassium *t*-butoxide was also demonstrated to produce the [^{18}F]$CuCF_3$ reagent. This was then reacted with aryl iodides or aryl boronic acids in DMF to produce the desired [^{18}F]trifluoromethylated product (**80-82)** in high RCY, with 10 examples (Scheme 1-22d).[102]

While this provides a brief summary of the variety of ^{18}F fluorination methods available, a more expansive review of fluorine-18 chemistry (and their applications to PET) may be found in, but is not limited to: Le Bars 2006, Schirrmacher et al *2007*, Miller *et al* 2008, Ametamey *et al* 2008, Cai *et* al 2008, Kilbourn and Shao 2009, Littich and Scott 2012, Campbell and Ritter 2014, Jacobson *et al* 2015, Campbell and Ritter 2015, Brooks *et al*, 2014, Cole *et al* 2014, Richter *et al* 2014, Gouverneur and Seppelt 2015, Liang *et al* 2014, Liang *et al* 2016, Preshlock *et al* 2016, and Taylor *et al* 2017.[31,42,43,61,62,85,104–115]

f. Carbon-11 Labeling From Cyclotron-Produced [^{11}C]CO_2

While fluorine-18 has many advantages such as a longer half-life and stability, carbon-11 is an attractive radionuclide for bioactive molecules because frequently its incorporation has minimal effect on biological activity. Moreover, the short half -life (20 min) allows multiple PET scans to be conducted in a single hospital visit (fluorine-18 scans are limited to 1 scan per day). Carbon-11 is produced *via* proton bombardment of

nitrogen-14, typically with small amounts of oxygen, through the $^{14}N(p,\alpha)^{11}C$ nuclear reaction. The $[^{11}C]CO_2$ is then delivered to a synthesis module with appropriate containment for the gaseous agent, where it is oftentimes trapped on a solid material (molecular sieves), then thermally released from the trap to the reactor or on to further transformation.

Specifically, from the cyclotron, $[^{11}C]CO_2$ destined to be $[^{11}C]CH_3I$ or $[^{11}C]CH_3OTf$, is trapped on a molecular sieve with nickel at room temperature. This is sealed and heated to 350°C with H_2 to reduce the $[^{11}C]CO_2$ to $[^{11}C]CH_4$, which is trapped on a carbosphere methane trap cooled to -75°C (with liquid N_2). When the carbosphere is heated to 80°C, it releases the $[^{11}C]CH_4$ which enters a circulation loop containing an iodine column at 100°C. The iodine, I_2, tube reactor is at 750°C and$[^{11}C]CH_4$ is circulated for 5 min to generate $[^{11}C]CH_3I$ which is trapped on a porapak column before being delivered to the reactor. If a more reactive methylating agent is required, $[^{11}C]CH_3I$ can be passed through a silver triflate at 190°C to generate $[^{11}C]CH_3OTf$. Following delivery to the reactor and

subsequent methylation, similar purification and reformulation using semi-preparative HPLC and solid-phase extraction are undertaken to generate the final dose.[116]

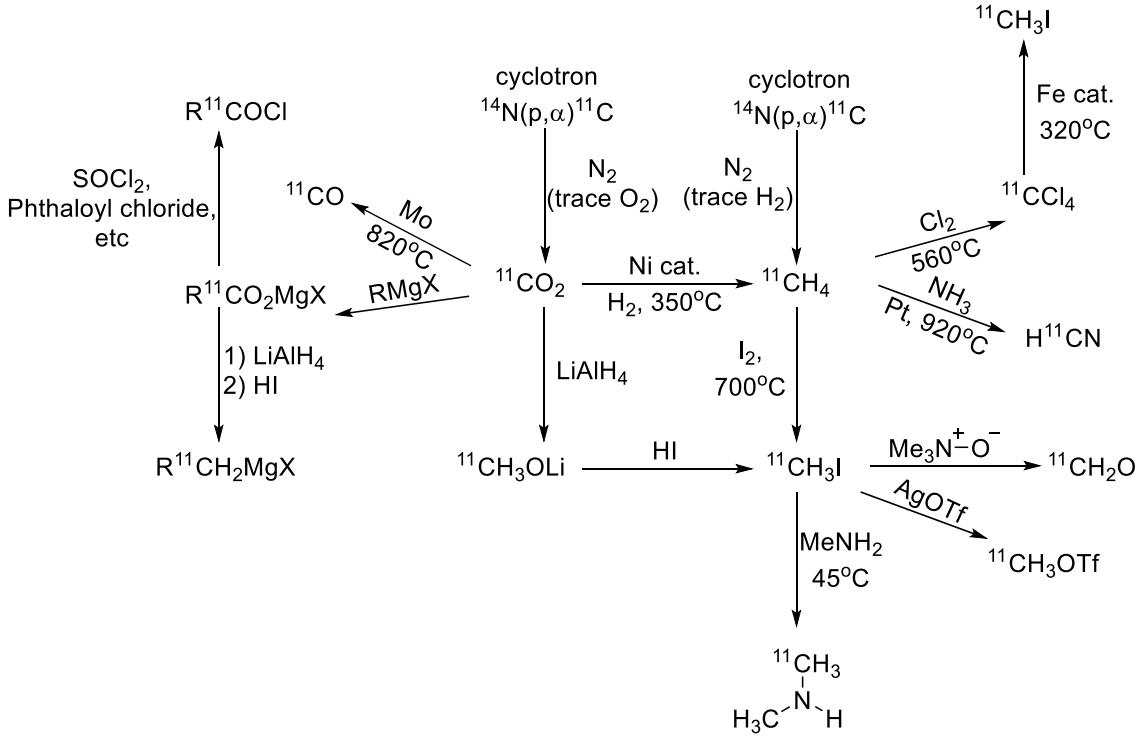

Scheme 1- 23 Carbon-11 Chemistry Summary. (Adapted from Scott, 2009)[117]

Common reagents as such include $[^{11}C]CO_2$, $[^{11}C]CO$, $[^{11}C]HCN$, $[^{11}C]COCl_2$, $[^{11}C]CH_3I$, $[^{11}C]CH_3OTf$ (Scheme 1- 23). Drawbacks of carbon-11 chemistry include competing side-reactions and by-products, and competition with atmospheric carbon-12, short half-life (20 min), and specific activity. Even though the most common strategy for ^{11}C labeling is through the production of the reactive methylating species ($[^{11}C]CH_3I$ and $[^{11}C]CH_3OTf$), $[^{11}C]CO_2$ is also an attractive reagent itself. $[^{11}C]CO_2$ can give access to

carboxylic aids, amides, ureas, carbamates, oxazolidinones, and other high oxidation state functional groups and their respective derivatives.[118]

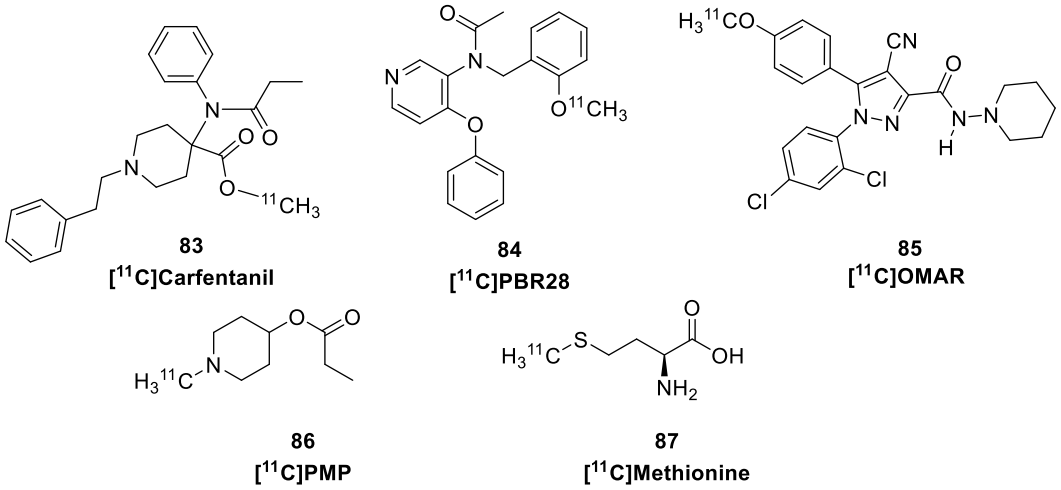

Figure 1-7 Selected C-11 Radiopharmaceuticals

Standard methylation at a heteroatom *via* [^{11}C]CH_3I, [^{11}C]CH_3OTf is a common strategy for production, and desirable for simplicity considering half-life, transfers, etc. This includes [^{11}C]Carfentanil (**83**), [^{11}C]PBR28 (**84**), [^{11}C]OMAR (**85**), [^{11}C]PMP (**86**), [^{11}C]Methionine (**87**), [^{11}C]CHL, [^{11}C]PIB, [^{11}C]DTBZ, [^{11}C]FMZ, [^{11}C]Raclopride (**91**) (from a TBA hydroxide/TBA salt (e.g. **90**), amine, phenol, etc) (Scheme 1- 24,Figure 1-7).[47,48]

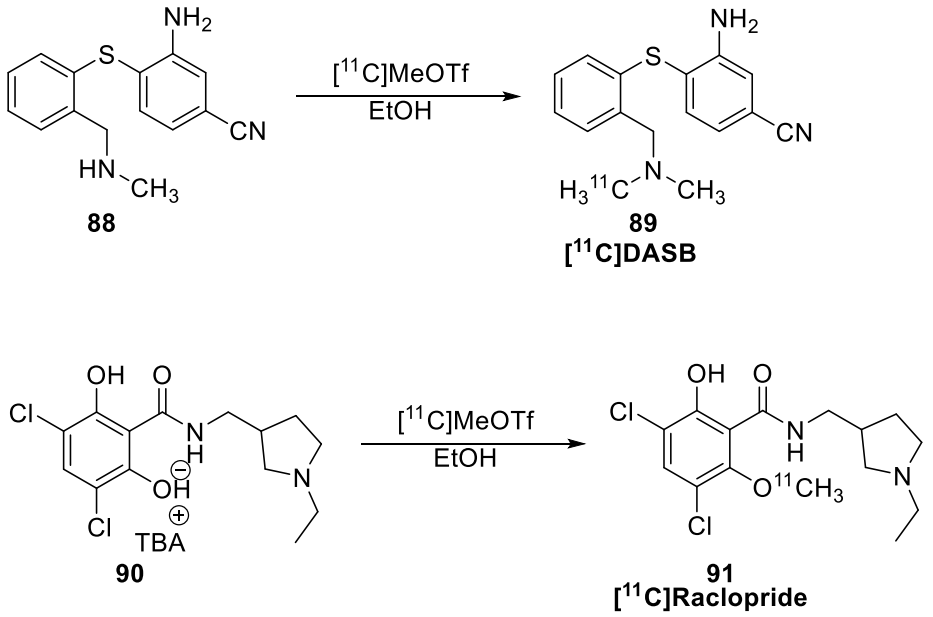

Scheme 1- 24 Synthesis of C-11 DASB and Raclopride

Other carbon-11 labeling strategies have been adapted from traditional organic chemistry techniques such as Huisgen cycloaddition, click chemistry, palladium-catalyzed cross-couplings (Stille, Suzuki, and Sonogashira reactions), and the use of organometallic reagents (Grignard, etc) to access carboxylic acids, amides (amines) and acyl chlorides have been adapted for these syntheses.[43,117–125]

One example of a more complicated carbon-11 labeling synthesis is for the dopamine D3 receptor-preferring radiopharmaceutical, (4aR,10bR)-4-(propyl-1-11C)-3,4,4a,5,6,10b-hexahydro-2H-naphtho[1,2-b][1,4]oxazin-9-ol ([^{11}C]PHNO, **97**). [^{11}C]PHNO is produced from the release of [^{11}C]CO_2 to ethylmagnesium bromide solution (**92**), then with treatment of phthaloyl dichloride; the resultant acyl chloride ([^{11}C]propionyl chloride, **94**) is reacted with the amine precursor (**95**) in TEA to form the [^{11}C]amide (**96**), and finally reduced with lithium aluminum hydride to give the desired product (**97**). Indeed

this complicated synthesis for such a short-lived isotope is not ideal, yet readily gives access to the desired scaffold (Scheme 1- 25).[48]

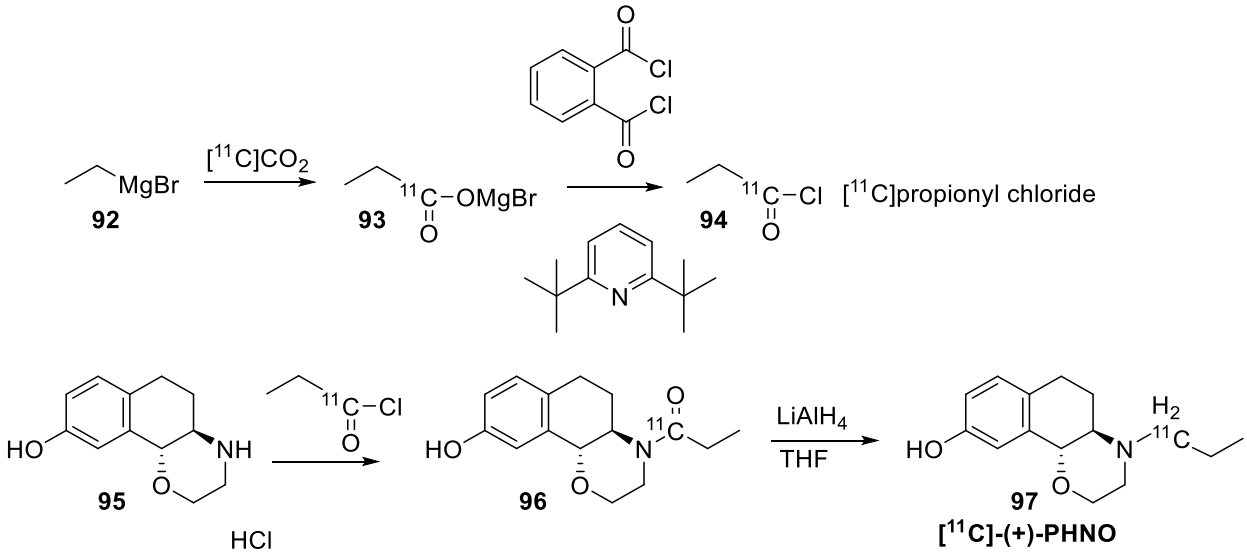

Scheme 1- 25 Synthesis of [^{11}C]-(+)-PHNO

[^{11}C]CO_2 fixation chemistry utilizing Grignard reagents (Scheme 1- 26 a), such as the synthesis of [^{11}C]-(+)-PHNO (**97**) mentioned above, as well other basic organometallic reagents include organolithium reagents (Scheme 1- 26b and c), and silanamines (Scheme 1- 26d). While organometallic/organosilicon species for [^{11}C]CO_2 fixation are feasible options they suffer from instability, and due to their reactivity, pose issues with reproducibility and automation required for translation to the clinic. Symmetrical and unsymmetrical ureas can also be prepared by [^{11}C]CO_2 fixation (Scheme 1- 27).[118] [^{11}C]Urea was synthesized by Chakraborty *et al* through LHMDS (**98**) in THF and bubbling in [^{11}C]CO_2 to afford **99**, followed by hydrolysis with aqueous ammonium chloride

provided [^{11}C]urea (**100**); this procedure was applied in the synthesis of [^{11}C]uracil (Scheme 1- 27a).[126] Moreover, [^{11}C]phosgene can been used to prepare ureas, as well as carbonates and isocyanates.[127] Phosphoryl chloride or thionyl chloride are another option to generate the acid chloride or isocyanate, highly electrophilic species, that could be used to prepare [^{11}C]diphenyl urea and [^{11}C]diphenyl carboiimide (Scheme 1- 27b).[128] Through careful manipulation, [^{11}C]ureas (**105, 107**) can be produced selectively through the use of $POCl_3$ to trap remaining amine on the [^{11}C]isocyanate (**104**) generated *in situ*; the reaction can also be controlled to favor unsymmetrical products (**107**) (Scheme 1- 27b, Scheme 1- 28).[118,129]

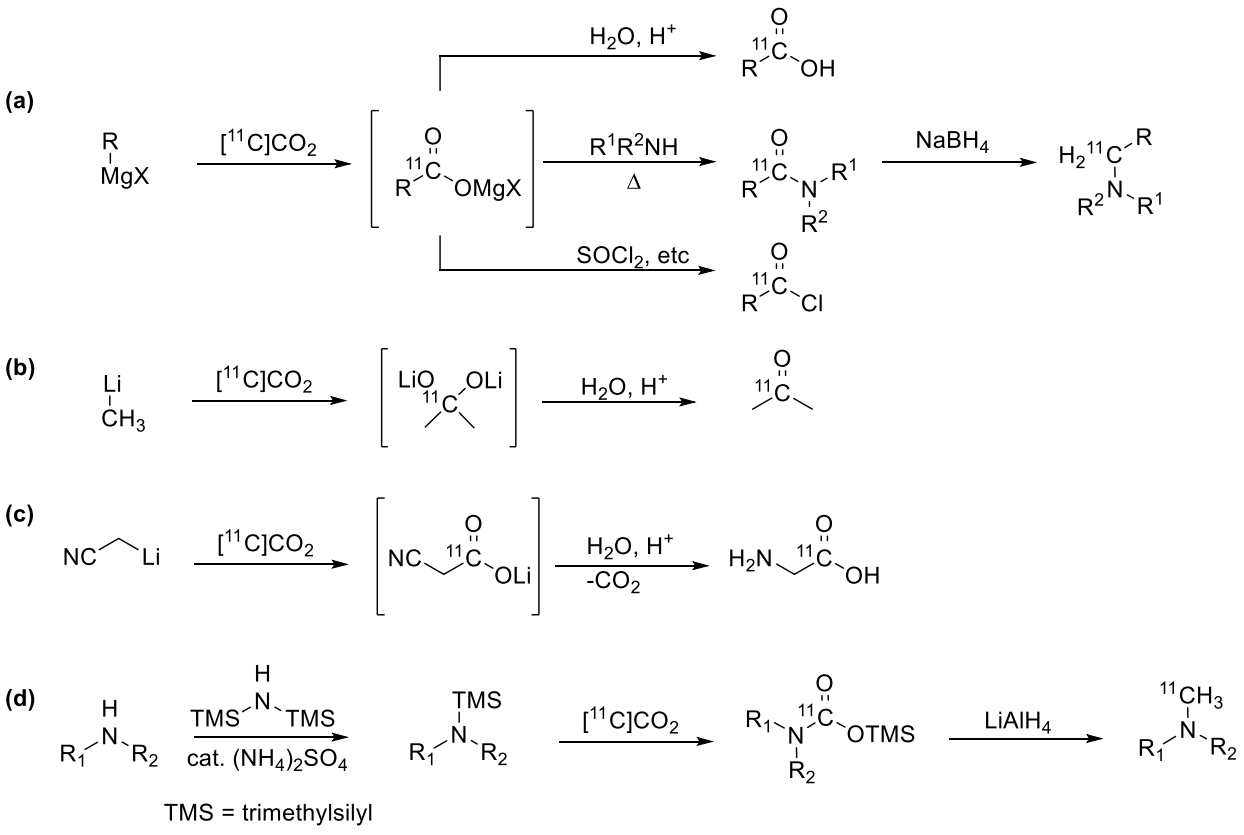

Scheme 1- 26 [^{11}C]CO_2 Fixation Reactions[118]

[^{11}C]CO_2 in this fashion was applied to radiolabeling a variety of structurally diverse drug-like molecules, including: [^{11}C]GR103545, [^{11}C]metergoline, [^{11}C]SL25.1188, [^{11}C-*carbonyl*]AR-A014418, [^{11}C]PF-0445785, to name a few.[118]

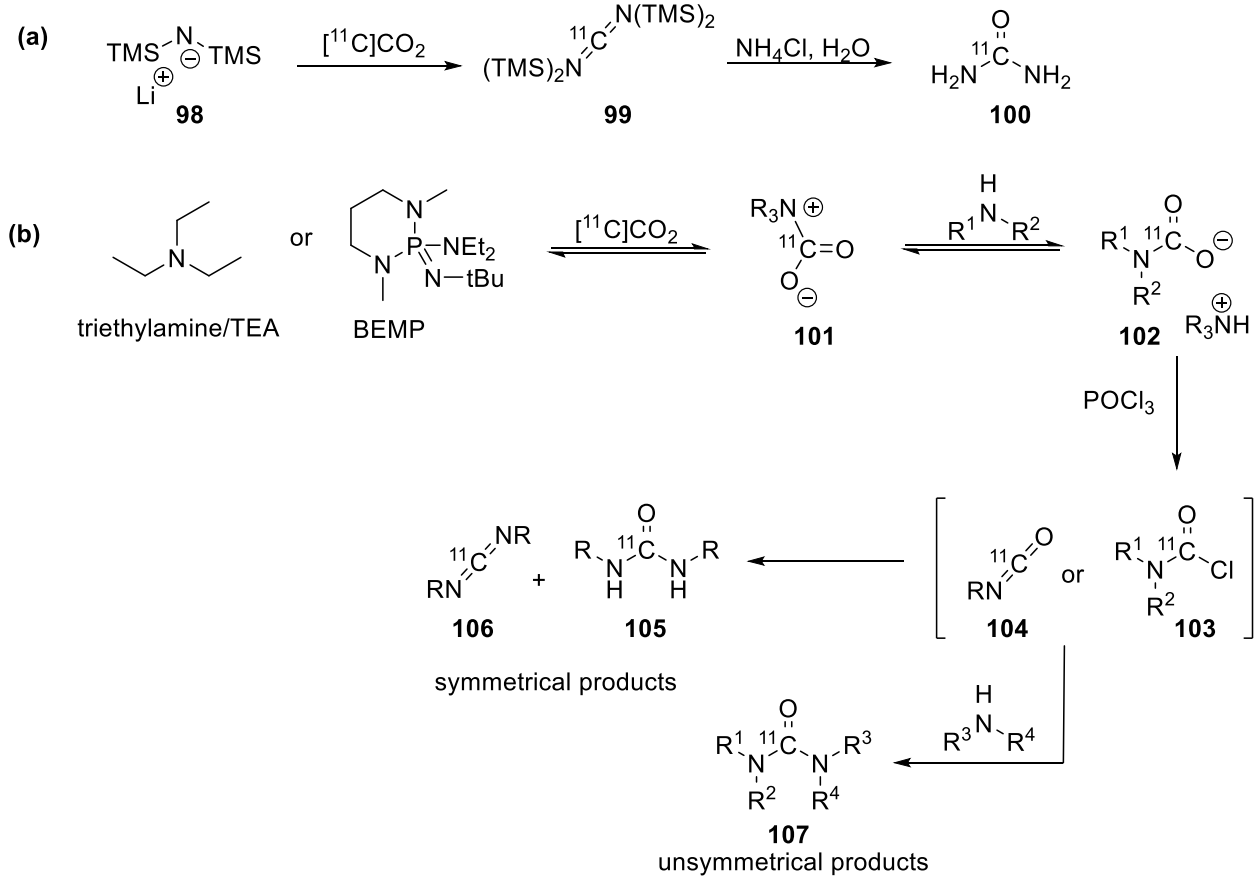

Scheme 1- 27 [^{11}C]CO_2 Fixation to Access [^{11}C]Ureas[118]

Condensation of phosphinimines with [^{11}C]CO_2 is another way to access [^{11}C]isocyanates. Phenyltriphosphinimine (**108**) is commercially available and can be used to prepare [^{11}C]urea (**110**) with aliphatic and aromatic amines (Scheme 1- 28). This procedure was reported in a one-pot fashion, with modest to good yields and short

reactions times (6 min). [^{11}C]CO_2 is trapped at -60^{o}C in THF and phosphinimine, amine, then heated to 60^{o}C to complete the transformation.[130]

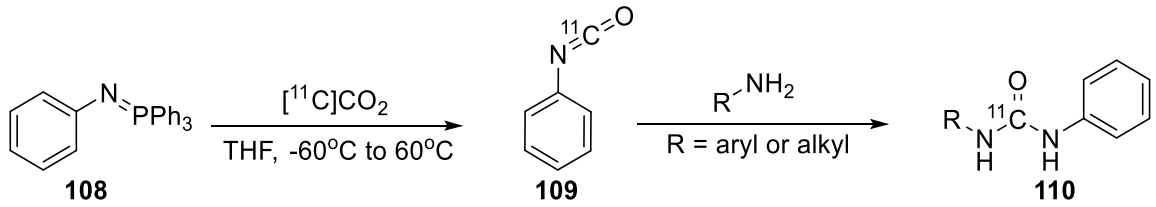

Scheme 1- 28 Synthesis of [^{11}C]phenylisocyanate and [^{11}C]ureas

Carbamates are also attractive functional groups and have been labeled using [^{11}C]phosgene and [^{11}C]carbon monoxide.[43] While [^{11}C]ureas require a carbamate salt intermediate when electrophiles are used, *O*-alkyl carbamates do not necessarily require this and was demonstrated by Hooker and Fowler in a one-pot procedure for [^{11}C]CO_2 into carbamates.[131] They identified 1,8-Diazabicyclo[5.4.0]undec-7-ene (DBU) as a trapping agent and catalyst, in MeCN, DMF, or DMSO, trapped >95% [^{11}C]CO_2. Benzyl and allyl chlorides were the best electrophiles, and reduction of the benzylamine (for example) was advantageous over reducing the concentrations of the other reagents (Scheme 1- 29).[118] [^{11}C]isocyanates are another option to access [^{11}C-*carbonyl*]-carbamates, through careful stoichiometric manipulation to prevent the formation of symmetrical [^{11}C]urea(s). This was demonstrated in the synthesis of [^{11}C]CURB, *via* [^{11}C]CO_2 fixation with cyclohexamine, 2-tert-Butylimino-2-diethylamino-1,3-dimethylperhydro-1,3,2-diazaphosphorine (BEMP), then formation of [^{11}C]isocyanate

with $POCl_3$, and quenching with the appropriate alcohol to provide the *O*-aryl carbamate tracer.[118,129]

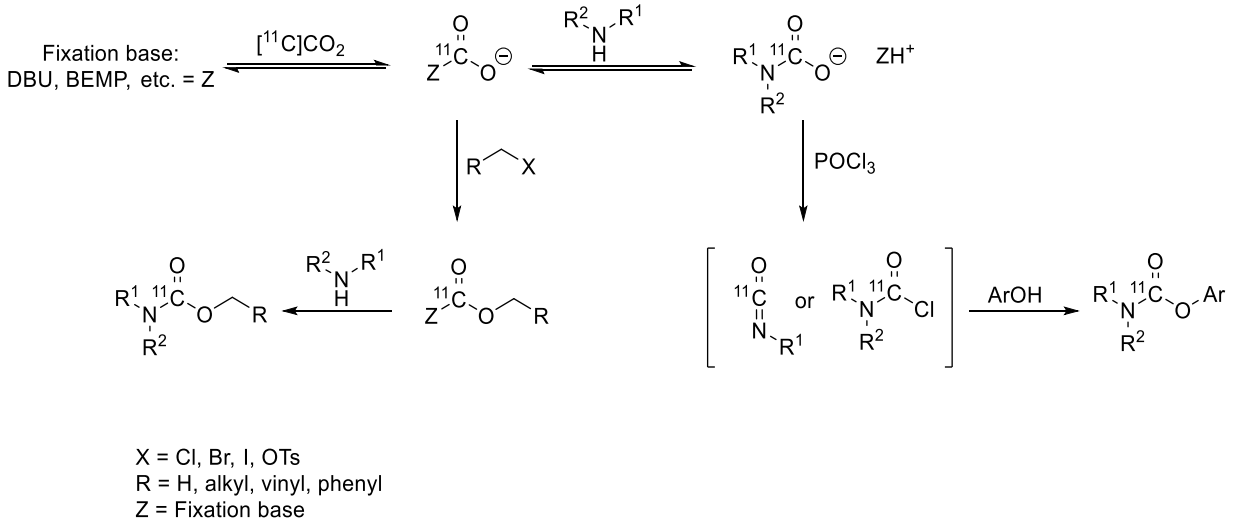

Scheme 1- 29 [^{11}C-*carbonyl*]carbamates from [^{11}C]CO_2 (left) trapping followed by amine substitution; (right) carbamate activation with $POCl_3$.[118]

[^{11}C-*carbonyl*]-oxazolidinones are another attractive functionality, found in many drug-like molecules, and is used in the synthesis of [^{11}C]SL25.1188, a reversible monoamine oxidase-B tracer.[132] Moreover, prefunctionalized metal-free conditions using organozinc and organoboron reagents have received attention recently and allowed access to [^{11}C]carboxylic acids ([^{11}C]ester and [^{11}C]amide).[133–135] Riss and colleagues reported a Cu-catalyzed (CuI-mediated) method for ^{11}C-carboxylation of boronic acid esters. This was extended to an amide *via* an acid chloride, a succinic ester *via* carbodiimide activation, as well as a methyl ester through iodomethane. These reactions

proceeded with [^{11}C]CO_2, TMEDA, KF, and crypt-222, and resulted in high specific activity [^{11}C]carboxylic acids.[118,136]

[^{11}C]CO_2 fixation chemistry has been covered, but some noteworthy techniques and summary(s) can be found in: Rotstein *et al* 2013, Perrio-Huard *et al* 2000, Scott 2009, and Mossine 2016. [117,118,137,138]

g. Automated Radiosynthesis for PET Radiochemistry

With a short review of ^{18}F and ^{11}C labeling strategies for PET radiopharmaceuticals in hand, a short discussion of the logistics involved in PET radiopharmaceutical production is necessary. As mentioned earlier, PET radiopharmaceutical production exists in a unique space, where a short-lived positron-emitting radionuclide (e.g. ^{18}F, $t_{1/2}$ = 110 min, or ^{11}C, $t_{1/2}$ = 20 min) is used to label (or tag) a bioactive molecule. These radionuclides, carbon-11 (^{14}N(p,α)^{11}C) and fluorine-18 (^{18}O(p,n)^{18}F), are produced in a medical cyclotron (at the University of Michigan, Ann Arbor, this is a General Electric (GE) PETTrace cyclotron) and delivered to lead-lined cells “hot cells” (Figure 1-8) for remote-controlled automation.

Figure 1-8 "Hot Cells" at the University of Michigan

As previously described, nucleophilic [^{18}F]fluoride is produced *via* ^{18}O(p,n)^{18}F, or proton bombardment of a [^{18}O]H_2O target. Typically, the $^{18}F^-$ anion is delivered in a bolus of [^{18}O]H_2O to a lead-lined “hot cell” with a TRACERLAB-Fx_{FN} synthesis module (Figure 1-9, Figure 1-10). The Remaining synthesis can be executed “manually” through a general labeling program, or a pre-programmed automation for a specific tracer. Then, the $^{18}F^-$ is loaded on to an ion-exchange column, typically a quaternary methyl ammonium (QMA) anion exchange cartridge to trap and recycle unused [^{18}O]H_2O. The $^{18}F^-$ is eluted to a cryptand, K_{222} (Kryptofix), an aminopolyether, which also acts as a phase transfer catalyst and used in conjunction with potassium carbonate to activate the [^{18}F]fluoride through the [^{18}F]KF·K_{222} complex (Figure 1-11). From here, the fluorine-18 (complex) is azeotropically dried (typically in water/MeCN) to remove residual water from the target, leaving an activated ^{18}F nucleophile. The ^{18}F nucleophile is then reacted with the precursor in aprotic, anhydrous solvents, such as MeCN and DMF.[46]

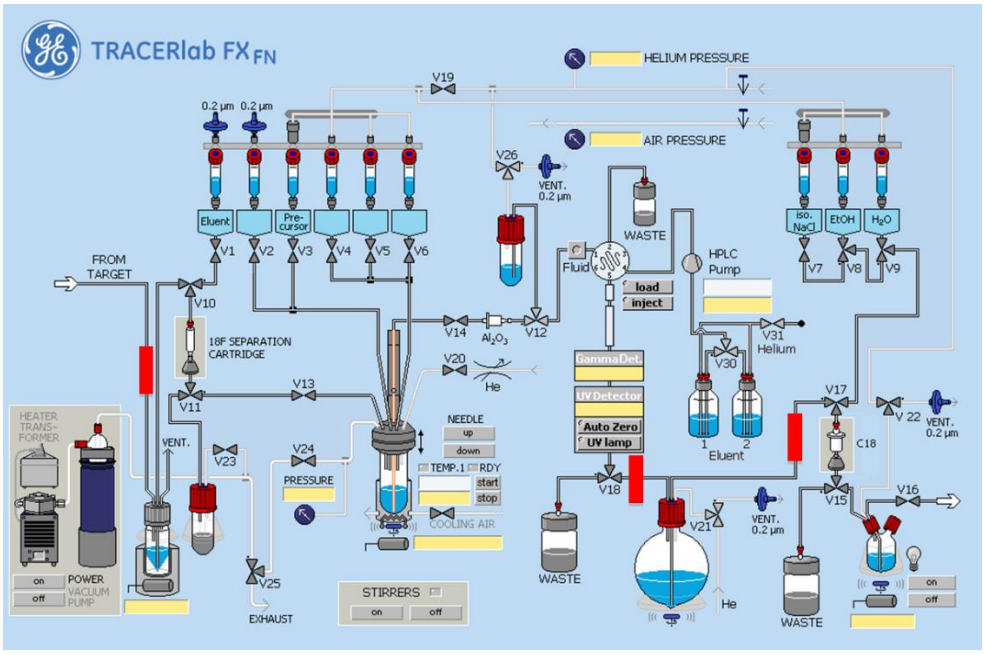

Figure 1-9 Fx_{FN} Synthesis Module for Fluorine-18

Figure 1-10 Fx_{FN} Synthesis Module for Fluorine-18 in a Hot Cell

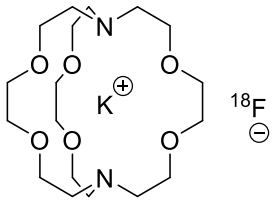

Figure 1-11 [^{18}F]KF-K_{222} Complex

Carbon-11 is prepared *via* the $^{14}N(p,\alpha)^{11}C$ nuclear reaction and delivered to a (GE)TRACERLAB-$Fx_{C\text{-}Pro}$ synthesis module (Figure 1-12, Figure 1-13) in the form of [^{11}C]CO_2. As previously described, [^{11}C]CO_2 can be used directly, or transformed into transformed into [^{11}C]CH_3I or [^{11}C]CH_3OTf for methylation at a hetero atom (i.e. N, S, O). The [^{11}C]CO_2 can be bubbled directly to a reactor containing another reagent (e.g. Grignard) before reacting with precursor, or trapped on a molecular sieve with carrier (CO_2) and used for subsequent chemistry.[116]

The production of [^{11}C]CH_3I or [^{11}C]CH_3OTf involves trapping [^{11}C]CO_2 from the cyclotron on a molecular sieve that is mixed with a nickel catalyst (Shimalite) at room temperature. The tube containing the sieve/nickel mixture is pressurized with H_2, sealed and heated to 350^{o}C to reduce [^{11}C]CO_2 to [^{11}C]CH_4, which is then trapped on a Carbosphere methane trap cooled to -75^{o}C with liquid N_2. The [^{11}C]CH_4 is thermally released when the Carbosphere is heated to 80^{o}C, and enters a circulation loop containing an iodine column at 100^{o}C. [^{11}C]CH_4 and iodine vapor circulate through a furnace at 750^{o}C for 5 min. to generate [^{11}C]CH_3I, which is trapped on a porapak column before delivery to the reactor. If a more reactive methylating agent is required, the

[^{11}C]CH_3I can be passed through a silver triflate column at 190°C to generate [^{11}C]CH_3OTf.[116]

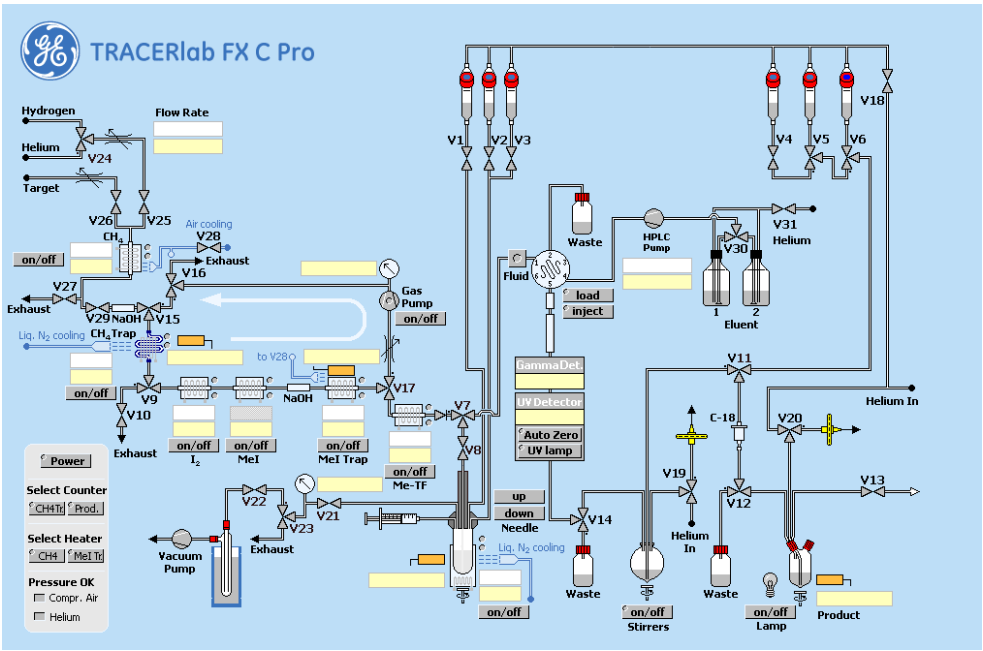

Figure 1-12 $Fx_{C\text{-}Pro}$ Synthesis Module for Carbon-11

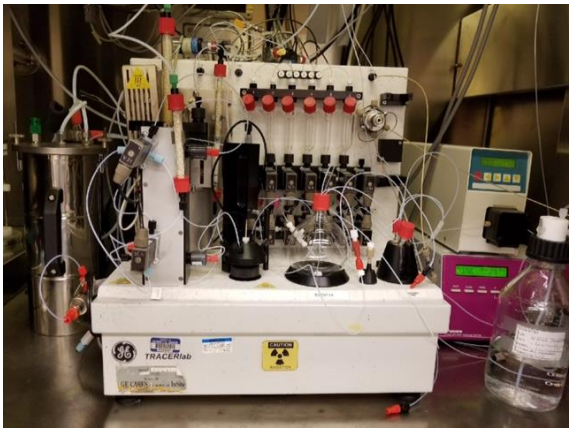

Figure 1-13 $Fx_{C\text{-}Pro}$ Synthesis Module for Carbon-11 in a Hot Cell

Carbon-11 chemistry has two core reaction methods: reactor and loop chemistry. The reactor chemistry is as briefly described earlier; this is such that $[^{11}C]CO_2$ $[^{11}C]CH_3I$ or $[^{11}C]CH_3OTf$ is bubbled into a reactor containing a reagent (such as an organometallic reagent) prior to reacting with precursor, or directly in a solution of solvent and precursor. Loop chemistry, on the other hand, reduces solvent volume through thin-film chemistry. The precursor, dissolved in ethanol, is loaded on the semi-preparative HPLC and conditioned with nitrogen gas to coat the loop. Following this, the methylating agent such as $[^{11}C]CH_3OTf$, is blown rapidly, 40 mL/min for ~3-5 min, through the loop containing the precursor.[139]

For the preparation of ^{18}F and ^{11}C-labeled PET radiopharmaceuticals, both undergo similar purification and reformulation, such as semi-preparative HPLC and solid-phase extraction to generate the final dose. The final dose is an ethanolic saline solution, suitable for IV injection, upon passing appropriate quality control (QC). Further discussion of PET radiopharmaceutical quality control can be found in **Chapter 3**.

h. An Introduction to PET Scan Data Acquisition: Photon Detection and Scintillation Detectors

The ^{18}F and ^{11}C-labeled PET radiopharmaceuticals decay *via* emission of a positron (β^+) and electron neutrino (ν_e). The positron travels in tissue, up to a couple mm depending on the radionuclide, until it loses enough energy to remain in the vicinity of its antiparticle, the electron (e^-), long enough to allow annihilation of the two particles to

occur. This event produces two 511 KeV gamma ray photons (γ) that project 180^{o} from the event location. If both photons of the pair are detected by the PET scanner (within ~5 nsec), this is termed a coincident event (Figure 1-14).[18,140] These annihilation events are detected when they reach the scanning device that uses scintillation crystals for absorbing the 511 KeV photons. Examples of scintillation crystals used in PET include: bismuth germanate/BGO, lutetium oxyorthosilicate doped with cerium/LSO, sodium iodide doped with thallium (NaI(Tl)), barium fluoride, yttrium oxyorthosilcate doped with cerium/YSO, and gadolinium oxyorthosilicate doped with cerium/GSO. A burst of light (visible or near UV) is then converted by photomultiplier tubes (Figure 1-15) to an electrical signal. The amount of light in these scintillation bursts is proportional to the energy deposited by the annihilation photon.[140,141]

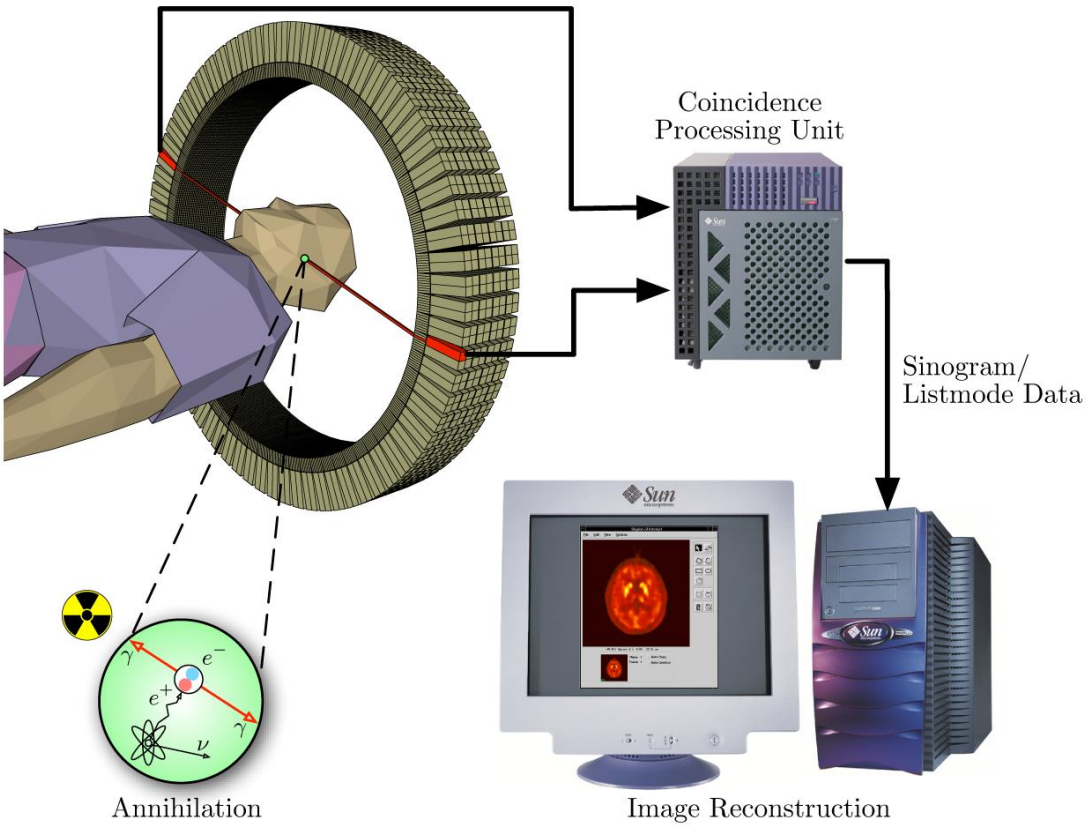

Figure 1-14 PET Scan Scheme © Public Domain, https://en.wikipedia.org/wiki/Positron_emission_tomography

In a standard PET scan, there are thousands of detectors configured in a series of rings around the patient (typically 400-600 crystals per ring, and 24-50 or more rings). All of these events/signals are fed through amplifiers and localized by storing which detectors recorded the pair of events.[141] The ~180^{o}, or co-linearity, path that these photons travel is the property that is exploited in PET, allowing a line-of-sight/coincidence (also called a Line of Response, or LOR) of the localized event to be determined (Figure 1-16).[18,140] In general, millions of these coincidence events give information on the spatial location and concentration of these positron emitters within the patient.[141]

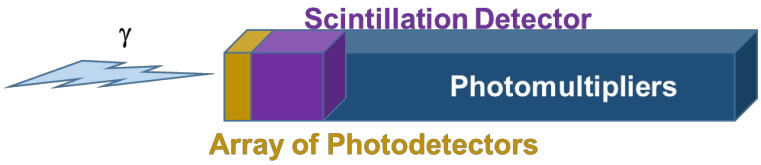

Figure 1-15 Simple PET Detector

In theory, these coincidence photons travel in opposite directions (180^{o}) from the annihilation event, and are called True Coincidences. In this case, the detector pair should produce signals simultaneously, or within 4-8 ns. If, however, unrelated coincidence events are registered within this time frame, they are called 'accidental' (or 'random') coincidences (Figure 1-16). These create noise and increased background within the PET scan images and need to be accounted for by removing them from the raw data measures.[141] Attenuation and the scattering of photons by a process called Compton scattering complicates the measured signal. Compton scattering is an interaction between a photon and a loosely bound electron, such that the out-going photon (after the interaction) is of lesser energy than the incoming photon and is diverted from the original direction ("scattered"); and is termed a 'scatter coincidence' and leads incorrectly assigned or misplaced LOR. These events make up roughly 40% of total recorded coincidences of a PET scan, but can be discriminated based on energy as measured by the light output from the scintillators.[141]

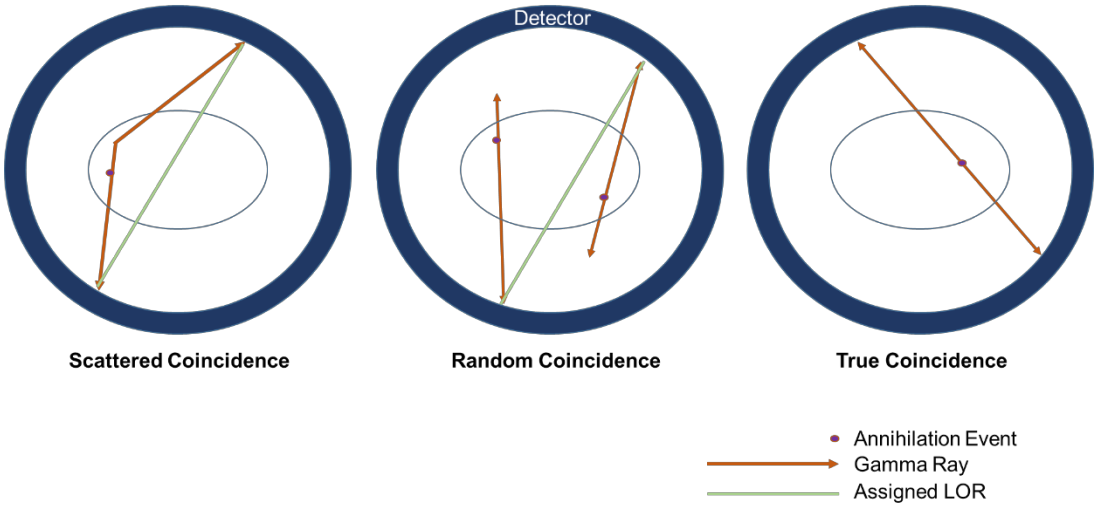

Figure 1-16 Types of Coincidence Events

The four main properties required of a PET detector/scintillator are: (1) light output, (2) signal decay time, (3) high probability for stopping or absorbing 511 KeV photons, (4) and its intrinsic energy resolution.

- (1,4) A high light output scintillator achieves higher energy resolution, and is related to the amount of light produced per each absorbed photon. Having good energy resolution is required to efficiently identify scattered events. With that, it is important to have only minor fluctuations in the measured energy of a detected photon (coupled with light output) to distinguish true coincidence photons from scattered photons.
- (2) The decay time of light determines how accurately in time the coincident photons are detected by the detectors; this is such that a faster production of signal is achieved after each complete photon absorption (shorter decay

constants to allow for higher photon counting rate). As the timing resolution improves, the signal-to-noise ratio improves.[18]

- (3) The sensitivity of the detector is related to the probability of absorbing a 511 KeV photon.[140,141]

As previously mentioned there are several available PET scintillators. BGO is a popular choice, as 95% of 511 KeV annihilated photons that enter a scintillation crystal are detected. Conversely, on the 3 cm block of the NaI detector, only 36% of the annihilated photons interact, yet it has a shorter decay time constant and the light output surpasses that of BGO. LSO, lutetium oxyorthosilicate, is another (newer and more expensive) option that has higher light output, hence better energy resolution (better discrimination of scattered events), as well as a shorter decay time constant.[141] Crystals (e.g. BGO) are limited by size (smaller size yields better spatial resolution), and as such, a matrix of crystals are often coupled to several photomultiplier tubes.

Following detection of these scintillation events, the next step in the process involves photomultiplier tubes (PMTs). PMTs are typically vacuum tubes with a photo cathode, whereby the incoming light signals are accelerated and amplified. The electrical current generated is proportional to the light output from the scintillation events, and by extension, to the initial annihilation photons in the initial scintillation crystals.[18]

Spatial resolution of PET is determined by many factors, including photon non-colinearity (photon trajectory deviating from the 180^{o}), positron range, as well as detector size. As previously discussed, non-colinearity (Figure 1-16) can produce error within the detected coincidence events and can deteriorate the resolution by ~0.2 cm. The positron range is the distance the positron travels in tissue before being annihilated, and this is

different for each radionuclide, and to a lesser extent, the tissue type. For example, the energies of positrons from ^{18}F have a maximum energy of 0.63 meV, and the error in spatial location can be ~0.2 mm – this is in stark contrast to ^{15}O that can have error as high as 1.2mm.[141]

i. General PET Scan Data Processing & Analysis

The raw data from the LORs are stored as sinograms, and these are the starting point for image reconstruction, data processing and analysis, and it is the sinograms where the necessary corrections are made prior to reconstruction.[32] The data required to produce reconstructed images from the raw data are the emission scan, a normalization scan, which corrects for detector non-uniformities, and a transmission/blank or CT scan, for calculating attenuation and scatter corrections. There are a variety of reconstruction algorithms available, including many iterative methods, and the analytic filtered back-projection (FBP) which was the long-time standard for both PET and CT. Reconstruction methods are beyond the scope of this introduction.[32,140,142,143] Localization of the radiopharmaceutical is thereby determined by reconstruction of all the annihilation events that occurred during a PET scan into a set of 2D images or 3D single image (Figure 1-14, Figure 1-17).[144]

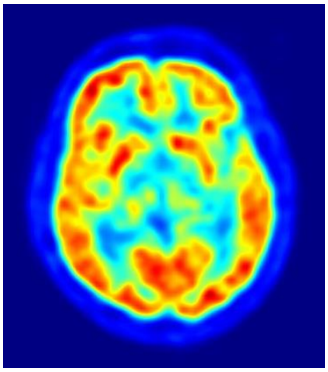

Figure 1-17 PET Scan of Human brain © Public Domain: https://en.wikipedia.org/wiki/Positron_emission_tomography

A Region of Interest (ROI) or voxel can be drawn around specific areas and a time-activity curve (TAC) generated (Figure 1-18). These values can be normalized to standard uptake values (SUV) to normalize for organism (patient) size and injected dose (Figure 1-19).[145]

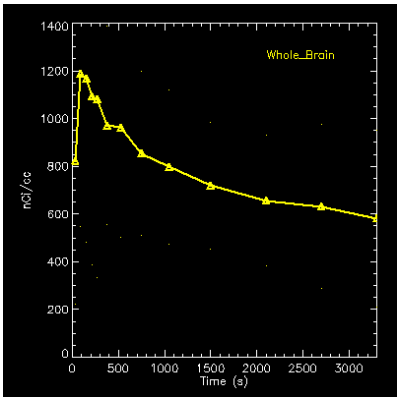

Figure 1-18 Time-Activity Curve (TAC)

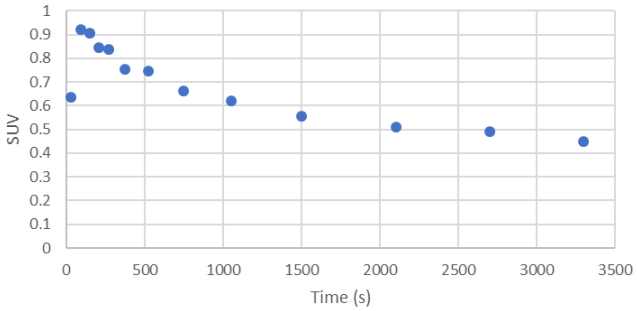

Figure 1-19 TAC in Standard Uptake Value (SUV)

PET scans can offer valuable information through static scans, to address spatial information (where are particular receptor populations, for example). With dynamic imaging data, kinetic modeling and quantitative, temporal information can be gained. This can include rate of trapping of the tracer, or how many receptors are in a volume of tissue.[146] Kinetic modeling and quantification of the tracer's *in vivo* behavior is an essential element in the development of new PET radiopharmaceuticals, imaging techniques, and their subsequent translation into clinical applications.[147]

The time-activity curves can be analyzed by a chosen pharmacokinetic model and modeled as a nonlinear function of rate parameters.[148] PET tracer kinetic modeling techniques can be model-driven or data-driven, to return the desired biologically based parameters.[147] Graphical analysis techniques for reversible and irreversible, include the

initial work in the Patlak plot for irreversible tracers, and an extended method to reversible kinetics called the Logan plot.[149,150]

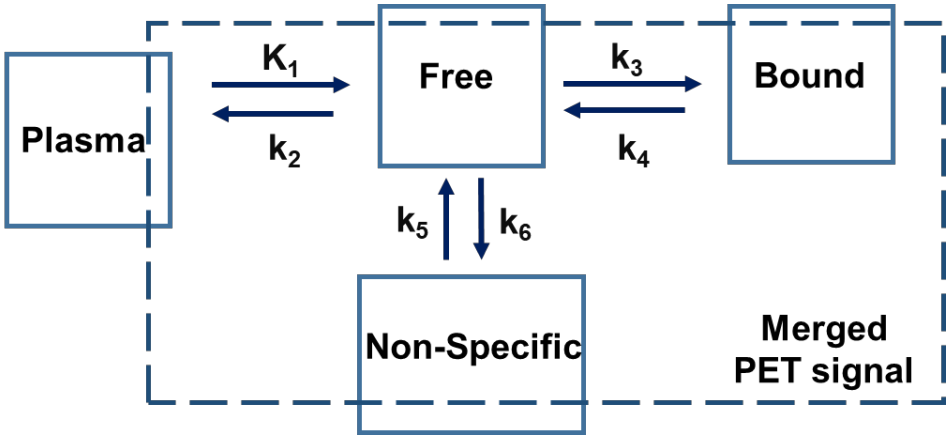

Figure 1-20 General Three-Compartment Model

Compartment models (such as Figure 1-20) are used to describe the dynamics of the PET scan – these are described by a series of differential equations with input functions and rate constants, or rather the entering/exiting of mass to/from (a) compartment, as previously shown. In PET tracer studies, several assumptions are made: the tracer amount injected is indeed a trace amount and does not elicit a change in physiology (this lends important to injecting high-specific activity PET radioligands), the tracer is in a steady state with the endogenous substrate, and the isotope does not inherently alter the tracer.[146] Several key values are of interest when describing tracer behavior. This includes distribution volume ratio (DVR): which is a ratio of the distribution volume of a region containing receptors to a nonreceptor region, to help determine receptor availability, or free receptor concentration. This is often done with an arterial input function, but can also be graphically modeled without the need for blood sampling.

This relates to the binding potential, or BP, which is proportional to the receptor density and binding affinity (K_D).[146,151–154]

Moreover, PET data helps bridge the gap between pharmacokinetics and pharmacodynamics through not just the determination of binding potential, but also receptor occupancy (taking the aforementioned BP a step further) and drug dosing.[152] Administration of the PET tracer, in a bolus injection, infusion (and etc) are other important characteristics to consider when planning a PET study and data analysis.[146] While the intricacies of compartmental modeling will not be discussed in this introduction, it is important to have an appreciation for the biomathematicians and kinetic modelers that describe the *in vivo* behavior of PET tracers.

j. Advancing Medicine and Drug Development Through PET

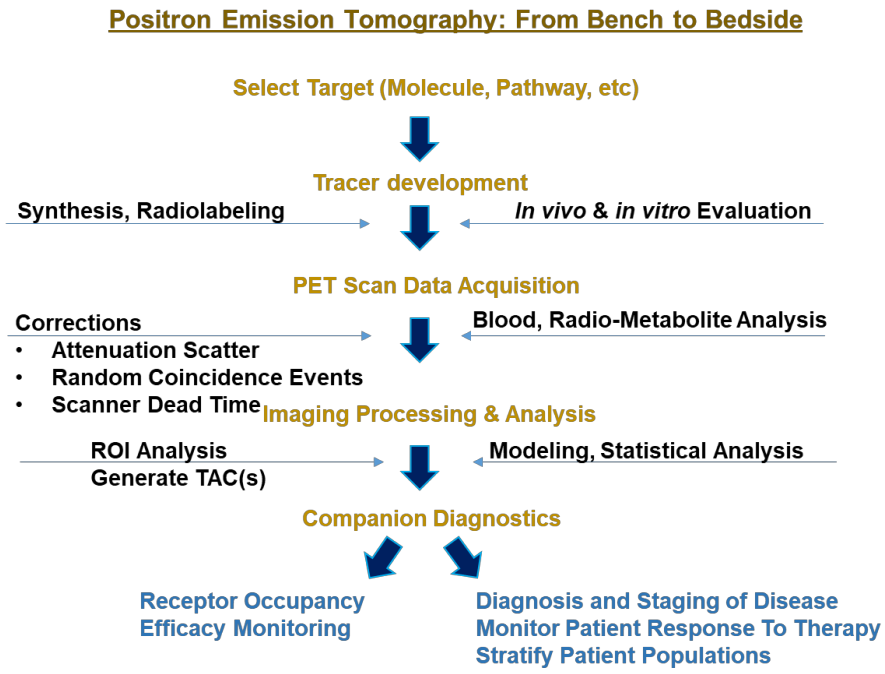

Figure 1-21 General PET Work Flow

Functional imaging offers unparalleled utility in drug development and medicine. PET differs fundamentally from other imaging modalities in that it deals at a molecular level, allowing one to see biochemical changes – and in many instances, chemical changes precede anatomical changes (as would be seen in other imaging modalities such as CT or MRI). A PET scan can assist nuclear medicine physicians, in the evaluation and staging of cancers, aid in the diagnosis and differentiation of dementias and related diseases/disorders, help identify damaged cardiac tissue and blood flow, aid in the planning of radiation therapy, and in monitoring patient response to therapy. It has applications in oncology, neurology, cardiology, infection and inflammation. Moreover, PET is a vital research tool to help understand (biochemically, physiologically, pharmacologically, etc) and "map" normal and diseased processes, and guide drug discovery programs.[18,21,140,155]

Formal training and education in nuclear medicine in the US is at a shortage, including radiopharmaceutical chemists. Most radiochemists are recruited from graduate and postgraduate training programs in organic, medicinal, and analytical chemistry, for example. Many doctoral studies are completed with a co-adviser in radiopharmaceutical chemistry, but lack formal training, and are relatively unspecialized. This means that radiochemical skills are gained largely at the postdoctoral training level. An estimated 5-10 new doctoral degrees in radiochemistry are awarded per year, and these values are declining. Even so, a recent study reported that an average of 2-3 positions per institution (in a survey of 20 institutions) went unfilled due to lack of unqualified applicants in radiopharmaceutical chemistry. The recruitment of students into radiopharmaceutical chemistry and nuclear medicine continues to be a challenge largely due to the fact that

many of the chemists in the field do not hold academic positions that have access to chemistry graduate students.[21]

It is with sincere gratitude that this work is put forth as the result of 5 years of mentorship and guidance by Professor Peter J.H. Scott, a radiopharmaceutical chemist and Director of PET Radiochemistry and Cyclotron Facility, and his appointment in the University of Michigan's Interdepartmental Program in Medicinal Chemistry. Without Dr. Scott's efforts to mentor chemistry graduate student(s) through their doctoral studies as the next generation of PET radiopharmaceutical chemists, this work would not have been possible.

References

(1) Röntgen, W. C. *Auf eine neueu Art von Strahlen (On a New Kind of Rays)*; 1895; Vol. 3.

(2) *Handbook of Radiopharmaceuticals: Radiochemistry and Applications*; Welch, M. J., Redvanly, C. S., Eds.; John Wiley & Sons, Ltd., 2003.

(3) Scatliff, J. H.; Morris, P. J. From roentgen to magnetic resonance imaging: the history of medical imaging. *N. C. Med. J.* **2014**, *75* (2), 111–113 DOI: 10.18043/ncm.75.2.111.

(4) Markel, H. “I Have Seen My Death”: How the World Discovered the X-Ray | PBS NewsHour https://www.pbs.org/newshour/health/i-have-seen-my-death-how-the-world-discovered-the-x-ray (accessed Nov 13, 2017).

(5) Thomson, J. J. Cathode Rays. *Philosophical Magazine and Journal of Science*. October 1897, pp 293–316.

(6) Wacławek, W.; Wacławek, M. Marie Skłodowska-Curie and her contributions to chemistry, radiochemistry and radiotherapy. *Anal. Bioanal. Chem.* **2011**, *400* (6), 1567–1575 DOI: 10.1007/s00216-011-4922-6.

(7) Röntgen, W. First medical X-ray by Wilhelm Röntgen of his wife Anna Bertha Ludwig’s hand https://commons.wikimedia.org/wiki/File:First_medical_X-ray_by_Wilhelm_Röntgen_of_his_wife_Anna_Bertha_Ludwig%27s_hand_-_18951222.gif (accessed Nov 13, 2017).

(8) Rutherford, E.; Soddy, F. Cause and Nature of Radioactivity, Part 1. *Philos. Mag.*

J. Sci. **1902**, *4* (6), 370–396.

(9) Rutherford, E.; Soddy, F. Cause and Nature of Radioactivity, Part 2. *Philos. Mag. J. Sci.* **1902**, *4* (6), 569–585.

(10) The Editors of Encyclopaedia Britannica. Frederic and Irene-Joliot-Curie. *Enclopaedia Britannica*; Encyclopaedia Brittanica, inc., 2016.

(11) Ter-Pogossian, M. M. The origins of positron emission tomography. *Semin. Nucl. Med.* **1992**, *22* (3), 140–149 DOI: 10.1016/S0001-2998(05)80142-4.

(12) Oliphant, M. L. E.; Harteck, P.; Rutherford, Lord. Transmutation Effects Observed with Heavy Hydrogen. *Proc. R. Soc. A Math. Phys. Eng. Sci.* **1934**, *144* (853), 692–703 DOI: 10.1098/rspa.1934.0077.

(13) Lappin, G. A historical perspective on radioisotopic tracers in metabolism and biochemistry. **2015**, *7*, 531–540 DOI: 10.4155/bio.14.286.

(14) Elmore, C. S.; Bragg, R. A. Isotope chemistry; A useful tool in the drug discovery arsenal. *Bioorganic Med. Chem. Lett.* **2015**, *25* (2), 167–171 DOI: 10.1016/j.bmcl.2014.11.051.

(15) Rubin, S.; Hassid, W. Z.; Kamen, M. D. Radioactive Carbon in Study of Photosynthesis. *J. Am. Chem. Soc.* **1939**, *61* (1), 661–663.

(16) Ruben, S.; Kamen, M. D. Radioactive Carbon of Long Half-Life. *Phys. Rev.* **1940**, *57* (6), 549–549 DOI: 10.1103/PhysRev.57.549.

(17) Yarris, L. Ernest Lawrence's Cyclotron: Invention for the Ages. **2017**, 2–5.

(18) Hoffman, E.J., Phelps, M. E. *Positron emission tomography*; 1979; Vol. 13.

(19) Nemenov, L. M. The history of the development of the cyclotron over fifty years (1930–1980). *Sov. Phys. Uspekhi* **1981**, *24* (3), 231–240 DOI: 10.1070/PU1981v024n03ABEH004773.

(20) Nemenov, L. M. Historical development of the cyclotron. *At. Energy* **1958**, *4* (2), 155–167 DOI: 10.1007/BF02207337.

(21) National Research Council; Institute of Medicine; Committee on State of the Science and Nuclear Medicine. *Advancing Nuclear Medicine Through Innovation*; National Academies Press: Washington, D.C., 2007.

(22) Cofield, C. Alpha Particles Target Cancer. *Am. Phys. Soc. APS News* **2014**, *23* (6).

(23) O'Donoghue, J. A.; Wheldon, T. E. Targeted radiotherapy using Auger electron emitters. *Phys. Med. Biol.* **1996**, *41* (10), 1973–1992.

(24) Jacobson, M. S.; Steichen, R. A.; Peller, P. J. PET Radiochemistry and Radiopharmacy. In *Dysphagia*; 2012; Vol. 39, pp 19–30.

(25) Nayak, T. K.; Brechbiel, M. W. Radioimmunoimaging with Longer-Lived Positron-Emitting Radionuclides: Potentials and Challenges. *Bioconjug. Chem.* **2009**, *20* (5), 825–841 DOI: 10.1021/bc800299f.

(26) Qaim, S. M.; Bisinger, T.; Hilgers, K.; Nayak, D.; Coenen, H. H. Positron emission intensities in the decay of 64Cu, 76Br and 124I. *Radiochim. Acta* **2007**, *95* (2), 67–73 DOI: 10.1524/ract.2007.95.2.67.

(27) Purrington, S. T.; Kagen, B. S.; Patrick, T. B. Application of elemental fluorine in organic synthesis. *Chem. Rev.* **1986**, *86* (6), 997–1018 DOI: 10.1021/cr00076a003.

(28) Solin, O.; Bergman, J. Production of [18F]F2 from [18O]O2. *J. Label. Comp. Radiopharm.* **1986**, *23*, 1202–1204.

(29) Nickles, R. J.; Daube, M. E.; Ruth, T. J. An 18O2 target for the production of [18F]F2. *Int. J. Appl. Radiat. Isot.* **1984**, *35* (2), 117–122 DOI: 10.1016/0020-708X(84)90194-7.

(30) Casella, V.; Wolf, A. P.; Fowler, J. S.; MacGregor, R. R.; Ruth, T. J. RADIOCHEMISTRY AND RADIOPHARMACEUT1CALS Anhydrous F-18 Labeled Elemental Fluorine for Radiopharmaceutical Preparation withdecreasIng. *J. Nucl. Med.* **1980**, *2*, 750–757.

(31) Cole, E.; Stewart, M.; Littich, R.; Hoareau, R.; Scott, P. Radiosyntheses using Fluorine-18: The Art and Science of Late Stage Fluorination. *Curr. Top. Med. Chem.* **2014**, *14* (7), 875–900 DOI: 10.2174/1568026614666140202205035.

(32) Schmitz, R. E.; Alessio, A. M.; Kinahan, P. E. *The Physics of PET/CT scanners*; 2009.

(33) Lasne, M.-C.; Perrio, C.; Rouden, J.; Barré, L.; Roeda, D.; Dolle, F.; Crouzel, C. Chemistry of β +-Emitting Compounds Based on Fluorine-18. In *Topics in Current Chemistry*; 2002; Vol. 222, pp 201–258.

(34) Eskola, O. *Fluorine and 18 F-Fluorine in Radiopharmaceutical Preparation*; 2013.

(35) O'Hagan, D. Understanding organofluorine chemistry. An introduction to the C-F bond. *Chem. Soc. Rev.* **2008**, *37* (2), 308–319 DOI: 10.1039/b711844a.

(36) Hagmann, W. K. The many roles for fluorine in medicinal chemistry. *J. Med. Chem.*

2008, *51* (15), 4359–4369 DOI: 10.1021/jm800219f.

(37) Purser, S.; Moore, P. R.; Swallow, S.; Gouverneur, V. Fluorine in medicinal chemistry. *Chem. Soc. Rev.* **2008**, *37* (2), 320–330 DOI: 10.1039/b610213c.

(38) Gillis, E. P.; Eastman, K. J.; Hill, M. D.; Donnelly, D. J.; Meanwell, N. A. Applications of Fluorine in Medicinal Chemistry. *J. Med. Chem.* **2015**, *58* (21), 8315–8359 DOI: 10.1021/acs.jmedchem.5b00258.

(39) Eskola, O.; Grönroos, T.; Bergman, J.; Haaparanta, M.; Marjamäki, P.; Lehikoinen, P.; Forsback, S.; Langer, O.; Hinnen, F.; Dollé, F.; et al. A novel electrophilic synthesis and evaluation of medium specific radioactivity (1R,2S)-4-[18F]fluorometaraminol, a tracer for the assessment of cardiac sympathetic nerve integrity with PET. *Nucl. Med. Biol.* **2004**, *31* (1), 103–110 DOI: 10.1016/S0969-8051(03)00098-2.

(40) Rosenblum, S. B.; Huynh, T.; Afonso, A.; Davis, H. R.; Yumibe, N.; Clader, J. W.; Burnett, D. A. Discovery of 1-(4-Fluorophenyl)-(3 R)-[3-(4-fluorophenyl)-(3 S)-hydroxypropyl]-(4 S)-(4-hydroxyphenyl)-2-azetidinone (SCH 58235): A Designed, Potent, Orally Active Inhibitor of Cholesterol Absorption. *J. Med. Chem.* **1998**, *41* (6), 973–980 DOI: 10.1021/jm970701f.

(41) Campbell, M. G.; Mercier, J.; Genicot, C.; Gouverneur, V.; Hooker, J. M.; Ritter, T. Bridging the gaps in 18F PET tracer development. *Nat. Chem.* **2016**, *9* (1), 1–3 DOI: 10.1038/nchem.2693.

(42) Brooks, A. F.; Topczewski, J. J.; Ichiishi, N.; Sanford, M. S.; Scott, P. J. H. Late-stage [^{18} F]fluorination: new solutions to old problems. *Chem. Sci.* **2014**, *5* (12),

4545–4553 DOI: 10.1039/C4SC02099E.

(43) Miller, P. W.; Long, N. J.; Vilar, R.; Gee, A. D. Synthesis of11C, 18F, 15O, and 13N radiolabels for positron emission tomography. *Angew. Chemie - Int. Ed.* **2008**, *47* (47), 8998–9033 DOI: 10.1002/anie.200800222.

(44) Hockley, B. G.; Scott, P. J. H. An automated method for preparation of [18F]sodium fluoride for injection, USP to address the technetium-99m isotope shortage. *Appl. Radiat. Isot.* **2010**, *68* (1), 117–119 DOI: 10.1016/j.apradiso.2009.08.012.

(45) Schirrmacher, R.; Wängler, B.; Bailey, J.; Bernard-Gauthier, V.; Schirrmacher, E.; Wängler, C. Small Prosthetic Groups in18F-Radiochemistry: Useful Auxiliaries for the Design of18F-PET Tracers. *Semin. Nucl. Med.* **2017**, *47* (5), 474–492 DOI: 10.1053/j.semnuclmed.2017.07.001.

(46) Shao, X.; Hoareau, R.; Hockley, B. G.; Tluczek, L. J. M.; Henderson, B. D.; Padgett, H. C.; Scott, P. J. H. Highlighting the versatility of the tracerlab synthesis modules. Part 1: fully automated production of [18F]labelled radiopharmaceuticals using a Tracerlab FXFN. *J. Label. Compd. Radiopharm.* **2011**, *54* (6), 292–307 DOI: 10.1002/jlcr.1865.

(47) *Radiochemical Syntheses Volume 1: Radiopharmaceuticals for Positron Emission Tomography*; Scott, P. J. H., Hockley, B. G., Eds.; John Wiley & Sons, Ltd: Hoboken, New Jersey, 2012.

(48) *Radiochemical Syntheses Volume 2: Further Radiopharmaceuticals for Positron Emission Tomography and New Strategies for Their Production*; Scott, P. J. H., Ed.; John Wiley & Sons, Ltd: Hoboken, New Jersey, 2015.

(49) Hollingworth, C.; Hazari, A.; Hopkinson, M. N.; Tredwell, M.; Benedetto, E.; Huiban, M.; Gee, A. D.; Brown, J. M.; Gouverneur, V. Palladium-catalyzed allylic fluorination. *Angew. Chemie - Int. Ed.* **2011**, *50* (11), 2613–2617 DOI: 10.1002/anie.201007307.

(50) Topczewski, J. J.; Tewson, T. J.; Nguyen, H. M. Iridium-catalyzed allylic fluorination of trichloroacetimidates. *J. Am. Chem. Soc.* **2011**, *133* (48), 19318–19321 DOI: 10.1021/ja2087213.

(51) Benedetto, E.; Tredwell, M.; Hollingworth, C.; Khotavivattana, T.; Brown, J. M.; Gouverneur, V. Regio- and stereoretentive synthesis of branched, linear (E)- and (Z)-allyl fluorides from allyl carbonates under Ir-catalysis. *Chem. Sci.* **2013**, *4* (1), 89–96 DOI: 10.1039/C2SC21789A.

(52) Ryzhikov, N.; Gomzina, N.; Fedorova, O.; Vasil'ev, D.; Kostikov, A.; Krasikova, R. Preparation of [18F]flumazenil, a potential radioligand for PET imaging of central 323 benzodiazepine receptors, by isotope exchange. *Radiochemistry* **2004**, *46*, 290–294.

(53) Tredwell, M.; Gouverneur, V. 18F labeling of arenes. *Angew. Chemie - Int. Ed.* **2012**, *51* (46), 11426–11437 DOI: 10.1002/anie.201204687.

(54) Ravert, H.; Holt, D.; Dannals, R. 2-([18F]fluoro-3-[(2S)-2-azetidinylmethoxy]pyridine ([18F]2FA). In *Radiochemical Syntheses Volume 1: Radiopharmaceuticals for Positron Emission Tomography*; Scott, P., Hockley, B., Eds.; John Wiley & Sons, Ltd: Hoboken, 2010.

(55) Hockley, B. G.; Stewart, M. N.; Sherman, P.; Quesada, C.; Kilbourn, M. R.; Albin,

R. L.; Scott, P. J. H. (-)-[18F]Flubatine: Evaluation in rhesus monkeys and a report of the first fully automated radiosynthesis validated for clinical use. *J. Label. Compd. Radiopharm.* **2013**, *56* (12), 595–599 DOI: 10.1002/jlcr.3069.

(56) Fischer, S.; Hiller, A.; Smits, R.; Hoepping, A.; Funke, U.; Wenzel, B.; Cumming, P.; Sabri, O.; Steinbach, J.; Brust, P. Radiosynthesis of racemic and enantiomerically pure (-)-[18F]flubatine-A promising PET radiotracer for neuroimaging of alpha4beta2 nicotinic acetylcholine receptors. *Appl. Radiat. Isot.* **2013**, *74*, 128–136 DOI: 10.1016/j.apradiso.2013.01.002.

(57) Alvarez, M.; LeBars, D. Synthesis of 4-(2'-methoxyphenyl)-1-[2'-(N-2'pyridinyl)-p-[18F]fluorobenzoamido]ethylpiperazine ([18F]MPPF). In *Radiochemical Syntheses Volume 1: Radiopharmaceuticals for Positron Emission Tomography*; Scott, P. J. H., Hockley, B., Eds.; John Wiley & Sons, Ltd: Hoboken, 2011; pp 87–94.

(58) Jackson, A.; Smith, G.; Brown, S.; Morrison-Iveson, V.; Chau, W.; Durrant, C.; Wilson, I. Radiosynthesis, Biodistribution and Metabolic Fate of Three PET Agents for Amyloid-Beta In Rats: [18F]Flutemetamol, florbetapir F18 (18F-AV-45) and florbetaben (BAY 94-9172) (PW012). *Eur. J. Nucl. Med. Mol. Imaging* **2011**, *38* (Suppl 2), S231–S232.

(59) Ekaeva, I.; Barre, L.; Lasne, M. C.; Gourand, F. 2- and 4-[18F]Fluorophenols from Baeyer-Villiger Oxidation of [18F]Fluorophenylketones and [18F]Fluorobenzaldehydes. *Appl. Radiat. Isot.* **1995**, *46* (8), 777–782 DOI: 10.1016/0969-8043(95)00022-6.

(60) Gao, Z.; Lim, Y. H.; Tredwell, M.; Li, L.; Verhoog, S.; Hopkinson, M.; Kaluza, W.;

Collier, T. L.; Passchier, J.; Huiban, M.; et al. Metal-free oxidative fluorination of phenols with [18F]fluoride. *Angew. Chemie - Int. Ed.* **2012**, *51* (27), 6733–6737 DOI: 10.1002/anie.201201502.

(61) Cai, L.; Lu, S.; Pike, V. W. Chemistry with [18F]fluoride ion. *European J. Org. Chem.* **2008**, No. 17, 2853–2873 DOI: 10.1002/ejoc.200800114.

(62) Jacobson, O.; Kiesewetter, D. O.; Chen, X. Fluorine-18 radiochemistry, labeling strategies and synthetic routes. *Bioconjug. Chem.* **2015**, *26* (1), 1–18 DOI: 10.1021/bc500475e.

(63) Pike, V. W.; Butt, F.; Shah, A.; Widdowson, D. a. Facile synthesis of substituted diaryliodonium tosylates by treatment of aryltributylstannanes with Koser's reagent. *J. Chem. Soc. Perkin Trans. 1* **1999**, No. 3, 245–248 DOI: 10.1039/a809349k.

(64) Carroll, M.; Jones, C.; Tang, S. Fluoridation of 2-thienyliodonium salts. *J Label Compd Radiopharm* **2007**, *50*, 450–451.

(65) Ross, T. L.; Ermert, J.; Hocke, C.; Coenen, H. H. Nucleophilic 18F-fluorination of heteroaromatic iodonium salts with no-carrier-added [18F]fluoride. *J. Am. Chem. Soc.* **2007**, *129* (25), 8018–8025 DOI: 10.1021/ja066850h.

(66) Telu, S.; Chun, J.; Simeon, F. G.; Lu, S.; Pike, V. W. Syntheses of mGluR5 PET radioligands through the radiofluorination of diaryliodonium tosylates. *Org. Biomol. Chem.* **2011**, *9* (19), 6629–6638 DOI: 10.1039/c1ob05555k.

(67) Cardinale, J.; Ermert, J.; Humpert, S.; Coenen, H. H. Iodonium ylides for one-step, no-carrier-added radiofluorination of electron rich arenes, exemplified with 4-(([^{18}

F]fluorophenoxy)-phenylmethyl)piperidine NET and SERT ligands. *RSC Adv.* **2014**, *4* (33), 17293–17299 DOI: 10.1039/C4RA00674G.

(68) Rotstein, B. H.; Stephenson, N. A.; Vasdev, N.; Liang, S. H. Spirocyclic hypervalent iodine(III)-mediated radiofluorination of non-activated and hindered aromatics. *Nat. Commun.* **2014**, *5* (May), 1–7 DOI: 10.1038/ncomms5365.

(69) Fischer, C.; Mu, L.; Holland, J.; Becaud, J.; Schubiger, P.; Schibli, R.; Ametamey, S.; Graham, K.; Stellfeld, T.; Dinkelborg, L.; et al. O-071: 18F-labeling of unactivated aromatic compounds using triarylsulfonium salts. *J Label Compd Radiopharm* **2011**, *54* (Suppl. 1), S71.

(70) Mu, L.; Fischer, C.; Holland, J.; Becaud, J.; Schubiger, P.; Schibli, R.; Ametamey, S.; Graham, K.; Stellfeld, T.; Dinkelborg, L.; et al. 18F-Radiolabeling of aromatic compounds using triarylsulfonium salts. *European J. Org. Chem.* **2012**, 889–892.

(71) Chun, J.-H.; Morse, C. L.; Chin, F. T.; Pike, V. W. No-carrier-added [18F]fluoroarenes from the radiofluorination of diaryl sulfoxides. *Chem. Commun.* **2013**, *49* (21), 2151 DOI: 10.1039/c3cc37795d.

(72) Chun, J.; Morse, C.; Chin, F.; Pike, V. O-070: No-carrier-added radiosyntheses of [18F]fluoroarenes from diaryl sulfoxides and [18F]fluoride ion. *J Label Compd Radiopharm* **2011**, *54* (Suppl. 1), S70.

(73) Narayanam, M. K.; Ma, G.; Champagne, P. A.; Houk, K. N.; Murphy, J. M. Synthesis of [18 F]Fluoroarenes by Nucleophilic Radiofluorination of N -Arylsydnones. *Angew. Chemie Int. Ed.* **2017**, 1–6 DOI: 10.1002/anie.201707274.

(74) Lee, E.; Kamlet, A. S.; Powers, D. C.; Neumann, C. N.; Boursalian, G. B.; Furuya, T.; Choi, D. C.; Hooker, J. M.; Ritter, T. A Fluoride-Derived Electrophilic Late-Stage Fluorination Reagent for PET Imaging. *Science (80-.).* **2011**, *334* (November), 639–642.

(75) Kamlet, A. S.; Neumann, C. N.; Lee, E.; Carlin, S. M.; Moseley, C. K.; Stephenson, N.; Hooker, J. M.; Ritter, T. Application of Palladium-Mediated 18F-Fluorination to PET Radiotracer Development: Overcoming Hurdles to Translation. *PLoS One* **2013**, *8* (3), 1–10 DOI: 10.1371/journal.pone.0059187.

(76) Brandt, J. R.; Lee, E.; Boursalian, G. B.; Ritter, T. Mechanism of electrophilic fluorination with Pd(<scp>iv</scp>): fluoride capture and subsequent oxidative fluoride transfer. *Chem. Sci.* **2014**, *5* (1), 169–179 DOI: 10.1039/C3SC52367E.

(77) Lee, E.; Hooker, J. M.; Ritter, T. Nickel-mediated oxidative fluorination for PET with aqueous [18F] fluoride. *J. Am. Chem. Soc.* **2012**, *134* (42), 17456–17458 DOI: 10.1021/ja3084797.

(78) Ren, H.; Wey, H. Y.; Strebl, M.; Neelamegam, R.; Ritter, T.; Hooker, J. M. Synthesis and imaging validation of [18F]MDL100907 enabled by Ni-mediated fluorination. *ACS Chem. Neurosci.* **2014**, *5* (7), 611–615 DOI: 10.1021/cn500078e.

(79) Neumann, C. N.; Hooker, J. M.; Ritter, T. Concerted nucleophilic aromatic substitution with 19F− and 18F−. *Nature* **2016**, *538* (7624), 274–274 DOI: 10.1038/nature19311.

(80) Sladojevich, F.; Arlow, S. I.; Tang, P.; Ritter, T. Late-stage deoxyfluorination of alcohols with phenofluor. *J. Am. Chem. Soc.* **2013**, *135* (7), 2470–2473 DOI:

10.1021/ja3125405.

(81) Tang, P.; Wang, W.; Ritter, T. Deoxyfluorination of phenols. *J. Am. Chem. Soc.* **2011**, *133* (30), 11482–11484 DOI: 10.1021/ja2048072.

(82) Goldberg, N. W.; Shen, X.; Li, J.; Ritter, T. AlkylFluor: Deoxyfluorination of Alcohols. *Org. Lett.* **2016**, *18* (23), 6102–6104 DOI: 10.1021/acs.orglett.6b03086.

(83) Fujimoto, T.; Ritter, T. PhenoFluorMix: Practical chemoselective deoxyfluorination of phenols. *Org. Lett.* **2015**, *17* (3), 544–547 DOI: 10.1021/ol5035518.

(84) Fujimoto, T.; Becker, F.; Ritter, T. PhenoFluor: Practical Synthesis, New Formulation, and Deoxy fl uorination of Heteroaromatics. **2014**, 10–13.

(85) Campbell, M. G.; Ritter, T. Late-stage formation of carbon-fluorine bonds. *Chem. Rec.* **2014**, *14* (3), 482–491 DOI: 10.1002/tcr.201402016.

(86) Ichiishi, N.; Canty, A. J.; Yates, B. F.; Sanford, M. S. Cu-catalyzed fluorination of diaryliodonium salts with KF. *Org. Lett.* **2013**, *15* (19), 5134–5137 DOI: 10.1021/ol4025716.

(87) Ichiishi, N.; Brooks, A. F.; Topczewski, J. J.; Rodnick, M. E.; Sanford, M. S.; Scott, P. J. H. Copper-Catalyzed [18F]Fluorination of (Mesityl)(aryl)iodonium Salts. *Org. Lett.* **2014**, *16* (12), 3224–3227 DOI: 10.1021/ol501243g.

(88) Ye, Y.; Schimler, S. D.; Hanley, P. S.; Sanford, M. S. Cu(OTf)2-mediated fluorination of aryltrifluoroborates with potassium fluoride. *J. Am. Chem. Soc.* **2013**, *135* (44), 16292–16295 DOI: 10.1021/ja408607r.

(89) Tredwell, M.; Preshlock, S. M.; Taylor, N. J.; Gruber, S.; Huiban, M.; Passchier, J.;

Mercier, J.; Génicot, C.; Gouverneur, V. A general copper-mediated nucleophilic 18F fluorination of arenes. *Angew. Chemie - Int. Ed.* **2014**, *53* (30), 7751–7755 DOI: 10.1002/anie.201404436.

(90) Mossine, A. V.; Brooks, A. F.; Makaravage, K. J.; Miller, J. M.; Ichiishi, N.; Sanford, M. S.; Scott, P. J. H. Synthesis of [^{18} F]Arenes via the Copper-Mediated [^{18} F]Fluorination of Boronic Acids. *Org. Lett.* **2015**, acs.orglett.5b02875 DOI: 10.1021/acs.orglett.5b02875.

(91) Gamache, R. F.; Waldmann, C.; Murphy, J. M. Copper-Mediated Oxidative Fluorination of Aryl Stannanes with Fluoride. *Org. Lett.* **2016**, *18* (18), 4522–4525 DOI: 10.1021/acs.orglett.6b02125.

(92) Makaravage, K. J.; Brooks, A. F.; Mossine, A. V.; Sanford, M. S.; Scott, P. J. H. Copper-Mediated Radiofluorination of Arylstannanes with [18F]KF. *Org. Lett.* **2016**, *18* (20), 5440–5443 DOI: 10.1021/acs.orglett.6b02911.

(93) Sanford, M. S.; Scott, P. J. H. Moving Metal-Mediated ^{18} F-Fluorination from Concept to Clinic. *ACS Cent. Sci.* **2016**, *2* (3), 128–130 DOI: 10.1021/acscentsci.6b00061.

(94) Hoover, A. J.; Lazari, M.; Ren, H.; Narayanam, M. K.; Murphy, J. M.; Van Dam, R. M.; Hooker, J. M.; Ritter, T. A Transmetalation Reaction Enables the Synthesis of [18F]5-Fluorouracil from [18F]Fluoride for Human PET Imaging. *Organometallics* **2016**, *35* (7), 1008–1014 DOI: 10.1021/acs.organomet.6b00059.

(95) Huang, X.; Liu, W.; Ren, H.; Neelamegam, R.; Hooker, J. M.; Groves, J. T. Late Stage Benzylic C–H Fluorination with [^{18} F]Fluoride for PET Imaging. *J. Am. Chem.*

Soc. **2014**, *136* (19), 6842–6845 DOI: 10.1021/ja5039819.

(96) McCammant, M. S.; Thompson, S.; Brooks, A. F.; Krska, S. W.; Scott, P. J. H.; Sanford, M. S. Cu-Mediated C-H 18 F-Fluorination of Electron-Rich (Hetero)arenes. *Org. Lett.* **2017**, acs.orglett.7b01902 DOI: 10.1021/acs.orglett.7b01902.

(97) Riss, P. J.; Aigbirhio, F. I. A simple, rapid procedure for nucleophilic radiosynthesis of aliphatic [18F]trifluoromethyl groups. *Chem. Commun.* **2011**, *47* (43), 11873 DOI: 10.1039/c1cc15342k.

(98) Riss, P. J.; Ferrari, V.; Brichard, L.; Burke, P.; Smith, R.; Aigbirhio, F. I. Direct, nucleophilic radiosynthesis of [18F]trifluoroalkyl tosylates: improved labelling procedures. *Org. Biomol. Chem.* **2012**, *10* (34), 6980–6986 DOI: 10.1039/c2ob25802a.

(99) Fawaz, M. V.; Brooks, A. F.; Rodnick, M. E.; Carpenter, G. M.; Shao, X.; Desmond, T. J.; Sherman, P.; Quesada, C. A.; Hockley, B. G.; Kilbourn, M. R.; et al. High affinity radiopharmaceuticals based upon lansoprazole for PET imaging of aggregated tau in alzheimer"s disease and progressive supranuclear palsy: Synthesis, preclinical evaluation, and lead selection. *ACS Chem. Neurosci.* **2014**, *5* (8), 718–730 DOI: 10.1021/cn500103u.

(100) Huiban, M.; Tredwell, M.; Mizuta, S.; Wan, Z.; Zhang, X.; Collier, T. L.; Gouverneur, V.; Passchier, J. A broadly applicable [18F]trifluoromethylation of aryl and heteroaryl iodides for PET imaging. *Nat. Chem.* **2013**, *5* (11), 941–944 DOI: 10.1038/nchem.1756.

(101) Rühl, T.; Rafique, W.; Lien, V. T.; Riss, P. J. Cu(<scp>i</scp>)-mediated ^{18} F-trifluoromethylation of arenes: Rapid synthesis of ^{18} F-labeled trifluoromethyl arenes. *Chem. Commun.* **2014**, *50* (45), 6056–6059 DOI: 10.1039/C4CC01641F.

(102) Ivashkin, P.; Lemonnier, G.; Cousin, J.; Gr??goire, V.; Labar, D.; Jubault, P.; Pannecoucke, X. CuCF3: A [18F]trifluoromethylating agent for arylboronic acids and aryl iodides. *Chem. - A Eur. J.* **2014**, *20* (31), 9514–9518 DOI: 10.1002/chem.201403630.

(103) Vanderborn, D.; Sewing, C.; Herscheid, J. D. M.; Windhorst, A. D.; Orru, R. V. A.; Vugts, D. J. A universal procedure for the [18F]trifluoromethylation of aryl iodides and aryl boronic acids with highly improved specific activity. *Angew. Chemie - Int. Ed.* **2014**, *53* (41), 11046–11050 DOI: 10.1002/anie.201406221.

(104) Richter, S.; Wuest, F. 18 F-labeled peptides: The future is bright. *Molecules* **2014**, *19* (12), 20536–20556 DOI: 10.3390/molecules191220536.

(105) Liang, S. H.; Vasdev, N. C(sp3)-18F Bond Formation by Transition-Metal-Based [18F]Fluorination. *Angew. Chemie - Int. Ed.* **2014**, *53* (43), 11416–11418 DOI: 10.1002/anie.201407065.

(106) Littich, R.; Scott, P. J. H. Novel strategies for fluorine-18 radiochemistry. *Angew. Chemie - Int. Ed.* **2012**, *51* (5), 1106–1109 DOI: 10.1002/anie.201106785.

(107) Ametamey, S. M.; Honer, M.; Schubiger, P. A. Molecular imaging with PET. *Chem. Rev.* **2008**, *108* (5), 1501–1516 DOI: 10.1021/cr0782426.

(108) Le Bars, D. Fluorine-18 and medical imaging: Radiopharmaceuticals for positron

emission tomography. *J. Fluor. Chem.* **2006**, *127* (11), 1488–1493 DOI: 10.1016/j.jfluchem.2006.09.015.

(109) Kilbourn, M. R.; Shao, X. Fluorine - 18 Radiopharmaceuticals. In *Fluorine in Medicinal Chemistry and Chemical Biology*; Ojima, I., Ed.; Blackwell publishing, Ltd., 2009; pp 361–388.

(110) Schirrmacher, R.; Wangler, C.; Schirrmacher, E. Recent Developments and Trends in 18F-Radiochemistry: Syntheses and Applications. *Mini. Rev. Org. Chem.* **2007**, *4* (4), 317–329 DOI: 10.2174/157019307782411699.

(111) Taylor, N.; Emer, E.; Preshlock, S.; Schedler, M.; Tredwell, M.; Verhoog, S.; Mercier, J.; Genicot, C.; Gouverneur, V. E. De-Risking the Cu-Mediated 18F-Fluorination of Heterocyclic PET Radioligands. *J. Am. Chem. Soc.* **2017**, jacs.7b03131 DOI: 10.1021/jacs.7b03131.

(112) Campbell, M. G.; Ritter, T. Late-stage fluorination: From fundamentals to application. *Org. Process Res. Dev.* **2014**, *18* (4), 474–480 DOI: 10.1021/op400349g.

(113) Liang, T.; Neumann, C. N.; Ritter, T. Introduction of fluorine and fluorine-containing functional groups. *Angew. Chemie - Int. Ed.* **2013**, *52* (32), 8214–8264 DOI: 10.1002/anie.201206566.

(114) Preshlock, S.; Tredwell, M.; Gouverneur, V. 18F-Labeling of Arenes and Heteroarenes for Applications in Positron Emission Tomography. *Chem. Rev.* **2016**, *116* (2), 719–766 DOI: 10.1021/acs.chemrev.5b00493.

(115) Gouverneur, V.; Seppelt, K. Introduction: Fluorine chemistry. *Chem. Rev.* **2015**, *115* (2), 563–565 DOI: 10.1021/cr500686k.

(116) Shao, X.; Hoareau, R.; Runkle, A. C.; Tluczek, L. J. M.; Hockley, B. G.; Henderson, B. D.; Scott, P. J. H. Highlighting the versatility of the Tracerlab synthesis modules. Part 2: fully automated production of [11C]-labeled radiopharmaceuticals using a Tracerlab FXC-Pro. *J. Label. Compd. Radiopharm.* **2011**, *54* (14), 819–838 DOI: 10.1002/jlcr.1937.

(117) Scott, P. J. H. Methods for the incorporation of carbon-11 to generate radiopharmaceuticals for PET imaging. *Angew. Chemie - Int. Ed.* **2009**, *48* (33), 6001–6004 DOI: 10.1002/anie.200901481.

(118) Rotstein, B. H.; Liang, S. H.; Holland, J. P.; Collier, T. L.; Hooker, J. M.; Wilson, A. a; Vasdev, N. 11CO2 fixation: a renaissance in PET radiochemistry. *Chem. Commun. (Camb).* **2013**, *49* (50), 5621–5629 DOI: 10.1039/c3cc42236d.

(119) Glaser, M.; Årstad, E. “Click labeling” with 2-[18F]fluoroethylazide for positron emission tomography. *Bioconjug. Chem.* **2007**, *18* (3), 989–993 DOI: 10.1021/bc060301j.

(120) Marik, J.; Sutcliffe, J. L. Click for PET: rapid preparation of [18F]fluoropeptides using CuI catalyzed 1,3-dipolar cycloaddition. *Tetrahedron Lett.* **2006**, *47* (37), 6681–6684 DOI: 10.1016/j.tetlet.2006.06.176.

(121) Hostetler, E. D.; Terry, G. E.; Burns, H. D. An improved synthesis of substituted [11C]toluenes via Suzuki coupling with [11C]methyl iodide. *J. Label. Compd. Radiopharm.* **2005**, *48* (9), 629–634 DOI: 10.1002/jlcr.953.

(122) Andersson, Y.; Cheng, A. P.; Langstrom, B. Palladium-Promoted Coupling Reactions of [C-11] Methyl-Iodide with Organotin and Organoboron Compounds. *Acta Chemica Scandinavica*. 1995, pp 683–688.

(123) Samuelsson, L.; Långström, B. Synthesis of 1-(2′-deoxy-2′-fluoro-β-D-arabinofuranosyl)-[methyl-11C]thymine ([11C]FMAU) via a stille cross-coupling reaction with [11C]methyl iodide. *J. Label. Compd. Radiopharm.* **2003**, *46* (3), 263–272 DOI: 10.1002/jlcr.668.

(124) Huang, Y.; Narendran, R. A Positron Emission Tomography Radioligand for the in Vivo Labeling of Metabotropic Glutamate 1 Receptor : 4-methoxycyclohexyl) methanone. *Society* **2005**, *47*, 5096–5099.

(125) Wuest, F. R.; Berndt, M. 11C-C bond formation by palladium-mediated cross-coupling of alkenylzirconocenes with [11C]methyl iodide. *J. Label. Compd. Radiopharm.* **2006**, *49* (2), 91–100 DOI: 10.1002/jlcr.1044.

(126) Chakraborty, P. K.; Mangner, T. J.; Chugani, H. T. The synthesis of No-carrier-added [< sup> 11</sup> C] Urea from [< sup> 11</sup> C] carbon dioxide and application to [< sup> 11</sup> C] uracil synthesis. *Appl. Radiat. Isot.* **1997**, *48* (5), 619–621.

(127) Roeda, D.; Dollé, F. [^{11}C]Phosgene: a versatile reagent for radioactive carbonyl insertion into medicinal radiotracers for positron emission tomography. *Curr. Top. Med. Chem.* **2010**, *10* (16), 1680–1700.

(128) Schirbel, A.; Holschbach, M. H.; Coenen, H. H. N.C.A. [11C]CO2 As A Safe Substitute for Phosgene In The Carbonylation of Primary Amines. *J Label Compd*

Radiopharm **1999**, *42*, 537–551 DOI: 10.1002/(SICI)1099-1344.

(129) Wilson, A. A.; Garcia, A.; Houle, S.; Sadovski, O.; Vasdev, N. Synthesis and application of isocyanates radiolabeled with carbon-11. *Chemistry* **2011**, *17* (1), 259–264 DOI: 10.1002/chem.201002345.

(130) Van Tilburg, E. W.; Windhorst, A. D.; Van Der Mey, M.; Herscheid, J. D. M. One-pot synthesis of [11C]ureas via triphenylphosphinimines. *J. Label. Compd. Radiopharm.* **2006**, *49* (4), 321–330 DOI: 10.1002/jlcr.1052.

(131) Hooker, J. M.; Reibel, A. T.; Hill, S. M.; Schueller, M. J.; Fowler, J. S.; Joanna, S. One-Pot, Direct Incorporation of [11 C]CO2 into Carbamates. *Angew. Chemie - Int. Ed.* **2009**, *48* (19), 3482–3485 DOI: 10.1002/anie.200900112.

(132) Vasdev, N.; Sadovski, O.; Garcia, A.; Dollé, F.; Meyer, J. H.; Houle, S.; Wilson, A. A. Radiosynthesis of [11C]SL25.1188 via [11C]CO 2 fixation for imaging monoamine oxidase B. *J. Label. Compd. Radiopharm.* **2011**, *54* (10), 678–680 DOI: 10.1002/jlcr.1908.

(133) Takaya, J.; Tadami, S.; Ukai, K.; Iwasawa, N. Copper(I)-catalyzed carboxylation of aryl- and alkenylboronic esters. *Org. Lett.* **2008**, *10* (13), 2697–2700 DOI: 10.1021/ol800829q.

(134) Kobayashi, K.; Kondo, Y. Transition-metal-free carboxylation of organozinc reagents using CO2 in DMF solvent. *Org. Lett.* **2009**, *11* (9), 2035–2037 DOI: 10.1021/ol900528h.

(135) Zhang, L.; Cheng, J.; Ohishi, T.; Hou, Z. Copper-catalyzed direct carboxylation of

C-H bonds with carbon dioxide. *Angew. Chem. Int. Ed. Engl.* **2010**, *49* (46), 8670–8673 DOI: 10.1002/anie.201003995.

(136) Riss, P. J.; Lu, S.; Telu, S.; Aigbirhio, F. I.; Pike, V. W. Cu I-Catalyzed 11C carboxylation of boronic acid esters: A rapid and convenient entry to 11C-labeled carboxylic acids, esters, and amides. *Angew. Chemie - Int. Ed.* **2012**, *51* (11), 2698–2702 DOI: 10.1002/anie.201107263.

(137) Perrio-Huard, C.; Aubert, C.; Lasne, M.-C. Reductive amination of carboxylic acids and [11C] magnesium halide carboxylates. *J. Chem. Soc., Perkin Trans. 1* **2000**, No. 3, 311–316.

(138) Mossine, A. V.; Brooks, A. F.; Jackson, I. M.; Quesada, C. A.; Sherman, P.; Cole, E. L.; Donnelly, D. J.; Scott, P. J. H.; Shao, X. Synthesis of Diverse 11C-Labeled PET Radiotracers via Direct Incorporation of [11C]CO2. *Bioconjug. Chem.* **2016**, *27* (5), 1382–1389 DOI: 10.1021/acs.bioconjchem.6b00163.

(139) Shao, X.; Schnau, P. L.; Fawaz, M. V.; Scott, P. J. H. Enhanced radiosyntheses of [11C]raclopride and [11C]DASB using ethanolic loop chemistry. *Nucl. Med. Biol.* **2013**, *40* (1), 109–116 DOI: 10.1016/j.nucmedbio.2012.09.008.

(140) *Positron emission tomography: basic sciences*; Bailey, D. L., Townsend, D. W., Valk, P. E., Maisey, M. N., Eds.; Springer-Verlag London, 2005.

(141) Shukla, A. K.; Kumar, U. Positron emission tomography: An overview. *J. Med. Phys.* **2006**, *31* (1), 13–21 DOI: 10.4103/0971-6203.25665.

(142) Fahey, F. H. Data acquisition in PET imaging. *J. Nucl. Med. Technol.* **2002**, *30* (2),

39–49.

(143) Shreve, P.; Townsend, D. W. Clinical PET-CT in radiology: Integrated imaging in oncology. *Clin. PET-CT Radiol. Integr. Imaging Oncol.* **2011**, 1–437 DOI: 10.1007/978-0-387-48902-5.

(144) Granov, A.; Tuitin, L.; Schwarz, T. *Positron Emission Tomography*; 2013.

(145) Gunn, R. N.; Slifstein, M.; Searle, G. E.; Price, J. C. Quantitative imaging of protein targets in the human brain with PET. *Phys. Med. Biol.* **2015**, *60* (22), R363–R411 DOI: 10.1088/0031-9155/60/22/R363.

(146) Morris, E. D.; Endres, C. J.; Schmidt, K. C.; Christian, B. T.; Muzic, R. F. J.; Fisher, R. E. Kinetic modeling in positron emission tomography. In *Emission Tomography*; Elsevier, 2004; Vol. 23, pp 499–540.

(147) Gunn, R. N.; Gunn, S. R.; Turkheimer, F. E.; Aston, J. A. D.; Cunningham, V. J. Positron Emission Tomography Compartmental Models: A Basis Pursuit Strategy for Kinetic Modeling. *J. Cereb. Blood Flow Metab.* **2002**, *22* (12), 1425–1439 DOI: 10.1097/01.wcb.0000045042.03034.42.

(148) Joshi, A.; Fessler, J. A.; Koeppe, R. A. Improving PET Receptor Binding Estimates from Logan Plots Using Principal Component Analysis. *J. Cereb. Blood Flow Metab.* **2008**, *28* (4), 852–865 DOI: 10.1038/sj.jcbfm.9600584.

(149) Logan, J. A review of graphical methods for tracer studies and strategies to reduce bias. *Nucl. Med. Biol.* **2003**, *30* (8), 833–844 DOI: 10.1016/S0969-8051(03)00114-8.

(150) Logan, J.; Fowler, J. S.; Volkow, N. D.; Wolf, A. P.; Dewey, S. L.; Schlyer, D. J.; MacGregor, R. R.; Hitzemann, R.; Bendriem, B.; Gatley, S. J. Graphical analysis of reversible radioligand binding from time-activity measurements applied to [N-11C-methyl]-(-)-cocaine PET studies in human subjects. *J. Cereb. Blood Flow Metab.* **1990**, *10* (5), 740–747 DOI: 10.1038/jcbfm.1990.127.

(151) Logan, J.; Fowler, J. S.; Volkow, N. D.; Wang, G.-J.; Ding, Y.-S.; Alexoff, D. L. Distribution Volume Ratios without Blood Sampling from Graphical Analysis of PET Data. *J. Cereb. Blood Flow Metab.* **1996**, *16* (5), 834–840 DOI: 10.1097/00004647-199609000-00008.

(152) Zhang, Y.; Fox, G. B. PET imaging for receptor occupancy: Meditations on calculation and simplification. *J. Biomed. Res.* **2012**, *26* (2), 69–76 DOI: 10.1016/S1674-8301(12)60014-1.

(153) Innis, R. B.; Cunningham, V. J.; Delforge, J.; Fujita, M.; Gjedde, A.; Gunn, R. N.; Holden, J.; Houle, S.; Huang, S.-C.; Ichise, M.; et al. Consensus Nomenclature for *in vivo* Imaging of Reversibly Binding Radioligands. *J. Cereb. Blood Flow Metab.* **2007**, *27* (9), 1533–1539 DOI: 10.1038/sj.jcbfm.9600493.

(154) Slifstein, M.; Laruelle, M. Models and methods for derivation of in vivo neuroreceptor parameters with PET and SPECT reversible radiotracers. *Nucl. Med. Biol.* **2001**, *28* (5), 595–608 DOI: 10.1016/S0969-8051(01)00214-1.

(155) Mason, N. S.; Mathis, C. A. Positron emission tomography radiochemistry. *Neuroimaging Clin. N. Am.* **2003**, *13* (4), 671–687 DOI: 10.1016/S1052-5149(03)00093-5.

Chapter 2

Motivation For This Work

The Scott lab is involved in all aspects of radiopharmaceutical development, including the development and optimization of novel radiolabeling methods for small molecules, the synthesis and pre-clinical evaluation of PET radiotracers for CNS diseases and disorders and the cGMP compliant production of PET radiotracers for clinical use. The work described in this thesis encompass, to some extent, each of these steps in the path to advance the field of nuclear medicine and human health. Firstly, a green approach to late-stage ^{18}F-fluorination (using only ethanol and water) of radiopharmaceuticals will be described. The goals were to (1) simplify quality control (QC) testing, (2) improve patient safety and (3) simplify waste disposal by eliminating hazardous solvents from ^{18}F-radiosynthesis. The work also raises important questions pertaining to the perceived reactivity of fluoride in green, protic solvents and/or aqueous media.

Secondly, PET radiotracer discovery for the interest of dopaminergic imaging in neurodegenerative diseases and disorders has been investigated. There exists a need to fully characterize the pharmacology at the dopamine-D_3 receptor and its utility in therapeutic application has yet to be fully explored and capitalized on. The availability of PET radiotracers for this purpose are limited and currently there are only non-selective tracers with affinity to both D_2 and D_3 receptors, including [^{11}C]raclopride and

[^{18}F]fallypride; even the more recent D_3 preferring radioligand [^{11}C](+)-PHNO offers only ~20-fold selectivity. Efforts to synthesize novel D_3 selective PET radioligands based upon pramipexole and BP-897 are described, as well as preliminary pre-clinical evaluation in rodents using *in vitro* autoradiography and *in vivo* microPET imaging.

Chapter 3

Applying the Principles of Green Chemistry to ^{18}F Fluorination

a. PET Radiopharmaceutical Production

[^{18}F]Fludeoxyglucose ([^{18}F]FDG (**3**)) is the most widely used PET radiopharmaceutical**,** at roughly 90% of the scans worldwide, making it nearly synonymous with PET (Figure 3- 1). [^{18}F]FDG is used widely in imaging oncology, neurology, and cardiology, with innovative uses for this tracer emerging every year. At the University of Michigan alone, [^{18}F]FDG is synthesized onsite twice daily and delivered to the clinic. This [^{18}F]FDG is used to scan approximately 20-30 patients every day, generating ~$40-60K/day in revenue. [^{18}F]FDG is a glucose analog that is preferentially taken up into cells with high energy requirements or high metabolic activity (brain, kidney, etc) by glucose transporters (in tumor cells, typically: GluT-1 and GluT-3) and phosphorylated by hexokinase, thus trapping it in the cell. This phosphorylated product, [^{18}F]FDG-6-phosphate, is unable to enter the glycolysis pathway and is not a substrate for glucose-6-phosphate isomerase, and so radioactivity gets trapped at a rate proportional to the consumption of glucose by the cell (Figure 3- 2). $^{18}F^-$ is converted to $^{18}O^-$ (please see pages **9-15** in **Chapter 1**for a discussion on nuclear decay), where it becomes protonated in its environment and becomes 2-^{18}O-deoxyglucose-6-phosphate.

Even with its heavy oxygen, it enter the glycolysis pathway where it is metabolized like glucose, with non-radioactive products.[13]

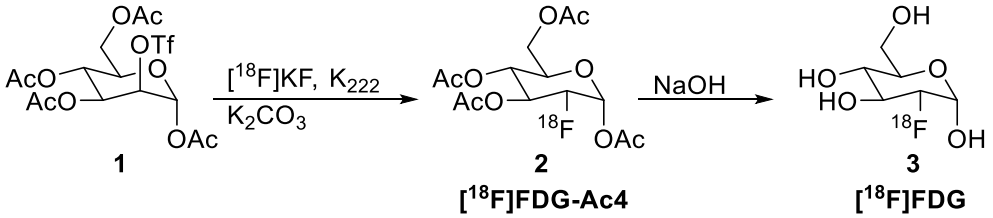

Figure 3- 1 Synthesis of [^{18}F]FDG

PETNET solutions, a subsidiary of Siemens Medical Solutions USA, and Cardinal Health are two industry-related entities that deliver minimally processed or "raw" radionuclide to facilities equipped to do radiochemical syntheses, or deliver already synthesized radiopharmaceuticals (e.g. [^{18}F]FDG) to a nearby facility with PET scanner(s). Other independent, privately or publicly owned medical facilities, such as universities and university-affiliated hospitals with an on-site cyclotron and/or generator can perform similar functions.

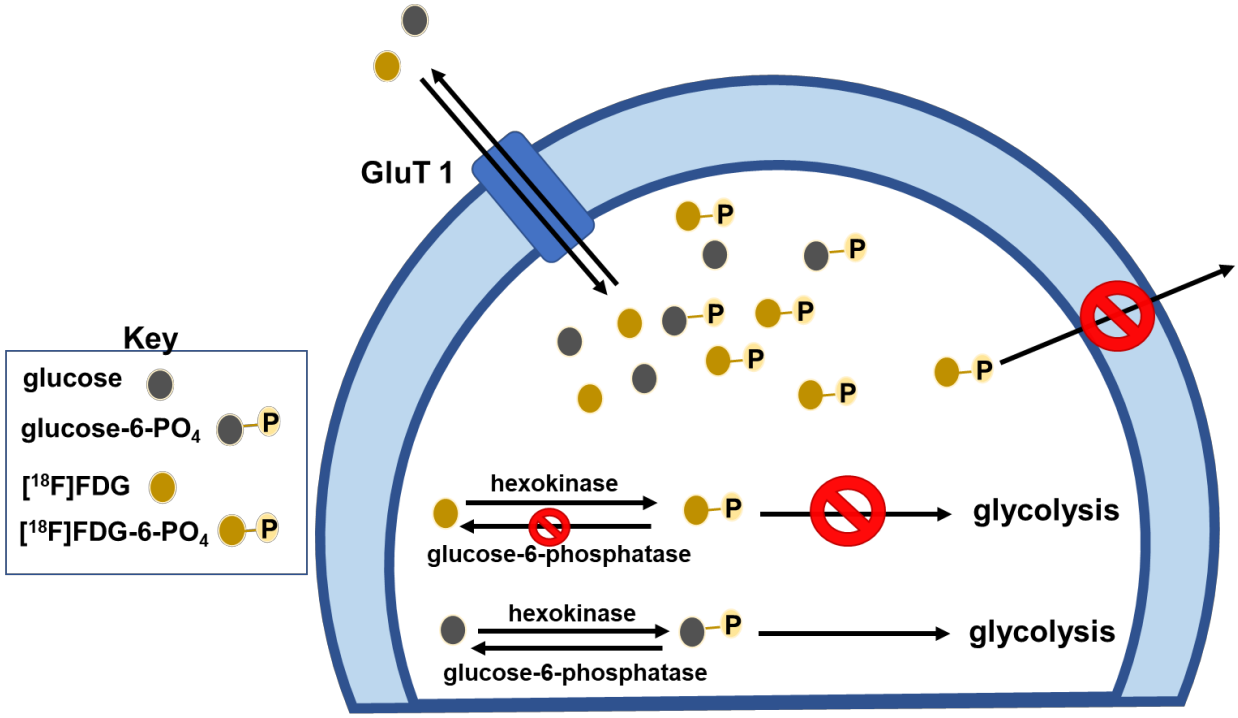

Figure 3- 2 Proposed Mechanism for [^{18}F]FDG

The approval of PET radiopharmaceuticals, their synthesis and use therein exists in a unique space compared to traditional pharmaceuticals. PET radiopharmaceuticals are administered in microdose amounts, typically nanomolar, (for radioactive and mass dose with carrier). As diagnostic pharmaceuticals, they do not elicit a pharmacological response and fall under unique federal, and otherwise related, guidelines for production and administration. Even with the use of animals in research, these tracer quantities still qualify animals as “pharmacologically naïve” and can be used for multiple experiments across a variety of PET probes and radiopharmaceuticals (unlike traditional pharmaceuticals which may permanently change receptor populations, etc.).

PET (diagnostic) radiopharmaceuticals manufactured in the USA under unique regulatory mechanisms and are regulated by the U.S. Food and Drug Administration

(FDA). In the case of investigational drug development, an exploratory IND (Investigational New Drug) application is required for clinical trials, just like any other pharmaceutical. Alternatively, PET radiopharmaceuticals already used safely in humans may be used for basic science clinical studies upon approval of an institutional Radioactive Drug Research Committee (RDRC).

Along the same lines of the use of traditional pharmaceuticals, a New Drug Application (NDA) allows PET radiopharmaceutical manufacturers authorization to market a particular radiopharmaceutical after completion of appropriate clinical trials (this information is from data gathered during the IND phase and includes information such as animal pharmacology, toxicology, clinical experience, trial outcomes etc.). The NDA documents the production and manufacturing of the PET drug, as well as its safety and efficacy profile, and describes specific indications for its use in the clinic. Once the NDA is reviewed by the FDA, the radiopharmaceutical may be approved for routine clinical use. An Abbreviated New Drug Application (ANDA) is another option that negates the need for the submission of preclinical and clinical data to meet the aforementioned safety concerns; instead this argues that the generic radiopharmaceutical will be prepared in the same manner as its innovator drug product approved under the parent NDA.[14]

All of these drug applications require that manufacturing is conducted in compliance with current Good Manufacturing Practice (cGMP). For studies under INDs, radiopharmaceutical need to be prepared according to the U.S. Pharmacopeia. However, once an NDA (or ANDA) is approved, more stringent manufacturing requirements are necessary, according to PET drug cGMP regulations issued in Title 21, *Code of Federal Regulations* part 212 (21 CFR 212).[15–17]

PET radiopharmaceutical production exists in a unique space. A short-lived positron-emitting radionuclide (e.g. ^{18}F, $t_{1/2}$ = 110 min, or ^{11}C, $t_{1/2}$ = 20 min) is used to label (or tag) a bioactive molecule. These radionuclides, carbon-11 ($^{14}N(p,\alpha)^{11}C$) and fluorine-18 ($^{18}O(p,n)^{18}F$), are produced in a medical cyclotron (General Electric PETTrace cyclotron) and delivered to lead-lined cells ("hot-cells") that contain an automated synthesis module. For a discussion of automated radiochemistry, synthesis modules, please see **Chapter 1.**

Fluorine-18 is delivered to a TRACERLab-Fx_{FN} synthesis module in a bolus of oxygen-18 water, trapped on a quaternary methyl ammonium (QMA) anion exchange cartridge to recycle the oxygen-18 water. The fluorine-18 is eluted with aqueous base, typically K_2CO_3,(to generate $K^{18}F$) into the reactor, and then azeotropically dried in MeCN with phase-transfer catalyst, Kryptofix-2.2.2 (K_{222}). The activated F-18 complex (Figure 3-3) is then used for subsequent nucleophilic fluorination with an appropriate precursor. These reactions typically take place in aprotic, anhydrous organic solvents. After subsequent deprotections (as needed), the reaction mixture is purified on semi-preparative HPLC. Solid-phase extraction on a C-18 cartridge allows reformulation into ethanolic saline, and sterile filtration through a 0.22 μm filter provides the final injectable dose as a sterile isotonic solution suitable for intravenous injection.

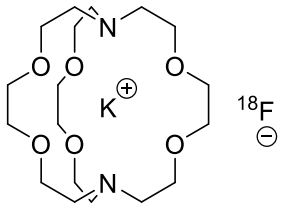

Figure 3- 3 [^{18}F]KF - K222 Complex

Carbon-11, on the other hand, is delivered to a TRACERLab-Fx$_{C\text{-}Pro}$ (**page 51)** in the form of [^{11}C]CO_2. If the [^{11}C]CO_2 is the desired reagent, this can be bubbled directly into a reactor containing another reagent (e.g. Grignard) before reacting with precursor, or trapped on a molecular sieve with carrier (CO_2) and utilized for further chemistry in a similar fashion. Typically, however, [^{11}C]CO_2 is transformed into [^{11}C]CH_3I or [^{11}C]CH_3OTf for methylation at a hetero atom (i.e. N, S, O).[18,19]

From the cyclotron [^{11}C]CO_2, destined to be converted to [^{11}C]CH_3I or [^{11}C]CH_3OTf, is trapped on a molecular sieve with nickel at room temperature. This is sealed and heated to 350^{o}C with H_2 to reduce the [^{11}C]CO_2 to [^{11}C]CH_4, which is trapped on a carbosphere methane trap cooled to -75^{o}C (with liquid N_2). When the carbosphere is heated to 80^{o}C, it releases the [^{11}C]CH_4 which enters a circulation loop containing an iodine column at 100^{o}C. The iodine, I_2, tube reactor is at 750^{o}C and[^{11}C]CH_4 is circulated for 5 min to generate [^{11}C]CH_3I which is trapped on a porapak column before being delivered to the reactor. If a more reactive methylating agent is required, [^{11}C]CH_3I can be passed through a silver triflate at 190^{o}C to generate [^{11}C]CH_3OTf. Following delivery to the reactor and subsequent methylation, similar purification and reformulation using

semi-preparative HPLC and solid-phase extraction are undertaken to generate the final dose.

The short shelf-life carbon-11 and fluorine-18 (20 and 110 min respectively) demand an on-site production at manufacturing facilities capable of these radiochemical syntheses, and in close range to a facility with a PET scanner. Current Good Manufacturing Practices (cGMPs), therefore, are complicated in terms of PET radiopharmaceuticals.

PET radiopharmaceutical quality control (QC) is completed in accordance with 21CFR212 – Current good Manufacturing Practice for Positron Emission Tomography Drugs or the U.S. Pharmacopeia Chapter 823 – Standards for PET drugs.[15–17] Radiopharmaceutical doses are analyzed as follows (including but not limited to): visual inspection, pH, chemical and radiochemical purity (HPLC or TLC), radionuclide identity (half-life), radionuclide purity, sterile filter integrity, bacterial endotoxins, sterility, and residual solvent analysis (GC). Failure of any of these check points (failed QC) means that the batch is rejected and the synthesis must be repeated.

In an effort to address failed doses as the result of failed QC due to contamination with residual solvents (Table 3- 1) used in the radiochemical synthesis, we sought to address the solvent selection. An extension of addressing the solvent selection, we pursued a green/sustainable approach to the design. While the definition of “green” chemistry and how it is applied is debatable, we sought to combine the principles of green chemistry and sustainability in the manufacturing of PET radiopharmaceuticals

b. Green Chemistry

Chemistry is “a science that deals with the composition, structure, and properties of substances and with the transformations that they undergo.”[20] The long history of organic chemistry, the foundation of the pharmaceutical industry, has largely been dictated by reactions roughly 50-100 years old, that did not necessarily take into account the large scale to which reactions are done today and how they are influence the world around us. These reliable reactions are inundated in chemistry curriculum and training, heralding the many synthetic procedures for atom efficiency. However, environmental and sustainable science, and toxicology are not a core course for traditional chemistry training.[21]

While the practice of green chemistry began years prior, ‘green chemistry’ is a relatively new term in the chemical sciences, adopted in the 1990s by the Environmental Protection Agency (EPA).[22] Green or sustainable chemistry is intentionally integrating hazard/toxin reduction in these transformations – it is not a form of chemistry unto itself, but is a practice that is incorporated into the chemical sciences.[23]

There are twelve principles of green chemistry, all guided by the idea that products and processes are “benign by design”.[24] The twelve principles of green chemistry, which also have the same underlying features of green engineering, can be summarized as follows[22,25,26]:

1. Waste prevention rather than remediation (avoid creating waste, rather than having to clean up to treat waste after its production).

2. Atom efficiency (synthetically design methods to maximize incorporation of all materials into the desired, final product).
3. Less hazardous chemicals (synthetic methods should be designed to produce materials that are benign or minimally toxic to the environment and human health).
4. “Benign by Design” (products should be designed such that serve their appropriate function and minimize toxicity).
5. Safer auxiliaries and solvents (make an innocuous choice for these elements whenever possible).
6. Design processes that are energy efficient (environmental and economic impacts should be minimized, and synthetic methods conducts at ambient temperature and pressure whenever possible).
7. Use renewable feedstocks or raw materials.
8. Avoid derivatization/shorter syntheses (lengthy syntheses utilizing many protection/deprotection and chemical/physical temporary modifications should be minimized as to avoid additional use of reagents and generation of waste).
9. Catalysis (catalytic reagents are preferred over stoichiometric reagents).
10. Design for Degradation (at the end of their function, chemical products should be designed to break down into innocuous degradation products).
11. Analysis for pollution prevention (analytical methodologies need to be developed and utilized to monitor and control prior to the formation of hazardous substances).
12. Inherently safer chemistry processes (substances and usage should be chosen and designed to minimize accidents, including explosions and fires).

Green/sustainable chemistry, therefore, challenges current chemical processes to drive a sense of responsibility and planning toward a safer future (environmental impact, while also considering chemical yield, cost of building blocks/solvents, energy demands, breakdown products, etc).

The initial applications of green chemistry had the environmental benefit as a mere side effect, taking backseat to efforts to minimize cost and optimizing efficiency.[23] In 2013, R&D costs were roughly $51.1 billion, compared to $1.2 billion in 1980. Costs are on the rise, with roughly 20% of drugs that make it to market return revenues that equal or surpass the R&D costs to get there. Cutting costs and reconstructing has become norm, with mergers and acquisitions (110 companies to roughly 30 companies over 30 years), decreasing R&D, minimizing risk by acquiring biotech/start-ups and experimental drugs already through initial evaluation. This includes Abbott spin off for R&D to create AbbVie, and significant downsizing at Lilly R&D (down 15-20%), and Merck personnel (20% reduction) from 2013-2014.[23]

While the drug discovery pipeline is one driven by timely and robust production and methodologies, something was surely missing.[21] In pharmaceutical chemistry, companies need “more bang for their buck”, and green chemistry lets you do just that.[23,27] Julie Manley summarizes this as:

> *“By viewing the entire life cycle of material and energy processes as an opportunity for design innovation, green chemistry enables the design of drug candidates to not just minimize unintended consequences, but more importantly to empower sustainability. Efficient and selective utilization of resources during the discovery,*

development, and manufacture of medicines enables the opportunity to meet the needs of today without limiting future generations to achieve theirs".[23]

Green chemistry was discussed in the 2000s, and met major players nearly 5 years later by the formation of the ACS GCI (American Chemical Society's Green Chemistry Institute®) Pharmaceutical Roundtable.[28] Beyond pharmaceutical chemistry, there are also roundtables for: Formulators', Chemical Manufacturers, Hydraulic Fracturing, and Biochemical Technology Leadership.[29] The Pharmaceutical Roundtable was developed as a partnership between the ACS GCI and industry to implement green chemistry and engineering in industrial practice. From 2005, Lilly, Merck and Pfizer, this non-competitive partnership has grown to 16 members in 2014. Some notable roundtable members include: Amgen, AstraZeneca, Boehringer Ingelheim, Bristol Myers Squibb, GlaxoSmithKline (GSK), Johnson & Johnson, Lilly, Merck, Novartis, Pfizer and F. Hoffman-La Roche Ltd.[23]

While membership in this roundtable does not necessarily correlate with active implementation of green chemistry principles, it opens up the conversation across corporations to address sustainability, meet environmental regulations, and cost saving measures for a common (noncompetitive) goal. It has sparked communication among these powerhouses to discuss collaborations, tool development, chemical alternatives and waste reduction. In 2015, the Roundtable sustainability report for Lilly reported the construction of a new 40-acre solar array to generate 12.6 million kWh of energy per year, improved their energy efficiency by 17%, reduced water intake by 35%, and reduced their waste to landfill by 73% from 2007-2013 alone.[30] Several publications regarding solvent selection, including those from Pfizer, GSK, and Astra Zeneca, are now touting words

often not associated with organic/medicinal chemistry. This includes a “holistic” approach to solvent selection, and releasing solvent and reagent guides for sustainability when planning syntheses.[21,31–33]

From industrial to academic institutions, green and sustainable initiatives are taking action to work toward this common goal. Environmental chemistry, green chemistry, and sustainability training are formally offered in 26 US states (and Puerto Rico) at the undergraduate and graduate training level.[34] This further extends to campus-wide initiatives across the US involving training and research laboratories, in reducing waste and energy requirements (including, but not limited to the University of Michigan, Ann Arbor).[35,36] By applying green chemistry principles, notably green alternative to reagents, solvents, and end products, “being green” offers itself as an alternative for both industry and manufacturing costs and safety, and as a way for chemistry to evolve with our increasing population and diminishing resources.

c. PET Radiopharmaceutical Production meets Green Chemistry: Carbon-11

This “benign by design” approach to chemical syntheses shares many qualities with a similar “quality by design” (QbD) approach to pharmaceutical development.[37] While the manufacturing of PET radiopharmaceuticals involves less use of mass materials and solvents than that of industrial levels of traditional therapeutics, applying the principles of green chemistry in the manufacturing of PET radiopharmaceuticals offers a unique space to explore quick syntheses and on-site QC considerations and safety.

Table 3- 1 Residual Solvents - Selected Guidelines

Class	Solvent	Exposure Limit (per dose)
1 Most Hazardous	Benzene	2 ppm
2 Limited Exposure	MeCN	410 ppm
	DMF	880 ppm
3 Lowest Toxic Potential	DMSO	5000 ppm
	EtOH	5000 ppm
U.S. Pharmacopeial Convention, General Chapter <467> Residual Solvents, ICH Guidelines on Residual Solvents[38]		

Previous work involving ethanolic "green" carbon-11 chemistry was recently reported by the Scott group in 2013 and 2014.[39,40] In these reports, ethanol (a "green" solvent) was the only organic solvent used throughout the entire synthesis, HPLC purification, reformulation, and module cleaning. This is in stark opposition from the usual solvents used for C-11 labeling: *N, N*-dimethylformamide (DMF), DMSO, 3-pentanone, methyl ethyl ketone, n-propanol, acetone, and MeCN. This extended to HPLC purification as well, as typically MeCN is used as the mobile phase, ethanol is a suitable HPLC mobile phase and a greener substitute for MeCN, and has been widely used throughout our lab for "green synthesis" as well as for other labile or sensitive compounds.

Using protic solvents with methylations is unusual, and typically thought of as incompatible with these reactions due to solvation of the nucleophile.[41] Nevertheless, [^{11}C]DASB (**89**) and [^{11}C]raclopride (**91**), were demonstrated by Shao and Scott in their C-11 ethanolic loop method (a discussion of loop chemistry can be found on **page 56**. Their method negated the need for residual solvent analysis, saved significant time during

synthesis which resulted in overall higher yields and specific activities for [^{11}C]raclopride, and similar yields for [^{11}C]DASB compared to traditional methods (Scheme 3- 1).[40]

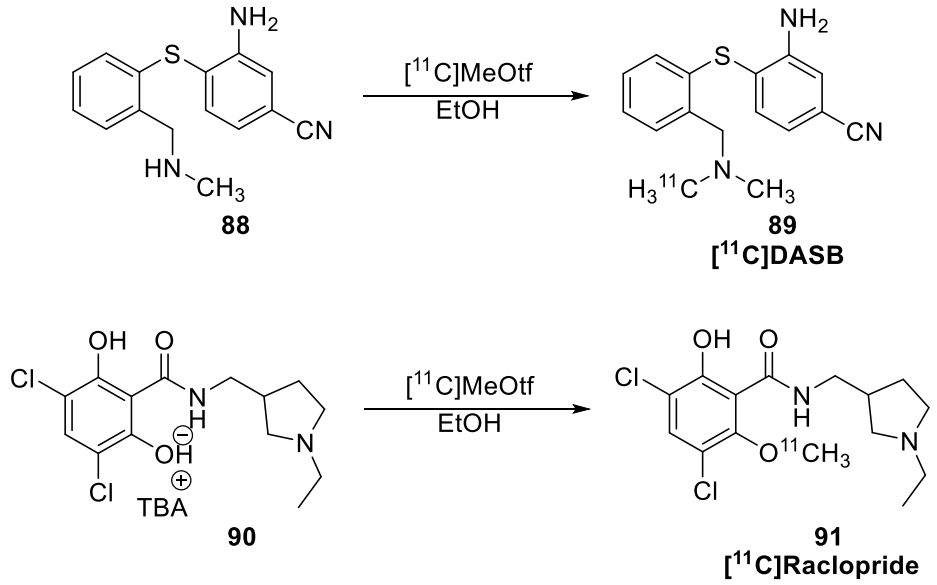

Scheme 3- 1 Green Carbon-11 Synthesis of [^{11}C]Raclopride and [^{11}C]DASB

Applying the proof-of-concept method utilizing ethanol through the entire manufacturing process of [^{11}C]raclopride and [^{11}C]DASB, this was then extended to several other radiopharmaceuticals routinely synthesized for clinical use. This was designed in part to move the manufacturing facility to a “green laboratory”, and explore the substrate compatibility (Figure 3- 4).[42]

Eleven different tracers were demonstrated, with radiochemical yields comparable to traditional methods, and radiochemical purities all above 95% (Figure 3- 4). The methylating agents and methods used were [^{11}C]MeOTf (loop, and reactor), and [^{11}C]MeI (reactor, and sep-pak) at several precursor preparations (including the free base and TBA salt). Here it was exciting to see that the C-11 loop method could be expanded to reactor

labeling of several tracers. The “Loop chemistry”, used for [^{11}C]DASB and [^{11}C]raclopride, is a special method that reduces solvent volume through thin-film chemistry; this is such that the precursor (dissolved in ethanol) is loaded on the semi-preparative HPLC loop (and conditioned with nitrogen gas for 20 sec at 10 mL/min), and [^{11}C]MeOTf blown rapidly through the loop (3 min at 40 mL/min). The reactor-based (5) and solid-support (sep-pak) (1) chemistry was demonstrated on 6 radiopharmaceuticals, and all produced doses suitable for clinical imaging at the end of synthesis.[40,42]

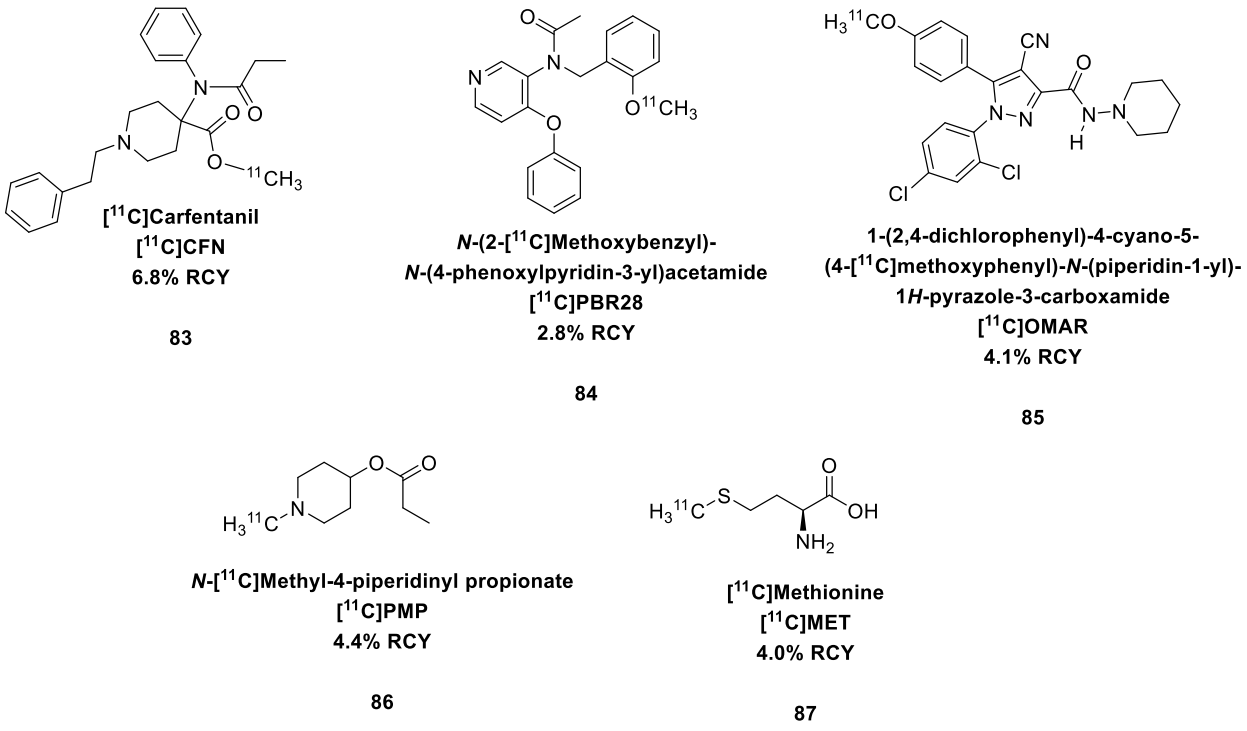

Figure 3- 4 Selected C-11 Radiopharmaceuticals Synthesized via "Green Radiochemistry"

Notable limitations to carbon-11 (ethanol) green chemistry is the solubility of the precursor in ethanol. Otherwise, these reactions were shown to proceed at room

temperature, in low solvent volumes, and simplified overall manufacturing in shortened synthesis time, and end of synthesis quality control (QC).[42] These mild reaction conditions are desirable for synthetic procedures, to not only save time and energy requirements (heating etc.), but also allows for more labile substrates to be evaluated.

d. PET Radiopharmaceutical Production meets Green Chemistry: ^{18}F and ^{19}F

The two most commonly used positron emitters used in PET radiopharmaceuticals (as small molecules), as mentioned before, are C-11 and F-18. While carbon-11 has many advantages including its incorporation having minimal biological effects in drug-like molecules, fluorine-18 PET diagnostics are widely used and desired for their longer half life (20 vs 110 min). Indeed, in synthetic organic chemistry, water is often considered a chemist's worst nightmare. Many of these synthetic transformations are typically sensitive to the presence of water, and often requires rigorous and pain-staking drying of glassware and solvents.

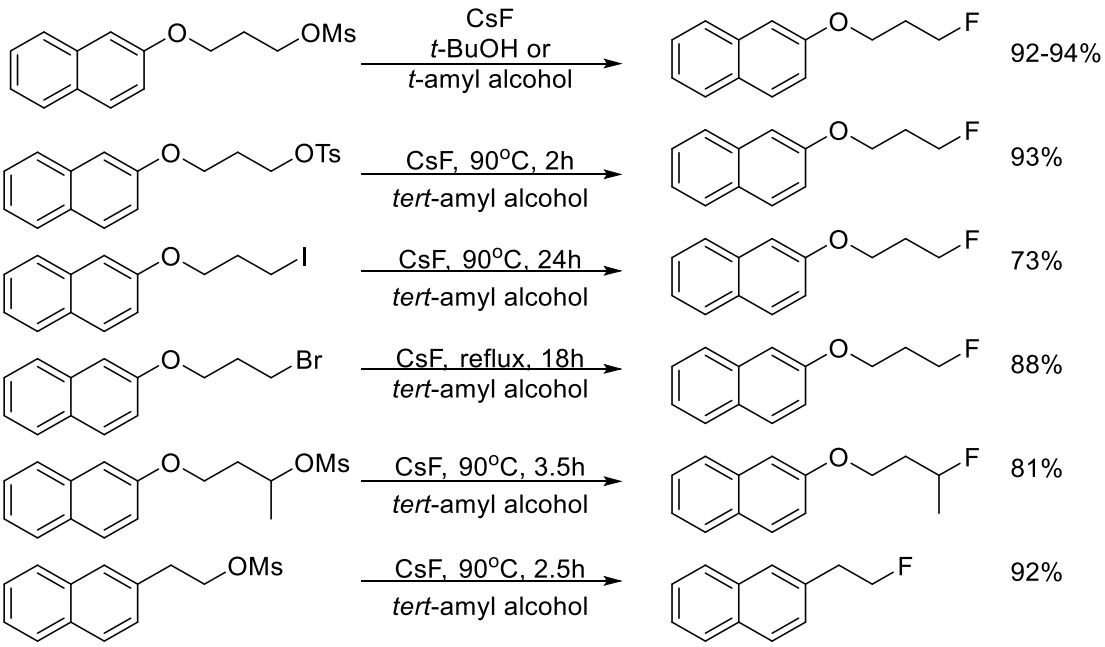

Scheme 3- 2 New set of S_N2 fluorinations catalyzed by protic solvents[43]

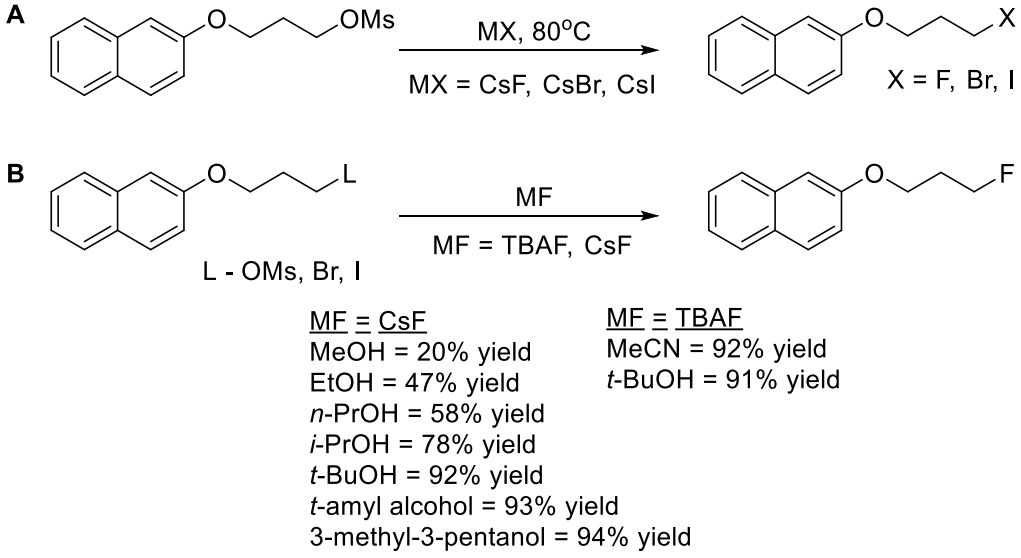

Scheme 3- 3 Nucleophilic Fluorinations in Alcohols[44]

Typically F-18 fluorinations ([^{18}F]KF) take place in aprotic, anhydrous solvents, as the fluoride anion is thought to be highly hydrated and, thus, poorly nucleophilic and poorly chemically reactive in protic solvents.[9] Indeed these reactions are typically done in MeCN, DMF (etc). As a result, the [^{18}F]fluoride is azeotropically dried to remove residual water left over from the oxygen-18 water from the target and the K_2CO_3 used to generate K^{18}F. Subsequent nucleophilic fluorination reactions are typically carried out in polar aprotic solvents such as MeCN, DMSO or DMF, usually with the inclusion of a phase-transfer catalyst for solubility considerations. Nevertheless, spurred on by the compatibility of carbon-11 methylations with ethanol, we investigated the possibility of developing green approaches for fluorine-18 radiochemistry.

Approaches to fluorine chemistry that fall under green, sustainable, or non-additive/metal-free have been previously explored.[45–47] We were gratified to see that methods challenging the need for rigorously dried [^{18}F]fluoride have been reported. For example, Chi reported S_N2 fluorinations in bulky, protic and alcohol-containing solvents (Scheme 3- 2,Scheme 3- 3).[43,44,48,49] These results show promising yields of the fluorinated product, with minor to modest formation of the elimination product in alcohol-containing solvents and alcohol-mixtures. Other work by Hooker and Ritter demonstrated nickel-mediated oxidative fluorination using aqueous ^{18}F (Scheme 3- 4). [50]

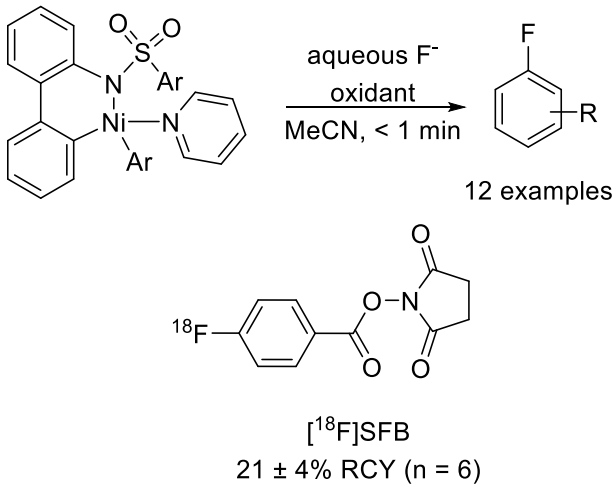

Scheme 3- 4 Nickel-Mediated Oxidative Fluorination with Aqueous ^{18}F

Additional work was done by Sergeev and van Dam that showed titanium nanoparticles can promote fluorination of tosylate precursors in aqueous-containing media (Scheme 3- 5). They demonstrated that titania nanoparticles in 1:1 (v/v) acetonitrile-thexyl alcohol solution and tetra-*n*-butylammonium bicarbonate allowed for direct nucleophilic ^{18}F fluorination without an azeotropic drying step. This was shown in aromatic, aliphatic, and cycloaliphatic tosylated starting materials, in addition to the synthesis of [^{18}F]Fallypride.[51]

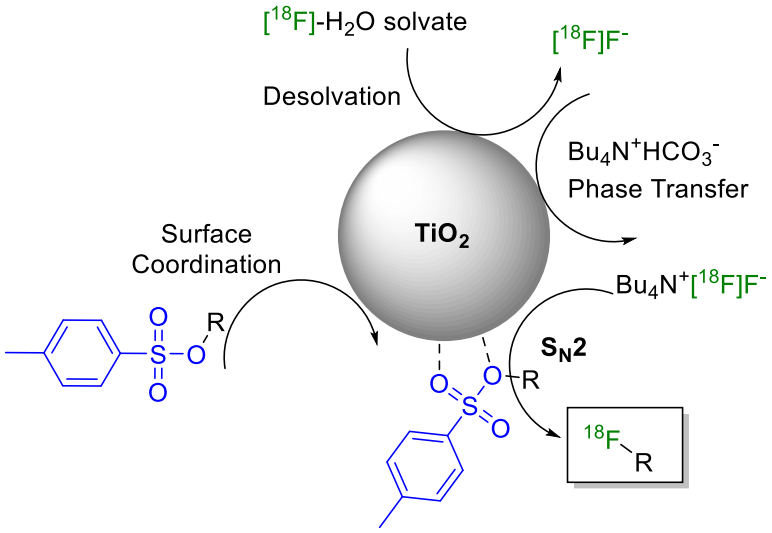

Scheme 3- 5 Titania-Catalyzed ^{18}F Fluorination of Tosylated Precursors in Highly Aqueous Media[51]

A report from Zhao and Gabbai, focused on nucleophilic fluorinations with aqueous fluoride ion solutions utilizing a cationic borane (2^+) to sequester F^- anions in aqueous conditions. Moreover, the 2+ species (Scheme 3- 6) is also being tested in [^{18}F]fluorination reactions.[52] Zhao and Gabbai's method was in part inspired by Sun and DiMagno's work with TBAF[53–55], as a way to offer a new fluorination method that could proceed in aqueous conditions.

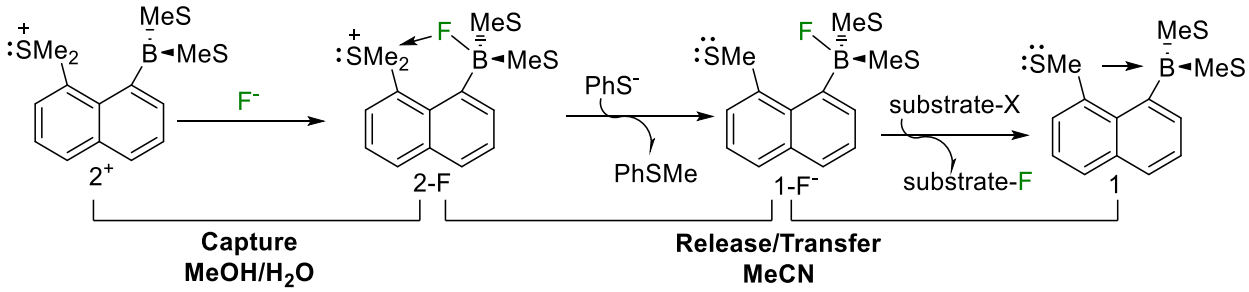

Scheme 3- 6 Aqueous Fluoride Ion Solutions and Nucleophilic Fluorination Reactions[52]

Sun and DiMagno showed that *in situ* generated TBAF is a powerful nucleophilic fluorinating reagent on a range of desirable substrates. One such work demonstrated fluorobenzene derivatives (**111**) with tetra-*n*-butylammonium cyanide (TBACN) in THF produced fluoride anions with "naked" character, denoted TBAF* (**113**) (Scheme 3- 7).[53] Sun and DiMagno went on to show that their TBAF* reagent was efficient in halex and fluorodenitration reactions.[55] By comparing TBAF* and KF side by side as fluorinating reagents, it was evident that KF(as KF-Kryptofix 222) was a poor reagent compared TBAF* - this is such that KF-Kryptofix 222 aromatic fluorodenitration reactions in DMSO at reflux in 10 min gave ~5% yield, to TBAF* at room temperature, >95% yield.[54,55]

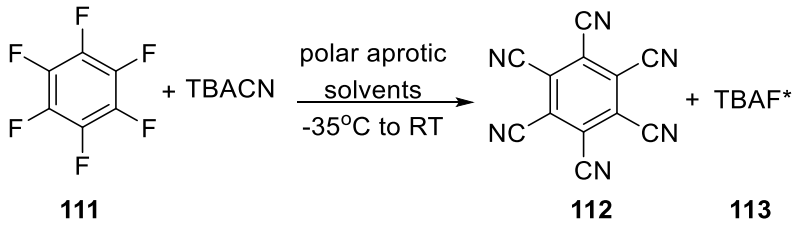

*Scheme 3- 7 Fluorinations in TBAF**[53]

The *in situ* generated TBAF* (**113**) reagent was then applied to the preparation of anhydrous tetraalkylammonium fluoride salts from KF. Sun and DiMagno describe the fluoride relay system as one such that the first fluoride is transferred from KF to a purifiable hydrophobic arene (**115**), the anhydrous fluoride salt is then generated from S_NAr with a cyanide salt (Scheme 3- *8*).[54]

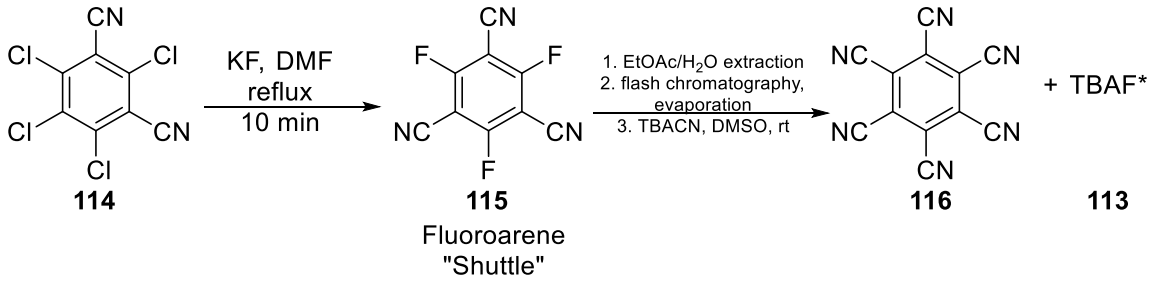

Examples

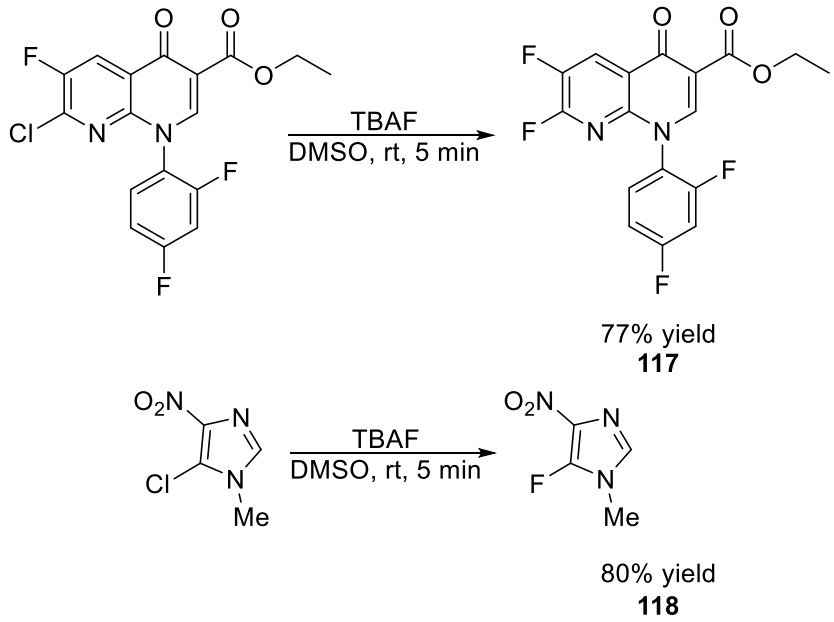

Scheme 3- 8 K and TBAF Fluoride Relay*[54]

A last interesting example was a recent work from Chun and Pike that reported F-18 fluorination of diaryliodonium tosylates in water-DMF mixtures, with 14-42% (v/v) water, without the use of a phase transfer catalyst (Scheme 3- 9).[56]

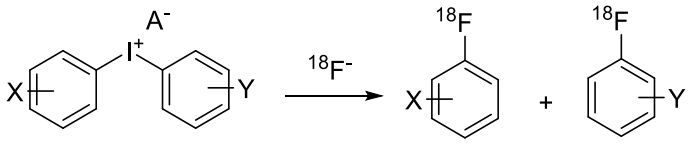

Scheme 3- 9 F-18 Fluorination of Diaryliodonium Tosylates in Aqueous-Containing Solvents[56]

When taken with other reports of nucleophilic fluorination reactions in aqueous media from the mainstream ^{19}F-fluorine chemistry literature[52], these remarkable results suggest the generally accepted incompatibility of fluoride with polar protic solvents does not hold up. While all of these reports provide valuable insight into the utility and nucleophilicity of the fluoride anion, there exists several imitations to radiopharmaceutical production. This includes the need to purify out catalysts (TiO_2), and to purify and remove residual solvents (DMF, thexOH, MeCN) and tetrabutylammonium cations. Aligned with the spirit of green chemistry, we sought to avoid these components all together. This fits in previous work within the group, as the group moves toward a green radiochemistry program for C-11 and F-18, with a new take on late-stage F-18 fluorinations.[39,40,57]

e. Results and Discussion:

i. Approaches to Late-Stage F-18 Fluorination in Ethanol/Water

The goal of this work is to explore [^{18}F]fluorinations in polar, protic solvents without additional additives (catalysts, etc). Aligned with green chemistry principles, we sought to use ethanol/water, avoiding hazardous solvents all together. Following azeotropic drying in MeCN, F-18 fluorinations are typically carried out in MeCN, DMF, and DMSO (Table 3-2), which require residual solvent analysis (RSA).[38] Using ethanol/water would negate this need for RSA.

Table 3- 2 Residual Solvent Analysis - and ^{18}F Tracer Examples

Class	Solvent	Exposure Limit (per dose)	Tracer Example
1 Most Hazardous	Benzene	2 ppm	
2 Limited Exposure	MeCN	410 ppm	[^{18}F]FDG, [^{18}F]FET
	DMF	880 ppm	[^{18}F]Flumazenil
3 Lowest Toxic Potential	DMSO	5000 ppm	[^{18}F]FAZA, [^{18}F]FLBT, [^{18}F]MPPF
	EtOH	50 mg/day	
U.S. Pharmacopeial Convention, General Chapter <467> Residual Solvents, ICH Guidelines on Residual Solvents[38]			

We sought to apply a step-wise approach to the development of green late-stage F-18 fluorination, (1) address the need for azeotropic drying of the [^{18}F]fluoride in MeCN, and (2) explore the reactivity of [^{18}F]fluoride in green solvents. Taken together, we sought to explore several fluorine-18 radiopharmaceuticals (Scheme 3- 10) commonly prepared at the UMich PET center ([^{18}F]FDG (**3**), [^{18}F]fluoroazomycin arabinoside ([^{18}F]FAZA) (**121**) , [^{18}F]fluoroethyl tosylate ([^{18}F]FET) (**64**) , [^{18}F]Flubatine (**13**), [^{18}F]Nifene (**125**), and 4-(2'-methoxyphenyl)-1-[2'(*N*-2''pyridinyl)-*p*-[^{18}F]fluorobenzoamido]ethylpiperazine ([^{18}F]MPPF) (**17**). As previously described, the fluorine-18 is eluted from a quaternary methylammonium (QMA) sep-pak using aqueous K_2CO_3 (3.5 mg in 0.5 mL water); to this is added Kryptofix/K_{222} (15 mg in 1 mL MeCN). This mixture is azeotropically dried to generate [^{18}F]KF.[58]

ii. Addressing Azeotropic Drying, from MeCN to EtOH

Table 3- 3 Azeotropic Drying: MeCN/water vs EtOH/water

Entry	Product	Azeotrope	Reaction Solvent	% RCY or % RCC
1	[^{18}F]FDG (**3**)	H_2O-MeCN	MeCN	74±12 (n = 3)[A]
2	[^{18}F]FDG (**3**)	H_2O-EtOH	MeCN	70±10 (n = 3)[A]
3	[^{18}F]FAZA (**121**)	H_2O-MeCN	DMSO	6±1 (n = 3)[B]
4	[^{18}F]FAZA (**121**)	H_2O-EtOH	DMSO	5±1 (n = 3)[B]
5	[^{18}F]FET (**64**)	H_2O-MeCN	MeCN	70±10 (n = 3)[C]
6	[^{18}F]FET (**64**)	H_2O-EtOH	MeCN	68±4 (n = 2)[C]
7	[^{18}F]Flubatine (**13**)	H_2O-MeCN	DMSO	25±10 (n = 3)[B]
8	[^{18}F]Flubatine (**13**)	H_2O-EtOH	DMSO	15±10 (n = 20)[B]
9	NBoc- [^{18}F]Nifene (**124**)	H_2O-MeCN	DMSO	50 (n = 1)[C]
10	NBoc- [^{18}F]Nifene (**124**)	H_2O-EtOH	DMSO	83 (n = 1)[C]
11	[^{18}F]MPPF (**17**)	H_2O-MeCN	DMSO	70±10 (n = 3)[C]
12	[^{18}F]MPPF (**17**)	H_2O-EtOH	DMSO	78±18 (n = 3)[C]

A) Radiochemical conversion (RCC) as determined by radioTLC
B) Isolated radiochemical yield (RCY)
C) RCC determined by radio-HPLC

First, we performed a straightforward switch of MeCN to ethanol, given that the azeotrope boiling points for these organic/water mixtures were comparable at 76.5^{o}C and 78.17^{o}C, and ethanol was our green solvent of choice.[59] As with the synthesis of [^{18}F]FDG (**3**), we saw comparable radiochemical conversions (RCC) from a water/MeCN azeotrope 74±12% to our new solvent system with water/ethanol 70±10% (Table 3- 3, Entries 1-2). By replacing MeCN with EtOH in the azeotropic drying without detrimental effects to final yield, we applied the same solvent replacement to the azeotropic drying step in the

synthesis of [^{18}F]FAZA (**121**), [^{18}F]FET (**64**), [^{18}F]Flubatine (**13**), [^{18}F]Nifene (**125**), and [^{18}F]MPPF (**17**), with similar results.

iii. Exploring [^{18}F]Fluorinations of Radiopharmaceuticals in EtOH & Aqueous EtOH

As the workhorse of PET imaging, [^{18}F]FDG (**3**) was chosen as the initial and major test substrate reaction conditions going forward. The next phase of this work was to investigate nucleophilic fluorination reactions in ethanol, or ethanol/water, as the primary reaction solvent. In neat ethanol, acetyl protected-[^{18}F]FDG ([^{18}F]FDG-Ac4 (**2**)) gave a notable 23±10% RCC (Table 3- 4, Entry 1). Even though the reaction in neat ethanol was lower than the same conditions in MeCN (Table 3- 3, Entry 2), we were encouraged to test the solvent tolerance further. With that, we sought to explore water/ethanol mixtures, to see if this would improve these reactions, as it was previously shown that small amounts of water can have a positive effect on fluorination reactions.[60]

We screened ethanol/water mixtures ranging from 3 to 100% water (Figure 3- 5) to explore how well water was tolerated. In this screen we found the optimal reaction solvent to be 15% water in 85% ethanol, (Figure 3- 5; Table 3- 4, Entry 2) and the RCC for [^{18}F]FDG-Ac4 (**2**)was 37±5% (n = 3). When the water content went above 15%, a steady drop in RCC was observed. Even more remarkable was that such fluorination reactions were still possible in neat water, albeit in low RCC of 2-3%. Since these reactions were proceeding with water in the reaction solvent, we were motivated to

explore the need to dry the [^{18}F]fluoride (the aforementioned reactions were performed using azeotropically dried [^{18}F]fluoride).

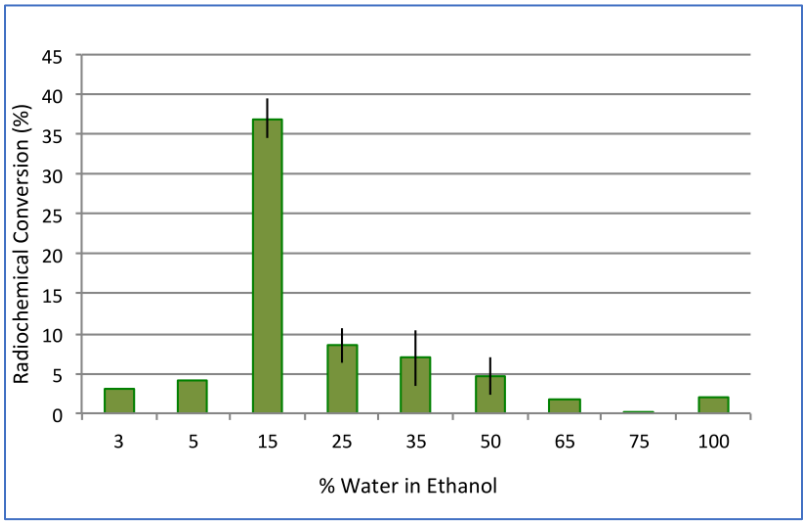

Figure 3- 5 Radiochemical Conversion of [^{18}F]FDG-Ac4 using different ethanol/water mixtures as the reaction solvent

Even though the role of water in improving these reactions yields is not clear, the need to dry the fluoride seems to be unnecessary if the addition of water (in these ethanol/water mixtures) show that these reactions still proceed. So we next explored the need to trap/release the [^{18}F]fluoride on the QMA cartridge, and subsequent drying step, by adding a solution of [^{18}F]fluoride in [^{18}O]water (0.15 mL) to a solution of K_2CO_3, K_{222} and mannose triflate precursor in ethanol (0.85 mL) to provide a final reaction solvent concentration of the optimal 15% water in ethanol. This resulted in 3±1% (n = 3) RCC to [^{18}F]FDG-Ac4 (**2**) and we attribute this to impurities, such as metal ions capable of sequestering [^{18}F]fluoride, in the cyclotron target water (Table 3- 4, Entry 3). To investigate this, the [^{18}F]fluoride was trapped on a QMA and eluted into the reactor using

a mixture of K_2CO_3/K_{222} in 15% water in ethanol (0.5 mL). The mannose triflate precursor was dissolved in 15% water in ethanol (0.5 mL) and added to the [^{18}F]fluoride / K_2CO_3 / K_{222} mixture, totaling 1 mL. This mixture was heated to 100^{0}C for 30 min to yield [^{18}F]FDG-Ac4 (**2**) in 58±5% (n = 3) RCC (Table 3- 4, Entry 4).

Table 3- 4 Nucleophilic Fluorinations in Ethanol/Water Mixtures

Entry	Product	QMA/Azeotrope	Reaction Solvent	% RCC
1	[^{18}F]FDG-Ac4 (**2**)	QMA/H_2O-EtOH	EtOH	23±10 (n = 3)
2	[^{18}F]FDG-Ac4 (**2**)	QMA/H_2O-EtOH	15% H_2O:85% EtOH	37±5 (n = 3)
3	[^{18}F]FDG-Ac4 (**2**)	No QMA/None	15% H_2O:85% EtOH	3±1 (n = 3)
4	[^{18}F]FDG-Ac4 (**2**)	QMA/None	15% H_2O:85% EtOH	58±5 (n = 3)
5	[^{18}F]FDG-Ac4 (**2**)	QMA/None	15% H_2O:85% EtOH[A]	16±4 (n = 3)
6	[^{18}F]FDG-Ac4 (**2**)	QMA/None	15% H_2O:85% EtOH[B]	4±1 (n = 3)
7	[^{18}F]FAZA (**121**)	QMA/None	15% H_2O:85% EtOH	3 (n = 1)
8	[^{18}F]FET (**64**)	QMA/None	EtOH + 1 drop DMSO	52 (n = 1)
9	NBoc- [^{18}F]Flubatine (**122**)	QMA/None	15% H_2O:85% EtOH	0 (n = 3)
10	NBoc- [^{18}F]Nifene (**124**)	QMA/None	15% H_2O:85% EtOH	0 (n = 1)
11	[^{18}F]MPPF (**17**)	QMA/None	EtOH	0 (n = 3)
11	[^{18}F]MPPF (**17**)	QMA/None	EtOH + DMSO[C]	0 (n = 3)

A) 2 mL reaction volume
B) Reaction without Kryptofix-K_{222}
C) DMSO added as co-solvent to improve precursor solubility

Increasing the reaction volume from 1 mL to 2 mL had detrimental effect on the reaction yields, providing only 16±4% RCC (n = 3) to [^{18}F]FDG-Ac4 (Table 3- 4, Entry 5), suggesting that reaction concentration is important. We also explored the need to include Kryptofix-K_{222} as a phase-transfer catalyst, and whether the aqueous conditions would

negate the need for a phase transfer catalyst. However, the RCC of [^{18}F]FDG-Ac4 (**2**) decreased significantly to 4±1% (n = 3) (Table 3- 4, Entry 6) when Kryptofix-K$_{222}$ was omitted. This result was likely the due to the improved nucleophilicity of the [^{18}F]fluoride as the result of the Kryptofix-K$_{222}$ complexing with the potassium counter ion, and not the phase transfer properties of the Kryptofix-K$_{222}$.

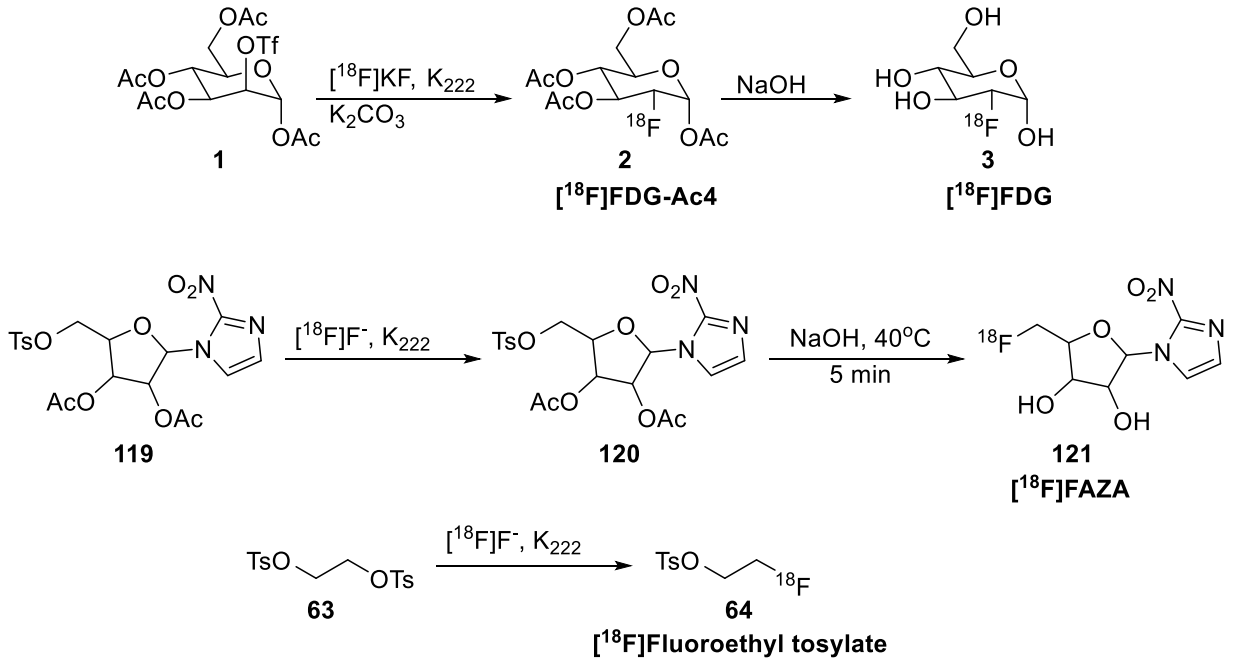

Scheme 3- 10 Green Radiosynthesis of [^{18}F]Radiotracers

Having shown that [^{18}F]FDG can be made with this methodology, we pursued to apply this radiofluorination to other radiopharmaceuticals of clinical relevance (Table 3-4). [^{18}F]FAZA (**121**) is used for imaging of hypoxia in tumors, as well as myocardia ischemia. 2-Nitroimidazoles are taken up in hypoxic environments and undergo intracellular reduction, where these fragments are trapped in the cell.[13] [^{18}F]FET (**64**) is a

prosthetic group, or “building block” [^{18}F]fluoroalkylating agent, and has been used to label a variety of PET tracers, including muscarinic receptor, *N*-methyl-*D*-aspartate (NMDA) receptor, dopamine D2 receptor, and gamma-aminobutyric acid (GABA) transporter ligands.[61] [^{18}F]Flubatine (**13**) and [^{18}F]nifene (**125**) are α4β2-nicotinic acetylcholine receptor (α4β2-nAChR) imaging agents for the staging and diagnosis of Alzheimer’s disease, dementia, and Parkinson’s disease.[62–64] [^{18}F]MPPF (**17**) is a PET radioligand for imaging serotonin-1A (5-HT$_{1A}$) receptors, in the case mood and other cognitive disorders (such as anxiety, depression, dementia, schizophrenia, etc).[13,65,66]

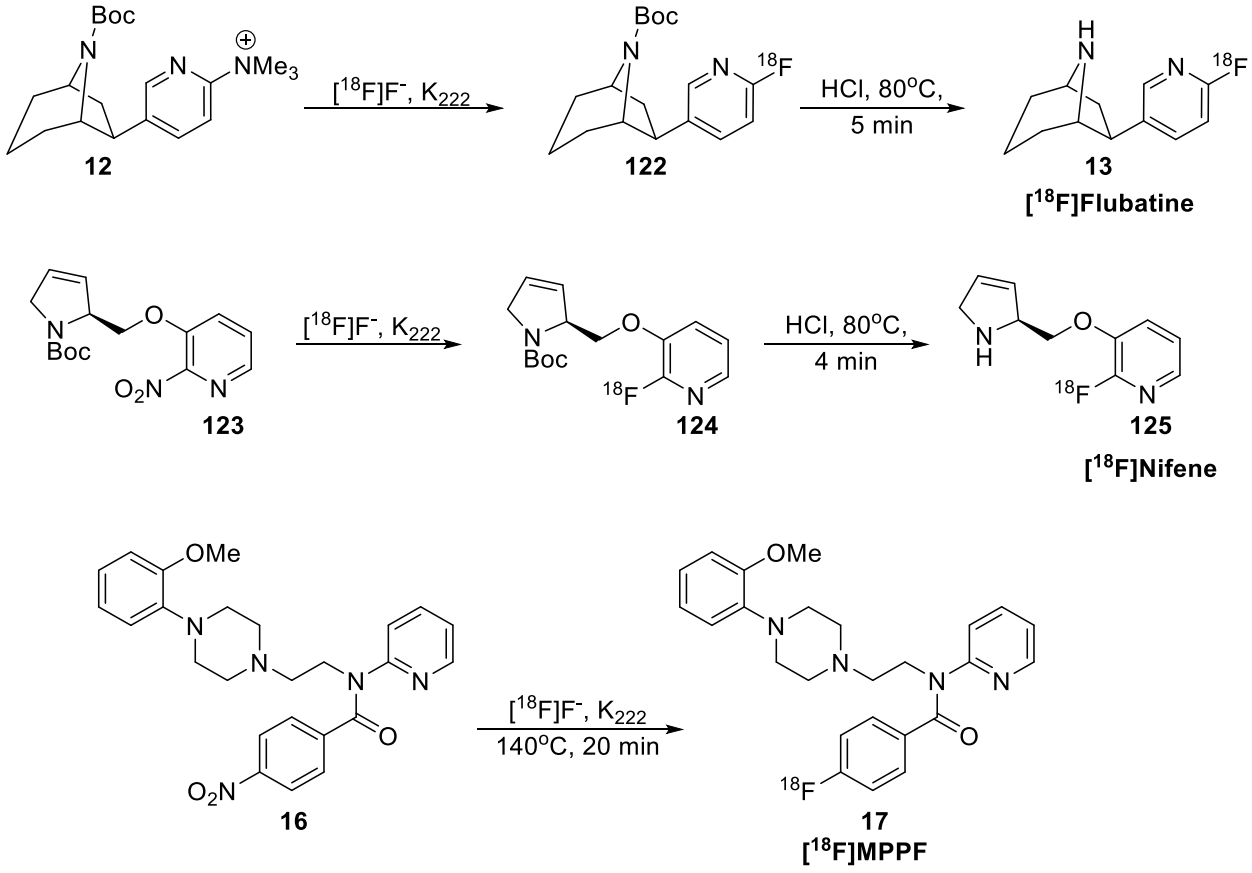

Scheme 3- 11 Applying the principles of green chemistry to S_NAr of [^{18}F]Radiopharmaceuticals

We next explored the synthesis of [^{18}F]FAZA (**121**) and [^{18}F]FET (**64**) *via* aliphatic fluorination. Green radiosynthesis of both [^{18}F]FAZA, (Table 3- 4, Entry 7, + 1 drop DMSO to help solubilize the precursor), and [^{18}F]FET (Table 3- 4, Entry 8) in ethanol or ethanol/water mixtures (etc) gave comparable yields to the traditional syntheses of these tracers conducted in DMSO (Table 3- 3, Entries 3 and 4) and MeCN (Table 3- 3, Entries 5 and 6). In the case of aromatic fluorination reactions (), such as the preparation of[^{18}F]Flubatine (**122**) (Table 3- 4, Entry 9), [^{18}F]nifene (**124**) (Table 3- 4, Entry 10), and [^{18}F]MPPF (**17**) (Table 3- 3, Entry 10), unfortunately no product was obtained.

For the [^{18}F]fluorination of [^{18}F]MPPF, we attribute this result to poor solubility of the precursor, even though attempts to use DMSO As a co-solvent with EtOH still did not improve the reaction. Additionally, S_NAr reactions are typically performed in DMSO at 120-150^{o}C for 15-30 min, but the boiling point for these water-ethanol mixtures are much lower at roughly 70-80^{o}C. As such, these conditions may simply be incompatible with the harsher fluorination conditions normally required for these substrates. Although, we acknowledge that lower temperature S_NAr reactions have been reported.[67]

In the essence of green chemistry, it should be noted that the fluoro(hetero)arene-containing products can be prepared in DMSO (Table 3- 3). DMSO is otherwise known as a bio-innocuous solvent, and one of the least toxic organic chemicals known, making it a green solvent.[68] The combination of azeotropic drying in water/ethanol and fluorination in DMSO also eliminates the need for residual solvent analysis during QC testing according to recent updates to the US Pharmacopeia (Table 3- 1). [69]

iv. Clinical Utility of Green [^{18}F]Fluorinations in Ethanol and Water/Ethanol

For our purposes and to apply this methodology to routine radiopharmaceutical production use in the clinical, these reactions should ideally be fully automated using a remote-controlled synthesis module. A General Electric TRACERLab FX_{FN} synthesis module was programmed to synthesize [^{18}F]FDG (**3**) using the optimized conditions described above (Table 3- 4, Entry 4). Following [^{18}F]fluorination, the acetate groups were deprotected by treatment with 1M NaOH at room temperature, followed by neutralization with 1M HCl, and formulation.[70] This yielded [^{18}F]FDG in 33±2% isolated and formulated radiochemical yield (decay corrected, n = 3), which compares to 68±1% isolated and formulated yields of [^{18}F]FDG using the traditional acetonitrile reaction solvent conditions (decay-corrected, n = 3).

While the green reaction yields are somewhat lower than the traditional method, and may be too low for routine and large commercial production of [^{18}F]FDG, they indeed demonstrate solid proof-of-concept for the use of water/mixture and ethanol-based reaction solvents in automated synthesis and production of clinical radiopharmaceuticals. One should note that these are preliminary studies and not had the benefit of decades of optimization work that has gone into the current synthesis and methods in practice to date.

As with the principles of green chemistry, one should also consider the balancing act one plays in choosing reagents for their transformations in regard to their “long term” application. Indeed time saving in this instance is a huge advantage of the traditional

methods (given no need for azeotropic drying, which is a 15-20 min procedure). Moreover, it may be worthwhile to sacrifice yield with the option to choose safer, less hazardous solvents associated with more straightforward QC testing. An instance would be with the goal of developing single automated modules for conducting QC testing, as a way to simplify radiopharmaceutical production in remote/developing/ markets that only have the need and requirement of producing a few doses a day or week, which could benefit significantly from negating the need for residual solvent analysis from the required (rather long) list of QC tests.[71]

v. Conclusions

With this work, preliminary studies and the exploration of green chemistry in late-stage fluorination for the synthesis of F-18 radiopharmaceuticals has been developed. This includes the preparation and activation of nucleophilic [^{18}F]fluoride in an ethanol-water azeotrope (in place of the traditional MeCN-water azeotrope) without detrimental effect on radiochemical yields. Aliphatic fluorination reactions can be conducted in ethanol/water mixtures with an optimal composition of 15% water and 85% ethanol. Even though these reaction yields are lower in polar protic solvents, this challenges the idea that nucleophilic fluoride is incompatible with polar protic reaction solvents. As such, this work encourages further exploration and studies in green fluorine chemistry and methodology.[72]

f. Experimental Methods and Supporting Data

i. General Considerations

[^{18}F]Fluoride (100 – 1500 mCi / 3.7 – 55.5 GBq) was produced via the ^{18}O(p,n)^{18}F nuclear reaction using a GE PETTrace cyclotron and dried using a TRACERLab FX_{FN} automated radiochemistry synthesis module (General Electric, GE). Production of fluorine-18 labeled radiotracers was carried out using the reaction vessel of the TRACERLab FX_{FN} or in bullet vials using a sand bath. Precursor solutions were gently warmed with a heat-gun to aid dissolution as needed. Radio-TLC analyses were conducted using Merck Glass-backed TLC Silica Gel 60 F_{254} plates and analyzed using a Bioscan AR-2000 TLC scanner. Radio-HPLC analyses were conducted on a Shimadzu LC-2010A HT system equipped with a Bioscan B-FC-1000 radiation detector using HPLC conditions outlined below. The identity of all ^{18}F product peaks were confirmed by comparison to unlabeled ^{19}F reference standards.

Unless otherwise stated, reagents and solvents were commercially available and used without further purification: sodium chloride, 0.9% USP and Sterile Water for Injection, USP were purchased from Hospira; ethanol was purchased from American Regent; anhydrous acetonitrile, potassium carbonate, kryptofix-2.2.2, sodium hydroxide, hydrochloric acid, sodium dihydrogenphosphate, ammonium acetate and DMSO were purchased from Sigma Aldrich; HPLC grade acetonitrile was purchased from Fisher Scientific.

Precursors and standards were commercially available as follows: FDG precursor

(mannose triflate), FET precursor (ditosyl methane) and reference standard, flubatine (standard and precursor), MPPF (standard and precursor) and nifene (standard and precursor) were purchased from ABX Advanced Biochemicals. FDG reference standard was purchased from Sigma Aldrich. FAZA precursor and reference standard were purchased from Prof. Friedrich Hammerschmidt (Universität Wien, Austria) and Prof. Hans-Jürgen Machulla (Steinbeis Transfer Center Radiopharmacy, Germany). All precursors and reference standards were used as received.

Other synthesis components were obtained as follows: sterile filters were obtained from Millipore; sterile product vials were purchased from Hollister-Stier; [^{18}O]H_2O was purchased from ABX Advanced Biochemical Compounds or Rotem Inc.; Alumina, C18-light and QMA-light Sep-Paks were purchased from Waters Corporation – C18-light and alumina Sep-Paks were flushed with 10 mL of ethanol followed by 10 mL of sterile water prior to use, while QMA-light Sep-Paks were flushed with 10 mL each of ethanol – water – 0.5 M sodium bicarbonate – water.

ii. Synthesis Procedures

General Procedure for Drying [^{18}F]Fluoride

[^{18}F]Fluoride was delivered to the synthesis module (in a 1.5 mL bolus of [^{18}O]water) and trapped on a QMA-light Sep-Pak to remove [^{18}O]water. [^{18}F]Fluoride was

then eluted into the reaction vessel using aqueous potassium carbonate (3.5 mg in 0.5 mL of water). A solution of kryptofix 2.2.2 (15 mg in 1 mL of acetonitrile or 1 mL of ethanol) was then added to the reaction vessel and the [^{18}F]fluoride was dried by evaporating the azeotrope. Azeotropic drying was achieved by heating the reaction vessel to 80 °C and drawing full vacuum for 4 min. After this time, the reaction vessel was cooled to 60 °C and subjected to both an argon stream and vacuum draw simultaneously for an additional 4 min.

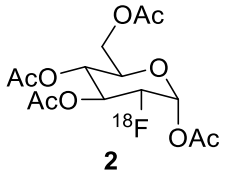

2

[^{18}F]FDG-Ac4

Table 3-4, Entry 1

[^{18}F]Fluoride was dried using the general method described above. Following drying, a solution of mannose triflate (40 mg) in ethanol (1 mL) was added to the reaction vessel and heated at 100 ^{o}C for 30 min. After this time, the crude reaction mixture was cooled and analyzed by radio-TLC (plate: silica gel TLC plate, solvent system: MeCN : H_2O = 95 : 5; R_f 0.008 = [^{18}F]fluoride, 0.650 = [^{18}F]FDG-Ac4a typical chromatogram is shown in Figure S1). Typical RCC were 23±10% (n = 3).

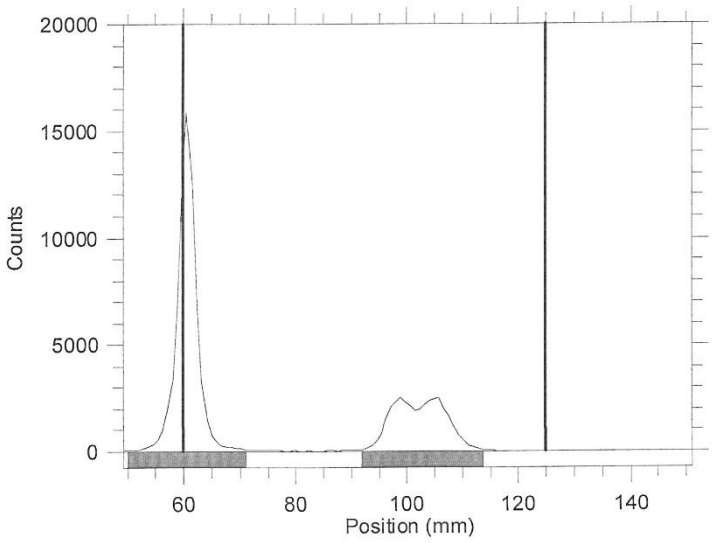

Reg	(mm) Start	(mm) Stop	(mm) Centroid	RF	Region Counts	Region CPM	% of Total	% of ROI
Rgn 1	50.2	71.0	60.5	0.008	68950.0	68950.0	64.90	66.35
Rgn 2	91.9	113.6	102.2	0.650	34975.0	34975.0	32.92	33.65
2 Peaks					103925.0	103925.0	97.82	100.00

Figure 3S- 1

Table 3-4, Entry 2

[^{18}F]Fluoride was dried using the general method described above. Following drying, a solution of mannose triflate (40 mg) in 15% water in ethanol (1 mL) was added to the reaction vessel and heated at 100 ^{o}C for 30 min. After this time, the crude reaction mixture was cooled and analyzed by radio-TLC (plate: silica gel TLC plate, solvent system: MeCN : H_2O = 95 : 5; R_f -0.004 = [^{18}F]fluoride, 0.779 = [^{18}F]FDG-Ac4; a typical chromatogram is shown in Figure S2). Typical RCC were 37±5% (n = 3).

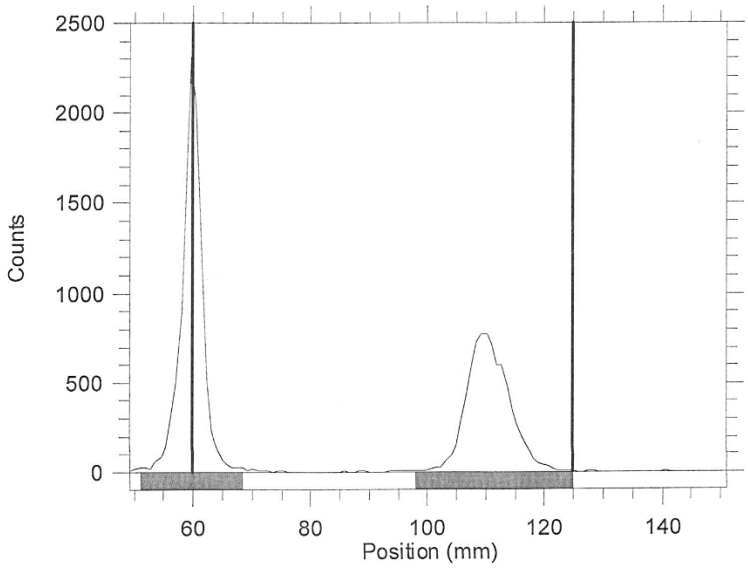

Reg	(mm) Start	(mm) Stop	(mm) Centroid	RF	Region Counts	Region CPM	% of Total	% of ROI
Rgn 1	51.0	68.4	59.7	-0.004	10170.0	10170.0	56.12	57.31
Rgn 2	98.0	125.0	110.6	0.779	7577.0	7577.0	41.81	42.69
2 Peaks					17747.0	17747.0	97.93	100.00

Figure 3S- 2

Table 3-4, Entry 3

A solution of [^{18}F]fluoride in [^{18}O]H_2O (0.15 mL) was added to the reaction vessel of the synthesis module. To this was added a mixture of potassium carbonate (3.5 mg), kryptofix (15 mg) and mannose triflate (40 mg) in ethanol (0.85 mL), and the reaction vessel was heated at 100 ^{o}C for 30 min. After this time, the crude reaction mixture was cooled and analyzed by radio-TLC (plate: silica gel TLC plate, solvent system: MeCN : H_2O = 95 : 5; R_f 0.009 = [^{18}F]fluoride, 0.864 = [^{18}F]FDG-Ac4; a typical chromatogram is shown in Figure S3). Typical RCC were 3±1% (n = 3).

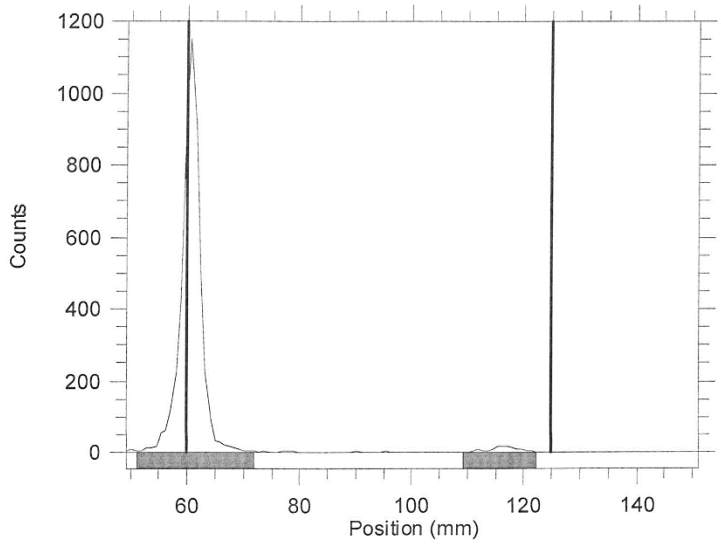

Reg	(mm) Start	(mm) Stop	(mm) Centroid	RF	Region Counts	Region CPM	% of Total	% of ROI
Rgn 1	51.0	71.9	60.6	0.009	4799.0	4799.0	96.11	97.68
Rgn 2	109.3	122.3	116.2	0.864	114.0	114.0	2.28	2.32
2 Peaks					4913.0	4913.0	98.40	100.00

Figure 3S- 3

Table 3-4, Entry 4

The [^{18}F]fluoride was delivered to the synthesis module (in a 1.5 mL bolus of [^{18}O]water) and trapped on a QMA-light Sep-Pak to remove [^{18}O]water. [^{18}F]Fluoride was then eluted into the reaction vessel using a solution of potassium carbonate (3.5 mg) and kryptofix (15 mg) in 15% water in ethanol (0.5 mL). A solution of mannose triflate (40 mg) in 15% water in ethanol (0.5 mL) was then added to the reaction vessel and the reaction was heated at 100 ^{o}C for 30 min. After this time, the crude reaction mixture was cooled and analyzed by radio-TLC (plate: silica gel TLC plate, solvent system: MeCN : H_2O = 95 : 5; R_f -0.011 = [^{18}F]fluoride, 0.824 = [^{18}F]FDG-Ac4; a typical chromatogram is shown in Figure S4). Typical RCC were 58±5% (n = 3).

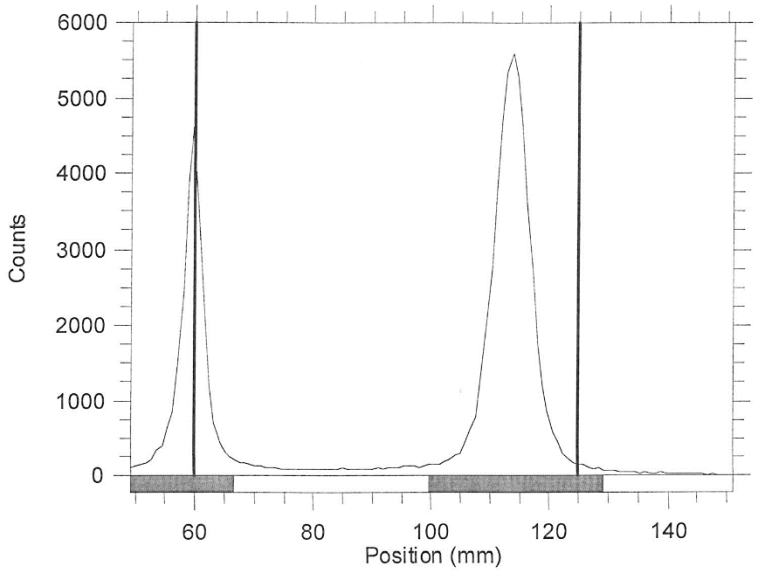

Reg	(mm) Start	(mm) Stop	(mm) Centroid	RF	Region Counts	Region CPM	% of Total	% of ROI
Rgn 1	49.3	66.7	59.3	-0.011	24128.0	24128.0	29.92	32.18
Rgn 2	99.7	129.3	113.6	0.824	50846.0	50846.0	63.05	67.82
2 Peaks					74974.0	74974.0	92.97	100.00

Figure 3S- 4

Table 3-4, Entry 5

The [^{18}F]fluoride was delivered to the synthesis module (in a 1.5 mL bolus of [^{18}O]water) and trapped on a QMA-light Sep-Pak to remove [^{18}O]water. [^{18}F]Fluoride was then eluted into the reaction vessel using a solution of potassium carbonate (3.5 mg) and kryptofix (15 mg) in 15% water in ethanol (1.0 mL). A solution of mannose triflate (40 mg) in 15% water in ethanol (1.0 mL) was then added to the reaction vessel and the reaction was heated at 100 ^{o}C for 30 min. After this time, the crude reaction mixture was cooled and analyzed by radio-TLC (plate: silica gel TLC plate, solvent system: MeCN : H_2O = 95 : 5; R_f -0.001 = [^{18}F]fluoride, 0.817 = [^{18}F]FDG-Ac4; a typical chromatogram is shown in Figure S5). Typical RCC were 16±4% (n = 3).

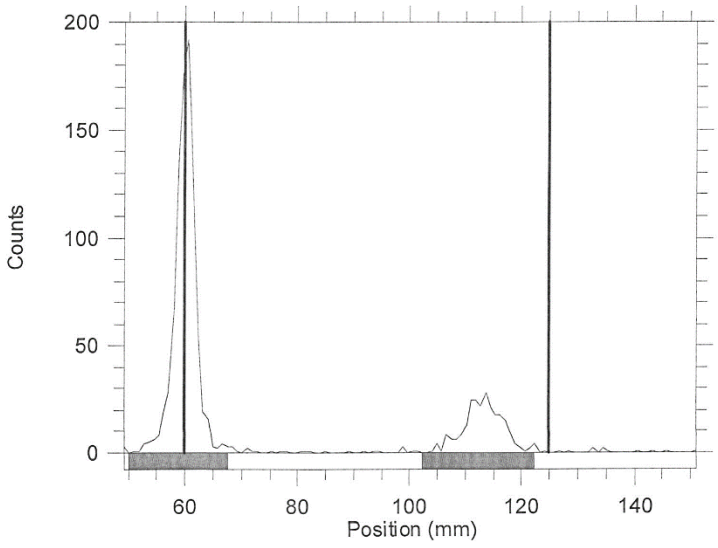

Reg	(mm) Start	(mm) Stop	(mm) Centroid	RF	Region Counts	Region CPM	% of Total	% of ROI
Rgn 1	50.2	67.5	59.9	-0.001	857.0	857.0	72.20	78.26
Rgn 2	102.3	122.3	113.1	0.817	238.0	238.0	20.05	21.74
2 Peaks					1095.0	1095.0	92.25	100.00

Figure 3S- 5

Table 3-4, Entry 6

The [^{18}F]fluoride was delivered to the synthesis module (in a 1.5 mL bolus of [^{18}O]water) and trapped on a QMA-light Sep-Pak to remove [^{18}O]water. [^{18}F]Fluoride was then eluted into the reaction vessel using a solution of potassium carbonate (3.5 mg) in 15% water in ethanol (0.5 mL). A solution of mannose triflate (40 mg) in 15% water in ethanol (0.5 mL) was then added to the reaction vessel and the reaction was heated at 100 ^{o}C for 30 min. After this time, the crude reaction mixture was cooled and analyzed by radio-TLC (plate: silica gel TLC plate, solvent system: MeCN : H_2O = 95 : 5; R_f 0.014 = [^{18}F]fluoride, 0.841 = [^{18}F]FDG-Ac4; a typical chromatogram is shown in Figure S6). Typical RCC were 4±1% (n = 3).

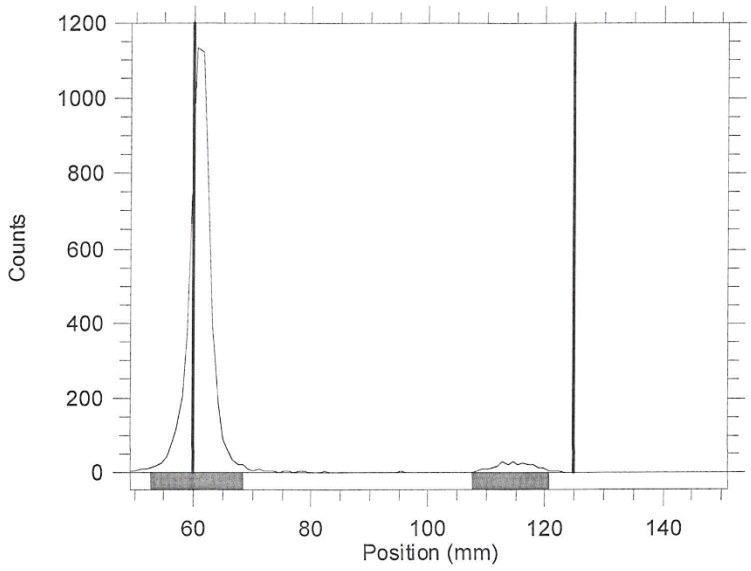

Reg	(mm) Start	(mm) Stop	(mm) Centroid	RF	Region Counts	Region CPM	% of Total	% of ROI
Rgn 1	52.8	68.4	60.9	0.014	5417.0	5417.0	92.39	95.81
Rgn 2	107.6	120.6	114.6	0.841	237.0	237.0	4.04	4.19
2 Peaks					5654.0	5654.0	96.44	100.00

Figure 3S- 6

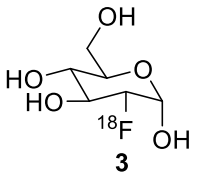

3

[^{18}F]FDG

Table 3-3, Entries 1 and 2

[^{18}F]Fluoride was dried using the general method described above. Following drying, a solution of mannose triflate (40 mg) in acetonitrile (1 mL) was added to the reaction vessel and heated at 100 ^{o}C for 30 min to yield [^{18}F]FDG-Ac4 (**2**). After this time, 1N NaOH was added and the reaction was stirred at room temperature (rt) for 5 min. Following neutralization (HCl/citrate buffer), the crude reaction mixture was analyzed by radio-TLC to determine RCC (plate: silica gel TLC plate, solvent system: MeCN : H_2O = 95 : 5, R_f -0.018 = [^{18}F]fluoride, 0.390 = [^{18}F]FDG; a typical chromatogram is shown in Figure S7). Typical RCC were 74±12% (H_2O-MeCN azeotrope, n = 3) or 70±10% (H_2O-EtOH azeotrope, n = 3).

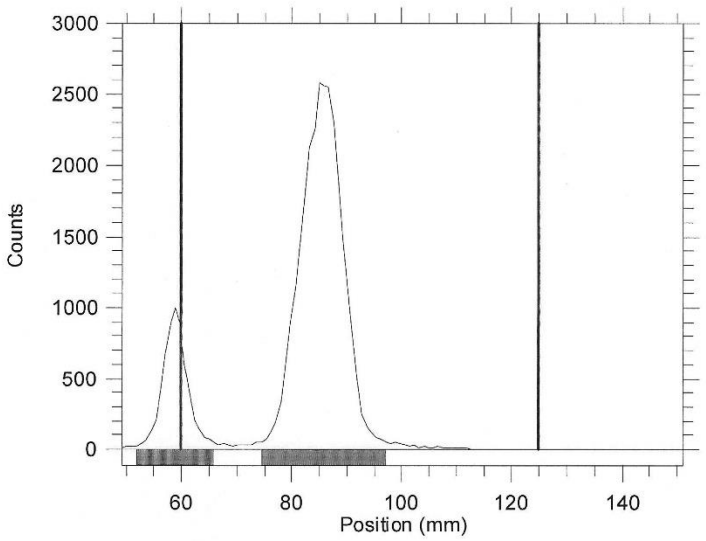

Reg	(mm) Start	(mm) Stop	(mm) Centroid	RF	Region Counts	Region CPM	% of Total	% of ROI
Rgn 1	51.9	65.8	58.9	-0.018	5838.0	5838.0	16.98	17.53
Rgn 2	74.5	97.1	85.3	0.390	27473.0	27473.0	79.93	82.47
2 Peaks					33311.0	33311.0	96.91	100.00

Figure 3S- 7

Fully-automated Synthesis of [^{18}F]FDG

The [^{18}F]fluoride was delivered to the synthesis module (in a 1.5 mL bolus of [^{18}O]water) and trapped on a QMA-light Sep-Pak to remove [^{18}O]water. [^{18}F]Fluoride was then eluted into the reaction vessel using a solution of potassium carbonate (3.5 mg) and kryptofix (15 mg) in 15% water in ethanol (0.5 mL). A solution of mannose triflate (40 mg) in 15% water in ethanol (0.5 mL) was then added to the reaction vessel and the reaction was heated at 100 ^{o}C for 30 min. After this time, 1N NaOH was added and the reaction was stirred at room temperature (rt) for 5 min. Following neutralization (HCl/citrate buffer), the crude reaction mixture was diluted and purified using alumina and C18 Sep-Paks, as previously described[70], to yield [^{18}F]FDG in 33±2% radiochemical yield (decay-corrected, n = 3). Analysis of the final product by radio-TLC confirmed product purity (plate: silica gel TLC plate, solvent system: MeCN : H_2O = 95 : 5, R_f 0.417 = [^{18}F]FDG; a typical chromatogram is shown in Figure S8).

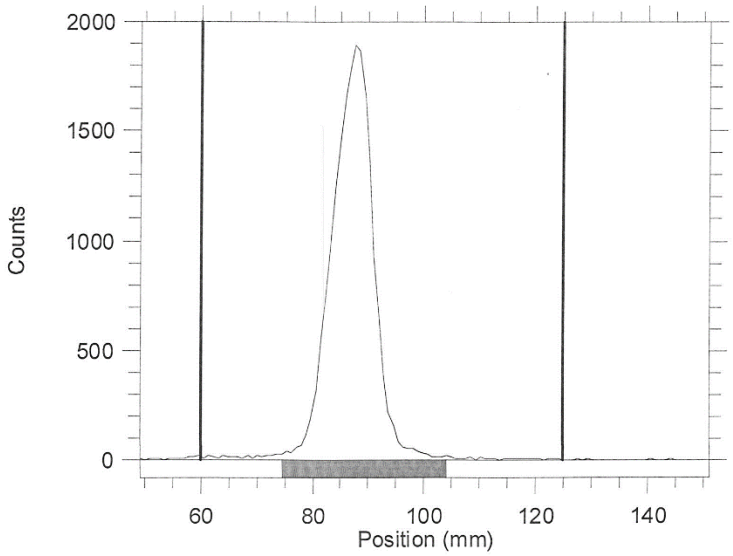

Reg	(mm) Start	(mm) Stop	(mm) Centroid	RF	Region Counts	Region CPM	% of Total	% of ROI
Rgn 1	74.5	104.1	87.1	0.417	18763.0	18763.0	97.16	100.00
1 Peaks					18763.0	18763.0	97.16	100.00

Figure 3S- 8

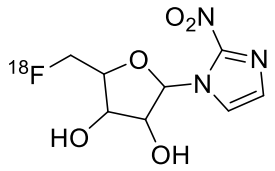

121

[^{18}F]FAZA

Table 3-3, Entries 3 and 4

[^{18}F]Fluoride was dried using the general method described above. [^{18}F]FAZA was then synthesized as previously described[58], and typical non-corrected radiochemical yields were 6% (H_2O-MeCN azeotrope, n = 3) or 5% (H_2O-EtOH azeotrope, n = 3). Radiochemical purity and identity were confirmed by radio-HPLC (column: Phenomonex Luna C8(2) 5µ, 100 x 2.0 mm; mobile phase: 5% acetonitrile: 95% 20mM aqueous ammonium acetate, pH 4.5; flow rate: 0.5 mL/min; UV wavelength = 254 nm; t_R [^{18}F]FAZA = 6.2 min; a typical chromatogram is shown in Figure S9).

UV

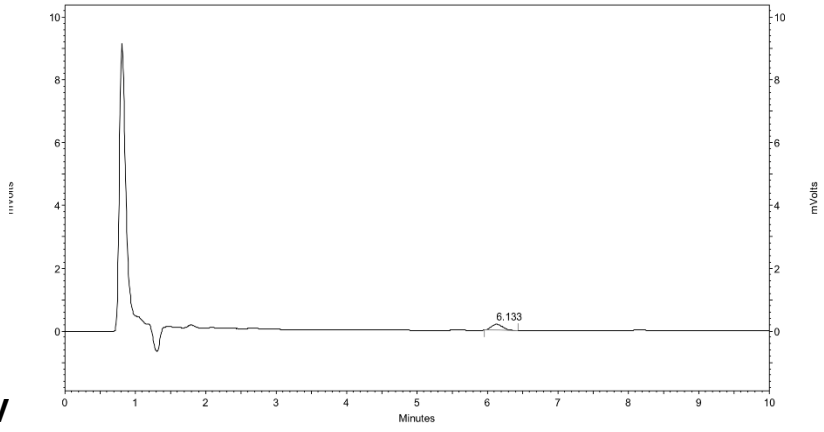

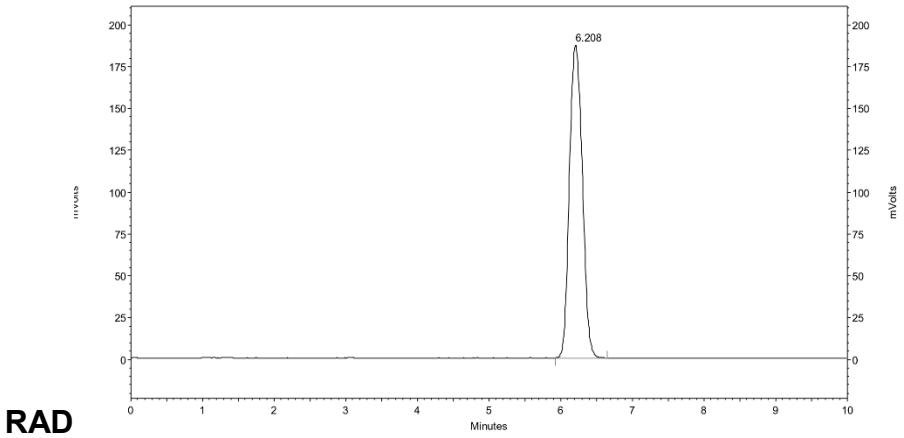

Figure 3S- 9

Table 3-4, Entry 7

[^{18}F]Fluoride was dried using the general method described above. Following drying, a solution of precursor **4** (8 mg) in 15% water in ethanol (2 mL) was added to the reaction vessel and heated at 100 ^{o}C for 10 min. After this time, the reaction was cooled to 40 ^{o}C and 0.1 M aqueous sodium hydroxide (1 mL) was added. The reaction was stirred for 5 min at 40 ^{o}C to hydrolyze the acetate protecting groups. The crude reaction mixture was then cooled and analyzed by radio-HPLC (column: Phenomonex Luna C8(2) 5µ, 100 x 2.0 mm; mobile phase: 15% acetonitrile: 85% 50mM aqueous ammonium acetate, pH 4.5; flow rate: 0.5 mL/min, UV = 254 nm, t_R [^{18}F]FAZA = 4.561 min; a typical chromatogram is shown in Figure S10). RCC was 3% (n = 1).

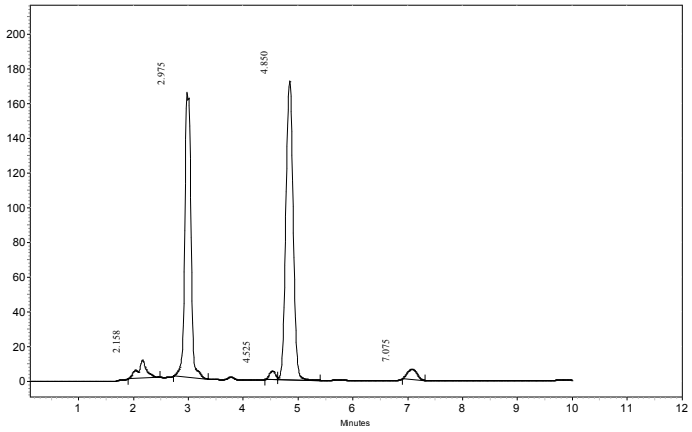

UV Detector Ch1-

254nm Results

Retention Time	Area	Area %	Height	Width	S/N (ASTM)
2.158	113813	4	10311	0.583	42.51
2.975	1283566	41	163832	0.625	675.45
4.525	38520	1	4877	0.233	4.71
4.850	1594457	51	171960	0.767	165.93
7.075	69664	2	5817	0.417	12.64

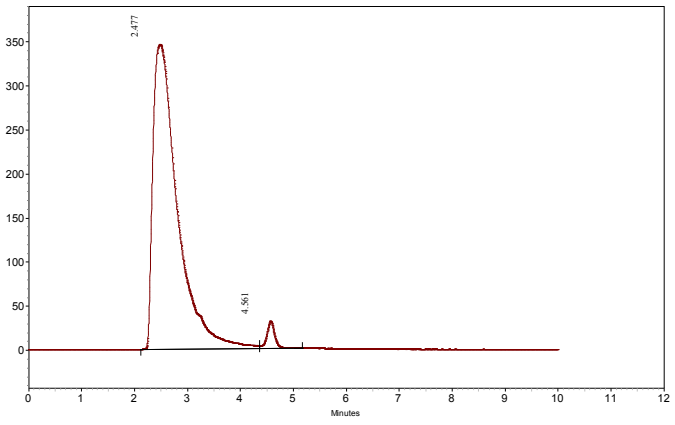

RAD Results

Retention Time	Area	Area %	Width
2.477	11058513	97	2.24
4.561	321900	3	0.81

Figure 3S- 10

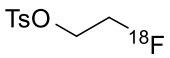

64

[^{18}F]Fluoroethyl tosylate ([^{18}F]FET)

Table 3-3, Entries 5 and 6

[^{18}F]Fluoride was dried using the general method described above. Following drying, a solution of ditosyl methane (5 mg) in acetonitrile (1 mL) was added to the reaction vessel and heated at 110 ^{o}C for 10 min. After this time, the crude reaction mixture was cooled and analyzed by radio-HPLC (column: Phenomenex Luna C18 150 x 4.6 mm, mobile phase: MeCN : H_2O = 60 : 40; flow rate: 1.0 mL/min; UV wavelength = 254 nm; t_R [^{18}F]FET = 2.608 min; a typical chromatogram is shown in Figure S11). Typical RCC were 70±10% (H_2O-MeCN azeotrope, n = 3) or 68±4% (H_2O-EtOH azeotrope, n = 2).

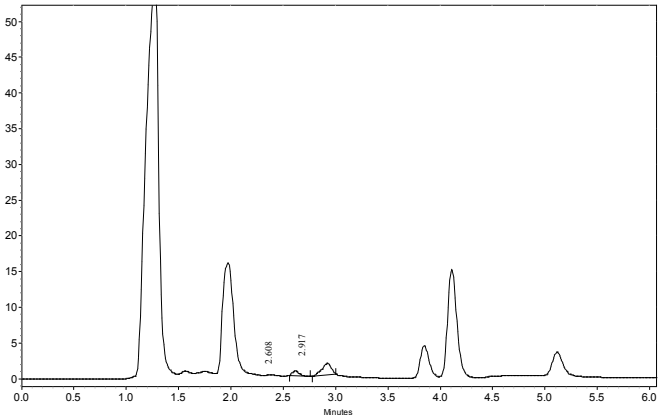

UV Detector Ch1-

254nm Results

Retention Time	Area	Area %	Height	Width	S/N (ASTM)
2.608	2998	23	647	0.200	0.04
2.917	10288	77	1635	0.225	0.1

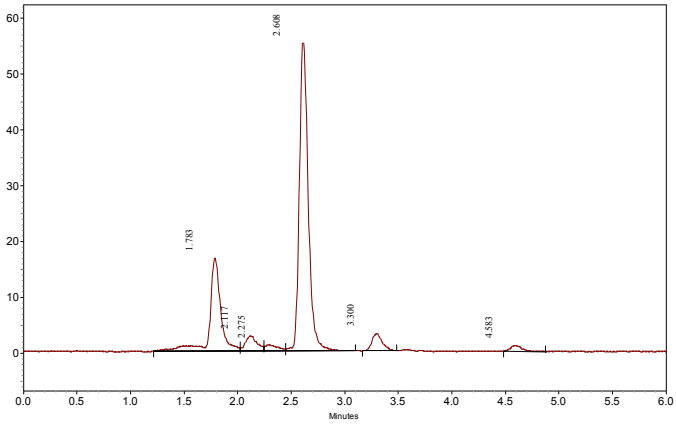

RAD Results

Retention Time	Area	Area %	Width
1.783	119733	24	0.81
2.117	20910	4	0.22
2.275	8823	2	0.20
2.608	318364	64	0.65
3.300	20543	4	0.32
4.583	7845	2	0.39

Figure 3S- 11

Table 3-4, Entry 8

[^{18}F]Fluoride was dried using the general method described above. Following drying, a solution of ditosyl methane (5 mg) in ethanol (1 mL) + 1 drop DMSO (to improve precursor solubility) was added to the reaction vessel and heated at 110 ^{o}C for 10 min. After this time, the crude reaction mixture was cooled and analyzed by radio-HPLC (column: Luna C18 150 x 4.6 mm, mobile phase: MeCN : H_2O = 50 : 50; t_R [^{18}F]FET = 4.87 min; chromatogram is shown in Figure S12). RCC was 52% (n = 1).

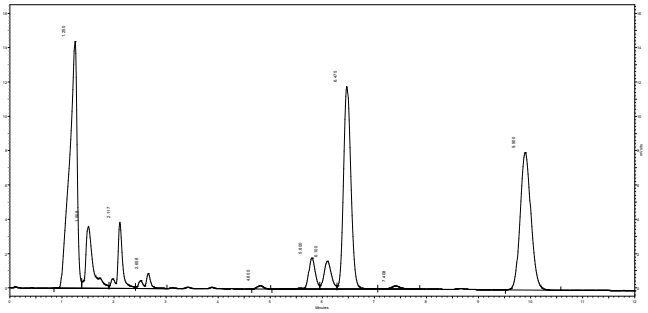

UV Detector Ch1-254nm

Results

Retention Time	Area	Area %
1.25	145548	30.32
1.51	33779	7.04
2.12	25435	5.30
2.66	7517	1.57

4.80	1641	0.34
5.80	16368	3.41
6.10	16152	3.36
6.47	114957	23.95
7.41	2488	0.52
9.90	116162	24.20

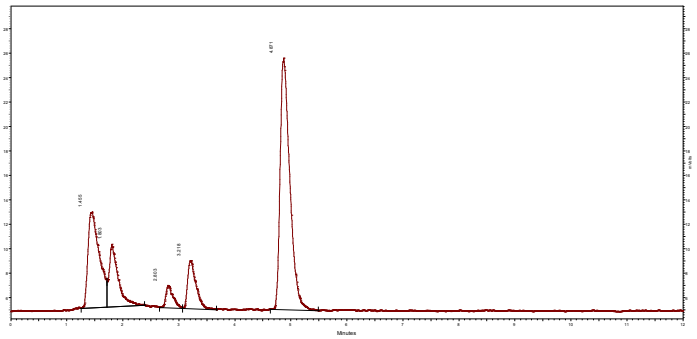

RAD Results

Retention Time	Area	Area %
1.45	111013	23.49
1.80	56964	12.06
2.80	16155	3.42
3.22	40485	8.57
4.87	247916	52.47

Figure 3S- 12

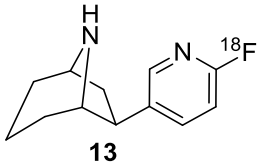

13

[^{18}F]Flubatine

Table 3-3, Entries 7 and 8

[^{18}F]Fluoride was dried using the general method described above. [^{18}F]Flubatine was then synthesized as previously described[62], and typical non-corrected radiochemical yields were 25±10% (H_2O-MeCN azeotrope, n = 3) or 15±10% (H_2O-EtOH azeotrope, n = 20). Radiochemical purity and identity were confirmed by radio-HPLC (column: Phenomonex Synergi Polar-RP 4 µ, 150 × 4.6 mm; mobile phase: 50% acetonitrile : 50% 0.1 M acetic acid; pH, 4.5; flow rate: 1.0 mL/min; oven temp: 40°C; UV wavelength: 254 nm; t_R = 5.0 min; a typical chromatogram is shown in Figure S13).

UV Detector Response

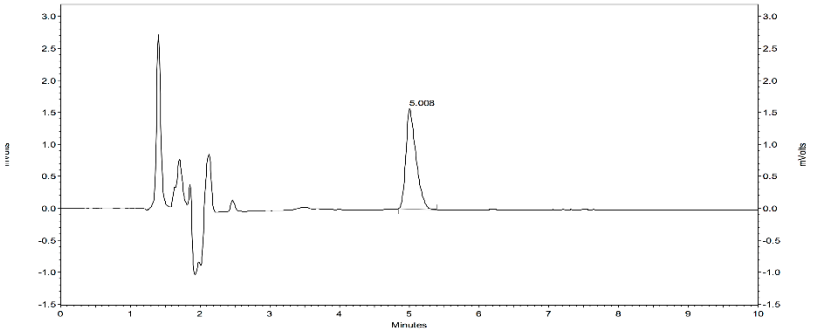

UV Detector Ch1-254nm Results

Retention Time	Area	Area %	Height	Width
5.008	15839	100.00	1570	0.57

Radioactivity Detector Response

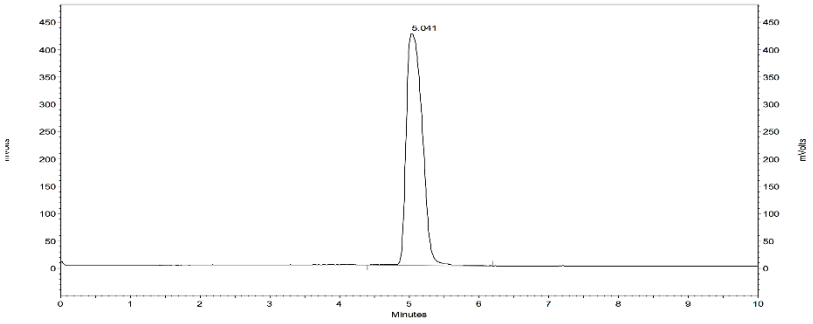

Bioscan RAD Results

Retention Time	Area	Area %
5.041	6721786	100.00

Figure 3S- 13

Table 3-4, Entry 9

[^{18}F]Fluoride was dried using the general method described above. It was then attempted to synthesize [^{18}F]flubatine as previously described,[3] but using ethanol or 15% H_2O : 85% EtOH as the reaction solvent (n = 3). In each case however, no product was formed as determined by radio-HPLC analysis (a typical chromatogram is shown in Figure S14, expected t_R of [^{18}F]flubatine = ~5 min).

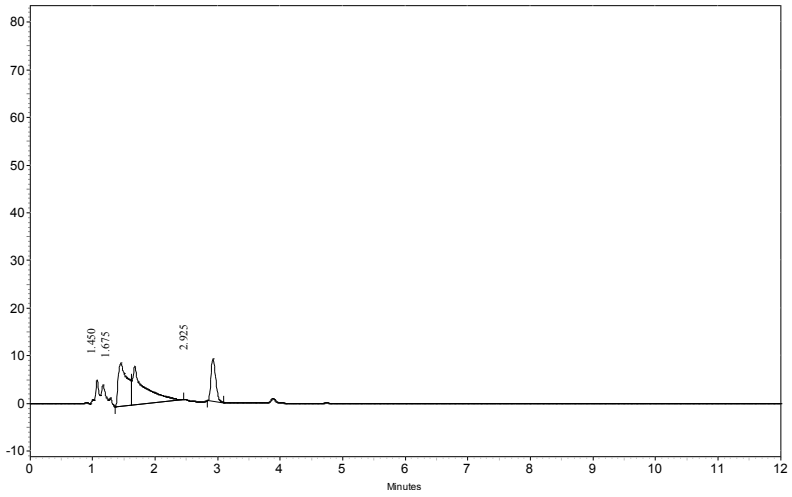

UV Detector Ch1-254nm Results

Retention Time	Area	Area %	Height	Width	S/N (ASTM)
1.450	90798	36	8990	0.267	2.97
1.675	113321	45	8025	0.833	2.66
2.925	46326	18	8848	0.267	2.93

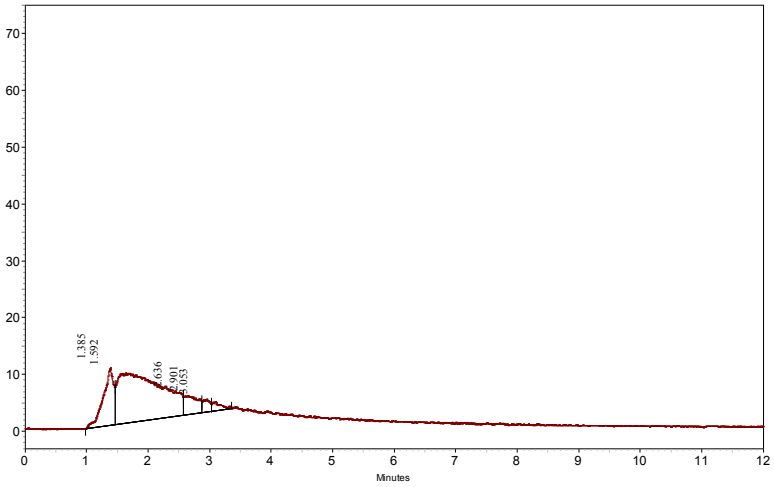

RAD Results

Retention Time	Area	Area %	Width
1.385	118835	19	0.48
1.592	436345	68	1.12
2.636	49635	8	0.30
2.901	17060	3	0.15
3.053	16097	3	0.33

Figure 3S- 14

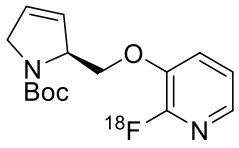

Boc-protected [^{18}F]Nifene

Table 3-3, Entries 9 and 10

[^{18}F]Fluoride was dried using the general method described above. Following drying, a solution of nifene precursor **12** (2 mg) in DMSO (1 mL) was added to the reaction vessel and heated at 125 ^{o}C for 30 min. After this time, the crude reaction mixture was cooled and analyzed by radio-HPLC (column: Phenomenex Synergi Polar RP 150 x 4.6 mm, mobile phase: MeCN : H_2O = 50 : 50 + 0.05% AcOH; flow rate: 1.0 mL/min; UV wavelength = 254 nm; t_R Bob-protected [^{18}F]nifene = 6.415 min; a typical chromatogram is shown in Figure S15). Typical RCC were 50% (H_2O-MeCN azeotrope, n = 1) or 83% (H_2O-EtOH azeotrope, n = 1).

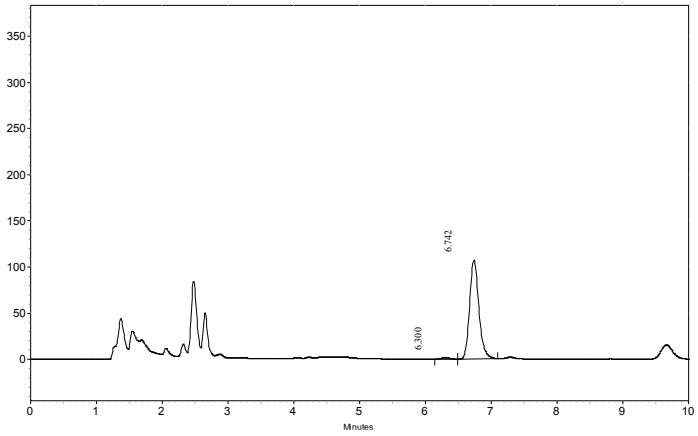

UV Detector Ch1-

254nm Results

Retention Time	Area	Area %	Height	Width	S/N (ASTM)
6.300	14160	1	1659	0.342	0.12
6.742	1048493	99	107059	0.608	7.42

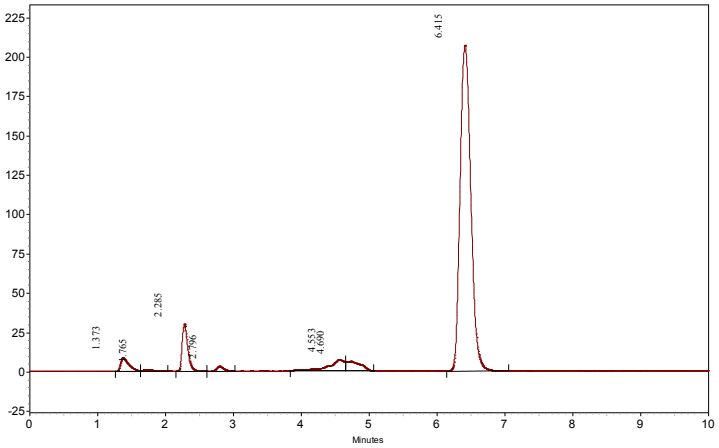

RAD Results

Retention Time	Area	Area %	Width
1.373	71187	3	0.37
1.765	8801	0	0.40

2.285	171173	6	0.45
2.796	22772	1	0.42
4.553	118687	4	0.81
4.690	86963	3	0.41
6.415	2274486	83	0.91

Figure 3S- 15

Table 3-4, Entry 10

[^{18}F]Fluoride was dried using the general method described above. It was then attempted to synthesize Bob-protected [^{18}F]nifene as described above, but using ethanol as the reaction solvent (n = 3). However, no product was formed as determined by radio-HPLC analysis (Figure S16, expected t_R of Boc-protected [^{18}F]nifene = ~6.4 min).

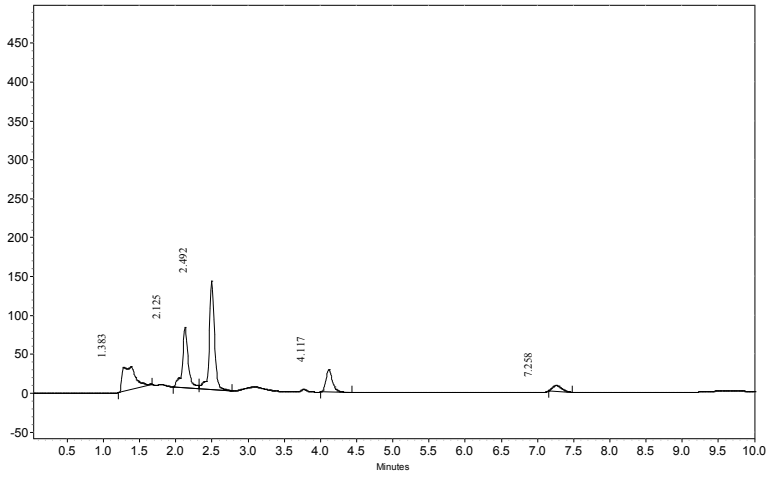

UV Detector Ch1-254nm Results

Retention Time	Area	Area %	Height	Width	S/N (ASTM)
1.383	372700	21	29380	0.458	119.37
2.125	444136	25	77651	0.358	315.49
2.492	699441	40	139470	0.450	566.66
4.117	176449	10	28736	0.433	9.67
7.258	61599	4	7243	0.333	13.65

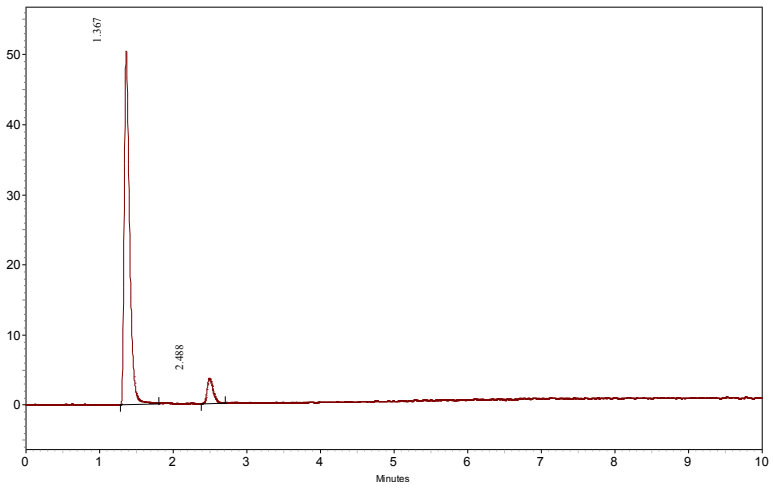

RAD Results

Retention Time	Area	Area %	Width
1.367	254428	93	0.52
2.488	20328	7	0.33

Figure 3S- 16

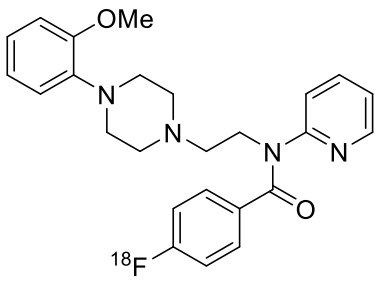

17

[^{18}F]MPPF

Table 3-3, Entries 11 and 12

[^{18}F]Fluoride was dried using the general method described above. MPPF precursor **15** (10 mg) in DMSO (0.5 mL) was added to the reactor, and the reaction was heated at 140 ^{o}C for 20 min. After this time, the crude reaction mixture was cooled and analyzed by radio-HPLC (column: Phenomenex Prodigy C8 5μ 150 x 4.6 mm; mobile phase: MeCN : 20 mM ammonium acetate = 35 : 50, pH 4.5; flow rate: 0.8 mL/min; oven temp: 40°C; UV wavelength: 254 nm; t_R [^{18}F]MPPF = 8.78 min; a typical chromatogram is shown in Figure S17). Typical RCC were 70±10% (H_2O-MeCN azeotrope, n = 3) or 78±18% (H_2O-EtOH azeotrope, n = 3).

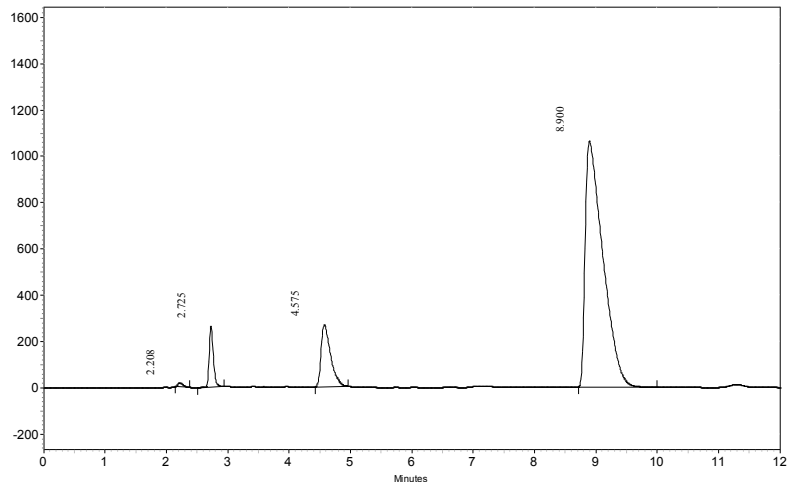

UV Detector Ch1-

254nm Results

Retention Time	Area	Area %	Height	Width	S/N (ASTM)
2.208	97806	0	17202	0.233	22.13
2.725	1268980	5	263342	0.425	338.76
4.575	2867369	11	266439	0.542	97.83
8.900	21201104	83	1061339	1.275	615.01

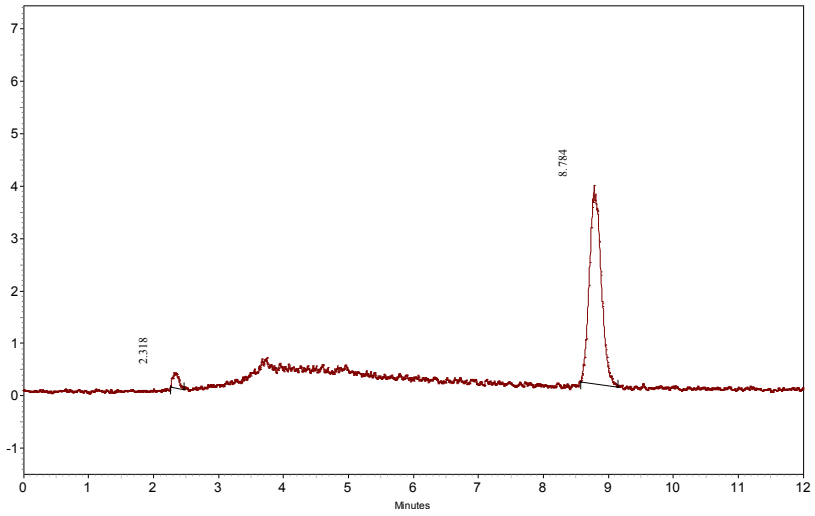

RAD Results

Retention Time	Area	Area %	Width
2.318	1967	4	0.21
8.784	47150	96	0.57

Figure 3S- 17

Table 3-4, Entry 11

[^{18}F]Fluoride was dried using the general method described above. It was then attempted to synthesize [^{18}F]MPPF as described above, but using ethanol (n = 3) or ethanol/DMSO [50:50] (n = 3) as the reaction solvent. However, no product was formed in either case as determined by radio-HPLC analysis (Figure S18, expected t_R of [^{18}F]MPPF = ~8.78 min).

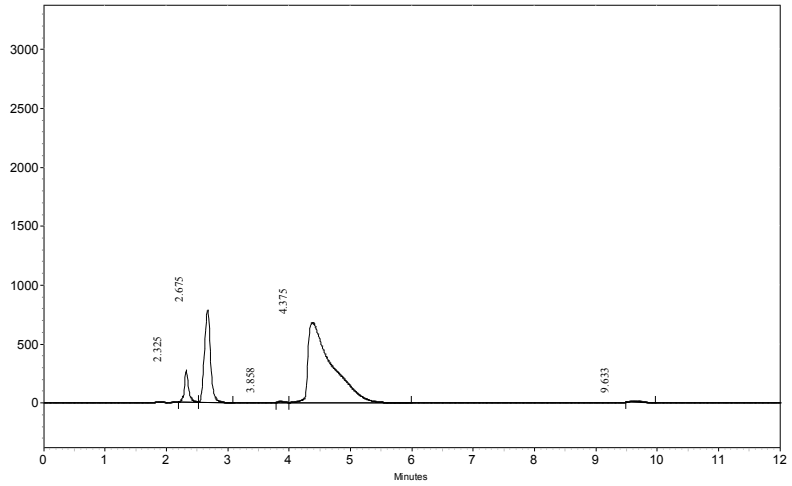

UV Detector Ch1-254nm Results

Retention Time	Area	Area %	Height	Width	S/N (ASTM)
2.325	1282831	5	271845	0.325	169.87
2.675	5381206	22	784338	0.558	490.12
3.858	54488	0	8850	0.208	4.01

4.375	18028968	72	680339	2.000	308.46
9.633	168280	1	13148	0.483	17.04

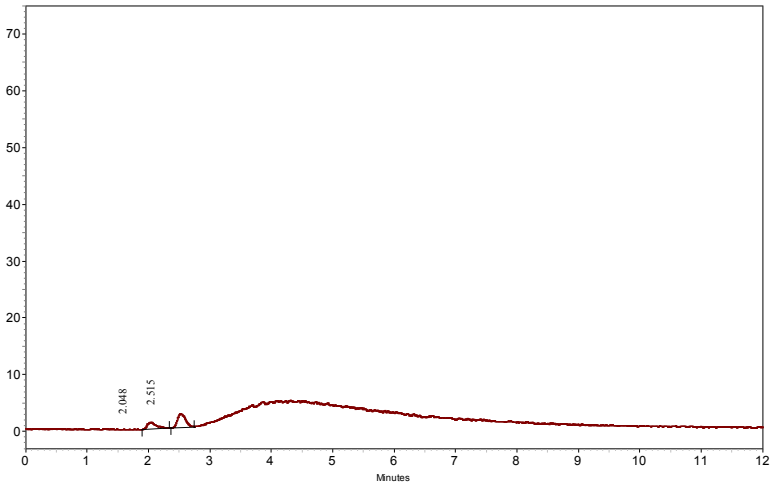

RAD Results

Retention Time	Area	Area %	Width
2.048	13238	37	0.44
2.515	22386	63	0.37

Figure 3S- 18

References

(1) Ametamey, S. M.; Honer, M.; Schubiger, P. A. Molecular imaging with PET. *Chem. Rev.* **2008**, *108* (5), 1501–1516 DOI: 10.1021/cr0782426.

(2) Pither, R. PET and the role of in vivo molecular imaging in personalized medicine. *Expert Rev. Mol. Diagn.* **2003**, *3* (6), 703–713 DOI: 10.1586/14737159.3.6.703.

(3) Matthews, P. M.; Rabiner, E. A.; Passchier, J.; Gunn, R. N. Positron emission tomography molecular imaging for drug development. *Br. J. Clin. Pharmacol.* **2012**, *73* (2), 175–186 DOI: 10.1111/j.1365-2125.2011.04085.x.

(4) Miller, P. W.; Long, N. J.; Vilar, R.; Gee, A. D. Synthesis of11C, 18F, 15O, and 13N radiolabels for positron emission tomography. *Angew. Chemie - Int. Ed.* **2008**, *47* (47), 8998–9033 DOI: 10.1002/anie.200800222.

(5) Scott, P. J. H. Methods for the incorporation of carbon-11 to generate radiopharmaceuticals for PET imaging. *Angew. Chemie - Int. Ed.* **2009**, *48* (33), 6001–6004 DOI: 10.1002/anie.200901481.

(6) Littich, R.; Scott, P. J. H. Novel strategies for fluorine-18 radiochemistry. *Angew. Chemie - Int. Ed.* **2012**, *51* (5), 1106–1109 DOI: 10.1002/anie.201106785.

(7) Brooks, A. F.; Topczewski, J. J.; Ichiishi, N.; Sanford, M. S.; Scott, P. J. H. Late-stage [^{18} F]fluorination: new solutions to old problems. *Chem. Sci.* **2014**, *5* (12), 4545–4553 DOI: 10.1039/C4SC02099E.

(8) Cole, E.; Stewart, M.; Littich, R.; Hoareau, R.; Scott, P. Radiosyntheses using Fluorine-18: The Art and Science of Late Stage Fluorination. *Curr. Top. Med.*

Chem. **2014**, *14* (7), 875–900 DOI: 10.2174/1568026614666140202205035.

(9) Cai, L.; Lu, S.; Pike, V. W. Chemistry with [18F]fluoride ion. *European J. Org. Chem.* **2008**, No. 17, 2853–2873 DOI: 10.1002/ejoc.200800114.

(10) Schirrmacher, R.; Wangler, C.; Schirrmacher, E. Recent Developments and Trends in 18F-Radiochemistry: Syntheses and Applications. *Mini. Rev. Org. Chem.* **2007**, *4* (4), 317–329 DOI: 10.2174/157019307782411699.

(11) Tredwell, M.; Gouverneur, V. 18F labeling of arenes. *Angew. Chemie - Int. Ed.* **2012**, *51* (46), 11426–11437 DOI: 10.1002/anie.201204687.

(12) Liang, S. H.; Vasdev, N. C(sp3)-18F Bond Formation by Transition-Metal-Based [18F]Fluorination. *Angew. Chemie - Int. Ed.* **2014**, *53* (43), 11416–11418 DOI: 10.1002/anie.201407065.

(13) *Radiochemical Syntheses Volume 1: Radiopharmaceuticals for Positron Emission Tomography*; Scott, P. J. H., Hockley, B. G., Eds.; John Wiley & Sons, Ltd: Hoboken, New Jersey, 2012.

(14) Vallabhajosula, S.; Solnes, L.; Vallabhajosula, B. A broad overview of positron emission tomography radiopharmaceuticals and clinical applications: What is new? *Semin. Nucl. Med.* **2011**, *41* (4), 246–264 DOI: 10.1053/j.semnuclmed.2011.02.003.

(15) Schwarz, S. W.; Dick, D.; VanBrocklin, H. F.; Hoffman, J. M. Regulatory Requirements for PET Drug Production. *J. Nucl. Med.* **2014**, *55* (7), 1132–1137 DOI: 10.2967/jnumed.113.132472.

(16) Bietendorf, J. FDG PET reimbursement. *J. Nucl. Med. Technol.* **2004**, *32*, 33–38.

(17) Wagner, H. N. PET is alive and well. *J. Nucl. Med.* **2007**, *48* (4), 495 DOI: 10.2967/jnumed.48.4.495.07.

(18) Shao, X.; Hoareau, R.; Runkle, A. C.; Tluczek, L. J. M.; Hockley, B. G.; Henderson, B. D.; Scott, P. J. H. Highlighting the versatility of the Tracerlab synthesis modules. Part 2: fully automated production of [11C]-labeled radiopharmaceuticals using a Tracerlab FXC-Pro. *J. Label. Compd. Radiopharm.* **2011**, *54* (14), 819–838 DOI: 10.1002/jlcr.1937.

(19) Rotstein, B. H.; Liang, S. H.; Holland, J. P.; Collier, T. L.; Hooker, J. M.; Wilson, A. a; Vasdev, N. 11CO2 fixation: a renaissance in PET radiochemistry. *Chem. Commun. (Camb).* **2013**, *49* (50), 5621–5629 DOI: 10.1039/c3cc42236d.

(20) Chemistry | Definition of Chemistry by Merriam-Webster https://www.merriam-webster.com/dictionary/chemistry (accessed Oct 27, 2017).

(21) Alfonsi, K.; Colberg, J.; Dunn, P. J.; Fevig, T.; Jennings, S.; Johnson, T. A.; Kleine, H. P.; Knight, C.; Nagy, M. A.; Perry, D. A.; et al. Green chemistry tools to influence a medicinal chemistry and research chemistry based organisation. *Green Chem.* **2008**, *10* (1), 31–36 DOI: 10.1039/B711717E.

(22) Anastas, P. T.; Warners, J. C. *Green Chemistry: Theory And Practice*; Oxford: Oxford University Press, 1998.

(23) Manley, J. B. Chapter 1. Introduction: The Five Ws of Pharmaceutical Green Chemistry. *RSC Drug Discov.* **2015**, *1* (46), 1–12 DOI: 10.1039/9781782622659-

00001.

(24) Anastas, P. T. Chapter 1 Benign by Design Chemistry. *Symp. A Q. J. Mod. Foreign Lit.* **1994**.

(25) Sheldon, R. A. Fundamentals of green chemistry: efficiency in reaction design. *Chem. Soc. Rev.* **2012**, *41* (4), 1437–1451 DOI: 10.1039/C1CS15219J.

(26) Anastas, P. T.; Zimmerman, J. B. Chapter 2: The Twelve Principles of Green Engineering as a Foundation for Sustainability BT - Sustainability Science and Engineering: Defining Principles. *Sustain. Sci. Eng. Defin. Princ.* **2006**, *2711* (5), 11–32 DOI: 10.1016/81871-2711(05)01002-0.

(27) *Green Techniques for Organic Synthesis and Medicinal Chemistry*; Zhang, W., Cue, B. W., Eds.; John Wiley & Sons, Ltd: Chichester, UK, 2012.

(28) History of the Green Chemistry Institute - American Chemical Society https://www.acs.org/content/acs/en/greenchemistry/about/history.html (accessed Oct 27, 2017).

(29) Green Chemistry: Industry & Business - American Chemical Society https://www.acs.org/content/acs/en/greenchemistry/industry-business.html (accessed Oct 27, 2017).

(30) Lechleiter, J. C. Business Roundtable: 2015 Sustainability Report: Lilly. **2015**.

(31) Alder, C. M.; Hayler, J. D.; Henderson, R. K.; Redman, A. M.; Shukla, L.; Shuster, L. E.; Sneddon, H. F. Updating and further expanding GSK's solvent sustainability guide. *Green Chem.* **2016**, *18* (13), 3879–3890 DOI: 10.1039/C6GC00611F.

(32) Adams, J. P.; Alder, C. M.; Andrews, I.; Bullion, A. M.; Campbell-Crawford, M.; Darcy, M. G.; Hayler, J. D.; Henderson, R. K.; Oare, C. A.; Pendrak, I.; et al. Development of GSK's reagent guides – embedding sustainability into reagent selection. *Green Chem.* **2013**, *15* (6), 1542 DOI: 10.1039/c3gc40225h.

(33) Diorazio, L. J.; Hose, D. R. J.; Adlington, N. K. Toward a More Holistic Framework for Solvent Selection. *Org. Process Res. Dev.* **2016**, *20* (4), 760–773 DOI: 10.1021/acs.oprd.6b00015.

(34) Green Chemistry Academic Programs - American Chemical Society https://www.acs.org/content/acs/en/greenchemistry/students-educators/academicprograms.html (accessed Oct 27, 2017).

(35) Office of Campus Sustainability | Planet Blue http://sustainability.umich.edu/ocs (accessed Oct 27, 2017).

(36) Sustainable Lab Recognition Program | Planet Blue http://sustainability.umich.edu/ocs/labs (accessed Oct 27, 2017).

(37) Yu, L. X.; Amidon, G.; Khan, M. A.; Hoag, S. W.; Polli, J.; Raju, G. K.; Woodcock, J. Understanding Pharmaceutical Quality by Design. *AAPS J.* **2014**, *16* (4), 771–783 DOI: 10.1208/s12248-014-9598-3.

(38) ICH-Q3C(R6). International Council for Harmonisation of Technical Requirements for Pharmaceuticals for Human Use Ich Harmonised Guideline Impurities: Guideline for Residual Solvents Q3C(R6). **2016**.

(39) Shao, X.; Fawaz, M. V.; Jang, K.; Scott, P. J. H. Ethanolic carbon-11 chemistry:

The introduction of green radiochemistry. *Appl. Radiat. Isot.* **2014**, *89*, 125–129 DOI: 10.1016/j.apradiso.2014.01.033.

(40) Shao, X.; Schnau, P. L.; Fawaz, M. V.; Scott, P. J. H. Enhanced radiosyntheses of [11C]raclopride and [11C]DASB using ethanolic loop chemistry. *Nucl. Med. Biol.* **2013**, *40* (1), 109–116 DOI: 10.1016/j.nucmedbio.2012.09.008.

(41) Effenberger, F. Electrophilic Reagents - Recent Developments and Their Preparative Application. *Angew. Chemie - Int. Ed.* **1980**, *19* (3), 151–230.

(42) Shao, X.; Fawaz, M. V.; Jang, K.; Scott, P. J. H. Ethanolic carbon-11 chemistry: The introduction of green radiochemistry. *Appl. Radiat. Isot.* **2014**, *89*, 125–129 DOI: 10.1016/j.apradiso.2014.01.033.

(43) Kim, D. W.; Ahn, D. S.; Oh, Y. H.; Lee, S.; Kil, H. S.; Oh, S. J.; Lee, S. J.; Kim, J. S.; Ryu, J. S.; Moon, D. H.; et al. A new class of SN2 reactions catalyzed by protic solvents: Facile fluorination for isotopic labeling of diagnostic molecules. *J. Am. Chem. Soc.* **2006**, *128* (50), 16394–16397 DOI: 10.1021/ja0646895.

(44) Kim, D. W.; Jeong; Lim, S. T.; Sohn, M.-H.; Katzenellenbogen, J. A.; Chi, D. Y. Facile Nucleophilic Fluorination Reactions Using tert -Alcohols as a Reaction Medium: Significantly Enhanced Reactivity of Alkali Metal Fluorides and Improved Selectivity. *J. Org. Chem.* **2008**, *73* (3), 957–962 DOI: 10.1021/jo7021229.

(45) Kitazume, T. Green chemistry development in fluorine science. *J. Fluor. Chem.* **2000**, *105* (2), 265–278 DOI: 10.1016/S0022-1139(99)00269-9.

(46) Harsanyi, A.; Sandford, G. Organofluorine chemistry: applications, sources and

sustainability. *Green Chem.* **2015**, *17* (4), 2081–2086 DOI: 10.1039/C4GC02166E.

(47) Tavener, S. J.; Clark, J. H. Can fluorine chemistry be green chemistry? *J. Fluor. Chem.* **2003**, *123* (1), 31–36 DOI: 10.1016/S0022-1139(03)00140-4.

(48) Lee, S. S.; Kim, H. S.; Hwang, T. K.; Oh, Y. H.; Park, S. W.; Lee, S.; Lee, B. S.; Chi, D. Y. Efficiency of bulky protic solvent for SN2 reaction. *Org. Lett.* **2008**, *10* (1), 61–64 DOI: 10.1021/ol702627m.

(49) Oh, Y. H.; Im, S.; Park, S. W.; Lee, S.; Chi, D. Y. SN2/E2 branching in protic solvents: A mechanistic study. *Bull. Korean Chem. Soc.* **2009**, *30* (7), 1535–1538 DOI: 10.5012/bkcs.2009.30.7.1535.

(50) Lee, E.; Hooker, J. M.; Ritter, T. Nickel-mediated oxidative fluorination for PET with aqueous [18F] fluoride. *J. Am. Chem. Soc.* **2012**, *134* (42), 17456–17458 DOI: 10.1021/ja3084797.

(51) Sergeev, M. E.; Morgia, F.; Lazari, M.; Jr, C. W.; Dam, R. M. Van. Titania-Catalyzed Radiofluorination of Tosylated P recursors in Highly Aqueous Media -SI. *J. Am. Chem. Soc.* **2015** DOI: 10.1021/jacs.5b02659.

(52) Zhao, H.; Gabbaï, F. P. Nucleophilic fluorination reactions starting from aqueous fluoride ion solutions. *Org. Lett.* **2011**, *13* (6), 1444–1446 DOI: 10.1021/ol200129q.

(53) Sun, H.; DiMagno, S. G. Anhydrous tetrabutylammonium fluoride. *J. Am. Chem. Soc.* **2005**, *127* (7), 2050–2051 DOI: 10.1021/ja0440497.

(54) Sun, H.; DiMagno, S. G. Fluoride relay: a new concept for the rapid preparation of anhydrous nucleophilic fluoride salts from KF. *Chem. Commun. (Camb).* **2007**, No.

5, 528–529 DOI: 10.1039/b614368g.

(55) Sun, H.; DiMagno, S. G. Room-temperature nucleophilic aromatic fluorination: Experimental and theoretical studies. *Angew. Chemie - Int. Ed.* **2006**, *45* (17), 2720–2725 DOI: 10.1002/anie.200504555.

(56) Chun, J.-H.; Telu, S.; Lu, S.; Pike, V. W. Radiofluorination of diaryliodonium tosylates under aqueous–organic and cryptand-free conditions. *Org. Biomol. Chem.* **2013**, *11* (31), 5094 DOI: 10.1039/c3ob40742j.

(57) Kilbourn, M. Green radiochemistry. *Nucl. Med. Biol.* **2014**, *41* (8), 651–652 DOI: 10.1016/j.nucmedbio.2014.04.128.

(58) Shao, X.; Hoareau, R.; Hockley, B. G.; Tluczek, L. J. M.; Henderson, B. D.; Padgett, H. C.; Scott, P. J. H. Highlighting the versatility of the tracerlab synthesis modules. Part 1: fully automated production of [18F]labelled radiopharmaceuticals using a Tracerlab FXFN. *J. Label. Compd. Radiopharm.* **2011**, *54* (6), 292–307 DOI: 10.1002/jlcr.1865.

(59) *CRC Handbook of Chemistry and Physics*, 73rd ed.; Lide, D. R., Ed.; CRC Press: Boca Raton, 1992.

(60) Pun, M.; Blecha, J.; Powell, J.; Joseph, S.; VanBrocklin, H. Solvent exchange radiofluorination: High yield production of fluorine-18 compounds without water evaporation. *J. Nucl. Med.* **2010**, *51* (Supplement 2), 534.

(61) Kniess, T.; Laube, M.; Brust, P.; Steinbach, J. 2-[18 F]Fluoroethyl tosylate – a versatile tool for building 18 F-based radiotracers for positron emission tomography.

Med. Chem. Commun. **2015**, *6* (10), 1714–1754 DOI: 10.1039/C5MD00303B.

(62) Hockley, B. G.; Stewart, M. N.; Sherman, P.; Quesada, C.; Kilbourn, M. R.; Albin, R. L.; Scott, P. J. H. (-)-[18F]Flubatine: Evaluation in rhesus monkeys and a report of the first fully automated radiosynthesis validated for clinical use. *J. Label. Compd. Radiopharm.* **2013**, *56* (12), 595–599 DOI: 10.1002/jlcr.3069.

(63) *Radiochemical Syntheses Volume 2: Further Radiopharmaceuticals for Positron Emission Tomography and New Strategies for Their Production*; Scott, P. J. H., Ed.; John Wiley & Sons, Ltd: Hoboken, New Jersey, 2015.

(64) Pichika, R.; Easwaramoorthy, B.; Collins, D.; Christian, B. T.; Shi, B.; Narayanan, T. K.; Potkin, S. G.; Mukherjee, J. Nicotinic α4β2 receptor imaging agents. *Nucl. Med. Biol.* **2006**, *33* (3), 295–304 DOI: 10.1016/j.nucmedbio.2005.12.017.

(65) Le Bars, D.; Lemaire, C.; Ginovart, N.; Plenevaux, A.; Aerts, J.; Brihaye, C.; Hassoun, W.; Leviel, V.; Mekhsian, P.; Weissmann, D.; et al. High-yield radiosynthesis and preliminary in vivo evaluation of p- [18F]MPPF, a fluoro analog of WAY-100635. *Nucl. Med. Biol.* **1998**, *25* (4), 343–350 DOI: 10.1016/S0969-8051(97)00229-1.

(66) Shiue, C.-Y.; Shiue, G. G.; Mozley, P. D.; Kung, M.-P.; Zhuang, Z.-P.; Kim, H.-J.; Kung, H. F. p-[18 F]-MPPF: A Potential Radioligand for PET Studies of 5-HT 1A Receptors in Humans. *Synapse* **1997**, *25* (March 1996), 147–154 DOI: 10.1002/(SICI)1098-2396(199702)25:2<147::AID-SYN5>3.0.CO;2-C.

(67) Haka, M. S.; Kilbourn, M. R.; Leonard Watkins, G.; Toorongian, S. A. Aryltrimethylammonium trifluoromethanesulfonates as precursors to aryl

[18F]fluorides: Improved synthesis of [18F]GBR-13119. *J. Label. Compd. Radiopharm.* **1989**, *27* (7), 823–833 DOI: 10.1002/jlcr.2580270711.

(68) Soroko, I.; Bhole, Y.; Livingston, A. G. Environmentally friendly route for the preparation of solvent resistant polyimide nanofiltration membranes. *Green Chem.* **2011**, *13* (1), 162 DOI: 10.1039/c0gc00155d.

(69) *USP 25 - NF 50 Chapter (823) Positron Emission Tomography Drugs for Compounding, Investigational,and Research Uses*; 2012.

(70) Richards, M. L.; Scott, P. J. H. Synthesis of [18F]Fluorodeoxyglucose ([18F]FDG). In *Radiochemical Syntheses Volume 1: Radiopharmaceuticals for Positron Emission Tomography*; Scott, P. J. H., Hockley, B. G., Eds.; John Wiley and Sons In.: Hoboken, New Jersey, 2012; pp 3–14.

(71) Anzellotti, A.; McFarland, A.; Brown-Proctor, C.; Hillesheim, D.; Khachaturian, M. Automated Quality Control System for Radiopharmaceuticals, 2015.

(72) Stewart, M. N.; Hockley, B. G.; Scott, P. J. H. Green approaches to late-stage fluorination: radiosyntheses of ^{18}F-labelled radiopharmaceuticals in ethanol and water. *Chem. Commun.* **2015**, *51* (79), 14805–14808 DOI: 10.1039/C5CC05919D.

Chapter 4

Synthesis & Initial Evaluation of a Dopamine D_3 Receptor-Selective PET Tracer

a. The Dopaminergic System & The Central Nervous System

The dopaminergic system and subsequent dysfunction in dopamine transmission is implicated in several neurologic, neurodegenerative, and psychiatric disorders; specifically, this includes depression, schizophrenia, Parkinson's disease (PD), and drug/substance abuse disorders. The receptors for this major neurotransmitter, dopamine (DA), are of interest because they are the principal target of drugs for these diseases and disorders.[1–4]

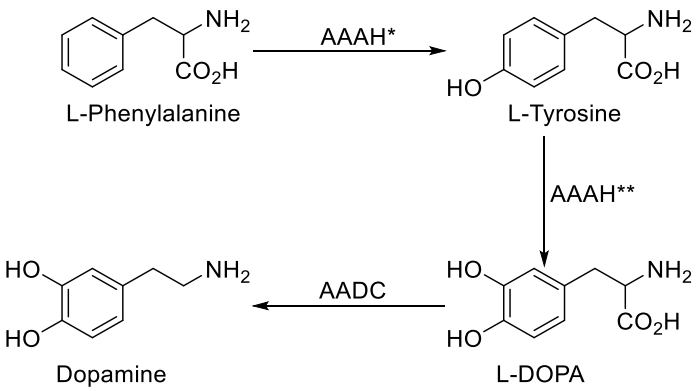

AAAH = biopterin-dependent aromatic amino acid hydroxylases
(*phenylalanine hydroxylase, **tyrosine hydroxylase)
AADC = aromatic L-amino acid decarboxylase
(DOPA-decarboxylase)

Scheme 4- 1 Biosynthesis of Dopamine

The biosynthesis of dopamine (Scheme 4-1) begins with the essential amino acid L-phenylalanine that is hydroxylated by a biopterin-dependent aromatic amino acid hydroxylase, AAAH (specifically phenylalanine hydroxylase) to form L-tyrosine. non-essential amino acid tyrosine (abbr. Tyr or Y). L-tyrosine is further hydroxylated by this same class of AAAH enzymes, specifically by tyrosine hydroxylase, in the rate-limiting step of catecholamine biosynthesis to form L-DOPA. L-DOPA, which cannot pass the Blood-Brain-Barrier (BBB), is then decarbcateoxylated by the aromatic L-amino acid decarboxylase, known as DOPA-decarboxylase, to produce dopamine. Dopamine is then packaged into vesicles to protect it from oxidation by monoamine oxidase (MAO) to await neurotransmission (Scheme 4- 1).[5,6] Mediated by an electrical impulse, these vesicles fuse with the presynaptic membrane and dopamine is released in to the synaptic cleft where it binds to its receptor(s).[7]

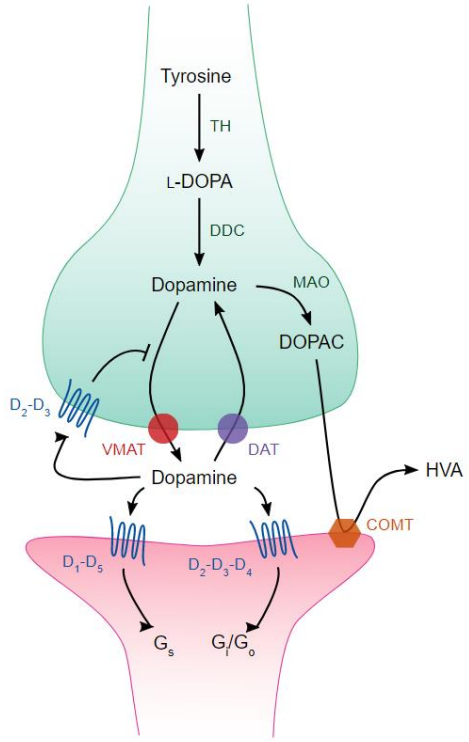

Figure 4- 1 Dopaminergic Synapse. Image: © Permissions granted from Creative Commons/Free Usage https://commons.wikimedia.org/wiki/File:Dopaminergic_synapse.svg

When dopamine is released into the synapse as the result of an action potential, it interacts with postsynaptic receptors. Dopamine concentrations are mediated *via* reuptake by the dopamine transporters (DAT). This regulation ensures the concentration of dopamine at the synapse to be low/nanomolar and at steady state concentrations. Moreover, dopamine is removed by MAO A or MAO B oxidation; this occurs in neurons (MAO A) and the glia (MAO B), which encompass the dopaminergic nerve terminals. Catecholamine O-methyltransferase (COMT) is another enzyme which inactivates DA by methylating at the catecholamine (donated by S-adenosyl methionine, aka SAM). In this situation, dopamine is transformed into 3-methoxytyramine by COMT (Figure 4- 1).[8,9] The final end product is homovanillic acid (HVA), which currently has no known biological

activity. Dopamine can also be transformed into norepinephrine by dopamine β-hydroxylase (DBH), which is then transformed into epinephrine by phenylethanolamine N-methyltransferase (PNMT).[9]

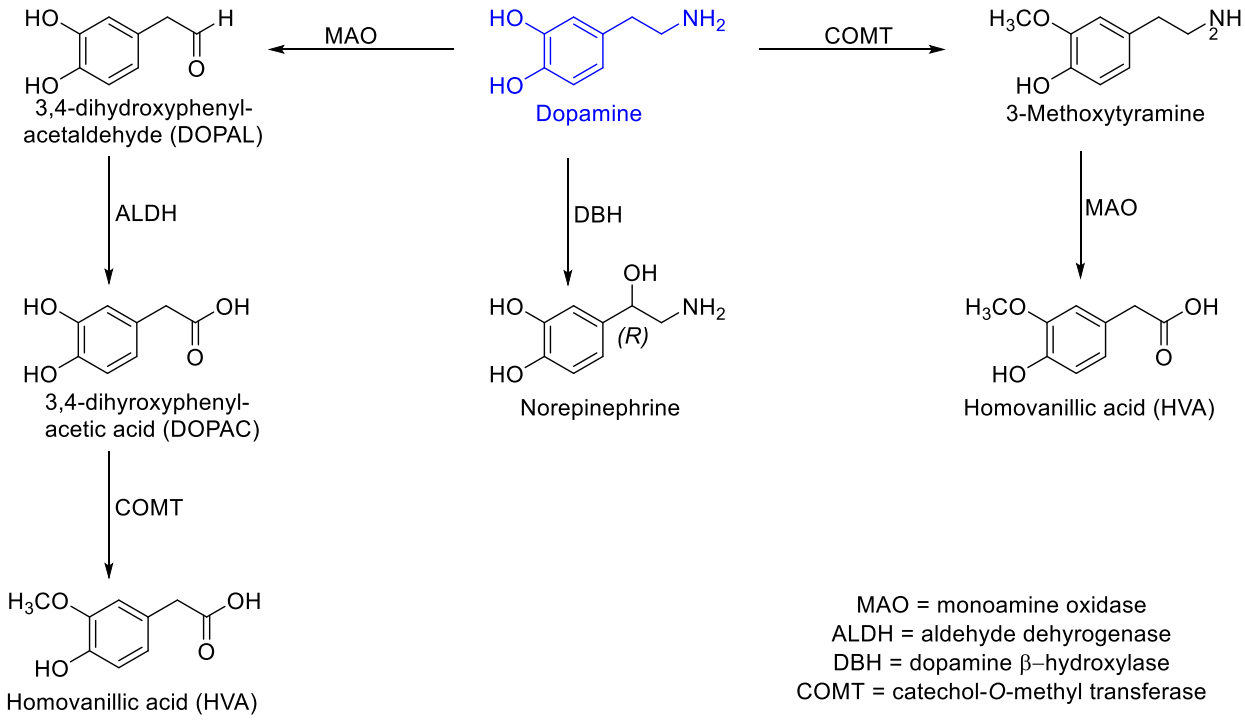

Scheme 4- 2 (General) Dopamine Metabolism

There are five dopamine receptors which mediate dopamine transmission, all of which are G protein-coupled receptors (GPCRs) with their characteristic 7-transmembrane domain region. These receptors are classified as D_1-like (D_1, D_5), and D_2-like (D_2, D_3, D_4). The dopamine receptor population were once thought to only include subtypes D_1 and D_2 until 1990.[10–12] Once the D_1 and D_2 receptor families were cloned,[13–15] the subtype receptors were later identified and cloned, D_3 and D_4, and D_5.[16–18] The D_3 receptor was cloned by Sokoloff in 1990 using rat cDNA and probes design from D_2

receptor sequence.[16] Not long behind was the human D_3 receptor cloned[19], then the murine D_3 receptor[20].[21] These are classified according to homology in sequence, and signal transduction and biochemistry (Figure 4- 2, Table 4- 1).[22–25]

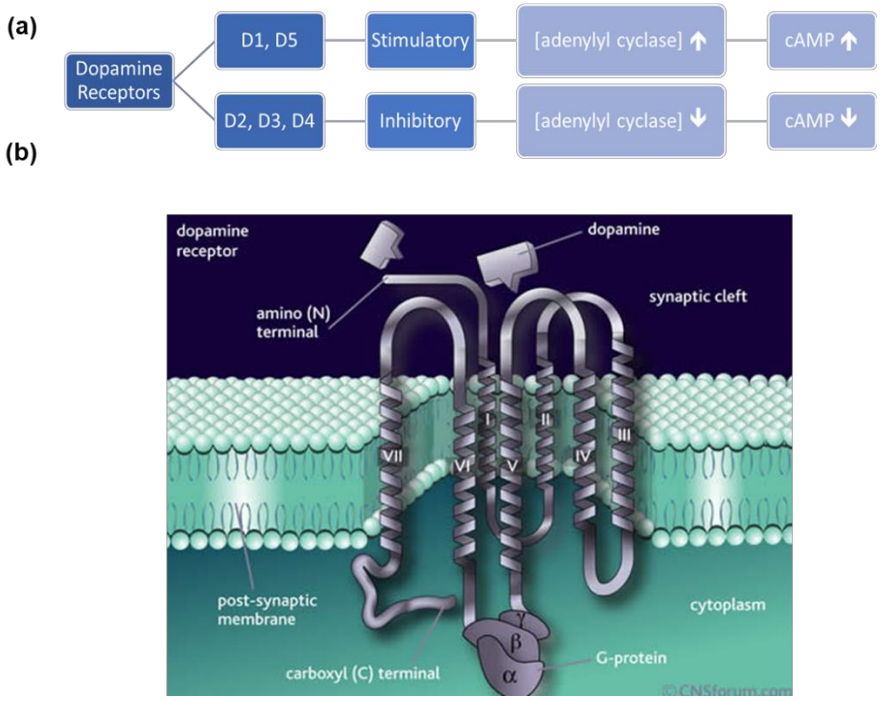

Figure 4- 2 (a) Classification of Dopamine Receptors (cAMP = cyclic adenosine monophosphate), (b) General Dopamine Receptor. Image: © CNSforum.com, Free Use.

Members of the same family share considerable homology In the D_1-like family, D_1, and D_5 share 80% identity in their trans-membrane domains. Within the D_2-like family, D_2 and D_3 receptors have a striking 75% identity; D_2 and D_4 receptors share 52% identity in their trans-membrane domains; this extends to D_2 and D_3 receptors sharing 39% and 41% homology with the D_4 receptor, respectively.[17,23,26] The presence/absence of introns is another key distinctive feature of these receptor subtype classifications (Table 4- 1).[22,27]

Moreover, these receptors are further classified based on their coupling to the effector adenylyl cyclase (AC): D_1-like receptors are positively coupled to AC through G-protein, G_s; D_2-like receptors inhibit AC through coupling to inhibitor G-proteins, G_i/G_o (Figure 4-2).[25]

Table 4- 1 Summary: Molecular Biology of the Dopamine Receptors[22,23]

	D_1-Like		**D_2-Like**		
	D_1	**D_5**	**D_2**	**D_3**	**D_4**
Chromosomal Localization	5q 35.1	4p 15.1-16.1	11q 22-23	3q 13.3	11p 15.5
Introns	No	No	6	5	3
Amino Acids	446 (rat) 446 (human)	457 (rat) 477 (human)	*415, **444 (rat) *414, **443 (human)	446 (rat) 400 (human)	385 (rat) 387 (human)
mRNA size	3.8 kb	3.0 kb	2.5 kb	8.3 kb	5.3 kb
D_2 isoforms: *short, ** long					

The dopaminergic neurons are defined by three main pathways: i) mesolimbic, ii) nigrostriatal, and iii) tuberoinfundibular. Dopaminergic neurons are localized mainly in the substantia nigra pars compact, the hypothalamus, and the ventral tegmental area.[28] The dopamine receptor subtypes can be troublesome to target in intact tissue due to their co-expression in the same brain region. However, molecular cloning has made it possible to isolate these receptors in cell lines and examine them *via* pharmacological agents.[23]

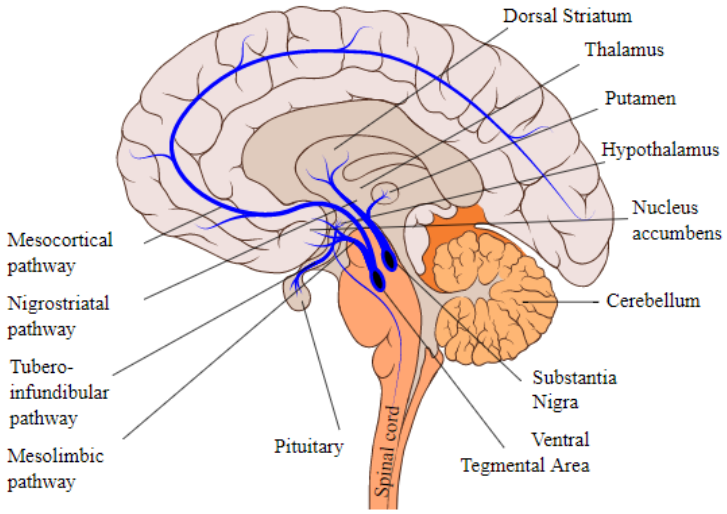

Figure 4- 3 Dopaminergic Pathways Image: © Permission granted from: GNU Free Documentation License, and Creative Commons https://commons.wikimedia.org/wiki/File:Dopaminergic_pathways.svg

A drawback to the *in vitro* approach is that the effectors and G-proteins present physiologically for these receptors may not be properly represented. For example, while a dopamine receptor may behave a certain way in cells, the behavior may not translate to an *in vivo* system where those G-proteins and effectors are differentially expressed.[22,29] Selective pharmacological agents are not readily available (for all subtypes), making traditional autoradiographic methods to determine dopamine receptor distribution challenging. However, a common, yet laborious, method to study the localization of the various receptor mRNAs is through *in situ* hybridization and has been used extensively for this purpose.[22] In the case of *in vivo* systems, competition with the endogenous ligand, dopamine, and confirming target engagement of these receptors by pharmacological means is similarly challenging due to limited BBB permeability, and for reasons mentioned above.[30–32]

The complete characterization and current understanding of dopamine receptors remains largely unknown due to the inability to selectively target these receptor(s). Given the clinical relevance of D_2-like receptors, the ability to utilize the pharmacological potential of these receptors is also largely unrealized.

b. The Dopamine D_2-Like Receptors: D_2 and D_3

In addition to the inhibition of cyclic adenosine monophosphate (cAMP), D_2-like receptors are known to modulate other second messenger pathways, such as ion channels, Na^+/H^+ exchanger, phosphatidylinositol hydrolysis, arachidonic acid release, and cell growth and differentiation.[22,23,33] D_2 receptors and, more prominently, the D_3 receptors also play an important role in the reinforcing properties of different drugs of abuse (e.g. cocaine), as well as in other neuropsychiatric disorders such as schizophrenia and depression.[33–37] The D_2-like receptors, more importantly the D_3/D_2 receptors, have a well-recognized clinical importance as a target for neuroleptic (antipsychotic) drugs based on the observed *in vitro* affinity for this compound class (Table 4- 2).[38]

The dopamine D_3 receptor was cloned and characterized by Sokoloff and coworkers in 1990.[16] This ground-breaking work not only expanded the family of the dopamine receptor subtype, but also reported a higher affinity for dopamine and its agonists for the D_3 receptors compared to the D_2 receptor.[16,19,22,38] The pivotal paper characterizing the D_3 receptor by Sokoloff reports a dopamine K_{iD2} 474±33 nM and K_{iD3} 25±3 nM, or roughly 19-fold (K_{iD2}/K_{iD3}) higher affinity at the D_3 receptor.[26] The D_2 receptors are found mainly in the nucleus accumbens, striatum, and olfactory tubercle, as well as

the substantia nigra pars compact and the ventral tegmental area (Figure 4- 3).[22,39] The D_3 receptor is expressed in brain regions associated with reward, motivation, emotion, and motion.[37,38,40] This includes a more restricted distribution in the nucleus accumbens and islands of Calleja, supporting its role in limbic brain functions.[29,32,38,41,42]

The dopamine D_2-like receptors exist in two states: a high affinity (D_2 high or D_{2High}) which is linked to second messenger systems (G-protein uncoupled) and a high affinity for agonists, and a low affinity state (D_2 low or D_{2Low}) which has a lower affinity for agonists and is functionally inert.[43] In this case, D_2R antagonists have equal affinity to both states, while the endogenous ligand dopamine, preferentially binds to the D_{2High}.[44,45] In the case of D_3 receptors, the existence of G protein-coupled/uncoupled and high vs. low affinity states is still debated and remains controversial.[26,46] This phenomena will be discussed further with regard to PET ligands. Regardless, it is well established that the D_3 receptors have roughly 20-fold higher affinity for dopamine than the D_2 receptor.[26]

Dopamine D_3 receptors also appear to function as autoreceptors (presynaptic receptor), with an inhibitory effect on dopamine release and on impulse flow.[47,48] This was further demonstrated in D_3R-null mice ($D_3R^{-/-}$), whereby these animals had extracellular dopamine twice as high as their wild-type littermates. Consistent with the idea that these receptors are also located presynaptically, the release of dopamine would be inhibited in the wild-type animal.[49–51]

Translating a nonselective D_2/D_3 ligand into a D_3 selective ligand has had mixed success. In addition to overcoming mixed binding of D_2/D_3, other major struggles to developing a D_3 selective PET tracer and pharmaceutical include off target binding to 5-HT receptors and/or sigma receptor subtypes, as well as BBB permeability.[33,52] Moreover,

the ability to study these receptors (D_2 and D_3) independently remains a challenge due to their high sequence homology (52%), and a striking 75% sequence homology in the 7 transmembrane domain (which contains the ligand binding domain).[26,33,38,52] The human D_3R (D_3 Receptor) was crystalized in 2010 by Chien and workers in complex with the D_2/D_3 antagonist eticlopride, with a resolution of 3.15 Å.[53] From here, structure-based drug design and structure-activity-relationship (SAR) studies were given a platform to blossom small molecule drug design off of.[32,53]

c. The Dopamine D_3 Receptor as a Drug Target

Neurotransmitter systems, such as the serotonergic and dopaminergic systems, are common pharmacological targets for therapeutics as well as PET imaging agents. Most antipsychotics do not show profound selectivity at the D_2/D_3R, but some show mixed binding or some D_3R preferring capacity (Table 4- 2) (a discussion of imaging agents at these systems is forthcoming).

Considerable work has been done in developing a D_3 selective ligand, building on computation screening of large compound libraries using a D_3R (D_3 Receptor) crystal structure or homology model, then utilizing a medicinal chemistry SAR approach to improve selectivity properties. Some notable groups targeting this receptor for substance use, neuropsychiatric disorders (for therapeutic or PET diagnostic purposes) include the Newman (largely therapeutic pursuits, with some interest in PET), Sokoloff (basic science and therapeutic interests), Micheli (therapeutic & diagnostic) and Mach (PET) group's.[3,19,26,32,35,36,53–77] PET is a valuable technique to quantify receptor populations and

confirm target engagement (a struggle with traditional drug design); as such, Mach and Volkow/Fowler are groups notable for their work in this area.[8,24,28,30,31,33,34,46,52,78–96] In an effort to identify vital pharmacophore features to develop D_3R selective agonists, extensive work has previously been done.[57,59,97–108] D_3R agonists, such as Pramipexole for treatment of Parkinson's Disease, mimic the action of dopamine at these receptors; D_3R antagonists essentially block this receptor and are typically antipsychotics used in such conditions as schizophrenia and bispolar disorder.[38,78,109,110] Even so, a distinct pharmacophore with full intrinsic activity and selective for the DA-D_3R has remained intangible.

Table 4- 2 Selected Antipsychotics & Binding (pK_i) to Serotonergic and Dopaminergic Receptors

pKi	5-HT_{1A}	5-HT_{2A}	5-HT_{2B}	5-HT_{2C}	D_1R	$D_{2L}R$	$D_{2S}R$	D_3R	D_4R	D_5R
Asenapine	8.6 (a)	10.15 (a)	9.75 (a)	10.46 (a)	8.85 (a)	8.9 (a)	8.84 (a)	9.38 (a)	8.95 (a)	ND
Aripiprazole	8.57 (a)	8.02 (a)	9.59 (a)	7.55 (a)	6.09 (a)	8.94 (a)	8.91 (a)	8.85 (a)	6.89 (a)	5.77 (b)
Ziprasidone	9.01 (a)	9.51 (a)	9.08 (a)	9.01 (a)	8.45 (a)	8.09 (a)	7.99 (a)	8.35 (a)	7.33 (a)	6.81 (b)
Quietapine	6.78 (a)	6.81 (a)	7.33 (a)	5.98 (a)	6.71 (a)	6.38 (a)	6.32 (a)	6.41 (a)	5.5 (a)	7.8 (b)
Olanzapine	5.82 (a)	8.88 (a)	8.41 (a)	8.41 (a)	7.93 (a)	7.67 (a)	7.58 (a)	7.46 (a)	7.75 (a)	7.04 (b)
Risperidone	6.75 (a)	9.69 (a)	7.99 (a)	8.17 (a)	7.68 (a)	8.21 (a)	8.07 (a)	8.16 (a)	8.21 (a)	7.8 (b)
Clozapine	7.06 (a)	8.39 (a)	8.79 (a)	8.56 (a)	7.64 (a)	6.87 (a)	6.81 (a)	6.66 (a)	7.33 (a)	6.63 (b)
Haloperidol	6.29 (a)	7.28 (a)	6.48 (a)	5.79 (a)	8.2 (a)	8.84 (a)	8.76 (a)	8.56 (a)	8.83 (a)	6.9 (b)
Amisulpride	5.8 (b)	5.08 (b)	7.88 (b)	5 (b)	5 (b)	8.89 (b)	ND	8.62 (b)	5.63 (b)	5 (b)
Sulpiride	5 (b)	ND	ND	ND	5 (b)	8 (b)	ND	8.07 (b)	7.26 (b)	ND
Remoxipride	ND	5.31 (b)	ND	ND	ND	7.21 (c)	ND	6.73 (c)	6 (b)	ND
Cariprazine	8.59 (d)	7.73 (d)	9.24 (d)	6.87 (d)	ND	9.31 (d)	9.16 (d)	10.07 (d)	ND	ND

Trazodone	6.93 (b)	7.35 (b)	7.11 (b)	6.65 (b)	5.42 (b)	5.38 (b)	ND	ND	6.15 (b)	5 (b)
Blonaserin	6.09 (e)	9.09 (e)	ND	7.57 (e)	5.97 (e)	9.84 (e)	ND	9.3 (e)	6.82 (e)	5.58 (e)
Buspirone	7.54 (b)	6.86 (b)	6.67 (b)	6.31 (b)	ND	7.2 (f)	ND	7.52 (f)	6.97 (b)	ND

Figure Adapted from Leggio, et al, 2016.[51]
(a) Shahid, 2009[111], (b) Roth 2000[112], (c) Burstein 2005[113], (d) Kiss 2010[114], (e) Tenjin 2013[115], (f) Leggio 2014[116], (ND) Not Determined

Shortly after the D_3 receptor was cloned, 7-hydroxy-N,N-di-n-propyl-2-aminotetralin (7-OH-DPAT, Figure 4- 4), an aminotetraline derivative, was reported as being D_3R selective and used for the design of antagonists.[117] However, this strategy was abandoned due to quick *in vivo* clearance.[37,51,117] However, another design strategy utilizing the alkyl-chain-linked phenylpiperazine of the (currently known as) "classic D_3 receptor agonists/antagonists" included compound **126**, which displayed a 122-fold selectivity over D_2 receptors and K_i = 1.75 nM.[118] The distribution of the D_3 receptor is more limited than the D_2 receptor and its distribution was elucidated through the use of [^{3}H](+)-7-[^{3}H]hydroxy-*N,N*-di-*n*-propyl-2-aminotetralin ([^{3}H]-7-OH-DPAT). In transfected Chinese hamster ovary (CHO) cells, it was found that [^{3}H]-7-OH-DPAT is 100-fold more selective for D_3 over D_2, and the resultant autoradiography showed D_3 populations restricted to the islands of Calleja, lobules 9 and 10 of the cerebellum, nucleus accumbens, and the olfactory tubercle; moreover, while the D_2 binding in the dorsal striatum is high, D_3 binding is significantly low.[42,117]

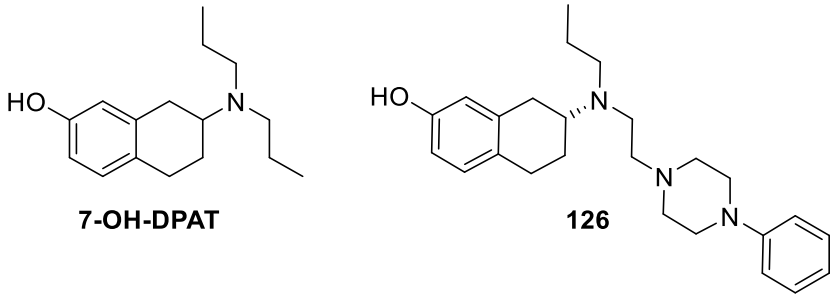

Figure 4- 4 D_3-selective 7-OH-DPAT

The tetrahydroisoquinoline derivative SB277011(A) was developed by GlaxoSmithKline (SmithKline Beecham) and characterized as a D_3R antagonist.[36,51,119,120] SB277011 was optimized to improve bioavailability and improve selectivity at the D_3 receptor (Figure 4- 7). To improve selectivity over 5-HT receptors, Stemp and colleagues added structural rigidity between the amide and azacyclic terminus, incorporated heteroatoms in the required aryl terminus, and included a cyano substitution to improve oral bioavailability and reduce lipophilicity.[36,120] Initial evaluation of this 2nd generation compound showed high D_3 receptor affinity (K_i = 10 nM) and > 100-fold selectivity over D_2, $5HT_{1B}$ and $5HT_{1D}$ receptors (Figure 4- 7).[36,119,120] However, this compound was not developed further as a therapeutic due to poor bioavailability in cynmolgus monkeys.[51,121]

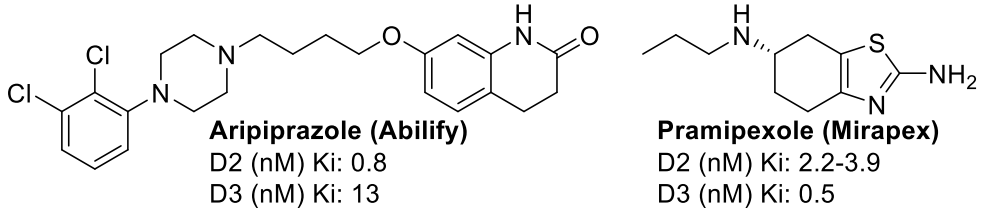

Figure 4- 5 Well-known D2/D3-preferring Pharmaceuticals

Regardless, the dopamine D_3R has proven to have therapeutic value for a variety of disorders (either by serendipity or design). For example, D_3 partial agonist aripiprazole (Abilify®) is used for treatment in schizophrenia, bipolar disorder, and manic depression, while agonist pramipexole (Mirapex®), an aminothiazole with negligible binding at serotonin receptors, is used for treating symptoms of Parkinson's disease (Figure 4-5).[122,123] Indeed major therapeutic interest for the D_3 receptor lies in Parkinson's disease, substance abuse/addiction, and other neurological diseases/disorders.[36,51,124,125] Based on promising findings with pramipexole, the scaffold has been utilized in several drug discovery programs to develop additional D_3 agonists / partial agonists (**127**, **128**) (Figure 4- 6).[126–130] The development of these compounds demonstrated the heteroaryl tolerance of binding selectively at the D_3 receptor (a summary of SAR at these receptors can be found in Figure 4- 9 and Figure 4- 10).[131–136]

Even with dedicated efforts by industry and academic research institutions (including 157 filed patents for novel D_3 antagonists from 2008-2012 alone), D_3-selective agonists and antagonists remain elusive and none are available for human therapeutic (or diagnostic) use.[124,137]

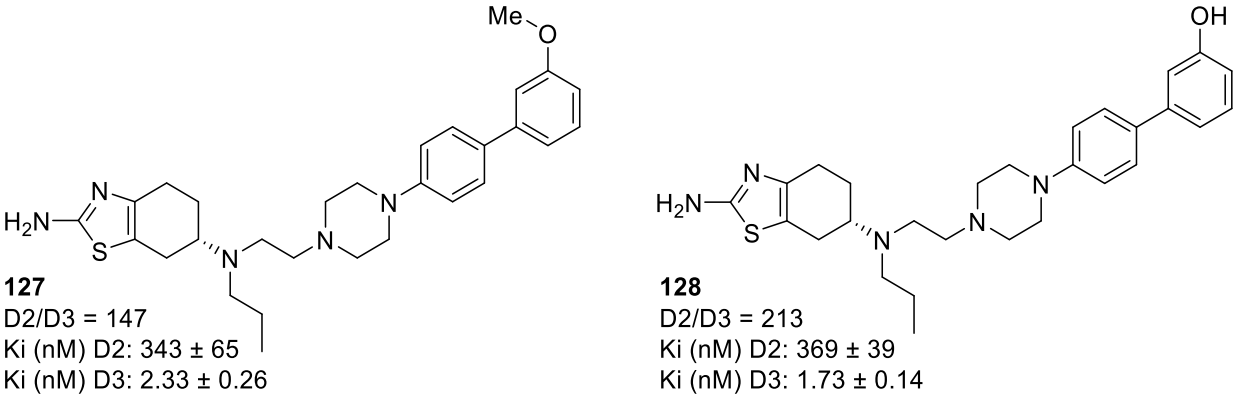

Figure 4- 6 Pramipexole-containing D3-selective compounds[130]

Some notable first generation D_3-selective agents include BP897 (Figure 4- 7), which was first reported in a French drug discovery program and identified as a dopamine D_3 receptor partial agonist. It was advertised to have potential in treating neuropsychiatric disorders, including depression, substance abuse and addiction, and Parkinson's disease.[36] Later, in 1999, BP897 was reported as a selective dopamine D_3 receptor partial agonist, exhibiting high-affinity binding at D_3 (K_i = 0.92 ± 0.2 nM), and 70-fold selectivity over D_2 receptors (K_i = 61 ± 0.2 nM). BP897 also has low affinities for D_1, D_4, α_1, α_2, $5HT_{1A}$, $5HT_7$, muscarinic, histamine, and opiate receptors. However, *in vivo* studies suggest that BP897 may behave as an antagonist.[55] Conflicting behavior *in vivo* and

discrepancies in ligand evaluation at the D_3 receptor across laboratories will be discussed later.

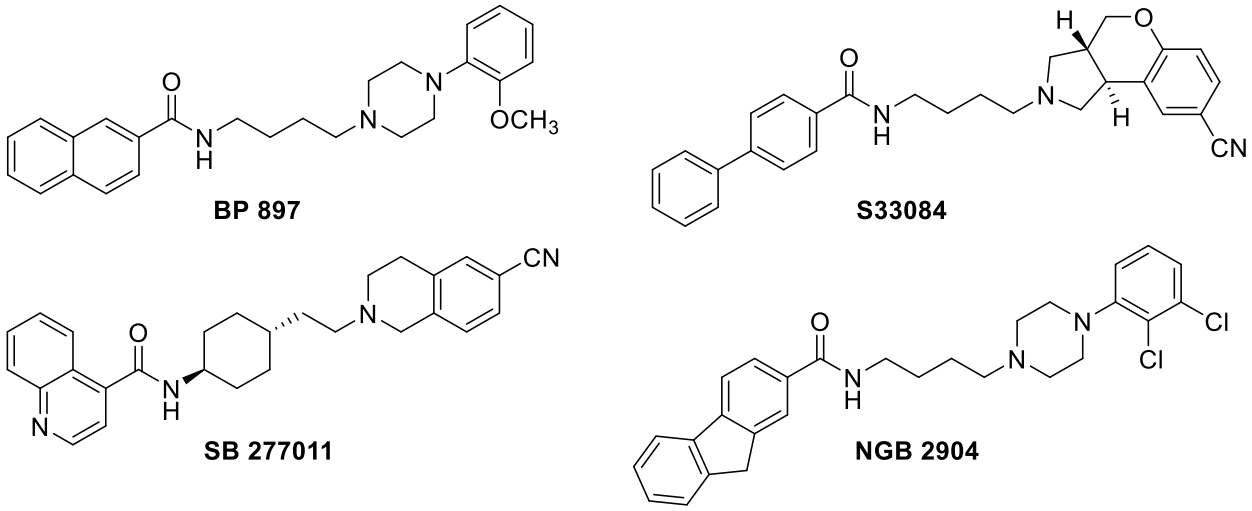

Figure 4- 7 "First Generation" D3-selective Agonists/Antagonists[36]

S33084 was defined as a potent, competitive, D_3-selective antagonist with >100-fold selectivity at the receptor, as demonstrated in over 20 receptor systems, characterized *in vitro* and *in vivo.* In a separate discovery synthetic drug discovery program, NG 2904 was identified as a lead for novel antipsychotic medications. NG 2904 shares the butylamide linker with BP897 and S33084, and demonstrated >150-fold selectivity over D_2 receptors (and similar selectivity over α1 and $5HT_2$ receptors). The butylamide functionality has shown to be optimal,[56,64,138] and reducing or increasing the linker length significantly decreases D_3 binding affinity and/or selectivity, as does the size of the terminal aromatic ring (Figure 4- 10).[36,64]

Moreover, Reilly and Mach recently reported a series of D_3 selective (264-905-fold selective over D_2) antagonists with diazaspiro alkane cores.[139]

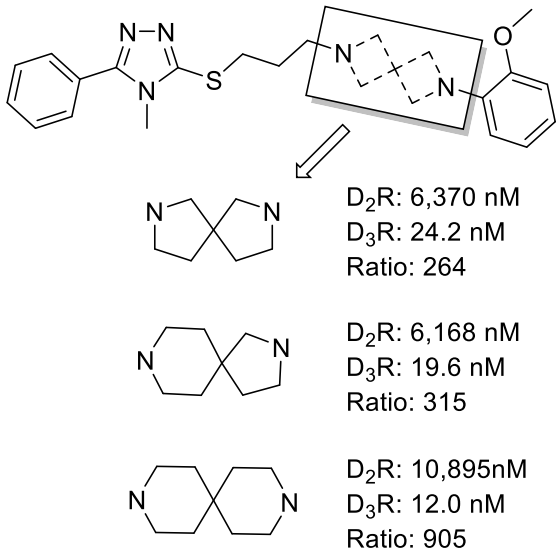

Figure 4- 8 Novel D3-Selective Antagonists With Diazaspiro Alkane Cores[139]

The SAR of the most selective D_3 compounds follow a strict skeleton. The phenyl piperazine, or 1,4-disubstituted aromatic piperadine/piperazine, is considered a "privileged scaffold" at these GPCRs, and the amide moiety is preferred for selectivity. The aryl ring system is tolerant of heteroatoms, to aid in optimizing logP and BBB permeability, and sometimes improving D_3 binding affinities (Figure 4- 9, Figure 4- 10). Constraints of the linker are associated with loss of selectivity at the receptor.[36] Computational and SAR studies to further explore the selectivity at these receptors continue to be reported.[89,102,107,131,132,140,141]

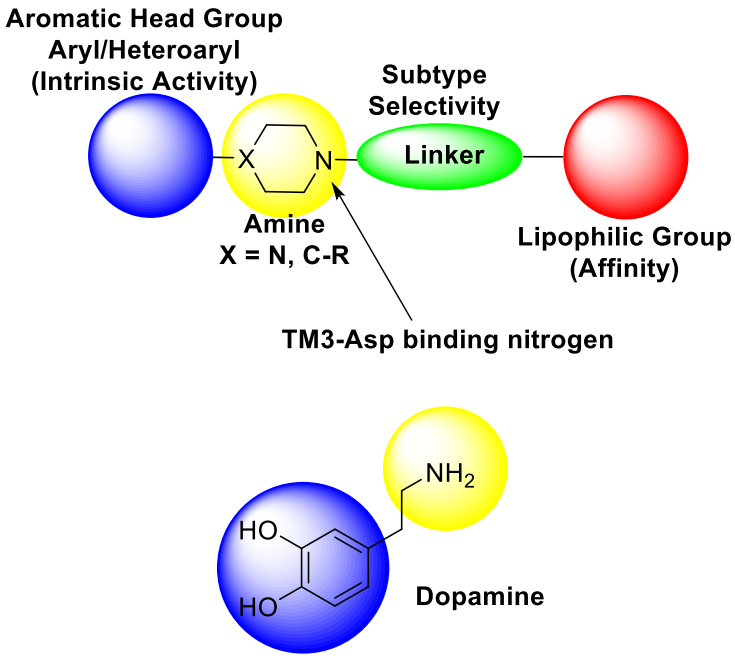

Figure 4- 9 Toward Dopamine Receptor Subtype Selectivity: The Anatomy of 1,4-disubstituted Aromatic Piperidines and Piperazines

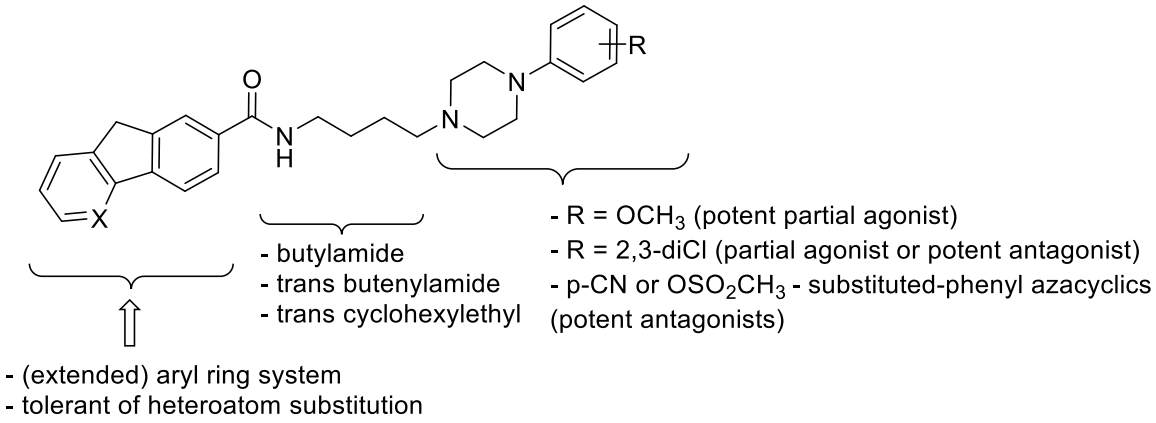

Figure 4- 10 General SAR of DAD3R Partial Agonists & Antagonists[36]

d. Challenges to The Development of a D_3-Selective Ligand

It should be noted that several discrepancies in binding affinities/selectivity's across laboratories have been reported. Comparing affinity and selectivity binding data

from *in vitro* to *in vivo* data, and with different assay conditions and model systems, have been vastly different. In short, "*[t]he absolute values were vastly different, which provides a significant challenge to medicinal chemists trying to identify pharmacophores and functional groups that will optimize both pharmacological specificity and bioavailability*" (Newman, et al 2005).[36] Newman and colleagues go on to argue that the binding data collected from cloned receptors expressed in cell lines and subsequently tested under non physiological conditions are useful tools to guide discovery; however, functional assays are more valuable predictors of *in vivo* action and selectivity at the receptor.[36,142]

A more creative approach to designing D_3 ligands is lacking, and is further limited by the narrow range from which the selectivity skeleton (pharmacophore) of these ligands rise from. Designing ligands that contain the desired pharmacophore features and which have reasonable lipophilicities for brain penetrance (cLogD < 5, or cLogP < 5) has proven difficult, and continues to challenge the utility of the currently available agents. Lastly, inconsistent *in vitro* and *in vivo* data across laboratories make comparisons and further development an ongoing challenge. Because of the limited and inconsistent evaluation of these ligands in multiple assays, *in vitro* and functional, utilizing SAR to predict selectivity and efficacy is deficient. All of these challenges have hindered the development of selective therapeutics and PET radioligands for *in vitro* assays in brain tissue instead of in cloned receptors.

Examining these receptors *in vivo* through PET and brain receptor occupancy studies has also been problematic (further hindered by inadequate selectivity and unfavorable lipophilicities). Non-selective D_2/D_3 PET ligands are available and may provide some insight. However, radioligands (as well as antipsychotic therapeutics, for

example) suffer from competition with endogenous dopamine at the receptor. This raises the concentration required to inhibit these receptors. In terms of therapeutics (e.g. antipsychotics), the drug concentration needed to occupy 75% of D_2 receptors is roughly three times higher than occupying 50% of the receptors.[143] Dopamine has a higher affinity for the D_3 receptor (vs D_2), further complicating the requirements to adequately engage the target of interest.[144,145]

"D_3-preferring" compounds are defined as those that bind primarily to D_3 receptors with at least 10-fold higher affinity than the second best target (*in vitro*).[124] Selectivity values for D_3 over D_2 are expressed as a ratio of D_2/D_3; in regard to *in vivo* selectivity, this ratio should be >100 fold.[36,39] Within this realm, the D_3-preferring D_2/D_3 mixed agonist pramipexole as well as ropinirole, can be dosed in the low effective dose range to primarily bind the D_3 receptors, and deliver the specific, desired pharmacodynamic effects; this was successfully shown with these compounds and in patients with restless leg syndrome.[124,146,147]

Dopamine receptors are a well-known target for antipsychotics, and as such, PET tracers can aid drug discovery by confirming target engagement and quantifying receptor occupancy. Roughly 75% receptor occupancy of the D_2 receptors at therapeutic maintenance (concentrations) of antipsychotics is required.[143,148] *In vitro* estimates of D_2:D_3 selectivity of selected antipsychotics and the predicted occupancy at these receptors were also reported (Table 4- 3), supporting a role for the D_3 receptor in the development of therapeutics.[21,42,43,149,150]

Table 4- 3 D2:D3 selectivity for selected antipsychotic drugs[42]

Antipsychotic	# Studies	D2:D3 Selectivity	D2 Occupancy	**D3 Occupancy
Clozapine	9	2.82 ± 2.01	60%	35%
Haloperidol	11	3.03 ± 4.42	75%	50%
Risperidone	3	4.9 ± 3.71	75%	38%
Olanzapine	1	3.18	75%	49%
Amisulpride lo	3	2.29 ± 0.58	67%	47%
Amisulpride hi	3	2.29 ± 0.58	80%	64%
Raclopride	3	1.16 ± 0.53	*	*
*No occupancy estimated for raclopride.**Predicted Values based on previous reports, Levant, 1997, Schotte, 1996.[21,150]				

A selective D_3 receptor PET ligand would provide insight in the pharmacological/therapeutic utility at this receptor, assess receptor occupancy in real time, and evaluate the effects of substance abuse (and further boost the development of therapeutics for this purpose).

e. Functional Imaging of Neurotransmitter Systems & Other Considerations

PET and SPECT are non-invasive, functional imaging techniques that can provide valuable information on receptor densities, neurotransmitter synthesis, and give insight into the underlying mechanisms and pathogenesis of diseases and disorders *in vivo*. Imaging neurotransmitter systems is widely conducted in nuclear medicine, and a variety of tracers exist for this purpose. These include radioligands for dopaminergic neurotransmission, serotoninergic neurotransmission, norepinephrine

neurotransmission, acetylcholine, central/peripheral or direct benzodiazepine site receptor ligands, glutamate neurotransmission, cannabinoid neurotransmission and opioid receptors. While all of these systems will not be discussed in depth, a representative list of PET radioligands used for functional neuroimaging is provided in Table 4- 4 (and Table 4- 5).[39,151,152]

Table 4- 4 Neurotransmitter System and Selected PET Radioligands[39,151]

Neurotransmitter System	Tracer/Ligand
Serotonin 5-HT_{1A}	[Carbonyl-^{11}C]-WAY-100635, [^{11}C]DWAY, [^{11}C]FCWAY, [^{11}C]NAD299, [^{18}F]MPPF
Serotonin 5-HT_{2A}	[^{11}C]NMSP, [^{11}C]MDL100907, [^{18}F]Altanserin, [^{18}F]Setoperone
Serotonin Transporter (5-HTT)	[^{11}C]DASB, [^{11}C]MADAM, [^{11}C]McN5652, [^{11}C]nor-β-CIT
Norepinephrine Transporter	[^{11}C]MENER, [^{18}F]FMeNER, [^{18}F]FD2MeNER, [^{11}C]Desipramine, [^{11}C]Talopram, [^{11}C]Talsupram
Glutamate	[^{11}C]MPEP, [^{11}C]JNJ-16567083
Opiate	[^{11}C]Diprenorphine, [^{11}C]Carfentanil, [^{18}F]Clyclofoxy, [^{11}C]LY2795050
Muscarinic	[^{11}C]NMPD, [^{11}C]3-MPB, [^{11}C]Benztropine
Nicotinic	[^{11}C]-Nicotine, [^{11}C]Mecamylamine, 2-[^{18}F]Fluoro-A-85380, [^{18}F]Nifene, (-)-[^{18}F]Flubatine
Histamine	[^{11}C]Doxepin, [^{11}C]Pyrilamine
Adenosine	[^{11}C]MDPX, [^{18}F]CDFPX
GABA-benzodiazepine	[^{11}C]-Flumazenil, [^{11}C]-RO 5-4513
Peripheral benzodiazepine	[^{11}C]-Vinpocetine, [^{11}C]DAA1106

For our purposes, as with any CNS drug discovery undertaking, certain considerations are taken when designing ligands or selecting lead compounds for further

evaluation. Important parameters to consider with regard to *in vivo* imaging of neurotransmitter systems with PET include, but are not limited to: selectivity (relative to competing binding sites, >100-fold is desired), and sufficient affinity to the target dependent on target expression level, binding potential (BP), occupancy, receptor saturation, target affinity/nonspecific affinity ratio, toxicity, low plasma protein binding, concentration in binding sites (B_{max}), low nonspecific binding, and BBB permeability (log P < 5). Considerations for logP are in terms of specific binding for functional PET radiotracer development, certainly as the range of logP for CNS therapeutics and tracers is wide ranging.[153] Other parameters and criteria include the presence of labeled metabolites. This is, such that if they occur, they are found in low concentrations, ideally do not penetrate the CNS and are cleared rapidly. This consideration follows the design of the compound such that the radiolabeled position is not subject to rapid metabolism and passes the BBB.[39]

f. Functional Imaging of the Dopaminergic System: PET & SPECT

Several radiotracers exist in imaging the dopaminergic system. This includes imaging dopamine synthesis and turnover, imaging the dopamine transporter (DAT), dopamine receptors, and the vesicular monoamine transporter type-2 (VMAT2) (Table 4-5.).

Table 4- 5 Selected PET and SPECT Tracers Targeting the Dopaminergic System

Target	PET or SPECT Tracer	Clinical studies/Relevance
Dopamine Synthesis & Turn Over	[^{18}F]DOPA	PD, gene therapy for PD, ADHD, Schizophrenia
	[^{18}F]FMT	Gene therapy for PD
Dopamine Transporter	[^{11}C]CFT	Heroine abuse
	[^{11}C]altropane	ADHD
	[^{123}I]-β-CIT (Dopascan)	PD, PM, cocaine abuse
	[^{123}I]-FP-CIT (DaTSCAN)	PM, ET, PD, DLB, ADHD, Schizophrenia
	[^{99m}Tc]-TRODAT-1	PD, MSA, PM, VP, DRD, PSP, genetic study of PD and MJD, cocaine and opiate abuse, nicotine dependence, ADHD
	[^{123}I]altropane	PD, ADHD
	[^{123}I]IPT	ADHD
Dopamine D1 Receptor	[^{11}C]NNC-112	Schizophrenia
	[^{11}C]SCH-23390	Schizophrenia
Dopamine D2 Receptor	[^{11}C]Raclopride	Drug abuse (cocaine, methamphetamine, opiate), alcohol dependence, ADHD, antipsychotics
	[^{123}I]IBZM	PM, schizophrenia, antipsychotics
Vesicular monoamine transporter type-2 (VMAT2)	[^{11}C]DTBZ	PD
	[^{18}F]RP-DTBZ (AV-133)	PD, DLB, AD

Abbreviations: Parkinson's Disease (PD), Parkinsonism (PM), multiple-system atrophy (MSA), progressive supranuclear palsy (PSP), essential tremor (ET), vascular Parkinsonism (VP), Machado-Joseph disease (MJD), DOPA-responsive dystonia (DRD), dementia with Lewy bodies disease (DLB), Alzheimer's disease (AD), attention deficit hyperactivity disorder (ADHD).

Table adapted and appropriate clinical references can be found in Shen et al, 2012.[154]

i. SPECT and DaTSCAN™

SPECT, while it is not as sensitive as PET (limited primarily by technology: collimators and detectors in gamma cameras), allows for a longer time window of observation due to the longer half-life of the single photon emitters.[155] SPECT is an attractive imaging modality due to the reduced scan cost, and availability of ligands (longer half-life makes for easier transport). A common SPECT radionuclide is iodine-123, which has a half-life of roughly 13 hours and produces 159 keV gamma photon energy.

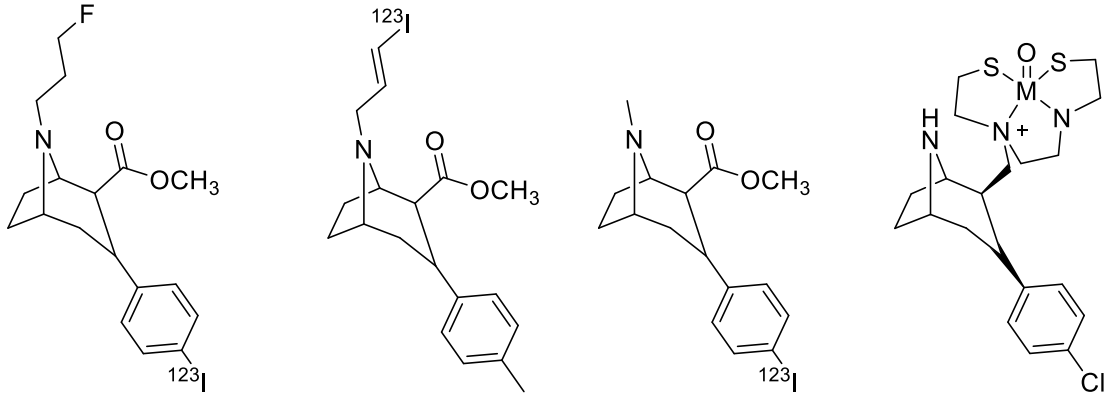

[^{123}I]-FP-CIT
^{123}I-ioflupane, DaTScan

[^{123}I]-PE21

[^{123}I]-β-CIT
Dopascan

[^{99}Tc]TRODAT-1
M = ^{99m}Tc

Figure 4- 11 Selected DAT Radioligands[156]

A hallmark of Parkinson's disease (PD) is a notable reduction in striatal dopaminergic neurons, as such, these imaging agents allow for a quantitative and spatial distribution of these transporters. SPECT ligands used clinically to detect high striatal DAT binding for the diagnosis of Parkinson's disease include: ^{123}I-β-CIT (Dopascan), ^{123}I-

PE21, ^{123}I-IPT, ^{123}I-FP-CIT (^{123}I-ioflupane, DaTScan^{TM}), and ^{99m}Tc-TRODAT-1 (Figure 4-11.[154,157] In the nigrostriatal pathway, the plasma membrane dopamine transporter (DAT) mediates dopamine re-uptake.[158]

^{123}I-β-CIT (Dopascan) was the first widely used DAT imaging agent, but suffered from lack of selectivity. ^{123}I-β-CIT (Dopascan) binds to DAT, as well as the serotonin transporter (SERT) and norepinephrine transporter (NET). The kinetics of this tracer are non-optimal, as scan times should be performed 20-30 hours post injection. The development of ^{123}I-FP-CIT (^{123}I-ioflupane, DaTScan^{TM}), a cocaine analog (Scheme 4- 3), helps combat these issues with faster kinetics which allow imaging as early as 3 hours following injection.[154] DaTSCAN is a relatively new imaging procedure, approved by the FDA in 2011, and is widely used to distinguish Parkinson's disease from essential tremor (Figure 4- 12).[159]

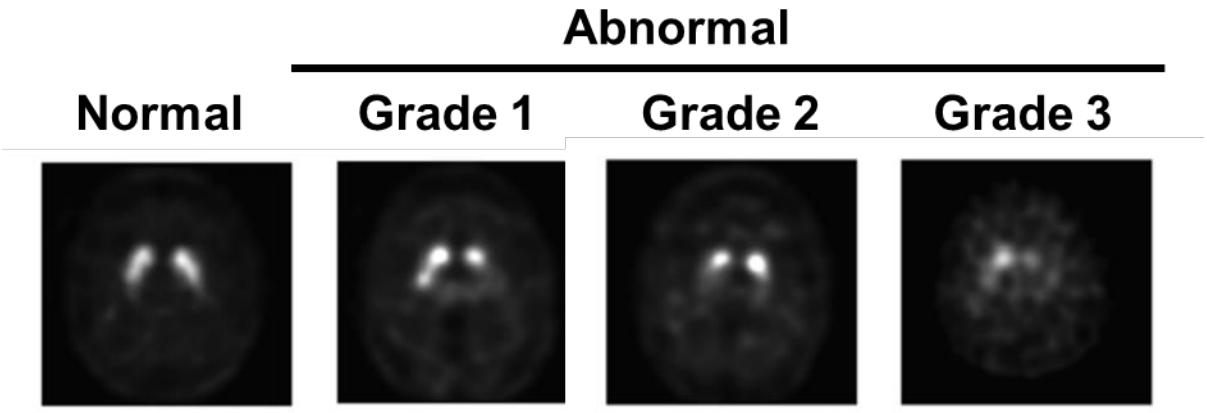

Figure 4- 12 DaTScan. Grades characterized by appearance of the striata, or the progressive loss of neurons in the caudate and putamen. Image: Public Domain © FDA prescribing website for DaTScan. https://www.accessdata.fda.gov/drugsatfda_docs/label/2015/022454Orig1s004lbl.pdf

While it has >97% diagnostic sensitivity for PD, other diseases that also experience a loss in dopaminergic neurons will be non-distinguishable with this method, including Progressive Supranuclear Palsy (PSP), Multiple Systems Atrophy (MSA) and Corticobasal Degeneration (CBD) (Michael J. Fox Foundation for Parkinson's Research). Other uses for DaTSCAN™ are being explored, including depression and other neuropsychiatric disorders, however patient heterogeneity continue to contribute to conflicting results.[160]

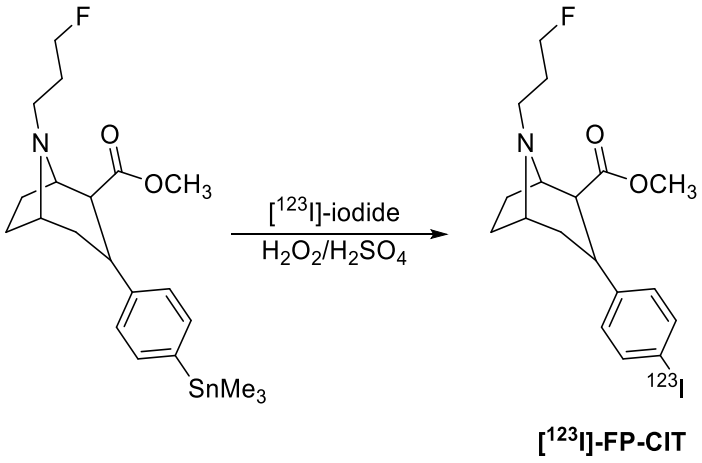

Scheme 4- 3 DaTSCAN™,[^{123}I]ioflupane

Another option for SPECT imaging of these neurons is [^{123}I]IBZM (Scheme 4- 4).[161] [^{123}I]IBZM is a D_2/D_3 (D_2 preferring) antagonist used to measure postsynaptic DA. It was used effectively to measure density in nonhuman primates and human SPECT studies.[162–165]

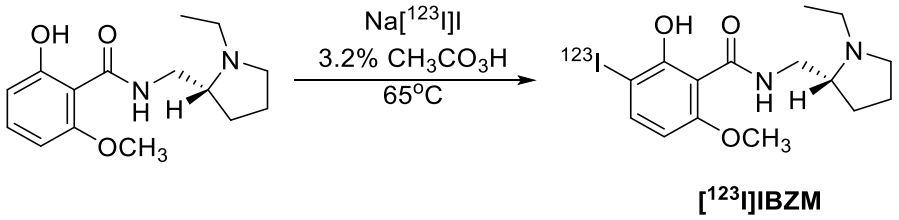

[^{123}I]IBZM

Scheme 4- 4 Electrophilic Iodination of [^{123}I]IBZM

ii. Positron Emission Tomography & The Dopaminergic System

PET offers a higher sensitivity (by two to three orders of magnitude) over SPECT, allowing for the ability to detect a higher number of emitted events. Spatial resolution in PET is limited by physics (whereas in SPECT it is limited by collimator design), such as photon non-collinearity and positron range; this, however, can be modeled in the reconstruction phase of imaging analysis. Another advantage of PET is the shorter half-lives of the radionuclides, which allows for higher activities injected in the patient. The concern here is radioactive accumulation over time with regard to dosing.[155] Multiple scans per day are also an option when using a radionuclide with a shorter half-life, such as carbon-11. PET has a clear advantage of quantitative instrumentation, versatile radionuclides, and selection of tracers. Moreover, PET is a useful tool in the development of CNS drugs to asses BBB permeability, target engagement, occupancy, and PD/PK considerations.[166] For these reasons, and due to the enhanced resolution and spatial clarity of PET, our focus is on developing a selective PET radioligand for imaging the D_3 receptor in neurological diseases and disorders,.[6]

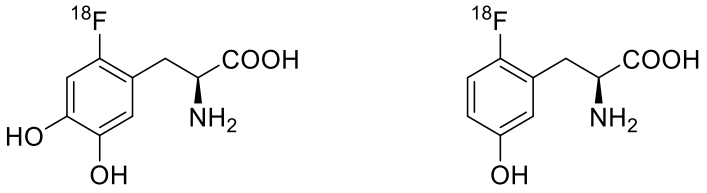

[^{18}F]FDOPA **[^{18}F]FMT**

Figure 4- 13 Pre-synaptic DA Imaging with [^{18}F]DOPA and [^{18}F]FMT

Pre-synaptically, 6-[^{18}F]fluoro-3,4-dihydroxyphenylalanine ([^{18}F]DOPA) is a widely used tracer for the imaging of dopaminergic metabolism and was first used in human studies in 1983.[167] [^{18}F]DOPA is an L-DOPA analog, and is used to visualize the activity of AAAD or AADC (aromatic L-amino acid decarboxylase (Scheme 4- 1, Figure 4- 13). When [^{18}F]DOPA is taken up in the dopaminergic neuron by the amino acid transporter, LAT-1 (large-neutral-amino-acid transporter), it is decarboxylated by AADC to generate [^{18}F]fluorodopamine (or [^{11}C]dopamine if [^{11}C]DOPA is used) which is stored in vesicles. However, a shortcoming of this approach is that [^{18}F]DOPA in the periphery and CNS is methylated by catecholamine-*O*-methyltransferase (COMT), producing 6-[^{18}F]fluoro-3-*O*-methyl-DOPA. This labeled product crosses the BBB and needs to be kinetically modeled to address its interference in imaging.

6-[^{18}F]Fluoro-L-*m* tyrosine ([^{18}F]FMT) is an alternative tracer that is still a substrate for AAAD/AADC, but not COMT, thus reducing the requirement for multicompartment kinetic modeling.[151,168] While AADC in dopaminergic neurons is of interest, it is important to note that this enzyme also plays a role in other monoamine transmitters (5-HT), and [^{18}F]DOPA and [^{18}F]FMT (Figure 4- 13) are also converted in serotonergic and noradrenergic neurons. Even so, the accumulation of these tracers in the striatum is predominantly in nigrostriatal dopaminergic neurons.[151]

In a more general sense, a useful way to image neurodegenerative diseases characteristic to the loss of a particular type of neuron (such as the loss of dopaminergic neurons in the basal ganglia as a marker of Parkinson's disease), is through targeting of the membrane-bound protein, vesicular monoamine transporter type 2 (VMAT2). Imaging of VMAT2 can be pursued *via* [^{11}C]DTBZ ((+)-α-[^{11}C]dihydrotetrabenazine). VMAT2 functions to transport monoamines from the cytosol into storage vesicles prior to release into the synapse – this transporter is not specific, but rather it is used in the handling of dopamine, norepinephrine, serotonin, and histamine.[151,169]

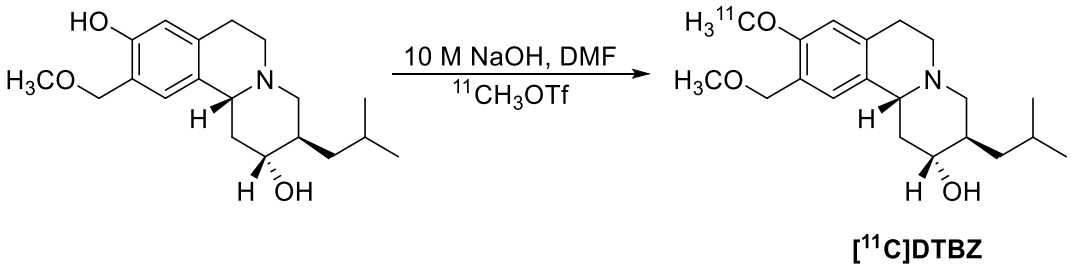

Scheme 4- 5 Synthesis of [^{11}C]DTBZ

The imaging of VMAT2 in neurodegenerative disease has significant utility due to the compartmentalization of the neuronal type in the human brain. [^{11}C]DTBZ (Scheme 4- 5) was developed out of the University of Michigan, Ann Arbor (Michael R. Kilbourn, Robert A. Koeppe, and David E. Kuhl). An analog labelled with fluorine-18, [^{18}F]Fluoropropyl-(+)-DTBZ, has also been developed for potential commercialization (the longer half-life of fluorine-18 is suited to transport). This tracer has been licensed to Avid Radiopharmaceuticals (as [^{18}F]AV-133), and has been employed in a number of clinical trials from 2012 to 2016 (including "A trial of 18F-AV-133 Positron Emission Tomography

(PET) Imaging to Differentiate Subjects with Parkinson's Disease (PD) From Other Movement Disorders"; Clinical Trials as reported by the U.S. National Institutes of Health, NCT01550484).[169]

Targeting the dopamine D_1 receptors is another ongoing pursuit in developing PET radioligands for the dopaminergic system. Even though the D_1 receptor was the first of the subtypes to be identified, the functional and pharmacological profile of this receptor is largely unknown.[170] The most widely used of the available radioligands antagonists including *(R)*-(+)-[^{11}C]SCH 23390, (+)-[^{11}C]NNC 112, and (+)-[^{11}C]A-69024, and full/partial agonists including the SKF series and *(S)*-[^{11}C]*N*-Methyl-NNC 010259 (Figure 4- 14).[171–175] The first of these, benzazepine [^{11}C]SCH 23390, showed only moderate D_1 to 5-HT_{2A} receptor selectivity *in vitro*, but was found to be D_1-selective *in vivo*. Radioligand [^{11}C]NNC 112 has better specific/nonspecific ratios in humans compared to [^{11}C]SCH 23390, but both ligands have been used to better understand dopamine activity in neuropsychiatric diseases/disorders, including schizophrenia.[176]

Unlike the D_2 receptors, the D_1 receptor does not show sensitivity to (pharmacological modulation of) endogenous dopamine release. This could be due to several reasons: (1) that these receptors are located largely extra-synaptically, (2) that these receptors have a lower affinity to their endogenous ligand, dopamine (compared to the D_2 receptor), and that (3) a small fraction of this receptor is in the high-affinity state.[171] Moreover, differences in the distribution of the D_1 receptors, as identified by agonists and antagonists, is not well understood. The affinity state of this receptor is speculated as the main reason for the discrepancy.

As with the D_2 receptor, the D_1 receptor also exists in a high or low affinity state. Richfield, et al[177] used quantitative autoradiography to determine the affinity states of the D_1 and D_2 receptor. They found that the D_1 receptor, without exogenous guanine nucleotides and nonselective dopamine competitors, is primarily in the low affinity agonist state (~80%), while the D_2 receptor exists primarily in the high affinity (agonist) state at ~77%. Receptor occupancy from D_1 to D_2 (with agonist or antagonist) did not influence the affinity states of either one, showing that an interaction between these two receptor types is not responsible for the different affinity states. Difficulties with assigning a specific role to the D_1 receptor may be the result of the low proportion of the receptor in the high affinity state.[177] The identification of D_2 selective ligands has shed light on the biological role of this receptor class, while the D_1 receptor still suffers from conflicting results due to many complicating factors in the dopaminergic system and behavior of these receptors.[176]

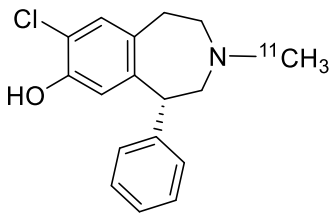

***(R)*-(+)-[^{11}C]SCH 23390**

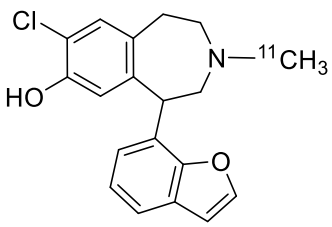

(+)-[^{11}C]NNC 112

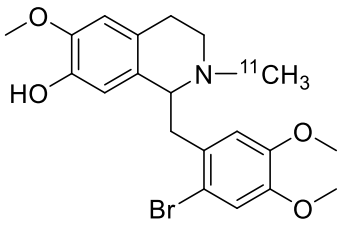

(+)-[^{11}C]A-69024

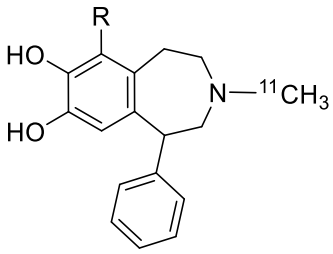

R = H (+)-[^{11}C]SKF 75670
R = Cl (+)-[^{11}C]SKF 82957

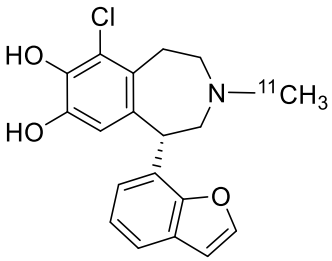

***(S)*-[^{11}C]*N*-Methyl-NNC 010259**

Authors report ambiguity with absolute configuration of these ligands.
These are largely identified and based on similarity with *(R)*-(+)-SCH 23390 configuration

Figure 4- 14 Dopamine D1 Receptor PET radioligands[171]

Post-synaptically, the dopamine D_2 receptor is most widely imaged *via* "the gold standard" [^{11}C]raclopride (previously known as S-(-)-[^{11}C]FLA 870), as well as [^{18}F]fallypride (an analog of epidepride), and [^{11}C]3-*N*-methyl-spiperone; and the dopamine D_3 receptor with 4aR,10bR)-4-(propyl-1-11C)-3,4,4a,5,6,10b-hexahydro-2H-naphtho[1,2-b][1,4]oxazin-9-ol ([^{11}C]-(+)-PHNO) (Figure 4- 15, Figure 4-16).[46,142,169,178,179]

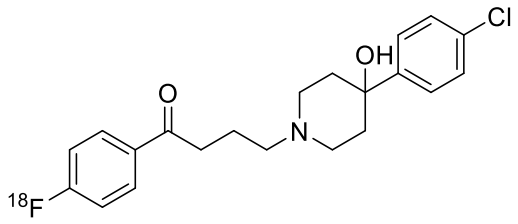

[^{18}F]Haloperidol
D_2: 1.4 nM
D_3: 2.0 nM

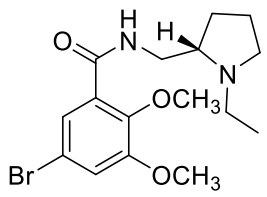

[^{18}F]FLB457
D_2: 0.02 nM
D_3: 0.017 nM

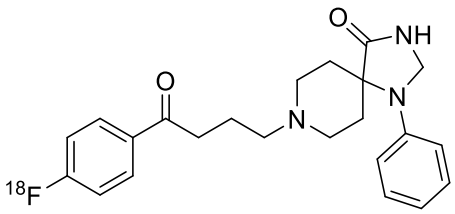

[^{18}F]Spiperone
D_2: 0.058 nM
D_3: 0.98 nM
5-HT$_2$: 0.45 nM

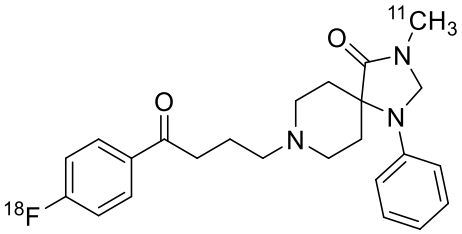

[^{18}F/^{11}C]N-methylspiperone
D_2: 0.12 nM
D_3: 1.4 nM
5-HT$_2$: 0.55 nM

Figure 4- 15 Other D2/D3 Radioligands[46]

The radiosyntheses of [^{11}C]raclopride (**91**) and [^{18}F]fallypride (**129**) are straightforward, with [^{11}C]MeOTf methylation at the tetrabutyl ammonium phenoxide precursor (**90**) for [^{11}C]raclopride (**91**), and a one-step aliphatic nucleophilic substitution of the tosylate precursor (**130**) with [^{18}F]KF for [^{18}F]fallypride (**129**) (Scheme 4- 6).[169] [^{18}F]Fallypride and [^{11}C]raclopride are high affinity D_2/D_3 antagonists. While (the gold standard) [^{11}C]raclopride is used for the imaging of D_2 receptors, it still has modest affinity for D_3 receptors (K_d D_2 =1.6 nM, and K_d D_3 = 18 nM as measured with [^{13}H]raclopride).[90,180]

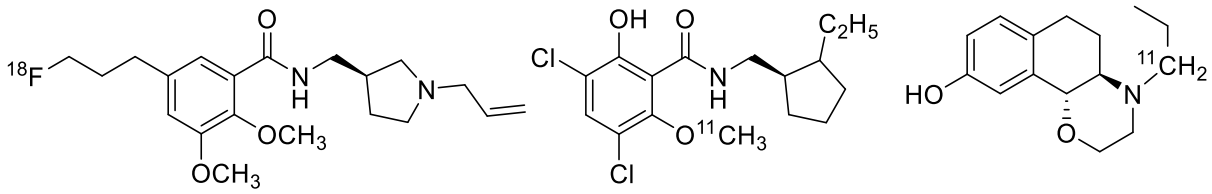

Figure 4- 16 Postsynaptic Dopamine Receptor Radiotracers: In the Clinic

[^{11}C]raclopride (**91**) is used extensively in the clinic to study neuropsychiatric disorders associated with D_2 receptors, including schizophrenia, Parkinson's disease, stress, and depression.[45,169,181–188] Other interests in imaging the dopamine receptors is in respect to understanding their underlying role in substance abuse, behavioral reinforcement and reward, and to support development of antipsychotic therapeutics.[185,189,190]

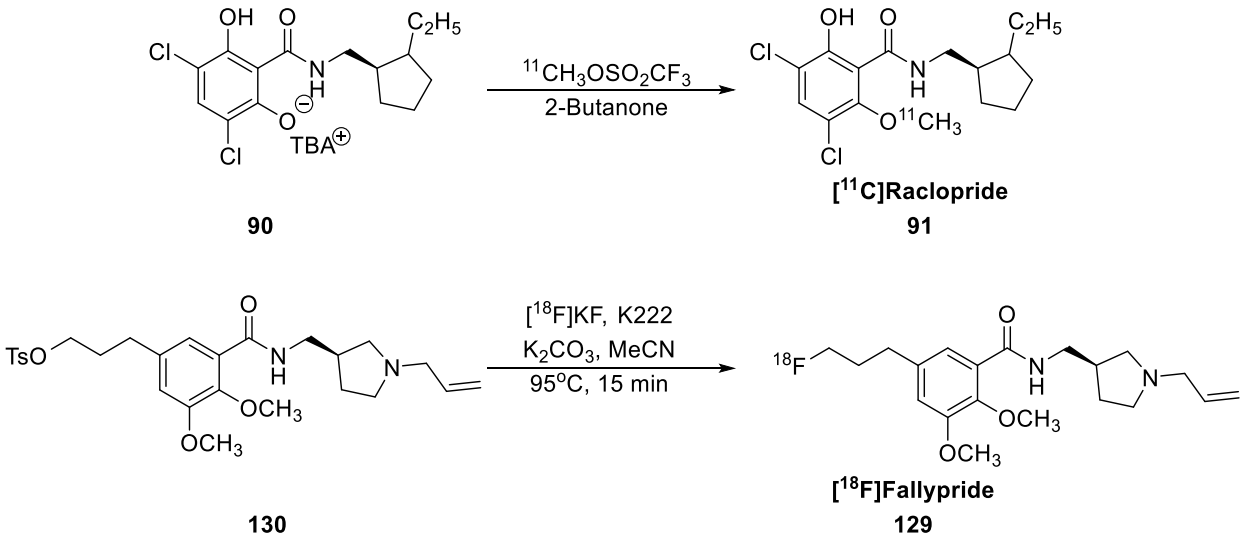

Scheme 4- 6 Radiosynthesis of [^{11}C]Raclopride and [^{18}F]Fallypride for Dopamine D2 Receptor PET Imaging

Similar to other G-protein-coupled receptors, dopamine D_2 receptors exist in a high- and low-affinity state for agonists (D_{2H} and D_{2L}), regardless of which type of G-protein they couple to (G_s, $G_{i/o}$, etc). Agonists bind with higher affinity to the G protein-coupled state, a process involving Mg^{2+} ions. This is such that Mg acts to lock the α unit of the G protein into conformation from where the $G\alpha$ dissociates from the $G\beta\gamma$.[191] In this way, Mg^{2+} and other cations (such as Na^+) act as allosteric modulators at GPCRs.[192,193] Interestingly, guanine nucleotides (guanosine diphosphate/GDP, guanosine triphosphate/GTP) were found to convert high affinity to low affinity D_2 receptor binding to agonist [^{3}H]spiperone.[194] Taken together, given the role of guanine nucleotides and ions, experimental conditions and methods can promote or hinder the detection of the high-affinity (dopamine) receptor state (Mg^{2+} to detect the high affinity state, and Na^+ to hinder the high-affinity state). While the D_3 receptor is not reported to have a high/low-affinity state, it is important to note experimental conditions when evaluating selectivity of these ligands from *in vitro* to *in vivo* behavior.[194–196] [^{11}C]-(+)-PHNO, an agonist, shows no preferential binding to the high or low affinity D_2 state, perhaps due to its preferential

binding at the D_3 receptor.[197] Selected radioligands that readily distinguish between the high and low-affinity D_2 state are listed in (Figure 4- 17).[46]

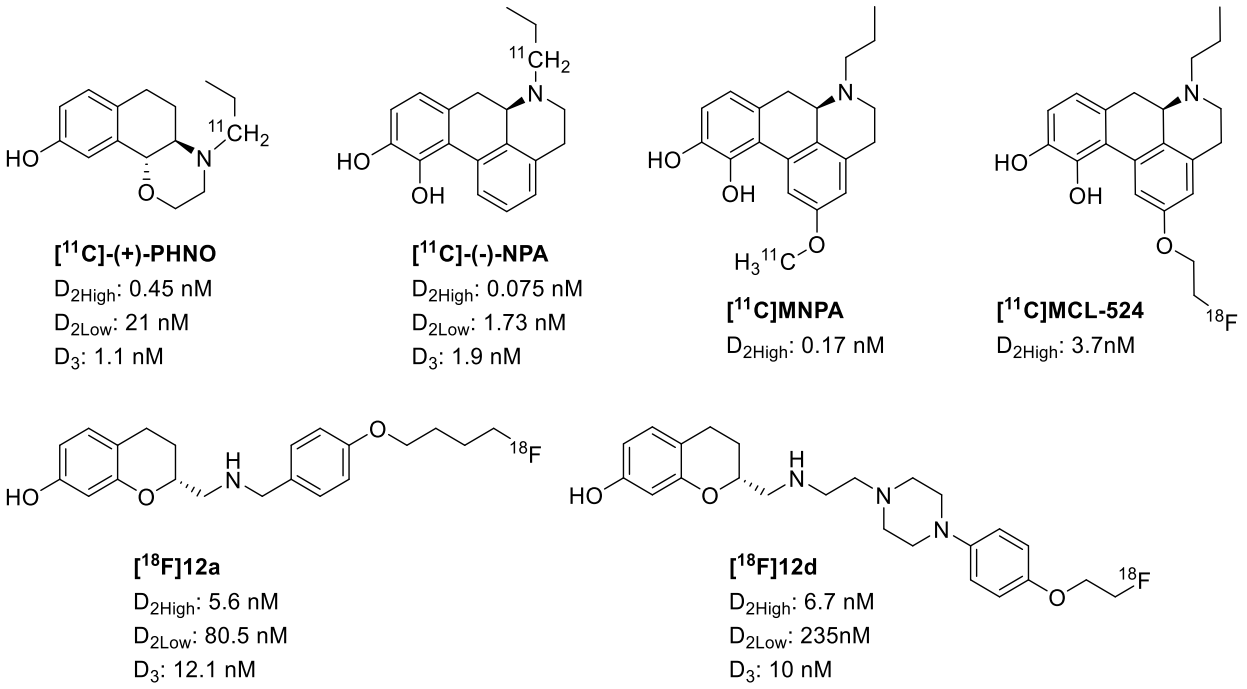

Figure 4- 17 Radioligand D2/D3 Agonists: D_{2High} vs D_{2Low}[46]

Other D_2-selective compounds, such as [^{18}F]N-Methylbenperidol and [^{11}C]SV-III-130 have shown recent improvement in efforts to develop a selective radioligand at the D_2 receptor. [^{18}F]N-Methylbenperidol was shown to be roughly 200-fold selective for the D_2 receptor over D_3, and initial PET studies have demonstrated that this tracer reflects a D_2 binding pattern, as opposed to D_2/D_3.[198] [^{11}C]SV-III-130 on the other hand has a roughly 60-fold D_2 preferring character, but also binds with high affinity to serotonergic receptors, hindering its progress as a selective tracer for dopamine receptors.[199]

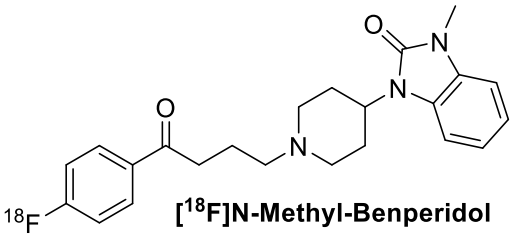

[^{18}F]N-Methyl-Benperidol
D_2: 0.58 nM
D_3: 114 nM

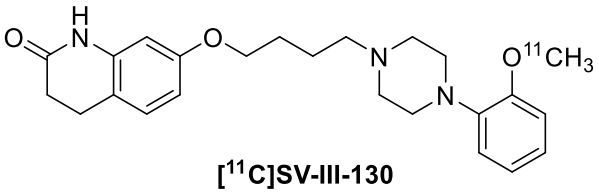

[^{11}C]SV-III-130
D_2: 0.22 nM
D_3: 13.1 nM
5-HT_{1A}: 0.28 nM

Figure 4- 18 Other D2-Selective Radioligands

iii. PET Imaging of the Dopamine D3 Receptor: [^{11}C]-(+)-PHNO & Recent Efforts

The current best clinical option in dopamine D_3 receptor imaging, with modest selectivity, at roughly 20-fold, is (4aR,10bR)-4-(propyl-1-11C)-3,4,4a,5,6,10b-hexahydro-2H-naphtho[1,2-b][1,4]oxazin-9-ol ([^{11}C]-(+)-PHNO, **97**), which was developed as a PET ligand in 2005 (Figure 4- 16, Scheme 4- 7).[200] The non-radioactive compound was initially developed as a therapy for Parkinson's disease in the 1990s.[201–203] Later it was labeled with tritium for autoradiography binding studies, and carbon-11 for PET imaging.[42,204] Wilson was the first to evaluate [^{11}C]-(+)-PHNO as a PET radioligand, reporting *in vivo* properties and tracer behavior.[200]

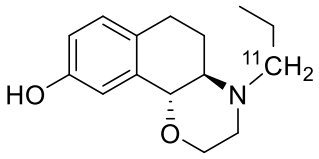

[^{11}C]-(+)-PHNO
97
D_{2High}: 0.45 nM
D_{2Low}: 21 nM
D_3: 1.1 nM

Figure 4- 19 [^{11}C]-(+)-PHNO and Dopamine Receptor D2/D3 Subtype Selectivity

The synthesis of [^{11}C]-(+)-PHNO begins with CO_2 insertion at an ethyl Grignard reagent (**92**), and consequent formation of the [^{11}C]propionyl chloride (**94**) through treatment with phthaloyl chloride; this is then reacted with the amine precursor (**95**) to form the amide that is subsequently reduced by $LiAlH_4$ to give the final N-propyl product (**97**) (Scheme 4- 7).[178]

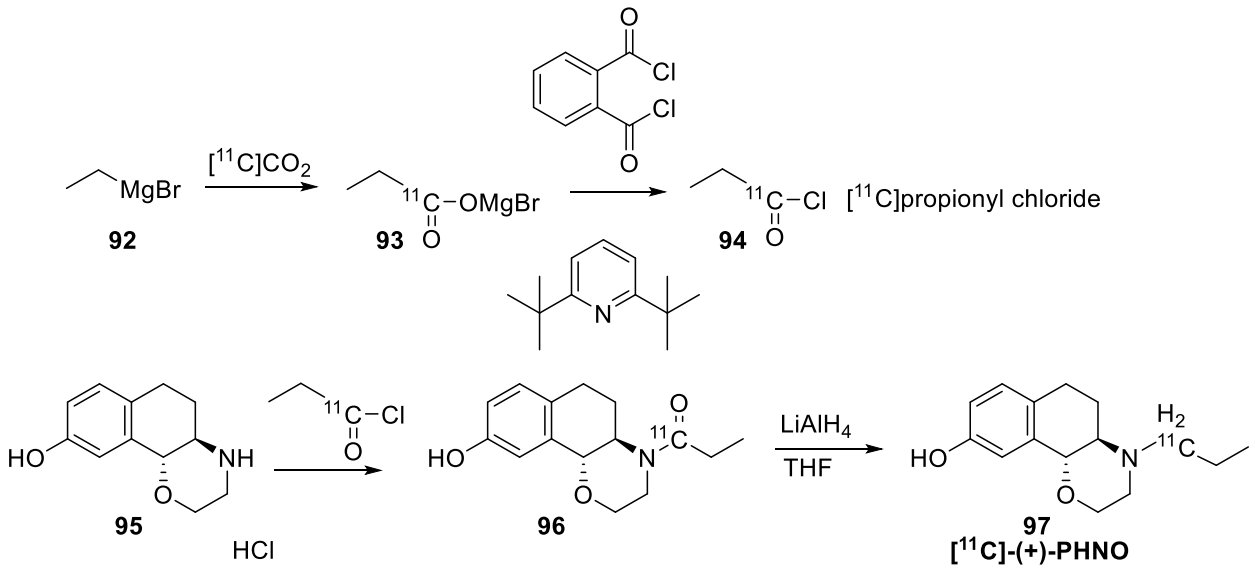

Scheme 4- 7 Radiosynthesis of D3-Preferring [^{11}C]-(+)-PHNO

Other valiant efforts have been ongoing to develop a D_3-preferring or D_3 selective radiotracer with desirable pharmacokinetic properties for *in vivo* imaging with PET, but [^{11}C]-(+)-PHNO (**97**) has been the only practical tracer for this purpose.[65,81,82,94,205,206] Extensive work has been done by the Hauck-Newman group at NIH to develop a robust medicinal chemistry program for identifying the major SAR for this receptor, as well as the Mach group at the University of Pennsylvania to develop a dopamine D_3 receptor ligand and adapt it for PET imaging (including a Phase 0 clinical trial for [^{18}F]fluortriopride in 2017).

Indeed, [^{11}C]-(+)-PHNO (**97**) is a D_2 receptor agonist, but its distribution and high binding in the globus pallidus suggests that it is D_3 preferring (consistent with postmortem human D_3 expression patterns). Moreover, the elucidation of whether agonist or antagonist tracers allow for an advantage in detecting affinity states (D_{2High}, D_{2Low}) is an active pursuit in PET and was encouraged by the development of this D_3 preferring ligand.[190,197,207–210] By utilizing other D_3 selective pharmacological agents, notably BP897, SB-277011, and GSK598809, as well as D_2 tracer [^{11}C]raclopride (or [^{3}H]raclopride), several groups were able to confirm the D_3-prefering nature of [^{11}C]-(+)-PHNO.[119,211–215] Even so, this tracer exhibits a considerably high affinity for the D_{2High} state (Figure 4- 19).[46]

As the result of these studies, it was concluded that [^{11}C]-(+)-PHNO (**97**) specific binding in the substantia nigra/ventral tegmental is due to D_3 receptors, whereas the binding in the putamen is due to D_2. Uptake in the globus pallidus, ventral striatum, and thalamus is attributed to mixed D_2/D_3 signals. The signal from the dopaminergic nuclei in the midbrain is due to D_3 receptors, however it cannot be measured precisely due to the small brain region and overall low specific binding of the radioligand.[42,148] Receptor

occupancy, D_3 vs D_2, was given a rough estimate by Gallezot et al in 2011, such that [^{11}C]-(+)-PHNO $K_D(D_3)$ = 0.02 - 0.05 nM, a very high affinity tracer.[215]

A great deal of work has gone into studying the pathophysiology of psychiatric illness as it pertains to the function of the dopamine D_3 receptor using [^{11}C]-(+)-PHNO (**97**). [^{11}C]-(+)-PHNO imaging is challenging in that it requires a multi-step radiosynthesis using a short-lived radionuclide (carbon-11, $t_{1/2}$ = 20 min), making high specific activity a concern. Pharmacokinetic quantification is also cumbersome due to its mixed affinity at the D_2 and D_3 receptors.[42]

Research efforts across groups in developing ligands based off the first reported D_3 agonist, BP897 (Figure 4- 7) have resulted in the production of carbon-11 and fluorine-18 compounds, Figure 4- 20, albeit with limited *in vitro* and *in vivo* data to evaluate their utility as PET ligands.[216–218] A structure-activity relationship study on a novel series of D_3 ligands on the aforementioned 2,3-dichloro scaffold (e.g. NGB 2904, Figure 4- 7) lead to a carbon-11 compound reported by Turolla and Perone (Figure 4- 20), also with structural similarity to BP897.[216,219,220] The result of this work was an optimization of carbon-11 labeling and preliminary *in vitro* and *in vivo* evaluation. The compounds were reported to cross the BBB, yet accumulated in areas uncharacteristic for D_3 receptors – despite the promising *in vitro* findings. This finding is not uncommon when comparing *in vitro* and *in vivo* behavior.[221,222] The ClogP of the compounds is argued to be the reason for poor specific binding, and noise as the result of high blood circulation causing image degradation.[219] This is further complicated by (potential) competition from endogenous dopamine at the receptor.[223] As such, these compounds were not deemed suitable for future *in vivo* imaging.[216]

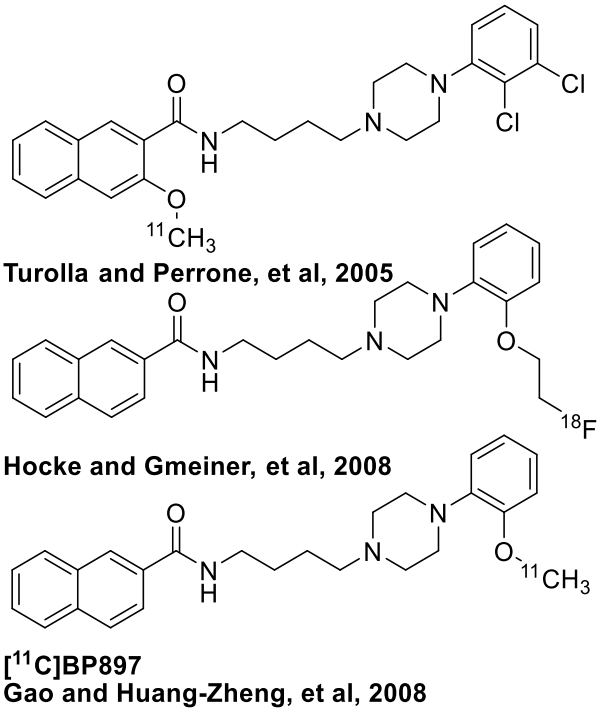

Figure 4- 20 Representative BP897 Derived Radioligands

Another development in BP897-derived ligands lead to [^{18}F]FAUC346, and another interesting work reported by Hocke and Gemeiner, et al (Figure 4- 21).[217] Receptor binding studies were performed and confirmed with 3D-QSAR models. These methods revealed sub-nanomolar D_3 affinities (K_i values 0.12-0.69 nM) and good selectivity's (> 100 fold) at these derivatives.[217] A series of other D_3 subtype selective compounds based on BP897 and FAUC346 were synthesized and initially evaluated[205,224–226]

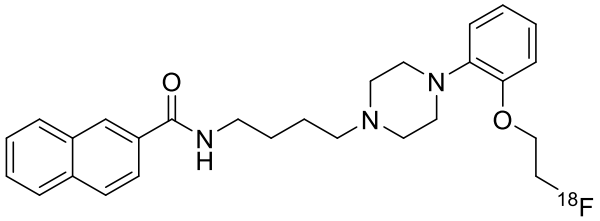

Hocke and Gmeiner, et al, 2008

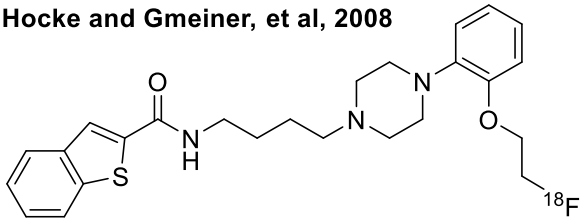

[^{18}F]FAUC 346

Figure 4- 21 [^{18}F]FAUC346 and BP897 derived ligands

The carboxamide BP897 derived series is, still, a common scaffold to pursue and modest SAR was pursued and labeling efforts reported in 2005 and 2008 by Gao and colleagues (**[^{11}C]BP897**, Figure 4- 20). High radiochemical yields and short synthesis times were reported, as well as drawing upon the previously biological data to encourage further *in vivo* evaluation.[218,227]

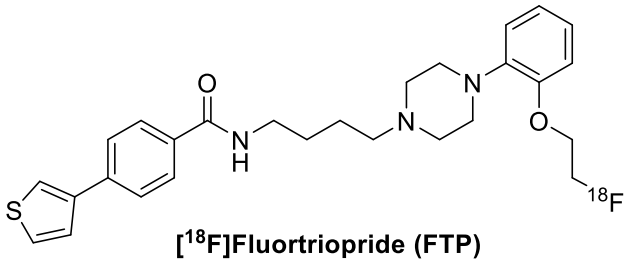

[^{18}F]Fluortriopride (FTP)
([^{18}F]LS-3-134)
D_2: 27.7 nM
D_3: 0.17nM
5-HT_{1A}: 10.3 nM
D2/D3: 163

Figure 4- 22 [^{18}F]Fluortriopride (FTP)

A considerable effort in the progress of a dopamine D_3 receptor-selective PET radioligand by the Mach group has resulted in the recent development of [^{18}F]fluortriopride ([^{18}F]LS-3-134) (Figure 4- 22). This potential PET tracer has sub-nanomolar affinity for the D_3 receptor (D_2 = 27.7 nM, D_3 = 0.17 nM) (and is >150-fold selective at the receptor (compared to D_2).[87] Currently this compound is being evaluated in a Phase 0 clinical trial, NIH ID 14119, at the University of Pennsylvania as of July 2017.[46,86]

g. Toward the Development of a Dopamine D_3 Receptor-Selective PET Radioligand

The identification of a specific, high affinity dopamine D_3 receptor PET radioligand is of urgent need in the field of nuclear medicine for the characterization and pharmacological evaluation of this receptor, to explore its role in disease, and as a way to fully utilize it as a diagnostic and therapeutic target. The development of a PET tracer will provide functional data and insight into three key areas: (1) this will provide functional data to support treatment efforts as well as valuable insight into normal and abnormal D_3 receptor activity as it relates to normal brain function, the aforementioned disorders, and any change that occurs *via* the result of drug therapy; (2) additionally, this will allow for better understanding of the differential availability between D_2 and D_3 receptors, previously complicated by dual receptor binding by currently available radioligands such as [^{11}C]-(+)-PHNO; (3) lastly, upon synthesis of a radioligand that shows *in vivo* sensitivity to endogenous levels of dopamine, the functional role of D_3 receptors would finally be accessible.

Several antagonists and agonists have been used to characterize the pharmacology of the D_3 receptor *in vitro*, but have fallen short due to the aforementioned homology and resultant specificity problems with the radioligand, as well as the expression system or tissue and assay system chosen for study. A list of the research groups who have done significant, notable work toward the development of D3 selective ligands for therapeutic or PET diagnostic purposes can be found in the "The Dopamine D_3 Receptor as a Drug Target" section of this chapter. With these shortcomings, however, the need for the development of a selective D3 agonist still exists.

Recently, several compounds have been identified that are selective agonists at the D_3 receptor with >100 fold selectivity for D_3 over D_2 and low nanomolar affinity.[107,108,130] The goal of the research described in this Chapter was to synthesize a series of selective D_3 receptor agonists and utilize them as lead compounds for the synthesis, radiosynthesis and initial evaluation of novel D_3-selective PET radioligands.

h. Results & Discussion Part 1: Pramipexole-Containing Compounds

i. Design & Synthesis

The D_3-prefering agonist, pramipexole, was used as the pharmacophore in a drug discovery program to develop a D_2/D_3 agonist for the treatment of Parkinson's disease, and was then used as it provided good selectivity at the D_3 receptor (as opposed to the naphthyl amide head group on BP897).[130,134,228–230]

As a result of these efforts, several potent D_3 preferring agonists emerged. These compounds, reported by Modi, Dutta and colleagues[130], contain the characteristic alkyl linker from the pramipexole moiety to the piperazine (bi)phenyl, and follows with good selectivity and affinity at the receptor: 3-methoxy **127** (D_2/D_3: 147; K_i = 2.33 ± 0.26 nM) or 3-hydroxy **128** (D_2/D_3: 213; K_i = 1.73 ± 0.14 nM) (Scheme 4- 8, Scheme 4- 11).[130]

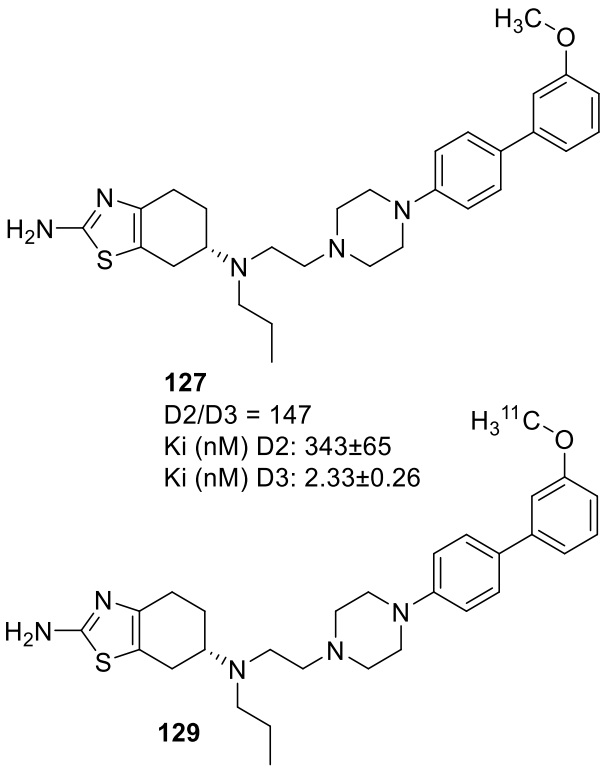

*Scheme 4- 8 Pramipexole-Containing C-11 Lead **127** and Proposed Radiotracer **129***

Using compound **128** as a starting point, we wished to synthesize the carbon-11 isotopalog **129** for PET imaging. The unlabeled reference standard, to confirm identity of the radiolabeled product by HPLC, was prepared as previously described (Scheme 4- 9)

from phenyl piperazine, and the carbon-11 precursor (also lead, **128**) prepared with modest variation (Scheme 4- 10).[231]

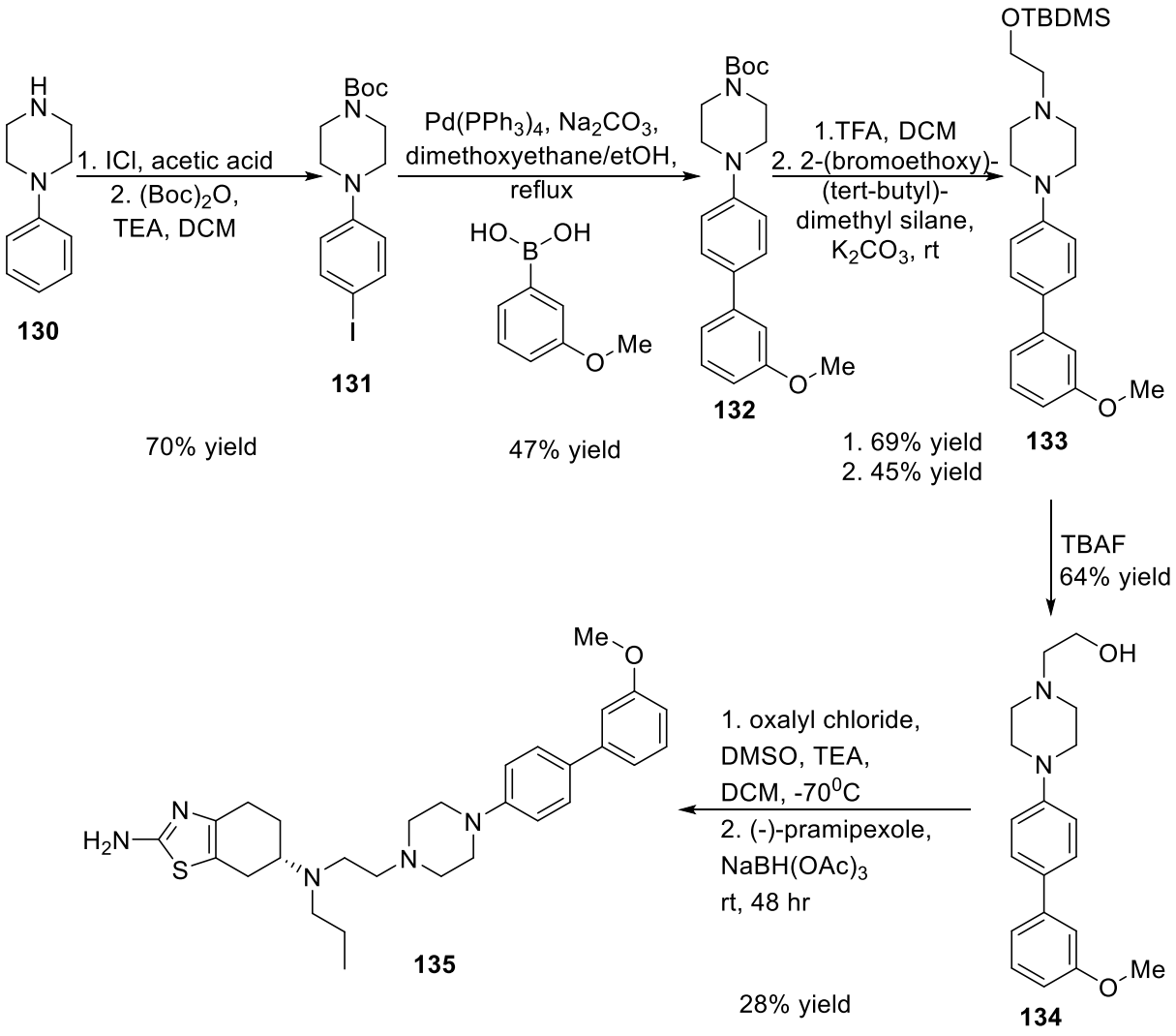

Scheme 4- 9 Synthesis of Standard 135[231]

Phenyl piperazine (**130**) was iodinated with ICl in acetic acid, followed by standard Boc protection of the piperazine amine, in 70% yield over two steps (**131**). Suzuki coupling with 3-methoxy phenyl boronic acid gave **132** in 47% yield. Deprotection of the amine in

TFA (69% isolated yield), followed by alkylation with 2-(bromoethoxy)-(tert-butyl)-dimethyl silane gave **133** in 45% yield. Deprotection in TBAF to the alcohol (**134**) (64% yield), followed by Swern oxidation gave the desired aldehyde (non-isolated), that was reacted with (S)-(5-methoxy-1,2,3,4-tetrahydro-naphthalen-2-yl)-propyl-amine (aka Pramipexole) in reductive amination conditions ($NaBH(OAc)_3$) to provide the final compound, **135**, in 28% yield.

To obtain labeling precursor **128**, O-demethylation of the carbon-12 standard (**135**) was initially pursued as previously reported[231], but was unsuccessful in our hands (reagents explored for demethylation: BBr_3, BCl_3, TMS-I). Protecting group compatibility was explored at the piperazine and phenyl boronic acid, including Fmoc, Boc and dioxolane, as well as the 3-hydroxyphenyl boronic acid and MOM-protected boronic acids. As a result, we took a similar approach with a MOM-protected boronic acid, and related synthetic approach thereafter (Scheme 4- 10).

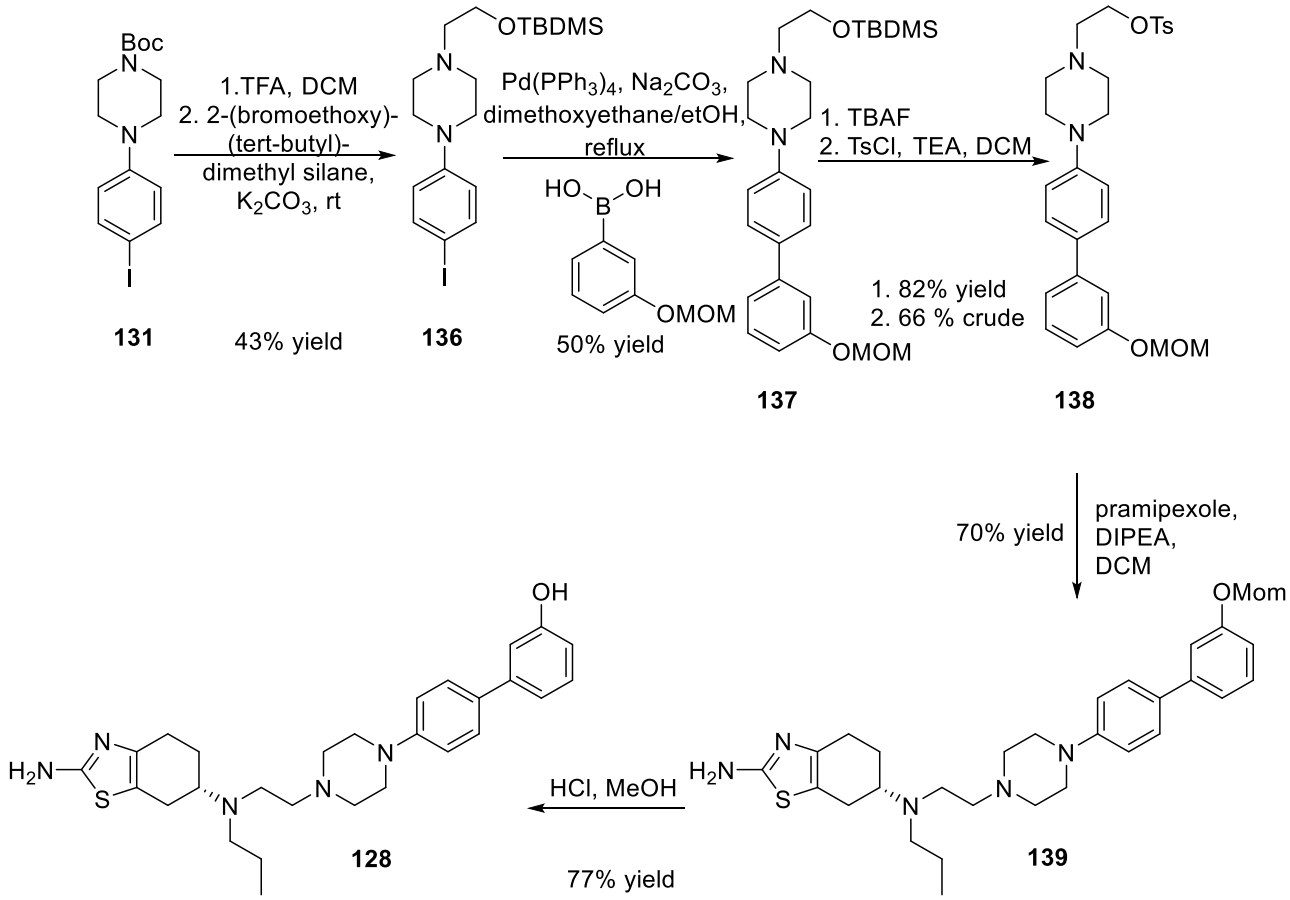

Scheme 4- 10 Synthesis of Precursor 139 and C-11 Labeling

Synthesis of the precursor **139** (Scheme 4- 10) therefore started with a common intermediate, **131**, and 2-(bromoethoxy)-(tert-butyl)-dimethyl silane was added to provide protected alcohol **136** (43% yield) prior to Suzuki coupling with MOM-protected phenyl boronic acid to generate **137** in 50% yield. While Swern oxidation followed by reductive amination with pramipexole was a robust option in previous reports[130], the formed aldehyde was not isolatable (unable to identify on NMR, and difficult to monitor *via* IR lead us to believe it was unstable) and the reductive amination was challenging. Therefore an alternative synthesis was developed. Following deprotection of **137** with TBAF (82% yield), the alcohol was converted to the tosylate (**138**) (66% crude yield). The tosylate

was not isolated but used directly in the alkylation with pramipexole to form the final product (before MOM deprotection), **139** in 70% yield. Final deprotection of the MOM ether in HCl/MeOH gave labeling precursor, **128**, in 77% yield.

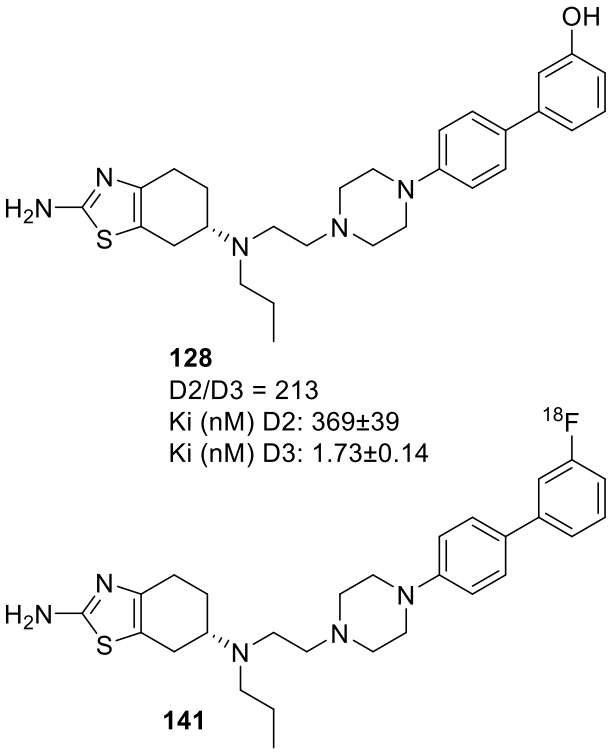

Scheme 4- 11 Pramipexole Containing Lead for F-18 Labeling

The synthesis of the fluorine-19 reference standard (Scheme 4- 12) was adapted from the previously reported procedure, and modified as follows: from the previously mentioned intermediate, *tert-butyl* 4-(4-iodophenyl)piperazine-1-carboxylate (**131**), Suzuki coupling with 3-fluoro phenyl boronic acid gave (**142**) in 43% yield. After deprotection with TFA (99%), alkylation with 1-bromo-2-chloroethane provided

intermediate **143**, which was directly reacted with pramipexole in base to provide the standard (**144**) in 31% over two steps.

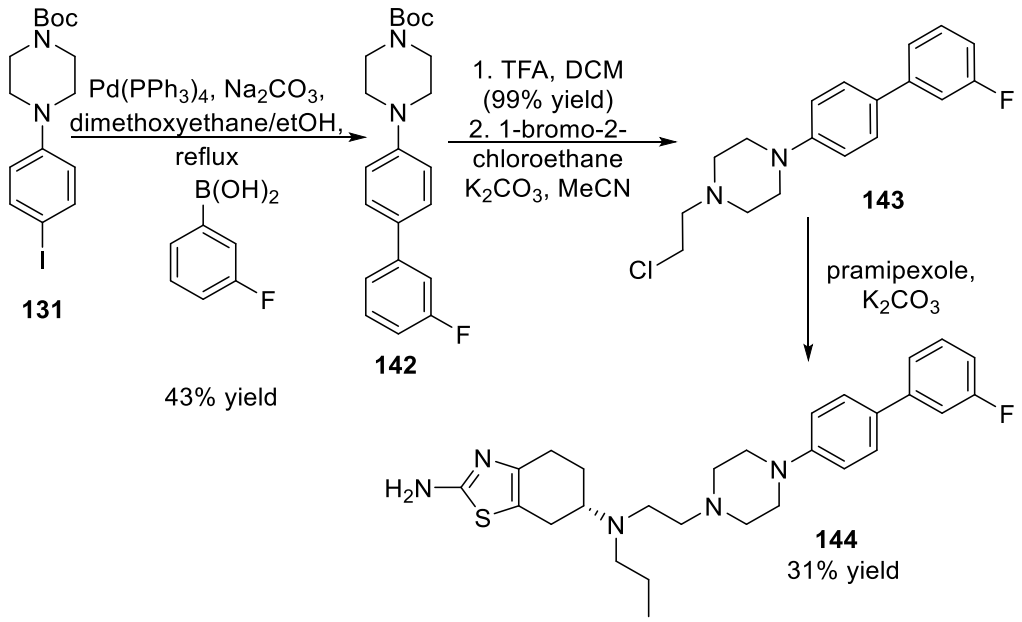

Scheme 4- 12 Synthesis of Fluorine-19 Standard

Radiofluorination of the unactivated arene, to generate the ^{18}F radiotracer (Scheme 4- 13) , was pursued through recently reported transition metal-mediated F-19/F-18 chemistry from Scott and Sanford utilizing stannane, boronic acid/Bpin (Bpin = boronic acid pinacol ester), or (mesityl)(aryl)iodonium salt precursors.[232–236] For our interests, we sought to pursue the Bpin and stannane precursors for F-18 fluorination (Scheme 4- 13). Initial attempts to synthesize the Bpin precursor for nucleophilic F-18 fluorination involved Suzuki coupling with a 1-3 di-Bpin on a common intermediate (**142**), however the desired product was never obtained and spectra analysis suggested dimerization of the products. Recent reports, however, demonstrate borylation *via* C-F bond cleavage.[237–240] As such, we sought to synthesize of the fluorine-19 reference

standard first, and to save on time and reagents, to form the Bpin precursor that would be used directly in nucleophilic [^{18}F]fluorination (Scheme 4- 14).

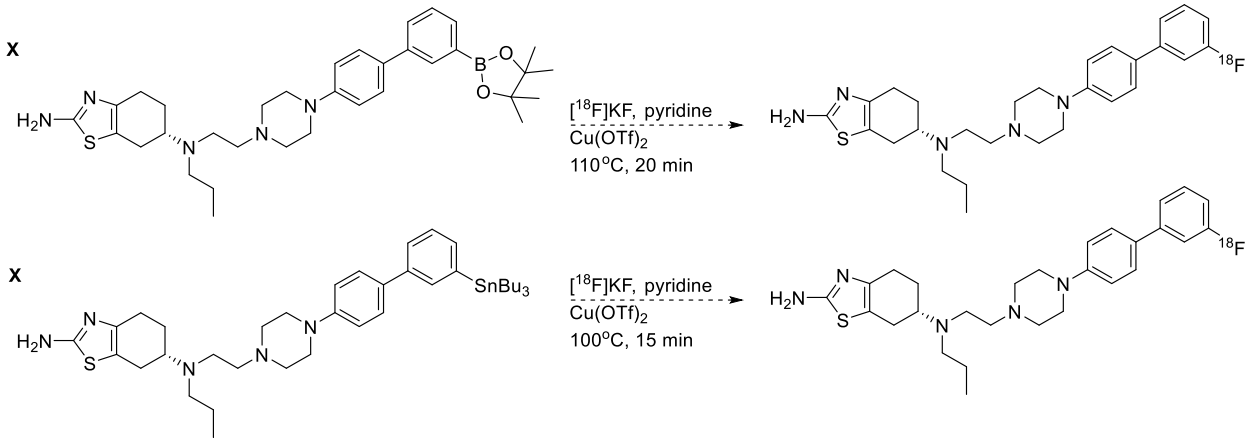

Scheme 4- 13 F-18 Fluorination Strategies

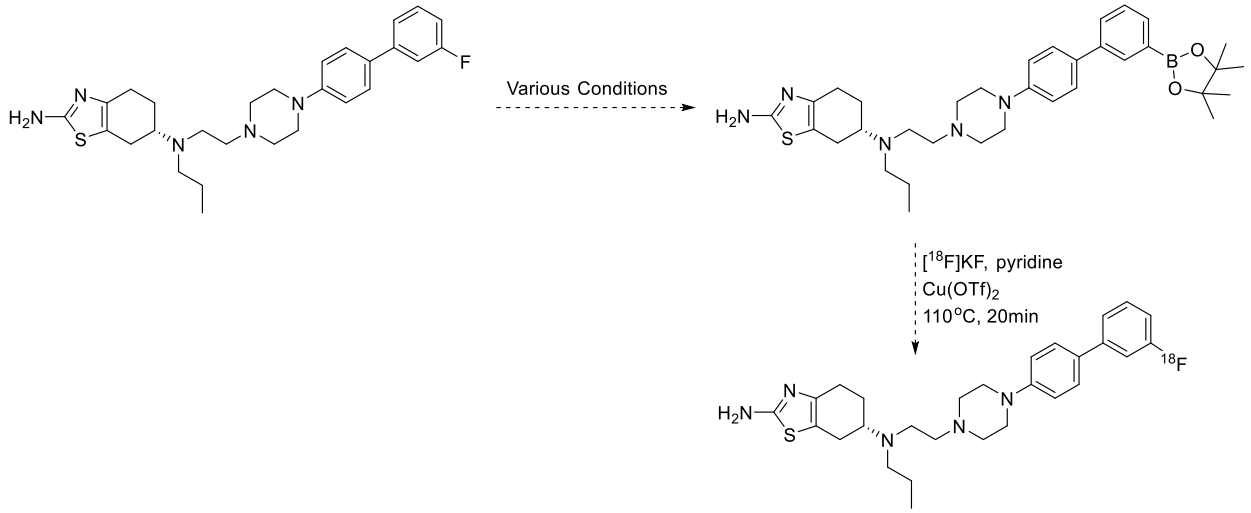

Scheme 4- 14 Strategy: Transition metal-mediate borylation via *C-F bond cleavage -To- F-18 fluorination*

In lieu of using precious standard, an appropriate intermediate was used to screen conditions (Scheme 4- 15).[237] Careful examination of the substrate scope defluoroborylation of haloarenes, 4-(4'-fluoro-[1,1'-biphenyl]-4-yl)morpholine and *tert*-

butyl (4-fluorophenyl)(methyl)carbamate is transformed into the appropriate Bpin using conditions described in Scheme 4- 15**A,** in 76% and 52% yield respectively (Scheme 4-15-**B**) and carry significant structural similarities to the intermediate of interest. Utilizing the conditions described, and extending the reaction from 24-72 h (Scheme 4- 15**A**, x = 1 and 3, x representing a multiplication factor of reagents described) on the model substrates, no desired Bpin was isolated, and starting material recovered (Scheme 4-15**C**, **D**). While most of these transition-metal mediated reactions require a glove box for working in an inert atmosphere, these were performed carefully in a standard fume hood. $Ni(cod)_2$ is known to rapidly oxidize to Ni^{2+} in the presence of air[241] (turning from a canary yellow to dark brown); and while this reagent did not have a rapid color change, this possibility should not be ruled out.

In another effort to obtain the Bpin precursor, another recent report demonstrated a metal and additive-free photoinduced borylation procedure of haloarenes.[240] Again, using a common intermediate, **142**, these conditions were tried using a 254 nm lamp under a closed and open vial system (Scheme 4- 16). While monitoring *via* TLC gave promising results, however after extraction and/or purification, starting material was recovered. Given the lamp used for this transformation is used for TLC analysis, and not specifically for photochemistry, it is likely that the 254 nm lamp used is not the optimum equipment required of this transformation.

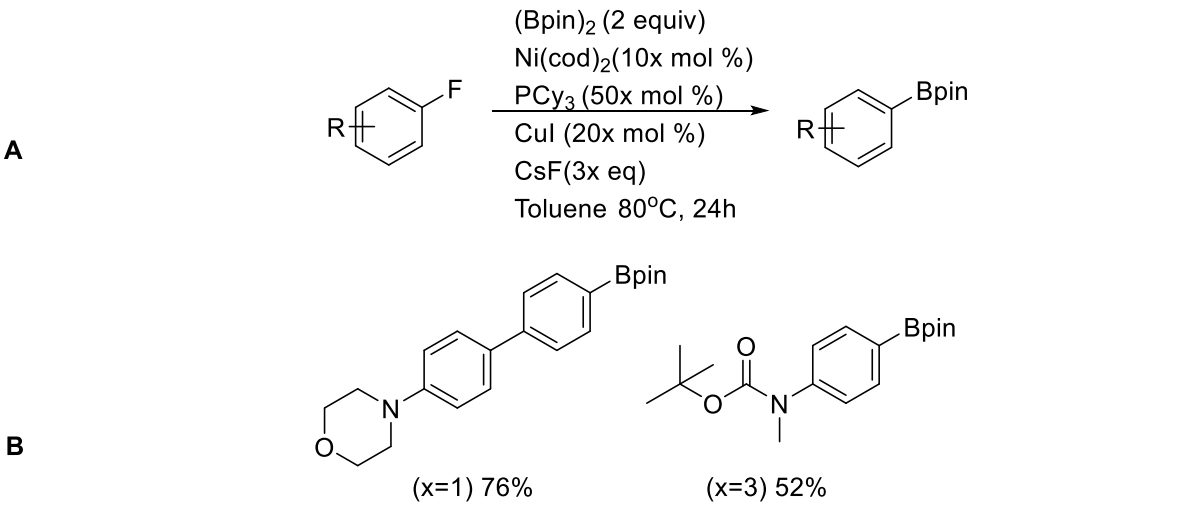

Scheme 4- 15 Toward a Bpin precursor via C-F bond cleavage

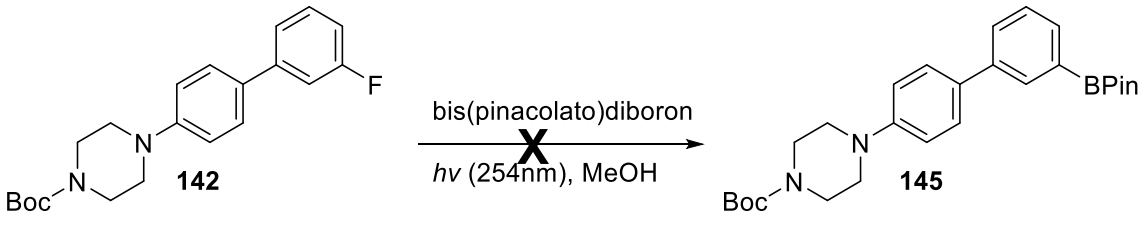

Scheme 4- 16 Toward a Bpin precursor: Metal and Additive-free, photoinduced borylation of haloarenes

Since access to BPin precursor **145** was proving challenging, the synthesis of 3-bromophenyl precursor **146** for end-stage stannylation was prepared. Starting from a common intermediate, **131**, Suzuki coupling with 3-bromophenyl boronic acid provided **148** in 26% yield. Deprotection of the N-Boc group using TFA (**149**), and subsequent alkylation with chloroacetyl chloride, gave **150** in 80% yield. To this was added base, catalytic KI and pramipexoleto produce **151** in over 50% yield. Reduction of the carbonyl in borane-THF provided bromide **146** in 68% yield.[136] This was, by far, the most robust and easy to purify means to access **146**. Unfortunately, efforts to stannylate **146** using a number of different conditions did not provide the desired product **147** (Scheme 4- 18).[232] (Scheme 4- 17).

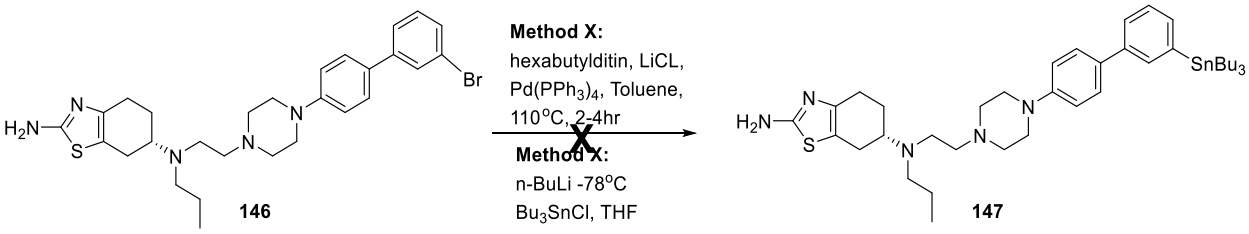

Scheme 4- 17 Other methods toward a stannane-containing precursor for F-18 fluorination

Intermediate, **148**, was then used to explore other means to produce the stannane. Stannylation of intermediate **148** with bis(tributyl)tin, $Pd(PPh_3)_4$ and LiCl proceeded in reasonable yield (20%) (Scheme 4- 19). However, deprotection of the Boc group in the presence of the stannane proved to be challenging. Reagents and conditions tried included: traditional Boc deprotection in TFA/DCM, which both deprotect and destannylated the product. DCM with a couple drops of TFA gave the destannylated product *via* TLC, but an intact Boc group. Other methods tried include water at 100°C and 150°C for 10-20 min but no reaction occurred under these conditions.[242,243]

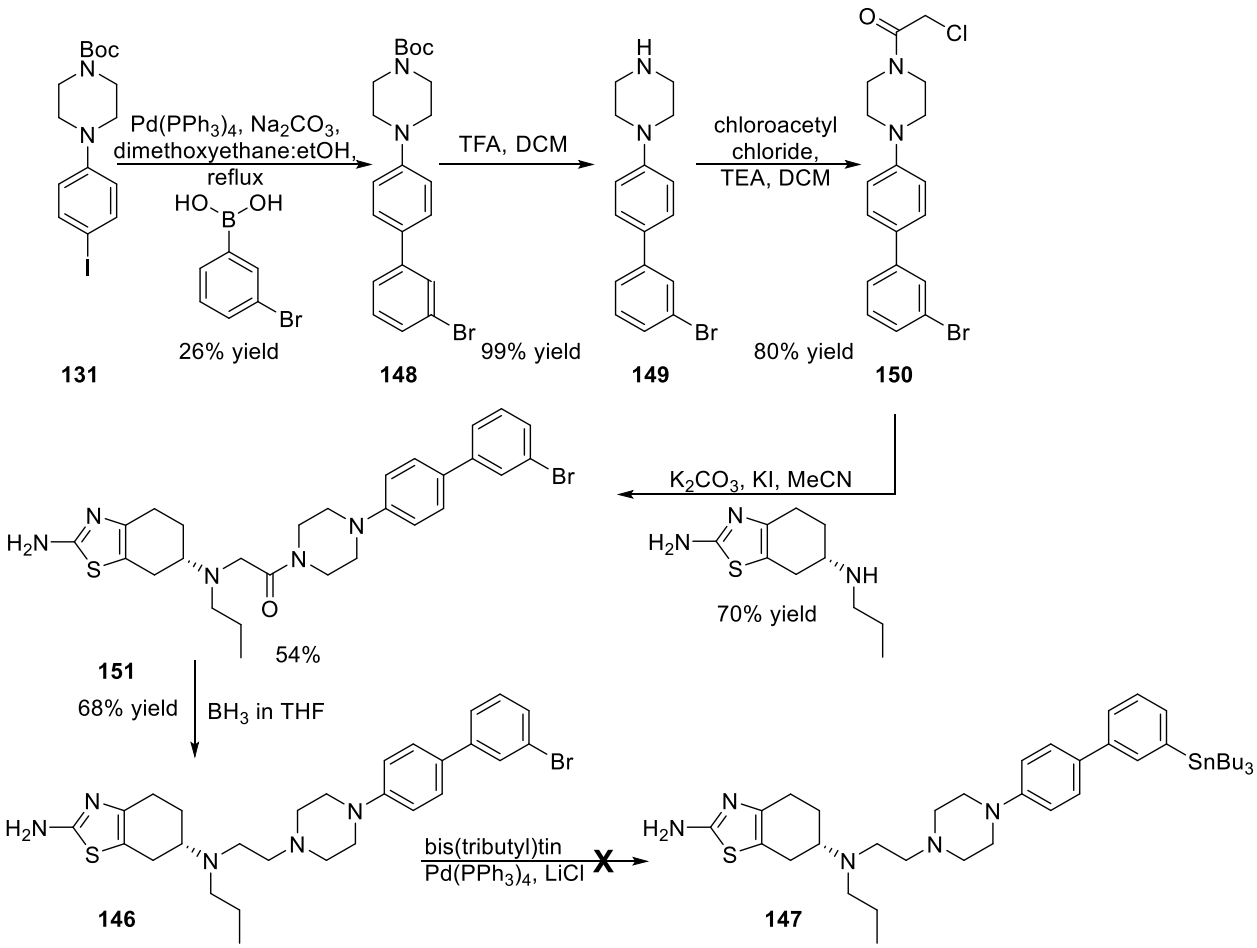

Scheme 4- 18 Toward a Stannane-containing precursor for F-18 Fluorination

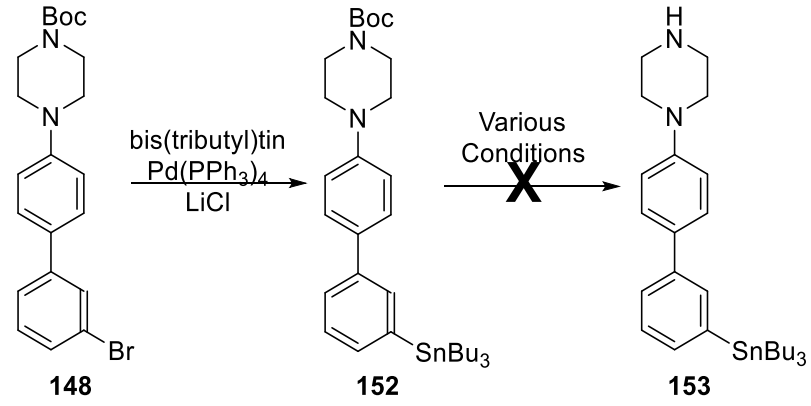

Scheme 4- 19 Stannane trial & error

Concurrent with these metal-mediated late-stage fluorination efforts, isotopic exchange with the fluorine-19 containing standard, **144**, was also being explored as a means of radiolabeling (Scheme 4- 21).

ii. Radiochemistry

Carbon-11 labeling of phenol precursor **128** was performed in a General Electric (GE) TracerLab $FX_{C\text{-}Pro}$ synthesis module. Initially, the carbon-11 was produced as $[^{11}C]CO_2$ with a GE PETTrace cyclotron *via* the $^{14}N(p\ \alpha)^{11}C$ nuclear reaction, and was delivered to the synthesis module for loop or reactor chemistry. Loop and reactor chemistry was performed and the synthesis modules modified as described by Shao and colleagues.[244] The carbon-11 sources utilized were standard $[^{11}C]CH_3I$ and $[^{11}C]CH_3OTf$ (a discussion of the formation of these carbon-11 methylating reagents can be found in the **Chapter 1**). Methylation of phenol **128**, using 1 mg of precursor, was pursued in DMSO or DMF, and using several bases (KOH, potassium carbonate, TBA-OH) or by formation of the TBA-salt (briefly, 1 mg precursor in 150 µl MeCN/water to 10 µl 1M tetrabutylammonium hydroxide in MeOH was added, vortexed, diluted with 5-6 mL water and passed through a C18 extraction disk; the disk was washed with water 2 x 5 mL and tried under nitrogen gas. The precursor was eluted in MeCN to a fresh vial after drying overnight in vacuum). In each instance, no product was obtained. Analysis of the reaction mixture following radiosyntheses confirmed intact precursor so it was not considered a stability issue. Alkylation at the free amine on the headgroup was not a concern, as the synthesis of pramipexole was previously reported, and the primary product was at the anticipated amine; while utilizing a protecting group in the pramipexole synthesis

decreased the mixture of products obtained, it was not required and the desired product was easily purified (Scheme 4- 20).[245]

*Table 4- 6 Carbon-11 Labeling of **128***

Methylating Agent	Solvent	Precursor	Method	Base	Reaction Notes	Result
[^{11}C]CH_3OTf	DMSO	1mg	Reactor	TBA-OH	3 min bubble through reactor	NR
[^{11}C]CH_3OTf	DMSO	1mg	Loop	TBA-OH	Addition of TBA, color change to yellow. 5 min through loop.	NR
[^{11}C]CH_3OTf	MeCN	1mg	Loop	TBA salt	5 min through loop.	NR
[^{11}C]CH_3I	DMSO	1mg	Reactor	KOH	Subtle color change after addition of base. 3 min bubble through reactor	NR
[^{11}C]CH_3I	DMSO	1mg	Reactor	KOH	3 min bubble through reactor, then heat 3 min, 85 ^{o}C	NR
[^{11}C]CH_3I	DMF	1mg	Reactor	K_2CO_3	Subtle color change after addition of base. Line cut from 31, bubbled into product vial.	NR
[^{11}C]CH_3I	DMF	1mg	Reactor	K_2CO_3	Line cut from 31, bubbled into product vial, then heat 5 min, 85 ^{o}C	NR
NR = No Reaction						

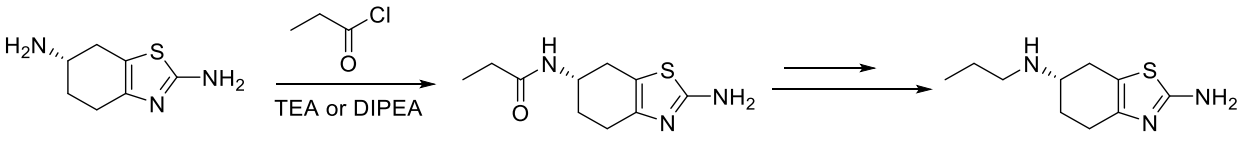

Scheme 4- 20 Synthesis of Pramipexole[245]

Similarly, the development of a fluorine-18 tracer at the D_3 receptor is highly desired due higher specific activity and longer half-life. The same group also reported a D_3 selective 3-hydroxy phenyl compound **128** with nanomolar affinity for D_3 and 213-fold over the D_2 receptor, (Scheme 4- 11).[130] Utilizing the -OH, **128** as a bioisostere for fluorine

(a discussion of fluorine as a bioisostere for this moiety in medicinal chemistry can be found in the **Chapter 1**), **144**, we sought to pursue this scaffold and utilize the recent advances in fluorine-18 chemistry to access unactivated arenes through transition-metal mediated F-18/F-19 fluorination methods.[232–234,246]

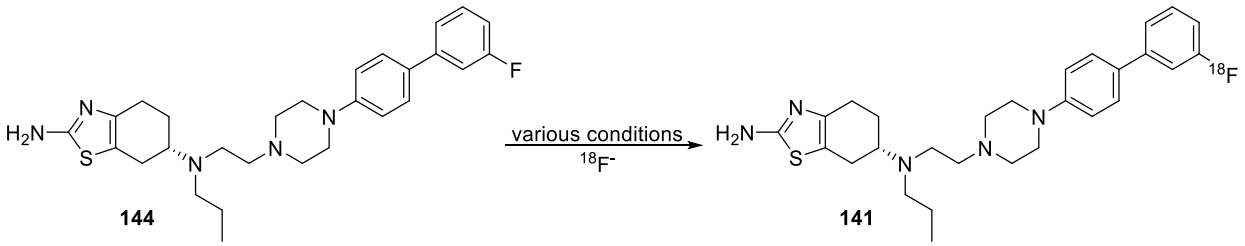

Scheme 4- 21 Isotopic Exchange: fluorine-19/fluorine-18

Fluorine-18 was produced as [^{18}F]fluoride with a GE PETTrace cyclotron *via* the ^{18}O(p,n)^{18}F nuclear reaction, and delivered to a TracerLab FX$_{FN}$ synthesis module in a 1.5 mL bolus of [^{18}O]H_2O. The process to prepare and activate the nucleophilic F-18 anion proceeds as follows:

1. This was delivered to TracerLab FX$_{FN}$ synthesis modules, where the fluorine-18 was trapped on a QMA light Sep-Pak to remove [^{18}O]H_2O. The QMA light Sep-Pak is preconditioned with 10 mL $NAHCO_3$ (10 mL deionized water, 10 mL ethanol, 10 mL deionized water – this is to aid is desorption (releasing) of the $^{18}F^-$ anion from the QMA resin).
2. Typically the $^{18}F^-$ is eluted into the reaction vessel using a solution of aqueous potassium carbonate (3-3.5 mg in 0.5 ml water), then a solution of kryptofix-2.2.2. (K_{222}) (15 mg in 1mL MeCN) added to the reaction vessel. Flourine-18 prep considerations: potassium carbon 3 mg per 15 mg K_{222}, or 1 mg per 10 mg are standard preparation. Moreover, TEA-HCO_3

(tetraethylammonium hydrogen carbonate) has proven to be a reliable fluorine-18 preparation for halex, or isotopic exchange (11-11.5 mg).

3. This mixture is then azeotropically dried by heating the reactor to 80°C, applying vacuum for 4 min, then cooled to 60°C and put under a stream of argon and under vacuum for another 4 min.

Azeotropic drying is performed to get rid of unwanted water from the initial radionuclide production and aqueous base elution. Otherwise, the fluorine-18 anion is thought to be hydrated and inadequately nucleophilic; as such, this drying process and complex with a phase transfer reagent enhances the fluorine-18 anion reactivity (Figure 4- 23 for [^{18}F]KF). [^{18}F]KF and [^{18}F]TEAF are the fluorine-18 discussed herein.

After azeotropic drying, the activated F-18 fluoride can be brought up into a desired solvent and used for use in multi-reactions manually, or the appropriate precursor (in an aprotic, anhydrous solvent) is added to the reactor and subsequent chemistry performed within the synthesis module of a lead-lined hot cell. For the current purpose, the fluorine-18 was brought up into DMSO or DMF and used for manual reactions.

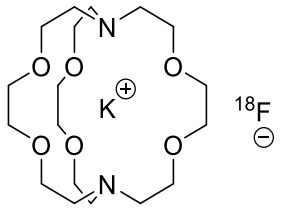

Figure 4- 23 "Exposed" F-18 anion as the result of the K222/K$^+$ complex

An exploration of solvent, precursor amount, and temperature yielded no desired fluorine-18 product, as demonstrated through radioTLC or HPLC. A summary of these conditions can be found in Table 4- 7.

*Table 4- 7 F-19/F-18 Isotopic Exchange on **144***

	[^{18}F]Fluoride Prep	Solvent	Precursor	Temp (°C)	Time	Reaction Notes	Result
1	15mg K_{222}, 3.5mg K_2CO_3, DMF	DMF, 0.5 mL	0.5 mg	120	20 min	TEA-HCO_3 11.5mg/reaction, 100uCi/reaction	NR
2	15mg K_{222}, 3.5mg K_2CO_3, DMF	DMSO,0.5mL	0.5 mg	170	20 min	TEA-HCO_3 11.5mg/reaction, 100uCi/reaction	NR
3	15mg K_{222}, 3.5mg K_2CO_3, DMF	DMF, 0.5 mL	1 mg	120	20 min	TEA-HCO_3 11.5mg/reaction, 100uCi/reaction	NR
4	15mg K_{222}, 3.5mg K_2CO_3, DMF	DMSO,0.5mL	1 mg	170	20 min	TEA-HCO_3 11.5mg/reaction, 100uCi/reaction	NR
5	11.5 mg TEA-HCO_3	DMSO, 1mL	1 mg	160	20 min	150 uL F-18/DMSO + 850 uL DMSO	NR
6	11.5 mg TEA-HCO_3	DMSO, 1mL	2 mg	170	20 min	150 uL F-18/DMSO + 850 uL DMSO	NR
7	11.5 mg TEA-HCO_3	DMSO, 1mL	1 mg	160	20 min	150 uL F-18/DMSO + 850 uL DMSO	NR
8	11.5 mg TEA-HCO_3	DMSO, 1mL	2 mg	170	20 min	150 uL F-18/DMSO + 850 uL DMSO	NR

In these initial F-18 radiolabeling test reactions, the stability of the F-19 compound, **144**, came into question. A curious phenomenon occurred in the stability of this compound in solution: DMSO or MeCN, as it decomposed to 68% and 31%, respectively. Aliquots of 1.5 mg of **144** were stirred with 11.5 mg TEA-HCO_3 in 1 mL DMSO, at 160°C for 0-60 min, and analyzed *via* HPLC. Decomposition of the standard was such that 21% of the standard was remaining after 5 min, and less than 1.5% was remaining after 1 hour (Table 4- 8, Table 4- 9). A prospective labile site may be from the piperazine to pramipexole, as the retention time of pramipexole in this system begins to increase as the standard appears to break down. The fragmentation of the standard is shown alongside 4 main

fragmentation peaks (Table 4- 9). Moreover, temperature, solvent, “cold” KF, and K_{222} were reacted with **144** and analyzed *via* HPLC, also showing breakdown of the standard.

*Table 4- 8 Stability of **144***

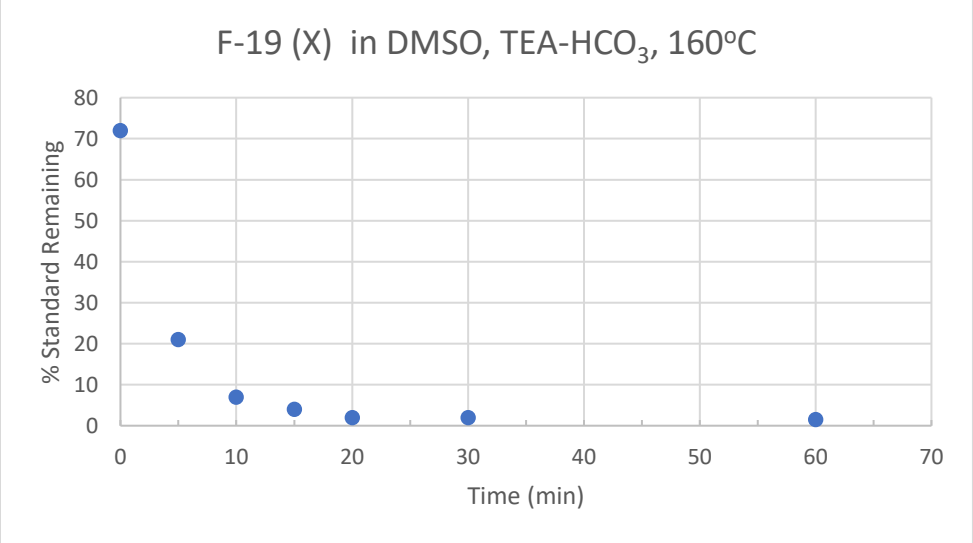

*Table 4- 9 F-19 Standard **144** in TEA-HCO_3 + DMSO*

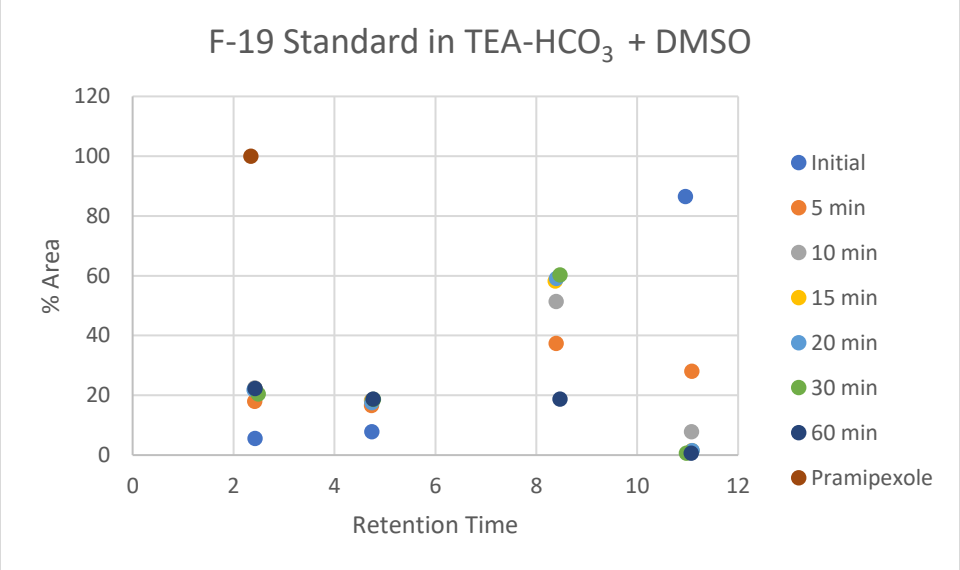

The cold Standard **144** was also heated to 145°C in K_{222} (15 mg/reaction) and cold KF (1-2 mg/reaction). The K_{222} and KF were added in MeCN and heated to 120°C under

a stream of argon to mimic the drying step in the traditional F-18 preparation. Dried fluoride was then mixed with precursor **144** (0.5 mg) in DMSO (0.5 mL), and heated to 145 ^{o}C. Samples were taken initially (after mixing), then at 20 and 40 minutes into the reaction. The K_{222}/KF/precursor mixture turned amber within 20 minutes, while the K_{222}/precursor mixture turned yellow within a similar time frame. Within 40 minutes, the K_{222}/KF/precursor mixture changed to a green/yellow, while the K_{222}/precursor turned from yellow to orange. These were analyzed on a Luna C8 5 micron, 100 Å, analytical HPLC column 150x4.6 mm, with 40% MeCN, 20 mM NH_4OAc, 2 mL HOAc, mobile phase.

*Table 4- 10 F-19 **144** Stability in Kryptofix-K222*

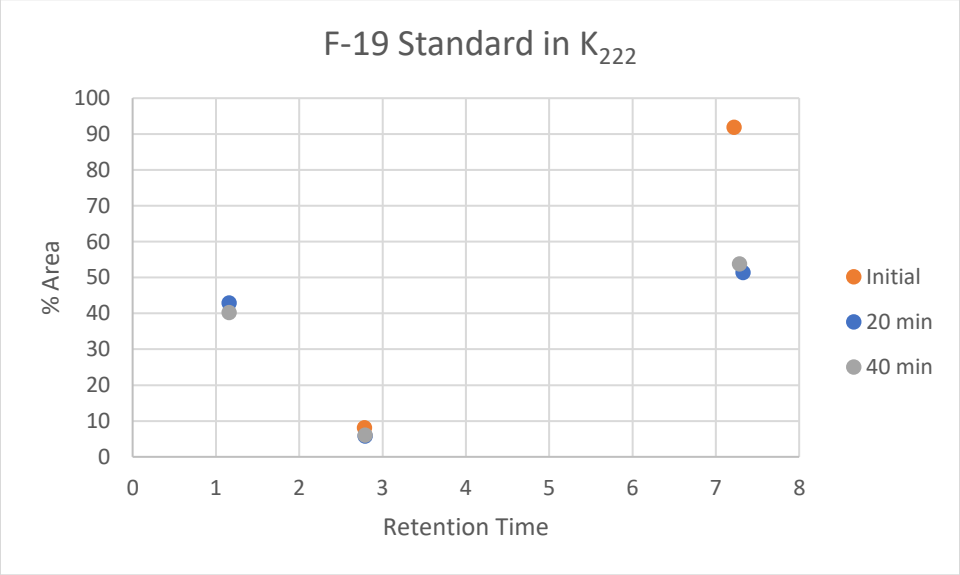

The stability of **144** in the presence of K_{222} was such that after initial mixing >90% of the compound was intact (retention time = 7.2 min). After 20 and 40 min, only 50% was remaining (Table 4- 10). A similar strategy was employed for the stability in K_{222}/KF (Table

4- 11). Upon initial mixing, 83% of the standard was intact, but was found to decompose after 20 and 40 min.

*Table 4- 11 F-19 **144** Standard Stability in Kryptofix-K222 and KF*

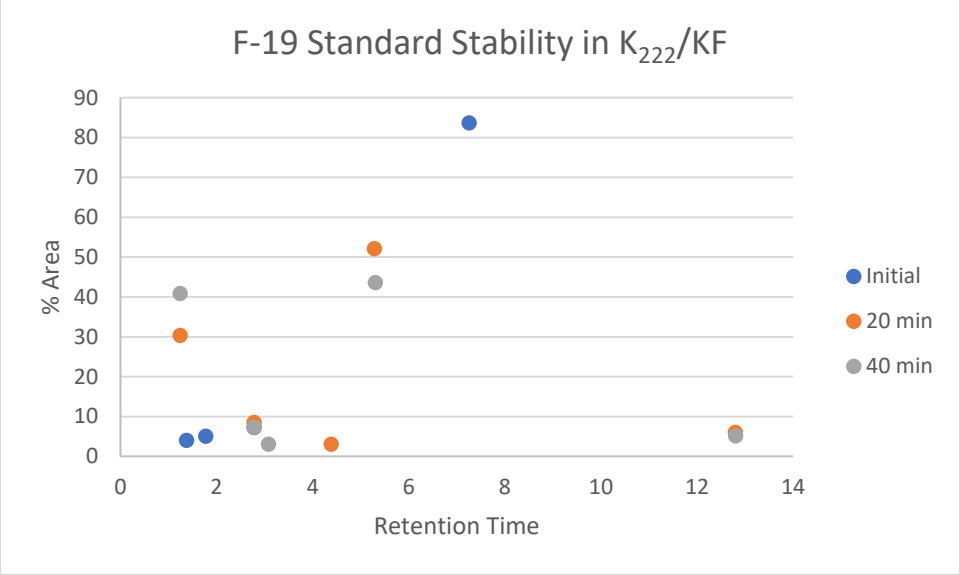

The pramipexole-containing compound, X, designed as a bioisostere out of the 3-hydroxy phenyl compound previously shown to be 213 -fold selective at the D3 receptor (Figure 4- 17) was also evaluated in whole rat brain tissue to explore the selectivity from OH to F substitution and that selectivity and affinity was not reproduced.[231]

iii. Summary

Given the instability of the precursors to a range of radiolabeling conditions, further efforts to develop D_3-selective radiotracers based upon this scaffold were abandoned. The selectivity of **144** at the D_3 and D_2 receptors was evaluated in whole rat brain tissue against [^{3}H]R-(+)-7-OH-DPAT and [^{3}H]Spiperone. In our system, **144** is roughly 5-fold selective at the D_3 receptor, compared to 213-fold of the 3-hydroxy phenyl in previous reports[106]; the affinity at these receptors are K_i 21.0 ± 11.4 nM, Bmax 0.2 ± 0.024 fmol/μg (D_3) and K_i 104.1 ± 34.2 nM, Bmax 0.363 ± 0.023 fmol/μg (D_2) respectively. A discussion on the differences in selectivity is forthcoming. Other scaffolds were then pursued as discussed below, building off previously reported D_3-selective compounds recently reported in the literature.

i. Carbon-11 Pramipexole

The pharmacophore for several of our previously explored compounds was the D_3-agonist, pramipexole (Figure 4- 24). To our knowledge, pramipexole itself has never never been radiolabeled for *in vivo* PET imaging. We reasoned that this could be accomplished using carbon-11, and enable us to explore the reactivity of the amine off the tetrahydrobenzothiazol moiety.

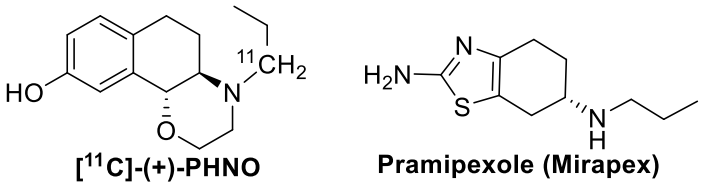

Figure 4- 24 Pramipexole

Our approach to synthesize [^{11}C]pramipexole was to employ a similar labeling strategy used for the preparation [^{11}C]-(+)-PHNO, although we recognize it has a "complicated synthesis" when considering the short half-life of carbon-11 (Scheme 4- 7, Figure 4- 25). Since the Scott group has applied complicated, multi-step, and water sensitive synthesis to carbon-11 labeling in this project and beyond,[247] we attempted to adapt the synthesis of [^{11}C]-(+)-PHNO to [^{11}C]pramipexole.

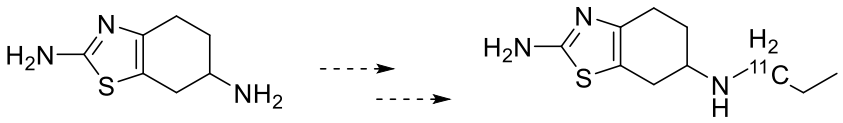

Figure 4- 25 General Strategy for C-11 labeling

The desired precursor and reference standard were both commercially available, and carbonyl-containing intermediate was synthesized as previously reported (Figure 4-25).[245] Two major strategies were employed, both starting with an ethyl Grignard and [^{11}C]CO_2 to produce [^{11}C]-magnesium bromide priopionate (Scheme 4- 22). Approach 1 planned to utilize thionyl chloride to produce [^{11}C]prionyl chloride that would be reacted

with the amine precursor in base to give the desired amide. Subsequent reduction with lithium aluminium hydride (LAH) would then provide [^{11}C]pramipexole. Approach 2, deviated at the point of the [^{11}C]-magnesium bromide priopionate where, treatment with HCl, would provide [^{11}C]propioninc acid. With amide coupling reagents, N-(3-Dimethylaminopropyl)-N′-ethylcarbodiimide (EDC)/1-Hydroxybenzotriazole hydrate (HOBt), and N-[(Dimethylamino)-1H-1,2,3-triazolo-[4,5-b]pyridin-1-ylmethylene]-N-methylmethanaminium hexafluorophosphate N-oxide (HATU) and the pramipexole amine precursor, this would give the amide intermediate. As with approach 1, this would also require another reduction step before producing the final [^{11}C]pramipexole.

Approach 1

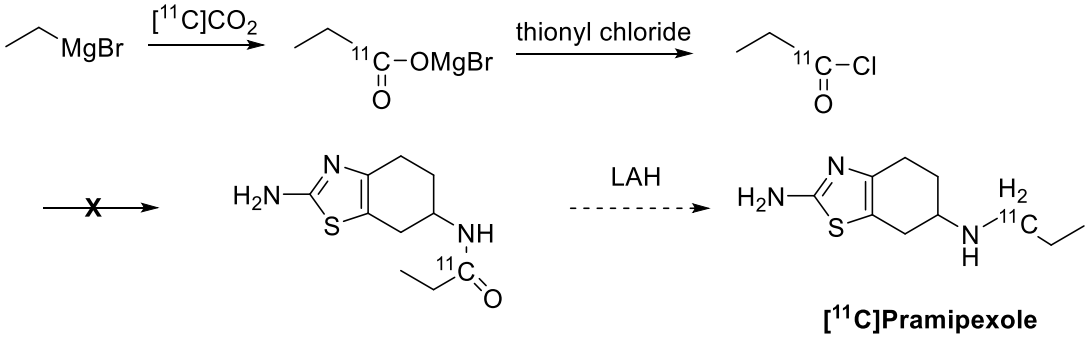

Approach 2

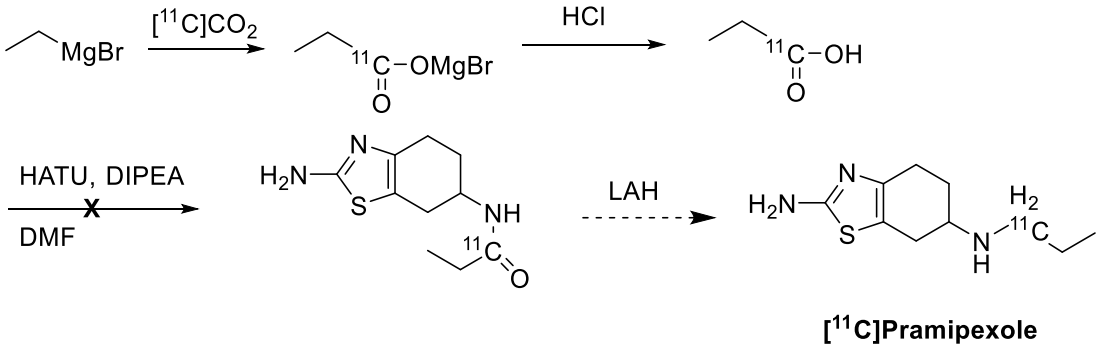

Scheme 4- 22 Approaches to [^{11}C]Pramipexole

These reactions were tackled in a stepwise formation, to show formation of new radiolabeled intermediates *via* HPLC. The formation of carbon-11 labeled N-(2-amino-4,5,6,7-tetrahydrobenzo[d]thiazol-6-yl)propionamide was monitored *via* HPLC alongside the previously synthesized cold standard intermediate; however it was never obtained. The coupling reagents, EDC (LDA, DMF, 2,3,4 eq) and HATU, alongside several amine and non-nucleophilic bases (TEA, DIPEA, DBU, LDA) and solvents (THF, DMF, 1,2 dimethoxyethane, 1,4-dioxane, trimethyl acetonitrile, 1,1,2,2-tetrachloroethane, 1,2 dichloroethane) were screened. Given that the carbon-11 amide intermediate was never obtained, no breakdown products were observed, the focus was shifted to another pramipexole-containing scaffold with superior selectivity at the D_3 receptor, in hopes that it would further shed light on the reactivity and stability of this compound class.

j. Results & Discussion Part 1: Pramipexole-Containing Compounds, Continued

Wang and colleagues reported a new series of pramipexole-containing compounds with exceptional selectivity and affinity at the D_3 receptor.[107] The compound of interest, has 451-fold selectivity at D_3 over D_2 and roughly 0.38 nM affinity (Figure 4-26). Given the 2-chloropyridine structure we sought to do a simple switch from chloro to fluoro without anticipation of a significant loss of affinity or selectivity. It should be noted that the chloro precursor and unlabeled fluorine standard were synthesized by the University of Michigan's Vahlteich Medicinal Chemistry Core.

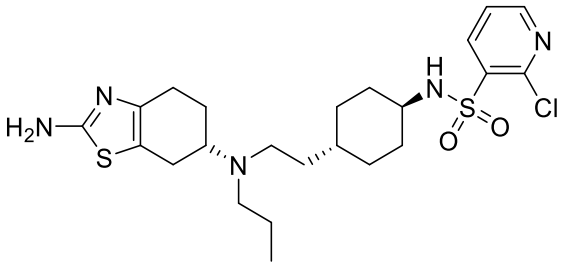

161
D2/D3 = 451
D2 K_i (nM) = 170 ± 19
D3 K_i (nM) = 0.38 ± 0.05

Figure 4- 26 Pramipexole-containing Compound for F-18 Fluorination

Like before, the screening of reaction conditions started with standard F-18 preparation in Kryptofix-222 and K_2CO_3, first in DMSO with no desired product (Entry 1-4, Table 4- 12). Using the same preparation of F-18, but changing solvent to DMF showed an initial 67% RCC (Entry 5), however this result could not be reproduced. Using :[^{18}F]-TEA-HCO_3, DMF, 120^{o}C, 40 min gave consistent and reproducible results from manual to automated synthesis, n = 3, 5.37±1.09% RCC (Table 4- 12, Entries 6-8).

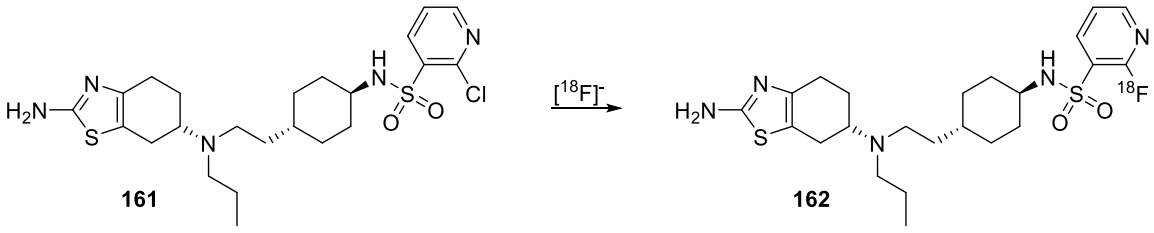

161 **162**

Scheme 4- 23 F-18 Fluorination of 161

Going forward, while the initial radiochemical conversions are promising, reaction conditions would benefit from further optimization. So far, no fragmentation or instability issues are apparent on HPLC or radioTLC from this pramipexole-containing compound from the standard or during radiolabeling. Prospective stability could be gained from replacement of the piperazine moiety.

*Table 4- 12 Preliminary F-18 Fluorination of Pramipexole-containing Compound **161***

Entry	RCC (%)	Precursor	Solvent	Prep	Solvent Volume	T (°C)	Time	Analysis	Type
1	X	1 mg	DMSO	K222, K_2CO_3	0.5 mL	100	15 min	HPLC	Automated
2	X	1 mg	DMSO	K222, K_2CO_3	1.0 mL	100	15 min	HPLC	Automated
3	X	1 mg	DMSO	K222, K_2CO_3	0.5 mL	100	20 min	HPLC	Automated
4	X	1 mg	DMSO	K222, K_2CO_3	1.0 mL	120	20 min	HPLC	Automated
5	67.21*	2 mg	DMF	K222, K_2CO_3	1 mL	130	30 min	HPLC	Automated
6	4.27	1 mg	DMF	TEA-HCO_3	1 mL	120	20 min	radioTLC	Manual
7	6.85	1 mg	DMF	TEA-HCO_3	1 mL	120	40 min	radioTLC	Manual
8	5	1 mg	DMF	TEA-HCO_3	1 mL	120	40 min	HPLC	Automated

*Non-reproducible
Non-isolated yields.
Syntheses of Standard/Precursor: Vahlteich Medicinal Chemistry Core

Given these synthetic difficulties due to suspected stability issues arising from the pramipexole moiety, we instead focused upon preparing radiotracers based upon the BP897-derived naphthamide derivative

k. Results & Discussion Part 2: Naphthylamide-containing Compounds

i. Design & Synthesis

BP897 is a potent and D_3-selective partial agonist first reported by Pilla and Sokoloff.[55] BP897 suffered in selectivity against the human adrenergic receptor, which ultimately limited its clinical potential. A systematic approach to explore the SAR at these receptors was undertaken in an effort to improve the selectivity (over the D_2 and adrenergic α-1 receptor, aka α), and several promising 2nd generation compounds were identified (Scheme 4- 24).[108]

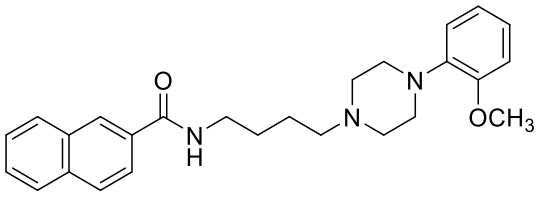

BP 897
D2/D3: 70
D3 K_i (nM): 0.92

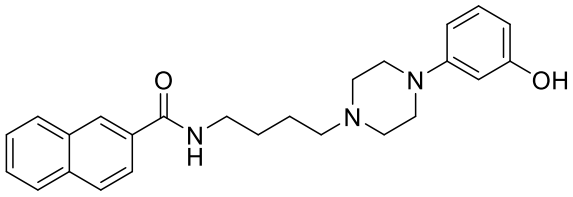

D2/D3: 1900
D3 K_i (nM): 0.2
D2 K_i (nM): 373
α K_i (nM): 1525
154

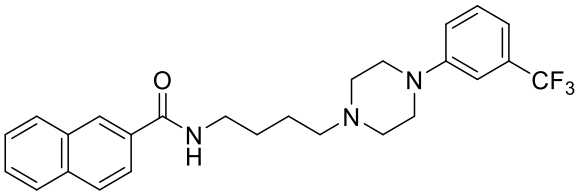

D2/D3: 1400
D2 K_i (nM): 1553
D3 K_i (nM): 1.1
α K_i (nM): 283
155c

Scheme 4- 24 Improving the selectivity of "BP897"

Building off of these reported compounds, several other leads were designed with logP and ease of radiolabeling in mind (Scheme 4- 25); the -CF_3 containing compound being a previously reported compound (Scheme 4- 24).[108]

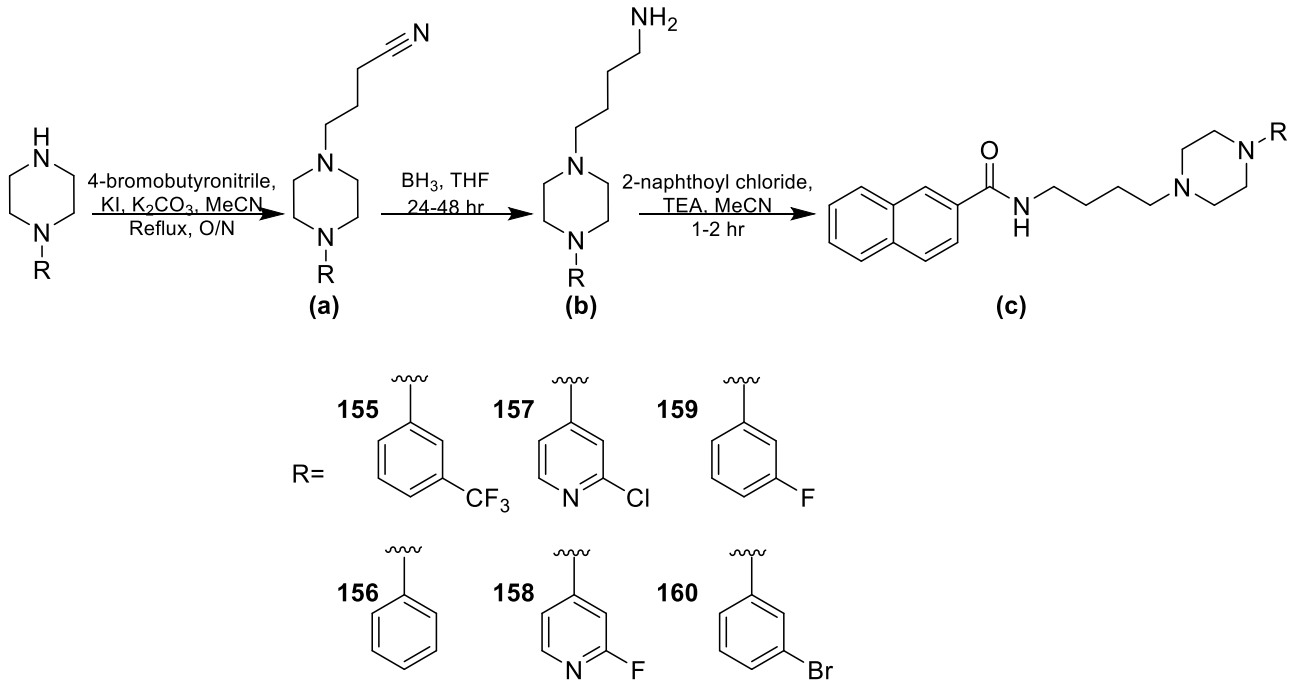

Scheme 4- 25 New D3-Selective Candidates & Synthesis

The compound with the most promising selectivity at the D_3 receptor is reported to have 1400-fold selectivity at the receptor, with a 1.1 nM affinity at D_3 (Ki = 1553 nM at D2). The synthesis of **155** was reported previously, and was remade for evaluation in this work in a similar fashion, but with some deviation (Scheme 4- 25).[108] The appropriately substituted phenyl (or pyridinyl) piperazines were commercially available. They were alkylated with 4-bromobutyronitrile, to form the intermediates (**155-160a**) in 68-98% yield. These were then reduced in borane-THF (26-72% yield) for 24-48 hr, to form amines **155-**

160b. The standards were synthesized by combing the amine in TEA with 2-naphtholyl chloride to form the amide series, **155-160c** (42-87%). A detailed discussion of methods and reagents can be found starting on **page 266**.

ii. *In Vitro* Evaluation of Selected Compounds in Whole Brain Rat Tissue

With cold reference standards in hand, we sought to confirm binding and selectivity of the compounds we prepared for the D_3 receptor using frozen whole rat brain tissue under conditions as close to physiological as possible. Binding assays were performed using the commercially available D_3 receptor agonist [^{3}H]-*R*-(+)-7-hydroxy-N,N-di-*n*-propyl-2-aminotetralin ([^{3}H]-*R*-(+)-7-OH-DPAT) and varying concentrations of the test compound in rat brain slices, with pramipexole used to identify non-specific binding. Similarly, D_2 receptor binding assays were performed with [^{3}H]spiperone, using (+)-butaclamol to identify non-specific binding.[20,23,135,248–250]

The naphthamide compounds (Scheme 4- 24), 155c (CF_3) was shown to be 1400-fold selective and the 3-hydroxy phenyl (bioisostere fluorine 101) to be 1900-fold selective at the receptor.[108] The compounds selected for *in vitro* evaluation were chosen to confirm currently available binding data for the previously reported compounds, and to evaluate novel compounds (Figure 4- 27).

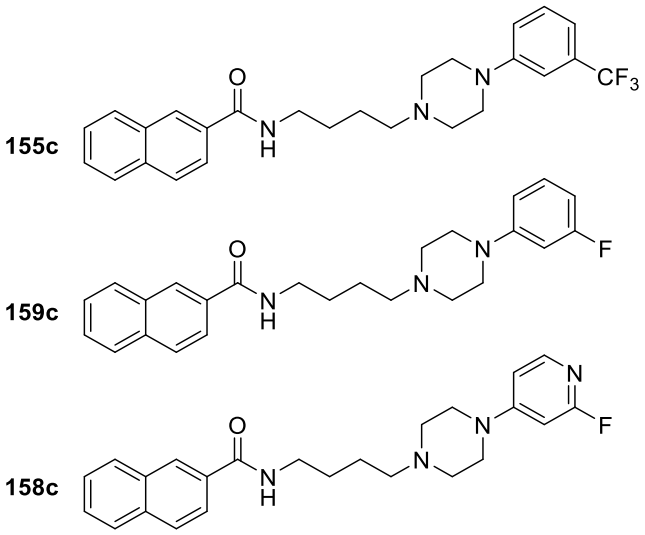

Figure 4- 27 Selected compounds for in vitro evaluation

iii. *In vitro* Results

In vitro evaluation of these compounds was performed with cold carbon-12 or fluorine-19 standards against tritiated pharmacological agents as previously described. Previous reports describe the use of other cofactors and additives, as discussed before.[36] We sought to perform assays under physiologically relevant conditions to mimic *in vivo* behavior, since many of these compounds perform well *in vitro* but fail *in vivo*. In our hands, selectivity for the D_3 receptor was apparent (Table 4- 13), but it was orders of magnitudes less than reported in the literature. This is in line with literature reports describing differences in binding and selectivity data between *in vitro* and *in vivo* experiments.[36]

Table 4- 13 Competition of cold standards with ^{3}H-pharmacological agents

Compound	[^{3}H]-7-OH-DPAT	[^{3}H]Spiperone	Reported Selectivity (D2/D3)	Selectivity in our system (D2/D3)
155c	K_i 46.5 ± 10.7 nM Bmax 0.230 ± 0.015 fmol/µg	K_i 647 ± 79 nM Bmax 0.627 ± 0.037 fmol/µg	1400[108]	14
158c	K_i 4.49 ± 0.31 µM Bmax 0.301 ± 0.007 fmol/µg	K_i 9.9 ± 1.120 µM Bmax 1.120 ± 0.0022 fmol/µg	N/A	2.2
159c	K_i of 48.0 +/- 10.2nM Bmax of 0.185 +/- 0.020 fmol/µg	K_i of 1.01 +/- 0.12 µM Bmax of 0.506 +/- 0.021 fmol/µg	1900[108]*	21
***bioisostere**				

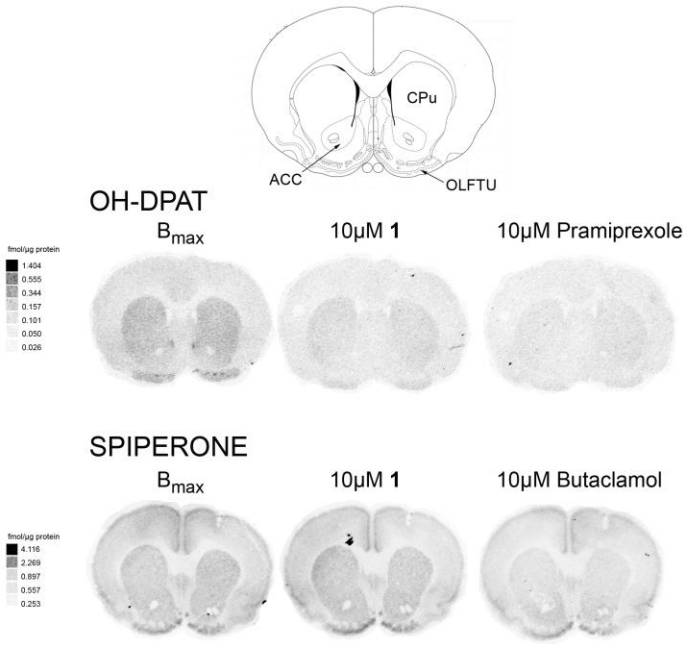

*Figure 4- 28 Rat Brain Autoradiography Studies of **155c** (CPu: caudate putamen, ACC: nucleus accumbens, OLFTU: olfactory tubercle)*

Our results demonstrate 14-fold selectivity of **155c** for D_3 receptors over D_2. We were encouraged to observe that the low nanomolar affinity and D_3 selectivity translated to *ex vivo* tissue samples, albeit with the expected losses in affinity and selectivity consistent with conducting binding affinity in true tissue samples. As expected, [^{3}H]R-(+)-7-OH-DPAT binding was highest in the caudate putamen (CPu), nucleus accumbens (ACC)

and olfactory tubercle (OLFTU), areas known to be rich in D_3 receptors (Figure 4- 28).[251] Reflecting the colocalization of D_2 and D_3 receptors in the rat brain, [^{3}H]spiperone binding was apparent in the same areas. Non-specific binding of [^{3}H]R-(+)-7-OH-DPAT was determined to be minimal (Panel C) by incubating with 10 μM pramipexole, a dopamine D_3 ligand.[252] Analogous identification of [^{3}H]spiperone non-specific binding was accomplished by co-incubating with 10 μM of the D2 antagonist butaclamol (Panel F).[21,252] Notably, incubating with 10 μM 1 was found to displace [^{3}H]R-(+)-7-OH-DPAT by a similar degree to pramipexole (Panel B), but did not displace [^{3}H]spiperone (Panel E), confirming good D_3 selectivity.

The large differences in selectivity between these experiments could be due to receptor availability. The literature values were largely from cell-derived (transfected HEK 293 cells) or membrane-based assays, whereas our system utilizes whole rat brain tissue (Table 4- 13).[108,130,253]Transfected cells are the main choice for the drug discovery platorm since they allow for more sophisticated functional assays to identify the action of compounds at GPCRs (non-radioactive, for HTS, and utilizes readouts such as Ca^{2+}, GTP binding, or cAMP).[254,255] Contrastingly, ligand binding is classically performed with a radioligand in whole tissue or membranes. Differences are expected since in assays utilizing cells transfected with human receptors (or membranes), it is possible that the receptor protein has been effectively concentrated and available binding sites more exposed than those in whole tissue, and this would account for our findings. Despite differences in magnitude of selectivity, we were nevertheless encouraged that the general trend in degree of selectivity was consistent between our data and the literature reports.

iv. Summary and Compound Selection

From literature reports and our own studies, the most promising compounds are **159c** and **155c**, owing to their high affinity for the D_3 receptor and good selectivity over the D_2 receptors. The remainder of this work focuses on the synthesis and evaluation of [^{11}C]155c. Moving this project forward, **159c** would be a promising candidate for ^{18}F-fluorination. Competition curves against [^{3}H]R-(+)-7-OH-DPAT and [^{3}H]Spiperone for both compounds can be found from **page 274**.

v. Synthesis of [^{11}C]155c

The general approach to labeling this scaffold was to utilize a naphthyl Grignard, to undergo [^{11}C]CO_2 insertion, followed by formation of the acyl chloride with thionyl chloride and catalytic DMF. The acyl chloride would then be combined with the amine precursor **155b**, in base, to form the amide, **155c** (Scheme 4- 27). This utilized an in-house Grignard prepared same-day, or commercially available naphthyl Grignard, **161**. In each case, the Grignard reagent was titrated with salicylaldehyde phenylhydrazone as described previously.[256]

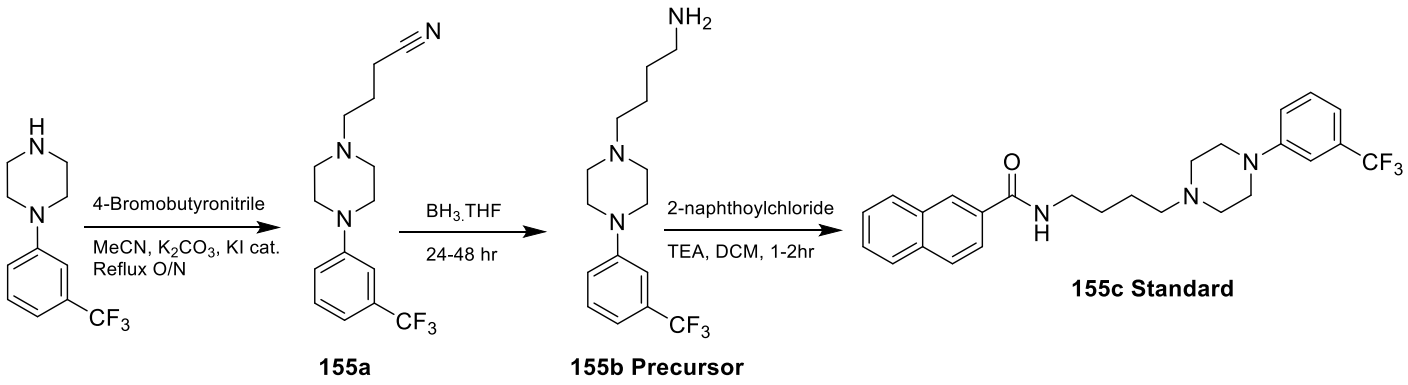

Scheme 4- 26 Synthesis of standard and precursor for [^{11}C]155c

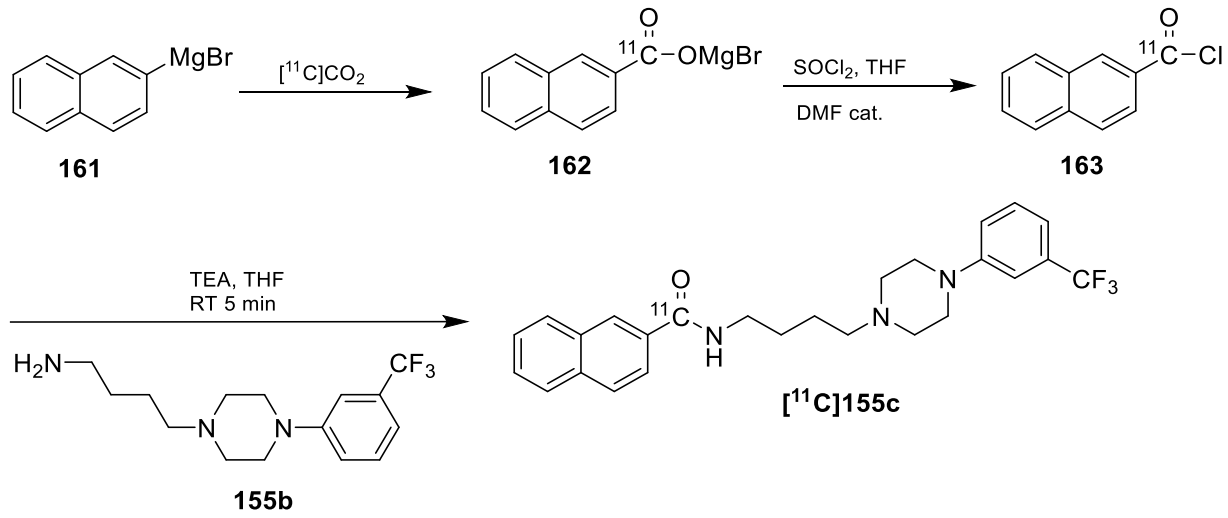

Scheme 4- 27 Synthetic strategy for C-11 labeling

Carbon-11 was produced *via* the $^{14}N(p,\alpha)^{11}C$ nuclear reaction, and ~40 min beam to produce roughly 3 Ci of carbon-11 as $[^{11}C]CO_2$. The preparation of **[^{11}C]155c** began by bubbling $[^{11}C]CO_2$ into a solution of the Grignard (in THF) for 5.5 min at 7 mL/min. This was followed by addition of thionyl chloride with cat. DMF in THF for 1.5-2 min. The precursor was then added and the reaction was stirred for 5 min. The stirring was turned off and the reaction mixture let settle for 1 min, before being passed through a Gelman

Acrodisc 13 CR PTFE 0.2 micron filter, and injected onto a semi-preparative C18 HPLC column (60% MeCN, 20mM NH_4OAc, 2 mL HOAc) at 2.5 mL/min. The desired peak was collected (R_T 10 – 11.5 min, Figure 4- 29). Chemistry optimization demonstrated good yield with carrier-added (1 mL CO_2), with radiochemical conversions (non-reformulated doses) of 23-26% (n=3), while non-carrier was 8-10% (n=2).

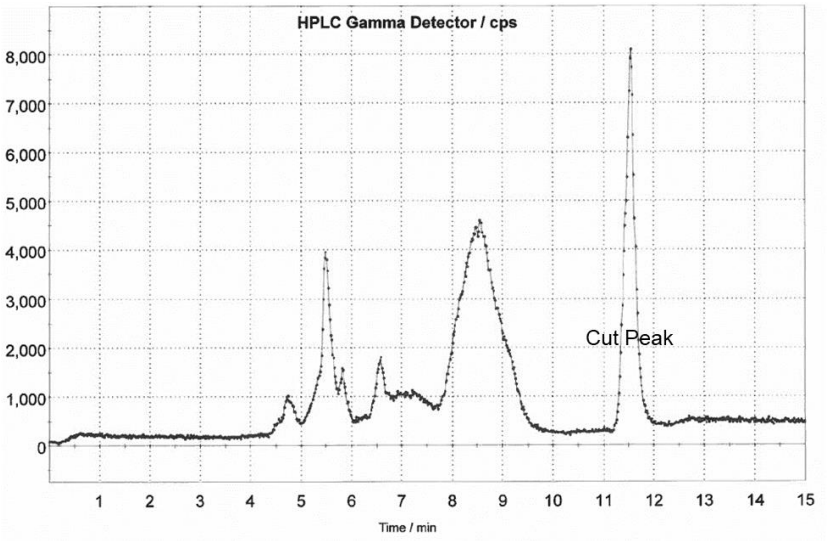

Figure 4- 29 Semi-preparative HPLC trace for [^{11}C]155c

Reformulation for preparation of an injectable dose for microPET imaging consisted of the following: compound **[^{11}C]155c** was diluted into 45 mL water containing 1mL 1% NH_4OH. This solution was passed through a C18 sep-pak (Waters), the cartridge was rinsed with another 2 mL water to remove residual HPLC mobile phase. Product **[^{11}C]155c** was eluted with ethanol (x mL – varied as a result of the desired final volume desired) and diluted with 0.9% saline to provide the final formulated product as a sterile isotonic product in 10% ethanolic saline solution (pH 5.5).

Non-carrier added synthesis were performed, and **[^{11}C]155c** was obtained in 0.8±0.2% decay-corrected radiochemical yield (RCY) (0.025 ±0.005% non-decay corrected) in 82±1% radiochemical purity (RCP), n=2. Carrier added syntheses were also attempted in which 1 mL of CO_2 was included in the synthesis of **[^{11}C]155c**. Product **[^{11}C]155c** was obtained in slightly higher RCYs (4.9±0.6% decay corrected RCY (0.11±-.01% non-decay corrected RCY)), in 100±0% RCP, n=2. Carrier-added synthesis gave modest specific activity of 133 Ci/mmol, while non-carrier specific activities were higher 1941 Ci/mmol. The imaging properties of both the carrier added and no-carrier added products were evaluated in female Sprague Dawley rats.

vi. MicroPET imaging: General Considerations

MicroPET imaging studies were conducted using a Concorde Microsystems P4 PET scanner (Figure 4- 30). Anesthesia was induced in healthy, female Sprague-Dawley rats (293-346 g) using isoflurane/O_2, and anesthesia was maintained with 2-4% isoflurane/O_2 throughout the experiment. Body temperature was maintained by a heating pad. A transmission scan for attenuation correction was acquired prior to administration of the radiolabeled compound of interest via tail vein injection (378-494 μCi).

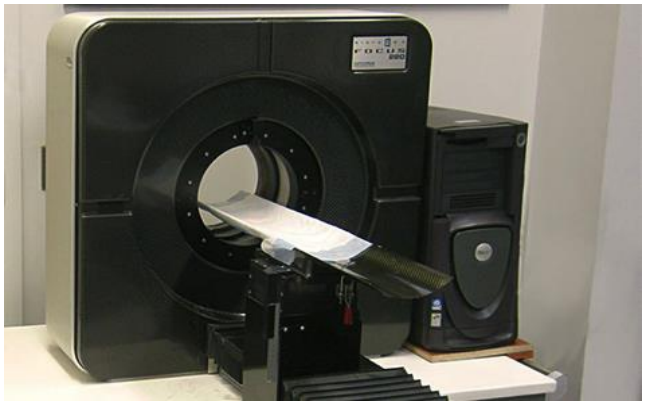

Figure 4- 30 Concorde Microsystems P4 PET scanner

Emission data were collected over 60 minutes. The emission data were corrected for attenuation, decay, dead time and random coincidences before reconstruction using an iterative ordered subset expectation maximization–maximum a posteriori (MAP) method to generate reconstructed images. The frames were summed, smoothed, and a region-of-interest was defined on several planes for the whole brain. The volumetric ROI was then applied to the full dynamic data set to obtain the brain tissue time-radioactivity data. Standardized uptake values (SUVs) were calculated for time-radioactivity data.

vii. MicroPET Imaging [^{11}C]155c: First Impressions

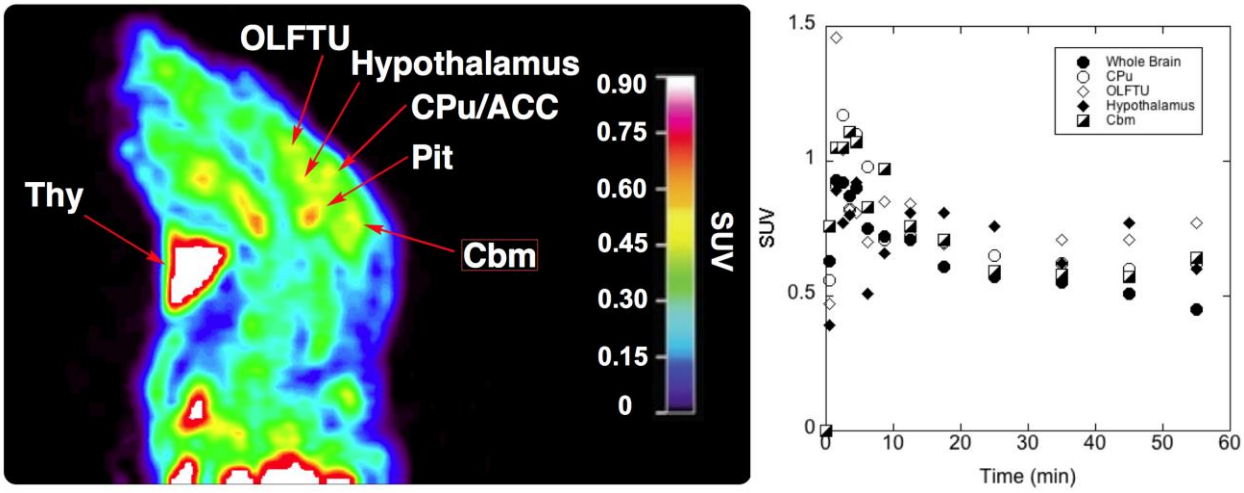

Figure 4- 31 Summed sagittal rodent image (0–60 min post-injection of [^{11}C]155c) and time-radioactivity curves for [^{11}C]155c (Cbm: cerebellum, CPu: caudate putamen, OLFTU: olfactory tubercle)

We were encouraged to see good CNS penetration of the radiotracer, as well as increased retention in identifiable brain regions. Notably, highest uptake was in the olfactory tubercle (peak SUV ~1.5), caudate putamen (including nuclear accumbens) region (peak SUV ~1.2) and hypothalamus (peak SUV ~0.9), known D_3-rich areas of the brain[251,257] that are consistent with the highest distribution of D_3 receptors identified in the [^{3}H]R-(+)-7-OH-DPAT autoradiography experiments described above. There was also uptake in the cerebellum (Cbm) that was lower (peak SUV ~1.0), and is also consistent with the known distribution of D3 receptors in the rat brain. D_3 receptors are found in the cerebellum, but at lower areas than, for example, the caudate putamen and olfactory tubercle.[257] There was also uptake of [^{11}C]155c in both the thyroid (Thy) and pituitary (Pit)

glands (Figure 4- 31), consistent with other radiotracers based upon the BP897 scaffold[21,216,258] and possibly indicative of non-specific binding.

Future experiments aimed at understanding the extent of non-specific binding, in vivo selectivity for D_3 over D_2 receptors, and sensitivity of the radiotracer to endogenous dopamine will occur following scale up and optimization of the radiosynthesis and translation of the radiotracer into nonhuman primates, where small D_3-rich areas of the brain are more accurately identifiable and quantifiable.

viii. MicroPET imaging with Carrier-Added [^{11}C]155c

Initial imaging was conducted using carrier added **[^{11}C]155c**. (raw data: Figure 4-32; adjusted to SUV: Figure 4- 33, PET:Figure 4- 34). While the imaging shows initial good uptake in the brain, clearance was not traditional and accumulation of a labeled entity was seen throughout the brain and the rest of the body of the rat. Whether this entity was the original (desired) compound, **[^{11}C]155c**, or a metabolite was of interest.

Whole Brain TAC 1094	Whole Brain Tac 1095
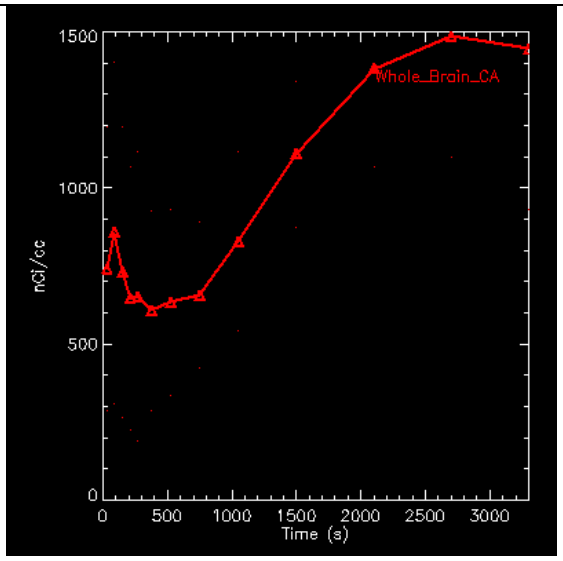	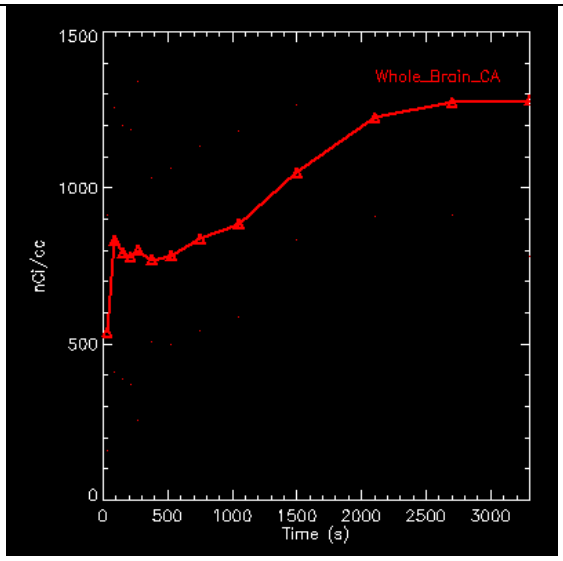

Figure 4- 32 Raw Whole Brain TACs for Carrier-Added Syntheses

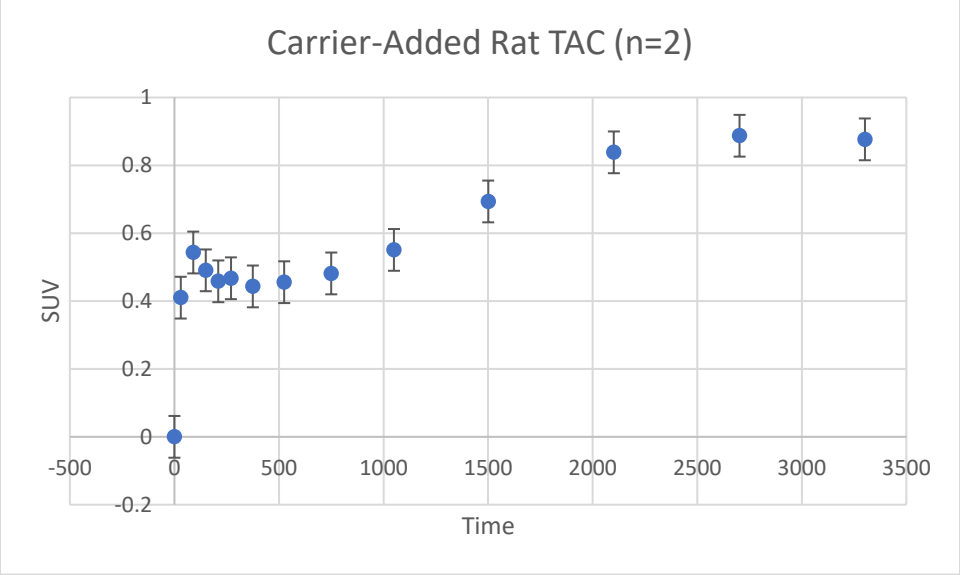

Figure 4- 33 CA Adjusted to SUV

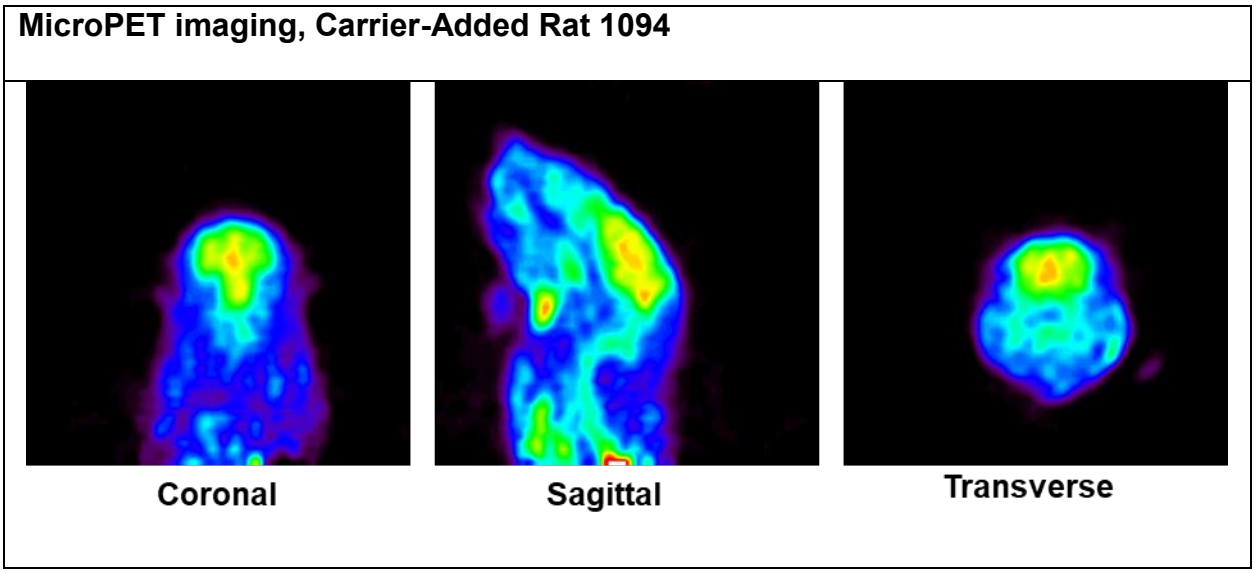

Figure 4- 34 MicroPET Rat 1094, Carrier-Added

ix. MicroPET imaging with No Carrier-Added [^{11}C]155c

We also conducted microPET imaging with no-carrier added **[^{11}C]155c** to not only produce a dose of higher specific activity, but to explore the role of cold mass in the final product and *in vivo* kinetics compared to the carrier-added synthesis. as well as blood stability of the carrier-added prepared compound. It should be noted that RCYs with carrier are traditionally higher than without carrier, and was apparent in this synthesis as well. Carrier-added synthesis produced activities around 3 mCi, while non-carrier products were regularly under 1 mCi.

Synthesis of **[^{11}C]155c** was performed as previously described, ROI's drawn for whole brain, and TACs generated. The *in vivo* behavior of the non-carrier added radiolabeled compound was as expected for a brain tracer with good uptake and washout in the whole brain (raw TAC: Figure 4- 35, adjusted to SUV: Figure 4- 36, PET: Figure 4-

37). While this behavior is desired, the non-carrier synthesis suffered with poor yields, regularly under 1 mCi.

Whole Brain TAC 1093	Whole Brain TAC 1101
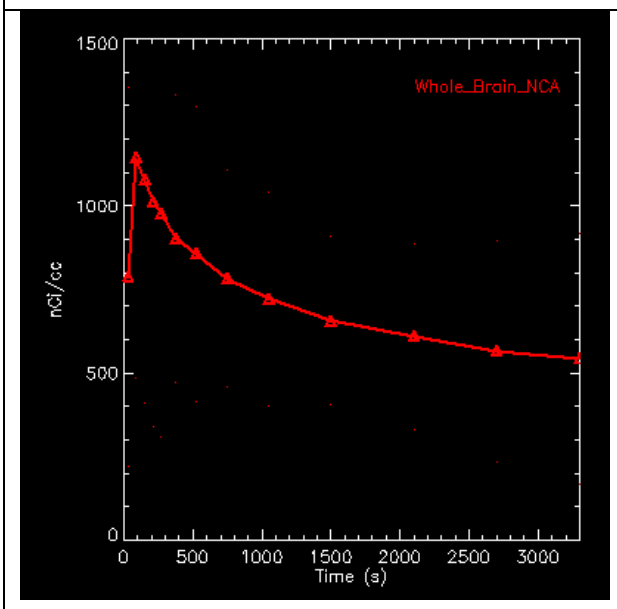	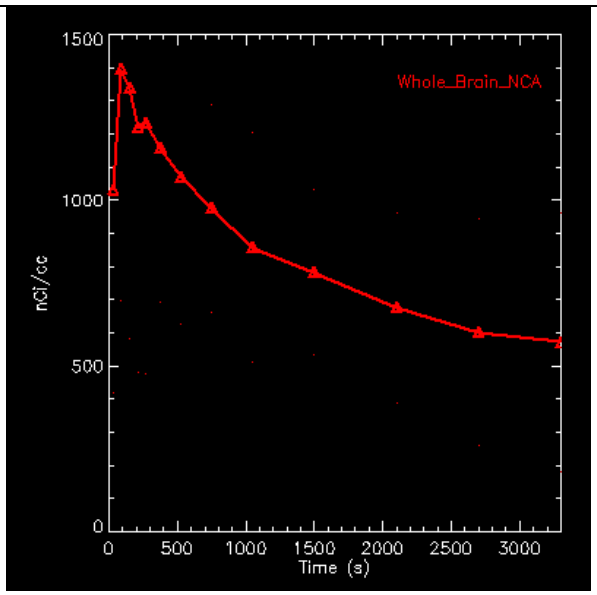

Figure 4- 35 Raw Whole Brain TACs for Non-Carrier Added Syntheses

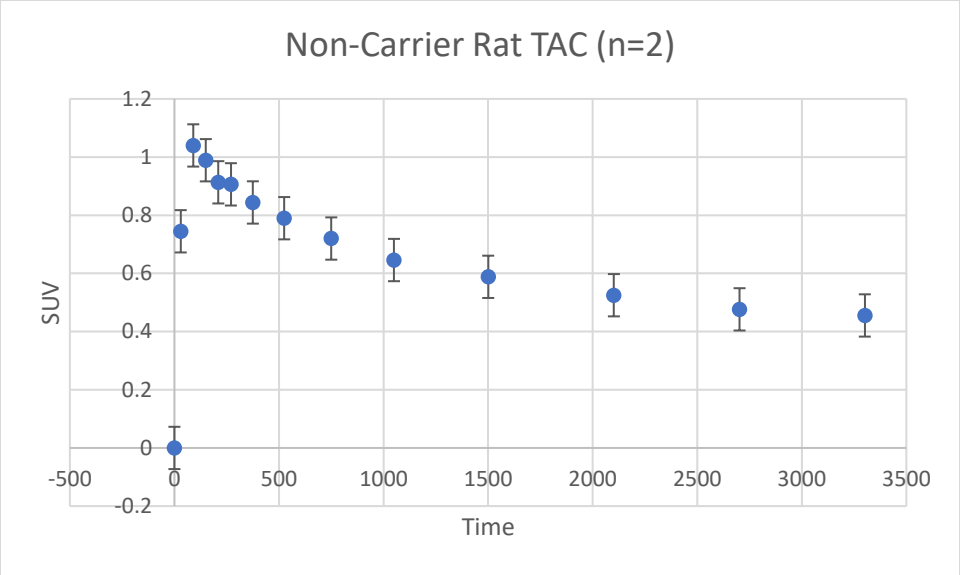

Figure 4- 36 NCA Adjusted to SUV

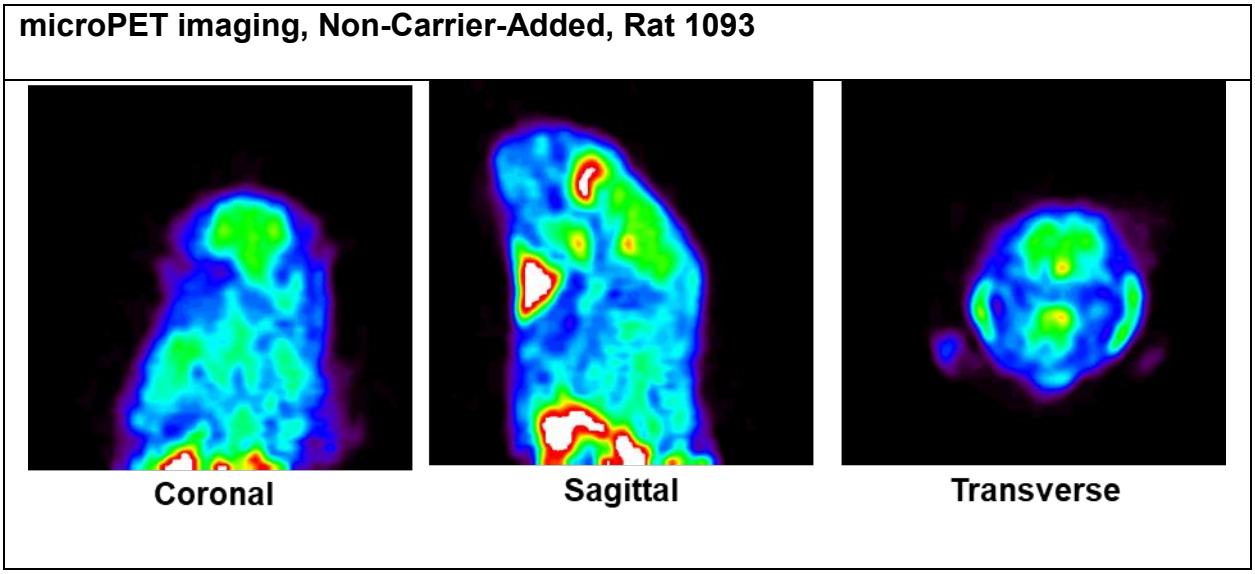

Figure 4- 37 microPET, NCA Rat 1101

Given the restricted expression of the dopamine D3 receptors in the brain, and resolution of PET, these regions cannot readily be identified in rodents. In order to thoroughly explore this potential radiotracer, target engagement and binding with

pharmacological agents and amphetamine challenge to stimulate endogenous dopamine release, non-human primate imaging in necessary. However, the low yields of the radiochemical syntheses are such that further *in vivo* studies in non-human primates are not currently feasible. Since >1 mCi of the dose is required for non-human primate imaging, it is necessary to further improved the radiosyntheses prior to imaging in higher species. This work extends beyond the scope of this thesis.

Given the clear discrepancy of *in vivo* behavior of these two compounds prepared with and without carrier, we sought to understand this by exploring the stability of **[^{11}C]155c** in human and rat blood.

x. [^{11}C]155c Stability Studies

1. General Methods

The stability of **[^{11}C]155c** was examined in female rat and female human plasma. Blood was collected up to three days prior to radiosynthesis; heparin was added and the blood stored at 8^{o}C, in the refrigerator, if it was not used same-day. Carrier-added **[^{11}C]155c** was synthesized as described above, and delivered in 10% ethanol/saline. Whole human blood (with heparin) was centrifuged at 1000xg (later experiments at 7500rpm) for 5 min, and the plasma/supernatant was transferred to a separate tube. **[^{11}C]155c (**100 µL) was added to 50 µL of plasma. stirred and incubated at RT for 5, 15 and 30min. After incubation, 50 µL samples were removed, diluted with 50 µL of EtOH

and mixed. This mixture was centrifuged for an additional 2 min and the supernatant was analyzed by radioTLC (silica TLC plates eluted with 10% MeOH/EtOAc).

2. Results & Discussion

RadioTLC was the chosen method for most of these stability studies, given the short half life of carbon-11 (20 minutes) and multiple incubation/extraction steps in the blood plasma. Several TLC plates could be run and analyzed back-to-back in a shorter time frame compared to a single HPLC run of 15 min (nearly 1 half life). The TLC plate could then be exposed on film for phosphorimaging. In this way, we wanted to be able to visualize the initial dose, co-spot, and product after incubation in blood at the same time.

To that end, **[^{11}C]155c** was prepared as before, but kept in semi-preparative HPLC buffer due to low activity (60% MeCN, 20 mM ammonium acetate, 2 mL HOAc). Roughly 1 mL of human and 1 mL rat blood was processed separately as follows: 172 µCi was delivered and 400-500 µl added to each blood sample (66.3 µCi and 24.7 µCi decay corrected to human and rat) and incubated for 10 minutes. These were centrifuged 7500 RPM for 5 minutes. The pellet (P) and supernatant (S) were isolated. S_{human} 21.2 µCi and P_{human} 15.7 µCi; and S_{rat} 17.5 µCi and P_{rat} 9.5 µCi (decay corrected). To the supernatant was added 500 µl absolute ethanol, sample was mixed thoroughly, then centrifuged 14,000 RPM for 5 min. The supernatant (S) and pellet (P) were isolated again and the

supernatant used for radioTLC analysis. S_{human} 27.2 µCi and P_{human} 6.7 µCi; and similarly for rat: S_{rat} 21.6 µCi and P_{rat} 6.7 µCi (decay corrected).

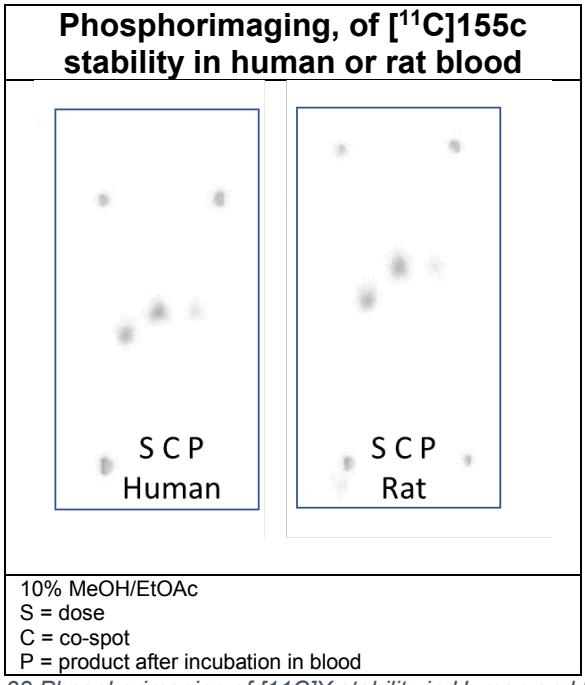

Figure 4- 38 Phosphorimaging of [11C]X stability in Human and Rat blood

While there appears to be a new product, across human and rat, the co-spot indicates a mere shift in the retention factor, and no actual breakdown in product (Figure 4- 38). We sought to explore the stability further with HPLC. A breakdown product was never obtained, as low activity in initial synthesis, and following blood incubation or after circulating *in vivo*, extraction, and injection on HPLC severely limited our detection. Isolation and identification of the breakdown product was not identified.

Further exploration and final investigation of dose stability in solution was explored on HPLC. **[^{11}C]155c** was prepared as before, aliquots taken in (1) semi-preparative HPLC

buffer, (2) 100% EtOH, (3) ethanolic saline and analyzed *via* analytical HPLC. Degradation of the parent compound under these conditions was not seen on HPLC

In conclusion, NCA **[^{11}C]155c** deserves further exploration as its possible utility a a D_3 radiotracer. There is a clear difference in uptake between NCA and CA syntheses, as there appears to be increased uptake in the thyroid or lymphatic glands, but good brain penetrance. While the TAC of the CA tracer provides what we initially suspected was evidence of metabolism, we were unable to isolate a metabolite for HPLC (during plasma stability studies) and, in contrast to initial radioTLC data, later radioTLC plasma stability studies reproducibly confirms that **[^{11}C]155c** is stable in plasma (also confirmed in HPLC: in semi-preparative HPLC buffer, ethanol, ethanolic/saline; please see methods from **page 266**). Therefore future efforts will optimize the radiosynthesis of **[^{11}C]155c** so that additional *in vivo* evaluation in non-human primates can be undertaken.

xi. Nucleophilic F-18 Fluorination of other Prospective D3 selective compounds

Other prospective dopamine D_3 receptor compounds were pursued and a selection of these will be discussed here. In the naphthylamide class, **157** and **158**, was designed to explore the SAR at this receptor. Indeed, while selectivity at the receptor was later found to be poor (Table 4- 13), initial labeling by nucleophilic F-18 fluorination was explored with standard F-18 preparation in K_{222}/K_2CO_3, as well as TEA-HCO_3 (Table 4- 14Scheme 4- 28).

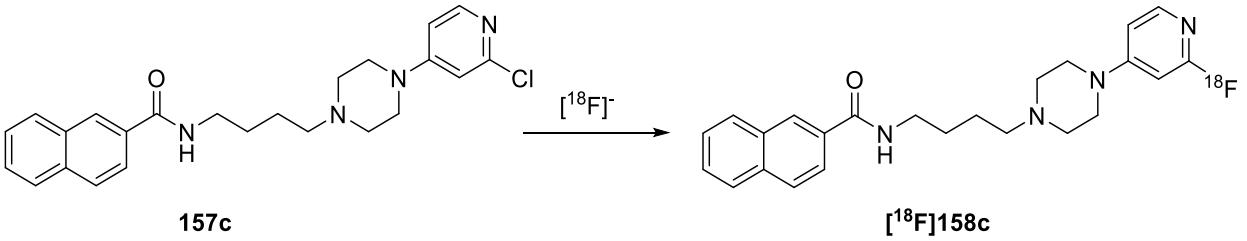

157c **[^{18}F]158c**

Scheme 4- 28 F-18 Fluorination of 157c

A brief screen of conditions, from F-18 fluoride prep, to precursor amount, temperature, and time was performed manually. Initial attempts utilized standard F-18 fluorination conditions for halex exchange at the pyridine ring, utilizing DMF, Kryptofix-222, and potassium carbonate at 100^{o}C and 120^{o}C for 20 min. While Entry 2 appeared promising (Table 4- 14) *via* HPLC, it was not easily reproduced. A different fluoride preparation with TEA-HCO_3 was pursued as it has good success in our lab with halex and isotopic exchange. With that, modest yields were obtained at 4 and 5% RCC manually (Entry 8-9) which surpassed the modest <2% RCC in the standard F-18 preparation (Entry 4-5). While this compound can be labeled, given the preliminary *in vitro* studies and more selective compounds identified, this potential tracer will not be pursued further.

*Table 4- 14 Preliminary F-18 Fluorination of **157c** to give **[^{18}F]158c***

Entry	RCC (%)	Precursor	Solvent	Prep	T (^{o}C)	Time	Notes	Analysis (crude rxn mix)
1	X*	2 mg	1 mL DMF	K_{222}, K_2CO_3	100	20 min	Manual	HPLC
2	74**	2 mg	1 mL DMF	K_{222}, K_2CO_3	120	20 min	Manual, broad peak	HPLC
3	1	2 mg	1 mL DMF	K_{222}, K_2CO_3	120	20 min	Manual	radioTLC
4	1.4	2 mg	1 mL DMF	K_{222}, K_2CO_3	120	20 min	Manual	radioTLC

5	1.6	2 mg	1 mL DMF	K_{222}, K_2CO_3	120	20 min	Manual	radioTLC
6	x	1 mg	1 mL DMSO	TEA-HCO_3	170	20 min	Manual	radioTLC
7	x	1 mg	1 mL DMSO	TEA-HCO_3	140	20 min	Manual	radioTLC
8	4.11	1 mg	1 mL DMF	TEA-HCO_3	120	20 min	Manual	radioTLC
9	5	1 mg	1 mL DMF	TEA-HCO_3	120	40 min	Manual	radioTLC
*malfunctioning hotplate, unlikely to be at 100°C **Non-reproducible 1 mL solvent volume								

xii. Conclusions and Future Considerations

The original goals of this project were to synthesize and evaluate potential PET radioligands selective for the dopamine D3 receptor. The original set of pramipexole-containing compounds proved to be difficult to not only synthesize, but stability issues in radiolabeling caused other scaffolds to be explored. The BP897 derived naphthylamide compounds, including preliminary microPET and evaluation of NCA **[^{11}C]155c** show promise as potential PET radioligands at the D3 receptor. The CA TAC could be the result of a miss injection such that, instead of a bolus injection (such as the NCA TAC), the dose could have been injected subcutaneously and not intravenously, which would cause activity to slowly acquire (resembling an infusion, instead of a bolus injection), as we see in the TAC. Even so, stability of **[^{11}C]155c** was explored in blood plasma using phosphorescence imaging and HPLC, which also suggest the compound to be stable (please see methods for HPLC traces of stability studies). Predicted metabolism of **[^{11}C]155c** does not suggest a brain penetrant metabolite, At this time, the differences in the CA and NCA images are unexplainable and require further investigation. With that,

the NCA **[^{11}C]155c** would be better pursued as a [^{18}F]CF_3-substituted tracer (**163**, Figure 4- 39). This would benefit from longer half life and prospective improved yields by negating the need for a water-sensitive organometallic reagent.

With regard to *in vivo* behavior, these radiolabeled compounds would be best evaluated in non-human primates through microPET imaging. Due to resolution limitations of imaging techniques, non-human primates as opposed to rodents will allow for identification of specific brain regions specific to D3 receptors: this includes the globus pallidus, substantia nigra/ventral tegmental areas and the thalamus. In addition, it is known that differences among species regarding the distribution of D3 receptors, brain permeability and subsequent radioligand metabolism varies and may result in misleading conclusions and for this reason, young mature female rhesus monkeys would be ideal. Baseline imaging studies will provide tissue time-radioactivity data for brain uptake/efflux determination and concurrent blood samples will be drawn at various time points during scan to determine radioligand metabolism.

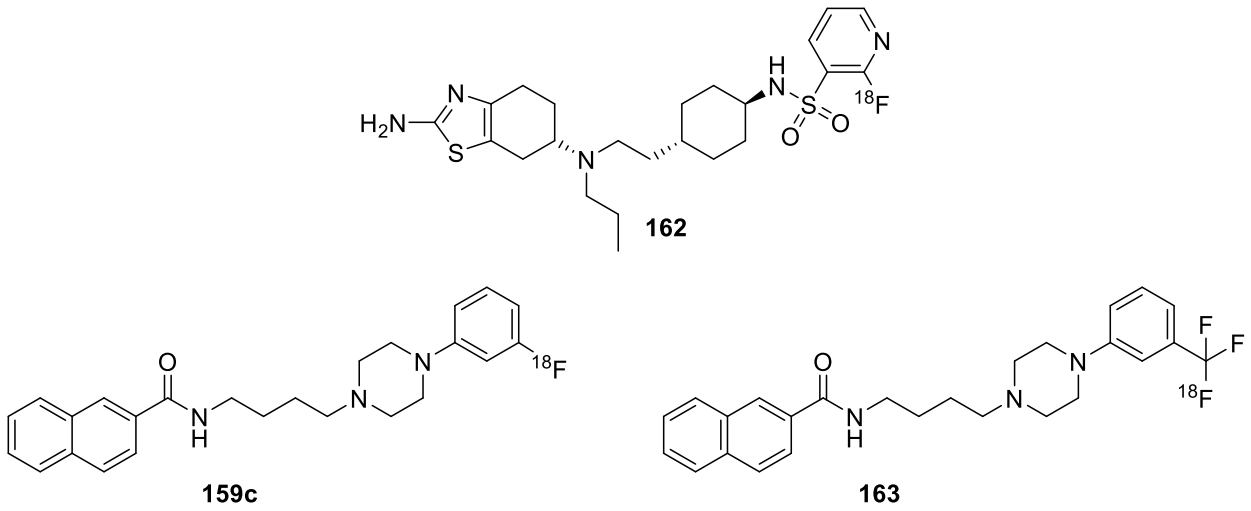

Figure 4- 39 Prospective D3 PET Radioligands that require further evaluation

Target engagement through the use of pharmacological blocking studies would be possible through the use of previously reported selective for the dopamine D2 or D3 receptor. Specific binding and non-specific binding of the radioligands will be assessed through procedures previously reported.[212] More specifically, microPET imaging will be utilized alongside chemical blockade *via* SB-277011, a selective D3 antagonist, as well as SV-156, a compound with no intrinsic activity but with 40-fold selectivity at the D2 receptor, alongside the fluorine-18 radioligands (Figure 4- 39).

Furthermore, microPET imaging in non-human primates to determine radioligand sensitivity to endogenous dopamine would provide further information on the *in vivo* behavior of these compounds. Behavioral manipulations[95,188,259–261] and pharmacological treatment[31,174,260,262,263] have been shown to produce a reduction in radioligand binding to dopamine D2/3 receptors when measured with PET (or SPECT). Interestingly,

amphetamine administration to patients with schizophrenia results in even greater reductions in D2 preferring antagonist [^{11}C]raclopride binding.[165,264–267]

As a result, fluctuations or changes in synaptic dopamine as a way to deduce changes in dopamine levels in the human brain can understood by measuring changes in radioligand binding. However, since these studies have proceeded with D2 or mixed D2/3 radioligands, a D3-selective radioligand is desirable. If shown to be sensitive to endogenous dopamine level fluctuations, the functional status or the D3 receptor may be better understood. MicroPET imaging following administration of amphetamine will be performed as previously described[267] with the expectation of reduced radioligand binding due to competition from endogenous dopamine at the receptor.

xiii. Experimental Methods, Considerations, and Supporting Data

1. Methods: Ligand Binding

D3 Receptor Saturation

Tissue sections were preincubated for five minutes in PBS, pH 7.4 at 25° C or 50mM Tris-HCl, pH 8.0, 50mM NaCl, 30mM EDTA at room temperature. The slides for total binding were then incubated in 5 - 60nM [^{3}H]R-(+)-7-OH-DPAT (American Radiochemical, Inc) in the above buffer for 15 minutes at room temperature. 10μM Pramipexole was added and an adjacent slide was incubated to define non-specific binding. Sections were washed twice for a total of two minutes in ice cold buffer then rinsed briefly in distilled water. Sections were air-dried before opposing to tritium sensitive phosphoimaging screen for three to five days.

D3 Receptor Displacement

Tissue sections were preincubated for five minutes in PBS, pH 7.4 at 25° C or 50mM Tris-HCl, pH 8.0 (± 150mM NaCl) at room temperature. Slides were then incubated in 35nM [^{3}H]R-(+)-7-OH-DPAT (American Radiochemical, Inc) with no addition (total binding) or various concentrations (300nM to 1mM, f.c.) of competing compound in the above buffer for 15 minutes at room temperature. 10μM Pramipexole was added and an adjacent slide was incubated to define non-specific binding. Sections were washed twice for a total of two minutes in ice cold buffer then rinsed briefly in distilled water. Sections

were air-dried before opposing to tritium sensitive phosphoimaging screen for three to five days.

D2 Receptor Saturation

Tissue sections were preincubated for five minutes in PBS, pH 7.4 at 25° C or 50mM Tris-HCl, pH 8.0, 50mM NaCl, 30mM EDTA at room temperature. The slides for total binding were then incubated in 0.5 - 50nM [^{3}H]Spiperone (American Radiochemical, Inc) in the above buffer for 30 minutes at room temperature. 10μM (+)Butaclamol was added and an adjacent slide was incubated to define non-specific binding. Sections were washed twice for a total of four minutes in ice cold buffer then rinsed briefly in distilled water. Sections were air-dried before opposing to tritium sensitive phosphoimaging screen for three to five days.

D2 Receptor Displacement

Tissue sections were preincubated for five minutes in PBS, pH 7.4 at 25° C or 50mM Tris-HCl, pH 8.0 (± 150mM NaCl) at room temperature. Slides were then incubated in 5nM [^{3}H]Spiperone (American Radiochemical, Inc) with no addition (total binding) or various concentrations (300nM to 1mM, f.c.) of competing compound in the above buffer for 30 minutes at room temperature. 10μM (+)Butaclamol was added and an adjacent slide was incubated to define non-specific binding. Sections were washed twice for a total of four minutes in ice cold buffer then rinsed briefly in distilled water. Sections were

air-dried before opposing to tritium sensitive phosphoimaging screen for three to five days.

2. **Densitometry**

Calibrated plastic radioactive standards were included with tissue sections to correct for variations in exposure. After development (Fuji Typhoon FLA 7000), images were analyzed with ImageQuant software (Fuji). Phosphoimager units were converted to femtomoles on the basis of image densities overlying the radioactive standards and the specific activity of the radioligand.

3. Competition Curves

144

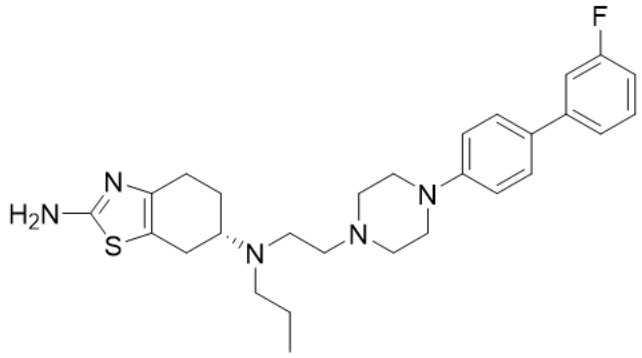

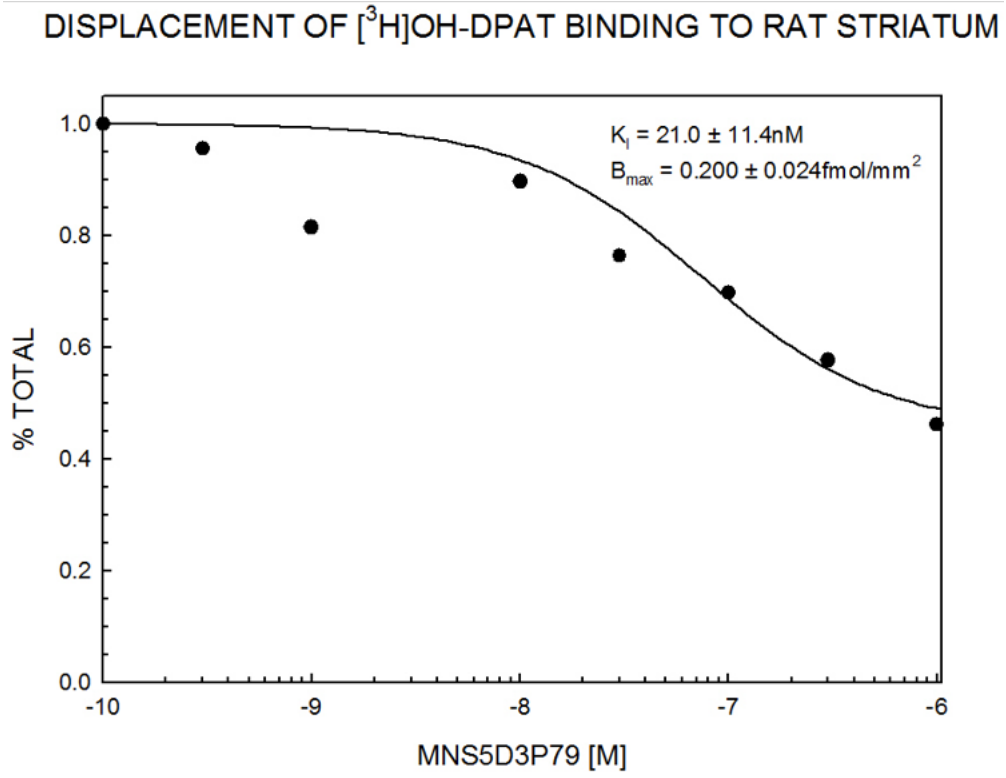

144

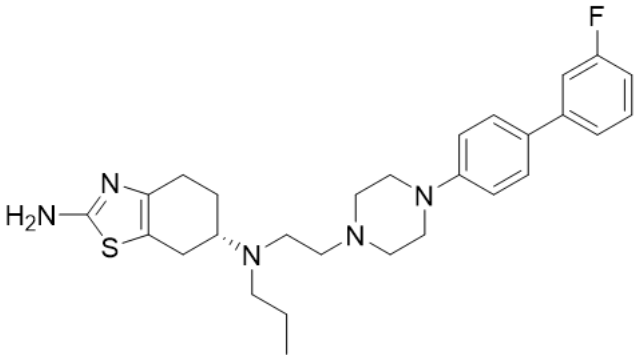

DISPLACEMENT OF [^{3}H]SPIPERONE BINDING TO RAT STRIATUM

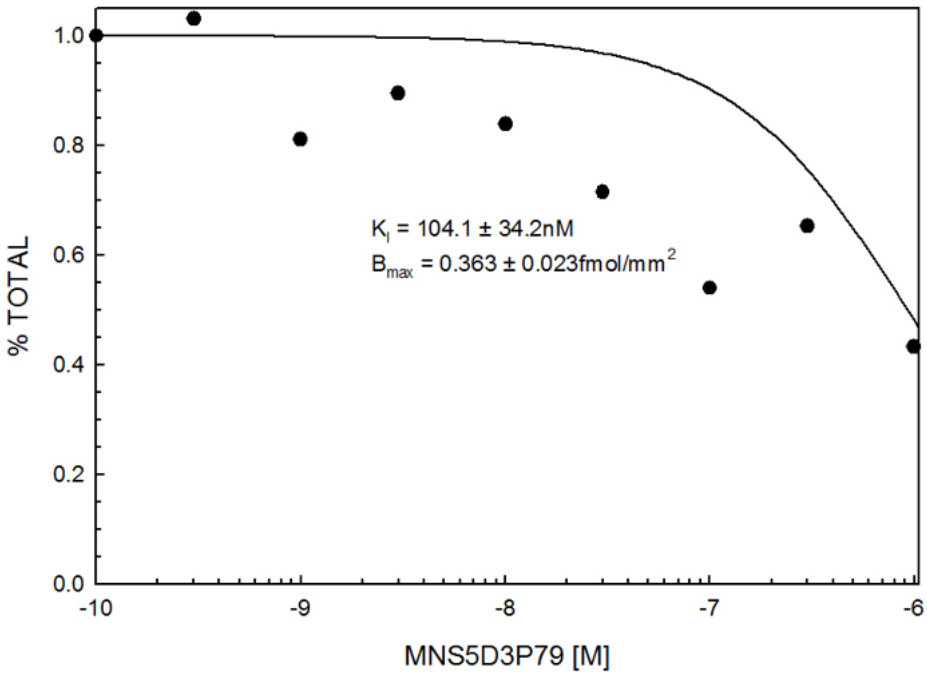

159c

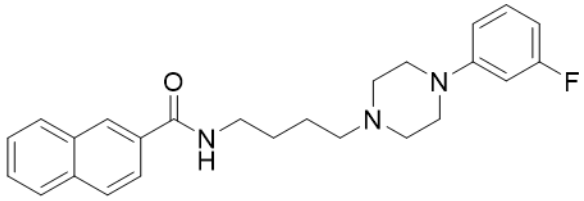

DISPLACEMENT OF [^{3}H]OH-DPAT BINDING TO RAT STRIATUM

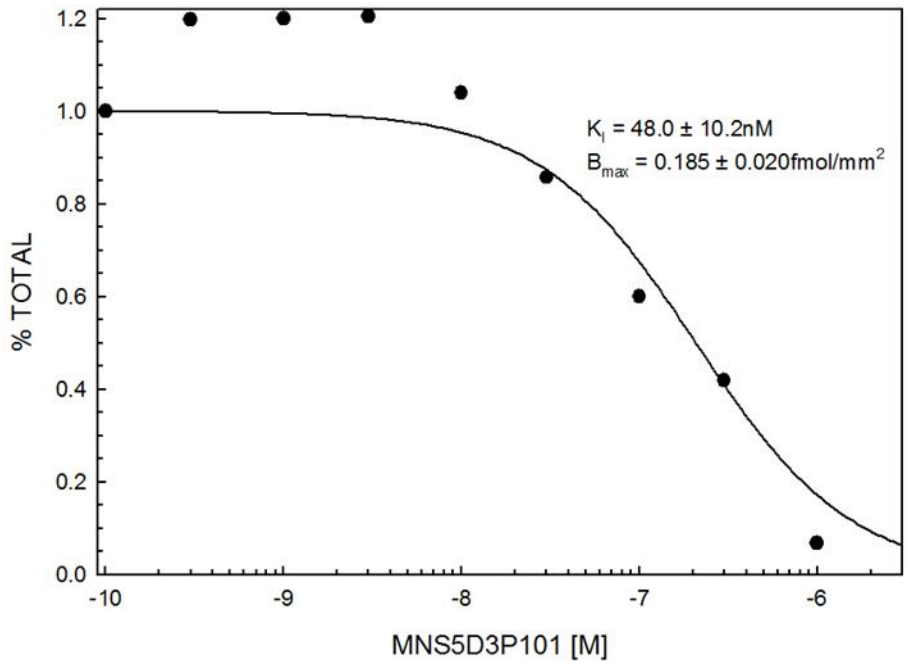

159c

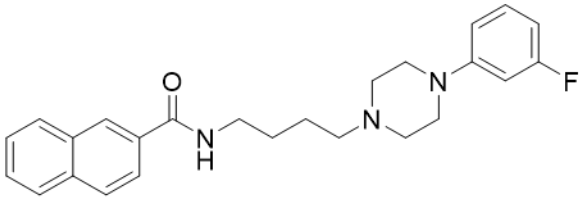

DISPLACEMENT OF [^{3}H]SPIPERONE BINDING TO RAT STRIATUM

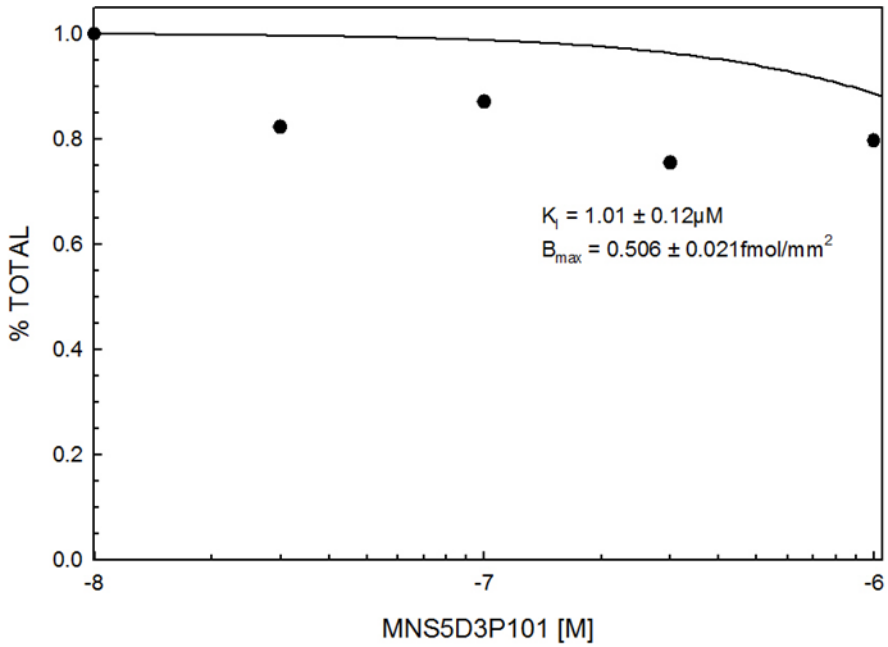

155c

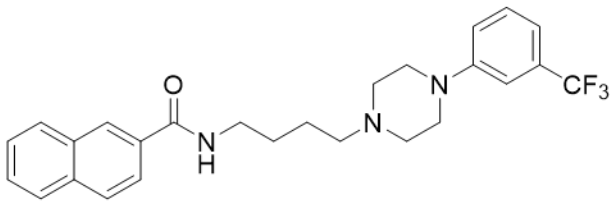

DISPLACEMENT OF [^{3}H]OH-DPAT BINDING TO RAT STRIATUM

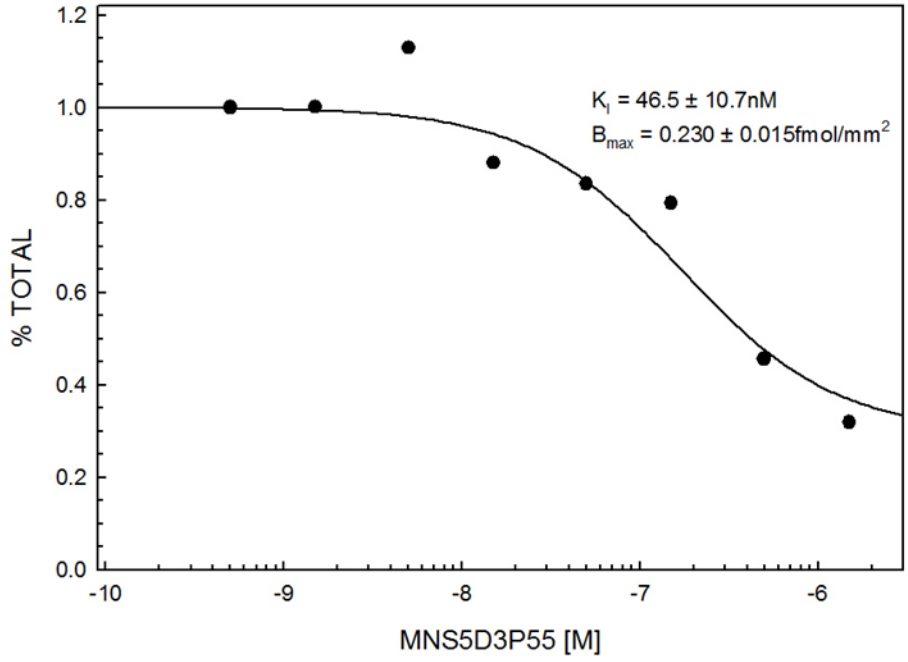

155c

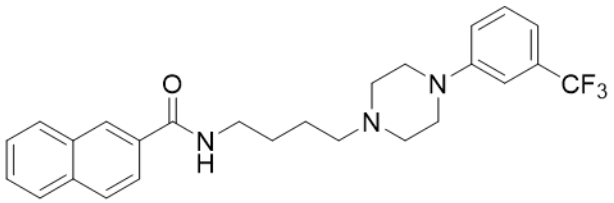

DISPLACEMENT OF [^{3}H]SPIPERONE BINDING TO RAT STRIATUM

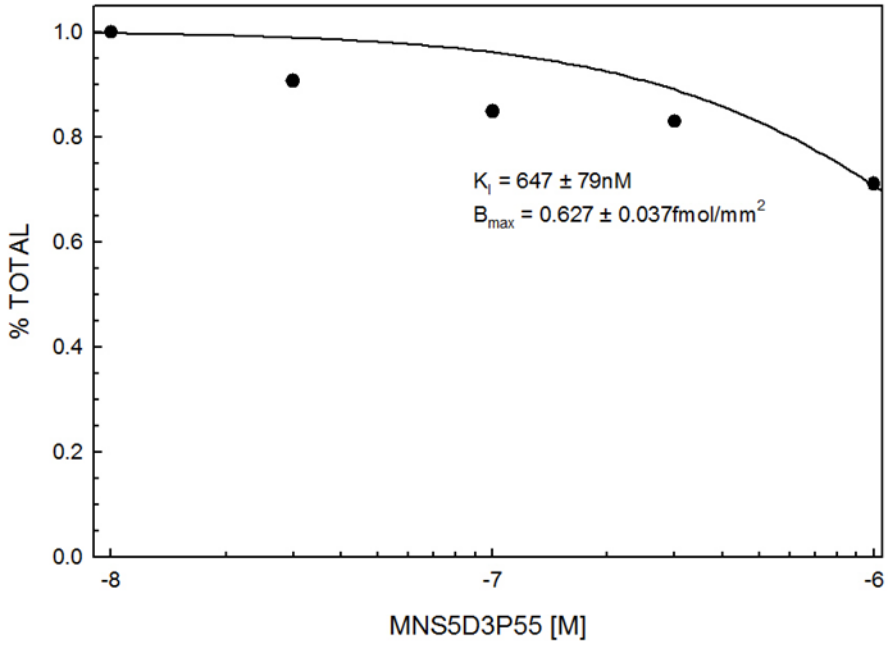

158c

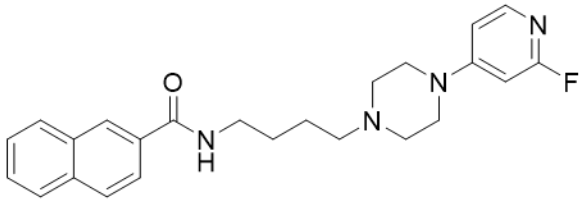

DISPLACEMENT OF [^{3}H]OH-DPAT BINDING TO RAT STRIATUM

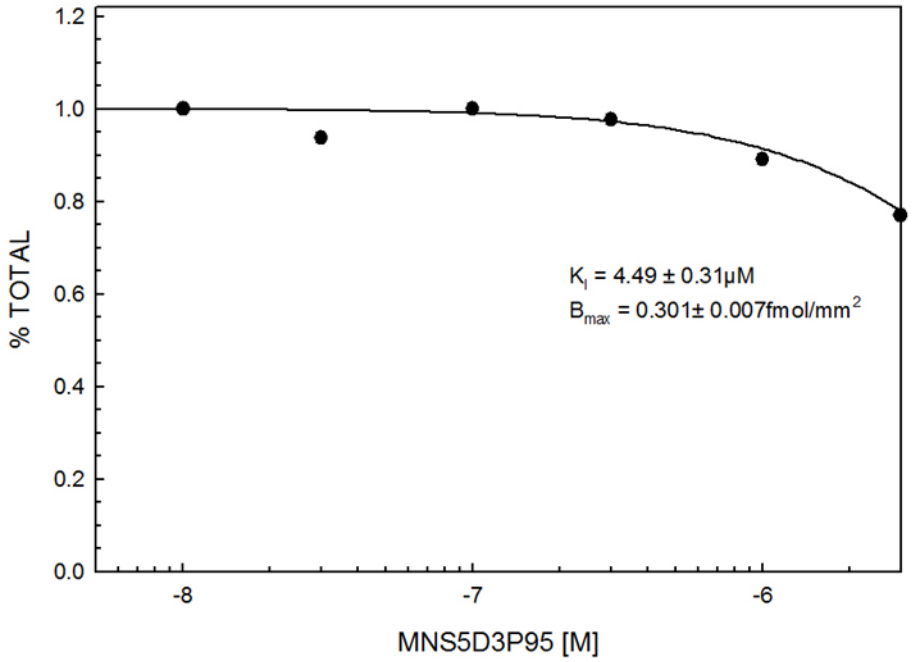

158c

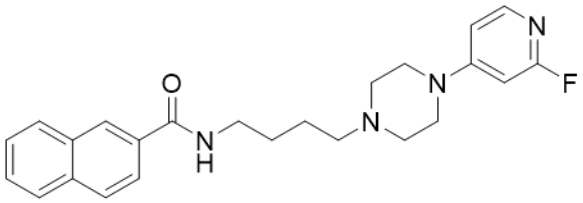

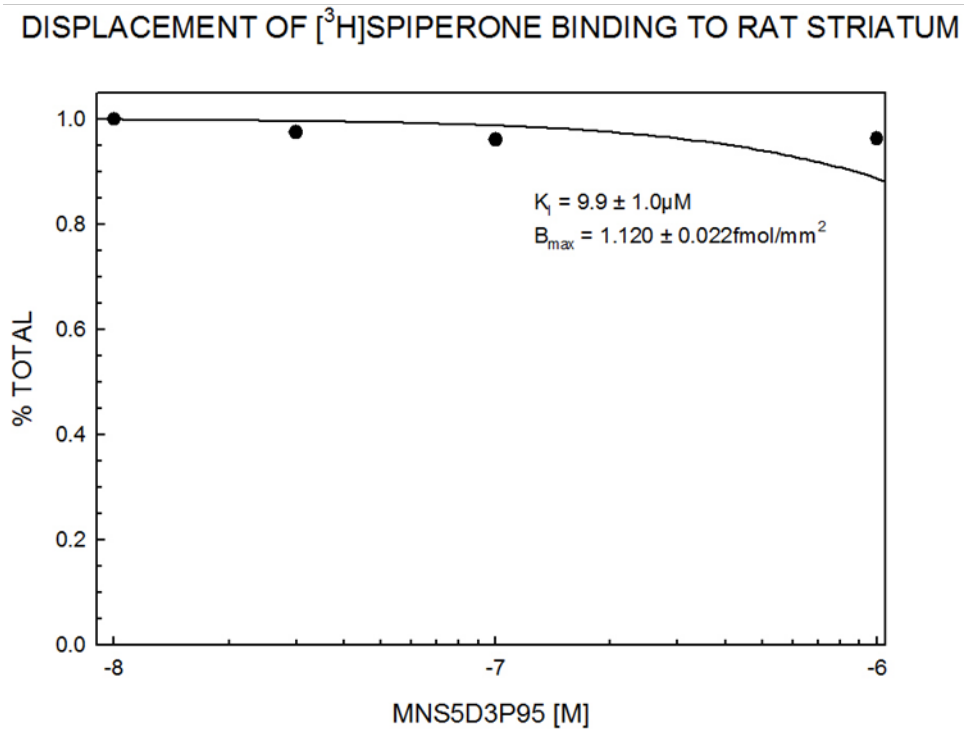

4. Additional Methods: Human/Rat Plasma Stability Studies

RadioTLC was performed in 20% MeOH/EtOAc with 0.5 µl of dose, 0.5 µl dose in human/rat blood, or 0.5 µl dose and 1.0 µl dose/blood co spot. These were spotted and LC performed as described, then exposed on film for 5-10 min before phosphorimaging.

5. Chemistry

a. Experimental Procedures

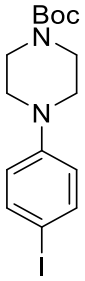

131

***tert*-butyl 4-(4-iodophenyl)piperazine-1-carboxylate (131**). This product was prepared as previously described.[231] The product was purified on SiO_2 in EtOAc/hexanes to give 11.76 g (70%) over two steps. R_f 0.5 (20% EtOAc/hexanes). The ^1H NMR was the same as previously described.[231]

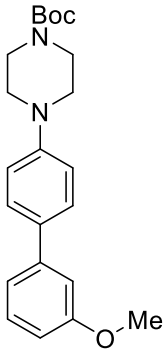

132

***tert*-butyl 4-(3'-methoxy-[1,1'-biphenyl]-4-yl)piperazine-1-carboxylate (132).** This product was prepared as previously described The product was purified on SiO_2 by column chromatography in EtOAc/hexanes in 1.1 g (47%). R_f 0.36 (20% EtOAc/hexanes). The ^1H NMR was the same as previously described.[231]

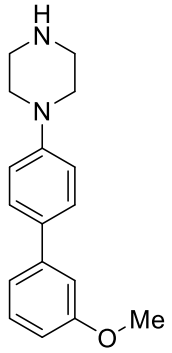

164

1-(3'-methoxy-[1,1'-biphenyl]-4-yl)piperazine (164). This product was prepared as previously described. The product was obtained 0.413 g (90%). The ^{1}H NMR was the same as previously described.[231]

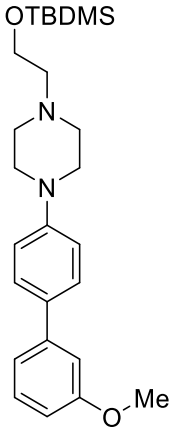

133

1-(2-((tert-butyldimethylsilyl)oxy)ethyl)-4-(3'-methoxy-[1,1'-biphenyl]-4-yl)piperazine (133).[231] This product was prepared as previously described. The product was purified on SiO_2 by column chromatography in EtOAc/hexanes to afford the final product, 0.617 g (72%). R_f 0.18 in (20% EtOAc/hexanes). The ^{1}H NMR was the same as previously described.[231]

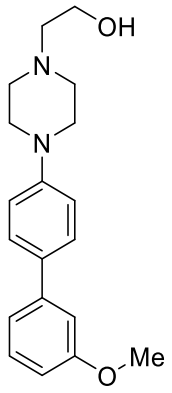

134

2-(4-(3′-Methoxybiphenyl-4-yl)piperazin-1-yl)ethanol (134). This product was prepared as previously described. The product was purified on SiO_2 by column chromatography in EtOAc/hexanes in 0.431 g (64%). R_f 0.67 (20% MeOH/DCM). The ^1H NMR was the same as previously described.[231]

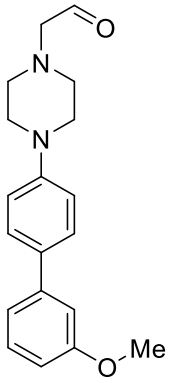

165

2-(4-(3′-Methoxybiphenyl-4-yl)piperazin-1-yl)- acetaldehyde (165). This product was prepared as previously described.[231] It was used without further purification to the next step. It was monitored *via* IR for peak appearance at ~2900 C=O, and peak disappearance at ~3250-3300 O-H to suggest aldehyde formation. The product was obtained 0.236 g (95%). R_f 0.83 ((20% MeOH/DCM).

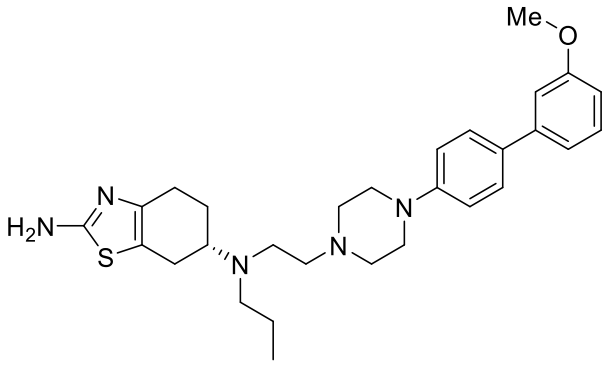

135

(S)-N6-(2-(4-(3'-methoxy-[1,1'-biphenyl]-4-yl)piperazin-1-yl)ethyl)-N6-propyl-4,5,6,7-tetrahydrobenzo[d]thiazole-2,6-diamine (135). This product was prepared as previously described.[231] The product was purified on SiO_2 by column chromatography in EtOAc/hexanes to afford the final product, 0.195 g (35%). R_f 0.24 (20% MeOH/EtOAc). The ^1H NMR was the same as previously described.[231] HPLC: Waters-Spherisorb 5µ-C8, 4.6x150mm, 35% 20mM NH_4OAc: 65% MeCN, 2mL HOAc, 1.5 mL/min, 30°C: R_t 8.3 min. Beckman Coulter – Ultrasphere 5µ-RP-C18, 10mm x 25 cm, 35% 20mM NH_4OAc: 65% MeCN, 2mL HOAc, 3 mL/min, 30°C: R_t 8.02 min.

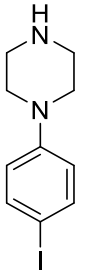

166

1-(4-iodophenyl)piperazine (166). This product was prepared as previously described.[231] The product was obtained in 17.6 g (46%). R_f 0.04 (1:1 EtOAc/hexanes). It was used without further purification to the next step.

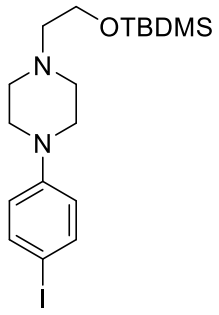

136

1-(2-((tert-butyldimethylsilyl)oxy)ethyl)-4-(4-iodophenyl)piperazine (136). A mixture of compound (**166**) (0.2 g, 0.7 mmol), (2-bromo-ethyl)-*tert*-butyldimethylsilane (0.411 g, 1.4 mmol), K_2CO_3 (0.3 g, 2.1 mmol) in CH_3CN (2.3 mL) was refluxed for 14 h. Acetonitrile was evaporated under vacuo and the crude material was purified on silica by column chromatography (hexanes/EtOAc) to afford the solid product 0.135 g (43%). R_f 0.54 (1:1 EtOAc/hexanes). ^{1}H NMR (400 MHz, Chloroform-*d*) δ 7.53 – 7.46 (m, 1H), 7.29 – 7.23 (m, 0H), 6.96 – 6.81 (m, 1H), 6.70 – 6.63 (m, 1H), 3.84 – 3.74 (m, 2H), 3.23 – 3.12 (m, 3H), 2.73 – 2.63 (m, 3H), 2.63 – 2.53 (m, 2H), 0.90 (d, *J* = 1.6 Hz, 10H), 0.11 – 0.04 (m, 7H); ^{13}C NMR (101 MHz, Chloroform-*d*) δ 150.89, 137.95, 137.45, 118.05, 117.81, 81.21, 61.36, 60.49, 53.87, 53.62, 48.89 (d, *J* = 45.0 Hz), 26.06, 25.71 (d, *J* = 24.1 Hz), -5.21. HRMS (ESI) *m/z*: $[M+H]^+$ calc for C18H31IN2OSi, 447.1323; found 447.1323.

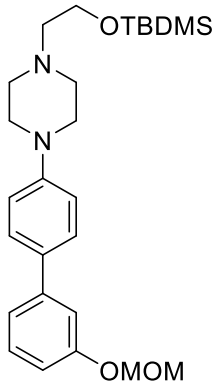

137

1-(2-((tert-butyldimethylsilyl)oxy)ethyl)-4-(3'-(methoxymethoxy)-[1,1'-biphenyl]-4-yl)piperazine (137). A suspension of (**136**) 2.23 g (5 mmol) and commercially avilable [3-(methoxymethoxy)phenyl]-boronic acid (1 g 5.5 mmol), Na_2CO_3 (5 mL, 10mmol, of 2M aqueous solution), $Pd(PPh_3)_4$ (0.433 mg, 0.375 mmol), in dimethoxy ethane/ethanol (7 mL: 7 mL) was refluxed 3-4 hours. The solvents were removed in vacuo, the palladium removed *via* fritted funnel filtration with SiO_2, and the crude product was concentrated. The product was purified on SiO_2 by column chromatography in hexanes/EtOAc. The product was obtained 1.28 g (45%). R_f 0.67 (20% EtOAc/hexanes). ^1H NMR was taken in Chloroform and K_2CO_3 to ensure intact MOM protecting group. ^1H NMR (400 MHz, Chloroform-d) δ 7.54 – 7.48 (m, 2H), 7.32 (t, J = 7.9 Hz, 1H), 7.27 – 7.18 (m, 3H), 7.01 – 6.93 (m, 3H), 5.22 (s, 2H), 3.82 (t, J = 6.3 Hz, 2H), 3.51 (s, 3H), 3.29 – 3.23 (m, 4H), 2.75 – 2.69 (m, 4H), 2.61 (t, J = 6.3 Hz, 2H), 0.91 (s, 9H), 0.08 (s, 6H). HRMS (ESI) *m/z*: $[M+H]^+$ calc for C26H40N2O3Si, 457.2881; found 457.2884.

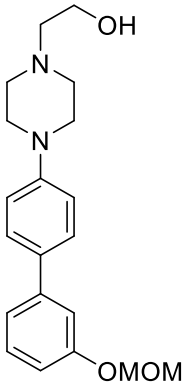

138

2-(4-(3'-(methoxymethoxy)-[1,1'-biphenyl]-4-yl)piperazin-1-yl)ethan-1-ol (138). In to a stirring solution of (**137**) (0.5 g, 1mmol) in anhydrous THF (8 mL), n-tetrabutylammonium fluoride (1.1 mL, 1 M solution in THF) was added at 0°C. The reaction mixture stirred for 1.5 hours at room temperature. THF was removed in vauo and

the crude reaction mixture was washed with water (15 mL) and extracted with methylene chloride (3 x 50 mL). The organic layer was washed with brine and dried over Na_2SO_4. The product was purified 2x on SiO_2 in EtOAc, then MeOH/DCM. TBAF proved challenging to remove, 0.519 g was recovered as a dark amber oil, and part was carried forward to the next step. R_f 0.18 (1:1 EtOAc/DCM). ^{1}H NMR (400 MHz, Chloroform-*d*) δ 7.52 – 7.42 (m, 3H), 7.34 – 7.16 (m, 4H), 7.05 (d, *J* = 8.4 Hz, 1H), 6.98 – 6.91 (m, 2H), 5.21 (s, 1H), 5.19 – 5.14 (m, 2H), 3.49 (s, 1H), 3.45 (s, 3H), 3.35 (t, *J* = 5.0 Hz, 3H), 3.18 – 3.09 (m, 4H), 2.99 – 2.74 (m, 3H).

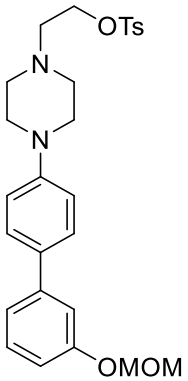

167

2-(4-(3'-(methoxymethoxy)-[1,1'-biphenyl]-4-yl)piperazin-1-yl)ethyl 4-methylbenzenesulfonate (167). At 0^{o}C, a solution of (**138**) (0.2 g, 0.58 mmol), DCM (1mL) and triethyl amine (0.147 g, 1.45 mmol) was added p-toluene sulfonyl chloride (0.166 g, 0.87 mmol) and stirred 12 h. The crude mixture was washed with water (20 mL) and extracted with methylene chloride (3 x 75 mL). To remove TBAF from the previous reaction, it was washed with Et_2O/H_2O 1:1 and NH_4Cl 5 times and dried over Na_2SO_4. The product was purified on silica plug, 0.19 g (66%). This was used directly in the next step. R_f 0.48 (1:1 EtOAc/hexanes), R_f 0.72 (DCM).

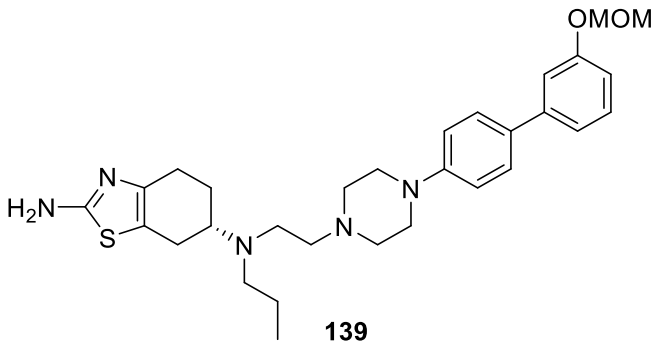

139

(S)-N6-(2-(4-(3'-(methoxymethoxy)-[1,1'-biphenyl]-4-yl)piperazin-1-yl)ethyl)-N6-propyl-4,5,6,7-tetrahydrobenzo[d]thiazole-2,6-diamine (139). In a stirring solution of tosylate (**167**) (0.190 g, 0.38 mmol) in methylene chloride (0.8 mL) was slowly added a solution of (S)-N6-propyl-4,5,6,7-tetrahydrobenzo[d]thiazole-2,6-diamine (0.161 g, 0.76 mmol) and *N,N*-Diisopropylethylamine (0.246 g, 1.9 mmol). This was stirred at room temp for 14 h. The reaction mixture was extracted with methylene chloride (3 x 75 mL), washed with brine, dried over Na_2SO_4 and concentrated. The product was purified on SiO_2 by column chromatography in Methanol/DCM to provide the product in 70% yield. ^{1}H NMR (400 MHz, Chloroform-*d*) δ 7.52 (dd, *J* = 13.0, 7.8 Hz, 2H), 7.32 (dd, *J* = 15.5, 7.5 Hz, 2H), 7.24 – 7.17 (m, 2H), 7.12 (t, *J* = 8.1 Hz, 1H), 6.98 (d, *J* = 6.0 Hz, 1H), 6.62 – 6.56 (m, 1H), 6.50 (d, *J* = 8.4 Hz, 1H), 5.14 (s, 2H), 3.49 (d, *J* = 5.6 Hz, 3H), 3.47 (d, *J* = 0.9 Hz, 4H), 3.38 – 3.09 (m, 8H), 2.70 (d, *J* = 6.6 Hz, 3H), 2.42 (d, *J* = 8.8 Hz, 2H), 1.25 (s, 4H), 1.02 (t, *J* = 7.3 Hz, 2H), 0.89 (s, 3H).HRMS (ESI) *m/z*: $[M+H]^+$ calc for C30H41N5O2S, 536.3054; found 536.3044. R_f 0.16 (20% MeOH/DCM).

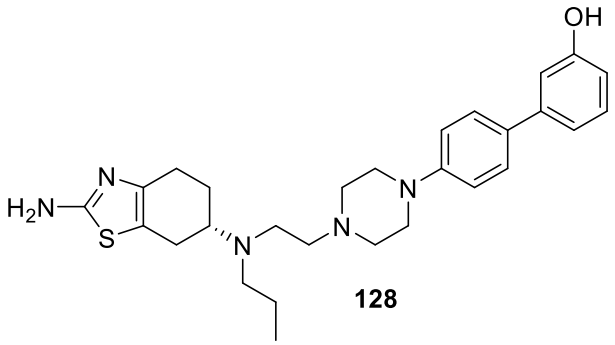

128

(S)-4'-(4-(2-((2-amino-4,5,6,7-tetrahydrobenzo[d]thiazol-6-yl)(propyl)amino)ethyl)piperazin-1-yl)-[1,1'-biphenyl]-3-ol (128). Compound (**139**) (0.05 g, 0.09 mmol) in Methanol (250 µl) was added a trace amount of concentrated HCl (3 drops), sealed and refluxed overnight. Reaction was neutralized with 1M KOH (1 mL), and extracted with methylene chloride (3 x 10 mL), and dried over Na_2SO_4. The product was purified on SiO_2 by column chromatography in Methanol/DCM. Product was obtained in 0.032 g (77%). R_f 0.03 (20% MeOH/DCM). HRMS (ESI) *m/z*: $[M+H]^+$ calc for C28H37N5OS, 492.2792; found 492.2786. HPLC: Waters-Spherisorb 5µ-C8, 4.6x150mm, 35% 20mM NH_4OAc: 65% MeCN, 2mL HOAc, 1.5 mL/min, 30°C: R_t 2.24 min. Beckman Coulter – Ultrasphere 5µ-RP-C18, 10mm x 25 cm, 35% 20mM NH_4OAc: 65% MeCN, 2mL HOAc, 3 mL/min, 30°C: R_t 3.67 min. ^{1}H NMR (400 MHz, Chloroform-*d*) δ 7.78 (d, *J* = 8.0 Hz, 2H), δ 7.52 (dd, *J* = 13.0, 7.8 Hz, 2H), 7.32 (dd, *J* = 15.5, 7.5 Hz, 2H), 7.12 (t, *J* = 8.1 Hz, 2H), 3.33 – 3.25 (m, 2H), 2.98 (dtd, *J* = 10.0, 5.2, 2.5 Hz, 4H), 2.85 (ddt, *J* = 15.4, 5.3, 1.4 Hz, 4H), 2.60 – 2.49 (m, 5H), 2.39 (dddd, *J* = 15.4, 8.4, 2.8, 1.8 Hz, 5H), 2.31 (s, 1H), 2.00 (q, *J* = 3.4, 2.5 Hz, 2H), 1.71 – 1.62 (m, 5H), 0.98 (t, *J* = 7.3 Hz, 3H).

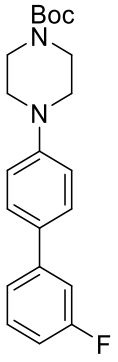

142

tert-butyl 4-(3'-fluoro-[1,1'-biphenyl]-4-yl)piperazine-1-carboxylate (142). A suspension of commercially available (3-fluorophenyl)boronic acid (1 eq), iodo compound (**131**) (1 eq), Na2CO3 (2 eq, 2M solution in water), and Pd(PPh3)4 (0.05 -0.075 eq) in dimethoxy ethane/ethanol (1:1) was refluxed for 1-4 hr. The solvents were removed in vacuo. The product was purified on SiO_2 by column chromatography in hexanes/ethyl acetate and the crude product was purified by flash chromatography using hexanes/EtOAC. to yield compound **(X)** (30%).^{1}H NMR (500 MHz, Chloroform-*d*) δ 7.51 (d, *J* = 8.8 Hz, 2H), 7.36 (dt, *J* = 13.9, 7.9 Hz, 2H), 7.30 – 7.23 (m, 2H), 7.02 – 6.97 (m, 2H), 3.64 – 3.58 (m, 4H), 3.25 – 3.17 (m, 4H), 1.50 (s, 9H). ^{19}F NMR (470 MHz, Chloroform-*d*) δ -113.38 (td, *J* = 9.3, 5.3 Hz). HRMS (ESI) *m/z*: $[M+H]^+$ calc for C21H25FN2O2, 357.1973; found 357.1973.

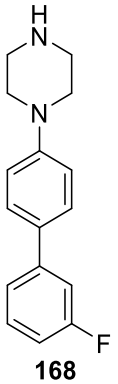

168

1-(3'-fluoro-[1,1'-biphenyl]-4-yl)piperazine (168) 1-(3′-fluoro-biphenyl-4-yl)piperazine (**10**). Into a stirring solution of compound **142** (1eq) in CH2Cl2 (0.4mmol/mL) and triethylsilane (1eq), TFA (28eq) was added slowly at room temperature, and the reaction mixture was stirred for 4 h. Unreacted TFA and solvent CH2Cl2 were removed in vacuo, and the salt formed was washed with diethyl ether. Saturated solution of sodium bicarbonate was added to the salt, and it was extracted with dichloromethane (3x). The combined organic layer was dried over Na2SO4, filtered, and evaporated in vacuo to provide the compound **10** (%). R_f 0.2 (1:1 EtOAc/hexanes). HRMS (ESI) *m/z*: $[M+H]^+$ calc for C16H17FN2, 257.1449; found 257.1449. ^{1}H NMR (500 MHz, Chloroform-*d*) δ 7.51 (d, *J* = 8.7 Hz, 1H), 7.39 – 7.22 (m, 3H), 6.99 (d, *J* = 8.9 Hz, 2H), 6.94 (d, *J* = 8.3 Hz, 2H), 3.29 (dd, *J* = 6.6, 3.5 Hz, 4H), 3.20 (dd, *J* = 6.4, 3.8 Hz, 4H).^{13}C NMR (126 MHz, Chloroform-*d*) δ 150.90, 129.26, 127.81, 120.79, 116.74, 116.52, 113.37, 48.75, 44.93, 44.76. 13C NMR (101 MHz, Chloroform-d) δ 164.45, 162.01, 151.40, 143.20, 130.74, 130.08 (d, J = 8.6 Hz), 127.68, 122.00, 115.97, 49.94, 46.05. ^{19}F NMR (376 MHz, Chloroform-*d*) δ -113.41.

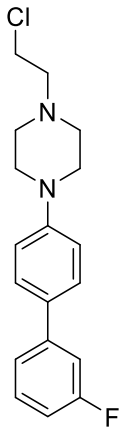

143

1-(2-chloroethyl)-4-(3'-fluoro-[1,1'-biphenyl]-4-yl)piperazine (143). At 0^{o}C, (**168**) (0.07 mg, 0.27 mmol), K_2CO_3 (0.075 g, 0.54 mmol), in acetonitrile (0.75 mL) was added 1-

bromo-2-chloroethane (0.043 g, 0.3 mmol). Reaction was monitored hourly *via* TLC for consumption of starting material and stirred at room temperature for 2 hours. R_f 0.7 (1:1 EtOAc/hexanes). This product was not isolated and used directly in next step.

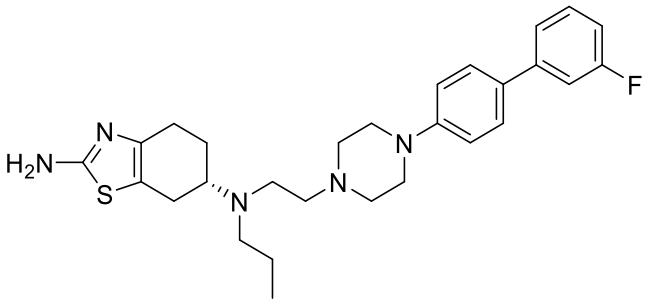

144

(S)-N6-(2-(4-(3'-fluoro-[1,1'-biphenyl]-4-yl)piperazin-1-yl)ethyl)-N6-propyl-4,5,6,7-tetrahydrobenzo[d]thiazole-2,6-diamine (144). To reaction mixture (**143**) was added (S)-N6-propyl-4,5,6,7-tetrahydrobenzo[d]thiazole-2,6-diamine (0.085 mg, 0.4 mmol) at room temperature and stirred 48 hours. Product was washed with water and extracted with methylene chloride (3 x 20 mL) and dried over sodium sulfate. It was purified over silica by column chromatography in methanol/EtOAc to afford the final product in 31% over two steps. R_f 0.2 (10% MeOH/EtOAc). HRMS (ESI) *m/z*: $[M+H]^+$ calc for C28H36FN5S, 494.2748; found 494.2751 and 494.2745. 1H NMR (400 MHz, Chloroform-d) δ 7.49 (d, J = 8.8 Hz, 2H), 7.38 – 7.30 (m, 2H), 7.26 (t, J = 1.7 Hz, 1H), 7.22 (d, J = 1.9 Hz, 1H), 6.97 (dt, J = 7.4, 2.6 Hz, 4H), 3.26 (t, J = 5.1 Hz, 5H), 3.05 (d, J = 4.7 Hz, 1H), 2.69 (dt, J = 14.0, 5.8 Hz, 9H), 2.61 – 2.44 (m, 6H), 2.07 – 1.96 (m, 2H), 1.77 – 1.65 (m, 1H), 1.48 (h, J = 7.3 Hz, 2H), 1.26 (t, J = 7.1 Hz, 1H), 0.89 (t, J = 7.3 Hz, 3H). 13C NMR (101 MHz, Chloroform-d) δ 165.49, 150.90, 145.00, 130.08, 130.00, 127.67, 121.98, 117.41, 115.86, 113.27, 113.05, 74.80, 58.68, 58.09, 53.66, 53.56, 48.67, 48.40, 41.55,

26.52, 25.84, 25.15, 22.36, 11.82. 19F NMR (376 MHz, Chloroform-d) δ -113.30 – -113.54 (m).

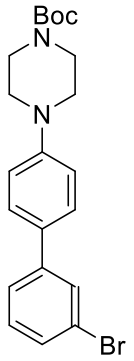

148

tert-butyl 4-(3'-bromo-[1,1'-biphenyl]-4-yl)piperazine-1-carboxylate (148). A suspension of commercially available (3-bromophenyl)boronic acid (0.142 g, 0.71 mmol), iodo compound (**131**) (0.25 g, 0.64 mmol), Na_2CO_3 (0.64 mL of 2M solution in water, 0.032 mmol), and $Pd(PPh_3)_4$ (0.05 -0.075 eq, 0.037 g, 0.032 mmol) in dimethoxy ethane/ethanol (1:1, 2mL) was refluxed for 1-4 hr. The solvents were removed in vacuo. the palladium removed *via* fritted funnel filtration with SiO_2, and the crude product was concentrated. The product was purified on SiO_2 by column chromatography in hexanes/EtOAc to yield compound **(X)** (50%). R_f 0.46 (20% EtOAc/hexanes). HRMS (ESI) *m/z*: $[M+H]^+$ calc for C21H25BrN2O2, 417.1172; found 417.1156. ^1H NMR (400 MHz, Chloroform-*d*) δ 7.69 (t, *J* = 1.8 Hz, 2H), 7.48 (dd, *J* = 8.2, 6.3 Hz, 3H), 7.42 – 7.38 (m, 1H), 6.98 (d, *J* = 8.7 Hz, 2H), 3.60 (t, *J* = 5.2 Hz, 4H), 3.20 (d, *J* = 5.4 Hz, 4H), 1.49 (s, 9H).

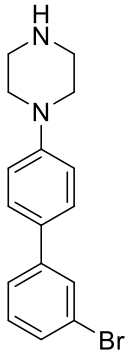

149

1-(4-(3'-bromo-[1,1'-biphenyl]-4-yl)piperazin-1-yl)-2-chloroethan-1-one (149). Into a stirring solution of compound **(148)** (0.13 g, 0.31 mmol)) in CH_2Cl_2 (1 mL) and triethylsilane (0.31 mmol), TFA (0.66 mL, 8.7 mmol) was added slowly at room temperature, and the reaction mixture was stirred for 4 h. Unreacted TFA and solvent CH2Cl2 were removed in vacuo, and the salt formed was washed with diethyl ether. Saturated solution of sodium bicarbonate was added to the salt, and it was extracted with dichloromethane (3 x 75 mL). The combined organic layer was dried over Na_2SO_4, filtered, and evaporated in vacuo to provide the compound **X** (0.103 g, 99%). HRMS (ESI) *m/z*: $[M+H]^+$ calc for C18H18BrClN2O, 314.0648; found 317.0653. 1H NMR (400 MHz, Chloroform-d) δ 7.70 (t, J = 1.9 Hz, 1H), 7.50 – 7.45 (m, 3H), 7.40 (ddd, J = 8.0, 2.0, 1.1 Hz, 1H), 7.27 (d, J = 7.8 Hz, 1H), 7.01 – 6.95 (m, 2H), 3.26 – 3.17 (m, 4H), 3.10 – 2.99 (m, 4H). 13C NMR (101 MHz, Chloroform-d) δ 151.36, 143.00, 130.19, 129.34 (d, J = 18.1 Hz), 127.72, 125.01, 122.85, 116.01, 49.87, 45.95.

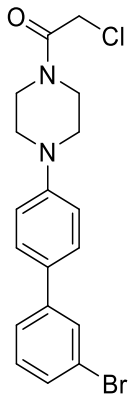

150

1-(4-(3'-bromo-[1,1'-biphenyl]-4-yl)piperazin-1-yl)-2-chloroethan-1-one (150). Into a solution of (**149**) (0.2 g, 0.63 mmol) at 0^{o}C, triethylamine (0.170 mL), methylene chloride (1 mL) was slowly added chloroacetyl chloride (0. 78 mg, 0.69 mmol). Reaction stirred and come to room temperature over 1 hour, then extracted with DCM (3 x 10 mL) and dried over Na_2SO_4. It was purified over SiO_2 by column chromatography in EtOAc/hexanes to afford the final product in 0.197 g (80%). R_f 0.18 (20% EtOAc/hexanes). 1H NMR (400 MHz, Chloroform-d) δ 7.69 (t, J = 1.9 Hz, 1H), 7.48 (td, J = 8.1, 7.4, 1.7 Hz, 2H), 7.41 (ddd, J = 8.0, 2.0, 1.0 Hz, 1H), 7.33 – 7.23 (m, 1H), 7.00 – 6.95 (m, 2H), 6.95 – 6.90 (m, 1H), 4.12 (d, J = 4.2 Hz, 2H), 3.79 (q, J = 5.5 Hz, 2H), 3.69 (dd, J = 6.3, 4.3 Hz, 2H), 3.28 (t, J = 5.2 Hz, 2H), 3.23 (dd, J = 6.4, 3.9 Hz, 2H). 13C NMR (101 MHz, Chloroform-d) δ 165.14, 150.32, 142.73, 131.63, 130.26 (d, J = 2.7 Hz), 129.52 (d, J = 4.9 Hz), 127.90, 125.10, 122.89, 116.70, 49.27, 48.87, 46.11, 41.97, 40.81. **6p59**

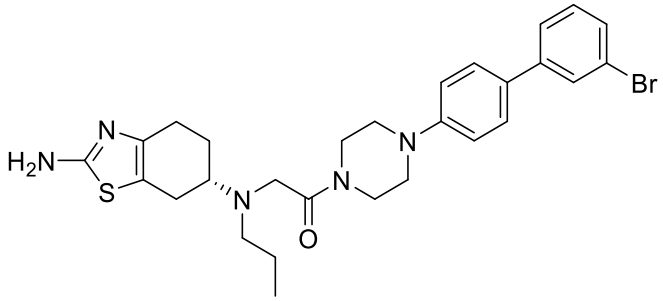

151

(S)-N-(2-amino-4,5,6,7-tetrahydrobenzo[d]thiazol-6-yl)-2-(4-(3'-bromo-[1,1'-biphenyl]-4-yl)piperazin-1-yl)-N-propylacetamide (151). In a suspension of (S)-N6-propyl-4,5,6,7-tetrahydrobenzo[d]thiazole-2,6-diamine (0.053 g, 0.25 mmol), K_2CO_3 (0.069 g, 0.5 mmol) and catalytic potassium iodide in acetonitrile (6 mL) was added (**149**) (0.15 g, 0.38 mmol) and refluxed for 3 h. The crude reaction mixture was filtered, washed with EtOAc and concentrated in vacuo. The product was purified on SiO_2 by column chromatography (EtOAc/MeOH) to give 0.053 g (70%). R_f 0.23 (95:5 EtOAc/MeOH). HRMS (ESI) *m/z*: $[M+H]^+$ calc for C28H34BrN5OS, 568.1740; found 568.1739.

^{1}H NMR (400 MHz, Chloroform-*d*) δ 7.68 (t, *J* = 1.8 Hz, 1H), 7.47 (dd, *J* = 9.0, 7.0 Hz, 3H), 7.42 – 7.38 (m, 1H), 7.26 (s, 2H), 6.98 (dd, *J* = 9.0, 2.4 Hz, 2H), 3.94 – 3.62 (m, 5H), 3.55 (s, 2H), 3.34 – 3.10 (m, 5H), 2.70 (d, *J* = 20.7 Hz, 3H), 2.60 (s, 4H), 2.03 (d, *J* = 5.9 Hz, 1H), 1.73-1.70 (m, 2H), 0.90 (t, *J* = 7.3 Hz, 3H). 13C NMR (101 MHz, Chloroform-d) δ 169.28, 165.89, 150.52, 142.78, 137.75, 131.30, 130.22, 129.48 (d, J = 6.8 Hz), 127.81, 125.07, 122.87, 116.40 (d, J = 16.8 Hz), 112.65, 58.26, 55.23, 52.95, 49.43, 48.90, 45.19, 41.79, 26.12, 25.54, 24.65, 21.38, 11.85.

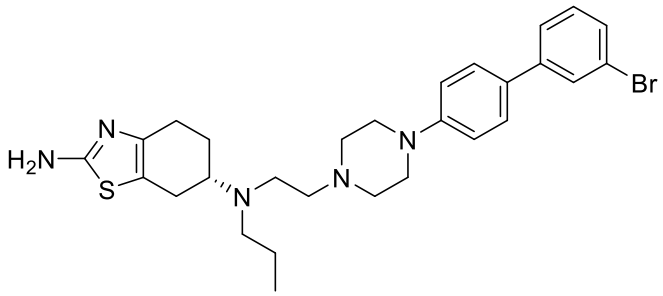

146

(S)-N6-(2-(4-(3'-bromo-[1,1'-biphenyl]-4-yl)piperazin-1-yl)ethyl)-N6-propyl-4,5,6,7-tetrahydrobenzo[d]thiazole-2,6-diamine (146). In a solution of (**151**) (0.053 g, 0.09 mmol) in anhydrous THF (0.7 mL) at 0°C, under argon, was slowly added borane-THF (0.545 mL, 1M solution). Reaction was then stirred at room temperature for 36 hours, then quenched with MeOH, and solvents removed in vacuo. The resultant solid was suspended in 6N HCl/MeOH (2 mL) and stirred for 2 h at room temperature. Methanol was removed in vacuo, and the pH was adjusted to alkaline with Na_2CO_3/$NaHCO_3$ and extracted with EtOAc, then methylene chloride. The product was dried over sodium sulfate and purified on SiO_2 by column chromatography. The desired product was isolated 0.043 mg (68%) in MeOH/EtOAc. R_f 0.12 (10% MeOH/EtOAc). HRMS (ESI) *m/z*: $[M+H]^+$ calc for C28H36BrN5S, 554.1948; found 554.1936. ^{1}H NMR (400 MHz, Chloroform-*d*) δ 7.68 (q, *J* = 1.8 Hz, 1H), 7.49 – 7.42 (m, 3H), 7.39 (ddd, *J* = 8.2, 2.3, 1.2 Hz, 1H), 7.25 (d, *J* = 4.6 Hz, 2H), 6.96 (dd, *J* = 8.9, 1.9 Hz, 2H), 3.77 – 3.58 (m, 2H), 3.28 (q, *J* = 7.2, 5.1 Hz, 5H), 2.87 (s, 3H), 2.70 (t, *J* = 13.4 Hz, 11H), 2.04 (s, 1H), 1.89 – 1.65 (m, 2H), 0.91 (td, *J* = 6.6, 5.8, 2.5 Hz, 3H). 13C NMR (101 MHz, Chloroform-d) δ 165.88, 150.71, 144.68, 142.94, 132.30, 130.57, 130.28, 129.34, 127.71 (d, J = 16.9 Hz), 125.00 (d, J = 16.8 Hz), 122.84, 116.18, 115.94, 58.71, 57.05, 53.45, 48.51, 47.61, 46.78, 26.32, 24.98 (d, J = 18.0 Hz), 21.40, 11.71.

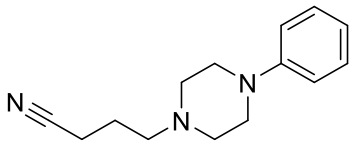

156a

4-(4-phenylpiperazin-1-yl)butanenitrile (156a). 1-pheynl piperazine (0.3 g, 1.85 mmol) in K_2CO_3 (0.28 g, 2.03 mmol), cat. KI, and anhydrous acetonitrile (9.25 mL) were stirred for 5 min at room temperature. Then 4-bromobutyronitrie (0.3 mg, 2.03 mmol) was added, the flask was sealed and the reaction refluxed for 14 h. Reaction was cooled, water added, and the product was extracted with methylene chloride and dried over Na_2SO_4The product was characterized and used directly in next step, 0.42 g, (99%). R_f 0.72 (20% MeOH/EtOAc). HRMS (ESI) *m/z* [M+H]+ calcd for C14H19N3, 230.1652, Found, 230.1652. 1H NMR (400 MHz, Chloroform-d) δ 7.27 (dd, J = 8.7, 7.2 Hz, 2H), 6.95 – 6.90 (m, 2H), 6.90 – 6.84 (m, 1H), 3.21 – 3.15 (m, 4H), 2.60 – 2.54 (m, 4H), 2.48 (t, J = 6.8 Hz, 2H), 2.40 (t, J = 7.1 Hz, 2H), 1.83 (q, J = 6.9 Hz, 2H). 13C NMR (101 MHz, Chloroform-d) δ 151.27, 129.33, 128.94, 119.90, 116.12, 56.27, 53.09, 49.07, 22.72, 14.90.

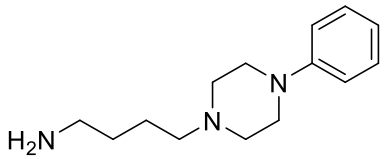

156b

4-(4-phenylpiperazin-1-yl)butan-1-amine (156b). To a mixture of nitrile (**156a**) (0.424 g, 1.85 mmol) in anhydrous THF (14 mL) at 0^{O}C, under argon, was slowly added borane-THF (11.1 mmol, 1M in THF) over 5 minutes. Reaction was let to come to room

temperature overnight and stirred for a total of 48 h. Mixture was cooled to 0^{O}C and quenched with methanol. The product was suspended in 6 HCl/MeOH and stirred for 2 hours at room temp, then concentrated. The pH was adjusted to alkaline with Na_2CO_3/$NaHCO_3$, extracted with ethyl acetate and dried over Na_2SO_4. The product was purified on silica by column chromatography with 20% methanol/ethyl acetate to give 0.25 g (58%). R_f 0.04 (20% MeOH/EtOAc). HRMS (ESI) *m/z* [M+H]+ calcd for C14H23N3, 234.1965, Found, 234.1968. 1H NMR (400 MHz, Chloroform-d) δ 7.21 (t, J = 7.8 Hz, 2H), 6.88 (d, J = 8.1 Hz, 2H), 6.80 (t, J = 7.3 Hz, 1H), 3.15 (t, J = 5.0 Hz, 4H), 2.90 – 2.75 (m, 2H), 2.69 (t, J = 6.6 Hz, 2H), 2.55 (t, J = 5.0 Hz, 4H), 2.36 (q, J = 7.6, 6.5 Hz, 2H), 1.59 – 1.41 (m, 4H). 13C NMR (101 MHz, Chloroform-d) δ 151.26, 129.14, 119.57, 115.91, 58.39, 53.22, 49.05, 41.72, 31.00, 24.27.

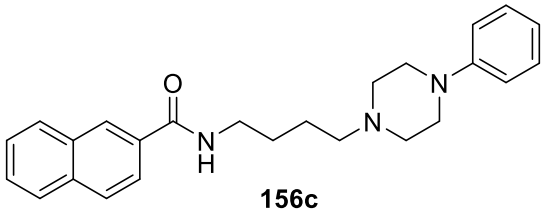

156c

N-(4-(4-phenylpiperazin-1-yl)butyl)-2-naphthamide (156c). In dry round bottom flask was added amine starting material (**156b**) (0.15 g, 0.64 mmol), anhydrous methylene chloride (1.5 mL) triethylamine (0.324 g, 3.2 mmol) for 5 min. To this was added 2-naphthoyl chloride (0.147 g, 0.77 mmol). Reaction was stirred at room temp for 1-2 hours, then extracted with methylene chloride (3 x 15 mL), dried over Na2SO4 and purified on SiO_2 by column chromatography. The product was obtained 0.154 g (62%). R_f 0.3 (20% MeOH/EtOAc). HRMS (ESI) *m/z* [M+H]+ calcd for C25H29N3O, 388.2383, Found, 388.2386. 1H NMR (400 MHz, Chloroform-d) δ 8.26 (d, J = 1.6 Hz, 1H), 7.85 (qd, J = 8.3,

1.9 Hz, 4H), 7.53 (dddd, J = 18.0, 8.2, 6.9, 1.4 Hz, 2H), 7.25 (dd, J = 8.7, 7.1 Hz, 2H), 6.92 (t, J = 5.5 Hz, 1H), 6.90 – 6.82 (m, 3H), 3.54 (q, J = 6.3 Hz, 2H), 3.18 – 3.11 (m, 4H), 2.58 (t, J = 5.0 Hz, 4H), 2.44 (t, J = 6.9 Hz, 2H), 1.77 – 1.63 (m, 4H). 13C NMR (101 MHz, Chloroform-d) δ 167.79, 151.21, 134.63, 132.57, 132.21, 129.12, 129.03, 128.87, 128.81, 128.41, 127.78, 127.72, 127.52, 127.24, 126.74, 126.66, 123.73, 119.70, 116.01, 57.96, 53.34, 53.23, 49.03, 40.09, 39.97, 27.45, 24.52.

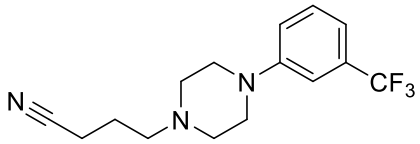

155a

4-(4-(3-(trifluoromethyl)phenyl)piperazin-1-yl)butanenitrile (155a). 1-(3-trifluoromethyl)phenylpiperazine (0.3 g, 1.3 mmol) in K_2CO_3 (0.198 g, 1.43 mmol), cat. KI, and anhydrous acetonitrile (6.5 mL) were stirred for 5 min at room temperature. Then 4-bromobutyronitrie (0.215 mg, 1.43 mmol) was added, the flask was sealed and the reaction refluxed for 14 h. Reaction was cooled, water added, and the product was extracted with methylene chloride and dried over Na_2SO_4. R_f 0.76 (20% MeOH/EtOAc). The product was characterized and used directly in next step, 0.42 g, (99%). HRMS (ESI) *m/z* [M+H]+ calcd for C15H18F3N3, 297.1526, Found, 298.1531. 1H NMR (400 MHz, Chloroform-d) δ 7.32 (t, J = 8.0 Hz, 1H), 7.09 (d, J = 2.0 Hz, 1H), 7.07 – 7.01 (m, 2H), 3.23 – 3.17 (m, 4H), 2.59 – 2.53 (m, 4H), 2.48 (t, J = 6.7 Hz, 2H), 2.42 (t, J = 7.1 Hz, 2H), 1.83 (q, J = 6.9 Hz, 2H). 13C NMR (101 MHz, Chloroform-d) δ 151.31, 131.41, 129.76, 119.80, 118.83, 115.88, 112.18, 56.12, 52.80, 48.54, 22.64, 14.83. 19F NMR (376 MHz, Chloroform-d) δ -62.59.

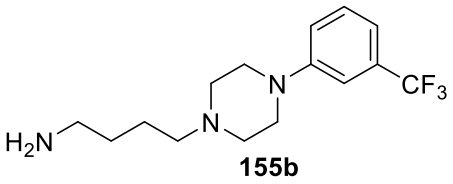

155b

4-(4-(3-(trifluoromethyl)phenyl)piperazin-1-yl)butan-1-amine (155b). To a mixture of nitrile (**155a**) (0.386 g, 1.3 mmol) in anhydrous THF (10 mL) at 0^{O}C, under argon, was slowly added borane-THF (7.8 mmol, 1M in THF) over 5 minutes. Reaction was let to come to room temperature overnight and stirred for a total of 48 h. Mixture was cooled to 0^{O}C and quenched with methanol. The product was suspended in 6 HCl/MeOH and stirred for 2 hours at room temp, then concentrated. The pH was adjusted to alkaline with Na_2CO_3/$NaHCO_3$, extracted with ethyl acetate and dried over Na_2SO_4. The product was purified on silica by column chromatography with 20% methanol/ethyl acetate to give 0.355g (72%). R_f 0.07 (20% MeOH/EtOAc). HRMS (ESI) *m/z* [M+H]+ calcd for C15H22F3N3, 301.1841, Found, 302.1841. 1H NMR (400 MHz, Chloroform-d) δ 7.24 (d, J = 15.7 Hz, 1H), 7.03 (s, 1H), 6.97 (t, J = 7.2 Hz, 2H), 3.44 (s, 2H), 3.14 (q, J = 8.5, 6.7 Hz, 4H), 2.67 (t, J = 6.5 Hz, 2H), 2.50 (q, J = 7.0, 6.0 Hz, 4H), 2.31 (q, J = 6.0, 5.4 Hz, 2H), 1.47 (th, J = 6.7, 3.4 Hz, 4H). 13C NMR (101 MHz, Chloroform-d) δ 151.28, 131.07, 129.55, 125.65, 118.52, 115.51, 111.97, 58.20, 52.91, 48.47, 41.66, 30.50, 24.07. 19F NMR (376 MHz, Chloroform-d) δ -62.68.

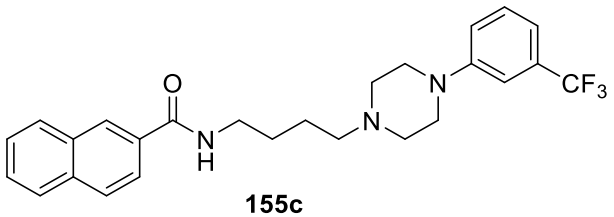

155c

N-(4-(4-(3-(trifluoromethyl)phenyl)piperazin-1-yl)butyl)-2-naphthamide (155c). In dry round bottom flask was added amine starting material (**155b**) (0.15 g, 0.5 mmol), anhydrous methylene chloride (1 mL) triethylamine (0.253 g, 2.5 mmol) for 5 min. To this was added 2-naphthoyl chloride (0.0.114 g, 0.6 mmol). Reaction was stirred at room temp for 1-2 hours, then extracted with methylene chloride (3 x 15 mL), dried over Na2SO4 and purified on SiO_2 by column chromatography. The product was obtained 0.197 g (87%). R_f 0.4 (20% MeOH/EtOAc). HRMS (ESI) *m/z* [M+H]+ calcd for C26H28F3N3O, 456.2257, Found, 456.2261. 1H NMR (400 MHz, Chloroform-d) δ 8.27 (d, J = 1.6 Hz, 1H), 7.85 – 7.79 (m, 4H), 7.52 (ddd, J = 8.1, 6.8, 1.4 Hz, 1H), 7.46 (ddd, J = 8.2, 6.9, 1.3 Hz, 1H), 7.32 (t, J = 7.9 Hz, 1H), 7.09 – 6.96 (m, 4H), 3.54 (q, J = 6.1 Hz, 2H), 3.21 (dd, J = 6.4, 3.8 Hz, 4H), 2.64 (dd, J = 6.2, 3.9 Hz, 4H), 2.51 (t, J = 6.8 Hz, 2H), 1.72 (dd, J = 6.3, 3.3 Hz, 4H). 13C NMR (101 MHz, Chloroform-d) δ 167.84, 151.10, 134.60, 132.54, 132.12, 129.63, 128.84, 128.37, 127.65, 127.28, 126.59, 123.72, 118.71, 116.02, 112.21, 57.64, 52.72, 48.19, 39.82, 27.29, 23.93. 19F NMR (376 MHz, Chloroform-d) δ -62.68.

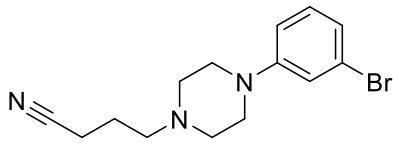

160a

4-(4-(3-bromophenyl)piperazin-1-yl)butanenitrile (160a). 1-(3-bromophenyl)piperazine (0.3 g, 1.25 mmol) in K_2CO_3 (0.19 g, 1.38 mmol), cat. KI, and anhydrous acetonitrile (6.25 mL) were stirred for 5 min at room temperature. Then 4-bromobutyronitrie (0.203 mg, 1.38 mmol) was added, the flask was sealed and the reaction refluxed for 14 h. Reaction was cooled, water added, and the product was extracted with methylene chloride and dried over Na_2SO_4. R_f 0.8 (20% MeOH/EtOAc).

The product was characterized and used directly in next step, 0.38 g (99%). HRMS (ESI) *m/z* [M+H]+ calcd for C14H18BrN3, 308.0757, Found, 308.0761, 310.0740. 1H NMR (400 MHz, Chloroform-d) δ 7.10 (t, J = 8.1 Hz, 1H), 7.03 (t, J = 2.1 Hz, 1H), 6.95 (ddd, J = 7.8, 1.8, 0.9 Hz, 1H), 6.82 (ddd, J = 8.4, 2.5, 0.9 Hz, 1H), 3.21 – 3.16 (m, 4H), 2.60 – 2.55 (m, 4H), 2.51 (t, J = 6.7 Hz, 2H), 2.46 (t, J = 7.1 Hz, 2H), 1.86 (p, J = 6.9 Hz, 2H). 13C NMR (101 MHz, Chloroform-d) δ 152.39, 130.31, 123.21, 122.25, 119.72, 118.67, 114.34, 56.18, 52.88, 48.64, 22.69, 14.93.

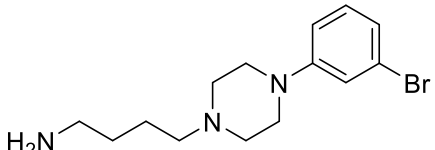

160b

4-(4-(3-bromophenyl)piperazin-1-yl)butan-1-amine (160b). To a mixture of nitrile (**160a**) (0.385 g, 1.25 mmol) in anhydrous THF (9.6 mL) at 0^{O}C, under argon, was slowly added borane-THF (7.5 mmol, 1M in THF) over 5 minutes. Reaction was let to come to room temperature overnight and stirred for a total of 48 h. Mixture was cooled to 0^{O}C and quenched with methanol. The product was suspended in 6 HCl/MeOH and stirred for 2 hours at room temp, then concentrated. The pH was adjusted to alkaline with Na_2CO_3/$NaHCO_3$, extracted with ethyl acetate and dried over Na_2SO_4. The product was purified on silica by column chromatography with 20% methanol/ethyl acetate to give 0.1g (26%). R_f 0.02 (20% MeOH/EtOAc). HRMS (ESI) *m/z* [M+H]+ calcd for C14H22BrN3, 312.107, Found, 312.107, 314.1054. 1H NMR (400 MHz, Chloroform-d) δ 6.99 (d, J = 8.1 Hz, 1H), 6.94 (t, J = 2.1 Hz, 1H), 6.85 (dd, J = 7.7, 1.8 Hz, 1H), 6.73 (dd, J = 8.3, 2.4 Hz, 1H), 3.38 (s, 2H), 3.10 (t, J = 5.1 Hz, 4H), 2.66 (t, J = 6.5 Hz, 1H), 2.58 (h, J = 4.9, 4.2 Hz, 1H), 2.49 (t, J = 5.2 Hz, 4H), 2.32 (dt, J = 11.7, 4.3 Hz, 2H), 1.55 – 1.41 (m, 4H), .

13C NMR (101 MHz, Chloroform-d) δ 152.33, 130.27, 123.12, 122.04, 118.47, 114.23, 58.16, 52.87, 48.41, 24.13, 22.23, 18.98, 13.94.

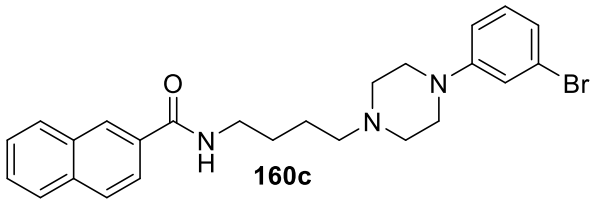

160c

N-(4-(4-(3-bromophenyl)piperazin-1-yl)butyl)-2-naphthamide (160c). In dry round bottom flask was added amine starting material (**160b**) (0.380 g, 1.23 mmol), anhydrous methylene chloride (2.5 mL) triethylamine (6.15 mmol) for 5 min. To this was added 2-naphthoyl chloride (0.0.191 g, 1.5 mmol). Reaction was stirred at room temp for 1-2 hours, then extracted with methylene chloride (3 x 15 mL), dried over Na2SO4 and purified on SiO_2 by column chromatography. The product was obtained 0.28 g (49%). R_f 0.33 (10% MeOH/EtOAc). HRMS (ESI) *m/z* [M+H]+ calcd for C25H28BrN3O, 466.1489, Found, 466.1488, 468.1470. 1H NMR (400 MHz, Chloroform-d) δ 8.26 (d, J = 1.6 Hz, 1H), 7.89 – 7.78 (m, 4H), 7.52 (dddd, J = 17.5, 8.1, 6.8, 1.4 Hz, 2H), 6.99 – 6.88 (m, 3H), 6.79 – 6.72 (m, 1H), 3.54 (q, J = 6.2 Hz, 2H), 3.19 – 3.09 (m, 4H), 2.60 – 2.53 (m, 4H), 2.45 (t, J = 6.9 Hz, 2H), 1.79 – 1.60 (m, 4H). 13C NMR (101 MHz, Chloroform-d) δ 167.82, 152.32, 134.62, 132.54, 132.17, 130.29, 128.80, 128.42, 127.75, 127.55, 127.23, 126.75, 123.71, 123.19, 122.23, 118.58, 114.30, 57.84, 52.93, 48.42, 40.01, 27.39, 24.33.

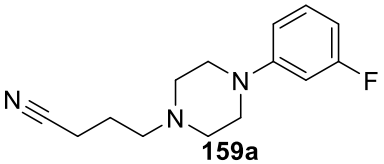

159a

4-(4-(3-fluorophenyl)piperazin-1-yl)butanenitrile (159a). 1-(3-bromophenyl)piperazine (0.3 g, 1.67 mmol) in K_2CO_3 (0.254 g, 1.84 mmol), cat. KI, and anhydrous acetonitrile (8.4 mL) were stirred for 5 min at room temperature. Then 4-bromobutyronitrie (0.272 mg, 1.84 mmol) was added, the flask was sealed and the reaction refluxed for 14 h. Reaction was cooled, water added, and the product was extracted with methylene chloride and dried over Na_2SO_4. R_f 0.8 (20% MeOH/EtOAc). The product was characterized and used directly in the next step, 0.413 g (99%). HRMS (ESI) *m/z* [M+H]+ calcd for C14H18FN3, 248.1588, Found, 248.1559. 1H NMR (400 MHz, Chloroform-d) δ 7.18 (td, J = 8.2, 7.0 Hz, 1H), 6.67 (ddd, J = 8.4, 2.4, 0.9 Hz, 1H), 6.58 (dt, J = 12.4, 2.4 Hz, 1H), 6.53 (tdd, J = 8.2, 2.4, 0.9 Hz, 1H), 3.22 – 3.17 (m, 4H), 2.58 (dq, J = 5.4, 2.7, 2.3 Hz, 4H), 2.52 (t, J = 6.8 Hz, 2H), 2.46 (t, J = 7.1 Hz, 2H), 1.87 (q, J = 6.9 Hz, 2H). 13C NMR (101 MHz, Chloroform-d) δ 165.02, 130.06, 119.71, 111.12, 105.98, 102.77, 56.18, 52.87, 48.58, 22.68, 14.93. 19F NMR (376 MHz, Chloroform-d) δ -112.37.

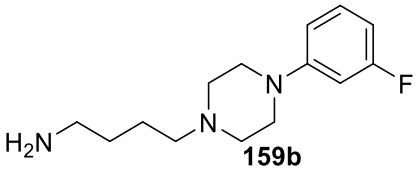

159b

4-(4-(3-fluorophenyl)piperazin-1-yl)butan-1-amine (159b) To a mixture of nitrile (**159a**) (0.413 g, 1.67 mmol) in anhydrous THF (12.8 mL) at 0^{O}C, under argon, was slowly added borane-THF (10 mmol, 1M in THF) over 5 minutes. Reaction was let to come to room temperature overnight and stirred for a total of 48 h. Mixture was cooled to 0^{O}C and quenched with methanol. The product was suspended in 6 HCl/MeOH and stirred for 2 hours at room temp, then concentrated. The pH was adjusted to alkaline with Na_2CO_3/$NaHCO_3$, extracted with ethyl acetate and dried over Na_2SO_4. The crude product

0.566 g (94%) was used directly in the next step. HRMS (ESI) *m/z* [M+H]+ calcd for C14H22FN3, 252.1871, Found, 252.1874. 1H NMR (400 MHz, Chloroform-d) δ 7.07 (q, J = 7.9 Hz, 1H), 6.56 (dd, J = 8.4, 2.3 Hz, 1H), 6.47 (dt, J = 12.4, 2.4 Hz, 1H), 6.40 (td, J = 8.2, 2.3 Hz, 1H), 3.39 (s, 2H), 3.09 (t, J = 5.1 Hz, 4H), 2.63 (t, J = 6.5 Hz, 2H), 2.33 – 2.25 (m, 2H), 1.50 – 1.38 (m, 4H). 13C NMR (101 MHz, Chloroform-d) δ 164.90, 162.49, 152.73, 129.94, 110.98, 105.72, 52.86, 48.35, 24.08, 22.24, 18.95, 13.87. 19F NMR (376 MHz, Chloroform-d) δ -112.38.

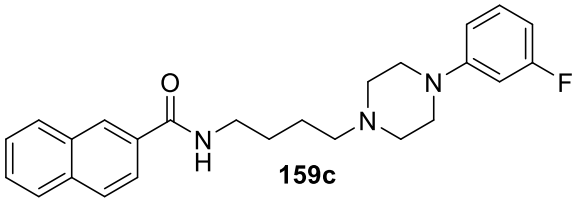

159c

N-(4-(4-(3-fluorophenyl)piperazin-1-yl)butyl)-2-naphthamide (159c) In dry round bottom flask was added amine starting material (**159b**) (0.42 g, 1.67 mmol), anhydrous methylene chloride (3.3 mL) triethylamine (8.35 mmol) for 5 min. To this was added 2-naphthoyl chloride (0.0.381 g, 2 mmol). Reaction was stirred at room temp for 1-2 hours, then extracted with methylene chloride (3 x 15 mL), dried over Na2SO4 and purified on SiO_2 by column chromatography. The product was obtained 0.3 g (42%). R_f 0.33 (10% MeOH/EtOAc). HRMS (ESI) *m/z* [M+H]+ calcd for C25H28FN3O, 406.2289, Found, 406.2292. 1H NMR (400 MHz, Chloroform-d) δ 8.26 (s, 1H), 7.88 – 7.79 (m, 4H), 7.51 (dddd, J = 20.8, 8.1, 6.9, 1.4 Hz, 3H), 7.16 (td, J = 8.5, 6.9 Hz, 1H), 6.96 (t, J = 5.6 Hz, 1H), 6.64 – 6.58 (m, 1H), 6.53 (dd, J = 5.9, 2.5 Hz, 1H), 6.50 (t, J = 1.8 Hz, 1H), 3.54 (q, J = 6.2 Hz, 2H), 3.15 (dd, J = 6.3, 3.8 Hz, 4H), 2.59 (dd, J = 6.3, 3.9 Hz, 4H), 2.47 (t, J = 6.9 Hz, 2H), 1.77 – 1.63 (m, 4H). 13C NMR (101 MHz, Chloroform-d) δ 167.82, 164.99, 152.79, 134.61, 132.54, 132.15, 130.08, 128.85, 128.40, 127.76, 127.26, 123.71, 57.78,

52.87, 48.32, 39.95, 27.37, 24.21. 19F NMR (376 MHz, Chloroform-d) δ -112.31 (d, J = 13.3 Hz).

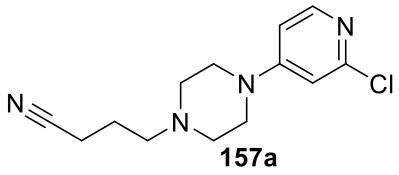

157a

4-(4-(2-chloropyridin-4-yl)piperazin-1-yl)butanenitrile (157a). 1-(2-chloropyridin-4-yl)piperazine (0.3 g, 1.52 mmol) in K_2CO_3 (0.23 g, 1.67 mmol), cat. KI, and anhydrous acetonitrile (7.6 mL) were stirred for 5 min at room temperature. Then 4-bromobutyronitrie (0.247 mg, 1.67 mmol) was added, the flask was sealed and the reaction refluxed for 14 h. Reaction was cooled, water added, and the product was extracted with methylene chloride and dried over Na_2SO_4. R_f 0.5 (20% MeOH/EtOAc). The product was characterized and used directly in the next step, 0.327 g (81%). HRMS (ESI) *m/z* [M+H]+ calcd for C13H17ClN4, 265.1215, [M+Na]+ 287.1034, Found, 265.1214. 1H NMR (400 MHz, Chloroform-d) δ 8.02 (d, J = 6.1 Hz, 1H), 6.65 (d, J = 2.4 Hz, 1H), 6.57 (dd, J = 6.1, 2.4 Hz, 1H), 3.36 – 3.31 (m, 4H), 2.58 – 2.53 (m, 4H), 2.51 (d, J = 6.7 Hz, 2H), 2.46 t, J = 7.0 Hz, 2H), 1.86 (p, J = 6.8 Hz, 2H). 13C NMR (101 MHz, Chloroform-d) δ 156.64, 152.72, 149.57, 119.60, 107.36, 107.34, 56.08, 52.36, 45.94, 22.58, 14.93.

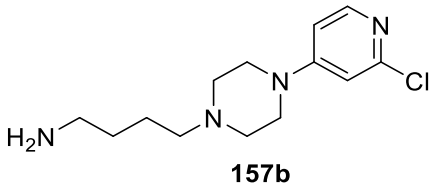

157b

4-(4-(2-chloropyridin-4-yl)piperazin-1-yl)butan-1-amine (157b). To a mixture of nitrile (**157a**) (0.325 g, 1.23 mmol) in anhydrous THF (9.5 mL) at 0^{O}C, under argon, was slowly

added borane-THF (7.36 mmol, 1M in THF) over 5 minutes. Reaction was let to come to room temperature overnight and stirred for a total of 48 h. Mixture was cooled to 0^{O}C and quenched with methanol. The product was suspended in 6 HCl/MeOH and stirred for 2 hours at room temp, then concentrated. The pH was adjusted to alkaline with Na_2CO_3/$NaHCO_3$, extracted with ethyl acetate and dried over Na_2SO_4. The crude product 0.33 g (99%) was used directly in the next step. HRMS (ESI) *m/z* [M+H]+ calcd for C13H21ClN4, 269.1528, Found, 269.1523. 1H NMR (400 MHz, Chloroform-d) δ 7.88 (d, J = 6.1 Hz, 1H), 6.52 (t, J = 2.1 Hz, 1H), 6.47 (dt, J = 6.1, 2.0 Hz, 1H), 3.50 (t, J = 6.7 Hz, 2H), 3.26 (dt, J = 18.6, 5.2 Hz, 4H), 2.63 (q, J = 6.8 Hz, 2H), 2.44 (q, J = 5.2 Hz, 4H), 2.30 (dt, J = 11.6, 6.6 Hz, 2H), 1.62 (p, J = 6.4 Hz, 2H), 1.52 (q, J = 6.2 Hz, 2H). 13C NMR (101 MHz, Chloroform-d) δ 156.59, 152.28, 149.27, 107.31, 107.11, 52.31, 45.71, 34.80, 27.59, 18.91, 13.87.

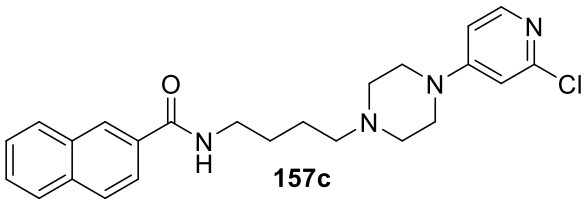

157c

N-(4-(4-(2-chloropyridin-4-yl)piperazin-1-yl)butyl)-2-naphthamide (157c). In dry round bottom flask was added amine starting material (**157b**) (0.33 g, 1.23 mmol), anhydrous methylene chloride (2.5 mL) triethylamine (6.15 mmol) for 5 min. To this was added 2-naphthoyl chloride (0.191 g, 1.5 mmol). Reaction was stirred at room temp for 1-2 hours, then extracted with methylene chloride (3 x 15 mL), dried over Na2SO4 and purified on SiO_2 by column chromatography. The product was obtained 0.282 g (54%). R_f

0.12 (10% MeOH/EtOAc). HRMS (ESI) *m/z* [M+H]+ calcd for C24H27ClN4O, 423.1946, [M+Na]+ 445.1766, Found, 423.1950, 445.1764. 1H NMR (400 MHz, Chloroform-d) δ 8.25 (d, J = 1.7 Hz, 1H), 7.99 (d, J = 6.1 Hz, 1H), 7.86 (t, J = 8.4 Hz, 4H), 7.81 (dd, J = 8.6, 1.8 Hz, 1H), 7.58 – 7.49 (m, 2H), 6.58 (d, J = 2.4 Hz, 1H), 6.51 (dd, J = 6.1, 2.4 Hz, 1H), 3.55 (q, J = 6.4 Hz, 2H), 3.30 – 3.24 (m, 4H), 2.58 – 2.51 (m, 4H), 2.46 (t, J = 7.0 Hz, 2H), 1.75 – 1.60 (m, 4H).

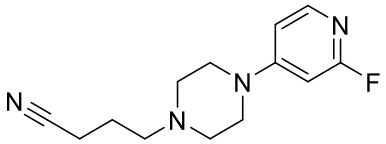

158a

4-(4-(2-fluoropyridin-4-yl)piperazin-1-yl)butanenitrile (158a). 1-(2-fluoropyridin-4-yl)piperazine (0.3 g, 1.66 mmol) in K_2CO_3 (0.253 g, 1.83 mmol), cat. KI, and anhydrous acetonitrile (8.3 mL) were stirred for 5 min at room temperature. Then 4-bromobutyronitrie (0.271 mg, 1.83 mmol) was added, the flask was sealed and the reaction refluxed for 14 h. Reaction was cooled, water added, and the product was extracted with methylene chloride and dried over Na_2SO_4. R_f 0.47 (10% MeOH/EtOAc). The product was purified on SiO_2 by column chromatography, to give 0.282 g (68%). HRMS (ESI) *m/z* [M+H]+ calcd for C13H17FN4, 249.151, [M+Na]+ 271.1329, Found, 249.1513, 271.1335. 1H NMR (400 MHz, Chloroform-d) δ 7.88 (d, J = 6.1 Hz, 1H), 6.54 (dt, J = 6.1, 1.9 Hz, 1H), 6.18 (dd, J = 2.3, 1.2 Hz, 1H), 3.37 – 3.32 (m, 4H), 2.56 (dd, J = 6.1, 4.2 Hz, 4H), 2.52 (t, J = 6.7 Hz, 2H), 2.46 (t, J = 7.0 Hz, 2H), 1.87 (q, J = 6.8 Hz, 2H). 13C NMR (101 MHz, Chloroform-d) δ 147.67, 147.48, 119.61, 106.57, 56.09, 52.37, 46.13, 22.59, 14.93. 19F NMR (376 MHz, Chloroform-d) δ -69.33.

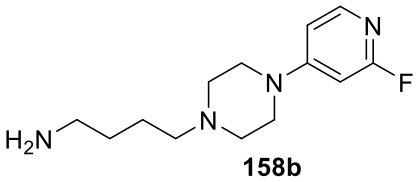

158b

4-(4-(2-fluoropyridin-4-yl)piperazin-1-yl)butan-1-amine (158b). To a mixture of nitrile (**158a**) (0.27 g, 1.1 mmol) in anhydrous THF (8.4 mL) at 0^{O}C, under argon, was slowly added borane-THF (6.53 mmol, 1M in THF) over 5 minutes. Reaction was let to come to room temperature overnight and stirred for a total of 48 h. Mixture was cooled to 0^{O}C and quenched with methanol. The product was suspended in 6 HCl/MeOH and stirred for 2 hours at room temp, then concentrated. The pH was adjusted to alkaline with Na_2CO_3/$NaHCO_3$, extracted with ethyl acetate and dried over Na_2SO_4. The crude product 0.28 g (99%) was used directly in the next step. HRMS (ESI) *m/z* [M+H]+ calcd for C13H21FN4, 353.1823, Found, 253.1828. 1H NMR (400 MHz, Chloroform-d) δ 7.83 (dd, J = 6.1, 2.2 Hz, 1H), 6.51 (dt, J = 6.0, 1.9 Hz, 1H), 6.14 (t, J = 1.7 Hz, 1H), 3.38 (t, J = 5.2 Hz, 2H), 3.31 (t, J = 5.3 Hz, 2H), 2.71 (dt, J = 13.5, 6.7 Hz, 2H), 2.53 (dt, J = 13.5, 5.1 Hz, 4H), 2.41 (t, J = 5.9 Hz, 2H), 1.70 (q, J = 6.2 Hz, 2H), 1.63 (q, J = 6.2 Hz, 2H), 1.56 – 1.45 (m, 2H).13C NMR (101 MHz, Chloroform-d) δ 106.64, 57.91, 52.35, 48.55, 45.86, 28.00, 24.71. 19F NMR (376 MHz, Chloroform-d) δ -69.59.

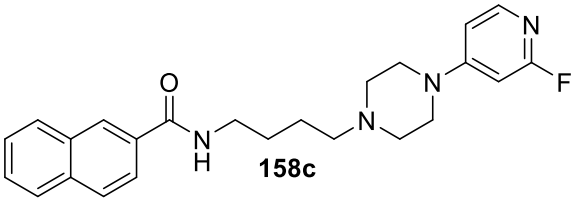

158c

N-(4-(4-(2-fluoropyridin-4-yl)piperazin-1-yl)butyl)-2-naphthamide (158c). In dry round bottom flask was added amine starting material (**158b**) (0.28 g, 1.1 mmol),

anhydrous methylene chloride (2.2 mL) triethylamine (5.5 mmol) for 5 min. To this was added 2-naphthoyl chloride (0.252 g, 1.32 mmol). Reaction was stirred at room temp for 1-2 hours, then extracted with methylene chloride (3 x 15 mL), dried over Na2SO4 and purified on SiO_2 by column chromatography. The product was obtained 0.239 g (53%). R_f 0.12 (10% MeOH/EtOAc). HRMS (ESI) *m/z* [M+H]+ calcd for C24H27FN4O, 407.2242, [M+Na]+ 429.2061, Found, 407.2248, 429.2067. 1H NMR (400 MHz, Chloroform-d) δ 8.26 (d, J = 1.4 Hz, 1H), 7.91 – 7.83 (m, 4H), 7.59 – 7.49 (m, 2H), 6.70 (s, 1H), 6.51 – 6.46 (m, 1H), 6.11 (d, J = 2.2 Hz, 1H), 3.56 (q, J = 6.3 Hz, 2H), 3.30 (t, J = 5.2 Hz, 4H), 2.56 (t, J = 5.2 Hz, 4H), 2.47 (t, J = 7.0 Hz, 2H), 1.71 (dq, J = 22.0, 7.3 Hz, 4H). 19F NMR (376 MHz, Chloroform-d) δ -69.42.

b. Spectral and Other Characterization Data

NMR spectra were recorded with a Varian 400 MHz or 500 MHz instrument at room temperature with tetramethylsilane (TMS) as an internal standard. Mass spectra were performed on an Agilent Q-TOF HPLC-MS or VG (Micromass) 70-250-S Magnetic sector mass spectrometer employing the electrospray ionization (ESI) method.

mns4d3p35_PROTON_01
mns4d3p35

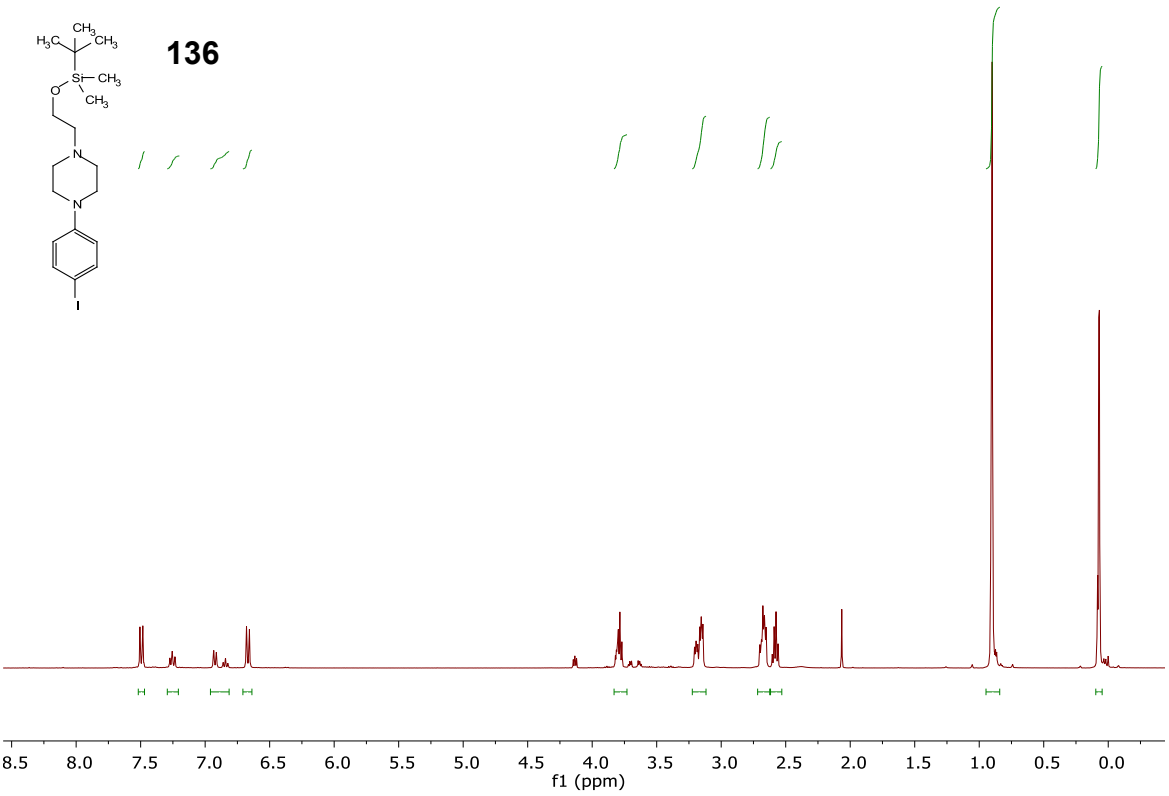

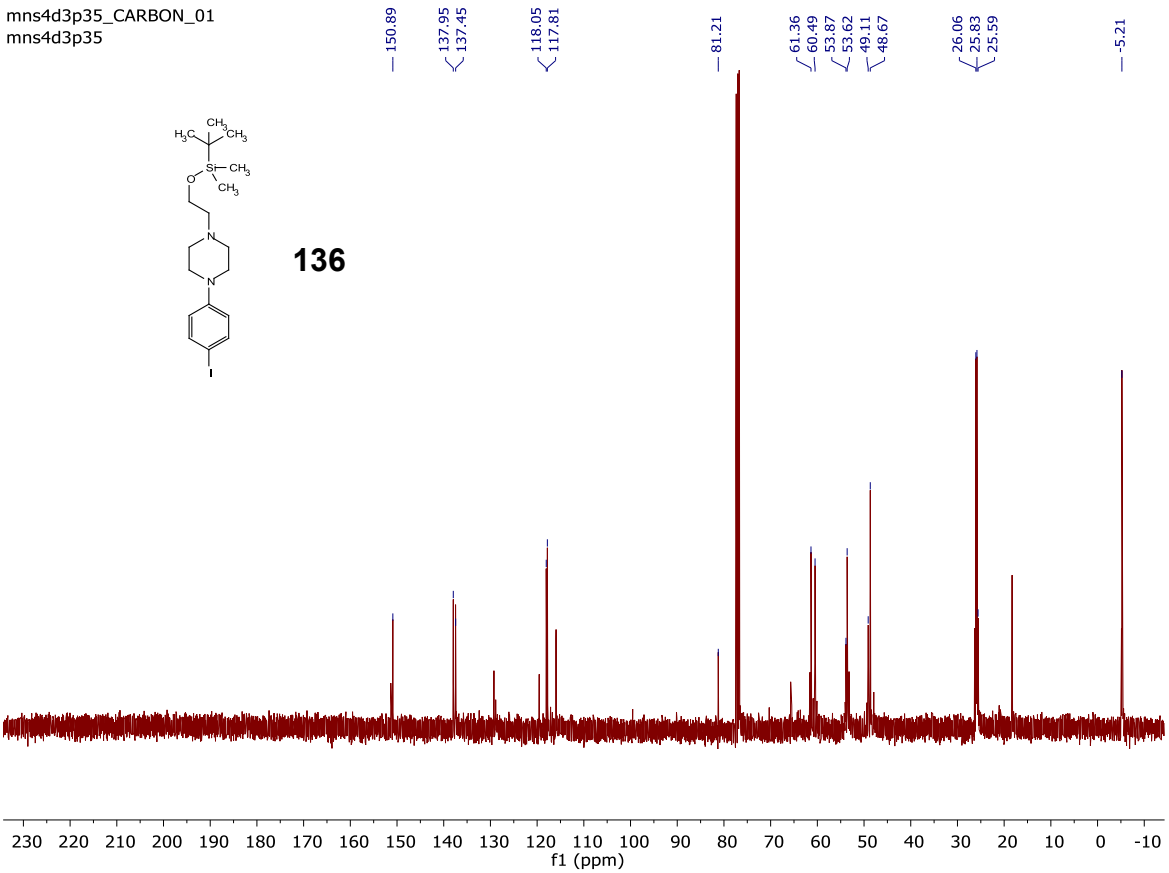
mns4d3p35_CARBON_01
mns4d3p35
150.89
137.95
137.45
118.05
117.81
81.21
61.36
60.49
53.87
53.62
49.11
48.67
26.06
25.83
25.59
-5.21
136
f1 (ppm)

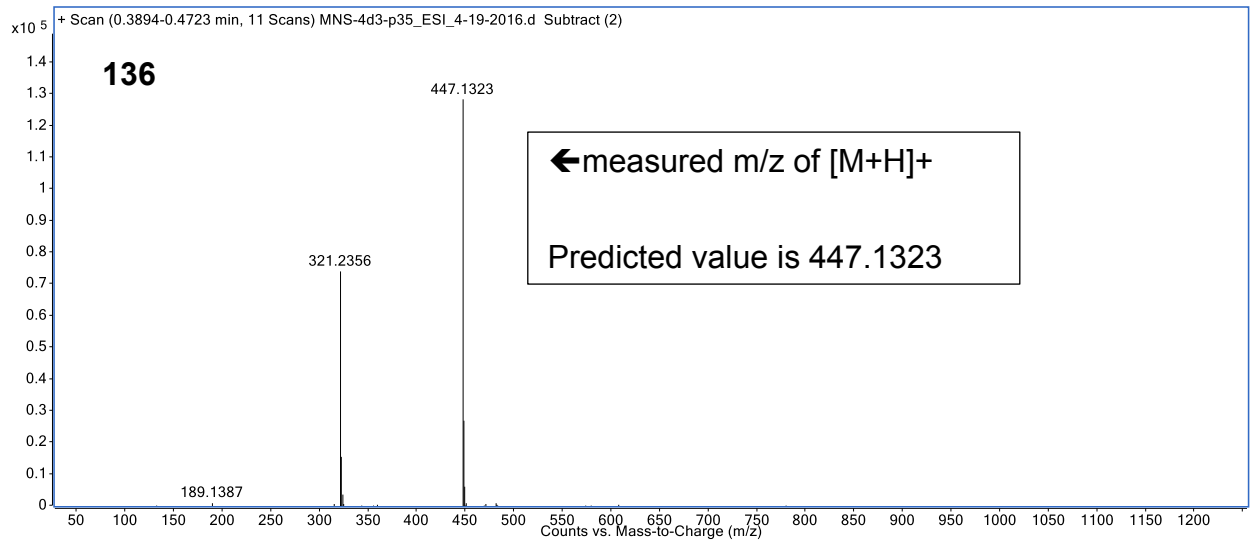
+ Scan (0.3894-0.4723 min, 11 Scans) MNS-4d3-p35_ESI_4-19-2016.d Subtract (2)
x10 5
136
447.1323
321.2356
189.1387
←measured m/z of [M+H]+
Predicted value is 447.1323
Counts vs. Mass-to-Charge (m/z)

mns4d3p39-3_PROTON_01
mns4d3p39-3

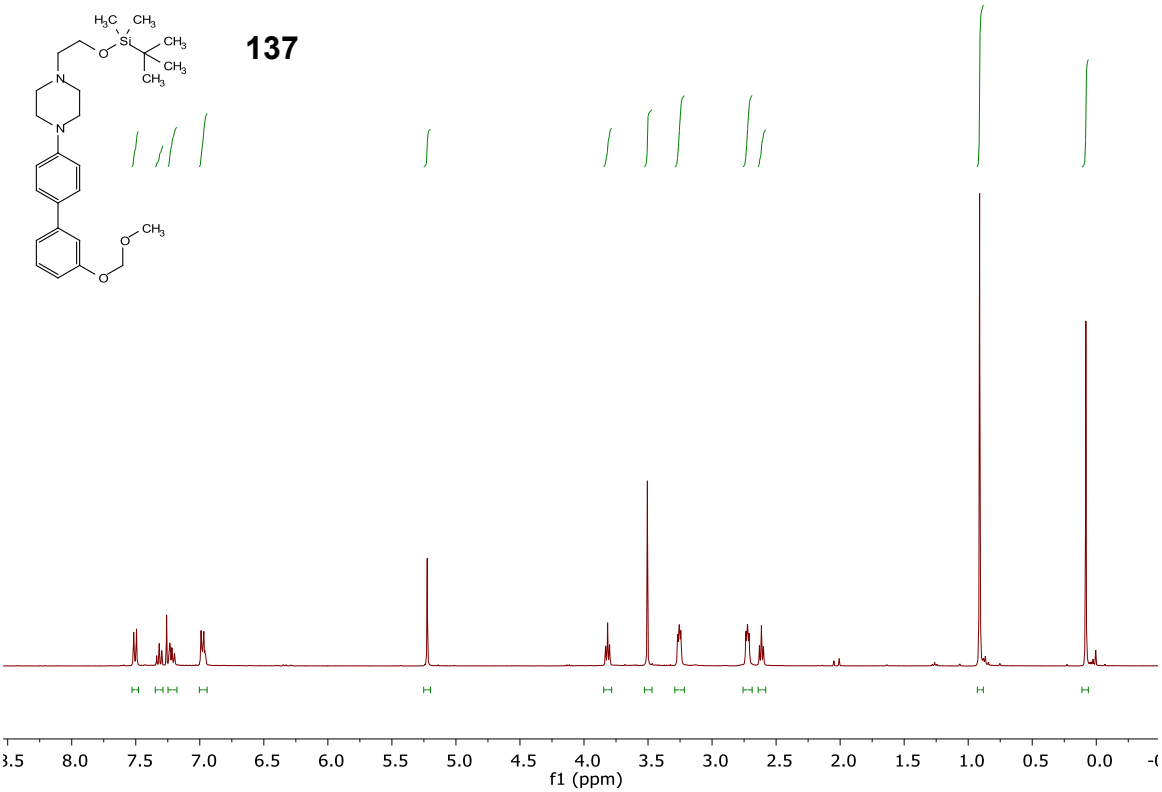

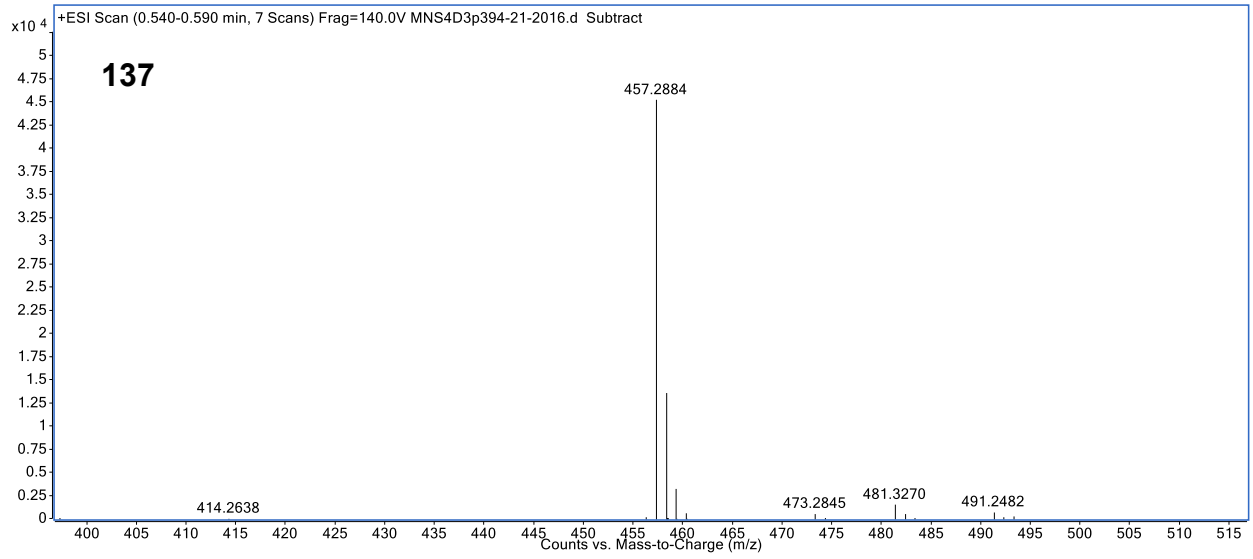

mns4d3p75-3_PROTON_01
mns4d3p75-3

139

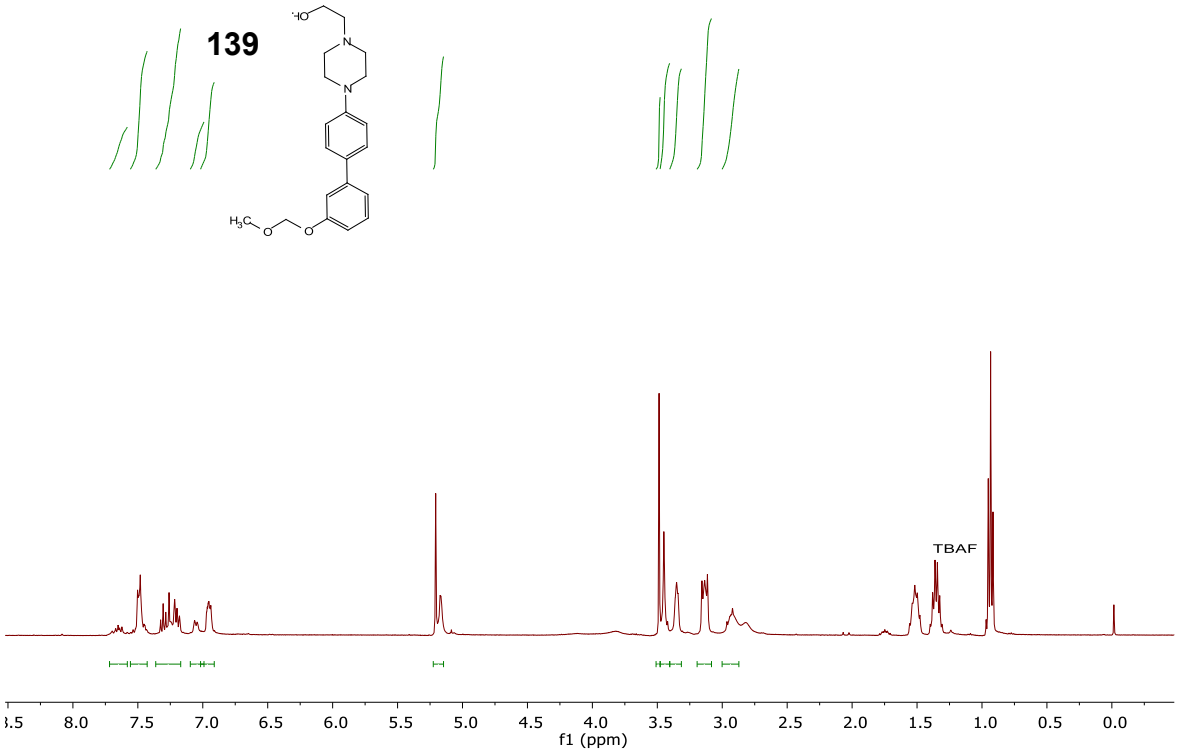

mns4d3p79-1_PROTON_01
mns4d3p79-1

138

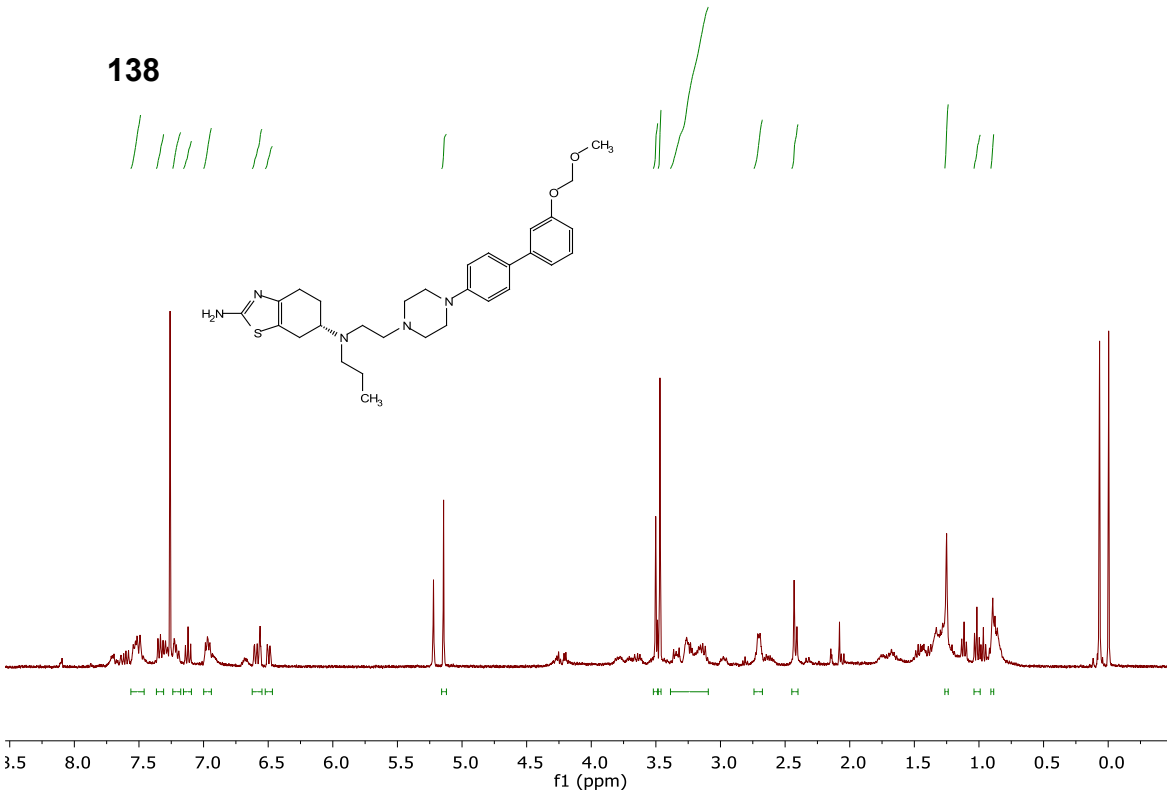

mns4d3p79-3_PROTON_01
mns4d3p79-3

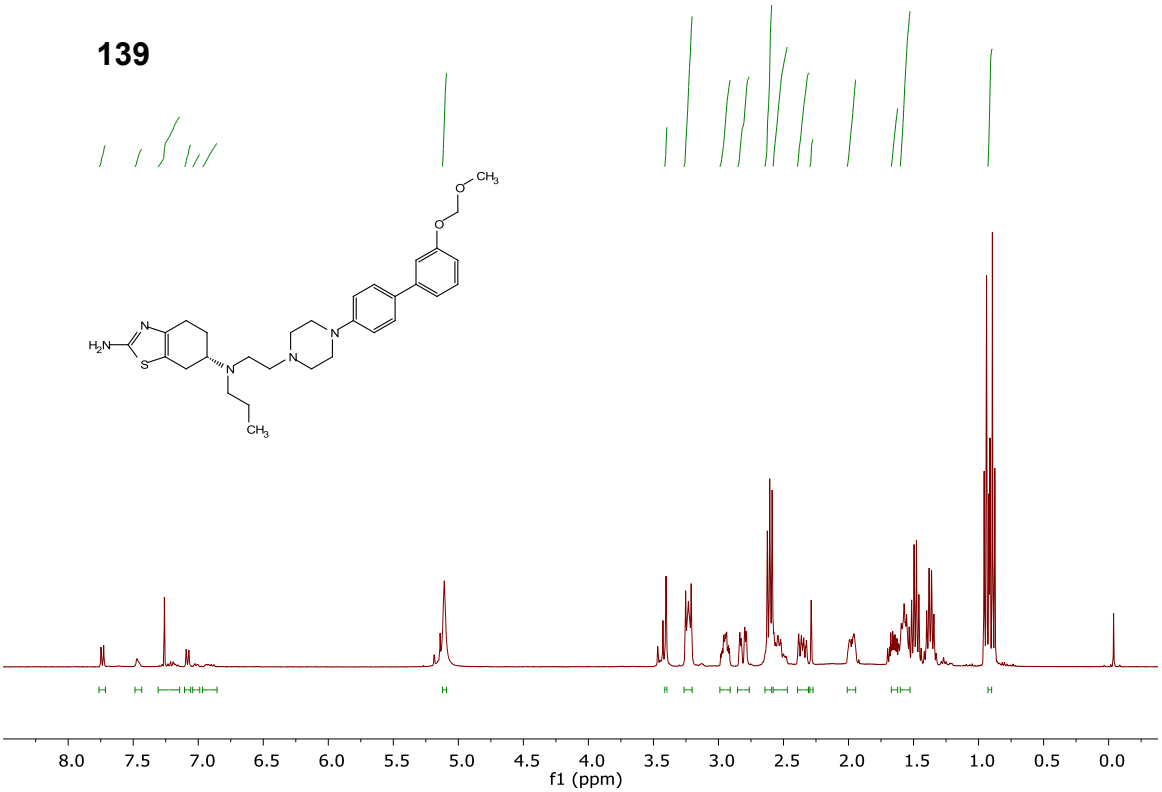

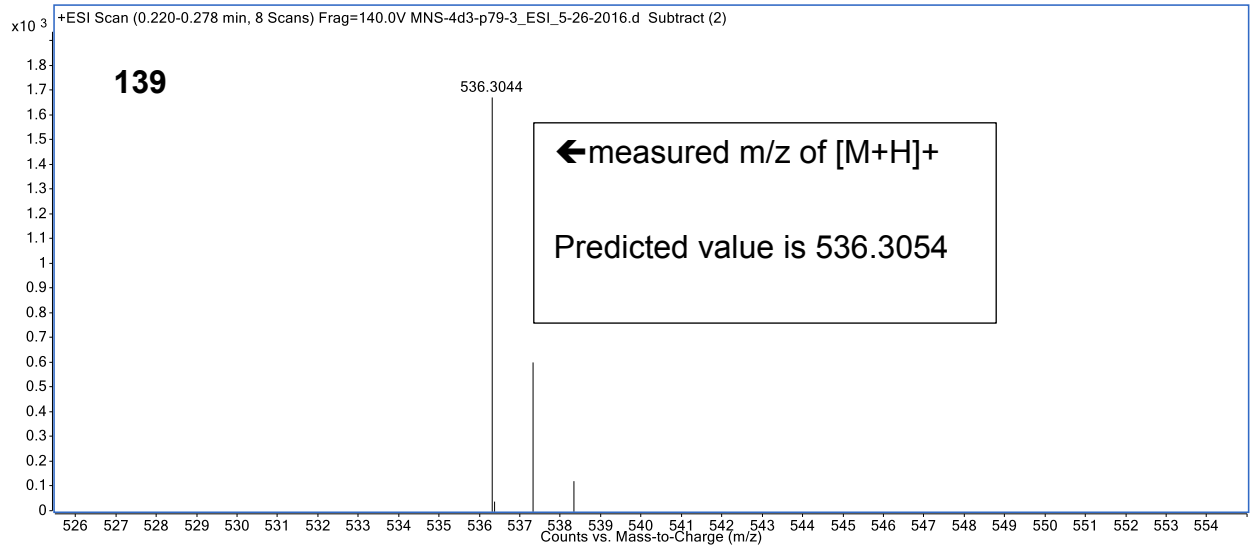

mns5d3p19_PROTON_01
mns5d3p19

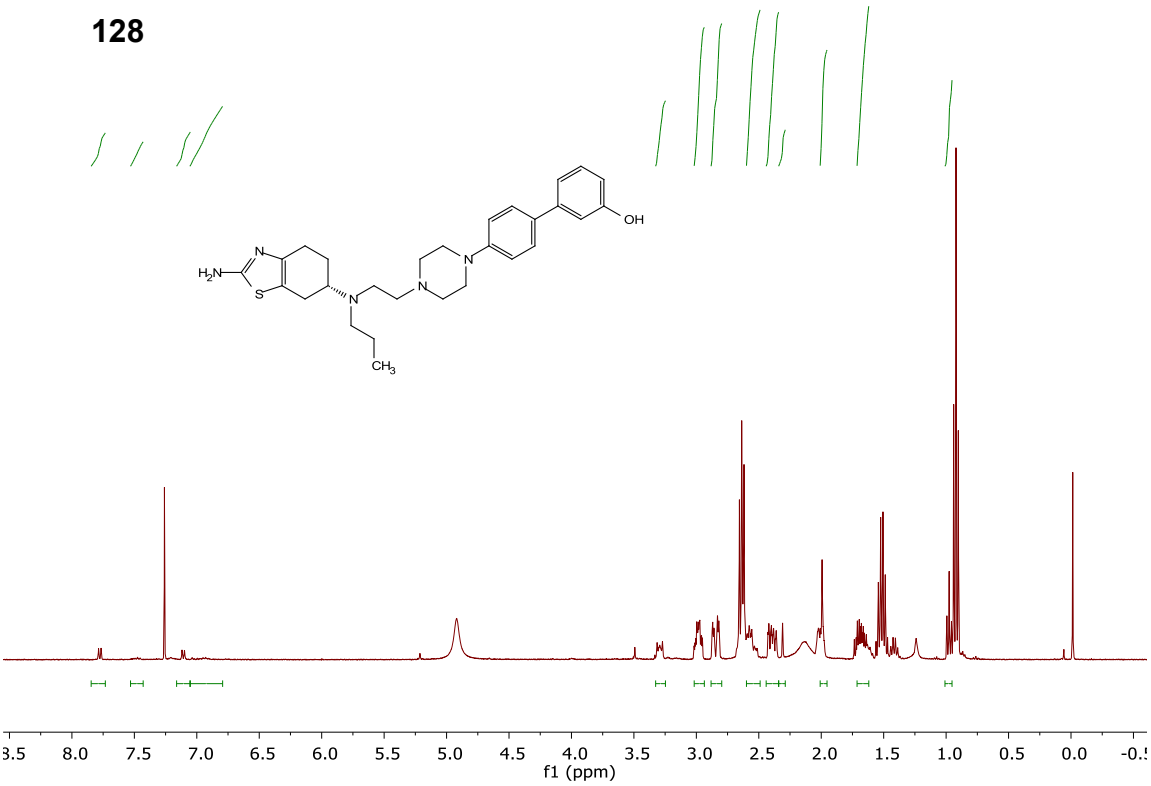

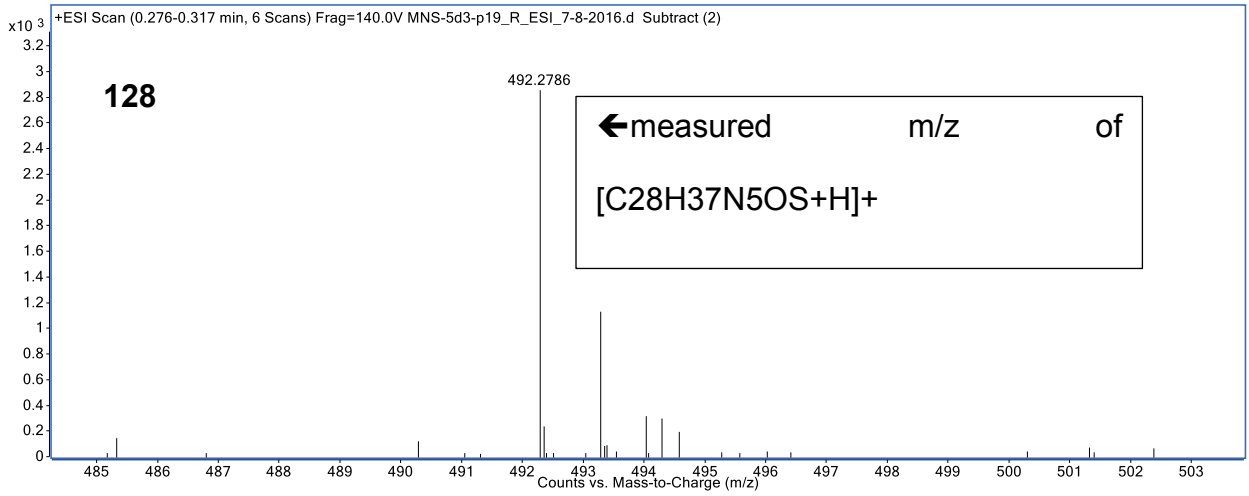

mns5d3p59_PROTON_01
mns5d3p59

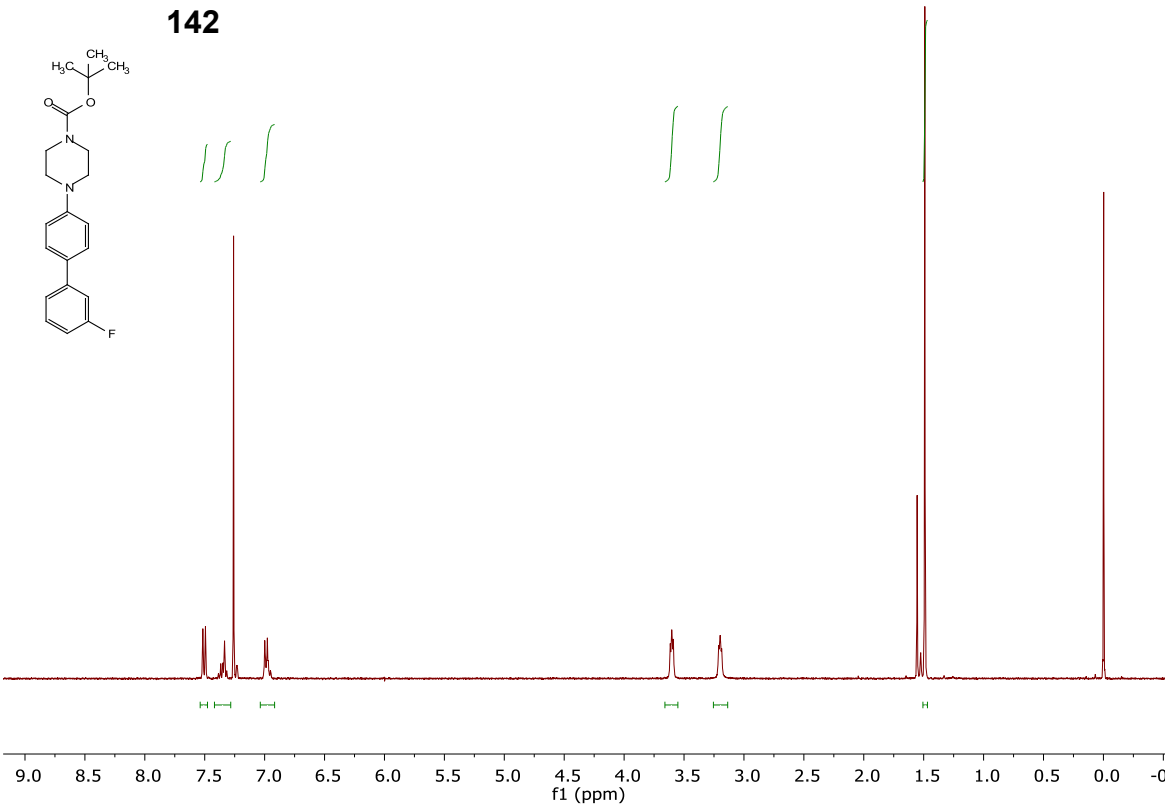

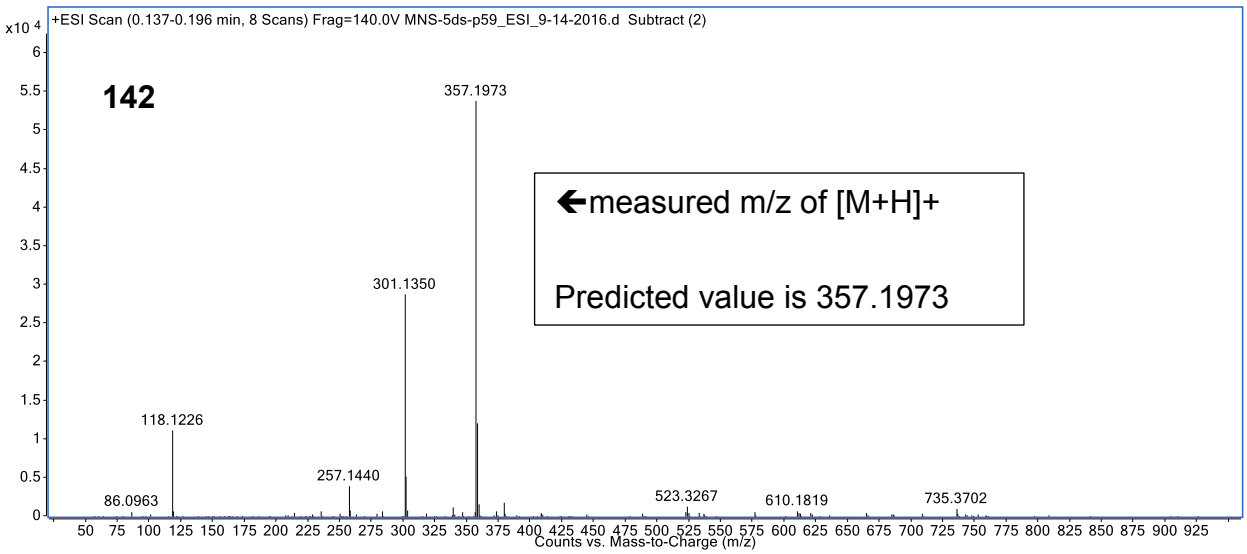

mns5d3p67_PROTON_01
mns5d3p67

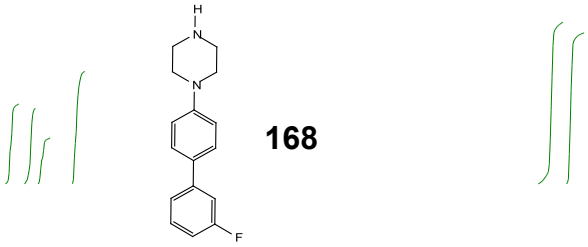

168

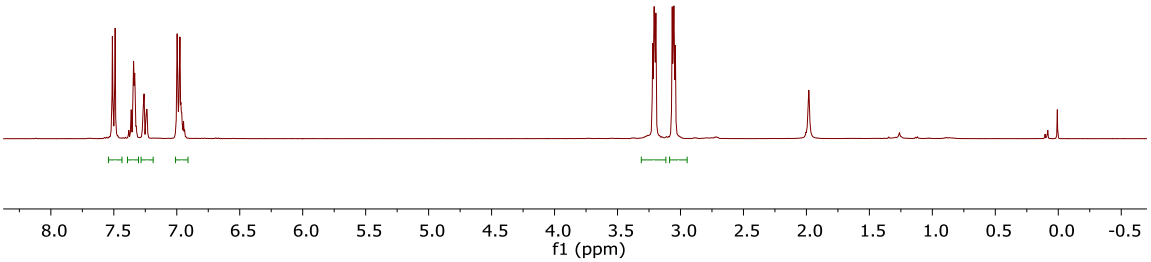

mns5d3p67_FLUORINE_01
mns5d3p67

168

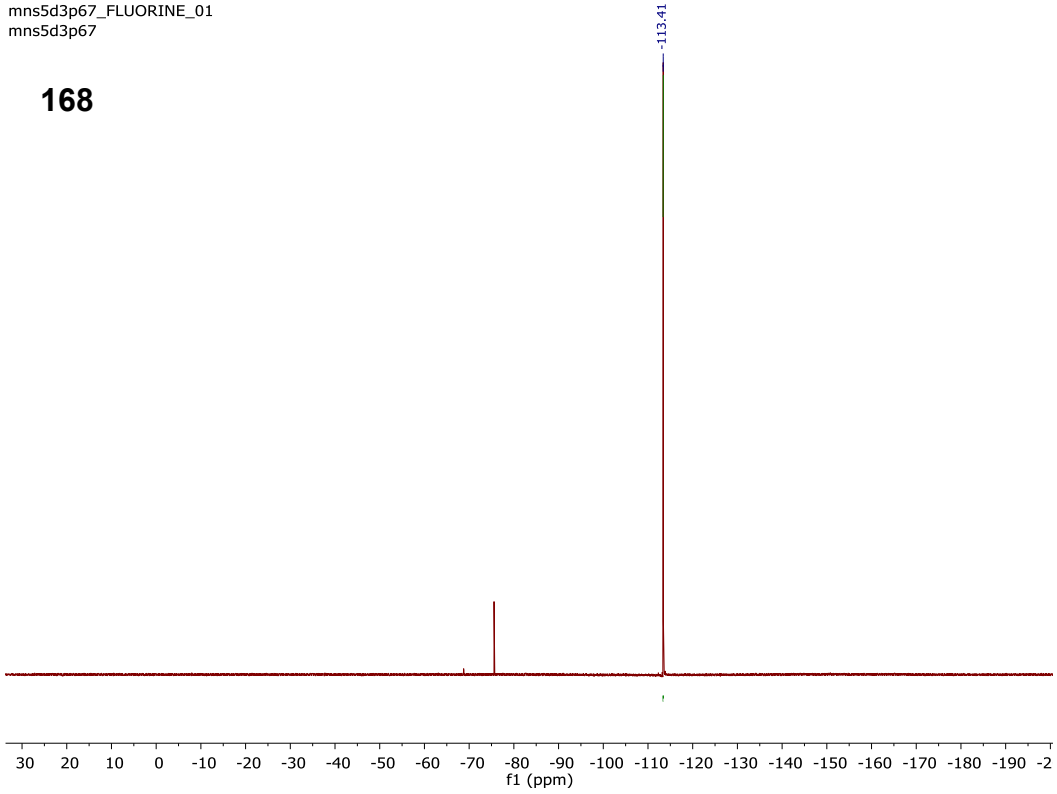

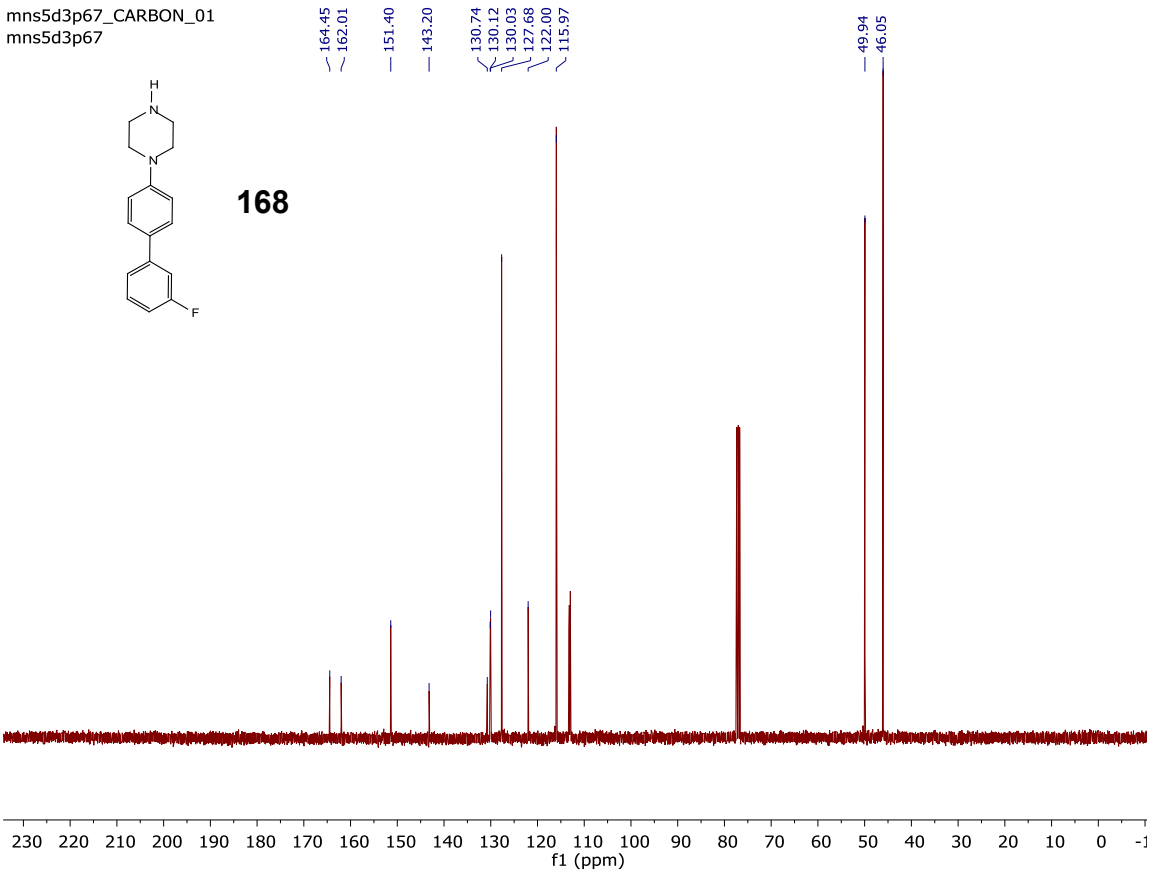
mns5d3p67_CARBON_01
mns5d3p67
164.45
162.01
151.40
143.20
130.74
130.12
130.03
127.68
122.00
115.97
49.94
46.05
168
f1 (ppm)

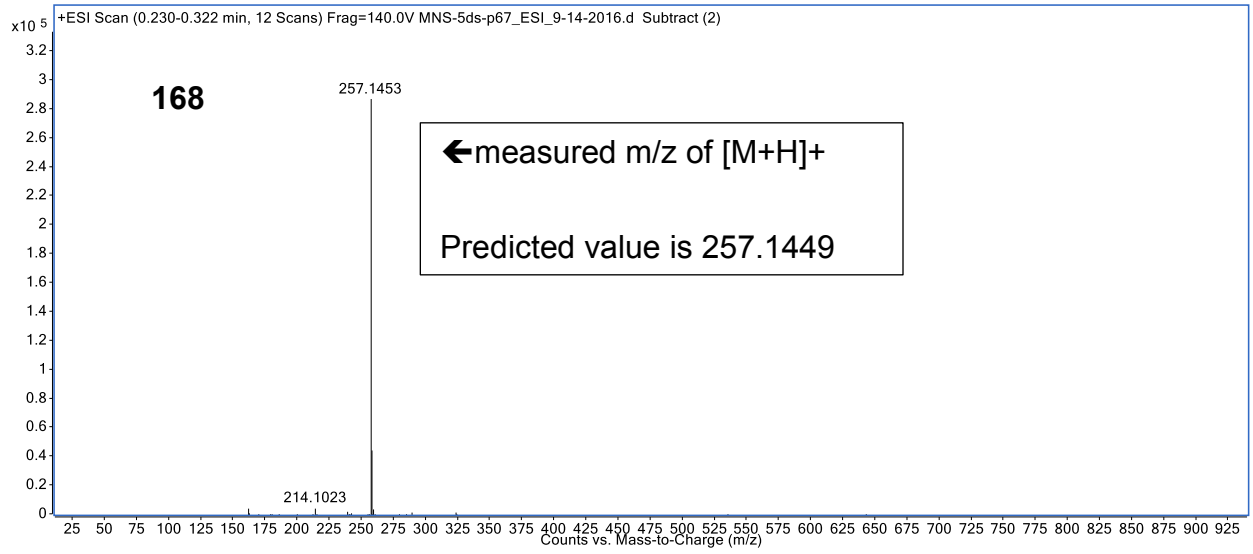
+ESI Scan (0.230-0.322 min, 12 Scans) Frag=140.0V MNS-5ds-p67_ESI_9-14-2016.d Subtract (2)
x10 5
168
257.1453
214.1023
←measured m/z of [M+H]+
Predicted value is 257.1449
Counts vs. Mass-to-Charge (m/z)

mns5d3p79-1_PROTON_01
mns5d3p79-1

144

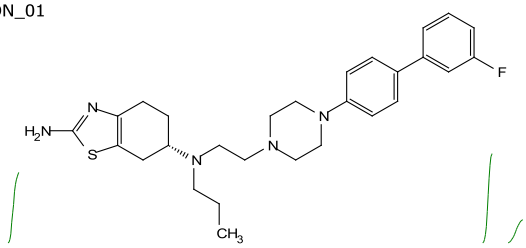

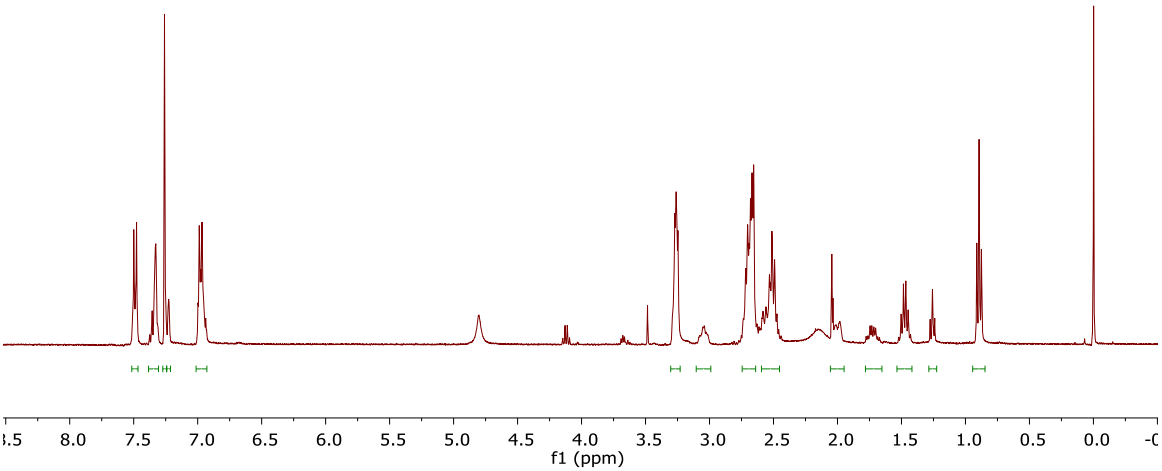

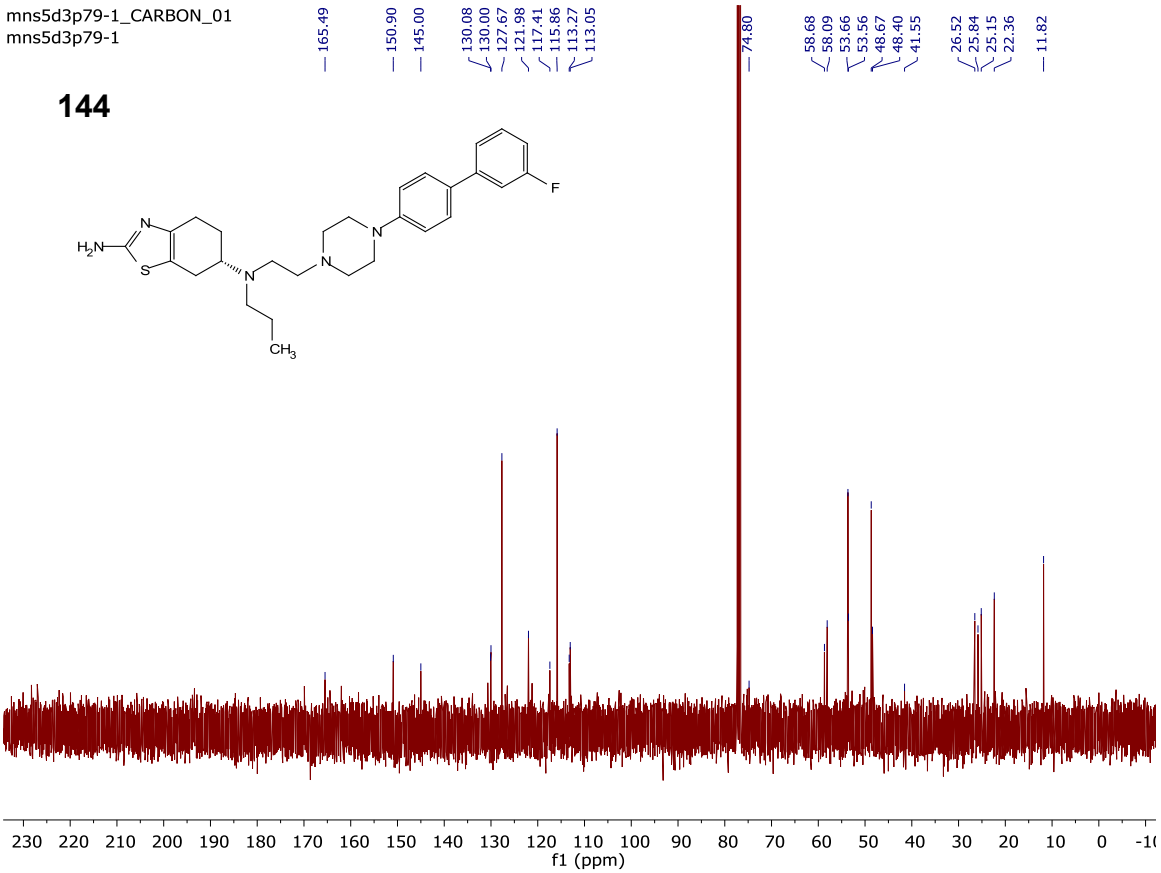
mns5d3p79-1_CARBON_01
mns5d3p79-1
144
165.49
150.90
145.00
130.08
130.00
127.67
121.98
117.41
115.86
113.27
113.05
74.80
58.68
58.09
53.66
53.56
48.67
48.40
41.55
26.52
25.84
25.15
22.36
11.82
F
N
H2N
S
N
N
N
CH3
230 220 210 200 190 180 170 160 150 140 130 120 110 100 90 80 70 60 50 40 30 20 10 0 -1(
f1 (ppm)

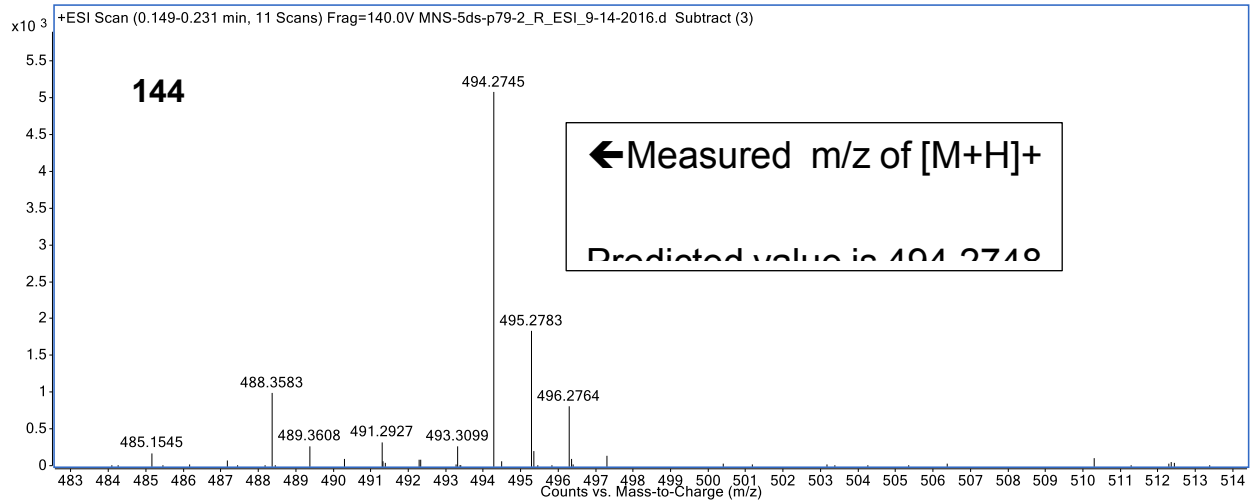
+ESI Scan (0.149-0.231 min, 11 Scans) Frag=140.0V MNS-5ds-p79-2_R_ESI_9-14-2016.d Subtract (3)
x10 3
144
494.2745
Measured m/z of [M+H]+
Predicted value is 494.2748
495.2783
496.2764
488.3583
489.3608
491.2927
493.3099
485.1545
Counts vs. Mass-to-Charge (m/z)

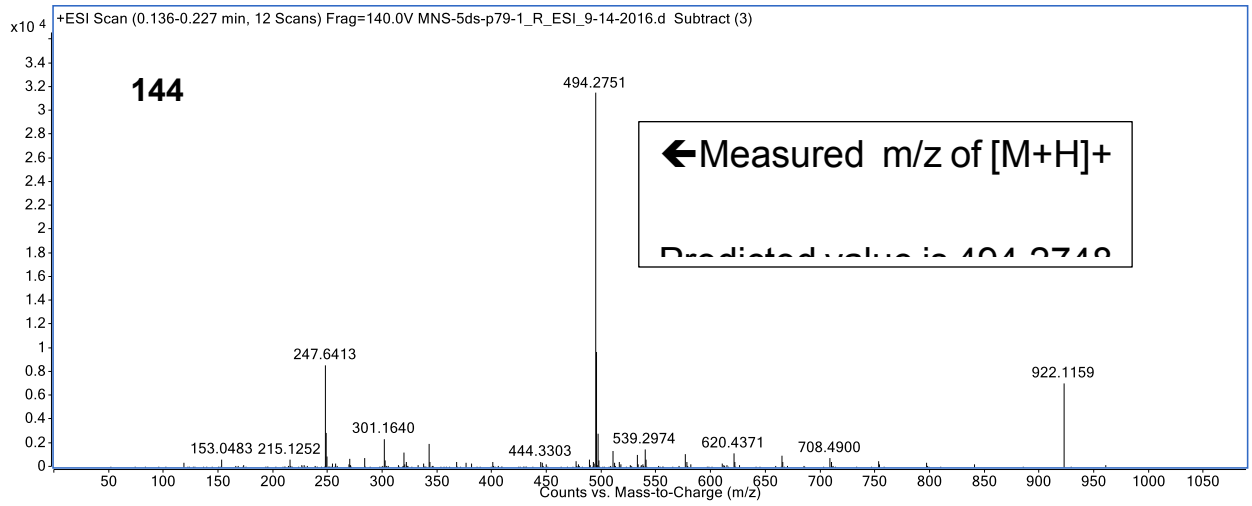

mns5d3p79-1_FLUORINE_01
mns5d3p79-1

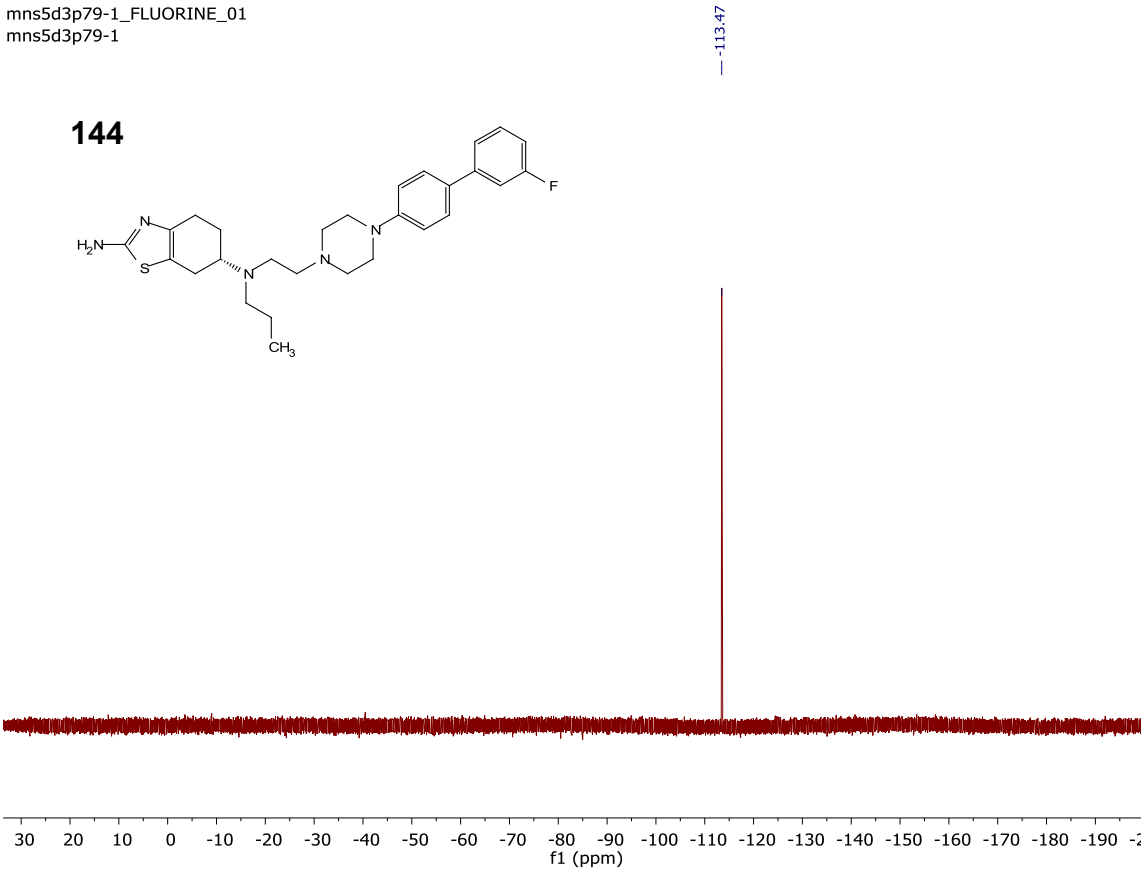

mns5d3p57_PROTON_01
mns5d3p57

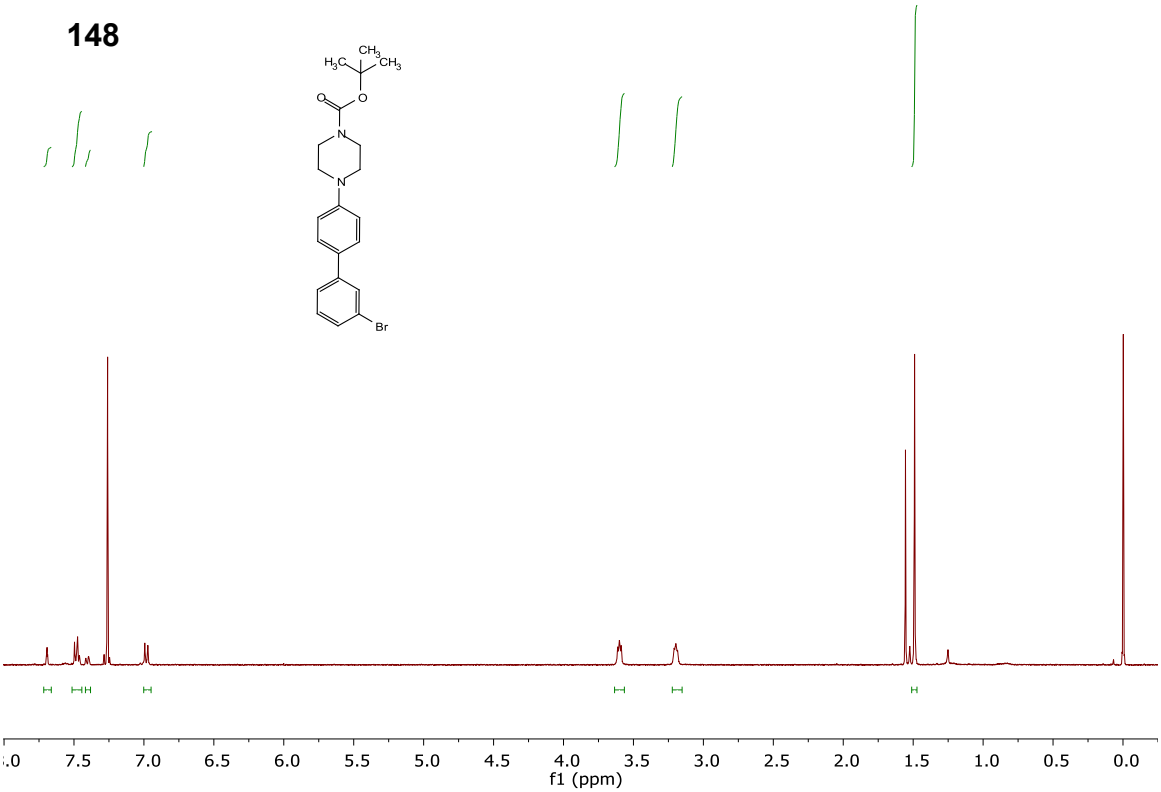

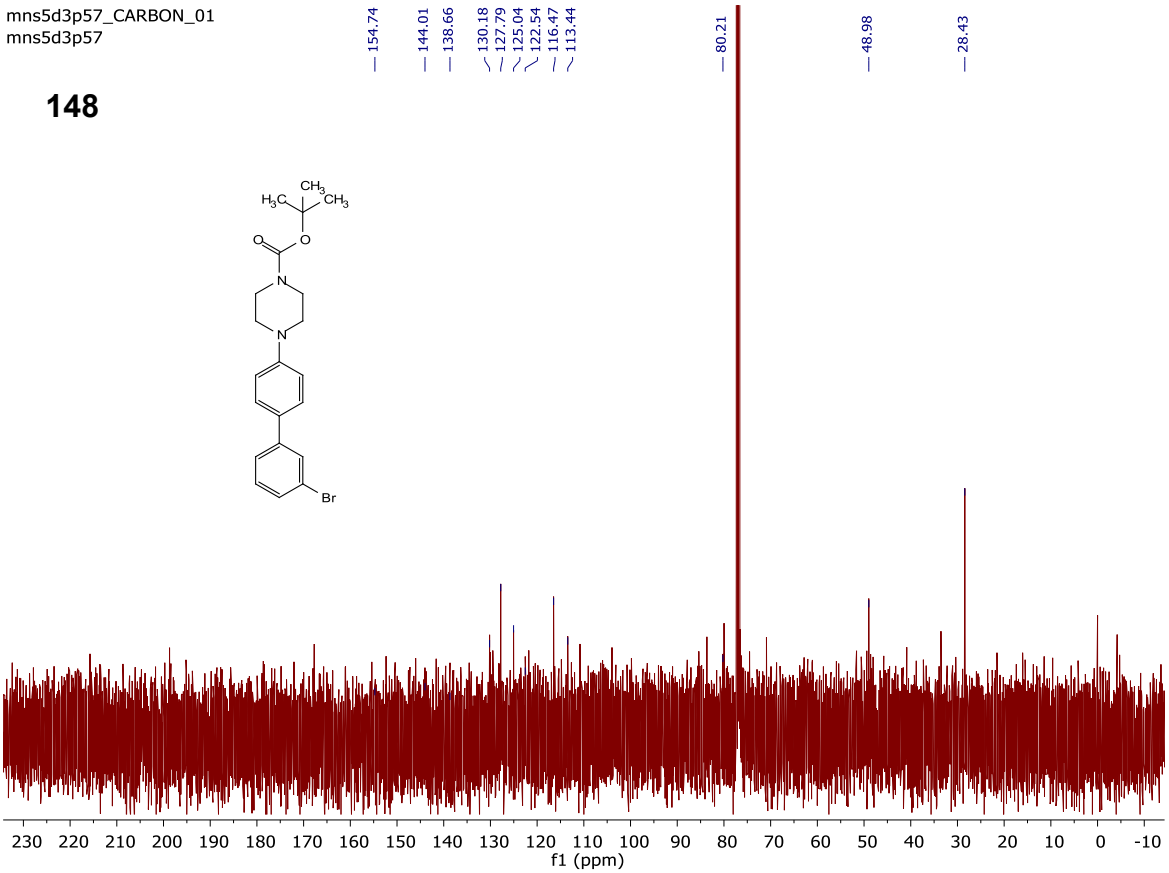
mns5d3p57_CARBON_01
mns5d3p57
154.74
144.01
138.66
130.18
127.79
125.04
122.54
116.47
113.44
80.21
48.98
28.43
148
Br
230 220 210 200 190 180 170 160 150 140 130 120 110 100 90 80 70 60 50 40 30 20 10 0 -10
f1 (ppm)

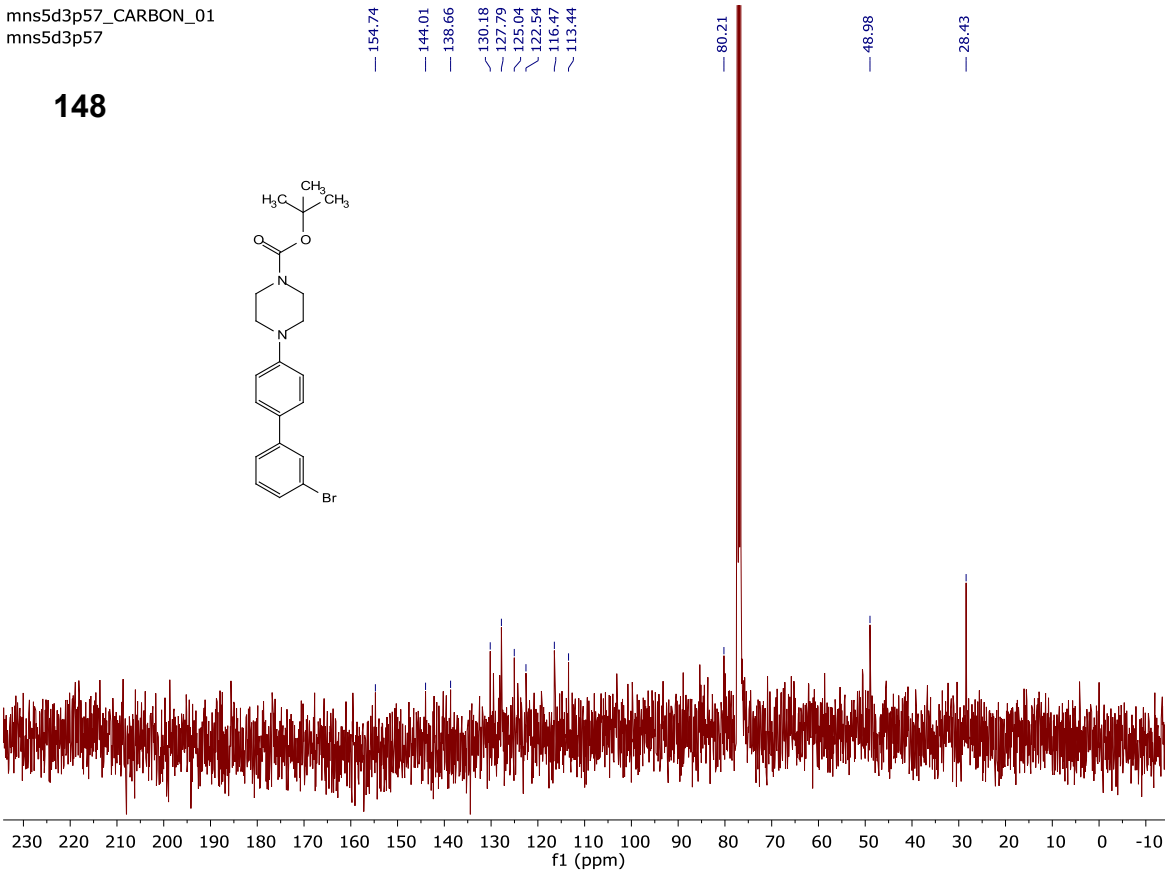
mns5d3p57_CARBON_01
mns5d3p57
148
154.74
144.01
138.66
130.18
127.79
125.04
122.54
116.47
113.44
80.21
48.98
28.43
Br
230 220 210 200 190 180 170 160 150 140 130 120 110 100 90 80 70 60 50 40 30 20 10 0 -10
f1 (ppm)

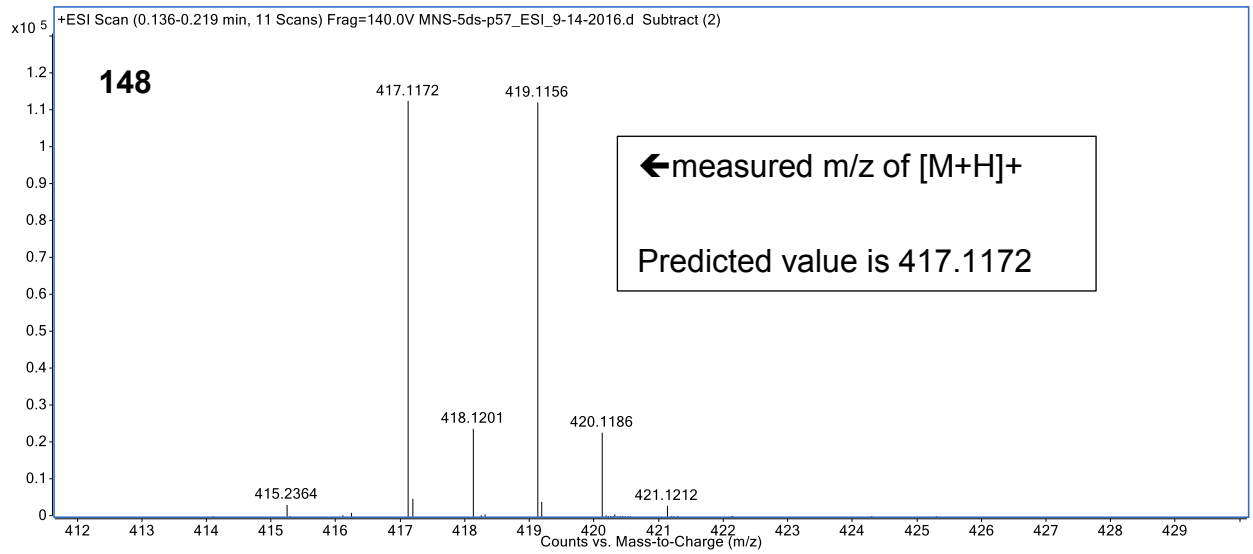
+ESI Scan (0.136-0.219 min, 11 Scans) Frag=140.0V MNS-5ds-p57_ESI_9-14-2016.d Subtract (2)
x10 5
148
417.1172
419.1156
418.1201
420.1186
415.2364
421.1212
←measured m/z of [M+H]+
Predicted value is 417.1172
Counts vs. Mass-to-Charge (m/z)

mns5d3p65_PROTON_01
mns5d3p65

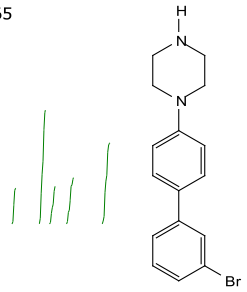

149

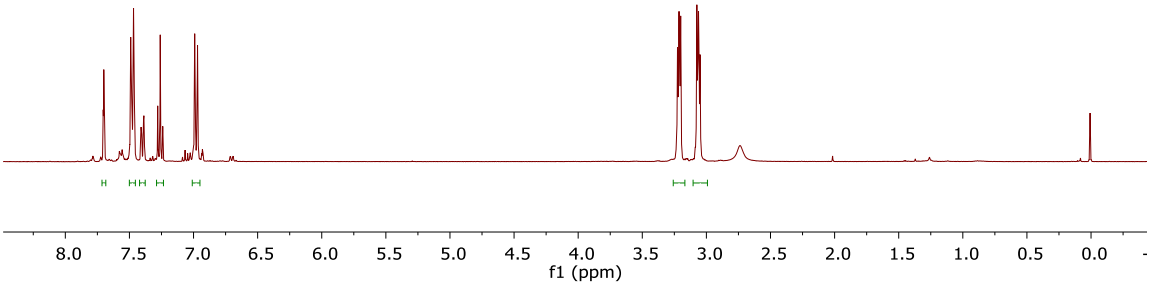

mns5d3p65_CARBON_01
mns5d3p65

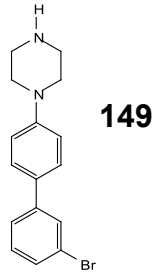

149

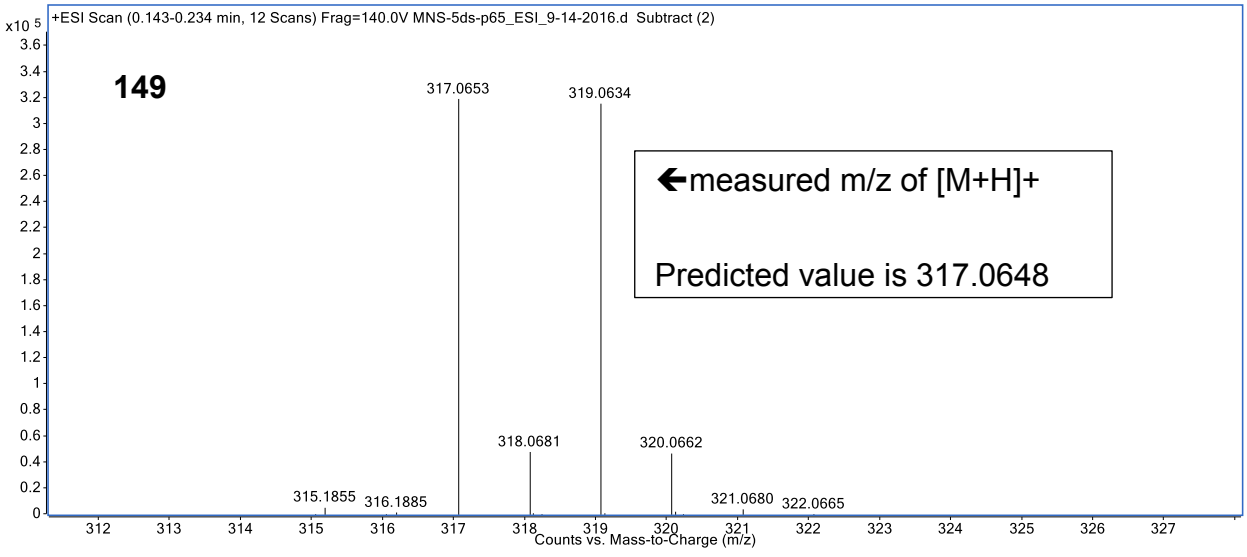

mns6d3p55-3_PROTON_01
mns6d3p55-3

150

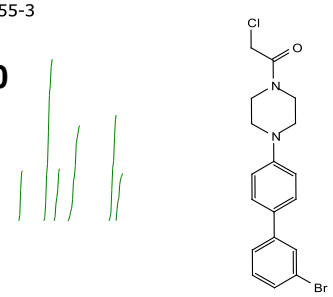

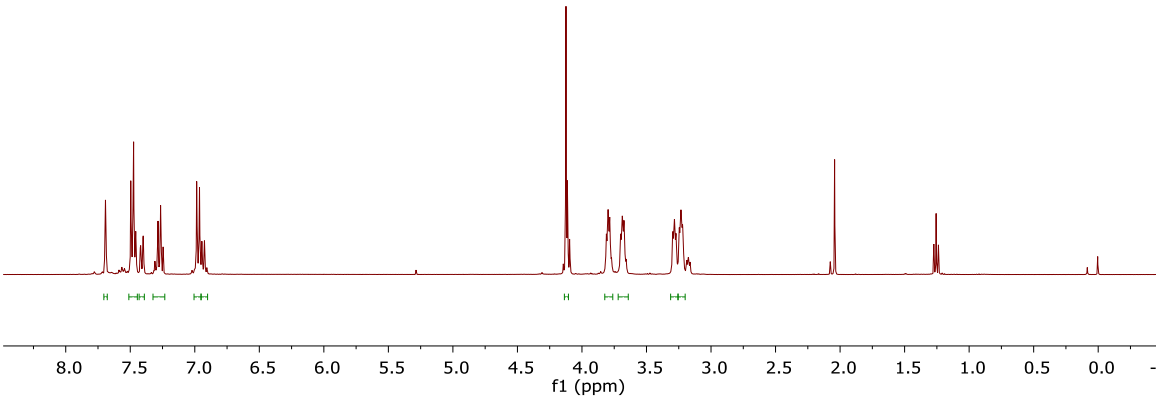

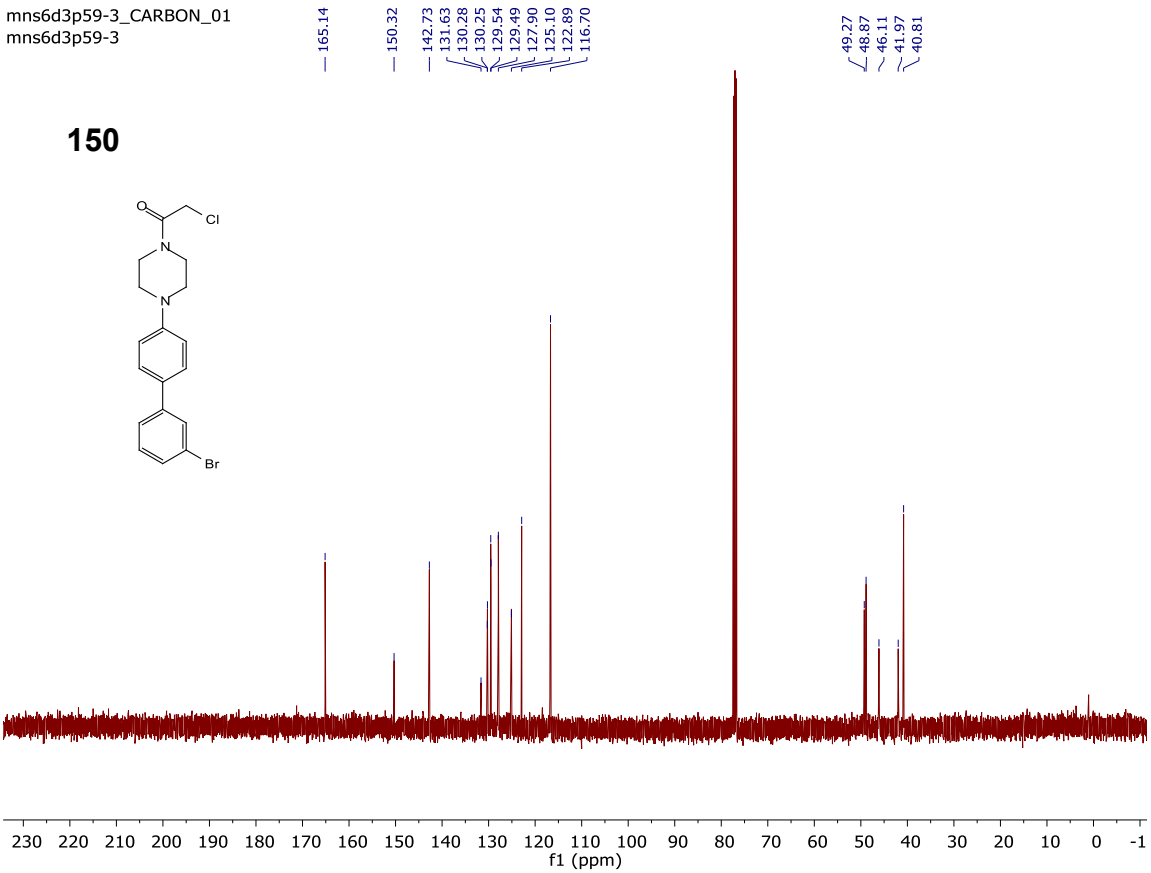
mns6d3p59-3_CARBON_01
mns6d3p59-3
165.14
150.32
142.73
131.63
130.28
130.25
129.54
129.49
127.90
125.10
122.89
116.70
49.27
48.87
46.11
41.97
40.81
150
O
Cl
N
N
Br
230 220 210 200 190 180 170 160 150 140 130 120 110 100 90 80 70 60 50 40 30 20 10 0 -1
f1 (ppm)

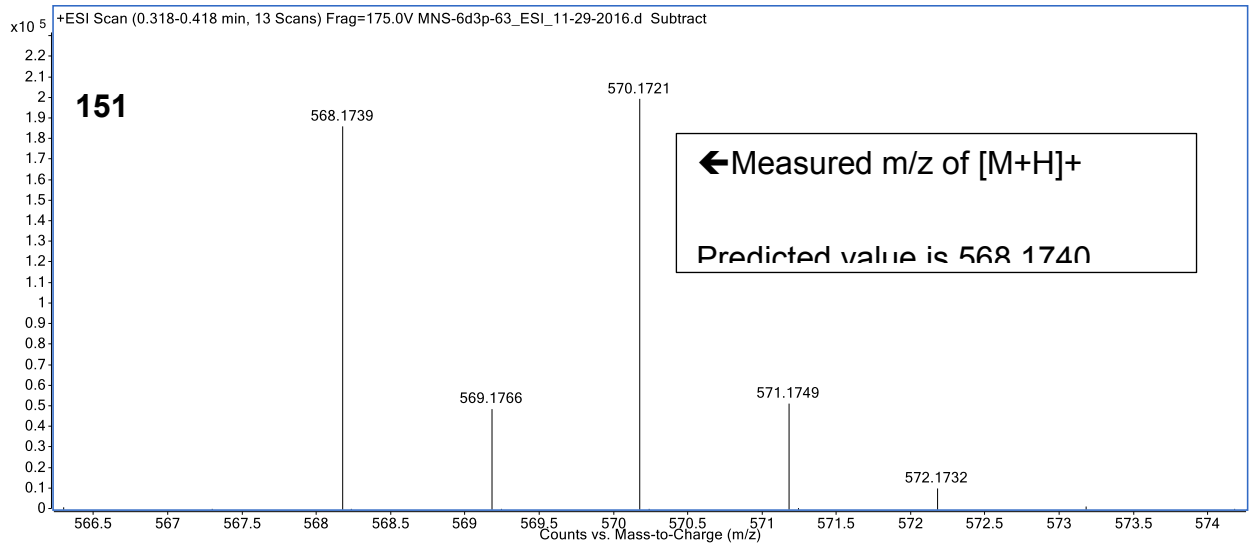

mns6d3p63_PROTON_01
mns6d3p63

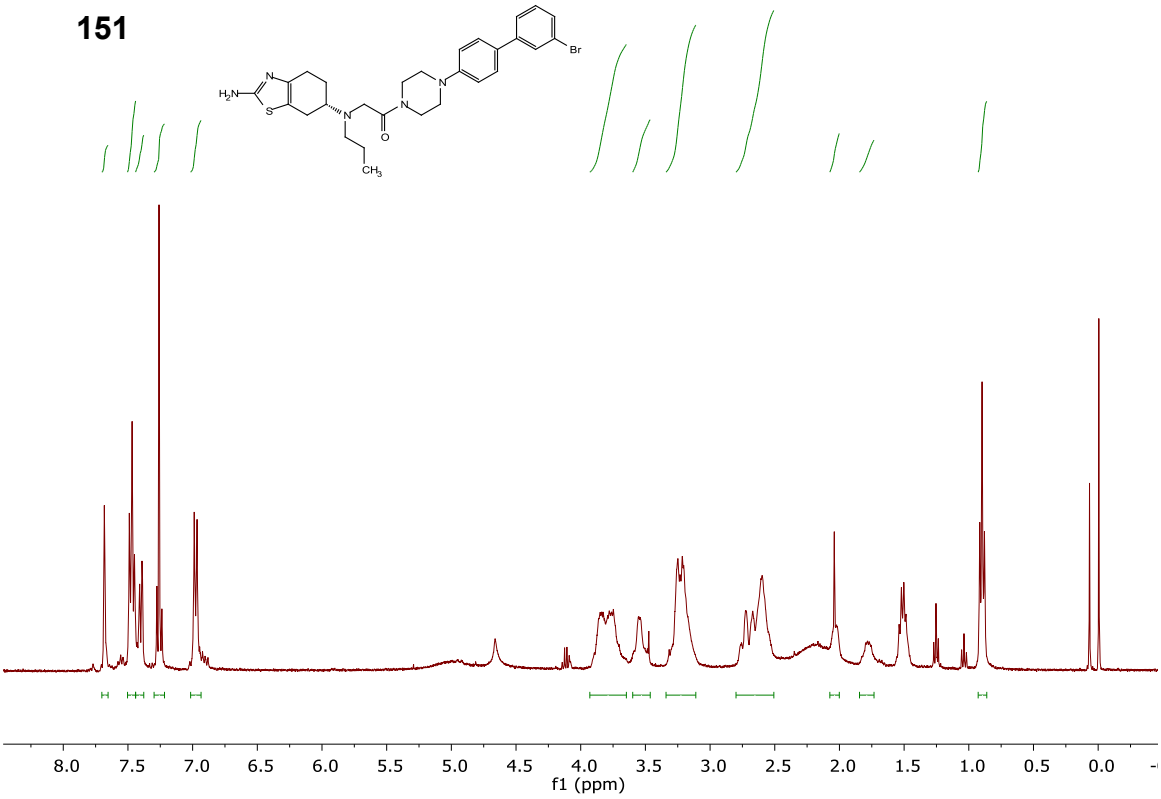

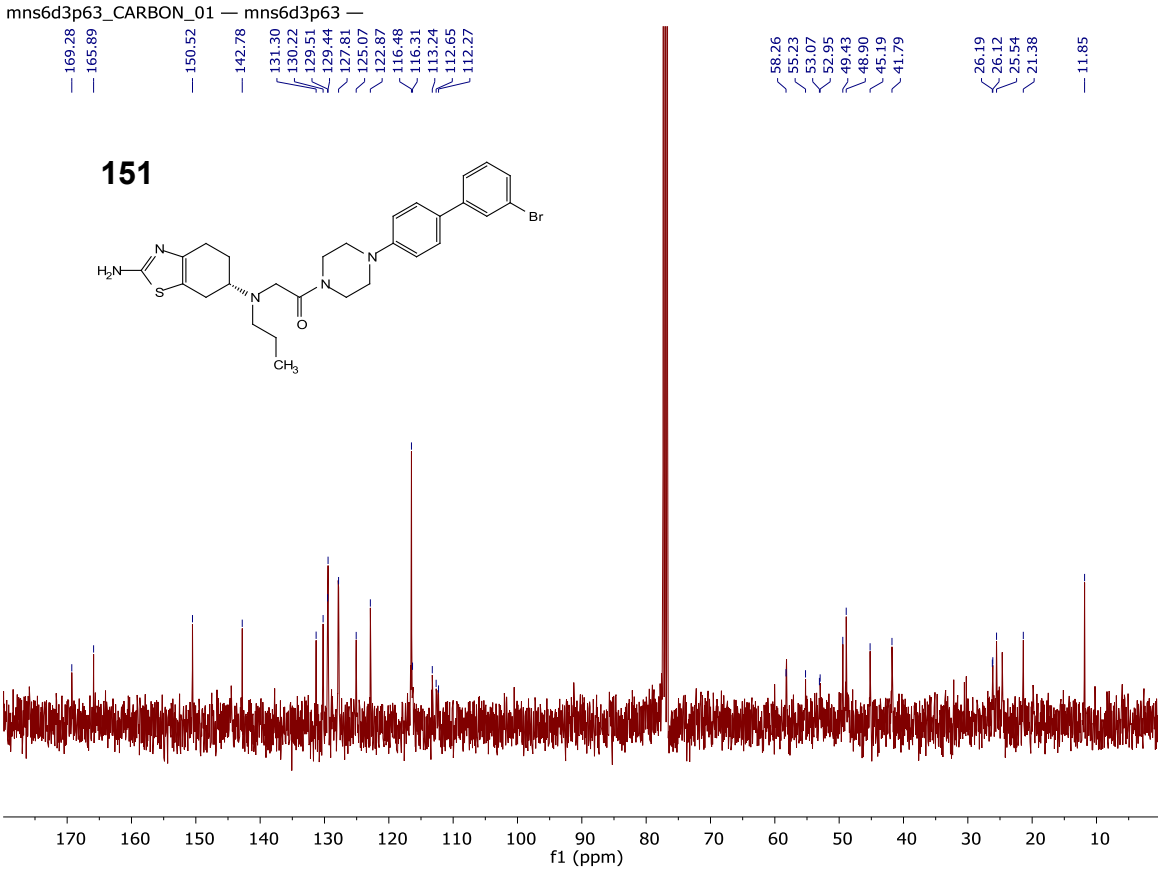
mns6d3p63_CARBON_01 — mns6d3p63 —
169.28
165.89
150.52
142.78
131.30
130.22
129.51
129.44
127.81
125.07
122.87
116.48
116.31
113.24
112.65
112.27
58.26
55.23
53.07
52.95
49.43
48.90
45.19
41.79
26.19
26.12
25.54
21.38
11.85
151
Br
N
H2N
S
N
N
N
O
CH3
170 160 150 140 130 120 110 100 90 80 70 60 50 40 30 20 10
f1 (ppm)

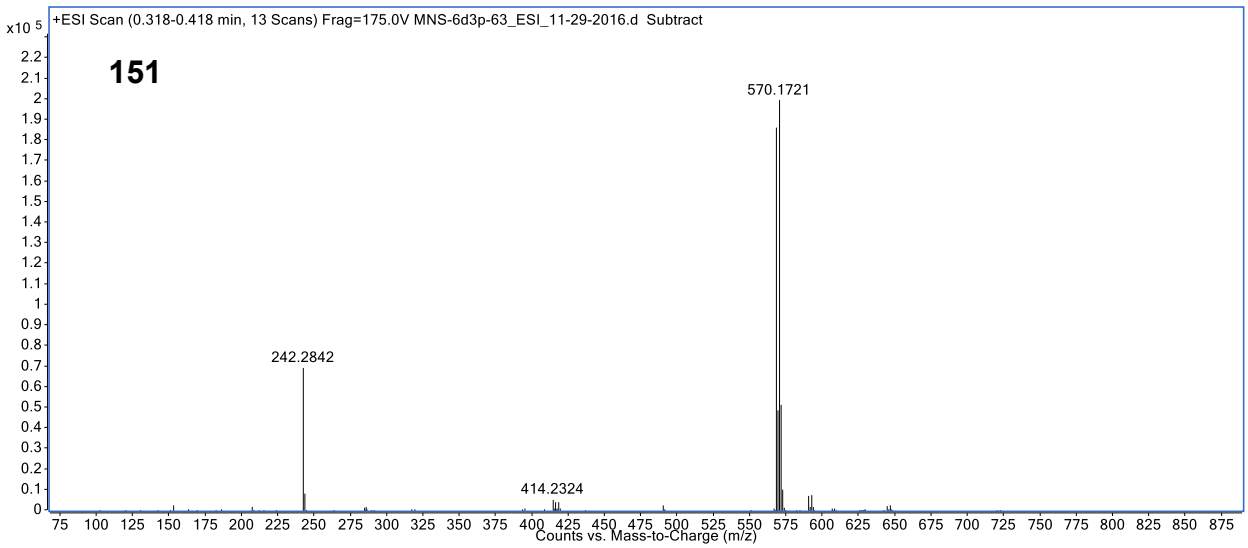
+ESI Scan (0.318-0.418 min, 13 Scans) Frag=175.0V MNS-6d3p-63_ESI_11-29-2016.d Subtract
x10 5
151
570.1721
242.2842
414.2324
Counts vs. Mass-to-Charge (m/z)

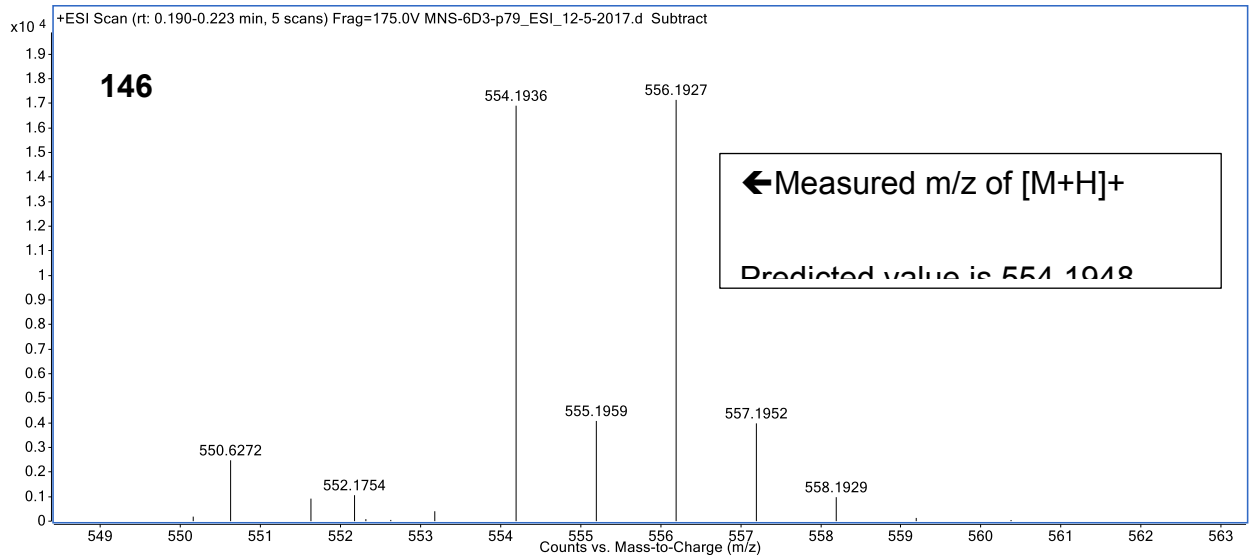
+ESI Scan (rt: 0.190-0.223 min, 5 scans) Frag=175.0V MNS-6D3-p79_ESI_12-5-2017.d Subtract
x10 4
146
554.1936
556.1927
Measured m/z of [M+H]+
555.1959
557.1952
550.6272
552.1754
558.1929
Counts vs. Mass-to-Charge (m/z)

ii

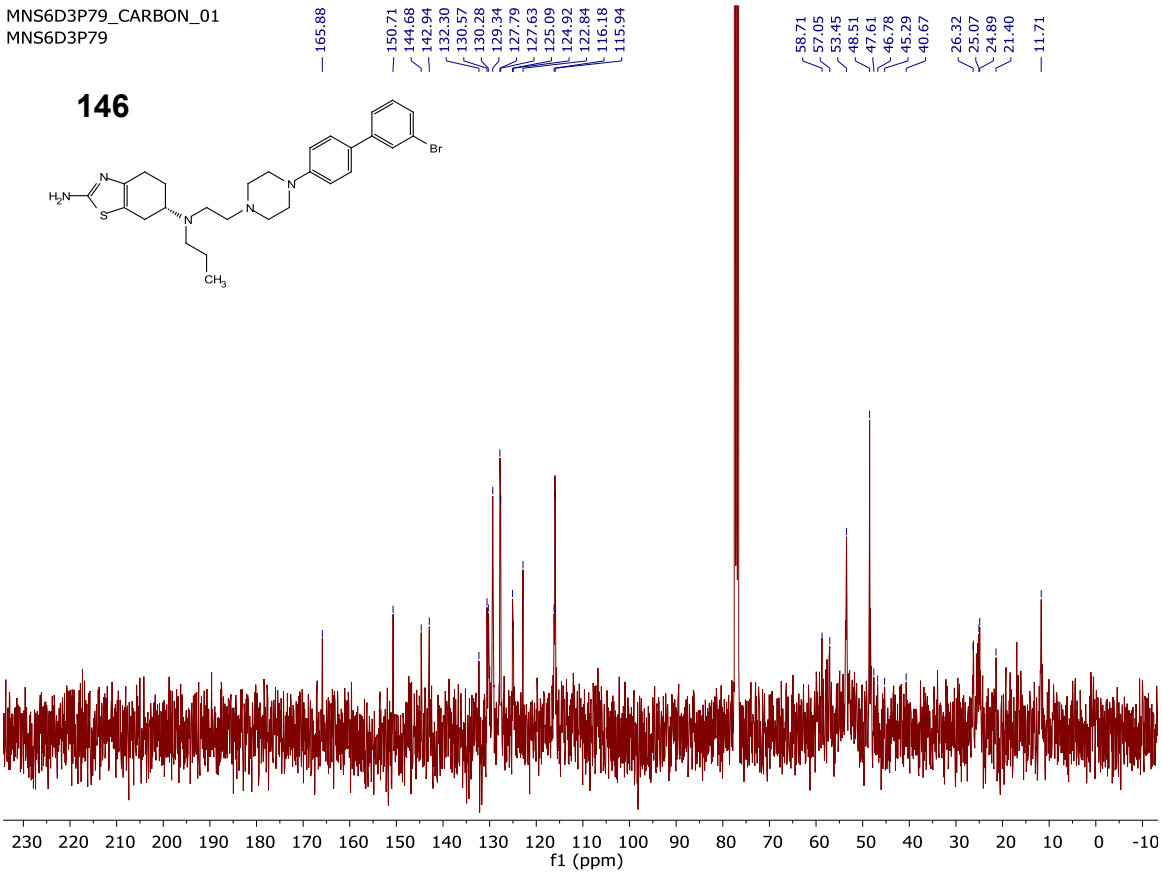
MNS6D3P79_CARBON_01
MNS6D3P79
146
165.88
150.71
144.68
142.94
132.30
130.57
130.28
129.34
127.79
127.63
125.09
124.92
122.84
116.18
115.94
58.71
57.05
53.45
48.51
47.61
46.78
45.29
40.67
26.32
25.07
24.89
21.40
11.71
f1 (ppm)

MNS6D3P79_PROTON_01
MNS6D3P79

146

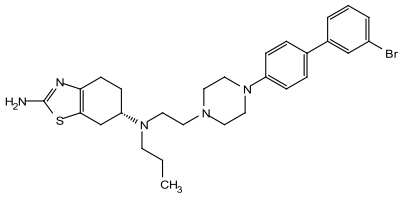

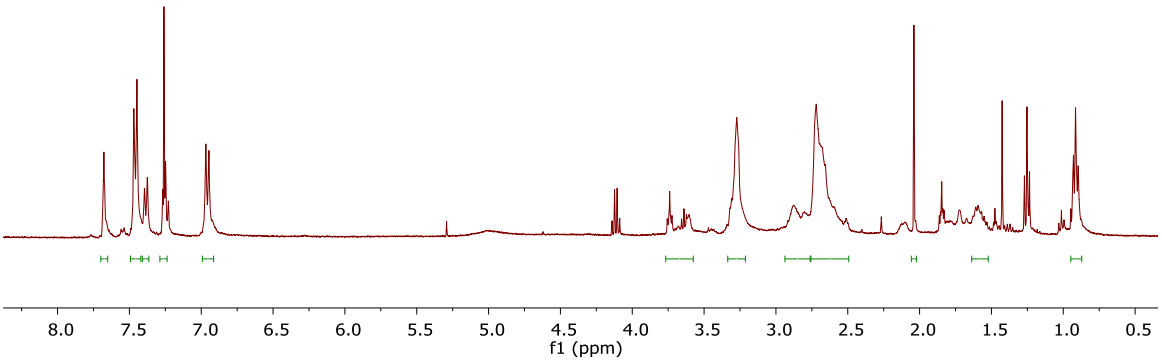

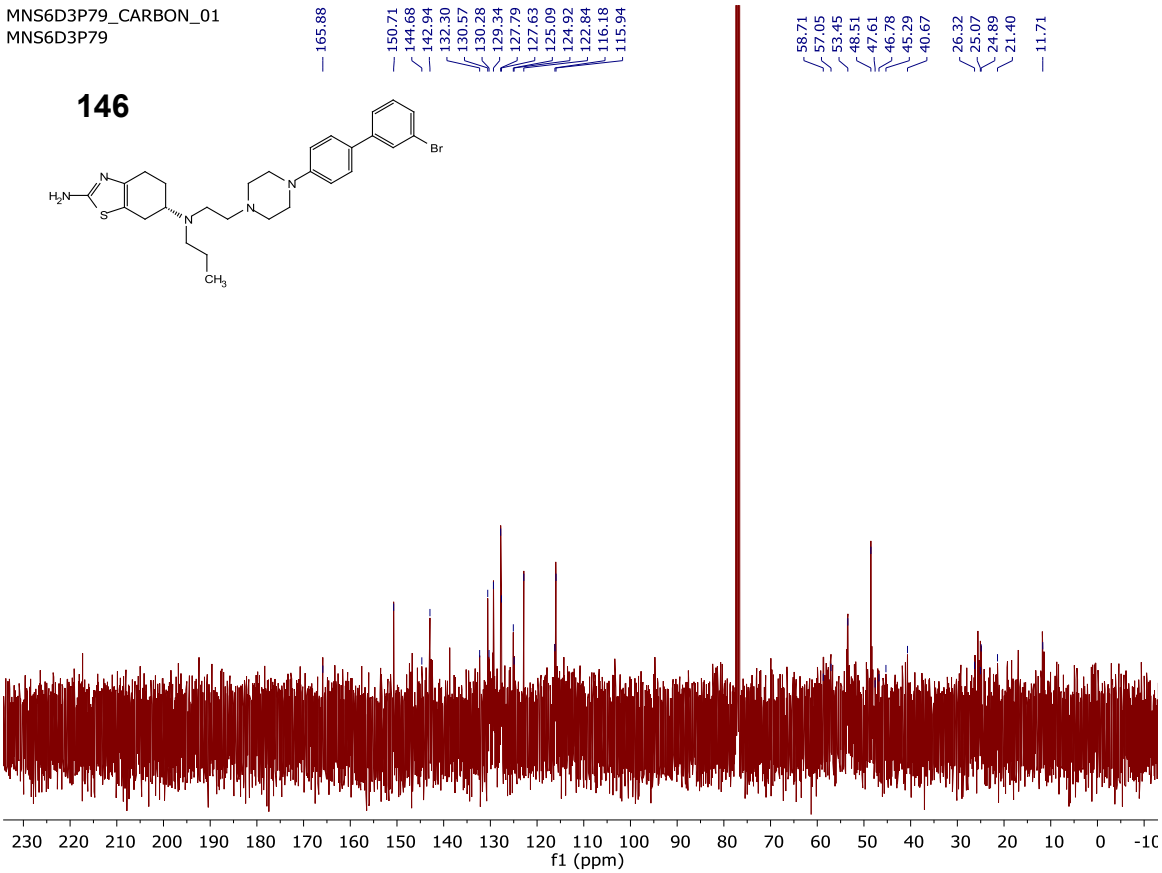
MNS6D3P79_CARBON_01
MNS6D3P79
146
165.88
150.71
144.68
142.94
132.30
130.57
130.28
129.34
127.79
127.63
125.09
124.92
122.84
116.18
115.94
58.71
57.05
53.45
48.51
47.61
46.78
45.29
40.67
26.32
25.07
24.89
21.40
11.71
Br
N
S
N
N
N
H_2N
CH_3
230 220 210 200 190 180 170 160 150 140 130 120 110 100 90 80 70 60 50 40 30 20 10 0 -10
f1 (ppm)

mns7d3p43_PROTON_01
mns7d3p43

156a

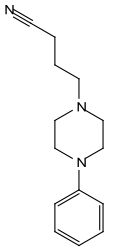

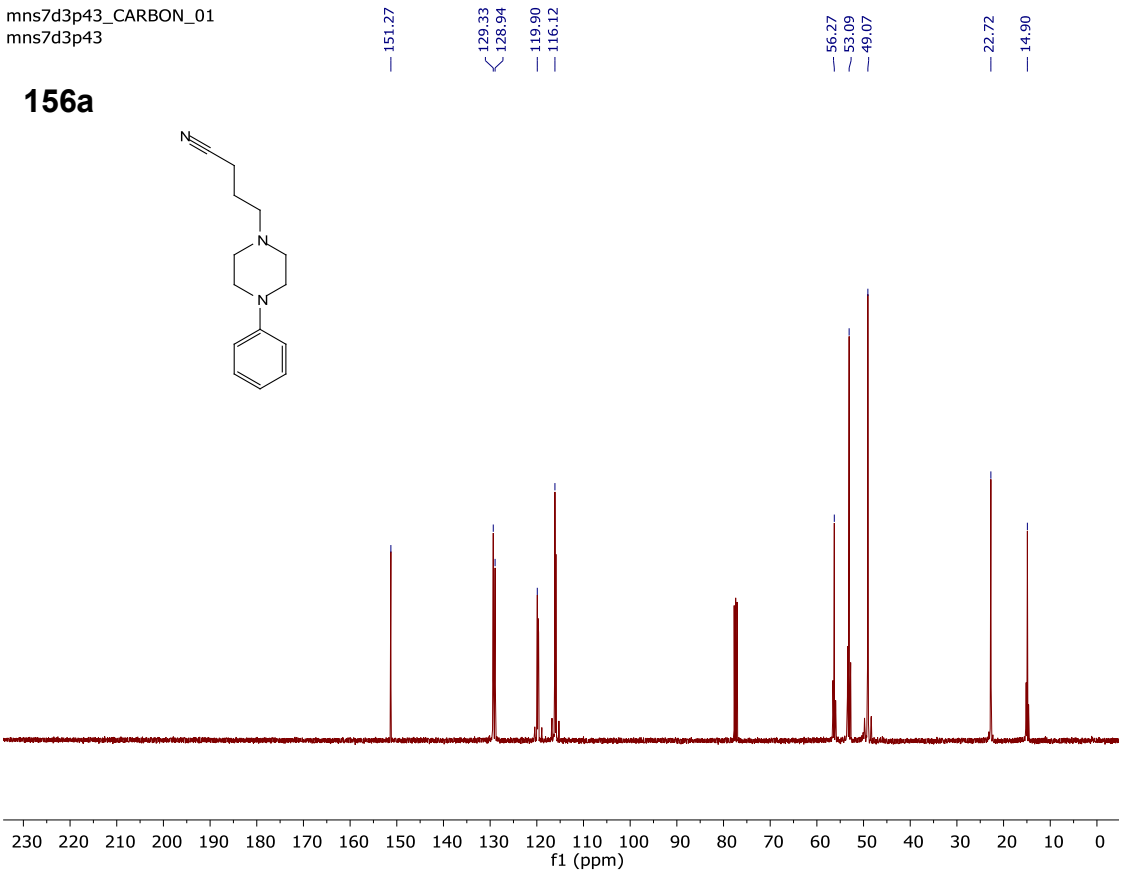
mns7d3p43_CARBON_01
mns7d3p43
151.27
129.33
128.94
119.90
116.12
56.27
53.09
49.07
22.72
14.90
156a
230 220 210 200 190 180 170 160 150 140 130 120 110 100 90 80 70 60 50 40 30 20 10 0
f1 (ppm)

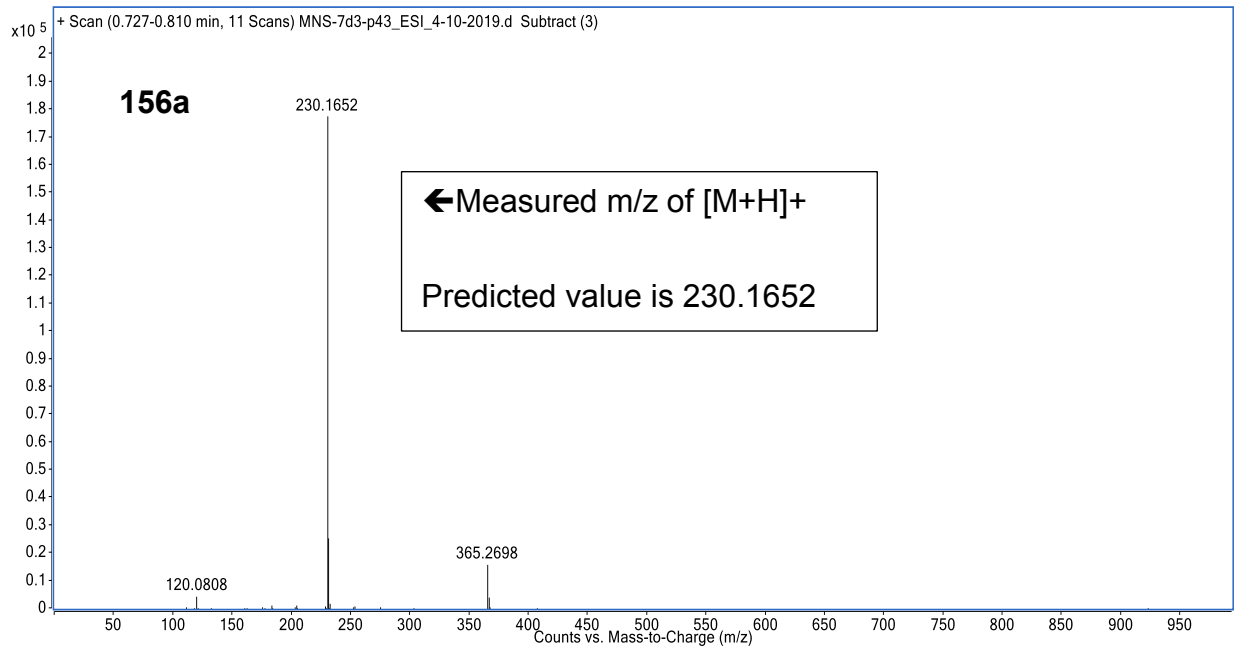
+ Scan (0.727-0.810 min, 11 Scans) MNS-7d3-p43_ESI_4-10-2019.d Subtract (3)
x10 5
156a
230.1652
365.2698
120.0808
←Measured m/z of [M+H]+
Predicted value is 230.1652
Counts vs. Mass-to-Charge (m/z)

mns7d3p47-2_PROTON_01
mns7d3p47-2

156b

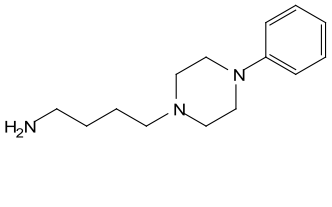

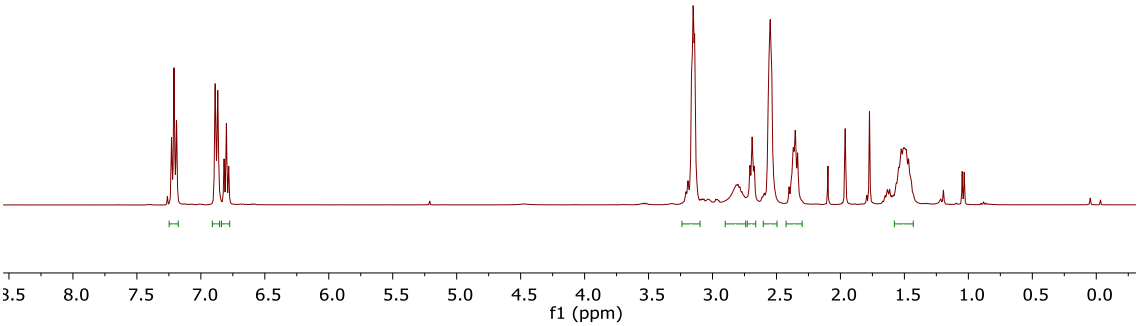

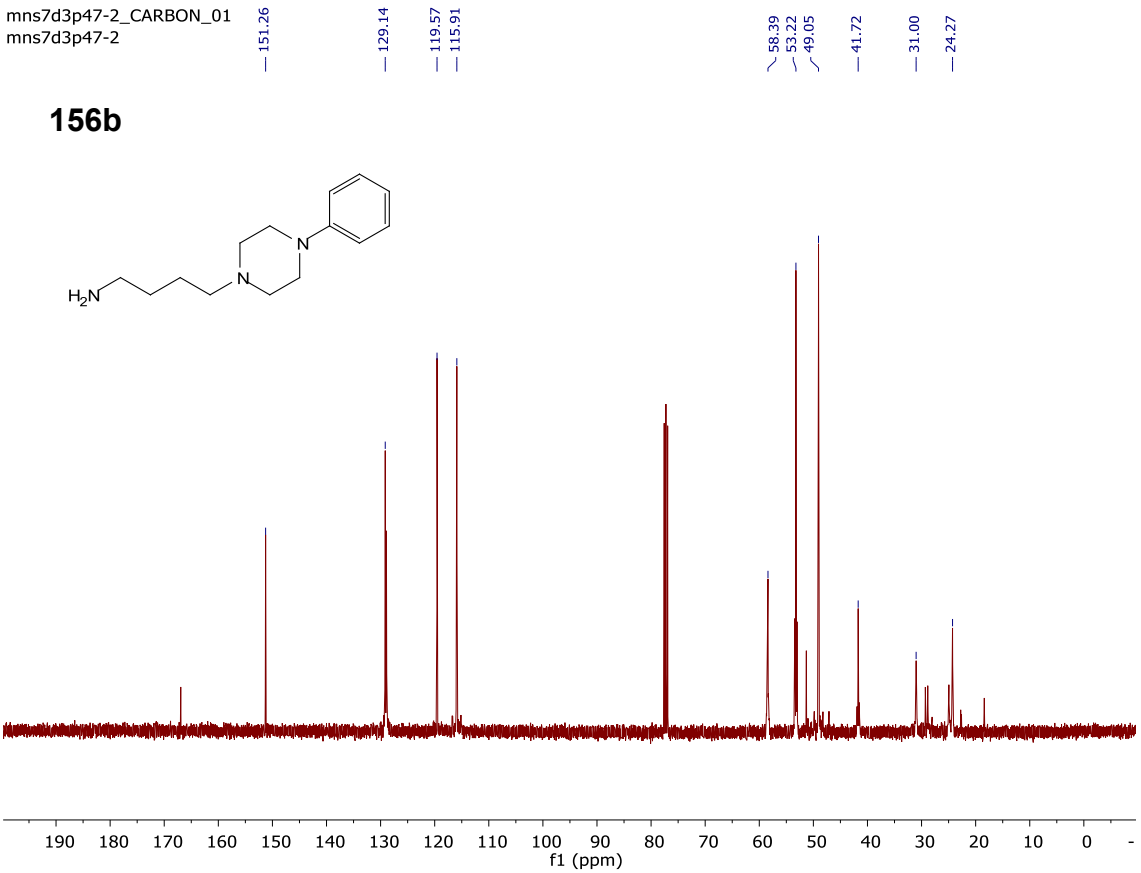
mns7d3p47-2_CARBON_01
mns7d3p47-2
151.26
129.14
119.57
115.91
58.39
53.22
49.05
41.72
31.00
24.27
156b
N
N
H2N
190 180 170 160 150 140 130 120 110 100 90 80 70 60 50 40 30 20 10 0 -
f1 (ppm)

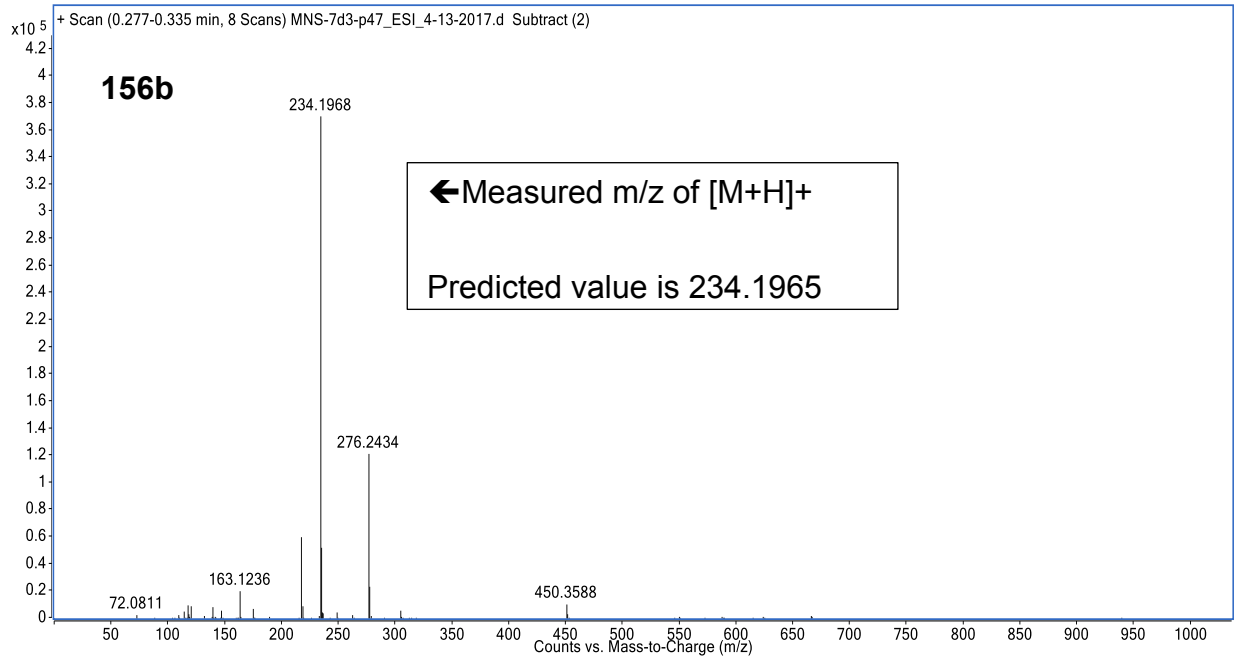
+ Scan (0.277-0.335 min, 8 Scans) MNS-7d3-p47_ESI_4-13-2017.d Subtract (2)
x10 5
156b
234.1968
276.2434
163.1236
72.0811
450.3588
←Measured m/z of [M+H]+
Predicted value is 234.1965
Counts vs. Mass-to-Charge (m/z)

mns7d3p53-2_PROTON_01
mns7d3p53-2

156c

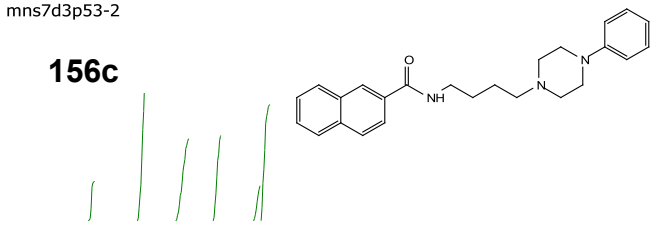

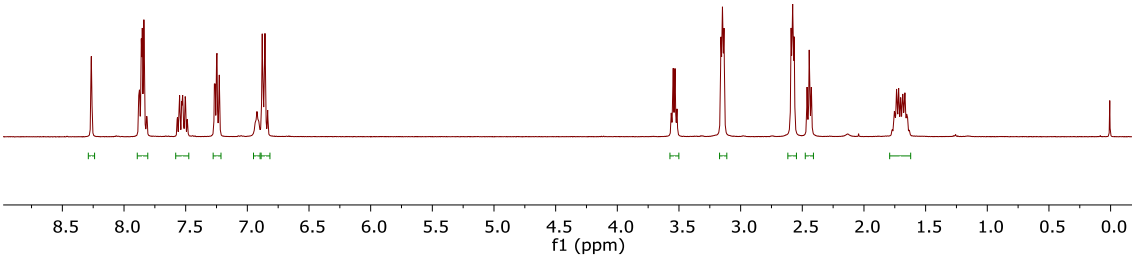

mns7d3p53-2_CARBON_01
mns7d3p53-2

167.79
151.21
134.63
132.57
132.21
129.12
129.03
128.87
128.81
128.41
127.78
127.72
127.52
127.24
126.74
126.66
123.73
119.70
116.01
57.96
53.34
53.23
49.03
40.09
39.97
27.45
24.52

156c

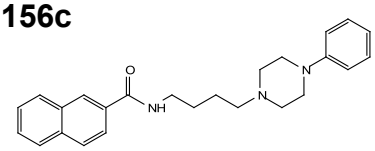

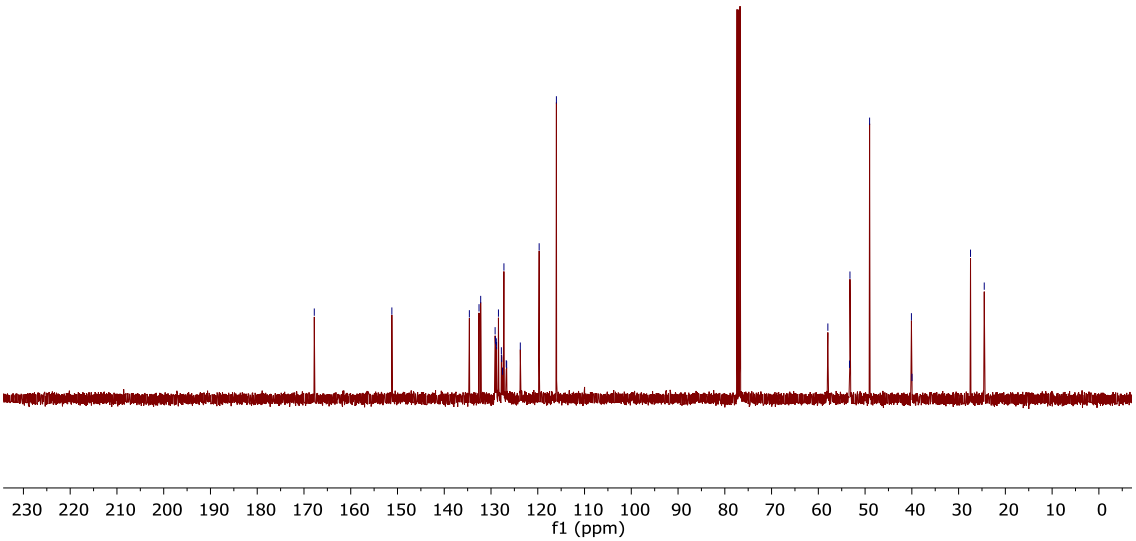

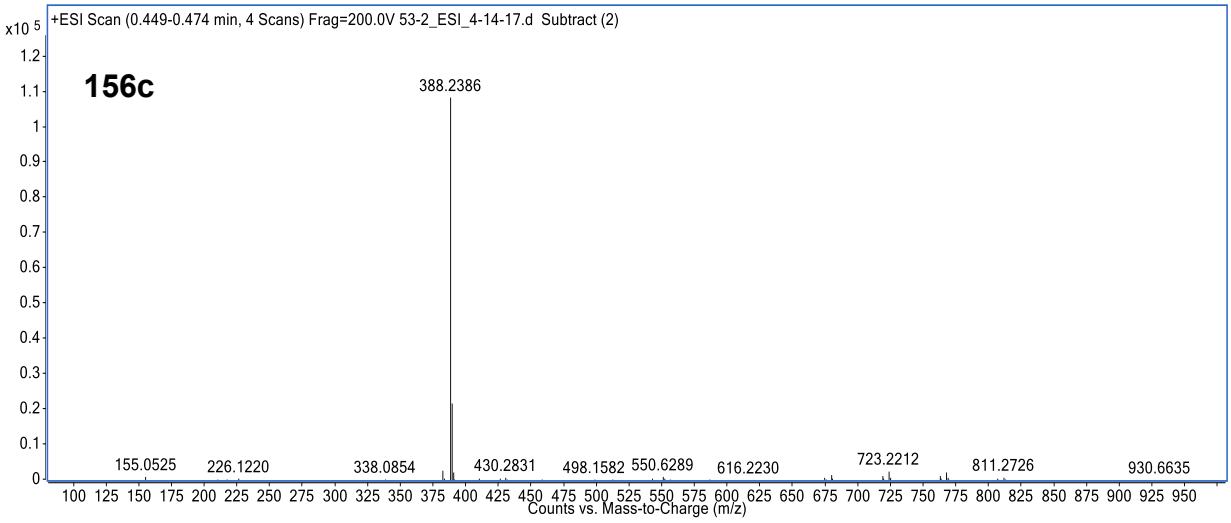

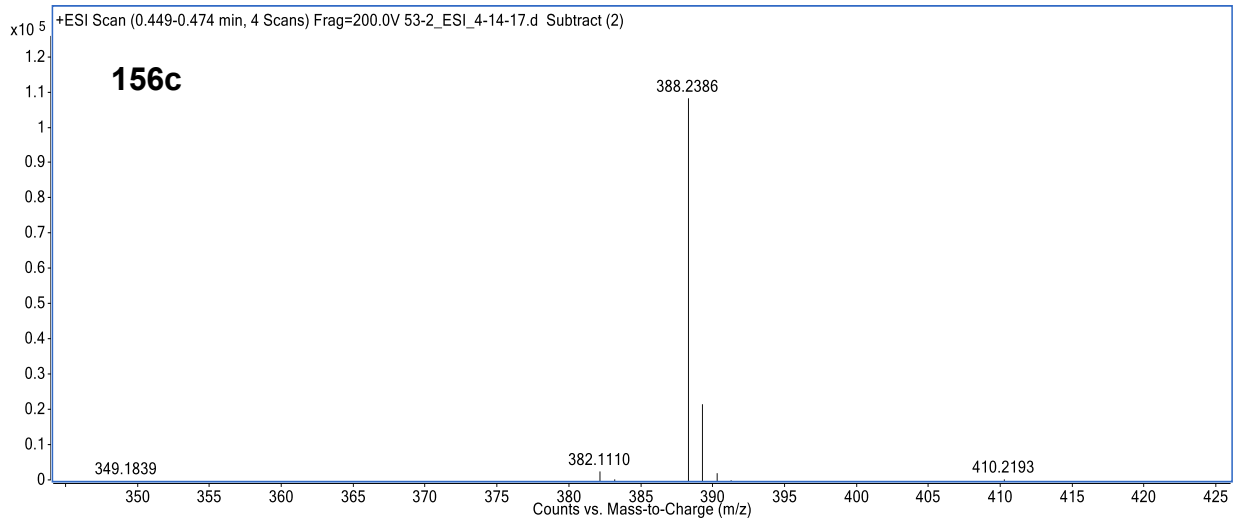

mns7d3p45_PROTON_01
mns7d3p45

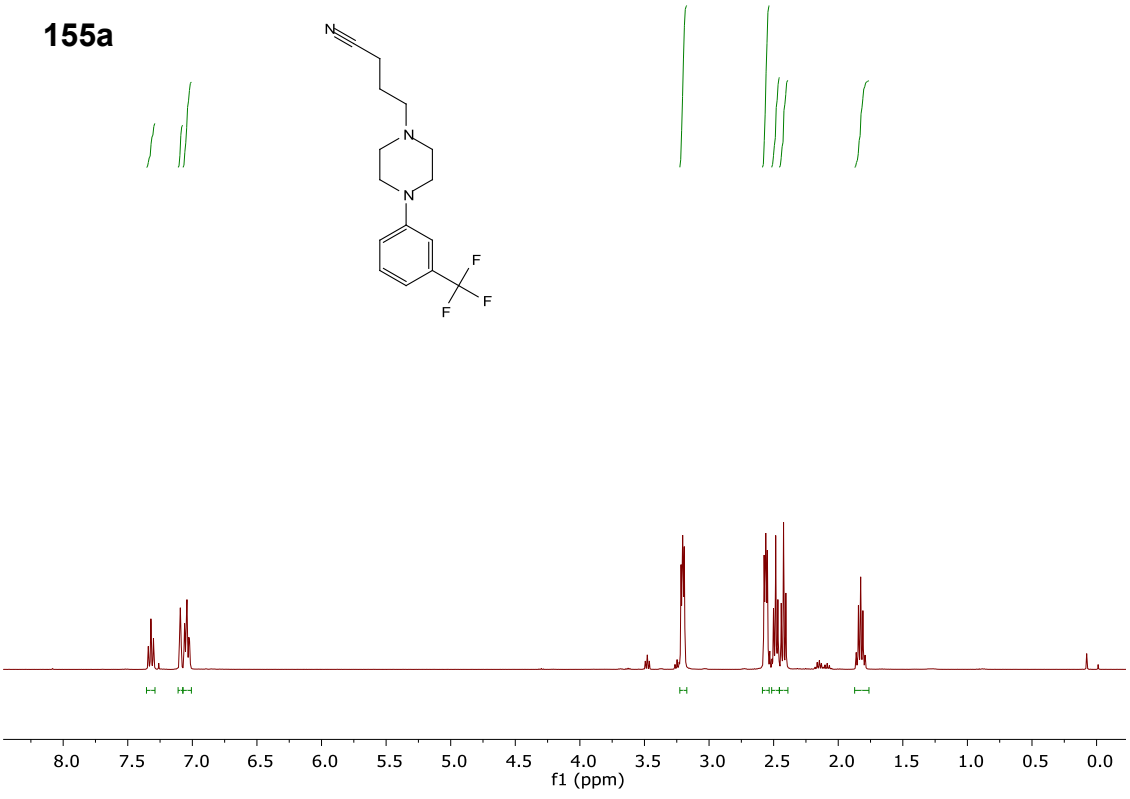

mns7d3p45_FLUORINE_01
mns7d3p45

155a

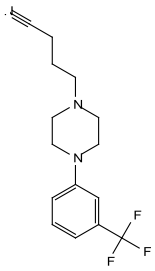

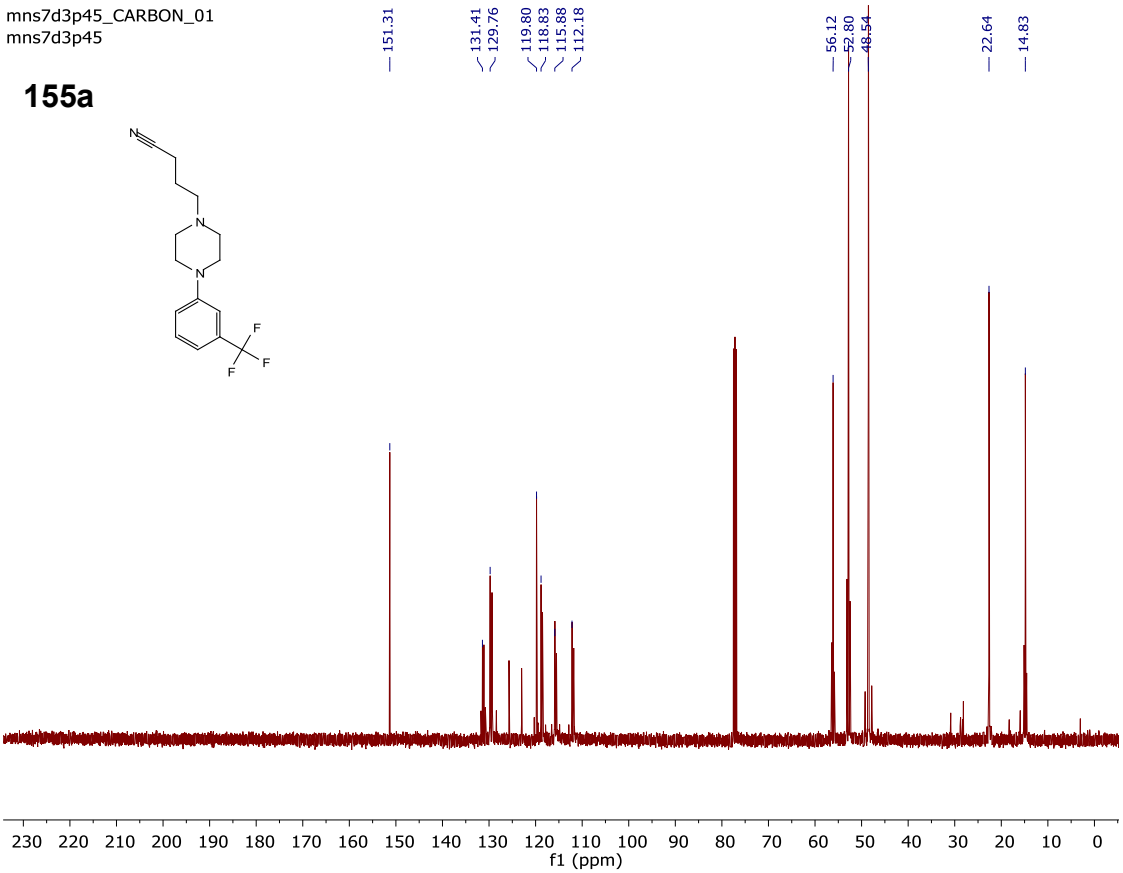
mns7d3p45_CARBON_01
mns7d3p45
155a
151.31
131.41
129.76
119.80
118.83
115.88
112.18
56.12
52.80
48.54
22.64
14.83
230 220 210 200 190 180 170 160 150 140 130 120 110 100 90 80 70 60 50 40 30 20 10 0
f1 (ppm)

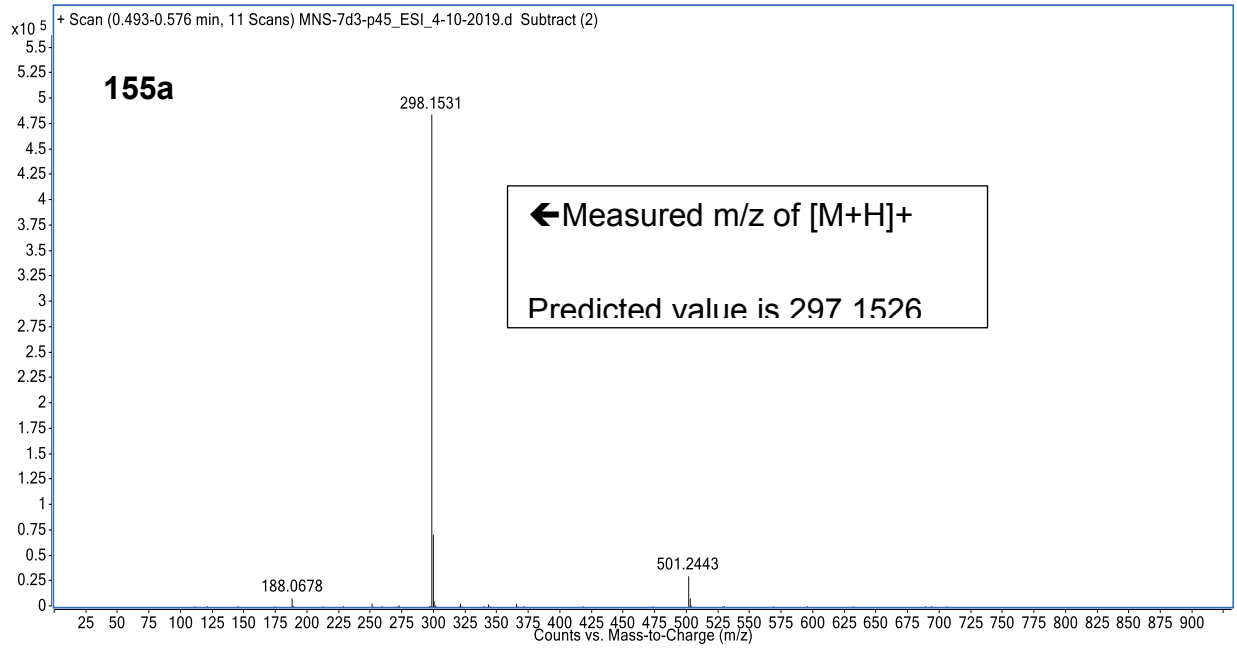
+ Scan (0.493-0.576 min, 11 Scans) MNS-7d3-p45_ESI_4-10-2019.d Subtract (2)
x10 5
155a
298.1531
188.0678
501.2443
←Measured m/z of [M+H]+
Predicted value is 297.1526
Counts vs. Mass-to-Charge (m/z)

mns7d3p49-2_PROTON_01
mns7d3p49-2

155b

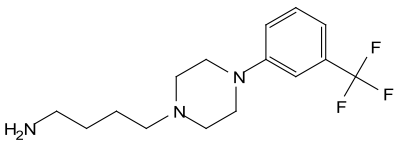

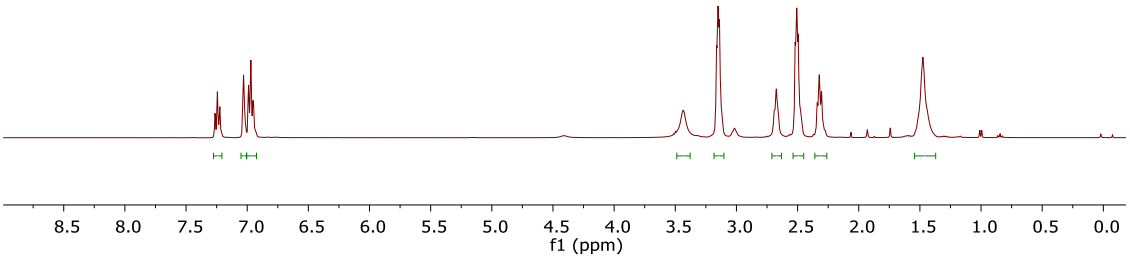

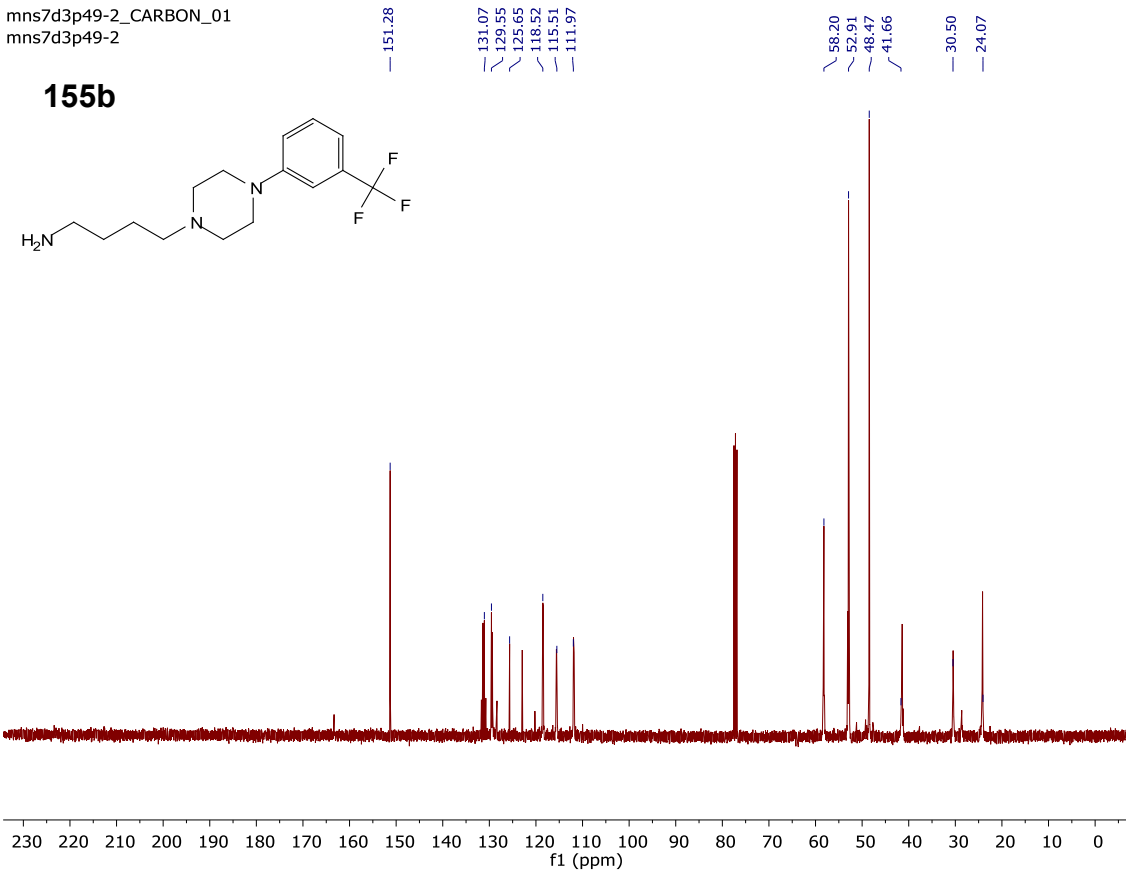
mns7d3p49-2_CARBON_01
mns7d3p49-2
155b
151.28
131.07
129.55
125.65
118.52
115.51
111.97
58.20
52.91
48.47
41.66
30.50
24.07
F
F
F
N
N
H2N
230 220 210 200 190 180 170 160 150 140 130 120 110 100 90 80 70 60 50 40 30 20 10 0
f1 (ppm)

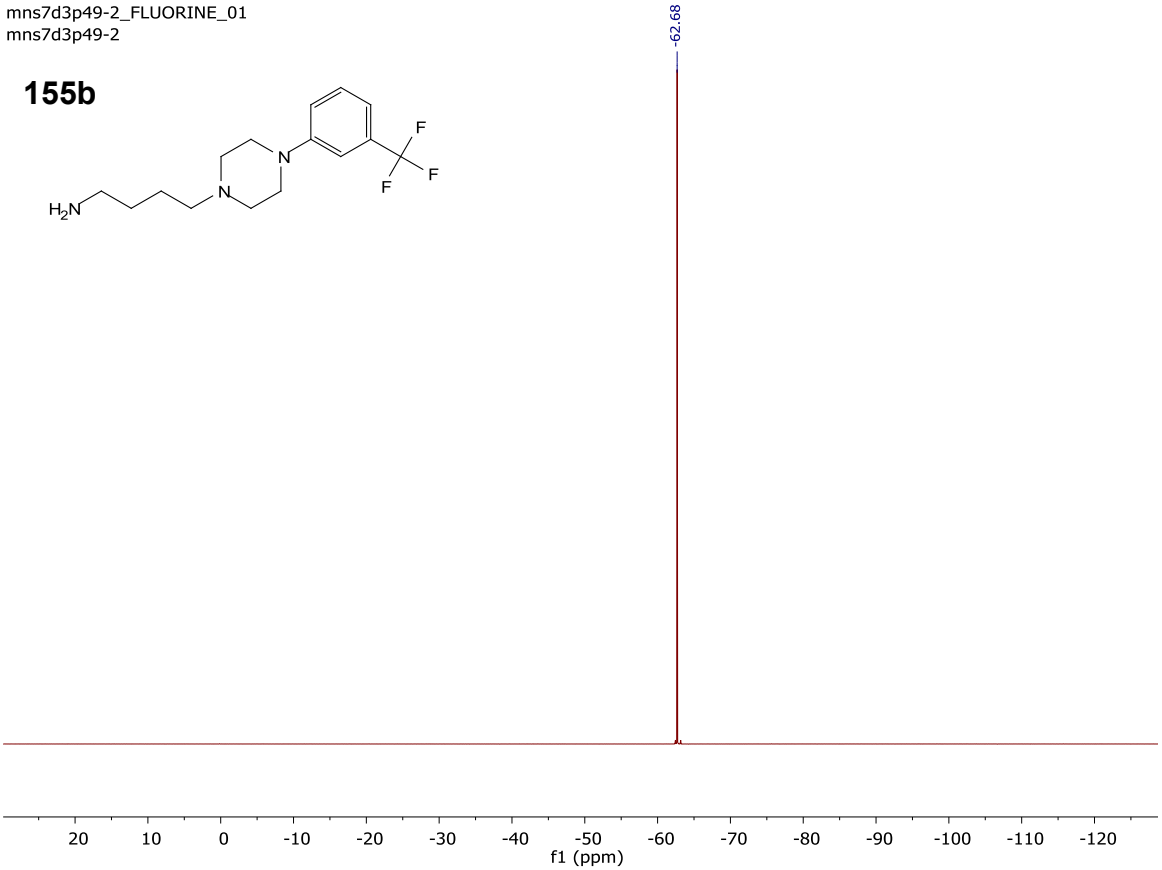
mns7d3p49-2_FLUORINE_01
mns7d3p49-2
155b
F
F
F
N
N
H2N
-62.68
20
10
0
-10
-20
-30
-40
-50
-60
-70
-80
-90
-100
-110
-120
f1 (ppm)

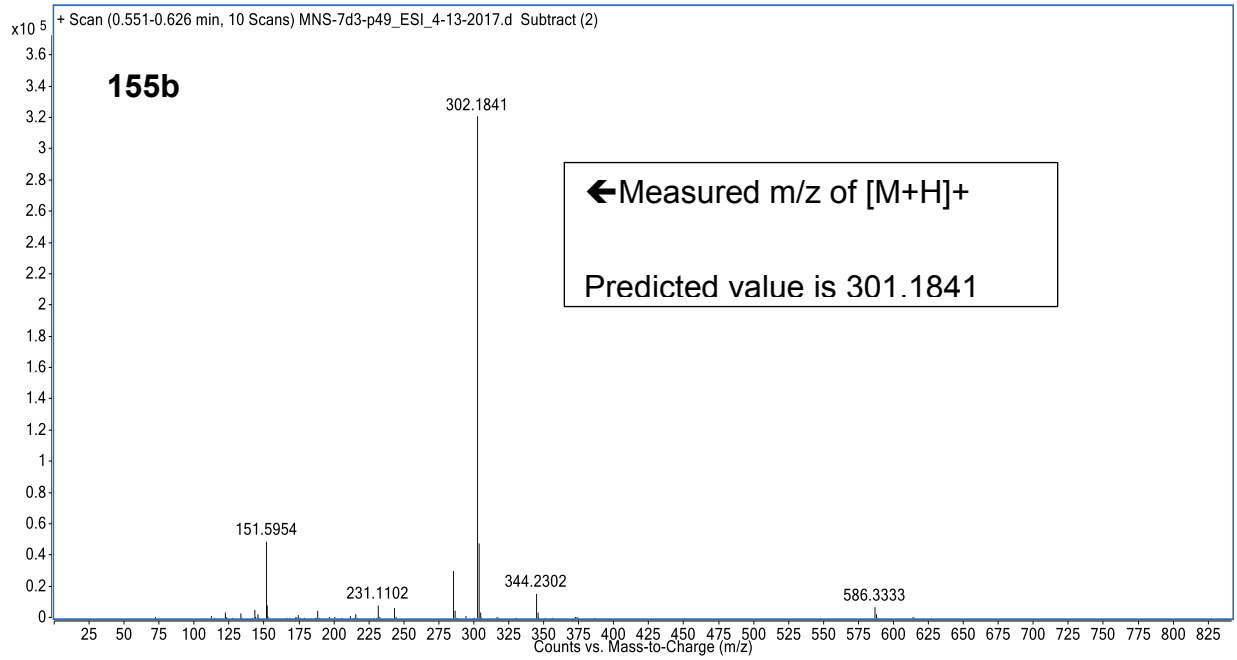
+ Scan (0.551-0.626 min, 10 Scans) MNS-7d3-p49_ESI_4-13-2017.d Subtract (2)
x10 5
155b
302.1841
151.5954
231.1102
344.2302
586.3333
←Measured m/z of [M+H]+
Predicted value is 301.1841
Counts vs. Mass-to-Charge (m/z)

mns7d3p55-2_PROTON_01
mns7d3p55-2

155c

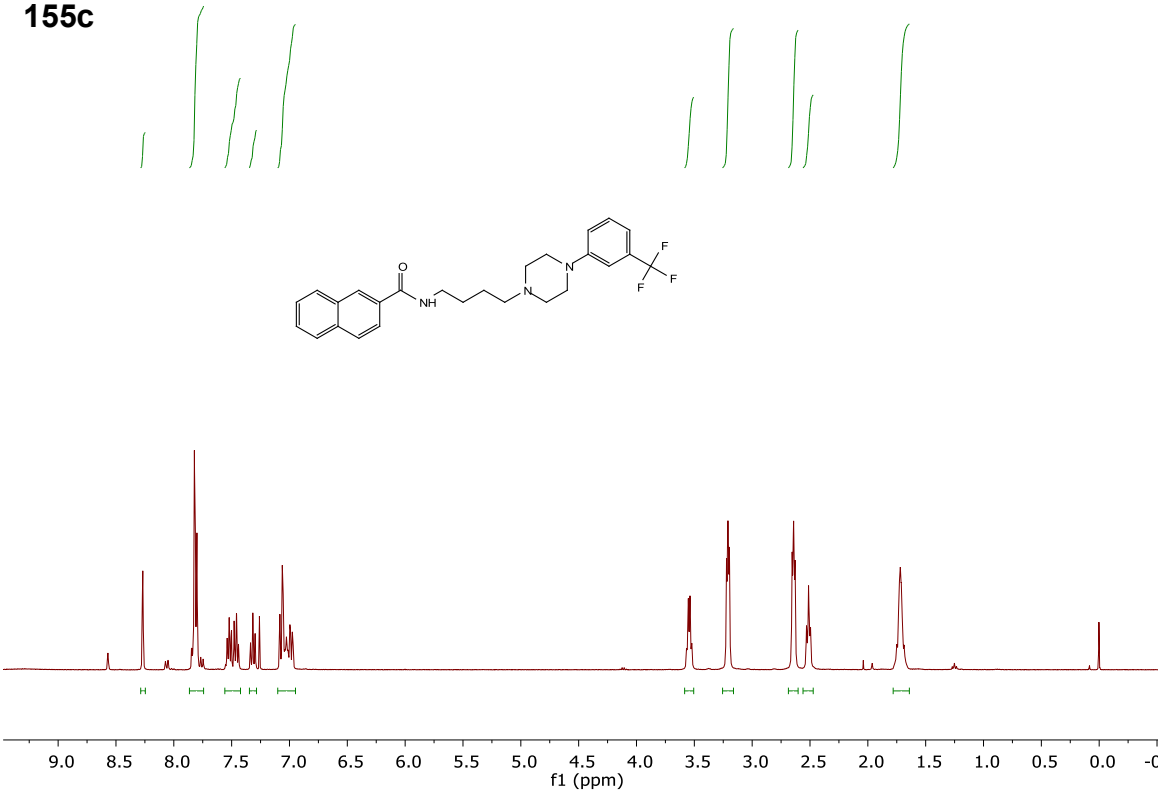

mns7d3p55-2_CARBON_01
mns7d3p55-2

167.84
151.10
134.60
132.54
132.12
131.51
131.20
129.63
128.84
128.37
127.65
127.28
126.59
123.72
122.93
118.71
116.02
112.21
57.64
52.72
48.19
39.82
27.29
23.93

155c

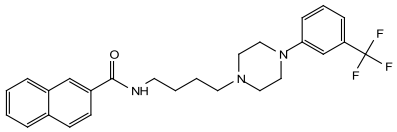

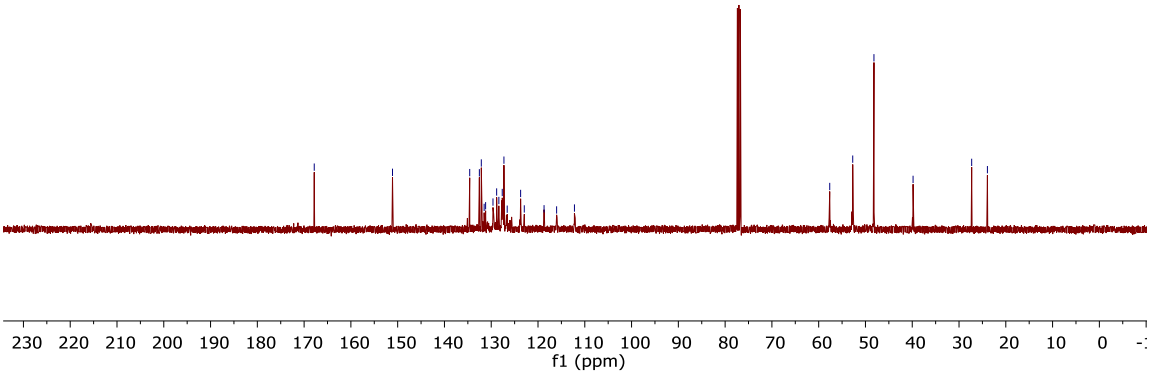

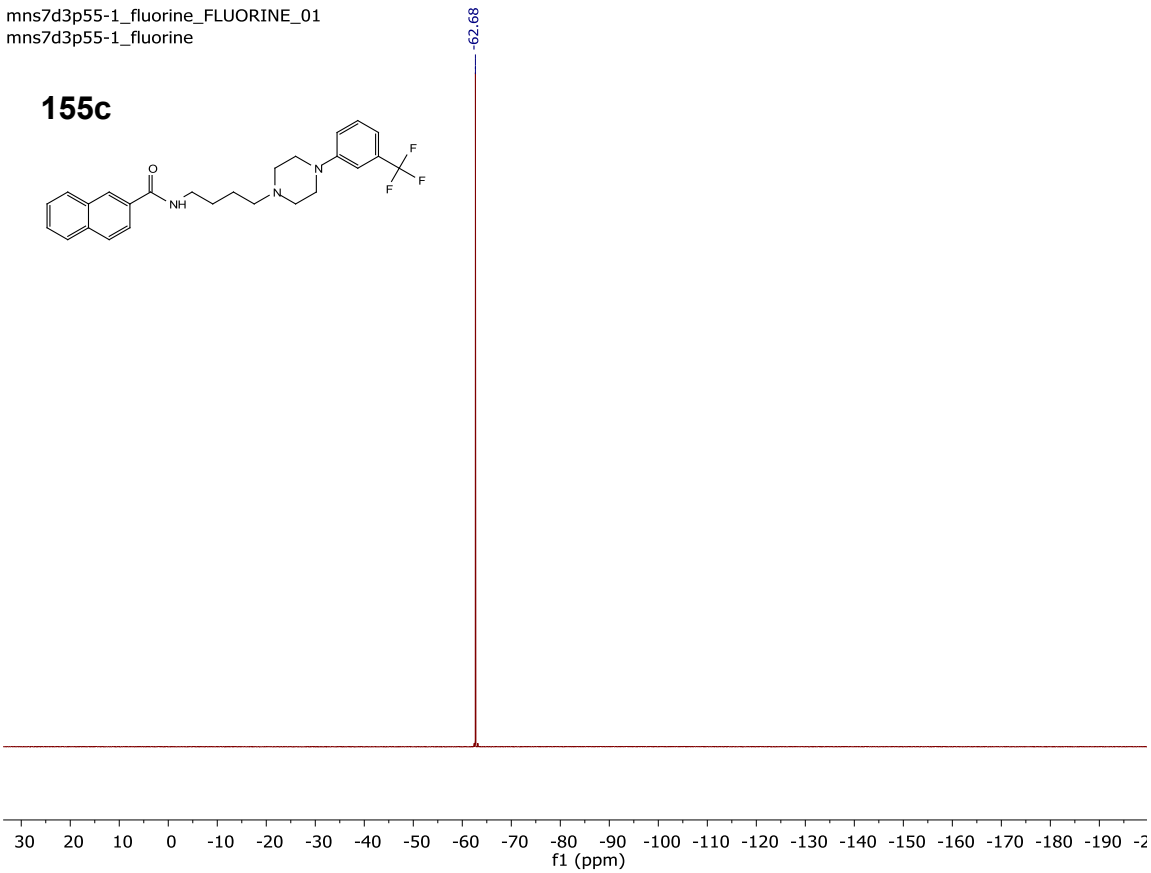
mns7d3p55-1_fluorine_FLUORINE_01
mns7d3p55-1_fluorine
155c
-62.68
30 20 10 0 -10 -20 -30 -40 -50 -60 -70 -80 -90 -100 -110 -120 -130 -140 -150 -160 -170 -180 -190 -2
f1 (ppm)

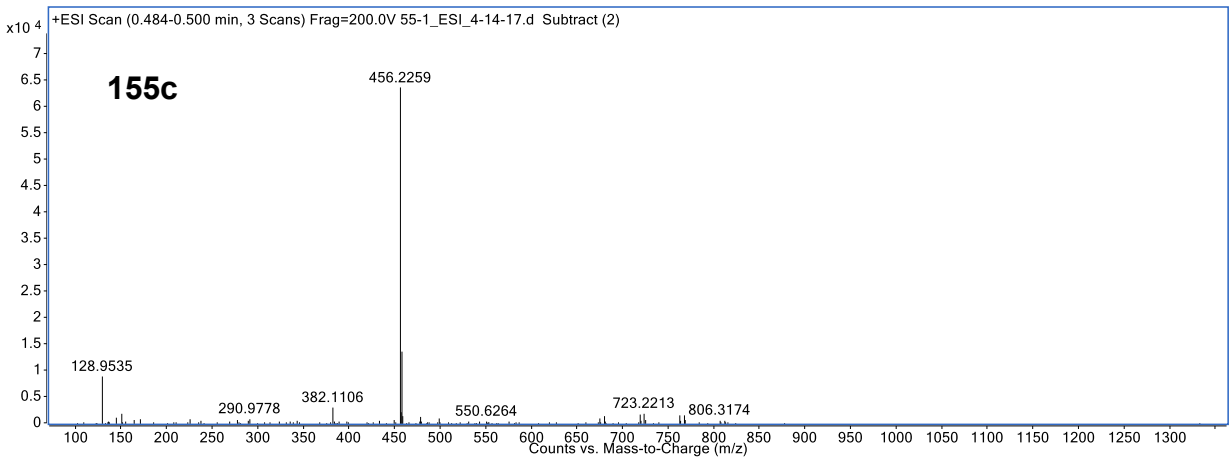
+ESI Scan (0.484-0.500 min, 3 Scans) Frag=200.0V 55-1_ESI_4-14-17.d Subtract (2)
x10 4
155c
456.2259
128.9535
290.9778
382.1106
550.6264
723.2213
806.3174
Counts vs. Mass-to-Charge (m/z)

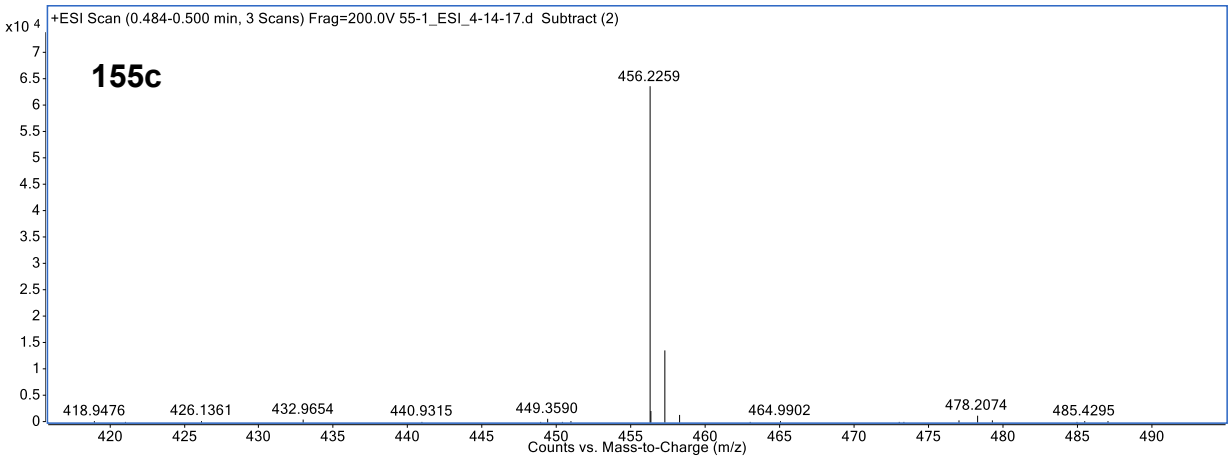
+ESI Scan (0.484-0.500 min, 3 Scans) Frag=200.0V 55-1_ESI_4-14-17.d Subtract (2)
x10 4
155c
456.2259
418.9476
426.1361
432.9654
440.9315
449.3590
464.9902
478.2074
485.4295
Counts vs. Mass-to-Charge (m/z)

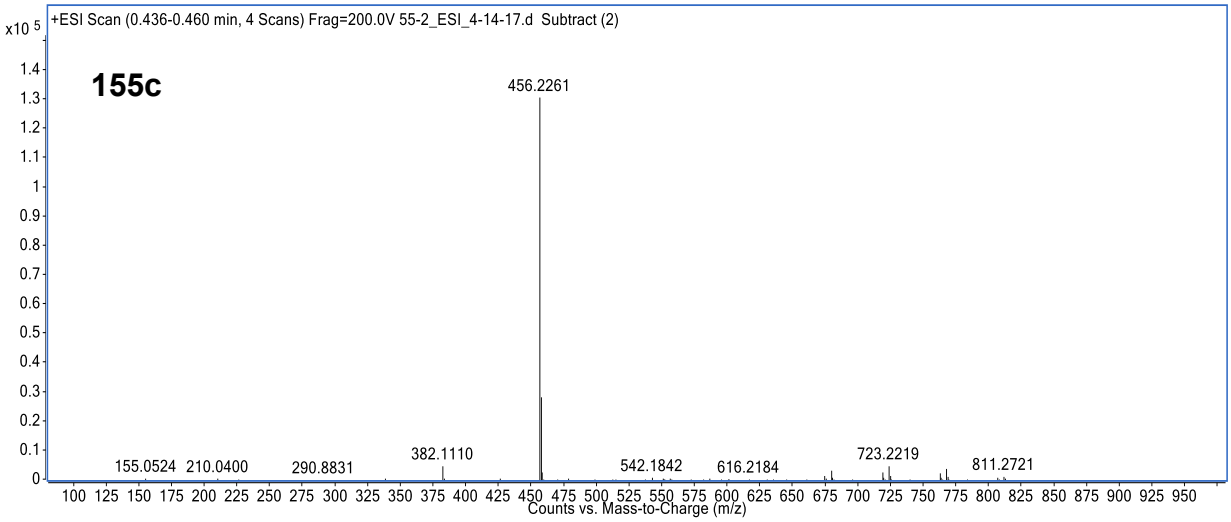
+ESI Scan (0.436-0.460 min, 4 Scans) Frag=200.0V 55-2_ESI_4-14-17.d Subtract (2)
x10 5
155c
456.2261
155.0524
210.0400
290.8831
382.1110
542.1842
616.2184
723.2219
811.2721
Counts vs. Mass-to-Charge (m/z)

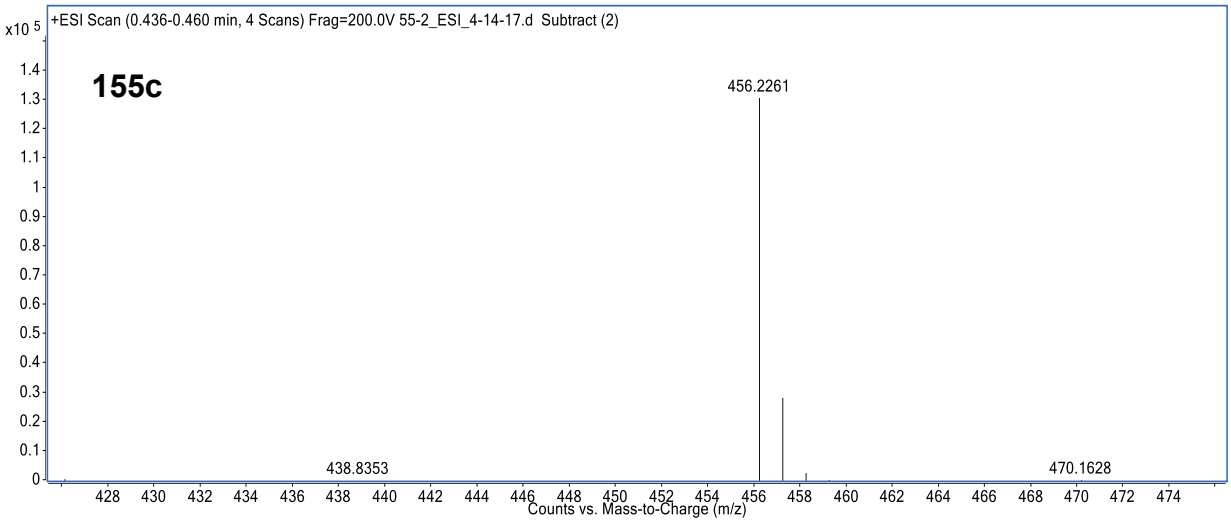
+ESI Scan (0.436-0.460 min, 4 Scans) Frag=200.0V 55-2_ESI_4-14-17.d Subtract (2)
x10 5
155c
456.2261
438.8353
470.1628
Counts vs. Mass-to-Charge (m/z)

MNS7NEWD3P65_PROTON_01
MNS7NEWD3P65

160a

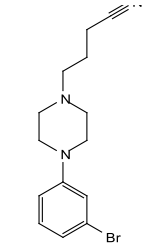

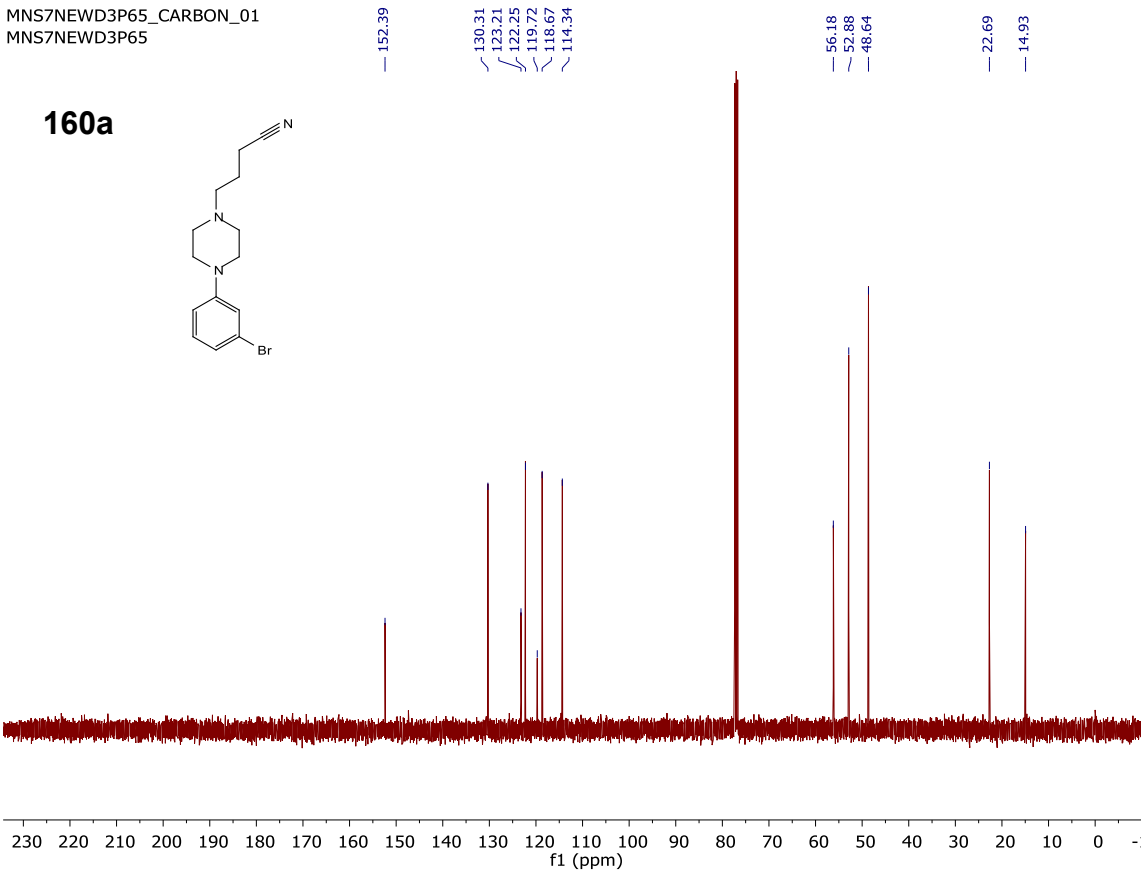
MNS7NEWD3P65_CARBON_01
MNS7NEWD3P65
160a
152.39
130.31
123.21
122.25
119.72
118.67
114.34
56.18
52.88
48.64
22.69
14.93
N
N
N
Br
230 220 210 200 190 180 170 160 150 140 130 120 110 100 90 80 70 60 50 40 30 20 10 0
f1 (ppm)

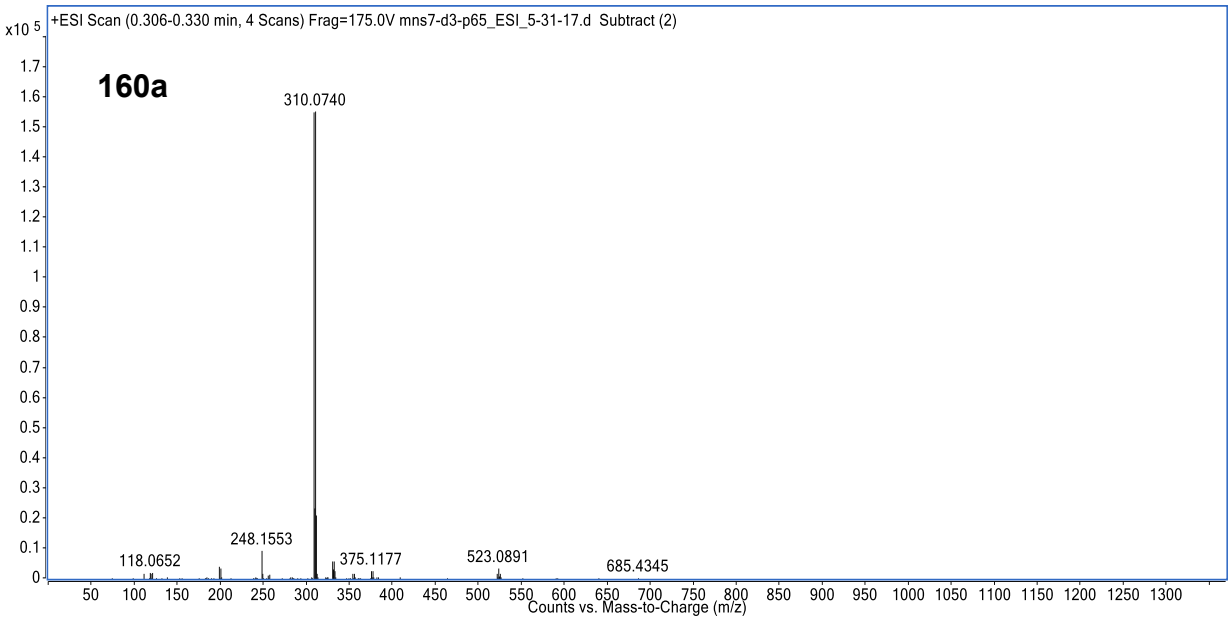
+ESI Scan (0.306-0.330 min, 4 Scans) Frag=175.0V mns7-d3-p65_ESI_5-31-17.d Subtract (2)
x10 5
160a
310.0740
248.1553
118.0652
375.1177
523.0891
685.4345
Counts vs. Mass-to-Charge (m/z)

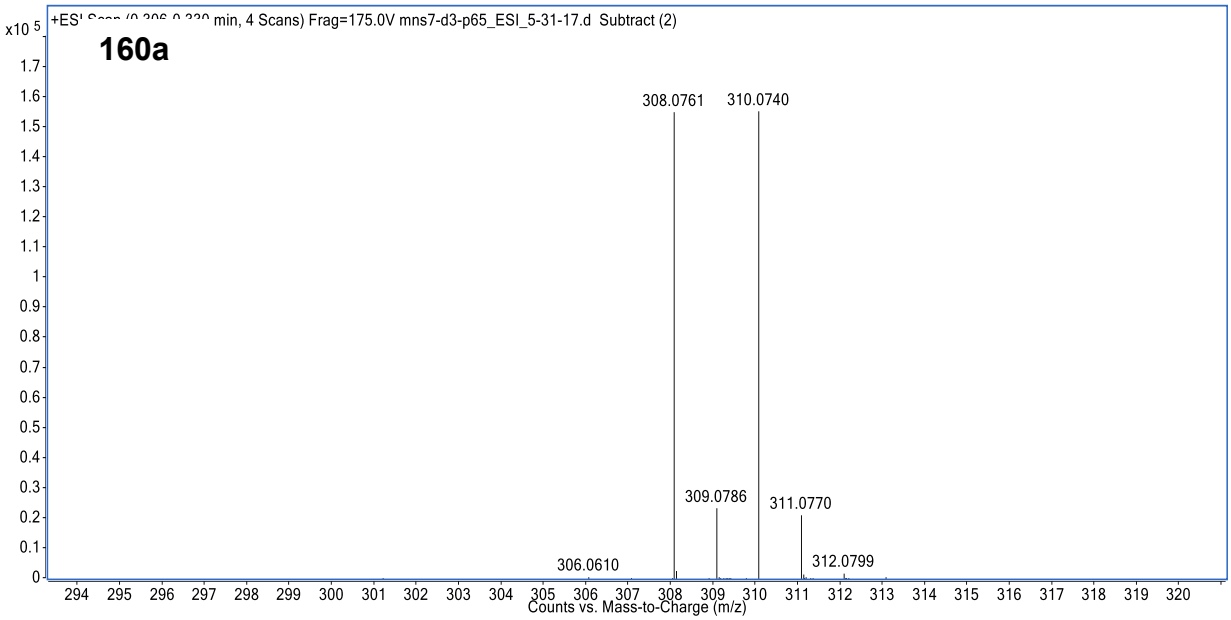
+ESI Scan (0.306-0.330 min, 4 Scans) Frag=175.0V mns7-d3-p65_ESI_5-31-17.d Subtract (2)
x10 5
160a
308.0761
310.0740
309.0786
311.0770
306.0610
312.0799
Counts vs. Mass-to-Charge (m/z)

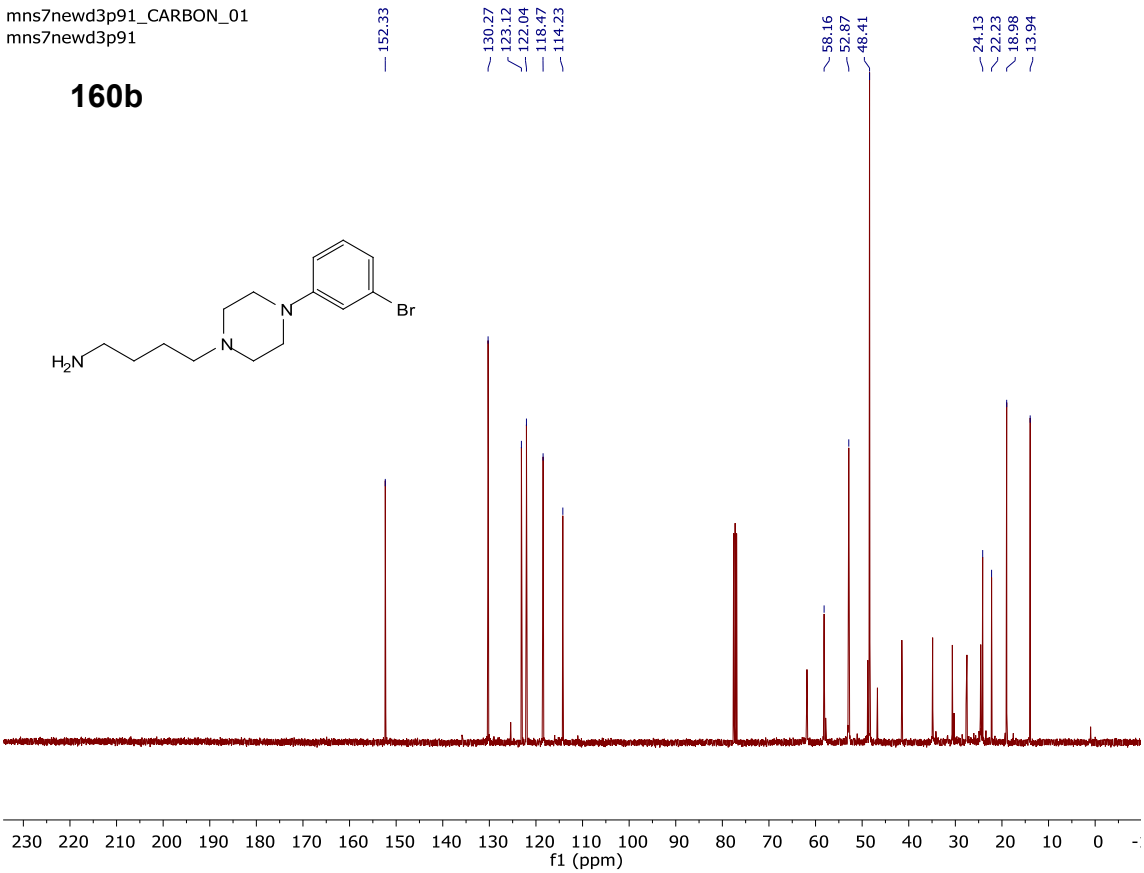
mns7newd3p91_CARBON_01
mns7newd3p91
160b
152.33
130.27
123.12
122.04
118.47
114.23
58.16
52.87
48.41
24.13
22.23
18.98
13.94
Br
N
N
H2N
230 220 210 200 190 180 170 160 150 140 130 120 110 100 90 80 70 60 50 40 30 20 10 0
f1 (ppm)

mns7newd3p91_PROTON_01
mns7newd3p91

160b

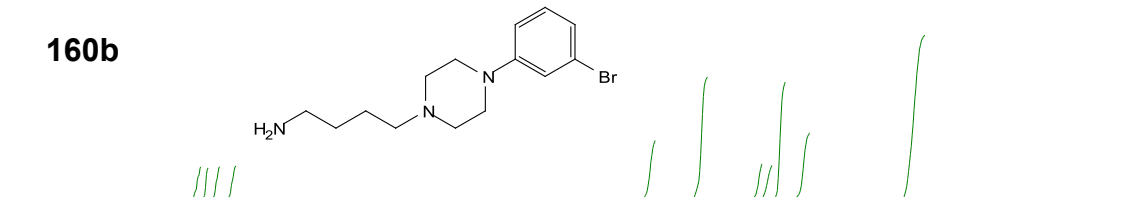

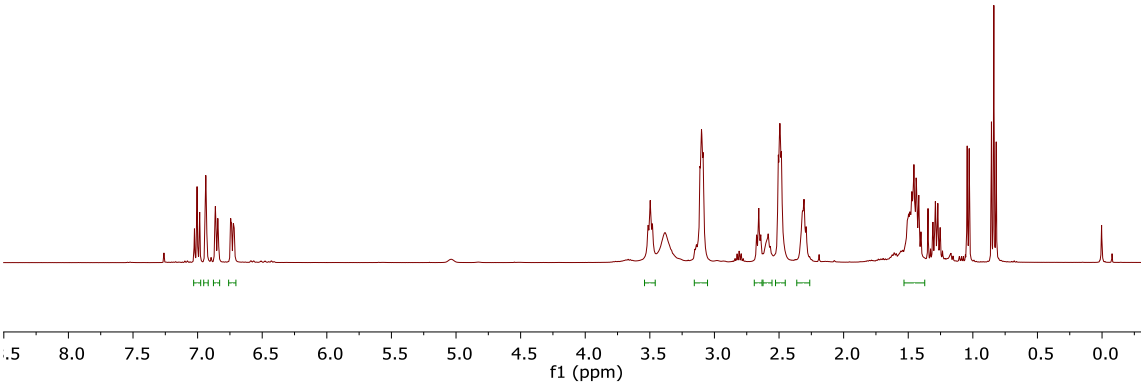

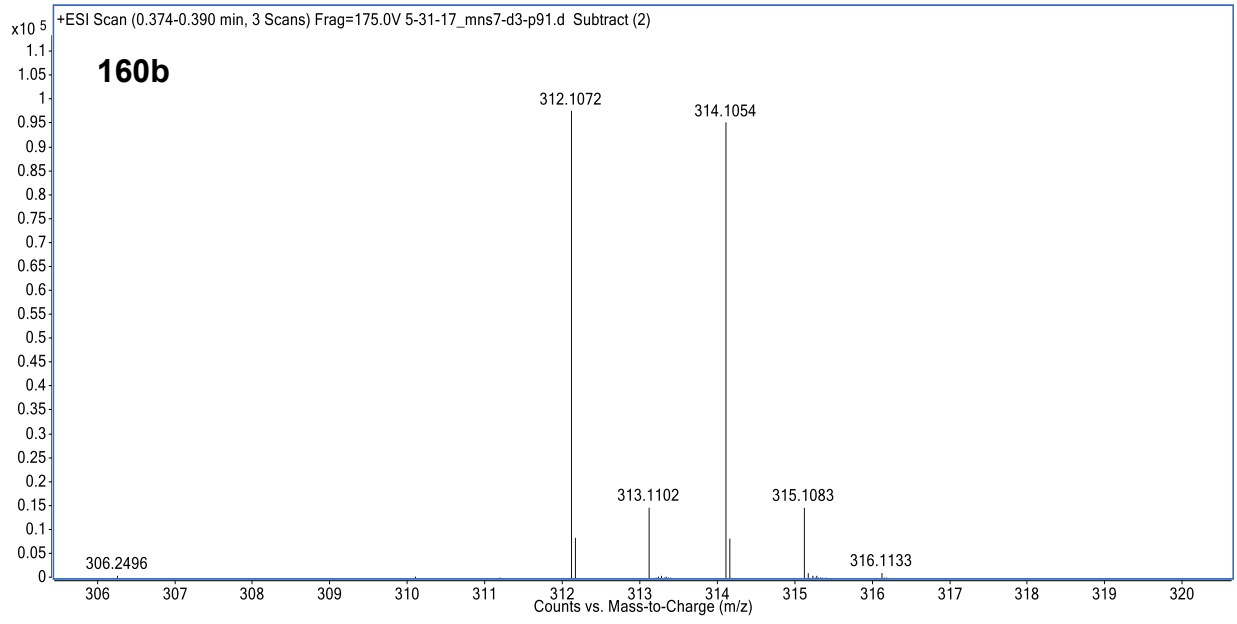

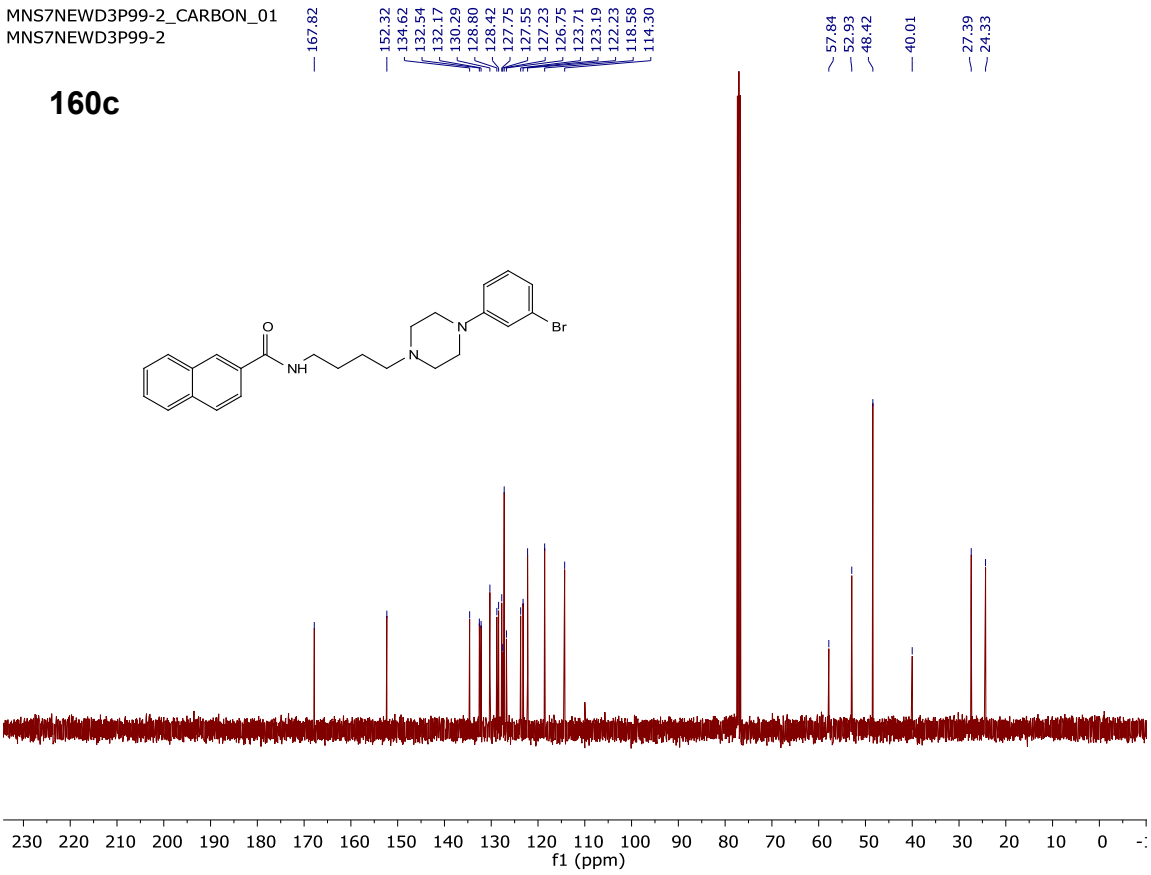
MNS7NEWD3P99-2_CARBON_01
MNS7NEWD3P99-2
160c
167.82
152.32
134.62
132.54
132.17
130.29
128.80
128.42
127.75
127.55
127.23
126.75
123.71
123.19
122.23
118.58
114.30
57.84
52.93
48.42
40.01
27.39
24.33
O
NH
N
N
Br
230 220 210 200 190 180 170 160 150 140 130 120 110 100 90 80 70 60 50 40 30 20 10 0
f1 (ppm)

MNS7NEWD3P99-2_PROTON_01
MNS7NEWD3P99-2

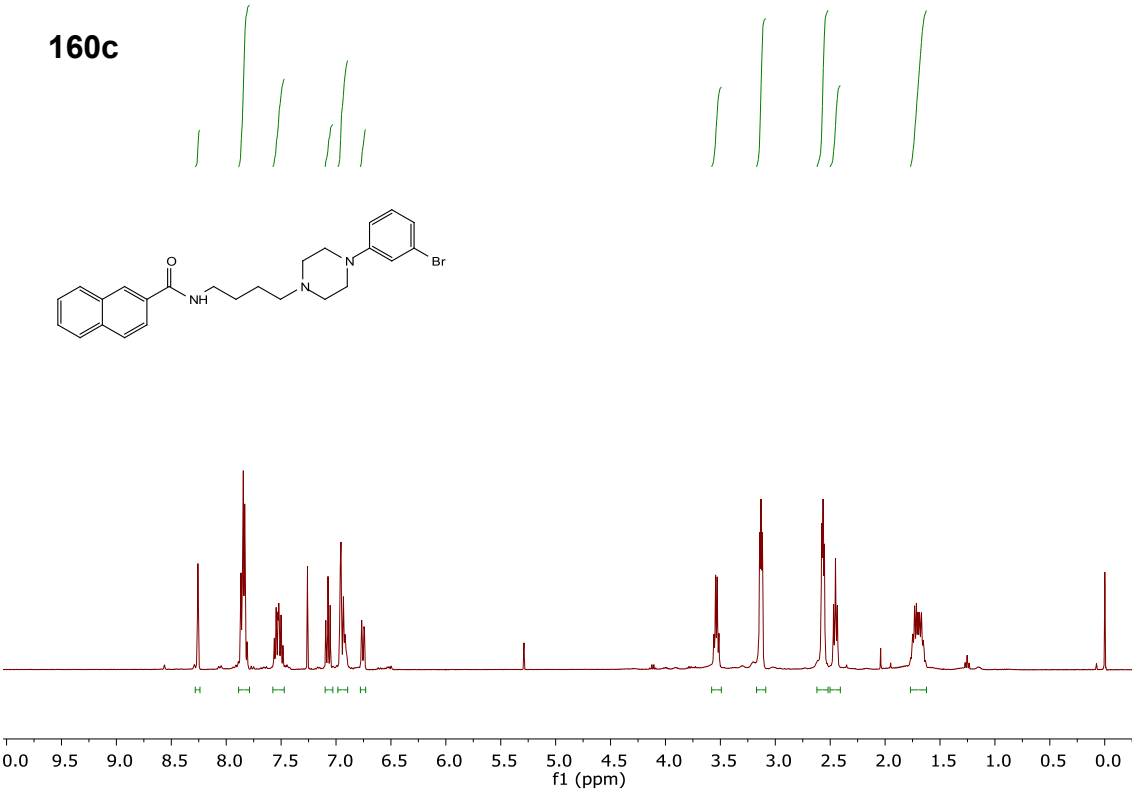

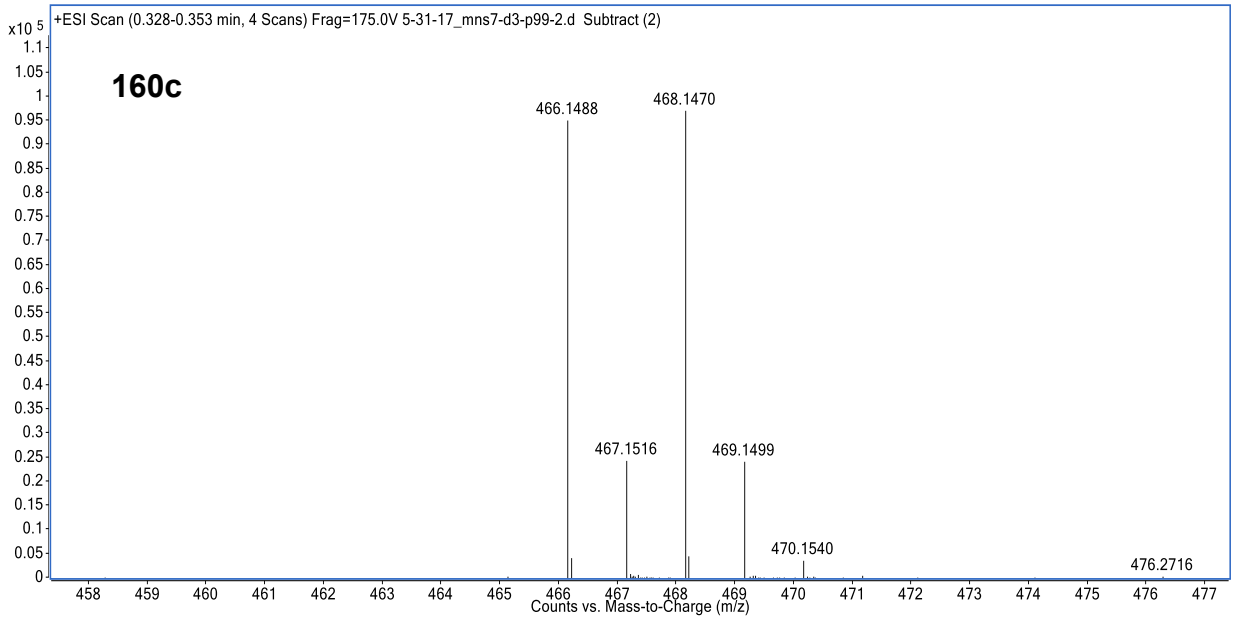

MNS7NEWD3P67_PROTON_01
MNS7NEWD3P67

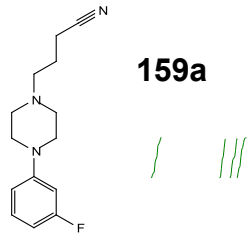

159a

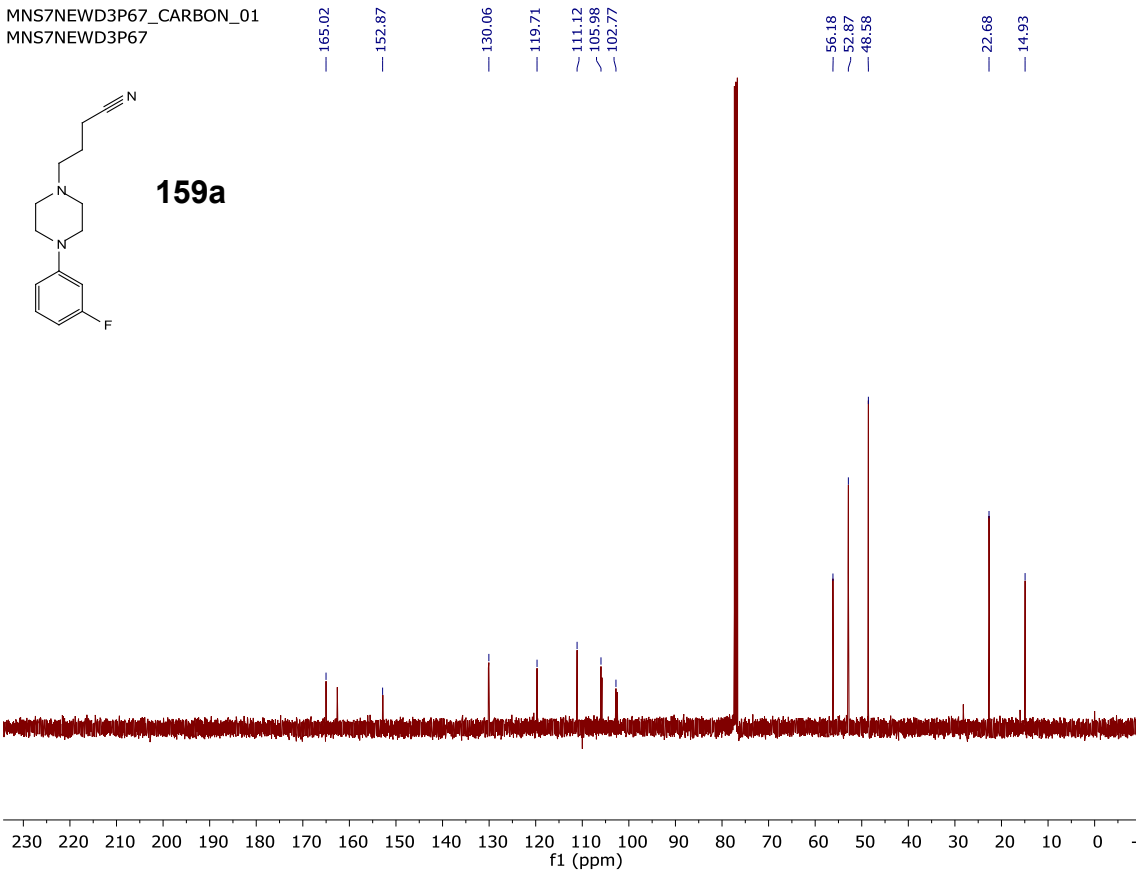
MNS7NEWD3P67_CARBON_01
MNS7NEWD3P67
165.02
152.87
130.06
119.71
111.12
105.98
102.77
56.18
52.87
48.58
22.68
14.93
159a
N
N
N
F
230 220 210 200 190 180 170 160 150 140 130 120 110 100 90 80 70 60 50 40 30 20 10 0
f1 (ppm)

mns7newd3p67-F_FLUORINE_01
mns7newd3p67-F

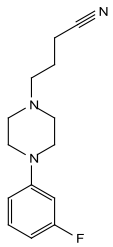

159a

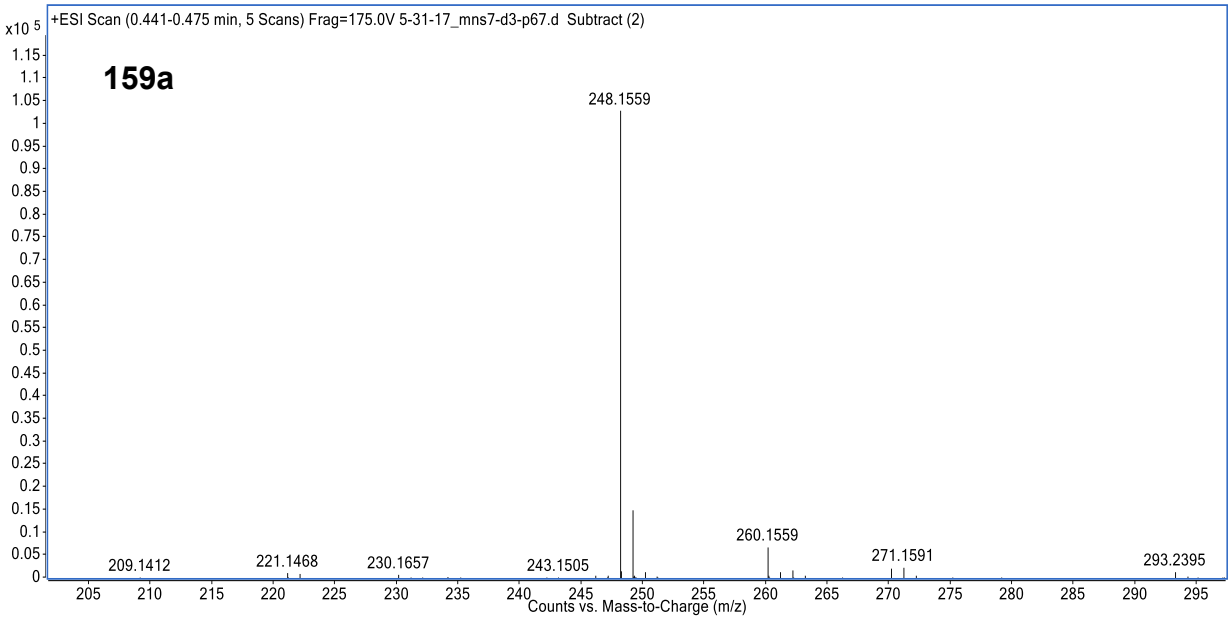

mns7newd3p93_PROTON_01
mns7newd3p93

159b

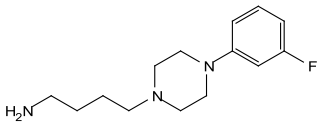

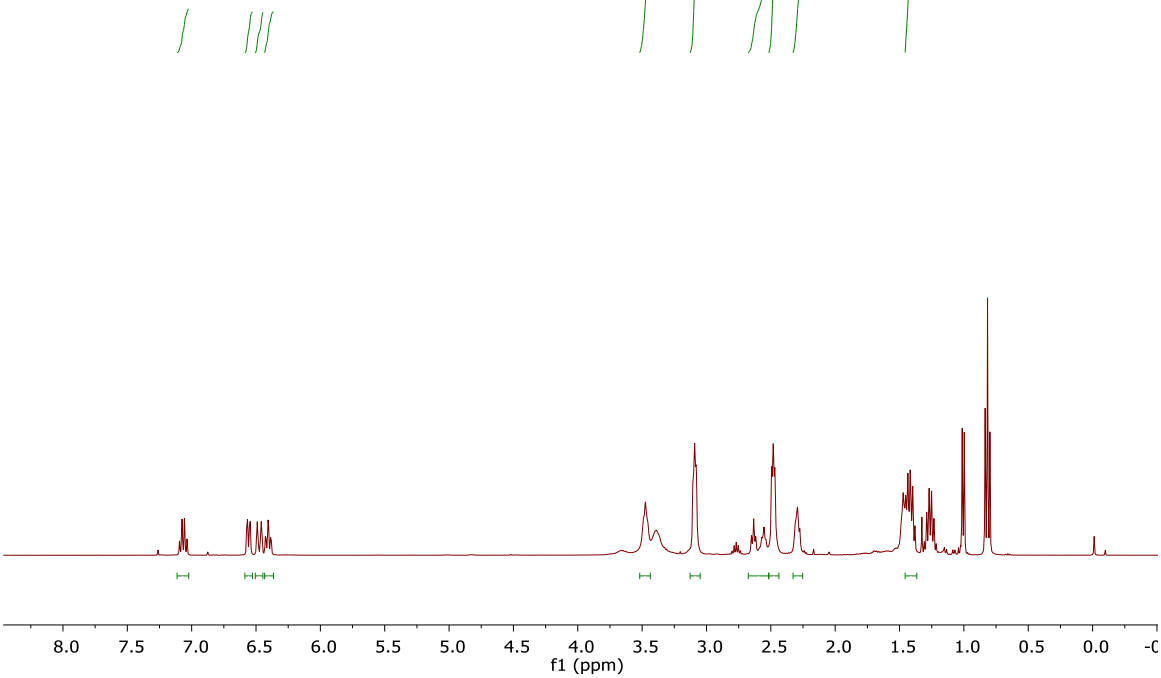

mns7newd3p93_FLUORINE_01
mns7newd3p93

159b

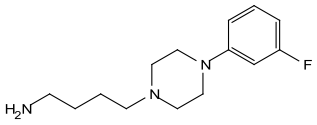

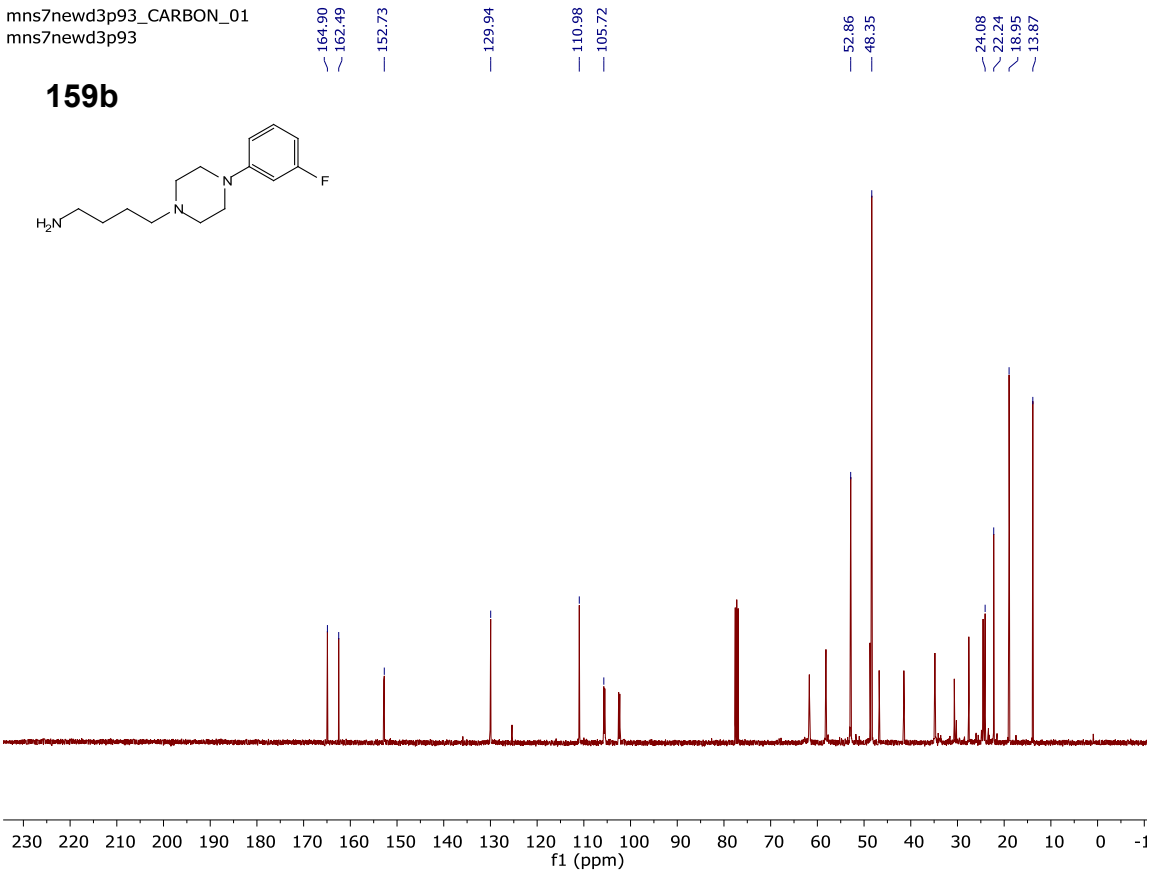
mns7newd3p93_CARBON_01
mns7newd3p93
164.90
162.49
152.73
129.94
110.98
105.72
52.86
48.35
24.08
22.24
18.95
13.87
159b
F
N
N
H2N
230 220 210 200 190 180 170 160 150 140 130 120 110 100 90 80 70 60 50 40 30 20 10 0 -1
f1 (ppm)

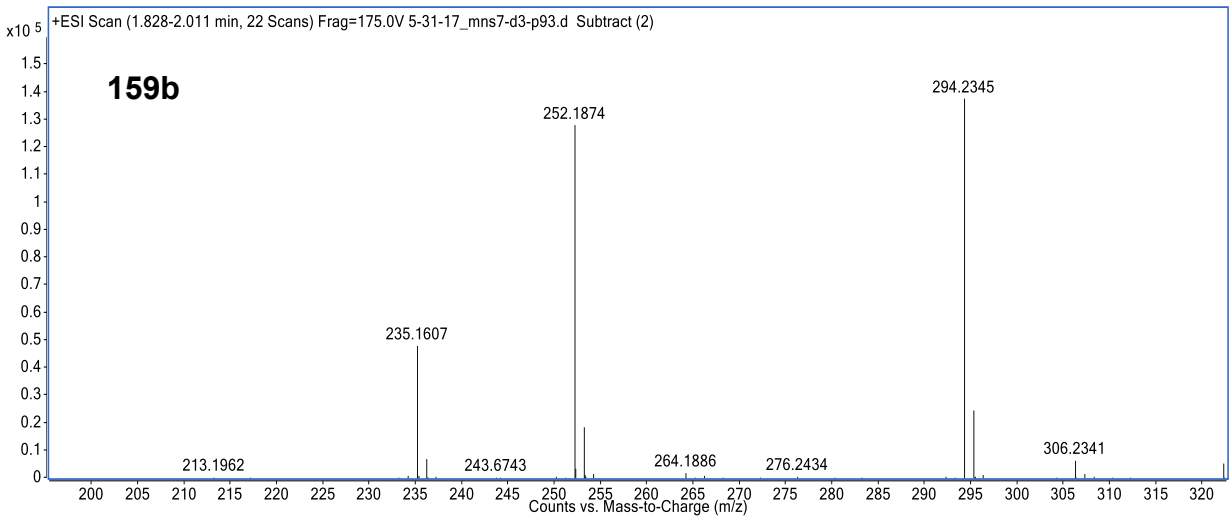
+ESI Scan (1.828-2.011 min, 22 Scans) Frag=175.0V 5-31-17_mns7-d3-p93.d Subtract (2)
x10 5
159b
294.2345
252.1874
235.1607
213.1962
243.6743
264.1886
276.2434
306.2341
Counts vs. Mass-to-Charge (m/z)

MNS7NEWD3P101-2_PROTON_01
MNS7NEWD3P101-2

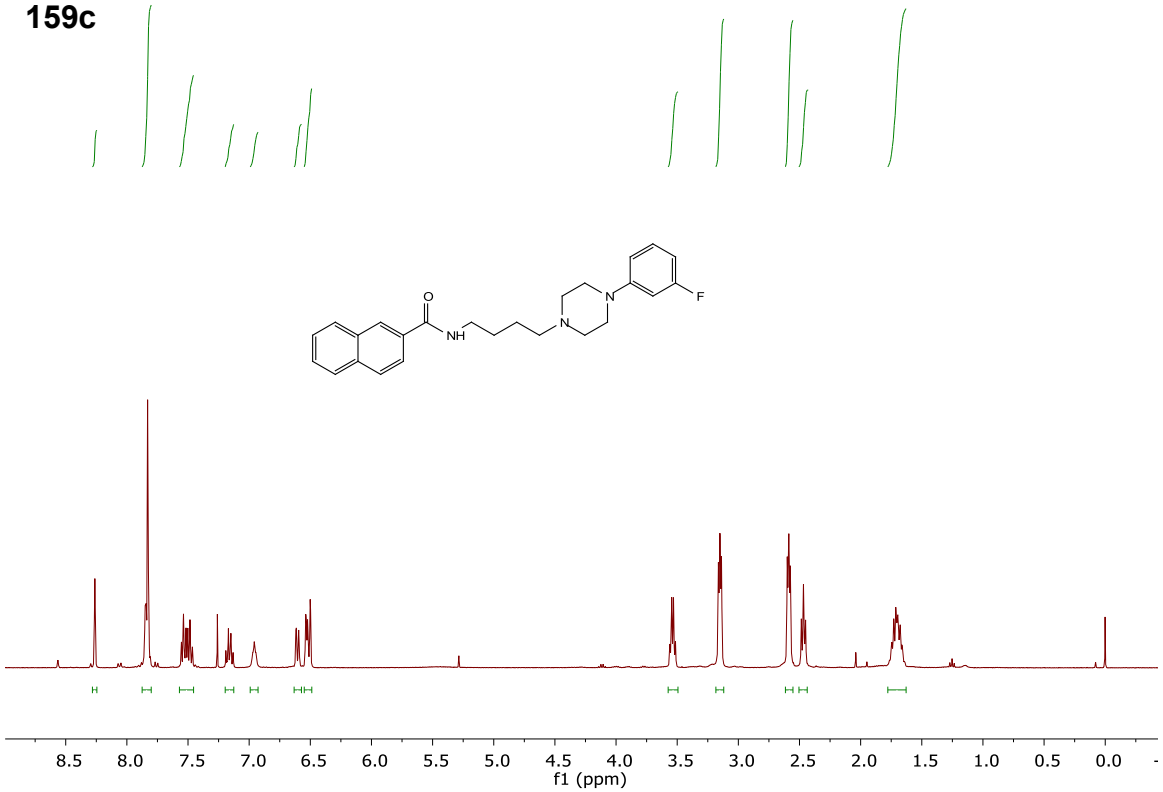

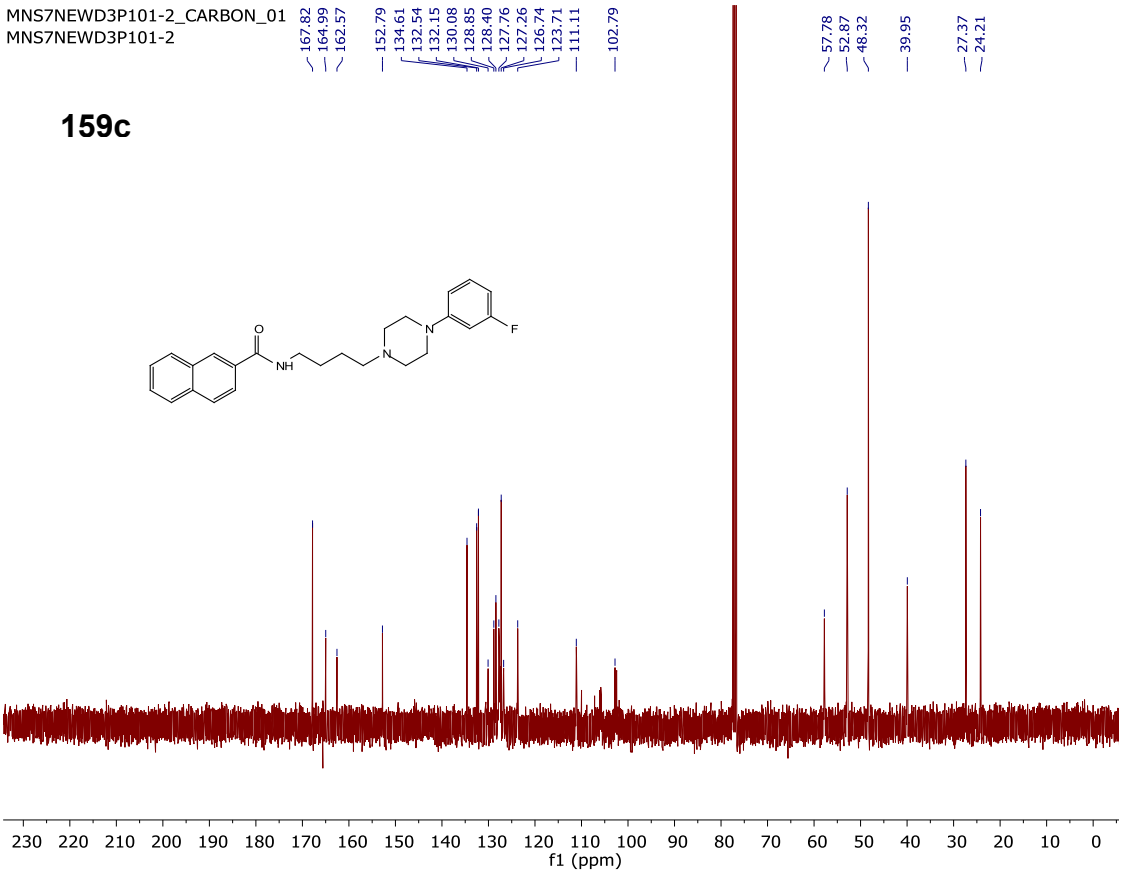
MNS7NEWD3P101-2_CARBON_01
MNS7NEWD3P101-2
167.82
164.99
162.57
152.79
134.61
132.54
132.15
130.08
128.85
128.40
127.76
127.26
126.74
123.71
111.11
102.79
57.78
52.87
48.32
39.95
27.37
24.21
159c
O
NH
N
N
F
230 220 210 200 190 180 170 160 150 140 130 120 110 100 90 80 70 60 50 40 30 20 10 0
f1 (ppm)

MNS7NEWD3P101-2-F_FLUORINE_01
MNS7NEWD3P101-2-F

-112.29
-112.33

159c

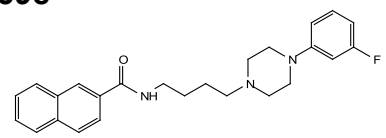

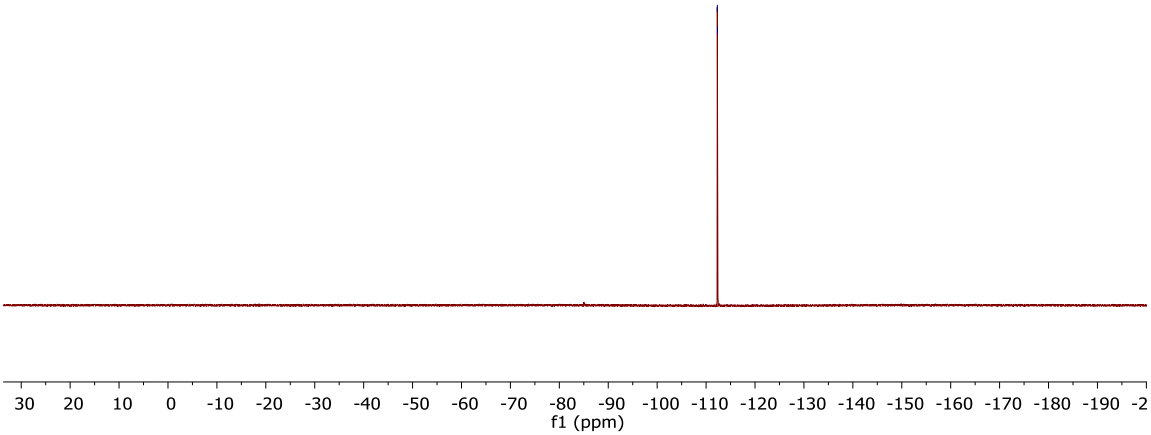

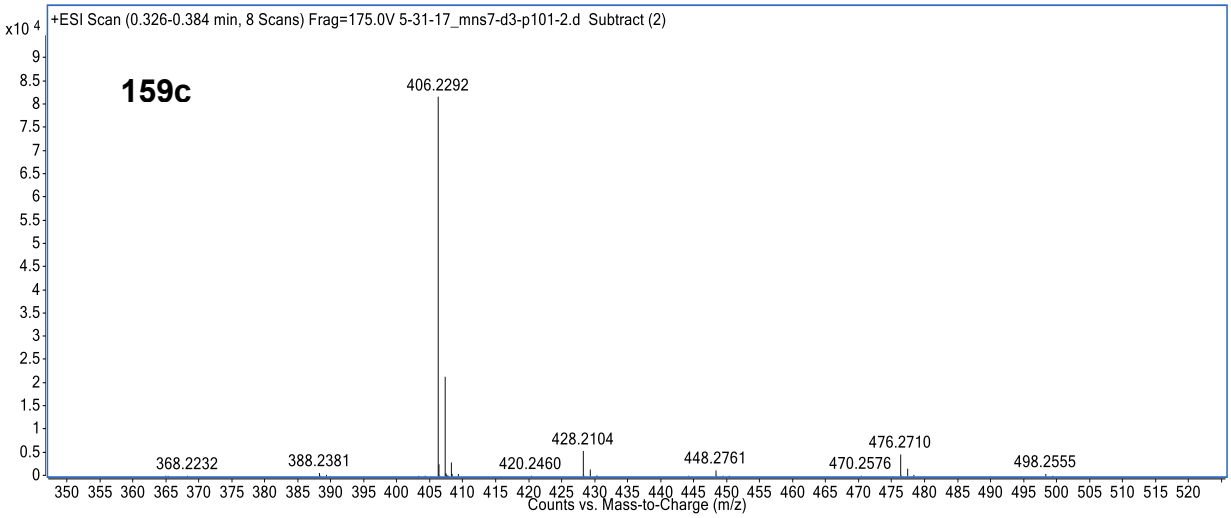

MNS7NEWD3P77_PROTON_01
MNS7NEWD3P77

157a

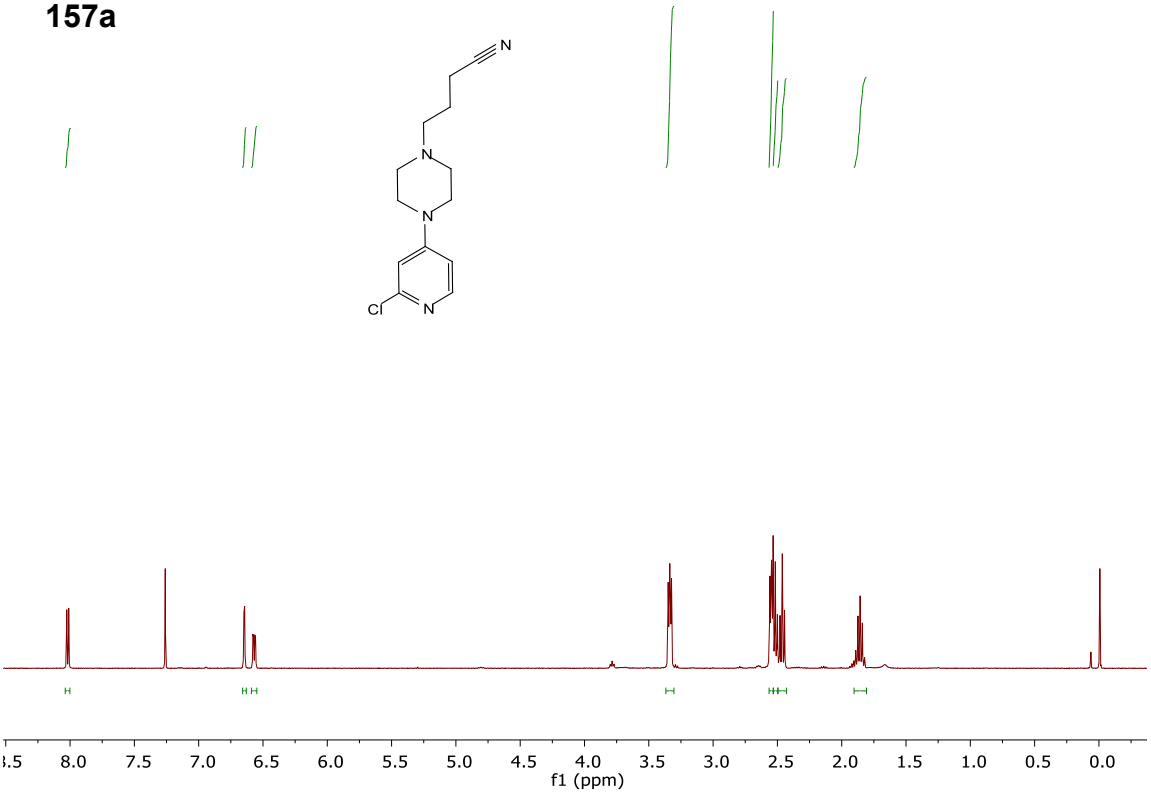

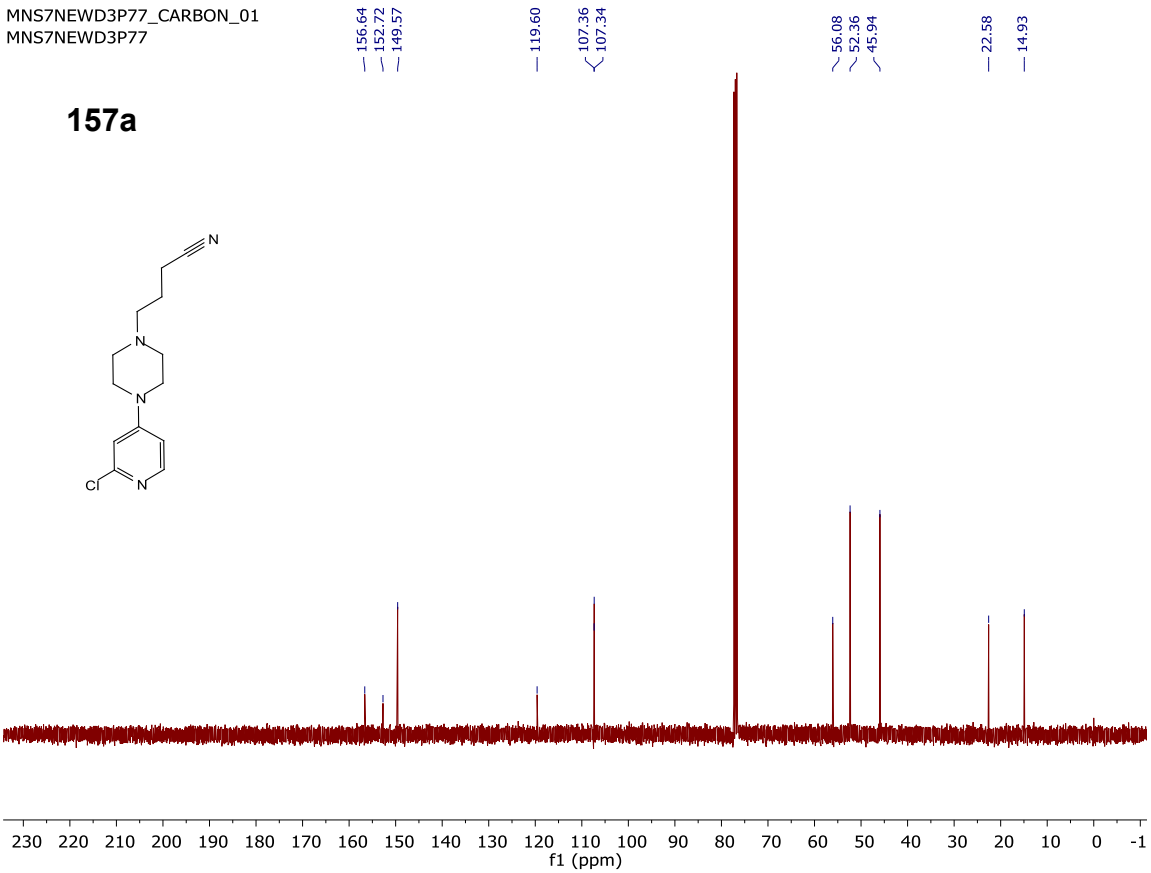
MNS7NEWD3P77_CARBON_01
MNS7NEWD3P77
156.64
152.72
149.57
119.60
107.36
107.34
56.08
52.36
45.94
22.58
14.93
157a
N
N
N
Cl
N
230 220 210 200 190 180 170 160 150 140 130 120 110 100 90 80 70 60 50 40 30 20 10 0 -1
f1 (ppm)

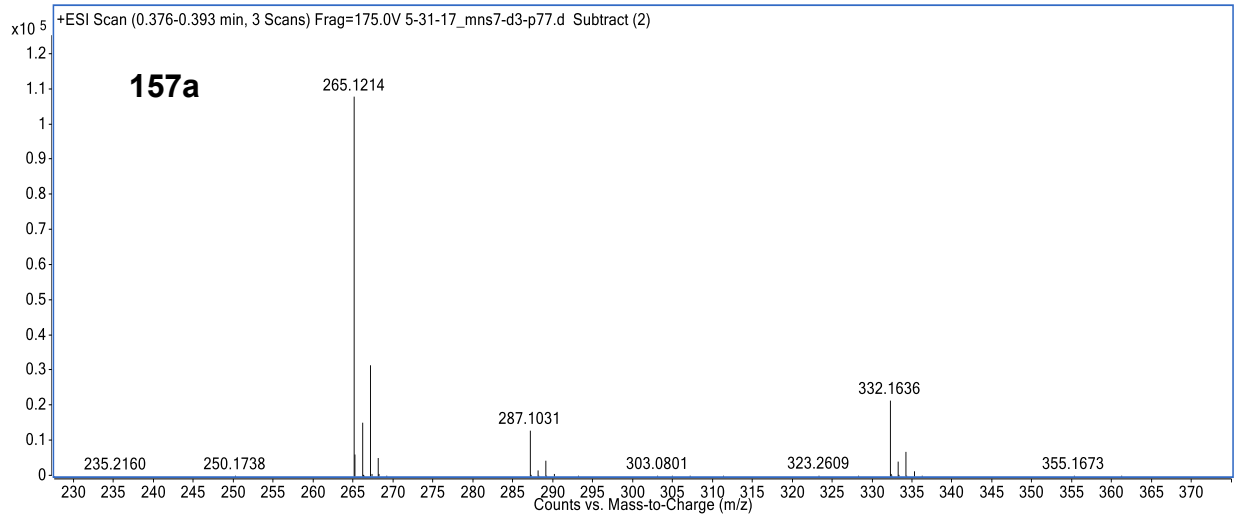
+ESI Scan (0.376-0.393 min, 3 Scans) Frag=175.0V 5-31-17_mns7-d3-p77.d Subtract (2)
x10 5
157a
265.1214
332.1636
287.1031
235.2160
250.1738
303.0801
323.2609
355.1673
Counts vs. Mass-to-Charge (m/z)

mns7newd3p89_PROTON_01
mns7newd3p89

157b

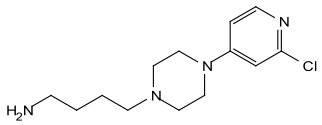

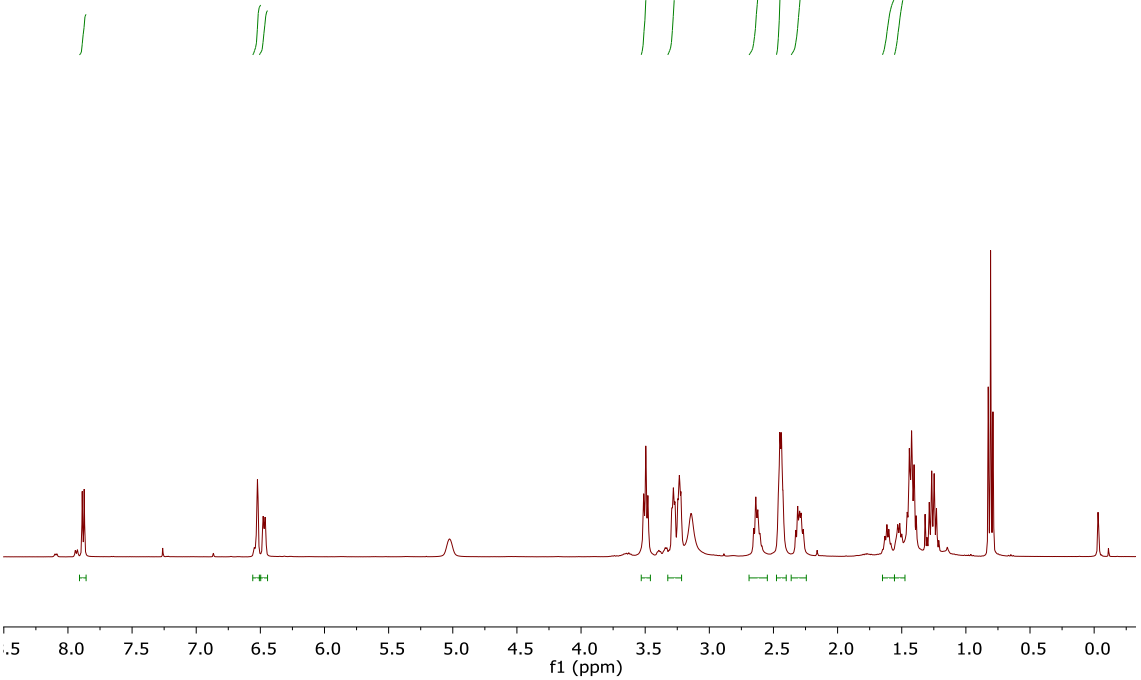

mns7newd3p89_CARBON_01
mns7newd3p89

156.59
152.28
149.27
107.31
107.11
52.31
45.71
34.80
27.59
18.91
13.87

157b

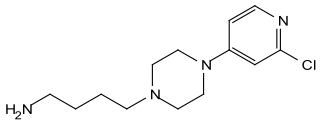

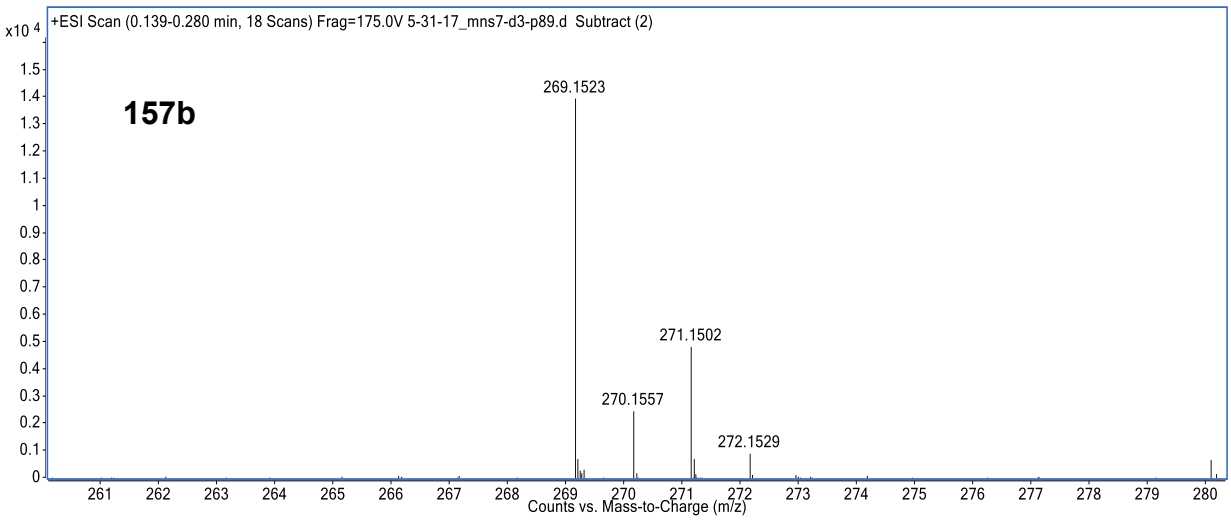

MNS7NEWD3P97_PROTON_01
MNS7NEWD3P97

157c

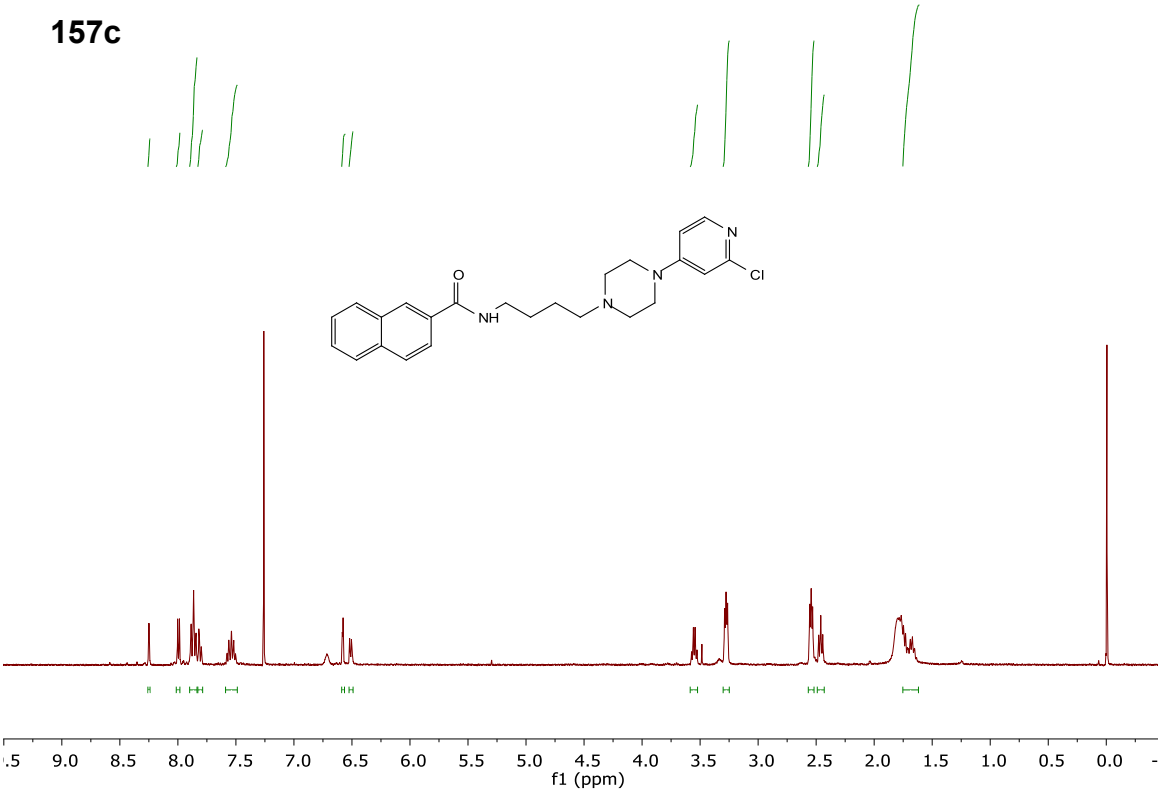

157b

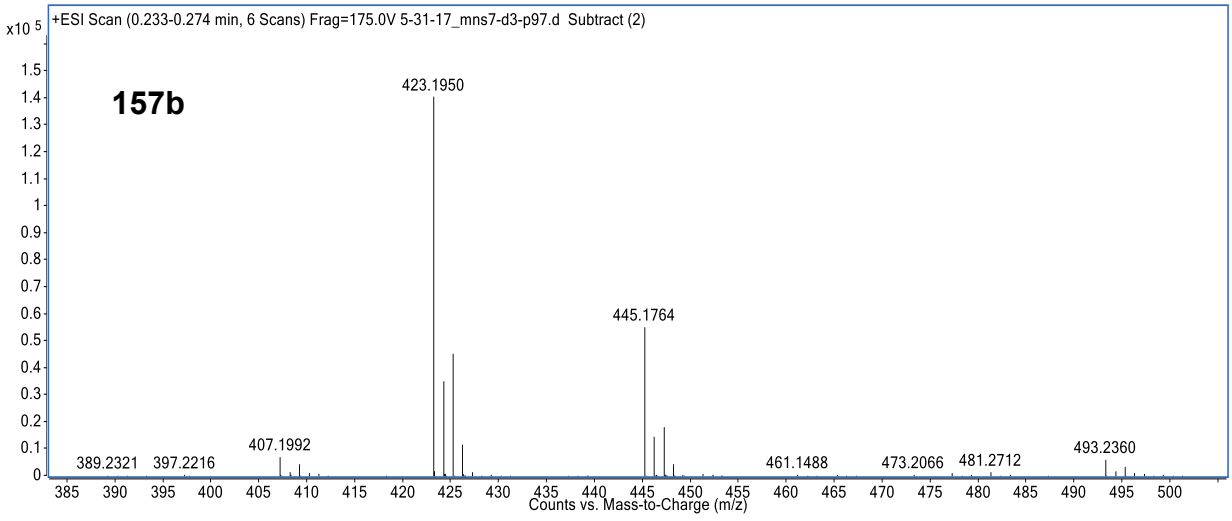

MNS7NEWD3P75_PROTON_01
MNS7NEWD3P75

158a

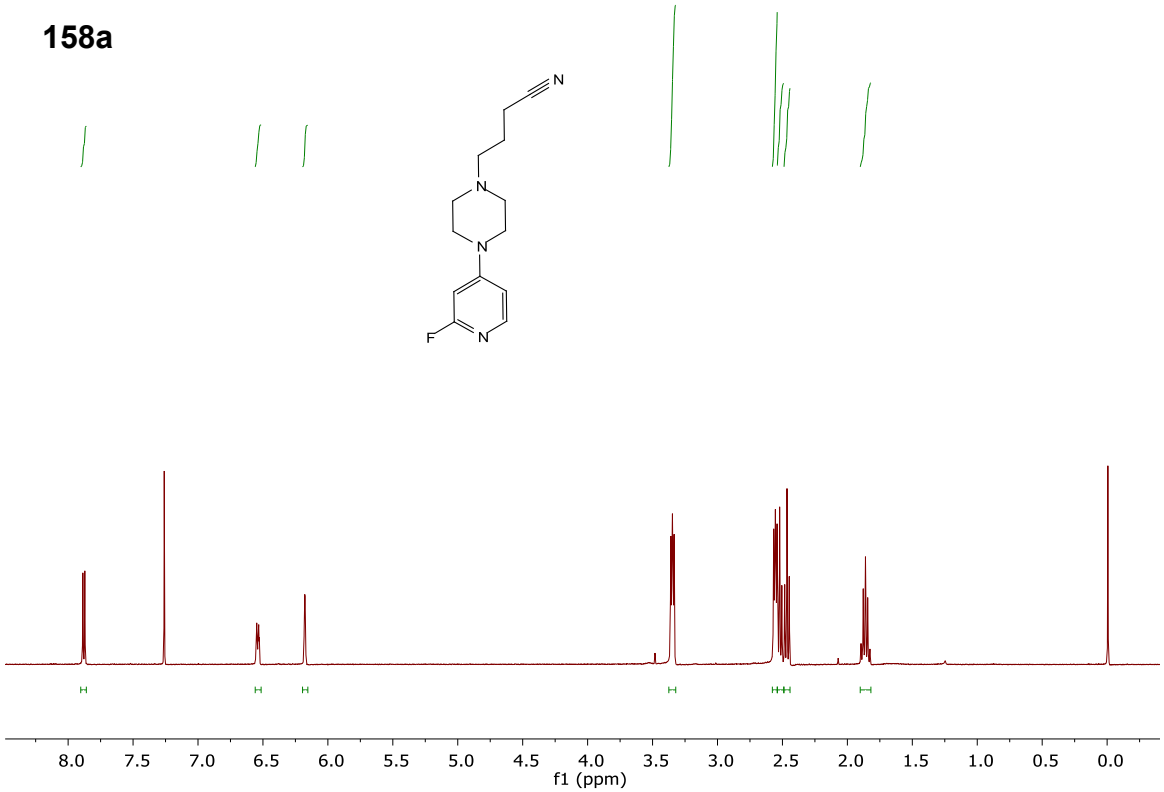

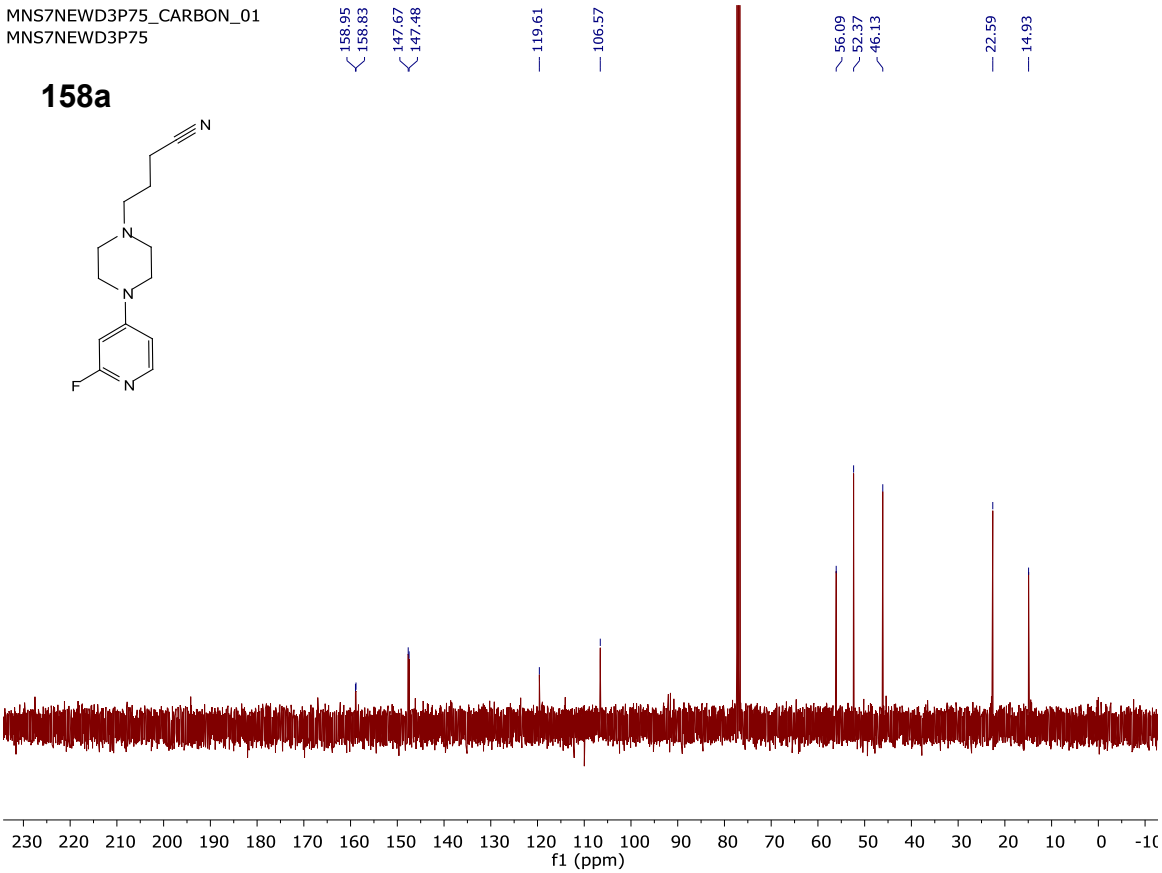
MNS7NEWD3P75_CARBON_01
MNS7NEWD3P75
158a
158.95
158.83
147.67
147.48
119.61
106.57
56.09
52.37
46.13
22.59
14.93
N
N
N
F
N
230 220 210 200 190 180 170 160 150 140 130 120 110 100 90 80 70 60 50 40 30 20 10 0 -10
f1 (ppm)

MNS7NEWD3P75_FLUORINE_01
MNS7NEWD3P75

158a

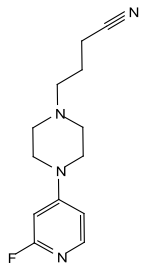

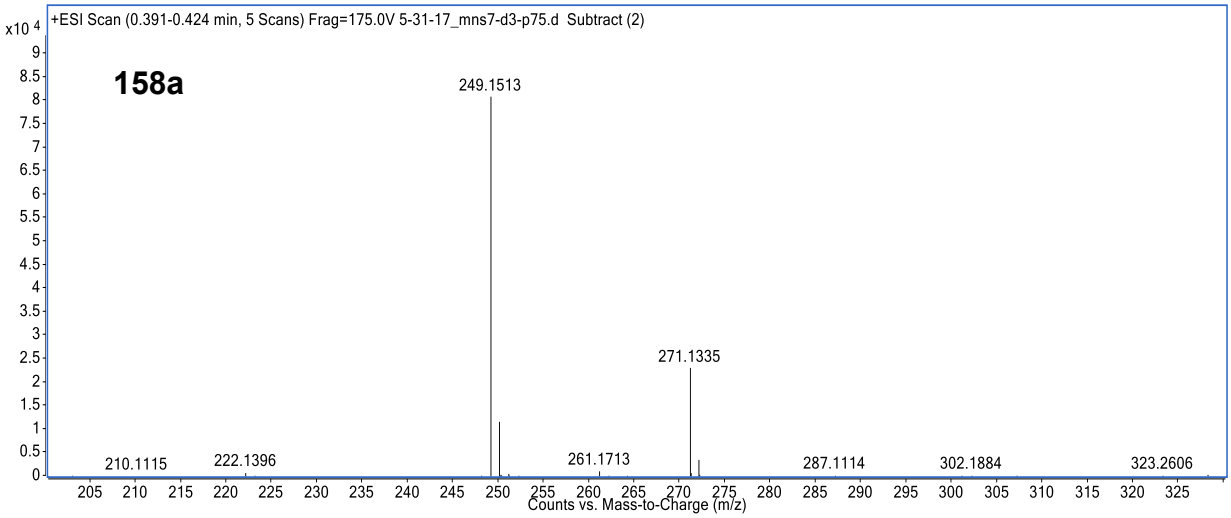

MNS7NEWD3P81_PROTON_01
MNS7NEWD3P81

158b

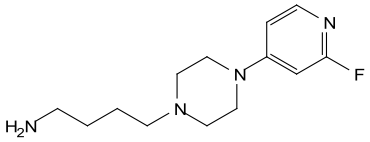

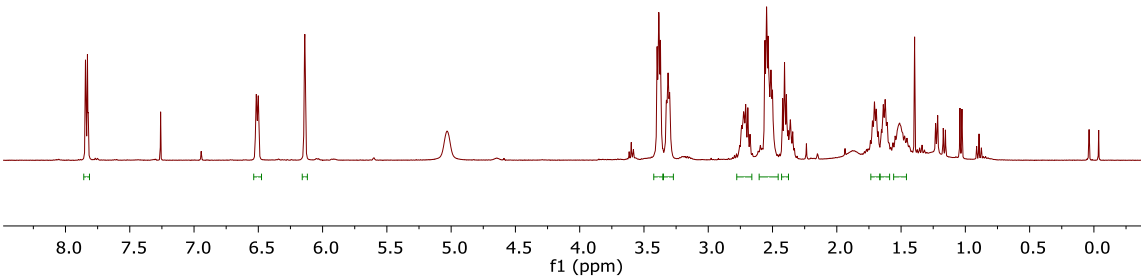

MNS7NEWD3P81_FLUORINE_01
MNS7NEWD3P81

158b

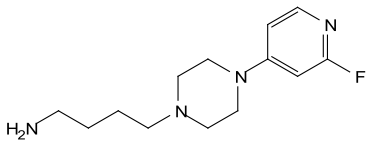

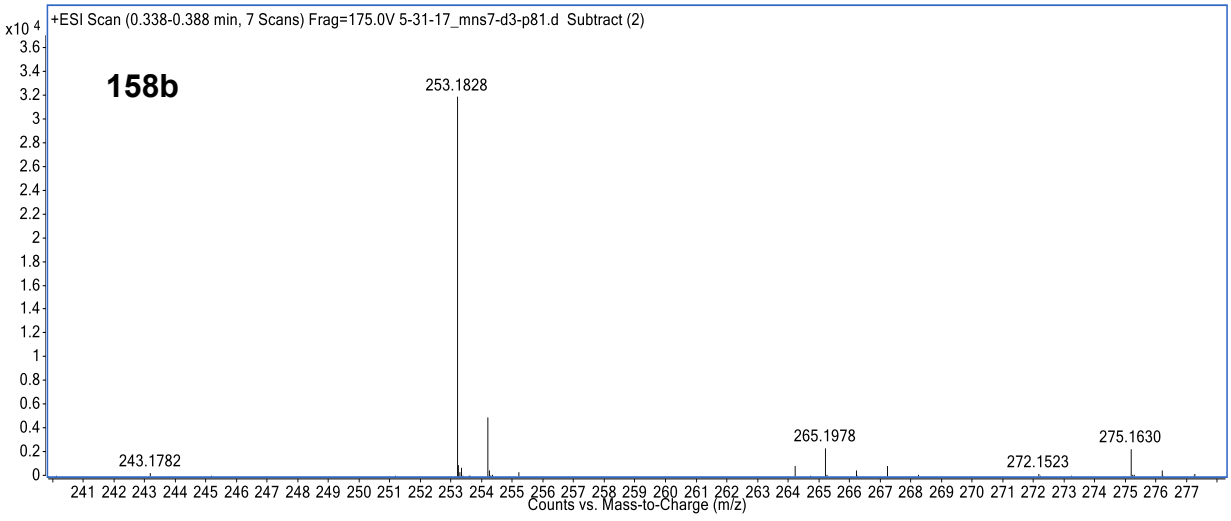

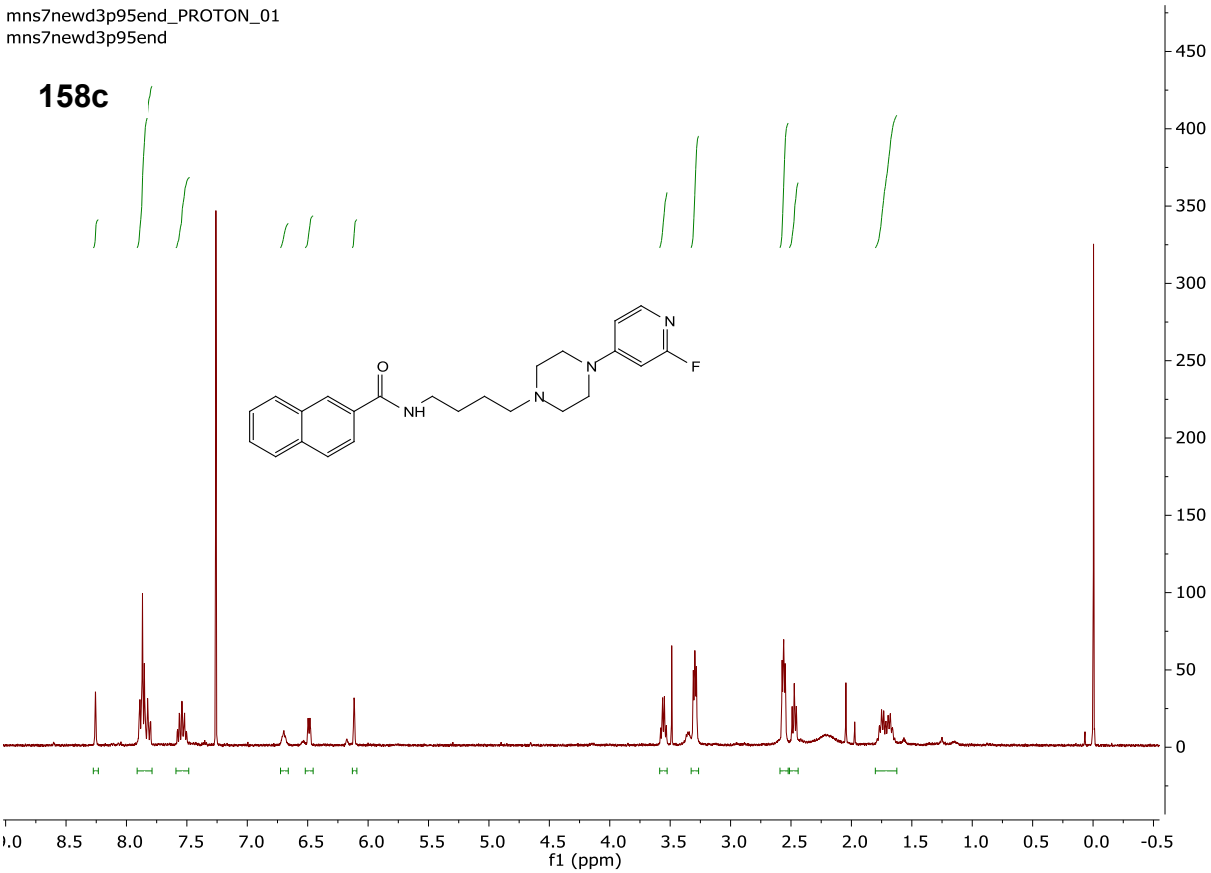
mns7newd3p95end_PROTON_01
mns7newd3p95end
158c
O
NH
N
N
N
F
450
400
350
300
250
200
150
100
50
0
8.5
8.0
7.5
7.0
6.5
6.0
5.5
5.0
4.5
4.0
3.5
3.0
2.5
2.0
1.5
1.0
0.5
0.0
-0.5
f1 (ppm)

MNS7NEWD3P95END-F_FLUORINE_01
MNS7NEWD3P95END-F

158c

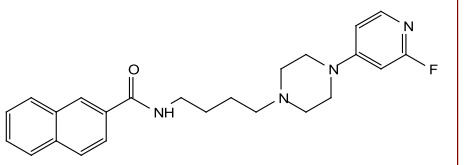

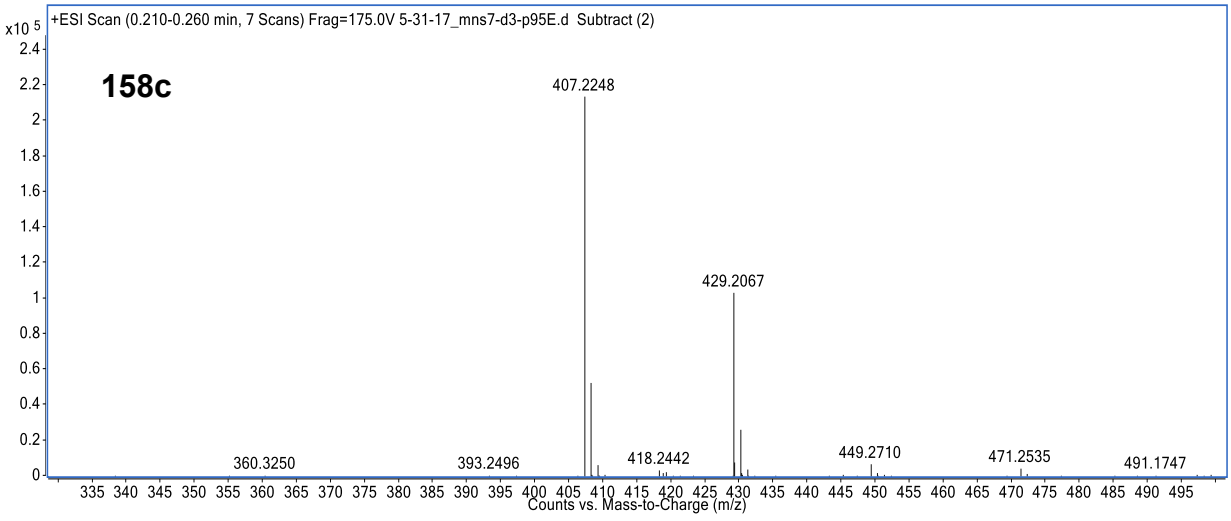

6. Radiochemistry Supporting Information for [^{11}C]155c

a. HPLC Conditions:

HPLC was performed using a Shimadzu LC-2010A HT system.

- Quality Control: 40% MeCN, 20mM NH_4OAc, 2 mL HOAc, 40^{o}C. Luna C18 100A, 150x4.6mm Phenomenex S/N H16-384835
- Semipreparative HPLC: 60% MeCN, 20mM NH_4OAc, 2 mL HOAc, 40^{o}C, 2.5 mL/min. Luna C18(2) 10 micron, 250x150mm, S/No 486505-1; 00G-4253-N0

HPLC Traces

- NCA Rat 1093
- NCA Rat 1101
- CA Rat 1094
- CA Rat 1095

PET scans, summed images, 3 views (coronal, sagittal, tranverse)

- NCA Rat 1093
- NCA Rat 1101
- CA Rat 1094
- CA Rat 1095

NCA Rat 1093

Cut Peak

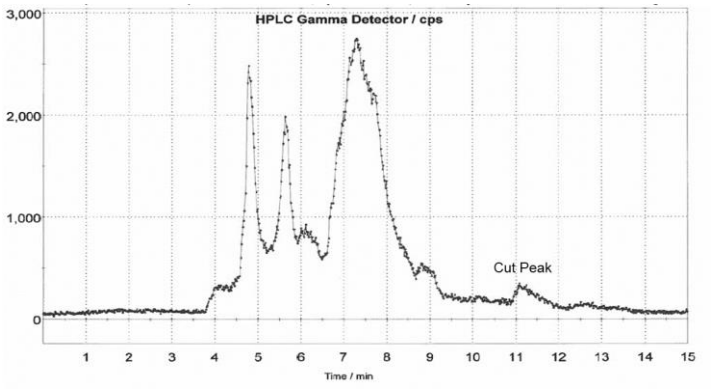

QC (93% RCP RCP**)**

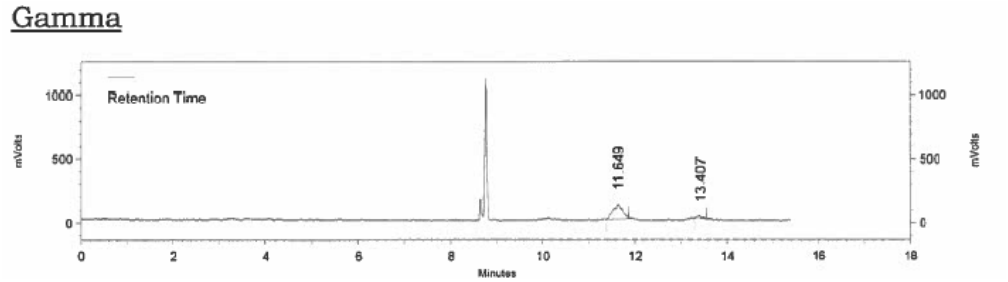

Coinjection (>80% RCP)

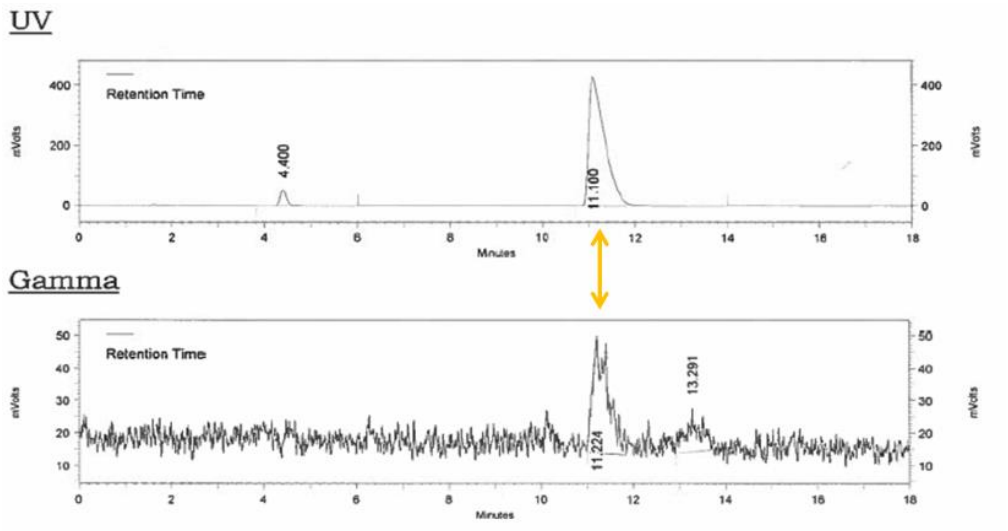

NCA Rac 1101

Cut Peak

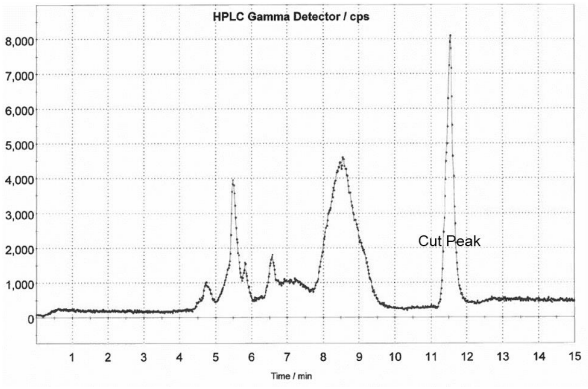

QC (82% RCP)

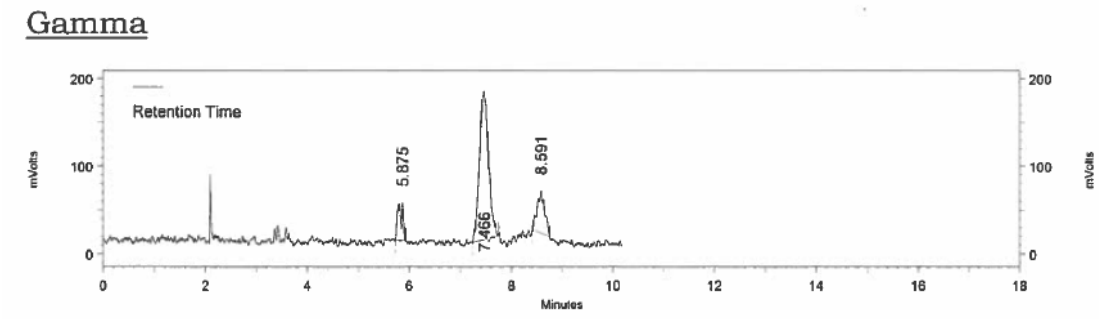

Coinjection (83% RCP)

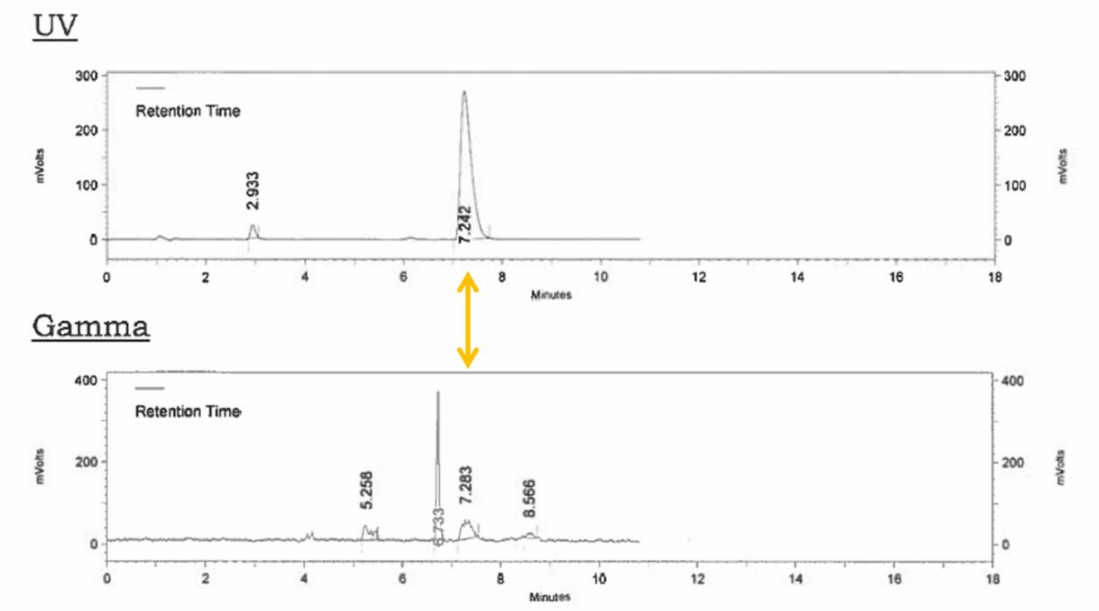

CA Rat 1094

Cut Peak

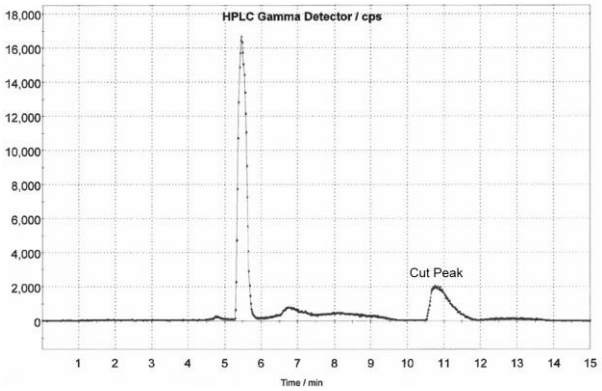

QC (>99% RCP)

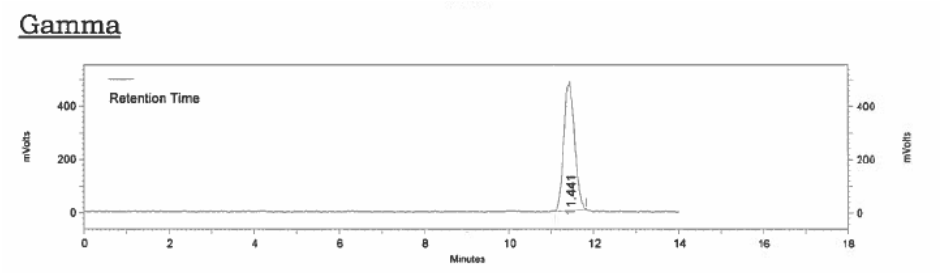

Coinjection (>99% RCP)

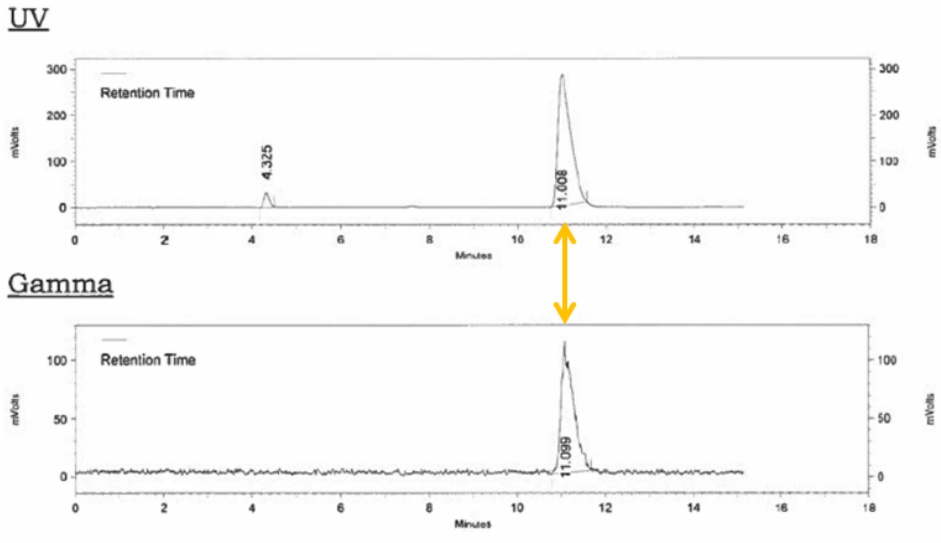

CA Rat 1095

Cut Peak

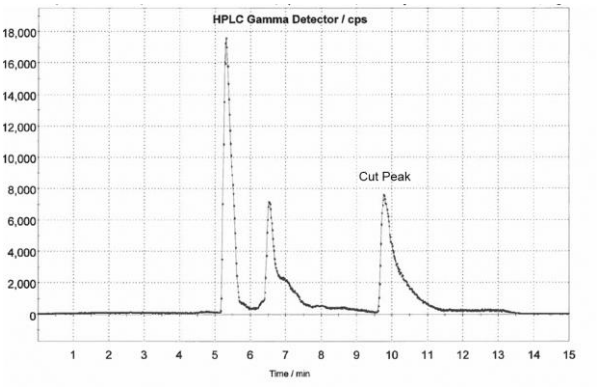

QC (>99% RCP)

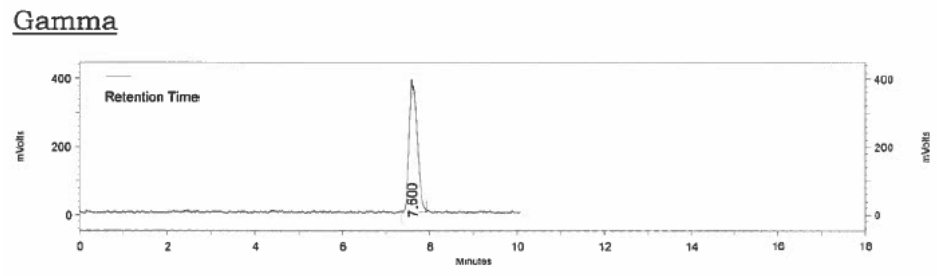

Coinjection (>99% RCP)

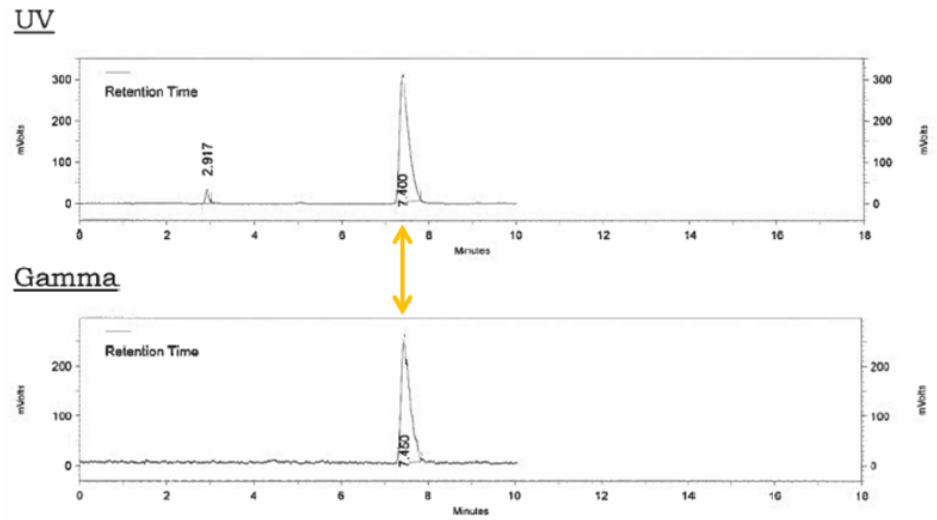

b. microPET scans for [^{11}C]155c

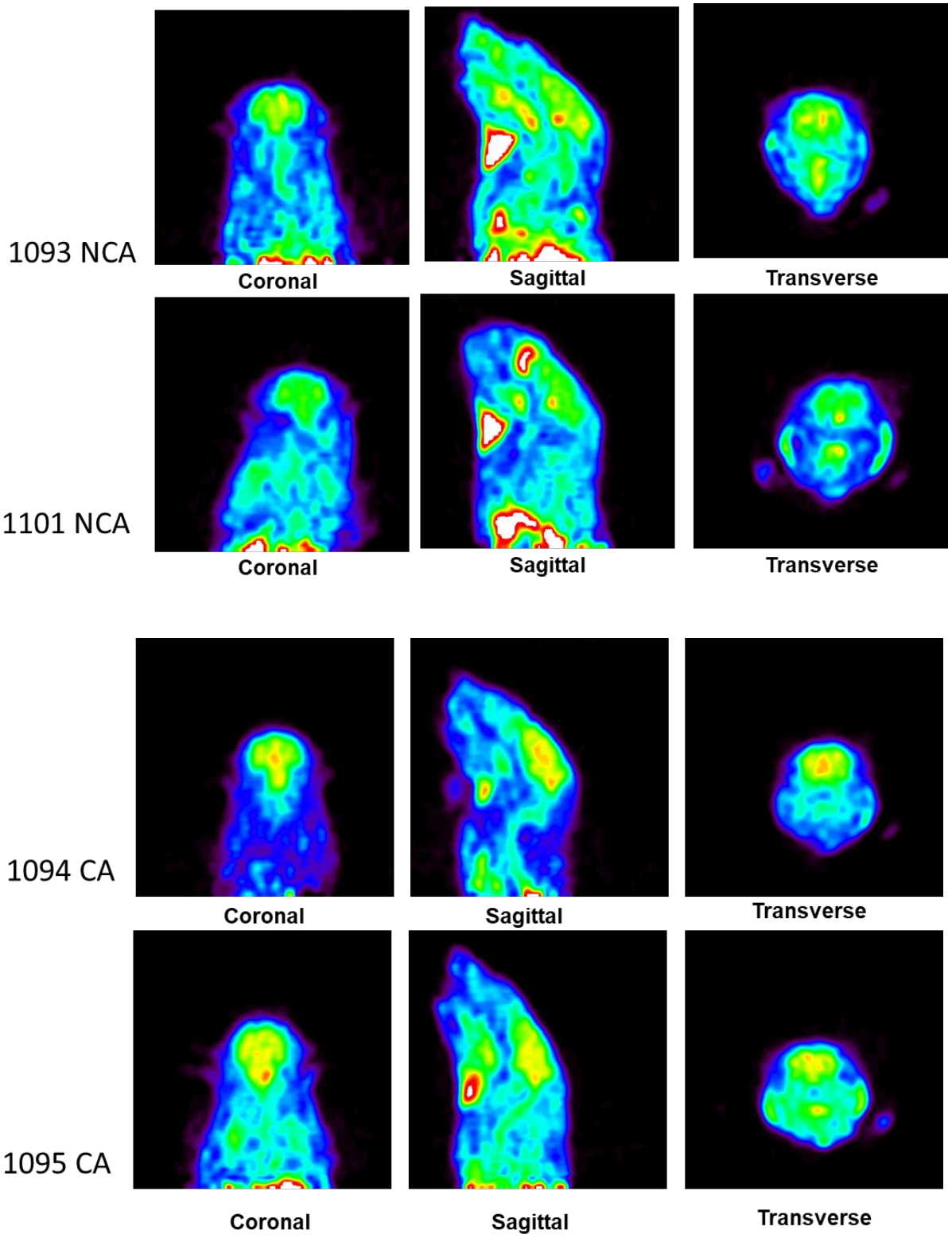

c. Stability Studies for [^{11}C]155c (Carrier Added)

40% MeCN, 20mM NH_4OAc, 2 mL HOAc, 40°C. Luna C18 100A, 150x4.6mm Phenomenex S/N H16-384835

Standard; 96% RCP

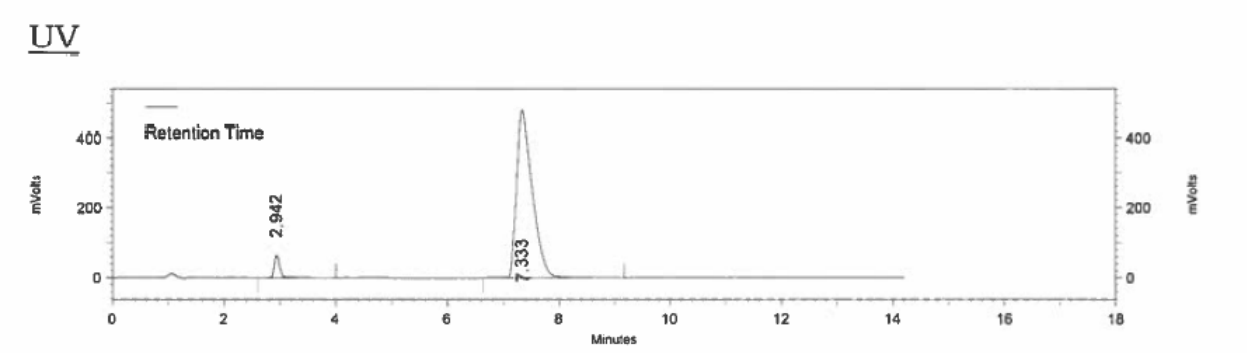

Reformulated Dose in semi-preparative HPLC Buffer; 96% RCP

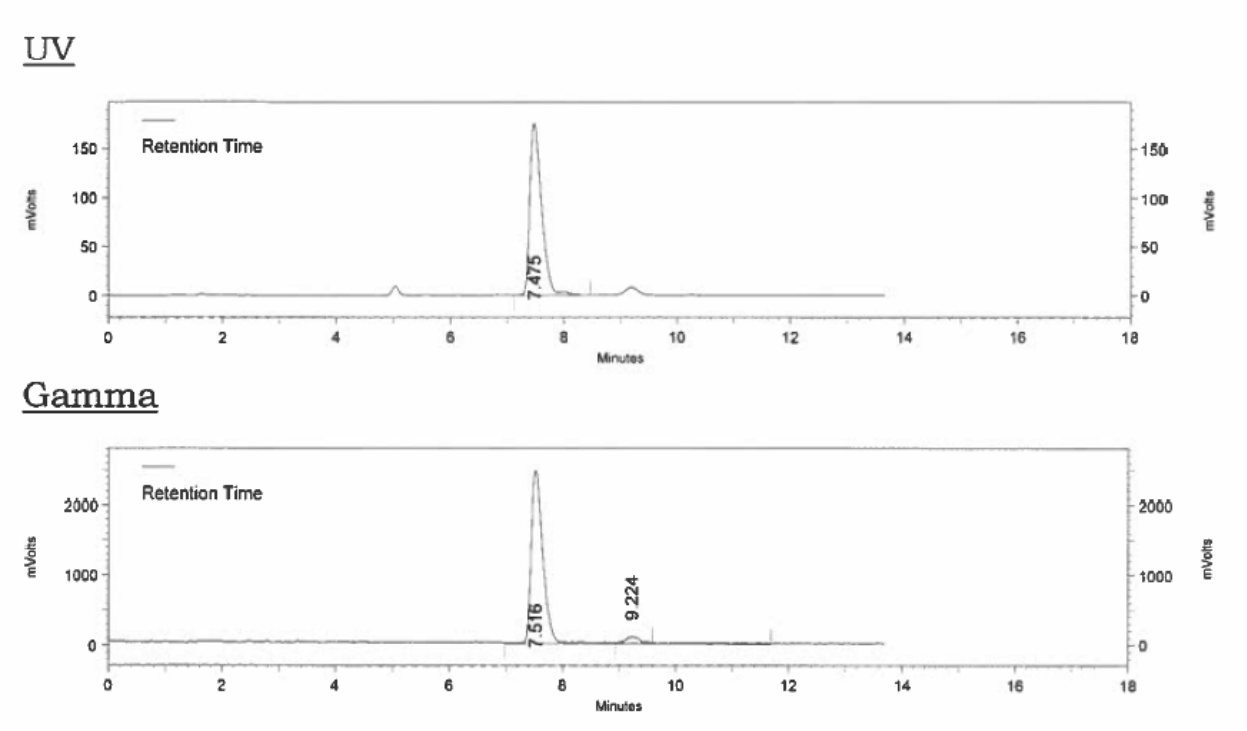

In 100% ethanol; Initial >99% RCP

UV

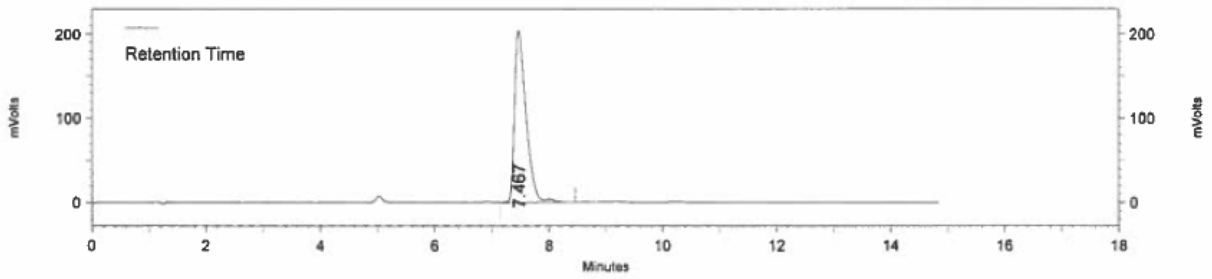

Gamma

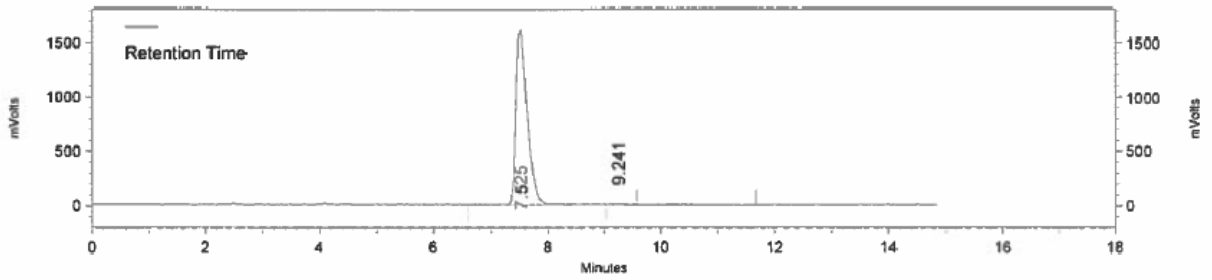

In 100% ethanol; After 1.5 hours, >99% RCP

UV

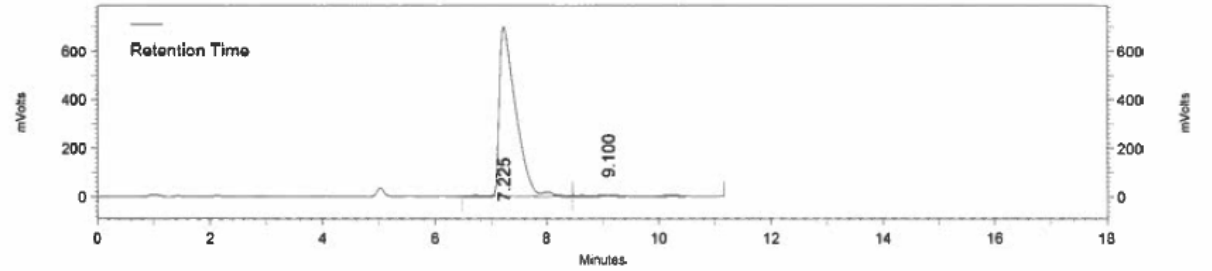

Gamma

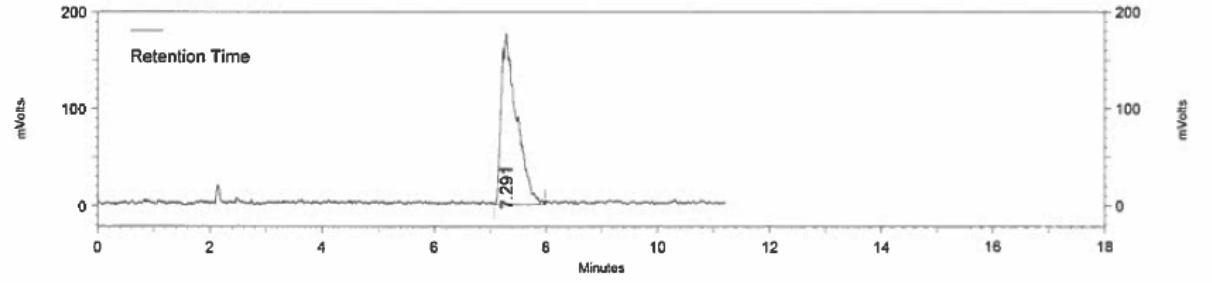

In 10% ethanolic saline; Initial >99% RCP

UV

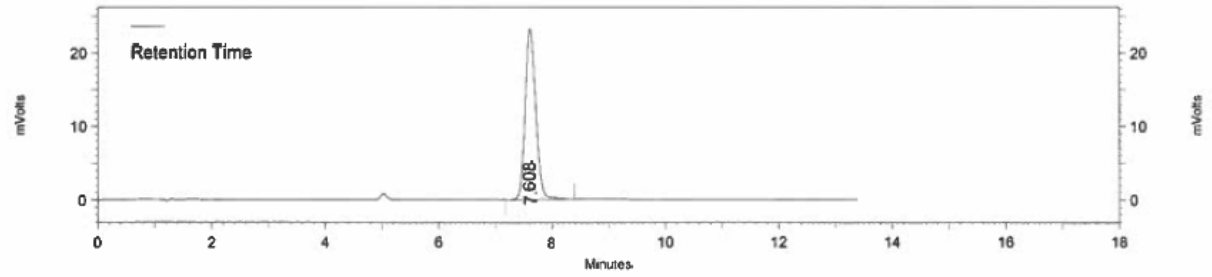

Gamma

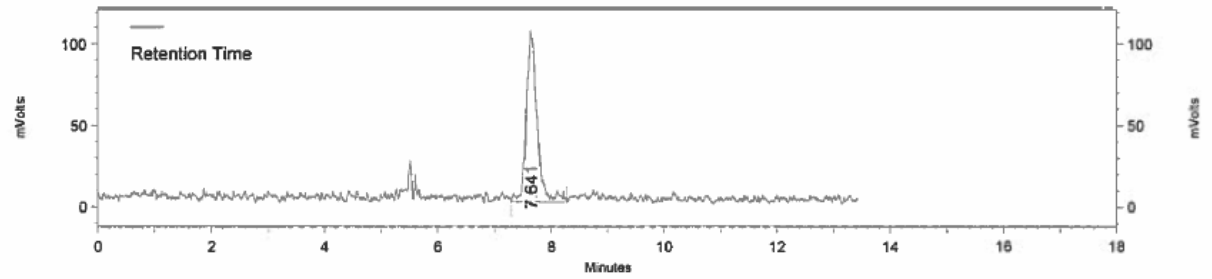

In 10% ethanolic saline; After 15 min from initial, 80% RCP

UV

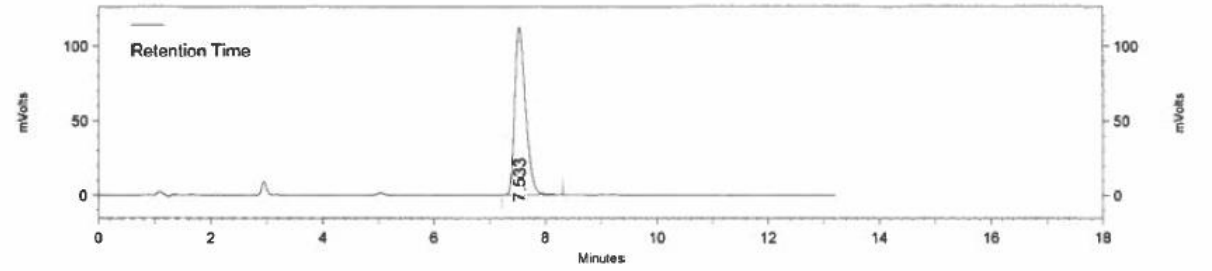

Gamma

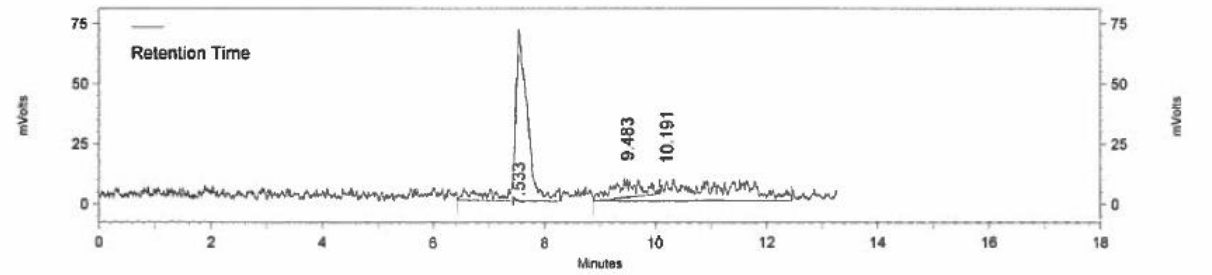

In 10% ethanolic saline; 1.5 hours from initial, 78% RCP

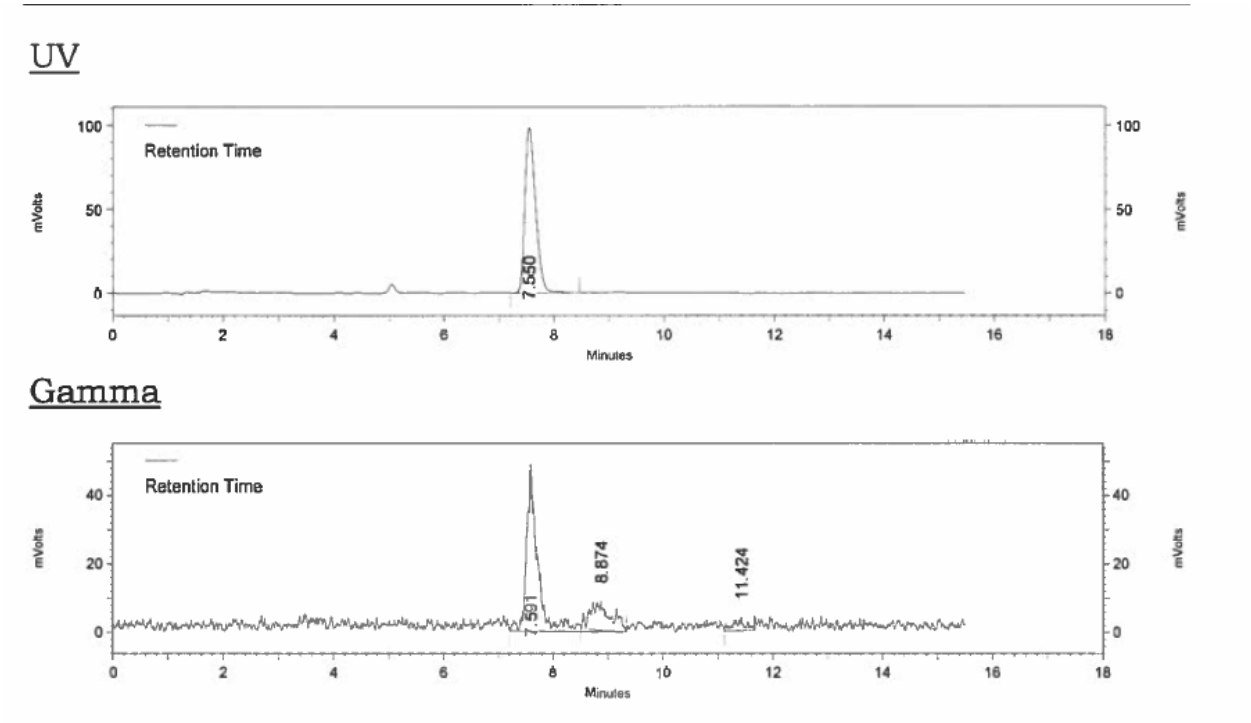

In 10% ethanolic saline; 2 hours from initial, 77% RCP

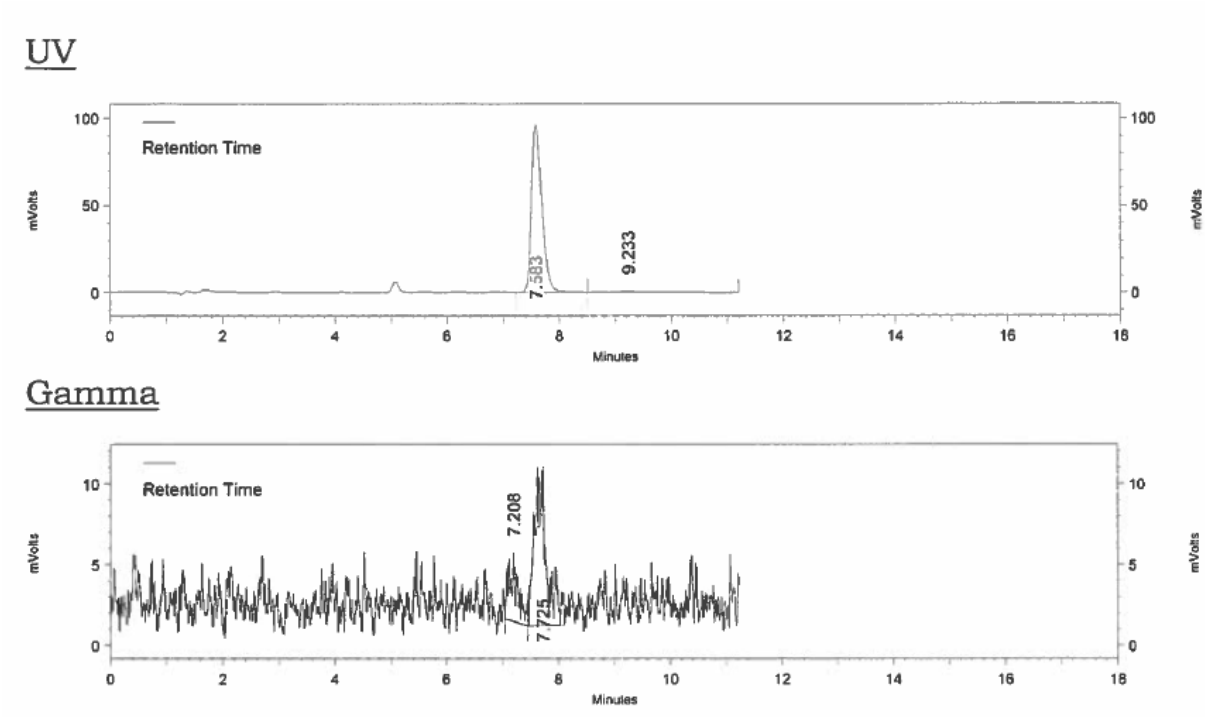

In 10% ethanolic saline; coinjection 2.5 hours after start; >99% RCP

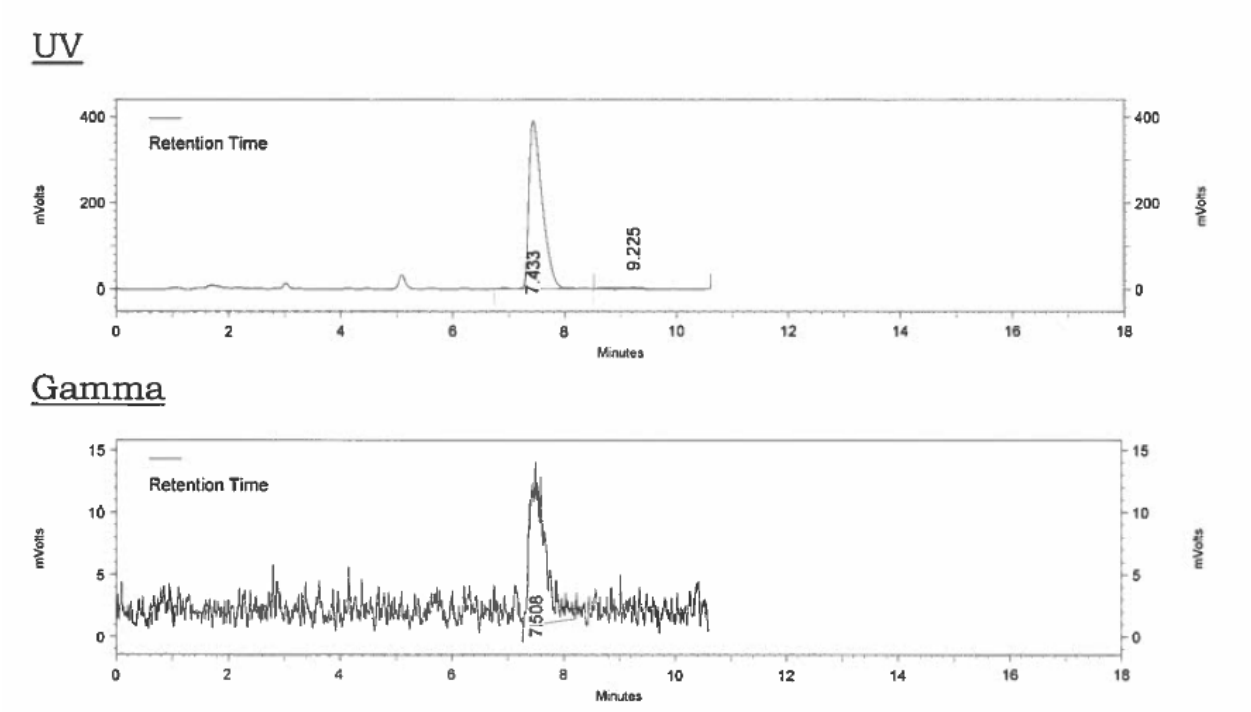

References

(1) Noble, E. P. Alcoholism and the dopaminergic system: a review. *Addict. Biol.* **1996**, *1* (4), 333–348 DOI: 10.1080/1355621961000124956.

(2) Joyce, J. N.; Millan, M. J. Dopamine D3 receptor agonists for protection and repair in Parkinson's disease. *Curr. Opin. Pharmacol.* **2007**, *7* (1), 100–105 DOI: 10.1016/j.coph.2006.11.004.

(3) Le Foll, B.; Collo, G.; Rabiner, E. A.; Boileau, I.; Merlo Pich, E.; Sokoloff, P. *Dopamine D3 receptor ligands for drug addiction treatment: Update on recent findings*, 1st ed.; Elsevier B.V., 2014; Vol. 211.

(4) Wang, G.-J. M.; Nora D. Volkow, M.; Panayotis K. Thanos, P.; Joanna S. Fowler, P. Imaging of Brain Dopamine Pathways: Implications for Understanding Obesity. *J Addict Med.* **2009**, *3* (1), 8–18 DOI: 10.1097/ADM.0b013e31819a86f7.Imaging.

(5) Daubner, S. C.; Le, T.; Wang, S. Tyrosine Hydroxylase and Regulation of Dopamine Synthesis. *Arch Biochem Biophys* **2012**, *508* (1), 1–12 DOI: 10.1016/j.abb.2010.12.017.Tyrosine.

(6) Volkow, N. D.; Fowler, J. S.; Gatley, S. J.; Logan, J.; Wang, G. J.; Ding, Y. S.; Dewey, S. PET evaluation of the dopamine system of the human brain. *J. Nucl. Med.* **1996**, *37* (7), 1242–1256.

(7) The Brain & Actions of Cocaine, Opiates, and Marijuana. *Natl. Institutes Heal. Natl. Inst. Drug Abus.* **2007**, No. January.

(8) Volkow, N. D.; Fowler, J. S.; Gatley, S. J.; Logan, J.; Wang, G.; Ding, Y.; Dewey,

S. PET Evaluation of the Dopamine System of the Human Brain. *J. Nucl. Med.* **1996**, *37* (7), 1242–1256.

(9) Eisenhofer, G. Catecholamine Metabolism: A Contemporary View with Implications for Physiology and Medicine. *Pharmacol. Rev.* **2004**, *56* (3), 331–349 DOI: 10.1124/pr.56.3.1.

(10) Seeman, P.; Grigoriadis, D. Dopamine receptors in brain and periphery. *Neurochem. Int.* **1987**, *10* (1), 1–25 DOI: 10.1016/0197-0186(87)90167-7.

(11) Vallar, L.; Meldolesi, J. Mechanisms of signal transduction at the dopamine D2 receptor. *Trends Pharmacol. Sci.* **1989**, *10* (2), 74–77 DOI: 10.1016/0165-6147(89)90082-5.

(12) Levant, B. Distribution of dopamine receptor subtypes in the CNS. In *CNS Neurotransmitters and Neuromodulators: Dopamine*; Stone, T. W., Ed.; CRC Press: Boca Raton, Florida, 1996; pp 77–87.

(13) Bunzow, J. R.; Tol, H. H. M. Van; Grandy, D. K.; Albert, P.; Salon, J.; Christie, M.; Machida, C. A.; Neve, K. A.; Civelli, O. Cloning and expression of a rat D2 dopamine receptor cDNA. *Nature* **1988**, *336* (6201), 783–787 DOI: 10.1038/336783a0.

(14) Monsma, F. J.; Mahan, L. C.; McVittie, L. D.; Gerfen, C. R.; Sibley, D. R. Molecular cloning and expression of a D1 dopamine receptor linked to adenylyl cyclase activation. *Proc. Natl. Acad. Sci. U. S. A.* **1990**, *87* (17), 6723–6727.

(15) Chu, W.; Zhou, D.; Gaba, V.; Liu, J.; Li, S.; Peng, X.; Xu, J.; Dhavale, D.; Bagchi, D. P.; D'Avignon, A.; et al. Design, Synthesis, and Characterization of 3-

(Benzylidene)indolin-2-one Derivatives as Ligands for ??-Synuclein Fibrils. *J. Med. Chem.* **2015**, *58* (15), 6002–6017 DOI: 10.1021/acs.jmedchem.5b00571.

(16) Sokoloff, P.; Giros, B.; Martres, M. P.; Bouthenet, M. L.; Schwartz, J. C. Molecular cloning and characterization of a novel dopamine receptor (D3) as a target for neuroleptics. *Nature* **1990**, *347* (6289), 146–151 DOI: 10.1038/347146a0.

(17) Van Tol, H. H.; Bunzow, J. R.; Guan, H. C.; Sunahara, R. K.; Seeman, P.; Niznik, H. B.; Civelli, O. Cloning of the gene for a human dopamine D4 receptor with high affinity for the antipsychotic clozapine. *Nature* **1991**, *350* (6319), 610–614 DOI: 10.1038/350610a0.

(18) Sunahara, R. K.; Guan, H. C.; O'Dowd, B. F.; Seeman, P.; Laurier, L. G.; Ng, G.; George, S. R.; Torchia, J.; Van Tol, H. H.; Niznik, H. B. Cloning of the gene for a human dopamine D5 receptor with higher affinity for dopamine than D1. *Nature* **1991**, *350* (6319), 614–619 DOI: 10.1038/350614a0.

(19) Giros, B.; Martres, M. P.; Sokoloff, P.; Schwartz, J. C. [Gene cloning of human dopaminergic D3 receptor and identification of its chromosome]. *C. R. Acad. Sci. III.* **1990**, *311* (13), 501–508.

(20) Fishburn, C. S.; Belleli, D.; David, C.; Carmon, S.; Fuchs, S. A novel short isoform of the D3 dopamine receptor generated by alternative splicing in the third cytoplasmic loop. *J. Biol. Chem.* **1993**, *268* (8), 5872–5878.

(21) Levant, B. The D3 dopamine receptor: neurobiology and potential clinical relevance. *Pharmacol. Rev.* **1997**, *49* (3), 231–252.

(22) Jaber, M.; Robinson, S. W.; Missale, C.; Caron, M. G. Dopamine receptors and brain function. *Neuropharmacology* **1997**, *35* (11), 1503–1519 DOI: 10.1016/S0028-3908(96)00100-1.

(23) Missale, C.; Nash, R. S.; Robinson, S. W.; Jaber, M.; Caron, M. G. Dopamine Receptors: From Structure to Function. *Physiol Rev* **1998**, *78* (1), 189–225.

(24) Li, A.; Mishra, Y.; Malik, M.; Wang, Q.; Li, S.; Taylor, M.; Reichert, D. E.; Luedtke, R. R.; MacH, R. H. Evaluation of N-phenyl homopiperazine analogs as potential dopamine D3 receptor selective ligands. *Bioorg. Med. Chem.* **2013**, *21* (11), 2988–2998 DOI: 10.1016/j.bmc.2013.03.074.

(25) Jackson, D. M.; Westlind-Danielsson, A. Dopamine receptors: molecular biology, biochemistry and behavioural aspects. *Pharmacol Ther* **1994**, *64* (2), 291–370 DOI: 10.1016/0163-7258(94)90041-8.

(26) Sokoloff, P.; Giros, B.; Martres, M.-P.; Bouthenet, M.-L.; Schwartz, J.-C. Molecular cloning and characterization of a novel dopamine receptor (D3) as a target for neuroleptics. *Nature* **1990**, *347* (6289), 146–151 DOI: 10.1038/347146a0.

(27) Kebabian, J. W.; Calne, D. B. Multiple receptors for dopamine. *Nature* **1979**, *277* (5692), 93–96.

(28) Rangel-Barajas, C.; Malik, M.; Taylor, M.; Neve, K. A.; Mach, R. H.; Luedtke, R. R. Characterization of [^{3}H]LS-3-134, a novel arylamide phenylpiperazine D3 dopamine receptor selective radioligand. *J. Neurochem.* **2014**, *131* (4), 418–431 DOI: 10.1111/jnc.12825.

(29) Sokoloff, P.; Schwartz, J. C. Novel dopamine receptors half a decade later. *Trends Pharmacol. Sci.* **1995**, *16* (8), 270–275 DOI: 10.1016/S0165-6147(00)89044-6.

(30) Mach, R. H.; Tu, Z.; Xu, J.; Li, S.; Jones, L. A.; Taylor, M.; Luedtke, R. R.; Derdeyn, C. P.; Perlmutter, J. S.; Mintun, M. A. Endogenous dopamine (DA) competes with the binding of a radiolabeled D3 receptor partial agonist in vivo: A positron emission tomography study. *Synapse* **2011**, *65* (8), 724–732 DOI: 10.1002/syn.20891.

(31) Volkow, N. D.; Wang, G.-J.; Fowler, J. S.; Logan, J.; Schlyer, D.; Hitzemann, R.; Lieberman, J.; Angrist, B.; Pappas, N.; MacGregor, R.; et al. Imaging endogenous dopamine competition with [11C]raclopride in the human brain. *Synapse* **1994**, *16* (4), 255–262 DOI: 10.1002/syn.890160402.

(32) Keck, T. M.; Burzynski, C.; Shi, L.; Newman, A. H. *Beyond small-molecule sar: Using the dopamine d3 receptor crystal structure to guide drug design*, 1st ed.; Elsevier Inc., 2014; Vol. 69.

(33) Mach, R. H.; Luedtke, R. R. Challenges in the Development of Dopamine D2- and D3-selective Radiotracers for PET Imaging Studies. *J. Label. Compd. Radiopharm.* **2017** DOI: 10.1002/jlcr.3558.

(34) Volkow, N. D.; Fowler, J. S.; Wang, G.-J.; Swanson, J. M. Dopamine in drug abuse and addiction: results from imaging studies and treatment implications. *Mol. Psychiatry* **2004**, *9* (6), 557–569 DOI: 10.1038/sj.mp.4001507.

(35) Keck, T. M.; John, W. S.; Czoty, P. W.; Nader, M. A.; Newman, A. H. Identifying Medication Targets for Psychostimulant Addiction: Unraveling the Dopamine D3 Receptor Hypothesis. *J. Med. Chem.* **2015**, *58* (14), 5361–5380 DOI:

10.1021/jm501512b.

(36) Newman, A. H.; Grundt, P.; Nader, M. A. Dopamine D3 Receptor Partial Agonists and Antagonists as Potential Drug Abuse Therapeutic Agents. *J. Med. Chem.* **2005**, *48* (11), 3663–3679 DOI: 10.1021/jm040190e.

(37) Hackling, A. E.; Stark, H. Dopamine D3 receptor ligands with antagonist properties. *Chembiochem* **2002**, *3* (10), 946–961 DOI: 10.1002/1439-7633(20021004)3:10<946::aid-cbic946>3.0.co;2-5.

(38) Sokoloff, P.; Le Foll, B. The dopamine D3 receptor, a quarter century later. *Eur. J. Neurosci.* **2017**, *45* (1), 2–19 DOI: 10.1111/ejn.13390.

(39) *Handbook of Neurochemistry and Molecular Neurobiology: Neurotransmitter Systems*; Lajtha, A., Vizi, E. S., Eds.; Springer Science+business Media, LLC, 2008.

(40) Sokoloff, P.; Le Foll, B.; Perachon, S.; Bordet, R.; Ridray, S.; Schwartz, J. C. The dopamine D3 receptor and drug addiction. *Neurotox Res* **2001**, *3* (5), 433–441 DOI: 10.1007/BF03033202.

(41) Schwartz, J. C.; Diaz, J.; Pilon, C.; Sokoloff, P. Possible implications of the dopamine D3 receptor in schizophrenia and in antipsychotic drug actions. *Brain Res. Rev.* **2000**, *31* (2–3), 277–287 DOI: 10.1016/S0165-0173(99)00043-0.

(42) Slifstein, M.; Rabiner, E. A.; Gunn, R. N. *Imaging the Dopamine D<inf>3</inf> Receptor In Vivo*; Elsevier, 2013.

(43) Graff-Guerrero, A.; Mizrahi, R.; Agid, O.; Marcon, H.; Barsoum, P.; Rusjan, P.;

Wilson, A. A.; Zipursky, R.; Kapur, S. The dopamine D2 receptors in high-affinity state and D3 receptors in schizophrenia: a clinical [11C]-(+)-PHNO PET study. *Neuropsychopharmacology* **2009**, *34* (4), 1078–1086 DOI: 10.1038/npp.2008.199.

(44) Kodaka, F.; Ito, H.; Takano, H.; Takahashi, H.; Arakawa, R.; Miyoshi, M.; Okumura, M.; Otsuka, T.; Nakayama, K.; Halldin, C.; et al. Effect of risperidone on high-affinity state of dopamine D2 receptors: a PET study with agonist ligand [11C](R)-2-CH3O-N-n-propylnorapomorphine. *Int. J. Neuropsychopharmacol.* **2011**, *14* (1), 83–89 DOI: 10.1017/S1461145710001148.

(45) Seneca, N.; Finnema, S. J.; Farde, L.; Gulyás, B.; Wikström, H. V.; Halldin, C.; Innis, R. B. Effect of amphetamine on dopamine D2 receptor binding in nonhuman primate brain: A Comparison of the agonist radioligand [11C]MNPA and antagonist [11C]raclopride. *Synapse* **2006**, *59* (5), 260–269 DOI: 10.1002/syn.20238.

(46) Mach, R. H. Small Molecule Receptor Ligands for PET Studies of the Central Nervous System—Focus on G Protein Coupled Receptors. *Semin. Nucl. Med.* **2017**, *47* (5), 524–535 DOI: 10.1053/j.semnuclmed.2017.05.002.

(47) Gobert, A.; Rivet, J.-M.; Audinot, V.; Cistarellie, L.; Spedding, M.; Vian, J.; Peglion, J.-L.; Millan, M. J. Functional Correlates of Dopamine D3 Receptor Actiation in the Rat In Vivo and Their Modulation by the Selective Antagonist, (+)-S 14297: II. Both D2 and “Silent” D3 Autoreceptors Control Synthesis and Release in Mesolimbic, Mesocortical and Nigrostriatal. *J. Pharmacol. Exp. Ther.* **1995**, *275* (2), 899–913.

(48) Tepper, J. M.; Sun, B. C.; Martin, L. P.; Creese, I. Functional roles of dopamine D2 and D3 autoreceptors on nigrostriatal neurons analyzed by antisense knockdown

in vivo. *J. Neurosci.* **1997**, *17* (7), 2519–2530.

(49) Koeltzow, T. E.; Xu, M.; Cooper, D. C.; Hu, X. T.; Tonegawa, S.; Wolf, M. E.; White, F. J. Alterations in dopamine release but not dopamine autoreceptor function in dopamine D3 receptor mutant mice. *J. Neurosci.* **1998**, *18* (6), 2231–2238.

(50) Joseph, J. D.; Wang, Y. M.; Miles, P. R.; Budygin, E. A.; Picetti, R.; Gainetdinov, R. R.; Caron, M. G.; Wightman, R. M. Dopamine autoreceptor regulation of release and uptake in mouse brain slices in the absence of D3 receptors. *Neuroscience* **2002**, *112* (1), 39–49 DOI: 10.1016/S0306-4522(02)00067-2.

(51) Leggio, G. M.; Bucolo, C.; Platania, C. B. M.; Salomone, S.; Drago, F. Current drug treatments targeting dopamine D3 receptor. *Pharmacol. Ther.* **2016**, *165*, 164–177 DOI: 10.1016/j.pharmthera.2016.06.007.

(52) Luedtke, R. R.; Rangel-Barajas, C.; Malik, M.; Reichert, D. E.; Mach, R. H. Bitropic D3 Dopamine Receptor Selective Compounds s Potential Antipsychotics. *Curr Pharm Des* **2015**, *21* (26), 3700–3724.

(53) Chien, E. Y. T.; Liu, W.; Zhao, Q.; Katritch, V.; Won Han, G.; Hanson, M. A.; Shi, L.; Newman, A. H.; Javitch, J. A.; Cherezov, V.; et al. Structure of the Human Dopamine D3 Receptor in Complex with a D2/D3 Selective Antagonist. *Science (80-.).* **2010**, *330* (6007), 1091–1095 DOI: 10.1126/science.1197410.

(54) Michino, M.; Boateng, C. A.; Donthamsetti, P.; Yano, H.; Bakare, O. M.; Bonifazi, A.; Ellenberger, M. P.; Keck, T. M.; Kumar, V.; Zhu, C.; et al. Toward understanding the structural basis of partial agonism at the dopamine D3 receptor. *J. Med. Chem.* **2017**, *60* (2), 580–593 DOI: 10.1021/acs.jmedchem.6b01148.

(55) Pilla, M.; Perachon, S.; Sautel, F.; Garrido, F.; Mann, A.; Wermuth, C. G.; Schwartz, J. C.; Everitt, B. J.; Sokoloff, P. Selective inhibition of cocaine-seeking behaviour by a partial dopamine D3 receptor agonist. *Nature* **1999**, *400* (6742), 371–375 DOI: 10.1038/43944.

(56) Newman, A. H.; Cao, J.; Bennett, C. J.; Robarge, M. J.; Freeman, R. A.; Luedtke, R. R. N-{4-[4-(2,3-Dichlorophenyl)piperazin-1-yl]butyl, Butenyl and Butynyl} arylcarboxamides as Novel Dopamine D3 Receptor Antagonists. *Bioorg. Med. Chem. Lett.* **2003**, *13*, 2179–2183 DOI: 10.1016/S0960-894X(03)00389-5.

(57) Banala, A. K.; Levy, B. A.; Khatri, S. S.; Furman, C. A.; Roof, R. A.; Mishra, Y.; Griffin, S. A.; Sibley, D. R.; Luedtke, R. R.; Newman, A. H. N-(3-fluoro-4-(4-(2-methoxy or 2,3-dichlorophenyl)piperazine-1-yl)butyl)arylcarboxamides as selective dopamine D3 receptor ligands: critical role of the carboxamide linker for D3 receptor selectivity. *J. Med. Chem.* **2011**, *54* (10), 3581–3594 DOI: 10.1021/jm200288r.

(58) Xi, Z.-X.; Newman, A. H.; Gilbert, J. G.; Pak, A. C.; Peng, X.-Q.; Ashby, C. R.; Gitajn, L.; Gardner, E. L. The novel dopamine D3 receptor antagonist NGB 2904 inhibits cocaine's rewarding effects and cocaine-induced reinstatement of drug-seeking behavior in rats. *Neuropsychopharmacology* **2006**, *31* (7), 1393–1405 DOI: 10.1038/sj.npp.1300912.

(59) Grundt, P.; Carlson, E. E.; Cao, J.; Bennett, C. J.; McElveen, E.; Taylor, M.; Luedtke, R. R.; Newman, A. H. Novel heterocyclic trans olefin analogues of N-{4-[4-(2,3-dichlorophenyl) piperazin-1-yl]butyl}arylcarboxamides as selective probes with high affinity for the dopamine D3 receptor. *J. Med. Chem.* **2005**, *48* (3), 839–

848 DOI: 10.1021/jm049465g.

(60) Kumar, V.; Moritz, A. E.; Keck, T. M.; Bonifazi, A.; Ellenberger, M. P.; Sibley, C. D.; Free, R. B.; Shi, L.; Lane, J. R.; Sibley, D. R.; et al. Synthesis and Pharmacological Characterization of Novel trans -Cyclopropylmethyl-Linked Bivalent Ligands That Exhibit Selectivity and Allosteric Pharmacology at the Dopamine D 3 Receptor (D 3 R). *J. Med. Chem.* **2017**, *60* (4), 1478–1494 DOI: 10.1021/acs.jmedchem.6b01688.

(61) Zou, M. F.; Keck, T. M.; Kumar, V.; Donthamsetti, P.; Michino, M.; Burzynski, C.; Schweppe, C.; Bonifazi, A.; Free, R. B.; Sibley, D. R.; et al. Novel Analogues of (R)-5-(Methylamino)-5,6-dihydro-4H-imidazo[4,5,1-ij]quinolin-2(1H)-one (Sumanirole) Provide Clues to Dopamine D2/D3 Receptor Agonist Selectivity. *J. Med. Chem.* **2016**, *59* (7), 2973–2988 DOI: 10.1021/acs.jmedchem.5b01612.

(62) Kumar, V.; Bonifazi, A.; Ellenberger, M. P.; Keck, T. M.; Pommier, E.; Rais, R.; Slusher, B. S.; Gardner, E.; You, Z. B.; Xi, Z. X.; et al. Highly selective dopamine D3 receptor (D3R) antagonists and partial agonists based on eticlopride and the D3R crystal structure: New leads for opioid dependence treatment. *J. Med. Chem.* **2016**, *59* (16), 7634–7650 DOI: 10.1021/acs.jmedchem.6b00860.

(63) Boateng, C. A.; Bakare, O. M.; Zhan, J.; Banala, A. K.; Burzynski, C.; Pommier, E.; Keck, T. M.; Donthamsetti, P.; Javitch, J. A.; Rais, R.; et al. High Affinity Dopamine D3 Receptor (D3R)-Selective Antagonists Attenuate Heroin Self-Administration in Wild-Type but not D3R Knockout Mice. *J. Med. Chem.* **2015**, *58* (15), 6195–6213 DOI: 10.1021/acs.jmedchem.5b00776.

(64) Robarge, M. J.; Husbands, S. M.; Kieltyka, A.; Brodbeck, R.; Thurkauf, A.; Newman, A. H. Design and Synthesis of [(2 , 3-Dichlorophenyl) piperazin-1-yl] alkylfluorenylcarboxamides as Novel Ligands Selective for the Dopamine D 3 Receptor Subtype. *J Med Chem* **2001**, *44*, 3175–3186 DOI: 10.1021/jm010146o.

(65) Bennacef, I.; Salinas, C. A.; Bonasera, T. A.; Gunn, R. N.; Audrain, H.; Jakobsen, S.; Nabulsi, N.; Weinzimmer, D.; Carson, R. E.; Huang, Y.; et al. Dopamine D3 receptor antagonists: The quest for a potentially selective PET ligand. Part 3: Radiosynthesis and in vivo studies. *Bioorganic Med. Chem. Lett.* **2009**, *19* (17), 5056–5059 DOI: 10.1016/j.bmcl.2009.07.055.

(66) Micheli, F. Recent advances in the development of dopamine D3 receptor antagonists: a medicinal chemistry perspective. *ChemMedChem* **2011**, *6* (7), 1152–1162 DOI: 10.1002/cmdc.201000538.

(67) Micheli, F.; Arista, L.; Bertani, B.; Braggio, S.; Capelli, A. M.; Cremonesi, S.; Di-Fabio, R.; Gelardi, G.; Gentile, G.; Marchioro, C.; et al. Exploration of the amine terminus in a novel series of 1,2,4-triazolo-3-yl-azabicyclo[3.1.0]hexanes as selective dopamine D3 receptor antagonists. *J. Med. Chem.* **2010**, *53* (19), 7129–7139 DOI: 10.1021/jm100832d.

(68) Micheli, F.; Andreotti, D.; Braggio, S.; Checchia, A. A specific and direct comparison of the trifluoromethyl and pentafluoro sulfanyl groups on the selective dopamine D(3) antagonist 3-(3-{[4-methyl-5-(4-methyl-1,3-oxazol-5-yl)-4H-1,2,4-triazol-3-yl]thio}propyl)-1-phenyl-3-azabicyclo[3.1.0]hexane template. *Bioorg. Med. Chem. Lett.* **2010**, *20* (15), 4566–4568 DOI: 10.1016/j.bmcl.2010.06.018.

(69) Micheli, F.; Bacchi, A.; Braggio, S.; Castelletti, L.; Cavallini, P.; Cavanni, P.; Cremonesi, S.; Dal Cin, M.; Feriani, A.; Gehanne, S.; et al. 1,2,4-Triazolyl 5-Azaspiro[2.4]heptanes: Lead Identification and Early Lead Optimization of a New Series of Potent and Selective Dopamine D3 Receptor Antagonists. *J. Med. Chem.* **2016**, *59* (18), 8549–8576 DOI: 10.1021/acs.jmedchem.6b00972.

(70) Micheli, F.; Cremonesi, S.; Semeraro, T.; Tarsi, L.; Tomelleri, S.; Cavanni, P.; Oliosi, B.; Perdonà, E.; Sava, A.; Zonzini, L.; et al. Novel morpholine scaffolds as selective dopamine (DA) D3 receptor antagonists. *Bioorg. Med. Chem. Lett.* **2016**, *26* (4), 1329–1332 DOI: 10.1016/j.bmcl.2015.12.081.

(71) Micheli, F.; Bernardelli, A.; Bianchi, F.; Braggio, S.; Castelletti, L.; Cavallini, P.; Cavanni, P.; Cremonesi, S.; Dal Cin, M.; Feriani, A.; et al. 1,2,4-Triazolyl octahydropyrrolo[2,3-b]pyrroles: A new series of potent and selective dopamine D3 receptor antagonists. *Bioorg. Med. Chem.* **2016**, *24* (8), 1619–1636 DOI: 10.1016/j.bmc.2016.02.031.

(72) Bonanomi, G.; Braggio, S.; Capelli, A. M.; Checchia, A.; Di Fabio, R.; Marchioro, C.; Tarsi, L.; Tedesco, G.; Terreni, S.; Worby, A.; et al. Triazolyl azabicyclo[3.1.0]hexanes: A class of potent and selective dopamine D(3) receptor antagonists. *ChemMedChem* **2010**, *5* (5), 705–715 DOI: 10.1002/cmdc.201000026.

(73) Holmes, I. P.; Blunt, R. J.; Lorthioir, O. E.; Blowers, S. M.; Gribble, A.; Payne, A. H.; Stansfield, I. G.; Wood, M.; Woollard, P. M.; Reavill, C.; et al. The identification of a selective dopamine D2 partial agonist, D3 antagonist displaying high levels of

brain exposure. *Bioorg. Med. Chem. Lett.* **2010**, *20* (6), 2013–2016 DOI: 10.1016/j.bmcl.2010.01.090.

(74) Holmes, I. P.; Micheli, F.; Gaines, S.; Lorthioir, O.; Watson, S. P.; Fabio, R. Di; Gentile, G.; Heidbreder, C.; Savoia, C.; Worby, A. Dopamine D3 receptor antagonists: the quest for a potentially selective PET ligand. Part one: lead identification. *Bioorg. Med. Chem. Lett.* **2009**, *19* (16), 4799–4801 DOI: 10.1016/j.bmcl.2009.06.043.

(75) Micheli, F.; Bonanomi, G.; Blaney, F. E.; Braggio, S.; Capelli, A. M.; Checchia, A.; Curcuruto, O.; Damiani, F.; Fabio, R. Di; Donati, D.; et al. 1,2,4-triazol-3-yl-thiopropyl-tetrahydrobenzazepines: a series of potent and selective dopamine D(3) receptor antagonists. *J. Med. Chem.* **2007**, *50* (21), 5076–5089 DOI: 10.1021/jm0705612.

(76) Micheli, F.; Bonanomi, G.; Braggio, S.; Capelli, A. M.; Damiani, F.; Di Fabio, R.; Donati, D.; Gentile, G.; Hamprecht, D.; Perini, O.; et al. New fused benzazepine as selective D3 receptor antagonists. Synthesis and biological evaluation. Part 2: [g]-fused and hetero-fused systems. *Bioorg. Med. Chem. Lett.* **2008**, *18* (3), 908–912 DOI: 10.1016/j.bmcl.2007.12.042.

(77) Micheli, F.; Holmes, I.; Arista, L.; Bonanomi, G.; Braggio, S.; Cardullo, F.; Di Fabio, R.; Donati, D.; Gentile, G.; Hamprecht, D.; et al. Dopamine D(3) receptor antagonists: The quest for a potentially selective PET ligand. Part two: Lead optimization. *Bioorg. Med. Chem. Lett.* **2009**, *19* (15), 4011–4013 DOI: 10.1016/j.bmcl.2009.06.028.

(78) Luedtke, R. R.; Mach, R. H. Progress in Developing D3 Dopamine Receptor Ligands as Potential Therapeutic Agents for Neurological and Neuropsychiatric Disorders. *Curr. Pharmaceu* **2003**, *9*, 643–671.

(79) Wang, Q.; Mach, R. H.; Luedtke, R. R.; Reichert, D. E. Subtype Selectivity of Dopamine Receptor Ligands: Insights from Structure and Ligand-Based Methods. *J. Chem. Inf. Model.* **2010**, *50* (11), 1970–1985 DOI: 10.1021/ci1002747.

(80) Huang, Y.; Luedtke, R. R.; Freeman, R. A.; Wu, L.; Mach, R. H. Synthesis and structure-activity relationships of naphthamides as dopamine D3 receptor ligands. *J. Med. Chem.* **2001**, *44* (11), 1815–1826 DOI: 10.1021/jm0100077.

(81) Mach, R. H.; Huang, Y.; Freeman, R. A.; Wu, L.; Vangveravong, S.; Luedtke, R. R. Conformationally-flexible benzamide analogues as dopamine D3 and σ2 receptor ligands. *Bioorg. Med. Chem. Lett.* **2004**, *14* (1), 195–202 DOI: 10.1016/j.bmcl.2003.09.083.

(82) Tu, Z.; Li, S.; Cui, J.; Xu, J.; Taylor, M.; Ho, D.; Luedtke, R. R.; Mach, R. H. Synthesis and Pharmacological Evaluation of Fluorine-Containing D 3 Dopamine Receptor Ligands. *J. Med. Chem.* **2011**, *54* (6), 1555–1564 DOI: 10.1021/jm101323b.

(83) Mach, R. H.; Luedtke, R. R.; Unsworth, C. D.; Boundy, V. a; Nowak, P. a; Scripko, J. G.; Elder, S. T.; Jackson, J. R.; Hoffman, P. L.; Evora, P. H. 18F-labeled benzamides for studying the dopamine D2 receptor with positron emission tomography. *J. Med. Chem.* **1993**, *36* (23), 3707–3720.

(84) Xu, J.; Chu, W.; Tu, Z.; Jones, L. A.; Luedtke, R. R.; Perlmutter, J. S.; Mintun, M.

A.; Mach, R. H. [3 H]4-(Dimethylamino)- N -[4-(4-(2-methoxyphenyl)piperazin- 1-yl)butyl]benzamide, a selective radioligand for dopamine D 3 receptors. I. In vitro characterization. *Synapse* **2009**, *63* (9), 717–728 DOI: 10.1002/syn.20652.

(85) Rangel-Barajas, C.; Malik, M.; Mach, R. H.; Luedtke, R. R. Pharmacological modulation of abnormal involuntary DOI-induced head twitch response movements in male DBA/2J mice: II. Effects of D3 dopamine receptor selective compounds. *Neuropharmacology* **2015**, *93*, 179–190 DOI: 10.1016/j.neuropharm.2014.10.030.

(86) Laforest, R.; Karimi, M.; Moerlein, S. M.; Xu, J.; Flores, H. P.; Bognar, C.; Li, A.; Mach, R. H.; Perlmutter, J. S.; Tu, Z. Absorbed radiation dosimetry of the D3-specific PET radioligand [18F]FluorTriopride estimated using rodent and nonhuman primate. *Am. J. Nucl. Med. Mol. Imaging* **2016**, *6* (6), 301–309.

(87) Mach, R. H.; Luedtke, R. R. Challenges in the Development of Dopamine D2- and D3-selective Radiotracers for PET Imaging Studies. *J. Label. Compd. Radiopharm.* **2017**, *9* (August), 1–8 DOI: 10.1002/jlcr.3558.

(88) Tu, Z.; Li, S.; Xu, J.; Chu, W.; Jones, L. A.; Luedtke, R. R.; Mach, R. H. Effect of cyclosporin A on the uptake of D3-selective PET radiotracers in rat brain. *Nucl. Med. Biol.* **2011**, *38* (5), 725–739 DOI: 10.1016/j.nucmedbio.2011.01.002.

(89) Peng, X.; Wang, Q.; Mishra, Y.; Xu, J.; Reichert, D. E.; Malik, M.; Taylor, M.; Luedtke, R. R.; Mach, R. H. Synthesis, pharmacological evaluation and molecular modeling studies of triazole containing dopamine D3 receptor ligands. *Bioorg. Med. Chem. Lett.* **2015**, *25* (3), 519–523 DOI: 10.1016/j.bmcl.2014.12.023.

(90) Sun, J.; Xu, J.; Cairns, N. J.; Perlmutter, J. S.; Mach, R. H. Dopamine D1, D2, D3

Receptors, Vesicular Monoamine Transporter Type-2 (VMAT2) and Dopamine Transporter (DAT) Densities in Aged Human Brain. *PLoS One* **2012**, *7* (11) DOI: 10.1371/journal.pone.0049483.

(91) Cheung, T. H.; Loriaux, A. L.; Weber, S. M.; Chandler, K. N.; Lenz, J. D.; Schaan, R. F.; Mach, R. H.; Luedtke, R. R.; Neisewander, J. L. Reduction of cocaine self-administration and D3 receptor-mediated behavior by two novel dopamine D3 receptor-selective partial agonists, OS-3-106 and WW-III-55. *J Pharmacol Exp Ther* **2013**, *347* (2), 410–423 DOI: 10.1124/jpet.112.202911.

(92) Cheung, T. H. C.; Nolan, B. C.; Hammerslag, L. R.; Weber, S. M.; Durbin, J. P.; Peartree, N. A.; Mach, R. H.; Luedtke, R. R.; Neisewander, J. L. Phenylpiperazine derivatives with selectivity for dopamine D3 receptors modulate cocaine self-administration in rats. *Neuropharmacology* **2012**, *63* (8), 1346–1359 DOI: 10.1016/j.neuropharm.2012.08.011.

(93) Kumar, R.; Riddle, L. R.; Griffin, S. A.; Chu, W.; Vangveravong, S.; Neisewander, J.; Mach, R. H.; Luedtke, R. R. Evaluation of D2 and D3 dopamine receptor selective compounds on l-dopa-dependent abnormal involuntary movements in rats. *Neuropharmacology* **2009**, *56* (6–7), 956–969 DOI: 10.1016/j.neuropharm.2009.01.019.

(94) Chu, W.; Tu, Z.; McElveen, E.; Xu, J.; Taylor, M.; Luedtke, R. R.; MacH, R. H. Synthesis and in vitro binding of N-phenyl piperazine analogs as potential dopamine D 3 receptor ligands. *Bioorganic Med. Chem.* **2005**, *13* (1), 77–87 DOI: 10.1016/j.bmc.2004.09.054.

(95) Volkow, N. D.; Wang, G.-J.; Telang, F.; Fowler, J. S.; Logan, J.; Childress, A.-R.; Jayne, M.; Ma, Y.; Wong, C. Cocaine Cues and Dopamine in Dorsal Striatum: Mechanism of Craving in Cocaine Addiction. *J. Neurosci.* **2006**, *26* (24), 6583–6588 DOI: 10.1523/JNEUROSCI.1544-06.2006.

(96) Kim, S. W.; Fowler, J. S.; Skolnick, P.; Muench, L.; Kang, Y.; Shea, C.; Logan, J.; Kim, D.; Carter, P.; King, P.; et al. Therapeutic doses of buspirone block D3 receptors in the living primate brain. *Int. J. Neuropsychopharmacol.* **2014**, *17* (8), 1257–1267 DOI: 10.1017/S1461145714000194.

(97) Boeckler, F.; Gmeiner, P. The structural evolution of dopamine D3 receptor ligands: Structure-activity relationships and selected neuropharmacological aspects. *Pharmacol. Ther.* **2006**, *112* (1), 281–333 DOI: 10.1016/j.pharmthera.2006.04.007.

(98) Elsner, J.; Boeckler, F.; Heinemann, F. W.; Hübner, H.; Gmeiner, P. Pharmacophore-guided drug discovery investigations leading to bioactive 5-aminotetrahydropyrazolopyridines. Implications for the binding mode of heterocyclic dopamine D3 receptor agonists. *J. Med. Chem.* **2005**, *48* (18), 5771–5779 DOI: 10.1021/jm0503805.

(99) Boeckler, F.; Gmeiner, P. Dopamine D3 receptor ligands—Recent advances in the control of subtype selectivity and intrinsic activity. *Biochim. Biophys. Acta - Biomembr.* **2007**, *1768* (4), 871–887 DOI: 10.1016/j.bbamem.2006.12.001.

(100) Ehrlich, K.; Gotz, A.; Bollinger, S.; Tschammer, N.; Bettinetti, L.; Harterich, S.; Hubner, H.; Lanig, H.; Gmeiner, P. Dopamine D2, D3, and D4 selective phenylpiperazines as molecular probes to explore the origins of subtype specific

receptor binding. *J. Med. Chem.* **2009**, *52* (15), 4923–4935 DOI: 10.1021/jm900690y.

(101) Gil-Mast, S.; Kortagere, S.; Kota, K.; Kuzhikandathil, E. V. An amino acid residue in the second extracellular loop determines the agonist-dependent tolerance property of the human D3 dopamine receptor. *ACS Chem. Neurosci.* **2013**, *4* (6), 940–951 DOI: 10.1021/cn3002202.

(102) Varady, J.; Wu, X.; Fang, X.; Min, J.; Hu, Z.; Levant, B.; Wang, S. Molecular modeling of the three-dimensional structure of dopamine 3 (D 3) subtype receptor: Discovery of novel and potent D3 ligands through a hybrid pharmacophore- and structure-based database searching approach. *J. Med. Chem.* **2003**, *46* (21), 4377–4392 DOI: 10.1021/jm030085p.

(103) Newman, A. H.; Beuming, T.; Banala, A. K.; Donthamsetti, P.; Pongetti, K.; LaBounty, A.; Levy, B.; Cao, J.; Michino, M.; Luedtke, R. R.; et al. Molecular Determinants of Selectivity and Efficacy at the Dopamine D3 Receptor. *J. Med. Chem.* **2012**, *55* (15), 6689–6699 DOI: 10.1021/jm300482h.

(104) Zhao, Y.; Lu, X.; Yang, C. Y.; Huang, Z.; Fu, W.; Hou, T.; Zhang, J. Computational modeling toward understanding agonist binding on dopamine 3. *J. Chem. Inf. Model.* **2010**, *50* (9), 1633–1643 DOI: 10.1021/ci1002119.

(105) Modi, G.; Voshavar, C.; Gogoi, S.; Shah, M.; Antonio, T.; Reith, M. E. A.; Dutta, A. K. Multifunctional D2/D3 agonist D-520 with high in vivo efficacy: Modulator of toxicity of alpha-synuclein aggregates. *ACS Chem. Neurosci.* **2014**, *5* (8), 700–717 DOI: 10.1021/cn500084x.

(106) Modi, G.; Antonio, T.; Reith, M.; Dutta, A. Structural Modifications of Neuroprotective Anti-Parkinsonian (−)- N 6-(2-(4-(Biphenyl-4-yl)piperazin-1-yl)-ethyl)- N 6-propyl-4,5,6,7-tetrahydrobenzo[d]thiazole-2,6-diamine (D-264): An Effort toward the Improvement of in Vivo Efficacy of the Parent Mol. *J. Med. Chem.* **2014**, *57* (4), 1557–1572 DOI: 10.1021/jm401883v.

(107) Chen, J.; Levant, B.; Wang, S. High-affinity and selective dopamine D3 receptor full agonists. *Bioorganic Med. Chem. Lett.* **2012**, *22* (17), 5612–5617 DOI: 10.1016/j.bmcl.2012.07.003.

(108) Capet, M.; Calmels, T.; Levoin, N.; Danvy, D.; Berrebi-Bertrand, I.; Stark, H.; Schwartz, J.-C.; Lecomte, J.-M. Improving selectivity of dopamine D3 receptor ligands. *Bioorg. Med. Chem. Lett.* **2015**, *26* (3), 10–13 DOI: 10.1016/j.bmcl.2015.12.068.

(109) Nord, M.; Farde, L. Antipsychotic Occupancy of Dopamine Receptors in Schizophrenia. *CNS Neurosci. Ther.* **2011**, *17* (2), 97–103 DOI: 10.1111/j.1755-5949.2010.00222.x.

(110) Nakajima, S.; Gerretsen, P.; Takeuchi, H.; Caravaggio, F.; Chow, T.; Le Foll, B.; Mulsant, B.; Pollock, B.; Graff-Guerrero, A. The potential role of dopamine D3 receptor neurotransmission in cognition. *Eur. Neuropsychopharmacol.* **2013**, *23* (8), 799–813 DOI: 10.1016/j.euroneuro.2013.05.006.

(111) Shahid, M.; Walker, G.; Zorn, S.; Wong, E. Asenapine: a novel psychopharmacologic agent with a unique human receptor signature. *J. Psychopharmacol.* **2009**, *23* (1), 65–73 DOI: 10.1177/0269881107082944.

(112) Roth, B. L.; Lopez, E.; Patel, S.; Kroeze, W. E. S. L. E. Y. K. The Mul ti plic ity of Se ro to nin Re cep tors : Use lessly Di verse Mol e cules or an Em bar rass ment of Riches ? **2000**.

(113) Burstein, E. S.; Ma, J.; Wong, S.; Gao, Y.; Pham, E.; Knapp, a. E.; Nash, N. R.; Olsson, R.; Davis, R. E.; Hacksell, U.; et al. Intrinsic Efficacy of Antipsychotics at Human D 2 , D 3 , and D 4 Dopamine Receptors : Identification of the Clozapine Metabolite N -Desmethylclozapine as a D 2 / D 3 Partial Agonist. *J. Pharmacol. Exp. Ther.* **2005**, *315* (3), 1278–1287 DOI: 10.1124/jpet.105.092155.dose.

(114) Kiss, B.; Horvath, A.; Nemethy, Z.; Schmidt, E.; Laszovszky, I.; Gubovics, G.; Fazekas, K.; Hornok, K.; Orosz, S.; Gyertyan, I.; et al. Cariprazine (RGH-188), a Dopamine D 3 Receptor-Preferring , D 3 / D 2 Dopamine Receptor Antagonist – Partial Agonist Antipsychotic Candidate : In Vitro and Neurochemical Profile. *J. Pharmacol. Exp. Ther.* **2010**, *333* (1), 328–340 DOI: 10.1124/jpet.109.160432.where.

(115) Tenjin, T.; Miyamoto, S.; Ninomiya, Y.; Kitajima, R.; Ogino, S.; Miyake, N.; Yamaguchi, N. Profile of blonanserin for the treatment of schizophrenia. *Neuropsychiatr. Dis. Treat.* **2013**, *9*, 587–594 DOI: 10.2147/NDT.S34433.

(116) Leggio, G. M.; Camillieri, G.; Platania, C. B. M.; Castorina, A.; Marrazzo, G.; Torrisi, S. A.; Nona, C. N.; D'Agata, V.; Nobrega, J.; Stark, H.; et al. Dopamine D3 Receptor Is Necessary for Ethanol Consumption: An Approach with Buspirone. *Neuropsychopharmacology* **2014**, *39* (8), 2017–2028 DOI: 10.1038/npp.2014.51.

(117) Lévesque, D.; Diaz, J.; Pilon, C.; Martres, M. P.; Giros, B.; Souil, E.; Schott, D.;

Morgat, J. L.; Schwartz, J. C.; Sokoloff, P. Identification, characterization, and localization of the dopamine D3 receptor in rat brain using 7-[3H]hydroxy-N,N-di-n-propyl-2-aminotetralin. *Proc. Natl. Acad. Sci. U. S. A.* **1992**, *89* (17), 8155–8159 DOI: 10.1073/pnas.89.17.8155.

(118) Dutta, A. K.; Fei, X.; Reith, M. E. A. A novel series of hybrid compounds derived by combining 2-aminotetralin and piperazine fragments: Binding activity at D2 and D3 receptors. *Bioorganic Med. Chem. Lett.* **2002**, *12* (4), 619–622 DOI: 10.1016/S0960-894X(01)00820-4.

(119) Reavill, C.; Taylor, S. G.; Wood, M. D.; Ashmeade, T.; Austin, N. E.; Avenell, K. Y.; Boyfield, I.; Branch, C. L.; Cilia, J.; Coldwell, M. C.; et al. Pharmacological actions of a novel, high-affinity, and selective human dopamine D(3) receptor antagonist, SB-277011-A. *J. Pharmacol. Exp. Ther.* **2000**, *294* (3), 1154–1165.

(120) Stemp, G.; Ashmeade, T.; Branch, C. L.; Hadley, M. S.; Hunter, A. J.; Johnson, C. N.; Nash, D. J.; Thewlis, K. M.; Vong, A. K.; Austin, N. E.; et al. Design and synthesis of trans-N-[4-[2-(6-cyano-1,2,3, 4-tetrahydroisoquinolin-2-yl)ethyl]cyclohexyl]-4-quinolinecarboxamide (SB-277011): A potent and selective dopamine D(3) receptor antagonist with high oral bioavailability and CNS penetration in the rat. *J. Med. Chem.* **2000**, *43* (9), 1878–1885 DOI: 10.1021/jm000090i.

(121) Austin, N. E.; Baldwin, S. J.; Cutler, L.; Deeks, N.; Kelly, P. J.; Nash, M.; Shardlow, C. E.; Stemp, G.; Thewlis, K.; Ayrton, A.; et al. Pharmacokinetics of the novel, high-affinity and selective dopamine D3 receptor antagonist SB-277011 in rat, dog and

monkey: in vitro/in vivo correlation and the role of aldehyde oxidase. *Xenobiotica* **2001**, *31* (8–9), 677–686 DOI: 10.1080/00498250110056531.

(122) Shapiro, D. a; Renock, S.; Arrington, E.; Chiodo, L. a; Liu, L.-X.; Sibley, D. R.; Roth, B. L.; Mailman, R. Aripiprazole, a novel atypical antipsychotic drug with a unique and robust pharmacology. *Neuropsychopharmacology* **2003**, *28* (8), 1400–1411 DOI: 10.1038/sj.npp.1300203.

(123) Piercey, M. F. Pharmacology of pramipexole, a dopamine D3-preferring agonist useful in treating Parkinson's disease. *Clin. Neuropharmacol. 21* (3), 141–151.

(124) Pich, E. M.; Collo, G. Pharmacological targeting of dopamine D3 receptors: Possible clinical applications of selective drugs. *Eur. Neuropsychopharmacol.* **2015**, *25* (9), 1437–1447 DOI: 10.1016/j.euroneuro.2015.07.012.

(125) Leggio, G. M.; Salomone, S.; Bucolo, C.; Platania, C.; Micale, V.; Caraci, F.; Drago, F. Dopamine D3 receptor as a new pharmacological target for the treatment of depression. *Eur. J. Pharmacol.* **2013**, *719* (1–3), 25–33 DOI: 10.1016/j.ejphar.2013.07.022.

(126) Chen, J.; Collins, G. T.; Zhang, J.; Yang, C. Y.; Levant, B.; Woods, J.; Wang, S. Design, synthesis, and evaluation of potent and selective ligands for the dopamine 3 (D3) receptor with a novel in vivo behavioral profile. *J. Med. Chem.* **2008**, *51* (19), 5905–5908 DOI: 10.1021/jm800471h.

(127) Ghosh, B.; Antonio, T.; Zhen, J.; Kharkar, P.; Reith, M. E. A.; Dutta, A. K. Development of (S)-N6-(2-(4-(isoquinolin-1-yl)piperazin-1-yl) ethyl)-N6-propyl-4,5,6,7-tetrahydrobenzo[d]-thiazole-2,6-diamine and its analogue as a D3 receptor

preferring agonist: Potent in vivo activity in Parkinson's disease animal models. *J. Med. Chem.* **2010**, *53* (3), 1023–1037 DOI: 10.1021/jm901184n.

(128) Sladojevich, F.; McNeill, E.; Börgel, J.; Zheng, S. L.; Ritter, T. Condensed-phase, halogen-bonded CF3I and C2F5I adducts for perfluoroalkylation reactions. *Angew. Chemie - Int. Ed.* **2015**, *54* (12), 3712–3716 DOI: 10.1002/anie.201410954.

(129) Zhen, J.; Antonio, T.; Jacob, J. C.; Grandy, D. K.; Reith, M. E. A.; Dutta, A. K.; Selley, D. E. Efficacy of Hybrid Tetrahydrobenzo[d]thiazole Based Aryl Piperazines D-264 and D-301 at D2 and D3 Receptors. *Neurochem. Res.* **2016**, *41* (1–2), 328–339 DOI: 10.1007/s11064-015-1808-6.

(130) Modi, G.; Antonio, T.; Reith, M.; Dutta, A. Structural Modifications of Neuroprotective Anti-Parkinsonian (−)- N 6-(2-(4-(Biphenyl-4-yl)piperazin-1-yl)-ethyl)- N 6-propyl-4,5,6,7-tetrahydrobenzo[d]thiazole-2,6-diamine (D-264): An Effort toward the Improvement of in Vivo Efficacy of the Parent Mol. *J. Med. Chem.* **2014**, *57* (4), 1557–1572 DOI: 10.1021/jm401883v.

(131) Löber, S.; Hübner, H.; Tschammer, N.; Gmeiner, P. Recent advances in the search for D 3- and D 4- selective drugs: Probes, models and candidates. *Trends Pharmacol. Sci.* **2011**, *32* (3), 148–157 DOI: 10.1016/j.tips.2010.12.003.

(132) Ananthan, S.; Saini, S. K.; Zhou, G.; Hobrath, J. V; Padmalayam, I.; Zhai, L.; Bostwick, J. R.; Antonio, T.; Reith, M. E.; McDowell, S.; et al. Design, synthesis, and structure-activity relationship studies of a series of [4-(4-carboxamidobutyl)]-1-arylpiperazines: insights into structural features contributing to dopamine D3 versus D2 receptor subtype selectivity. *J Med Chem* **2014**, *57* (16), 7042–7060 DOI:

10.1021/jm500801r.

(133) Biswas, S.; Hazeldine, S.; Ghosh, B.; Parrington, I.; Kuzhikandathil, E.; Reith, M. E. a; Dutta, A. K. Bioisosteric heterocyclic versions of 7-{[2-(4-phenyl-piperazin-1-yl)ethyl]propylamino}-5,6,7,8-tetrahydronaphthalen-2-ol: identification of highly potent and selective agonists for dopamine D3 receptor with potent in vivo activity. *J. Med. Chem.* **2008**, *51* (10), 3005–3019 DOI: 10.1021/jm701524h.

(134) Li, C.; Biswas, S.; Li, X.; Dutta, A. K.; Le, W. Novel D3 dopamine receptor-preferring agonist D-264: Evidence of neuroprotective property in Parkinson's disease animal models induced by 1-methyl-4-phenyl-1,2,3,6-tetrahydropyridine and lactacystin. *J. Neurosci. Res.* **2010**, *88* (11), 2513–2523 DOI: 10.1002/jnr.22405.

(135) Biswas, S.; Zhang, S.; Fernandez, F.; Ghosh, B.; Zhen, J.; Kuzhikandathil, E. Further Structure – Activity Relationships Study of Hybrid 7- {[2- (4-Phenylpiperazin-1-yl) ethyl] propylamino } - Agonist with Potent in Vivo Activity with Long Duration of Action. *J. Med. Chem.* **2007**, *51*, 101–117.

(136) Brown, D. A.; Mishra, M.; Zhang, S.; Biswas, S.; Parrington, I.; Antonio, T.; Reith, M. E. A.; Dutta, A. K. Investigation of various N-heterocyclic substituted piperazine versions of 5/7-{[2-(4-aryl-piperazin-1-yl)-ethyl]-propyl-amino}-5,6,7,8-tetrahydro-naphthalen-2-ol: Effect on affinity and selectivity for dopamine D3 receptor. *Bioorg. Med. Chem.* **2009**, *17* (11), 3923–3933 DOI: 10.1016/j.bmc.2009.04.031.

(137) Micheli, F.; Heidbreder, C. Dopamine D3 receptor antagonists: a patent review (2007 – 2012). *Expert Opin. Ther. Pat.* **2013**, *23* (3), 363–381 DOI: 10.1517/13543776.2013.757593.

(138) Bettinetti, L.; Schlotter, K.; Hubner, H.; Gmeiner, P. Interactive SAR Studies : Rational Discovery of Super-Potent and Highly Selective Dopamine D3 Receptor Antagonists and Partial Agonists. *J. Med. Chem.* **2002**, *45*, 4594–4597 DOI: 10.1021/jm025558r.

(139) Reilly, S. W.; Griffin, S.; Taylor, M.; Sahlholm, K.; Weng, C.-C.; Xu, K.; Jacome, D. A.; Luedtke, R. R.; Mach, R. H. Highly Selective Dopamine D $_3$ Receptor Antagonists with Arylated Diazaspiro Alkane Cores. *J. Med. Chem.* **2017**, acs.jmedchem.7b01248 DOI: 10.1021/acs.jmedchem.7b01248.

(140) Chen, J.; Jiang, C.; Levant, B.; Li, X.; Zhao, T.; Wen, B.; Luo, R.; Sun, D.; Wang, S. Pramipexole Derivatives as Potent and Selective Dopamine D 3 Receptor Agonists with Improved Human Microsomal Stability. *ChemMedChem* **2014**, *9* (12), 2653–2660 DOI: 10.1002/cmdc.201402398.

(141) Luedtke, R. R.; Mishra, Y.; Wang, Q.; Gri, S. A.; Bell-horner, C.; Taylor, M.; Vangveravong, S.; Dillon, G. H.; Huang, R.; Reichert, D. E.; et al. Comparison of the Binding and Functional Properties of Two Structurally Di ff erent D2 Dopamine Receptor Subtype Selective Compounds. **2012**.

(142) Kanthan, M.; Cumming, P.; Hooker, J. M.; Vasdev, N. Classics in Neuroimaging: Imaging the Dopaminergic Pathway with PET. **2017**, 10–12 DOI: 10.1021/acschemneuro.7b00252.

(143) Seeman, P. Antipsychotic drugs, dopamine receptors, and schizophrenia. *Clin. Neurosci. Res.* **2001**, *1* (1–2), 53–60 DOI: 10.1016/S1566-2772(00)00007-4.

(144) Le Foll, B.; Payer, D.; Di Ciano, P.; Guranda, M.; Nakajima, S.; Tong, J.; Mansouri,

E.; Wilson, A. A.; Houle, S.; Meyer, J. H.; et al. Occupancy of Dopamine D3 and D2 Receptors by Buspirone: A [11C]-(+)-PHNO PET Study in Humans. *Neuropsychopharmacology* **2016**, *41* (2), 529–537 DOI: 10.1038/npp.2015.177.

(145) Cumming, P.; Wong, D. F.; Dannals, R. F.; Gillings, N.; Hilton, J.; Scheffel, U.; Gjedde, A. The competition between endogenous dopamine and radioligands for specific binding to dopamine receptors. *Ann. N. Y. Acad. Sci.* **2002**, *965*, 440–450 DOI: 10.1111/j.1749-6632.2002.tb04185.x.

(146) Manconi, M.; Ferri, R.; Zucconi, M.; Clemens, S.; Giarolli, L.; Bottasini, V.; Ferini-Strambi, L. Preferential D2 or preferential D3 dopamine agonists in restless legs syndrome. *Neurology* **2011**, *77* (2), 110–117 DOI: 10.1212/WNL.0b013e3182242d91.

(147) Kushida, C. A. Ropinirole: For the treatment of restless legs syndrome. *Neuropsychiatr. Dis. Treat.* **2006**, *2* (4), 407–419 DOI: 10.2165/00023210-200418110-00004.

(148) Girgis, R. R.; Slifstein, M.; D'Souza, D.; Lee, Y.; Periclou, A.; Ghahramani, P.; Laszlovszky, I.; Durgam, S.; Adham, N.; Nabulsi, N.; et al. Preferential binding to dopamine D3 over D2 receptors by cariprazine in patients with schizophrenia using PET with the D3/D2 receptor ligand [11C]-(+)-PHNO. *Psychopharmacology (Berl).* **2016**, *233* (19–20), 3503–3512 DOI: 10.1007/s00213-016-4382-y.

(149) Girgis, R. R.; Xu, X.; Miyake, N.; Easwaramoorthy, B.; Gunn, R. N.; Rabiner, E. A.; Abi-Dargham, A.; Slifstein, M. In Vivo Binding of Antipsychotics to D3 and D2 Receptors: A PET Study in Baboons with [11C]-(+)-PHNO.

Neuropsychopharmacology **2011**, *36* (4), 887–895 DOI: 10.1038/npp.2010.228.

(150) Schotte, A.; Janssen, P. F. M.; Gommeren, W.; Luyten, W. H. M. L.; Van Gompel, P.; Lesage, A. S.; De Loore, K.; Leysen, J. E. Risperidone compared with new and reference antipsychotic drugs: In vitro and in vivo receptor binding. *Psychopharmacology (Berl).* **1996**, *124* (1–2), 57–73 DOI: 10.1007/BF02245606.

(151) Otte, A.; Vries, E. F. J. De; Waarde, A. Van; Luiten, P. G. M. *PET and SPECT of Neurobiological Systems*; Dierckx, R. A. J. ., Otte, A., de Vries, E. F. J., van Waarde, A., Eds.; Springer-Verlag Berlin Heidelberg, 2014.

(152) Jones, T.; Rabiner, E. A. The development, past achievements, and future directions of brain PET. *J. Cereb. Blood Flow Metab.* **2012**, *32* (7), 1426–1454 DOI: 10.1038/jcbfm.2012.20.

(153) Kilbourn, M. R.; Scott, P. J. H. Is LogP Truly Dead? *Nucl. Med. Biol.* **2017** DOI: 10.1016/j.nucmedbio.2017.08.006.

(154) Shen, L. H.; Liao, M. H.; Tseng, Y. C. Recent advances in imaging of dopaminergic neurons for evaluation of neuropsychiatric disorders. *J. Biomed. Biotechnol.* **2012**, *2012* DOI: 10.1155/2012/259349.

(155) Rahmim, A.; Zaidi, H. PET versus SPECT: strengths, limitations and challenges. *Nucl. Med. Commun.* **2008**, *29* (3), 193–207 DOI: 10.1097/MNM.0b013e3282f3a515.

(156) Wu, X.; Cai, H.; Ge, R.; Li, L.; Jia, Z. Recent progress of imaging agents for Parkinson’s disease. *Curr. Neuropharmacol.* **2014**, *12* (6), 551–563 DOI:

10.2174/1570159X13666141204221238.

(157) Wang, L.; Zhang, Q.; Li, H.; Zhang, H. SPECT molecular imaging in Parkinson's disease. *J. Biomed. Biotechnol.* **2012**, *2012* DOI: 10.1155/2012/412486.

(158) Cumming, P.; Maschauer, S.; Riss, P. J.; Tschammer, N.; Fehler, S. K.; Heinrich, M. R.; Kuwert, T.; Prante, O. Radiosynthesis and validation of ^{18}F-FP-CMT, a phenyltropane with superior properties for imaging the dopamine transporter in living brain. *J. Cereb. Blood Flow Metab.* **2014**, *34* (7), 1148–1156 DOI: 10.1038/jcbfm.2014.63.

(159) Bajaj, N.; Hauser, R. A.; Grachev, I. D. Clinical utility of dopamine transporter single photon emission CT (DaT-SPECT) with (123I) ioflupane in diagnosis of parkinsonian syndromes. *J. Neurol. Neurosurg. Psychiatry* **2013**, *84* (11), 1288–1295 DOI: 10.1136/jnnp-2012-304436.

(160) Camardese, G.; Di Giuda, D.; Di Nicola, M.; Cocciolillo, F.; Giordano, A.; Janiri, L.; Guglielmo, R. Imaging studies on dopamine transporter and depression: A review of literature and suggestions for future research. *J. Psychiatr. Res.* **2014**, *51* (1), 7–18 DOI: 10.1016/j.jpsychires.2013.12.006.

(161) Zea-ponce, Y.; Laruelle, M. Synthesis of [123 I] IBZM : A Reliable Procedure for Routine Clinical Studies. *Nucl. Med. Biol.* **1999**, *26* (April), 661–665.

(162) Kung, H. F.; Guo, Y. Z.; Billings, J.; Xu, X.; Mach, R. H.; Blau, M.; Ackerhalt, R. E. Preparation and biodistribution of [125I]IBZM: A potential CNS D-2 dopamine receptor imaging agent. *Int. J. Radiat. Appl. Instrumentation.* **1988**, *15* (2), 0–5 DOI: 10.1016/0883-2897(88)90088-8.

(163) Li, H.; Gildehaus, F. J.; Dresel, S.; Patt, J. T.; Shen, M.; Zhu, T.; Liu, B.; Tang, Z.; Tatsch, K.; Hahn, K. Comparison of in vivo dopamine D2 receptor binding of [(123)I]AIBZM and [(123)I]IBZM in rat brain. *Nucl Med Biol* **2001**, *28* (4), 383–389.

(164) Innis, R. B.; Malison, R. T.; Al-Tikriti, M.; Hoffer, P. B.; Sybirska, E. H.; Seibyl, J. P.; Zoghbi, S. S.; Baldwin, R. M.; Laruelle, M.; Smith, E. O.; et al. Amphetamine-stimulated dopamine release competes in vivo for [123I]IBZM binding to the D2 receptor in nonhuman primates. *Synapse* **1992**, *10* (3), 177–184 DOI: 10.1002/syn.890100302.

(165) Laruelle, M.; Abi-Dargham, a; van Dyck, C. H.; Gil, R.; D'Souza, C. D.; Erdos, J.; McCance, E.; Rosenblatt, W.; Fingado, C.; Zoghbi, S. S.; et al. Single photon emission computerized tomography imaging of amphetamine-induced dopamine release in drug-free schizophrenic subjects. *Proc. Natl. Acad. Sci. U. S. A.* **1996**, *93* (17), 9235–9240 DOI: 10.1073/pnas.93.17.9235.

(166) Lee, C.-M.; Farde, L. Using positron emission tomography to facilitate CNS drug development. *Trends Pharmacol. Sci.* **2006**, *27* (6), 310–316 DOI: 10.1016/j.tips.2006.04.004.

(167) Garnett, E. S.; Firnau, G.; Nahmias, C. Dopamine visualized in the basal ganglia of living man. *Nature*. 1983, pp 137–138.

(168) Vanbrocklin, H. F.; Blagoev, M.; Hoepping, A.; Neil, J. P. O.; Klose, M.; Schubiger, P. A.; Ametamey, S. A new precursor for the preparation of 6- [18F] Fluoro-l-m-tyrosine ([18 F] FMT): efficient synthesis and comparison of radiolabeling. *Appl. Radiat. Isot.* **2004**, *61*, 1289–1294 DOI: 10.1016/j.apradiso.2004.04.008.

(169) *Radiochemical Syntheses Volume 1: Radiopharmaceuticals for Positron Emission Tomography*; Scott, P. J. H., Hockley, B. G., Eds.; John Wiley & Sons, Ltd: Hoboken, New Jersey, 2012.

(170) Farde, L.; Halldin, C.; Stone-Elander, S.; Sedvall, G. Psychopharmacology PET analysis of human dopamine receptor subtypes using 11C-SCH 23390 and 1 C-raclopride. *Psychopharmacology (Berl).* **1987**, *92*, 278–284.

(171) Finnema, S. J.; Bang-Andersen, B.; Jørgensen, M.; Christoffersen, C. T.; Gulyás, B.; Wikström, H. V.; Farde, L.; Halldin, C. The dopamine D1 receptor agonist (S)-[11C]N-methyl-NNC 01-0259 is not sensitive to changes in dopamine concentration-a positron emission tomography examination in the monkey brain. *Synapse* **2013**, *67* (9), 586–595 DOI: 10.1002/syn.21664.

(172) Dejesus, T.; Van Moffaert, J. C.; Friedman, M. Synthesis of [11C]SCH 23390 for Dopamine D 1 Receptor Studies. *Appl. Radiat. Isot.* **1987**, *38* (5), 345–348.

(173) Halldin, C.; Foged, C.; Chou, Y. H.; Karlsson, P.; Swahn, C. G.; Sandell, J.; Sedvall, G.; Farde, L. Carbon-11-NNC 112: a radioligand for PET examination of striatal and neocortical D1-dopamine receptors. *J. Nucl. Med.* **1998**, *39* (12), 2061–2068.

(174) Farde, L.; Nordström, A.-L.; Wiesel, F.-A.; Pauli, S.; Halldin, C.; Sedvall, G.; Carlsson A, L. M.; JM, V. R.; Andén NE, B. S. C. H. F. K. U. U.; Seeman P, L. T. C.-W. M. W. K.; et al. Positron Emission Tomographic Analysis of Central D1 and D2 Dopamine Receptor Occupancy in Patients Treated With Classical Neuroleptics and Clozapine. *Arch. Gen. Psychiatry* **1992**, *49* (7), 538 DOI: 10.1001/archpsyc.1992.01820070032005.

(175) Kassiou, M.; Scheffel, U.; Ravert, H. T.; Mathews, W. B.; Musachio, J. L.; Lambrecht, R. M.; Dannals, R. F. [C-11]A-69024: a potent and selective non-benzazepine radiotracer for in vivo studies of dopamine D1 receptors. *Nucl. Med. Biol.* **1995**, *22* (2), 221–226.

(176) Guo, N.; Hwang, D.; Lo, E.; Huang, Y.; Laruelle, M.; Abi-dargham, A. Dopamine Depletion and In Vivo Binding of PET D 1 Receptor Radioligands : Implications for Imaging Studies in Schizophrenia. **2003**, 1703–1711 DOI: 10.1038/sj.npp.1300224.

(177) Richfield, E. K.; Penney, J. B.; Young, A. B. Anatomical and affinity state comparisons between dopamine D1 and D2 receptors in the rat central nervous system. *Neuroscience* **1989**, *30* (3), 767–777 DOI: 10.1016/0306-4522(89)90168-1.

(178) *Radiochemical Syntheses Volume 2: Further Radiopharmaceuticals for Positron Emission Tomography and New Strategies for Their Production*; Scott, P. J. H., Ed.; John Wiley & Sons, Ltd: Hoboken, New Jersey, 2015.

(179) Ehrin, E.; Farde, L.; de Paulis, T.; Eriksson, L.; Greitz, T.; Johnström, P.; Litton, J. E.; Nilsson, J. L. G.; Sedvall, G.; Stone-Elander, S.; et al. Preparation of 11C-labelled raclopride, a new potent dopamine receptor antagonist: Preliminary PET studies of cerebral dopamine receptors in the monkey. *Int. J. Appl. Radiat. Isot.* **1985**, *36* (4), 269–273 DOI: 10.1016/0020-708X(85)90083-3.

(180) Xu, J.; Hassanzadeh, B.; Chu, W.; Tu, Z.; Jones, L. A.; Luedtke, R. R.; Perlmutter, J. S.; Mintun, M. A.; Mach, R. H. [3 H]4-(dimethylamino)- N -(4-(4-(2-methoxyphenyl)piperazin-1-yl) butyl)benzamide: A selective radioligand for

dopamine D 3 receptors. II. Quantitative analysis of dopamine D 3 and D 2 receptor density ratio in the caudate-putamen. *Synapse* **2010**, *64* (6), 449–459 DOI: 10.1002/syn.20748.

(181) Nordstrom, A.; Farde, L.; Wiesel, F. : Central D2- dopamine receptor occupancy in relation to antipsychotic drug effects: a double-blind PET study of schizophrenic patients. *Biol Psychiatry* **1993**, *33*, 227–235.

(182) Farde, L.; Hall, H.; Ehrin, E.; Sedvall, G. Quantitative analysis of D2 dopamine receptor binding in the living human brain by PET. *Science (80-.).* **1986**, *231* (4735), 258–261 DOI: 10.1126/science.2867601.

(183) Rinne, J. O.; Laihinen, A.; Rinne, U. K.; Någren, K.; Bergman, J.; Ruotsalainen, U. PET study on striatal dopamine D2 receptor changes during the progression of early Parkinson's disease. *Mov. Disord.* **1993**, *8* (2), 134–138 DOI: 10.1002/mds.870080203.

(184) Yasuno, F.; Suhara, T.; Okubo, Y.; Sudo, Y.; Inoue, M.; Ichimiya, T.; Takano, A.; Nakayama, K.; Halldin, C.; Farde, L. Low dopamine D2 receptor binding in subregions of the thalamus in schizophrenia. *Am. J. Psychiatry* **2004**, *161* (6), 1016–1022 DOI: 10.1176/appi.ajp.161.6.1016.

(185) Dewey, S. L.; Smith, G. S.; Logan, J.; Brodie, J. D.; Fowler, J. S.; Wolf, A. P. Striatal binding of the PET ligand 11C-raclopride is altered by drugs that modify synaptic dopamine levels. *Synapse* **1993**, *13* (4), 350–356 DOI: 10.1002/syn.890130407.

(186) Kuroda, Y.; Motohashi, N.; Ito, H.; Ito, S.; Takano, A.; Nishikawa, T.; Suhara, T. Effects of repetitive transcranial magnetic stimulation on [11C] raclopride binding

and cognitive function in patients with depression. *J. Affect. Disord.* **2006**, *95*, 35–42 DOI: 10.1016/j.jad.2006.03.029.

(187) Mizrahi, R. Advances in PET analyses of stress and dopamine. *Neuropsychopharmacology* **2010**, *35* (1), 472–476 DOI: 10.1038/npp.2009.108.

(188) Pruessner, J. C.; Champagne, F.; Meaney, M. J.; Dagher, A. Dopamine Release in Response to a Psychological Stress in Humans and Its Relationship to Early Life Maternal Care: A Positron Emission Tomography Study Using [11C]Raclopride. *J. Neurosci.* **2004**, *24* (11), 2825–2831 DOI: 10.1523/jneurosci.3422-03.2004.

(189) Drevets, W. C.; Gautier, C.; Price, J. C.; Kupfer, D. J.; Kinahan, P. E.; Grace, A. A.; Price, J. L.; Mathis, C. A. Amphetamine-induced dopamine release in human ventral striatum correlates with euphoria. *Biol. Psychiatry* **2001**, *49* (2), 81–96 DOI: 10.1016/S0006-3223(00)01038-6.

(190) Finnema, S. J.; Halldin, C.; Bang-Andersen, B.; Gulyás, B.; Bundgaard, C.; Wikström, H. V.; Farde, L. Dopamine D2/3 receptor occupancy of apomorphine in the nonhuman primate brain - A comparative PET study with [11C]raclopride and [11C]MNPA. *Synapse* **2009**, *63* (5), 378–389 DOI: 10.1002/syn.20615.

(191) Birnbaumer, L.; Zurita, A. R. On the roles of Mg in the activation of G proteins. *J. Recept. Signal Transduct. Res.* **2010**, *30* (6), 372–375 DOI: 10.3109/10799893.2010.508165.

(192) van der Westhuizen, E. T.; Valant, C.; Sexton, P. M.; Christopoulos, A. Endogenous Allosteric Modulators of G Protein-Coupled Receptors. *J. Pharmacol. Exp. Ther.* **2015**, *353* (2), 246–260 DOI: 10.1124/jpet.114.221606.

(193) Rodriguez, F. D.; Bardaji, E.; Traynor, J. R. Differential Effects of Mg2+ and Other Divalent Cations on the Binding of Tritiated Opioid Ligands. *J. Neurochem.* **1992**, *59* (2), 467–472 DOI: 10.1111/j.1471-4159.1992.tb09393.x.

(194) Van Wieringen, J. P.; Booij, J.; Shalgunov, V.; Elsinga, P.; Michel, M. C. Agonist high- and low-affinity states of dopamine D2 receptors: Methods of detection and clinical implications. *Naunyn. Schmiedebergs. Arch. Pharmacol.* **2013**, *386* (2), 135–154 DOI: 10.1007/s00210-012-0817-0.

(195) van Wieringen, J.-P.; Michel, M. C.; Janssen, H. M.; Janssen, A. G.; Elsinga, P. H.; Booij, J. Agonist signalling properties of radiotracers used for imaging of dopamine D2/3 receptors. *EJNMMI Res.* **2014**, *4* (1), 53 DOI: 10.1186/s13550-014-0053-3.

(196) Di Paolo, T.; Lévesque, D. Sodium and guanine nucleotide regulation of dopamine receptor agonist and antagonist binding sites in MtTW15 pituitary tumors. *Can. J. Physiol. Pharmacol.* **1988**, *66* (3), 246–249.

(197) Seeman, P. Dopamine agonist radioligand binds to both D2High and D2Low receptors, explaining why alterations in D2High are not detected in human brain scans. *Synapse* **2012**, *66* (1), 88–93 DOI: 10.1002/syn.20987.

(198) Karimi, M.; Moerlein, S. M.; Videen, T. O.; Luedtke, R. R.; Taylor, M.; Mach, R. H.; Perlmutter, J. S. Decreased striatal dopamine receptor binding in primary focal dystonia: A D2 or D3 defect? *Mov. Disord.* **2011**, *26* (1), 100–106 DOI: 10.1002/mds.23401.

(199) Xu, J.; Vangveravong, S.; Li, S.; Fan, J.; Jones, L. A.; Cui, J.; Wang, R.; Tu, Z.; Chu, W.; Perlmutter, J. S.; et al. Positron emission tomography imaging of

dopamine D2 receptors using a highly selective radiolabeled D2 receptor partial agonist. *Neuroimage* **2013**, *71* (5), 168–174 DOI: 10.1016/j.neuroimage.2013.01.007.

(200) Wilson, A. A.; McCormick, P.; Kapur, S.; Willeit, M.; Garcia, A.; Hussey, D.; Houle, S.; Seeman, P.; Ginovart, N. Radiosynthesis and evaluation of [11C]-(+)-4-propyl-3,4,4a,5,6, 10b-hexahydro-2H-naphtho[1,2-b][1,4]oxazin-9-ol as a potential radiotracer for in vivo imaging of the dopamine D2 high-affinity state with positron emission tomography. *J. Med. Chem.* **2005**, *48* (12), 4153–4160 DOI: 10.1021/jm050155n.

(201) Ahlskog, J. E.; Muenter, M. D.; Bailey, P. A.; Miller, P. M. Parkinson's disease monotherapy with controlled-release MK-458 (PHNO): double-blind study and comparison to carbidopa/levodopa. *Clinical neuropharmacology*. 1991, pp 214–227.

(202) Dykstra, D.; Hazelhoff, B.; Mulder, T. B. .; Devries, J. B.; Wynberg, H.; Horn, A. S. Sythesis and pharmacological activity of the hexahydro-4H-naphth[1,2b][1,4]-oxazines: A new series of potent dopamine receptor agonists. *Eur. J. Med. Chem.* **1985**, *20* (3), 247–250.

(203) Jones, J. H.; Anderson, P. S.; Baldwin, J. J.; Clineschmidt, B. V; McClure, D. E.; Lundell, G. F.; Randall, W. C.; Martin, G. E.; Williams, M.; Hirshfield, J. M.; et al. Synthesis of 4-substituted 2H-naphth[1,2-b]-1,4-oxazines, a new class of dopamine agonists. *J Med Chem* **1984**, *27* (12), 1607–1613 DOI: 10.1021/jm00378a014.

(204) Seeman, P.; Ulpian, C.; Larsen, R. D.; Anderson, P. S. Dopamine receptors

labelled by PHNO. *Synapse* **1993**, *14* (4), 254–262 DOI: 10.1002/syn.890140403.

(205) Hocke, C.; Maschauer, S.; Hübner, H.; Löber, S.; Utz, W.; Kuwert, T.; Gmeiner, P.; Prante, O. A series of 18F-labelled pyridinylphenyl amides as subtype-selective radioligands for the dopamine D3 receptor. *ChemMedChem* **2010**, *5* (6), 941–948 DOI: 10.1002/cmdc.201000067.

(206) Höfling, S. B.; Maschauer, S.; Hübner, H.; Gmeiner, P.; Wester, H. J.; Prante, O.; Heinrich, M. R. Synthesis, biological evaluation and radiolabelling by 18F-fluoroarylation of a dopamine D3-selective ligand as prospective imaging probe for PET. *Bioorganic Med. Chem. Lett.* **2010**, *20* (23), 6933–6937 DOI: 10.1016/j.bmcl.2010.09.142.

(207) McCormick, P. N.; Kapur, S.; Seeman, P.; Wilson, A. A. Dopamine D2 receptor radiotracers [11C](+)-PHNO and [3H]raclopride are indistinguishably inhibited by D2 agonists and antagonists ex vivo. *Nucl. Med. Biol.* **2008**, *35* (1), 11–17 DOI: 10.1016/j.nucmedbio.2007.08.005.

(208) Narendran, R.; Mason, N. S.; Laymon, C. M.; Lopresti, B. J.; Velasquez, N. D.; May, M. a; Kendro, S.; Martinez, D.; Mathis, C. a; Frankle, W. G. A Comparative Evaluation of the Dopamine D 2 / 3 Agonist Radiotracer [11 C](ⵞ) - N -Propyl-norapomorphine and Antagonist [11 C] Raclopride to Measure Amphetamine-Induced Dopamine Release in the Human Striatum. *J. Pharmacol. Exp. Ther.* **2010**, *333* (2), 533–539 DOI: 10.1124/jpet.109.163501.increased.

(209) Shotbolt, P.; Tziortzi, A. C.; Searle, G. E.; Colasanti, A.; van der Aart, J.; Abanades, S.; Plisson, C.; Miller, S. R.; Huiban, M.; Beaver, J. D.; et al. Within-Subject

Comparison of [^{11} C]-(+)-PHNO and [^{11} C]raclopride Sensitivity to Acute Amphetamine Challenge in Healthy Humans. *J. Cereb. Blood Flow Metab.* **2012**, *32* (1), 127–136 DOI: 10.1038/jcbfm.2011.115.

(210) Skinbjerg, M.; Sibley, D. R.; Javitch, J. A.; Abi-Dargham, A. Imaging the high-affinity state of the dopamine D 2 receptor in vivo: Fact or fiction? *Biochem. Pharmacol.* **2012**, *83* (2), 193–198 DOI: 10.1016/j.bcp.2011.09.008.

(211) Seeman, P.; Wilson, A.; Gmeiner, P.; Kapur, S. Dopamine D2 and D3 receptors in human putamen, caudate nucleus, and globus pallidus. *Synapse* **2006**, *60* (3), 205–211 DOI: 10.1002/syn.20298.

(212) Rabiner, E. A.; Slifstein, M.; Nobrega, J.; Plisson, C.; Huiban, M.; Raymond, R.; Diwan, M.; Wilson, A. A.; McCormick, P.; Gentile, G.; et al. In vivo quantification of regional dopamine-D3 receptor binding potential of (+)-PHNO: Studies in non-human primates and transgenic mice. *Synapse* **2009**, *63* (9), 782–793 DOI: 10.1002/syn.20658.

(213) Searle, G.; Beaver, J. D.; Comley, R. A.; Bani, M.; Tziortzi, A.; Slifstein, M.; Mugnaini, M.; Griffante, C.; Wilson, A. A.; Merlo-Pich, E.; et al. Imaging dopamine D3 receptors in the human brain with positron emission tomography, [11C]PHNO, and a selective D3 receptor antagonist. *Biol. Psychiatry* **2010**, *68* (4), 392–399 DOI: 10.1016/j.biopsych.2010.04.038.

(214) Tziortzi, A. C.; Searle, G. E.; Tzimopoulou, S.; Salinas, C.; Beaver, J. D.; Jenkinson, M.; Laruelle, M.; Rabiner, E. A.; Gunn, R. N. Imaging dopamine receptors in humans with [11C]-(+)-PHNO: Dissection of D3 signal and anatomy. *Neuroimage*

2011, *54* (1), 264–277 DOI: 10.1016/j.neuroimage.2010.06.044.

(215) Gallezot, J. D.; Beaver, J. D.; Gunn, R. N.; Nabulsi, N.; Weinzimmer, D.; Singhal, T.; Slifstein, M.; Fowles, K.; Ding, Y. S.; Huang, Y.; et al. Affinity and selectivity of [11C]-(+)-PHNO for the D3 and D2 receptors in the rhesus monkey brain in vivo. *Synapse* **2012**, *66* (6), 489–500 DOI: 10.1002/syn.21535.

(216) Turolla, E. a; Matarrese, M.; Belloli, S.; Moresco, R. M.; Simonelli, P.; Todde, S.; Fazio, F.; Magni, F.; Kienle, M. G.; Leopoldo, M.; et al. 11C-labeling of n-[4-[4-(2,3-dichlorophenyl)piperazin-1-yl]butyl]arylcarboxamide derivatives and evaluation as potential radioligands for PET imaging of dopamine D3 receptors. *J. Med. Chem.* **2005**, *48* (22), 7018–7023 DOI: 10.1021/jm050171k.

(217) Hocke, C.; Prante, O.; Salama, I.; Hübner, H.; Löber, S.; Kuwert, T.; Gmeiner, P. 18F-labeled FAUC 346 and BP 897 derivatives as subtype-selective potential PET radioligands for the dopamine D3 receptor. *ChemMedChem* **2008**, *3* (5), 788–793 DOI: 10.1002/cmdc.200700327.

(218) Gao, M.; Wang, M.; Hutchins, G. D.; Zheng, Q. H. Synthesis of new carbon-11-labeled carboxamide derivatives as potential PET dopamine D3 receptor radioligands. *Appl. Radiat. Isot.* **2008**, *66* (12), 1891–1897 DOI: 10.1016/j.apradiso.2008.05.010.

(219) Leopoldo, M.; Berardi, F.; Colabufo, N. A.; De Giorgio, P.; Lacivita, E.; Perrone, R.; Tortorella, V. Structure-affinity relationship study on N-[4-(4-arylpiperazin-1-yl)butyl]arylcarboxamides as potent and selective dopamine D3 receptor ligands. *J. Med. Chem.* **2002**, *45* (26), 5727–5735 DOI: 10.1021/jm020952a.

(220) Leopoldo, M.; Lacivita, E.; De Giorgio, P.; Colabufo, N. A.; Niso, M.; Berardi, F.; Perrone, R. Design, Synthesis, and Binding Affinities of Potential Positron Emission Tomography (PET) Ligands for Visualization of Brain Dopamine D 3 Receptors. *J. Med. Chem.* **2006**, *49* (1), 358–365 DOI: 10.1021/jm050734s.

(221) Sóvágó, J.; Farde, L.; Halldin, C.; Langer, O.; Laszlovszky, I.; Kiss, B.; Gulyás, B. Positron emission tomographic evaluation of the putative dopamine-D3 receptor ligand, [11C]RGH-1756 in the monkey brain. *Neurochem. Int.* **2004**, *45* (5), 609–617 DOI: 10.1016/j.neuint.2004.04.004.

(222) Sóvágó, J.; Farde, L.; Halldin, C.; Schukin, E.; Schou, M.; Laszlovszky, I.; Kiss, B.; Gulyás, B. Lack of effect of reserpine-induced dopamine depletion on the binding of the dopamine-D3 selective radioligand, [11C]RGH-1756. *Brain Res. Bull.* **2005**, *67* (3), 219–224 DOI: 10.1016/j.brainresbull.2005.06.034.

(223) Schotte, A.; Janssen, P. F.; Bonaventure, P.; Leysen, J. E. Endogenous dopamine limits the binding of antipsychotic drugs to D3 receptors in the rat brain: a quantitative autoradiographic study. *Histochem. J.* **1996**, *28*, 791–799.

(224) Nebel, N.; Maschauer, S.; Hocke, C.; Hübner, H.; Gmeiner, P.; Prante, O. Optimization and synthesis of an ^{18}F-labeled dopamine D$_3$ receptor ligand using [^{18}F]fluorophenylazocarboxylic *tert* -butylester. *J. Label. Compd. Radiopharm.* **2016**, *59* (2), 48–53 DOI: 10.1002/jlcr.3361.

(225) Nebel, N.; Maschauer, S.; Bartuschat, A. L.; Fehler, S. K.; Hübner, H.; Gmeiner, P.; Kuwert, T.; Heinrich, M. R.; Prante, O.; Hocke, C. Synthesis and evaluation of fluoro substituted pyridinylcarboxamides and their phenylazo analogues for potential

dopamine D3 receptor PET imaging. *Bioorg. Med. Chem. Lett.* **2014**, *24* (23), 5399–5403 DOI: 10.1016/j.bmcl.2014.10.043.

(226) Hocke, C.; Cumming, P.; Maschauer, S.; Kuwert, T.; Gmeiner, P.; Prante, O. Biodistribution studies of two 18F-labeled pyridinylphenyl amides as subtype selective radioligands for the dopamine D3 receptor. *Nucl. Med. Biol.* **2014**, *41* (3), 223–228 DOI: 10.1016/j.nucmedbio.2013.12.014.

(227) Gao, M.; Mock, B. H.; Hutchins, G. D.; Zheng, Q.-H. Synthesis and initial PET imaging of new potential dopamine D3 receptor radioligands (E)-4,3,2-[11C]methoxy-N-4-(4-(2-methoxyphenyl)piperazin-1-yl)butyl-cinnamoylamides. *Bioorg. Med. Chem.* **2005**, *13* (22), 6233–6243 DOI: 10.1016/j.bmc.2005.06.055.

(228) Johnson, M.; Antonio, T.; Reith, M. E. A.; Dutta, A. K. Structure-activity relationship study of N 6-(2-(4-(1 H -Indol-5-yl)piperazin-1-yl)ethyl)- N 6-propyl-4,5,6,7-tetrahydrobenzo[d]thiazole-2,6-diamine analogues: Development of highly selective D3 dopamine receptor agonists along with a highly potent D2/. *J. Med. Chem.* **2012**, *55* (12), 5826–5840 DOI: 10.1021/jm300268s.

(229) Ghoshs, B.; Antonio, T.; Reith, M. E. A.; Dutta, A. K. Discovery of 4-(4-(2-((5-Hydroxy-1,2,3,4-tetrahydronaphthalen-2-yl)(propyl) amino)ethyl)piperazin-1-yl)quinolin-8-ol and its analogues as highly potent dopamine D2/D3 agonists and as iron chelator: In vivo activity indicates potential application in sympt. *J. Med. Chem.* **2010**, *53* (5), 2114–2125 DOI: 10.1021/jm901618d.

(230) Dutta, A. K.; Venkataraman, S. K.; Fei, X. S.; Kolhatkar, R.; Zhang, S.; Reith, M. E. A. Synthesis and biological characterization of novel hybrid 7-{[2-(4-phenyl-

piperazin-1-yl)-ethyl]-propyl-amino}-5,6,7,8-tetrahydro- naphthalen-2-ol and their heterocyclic bioisosteric analogues for dopamine D2 and D3 receptors. *Bioorganic Med. Chem.* **2004**, *12* (16), 4361–4373 DOI: 10.1016/j.bmc.2004.06.019.

(231) Modi, G.; Antonio, T.; Reith, M.; Dutta, A. Structural modifications of neuroprotective anti-parkinsonian (-)-N6-(2-(4-(biphenyl-4-yl)piperazin-1-yl)-ethyl)-N6-propyl-4,5,6, 7-tetrahydrobenzo[d]thiazole-2,6-diamine (D-264): An effort toward the improvement of in vivo efficacy of the parent molecule. *J. Med. Chem.* **2014**, *57* (4), 1557–1572 DOI: 10.1021/jm401883v.

(232) Makaravage, K. J.; Brooks, A. F.; Mossine, A. V.; Sanford, M. S.; Scott, P. J. H. Copper-Mediated Radiofluorination of Arylstannanes with [18F]KF. *Org. Lett.* **2016**, *18* (20), 5440–5443 DOI: 10.1021/acs.orglett.6b02911.

(233) Mossine, A. V.; Brooks, A. F.; Makaravage, K. J.; Miller, J. M.; Ichiishi, N.; Sanford, M. S.; Scott, P. J. H. Synthesis of [18F]Arenes via the Copper-Mediated [18F]Fluorination of Boronic Acids. *Org. Lett.* **2015**, *17* (23), 5780–5783 DOI: 10.1021/acs.orglett.5b02875.

(234) Gamache, R. F.; Waldmann, C.; Murphy, J. M. Copper-Mediated Oxidative Fluorination of Aryl Stannanes with Fluoride. *Org. Lett.* **2016**, *18* (18), 4522–4525 DOI: 10.1021/acs.orglett.6b02125.

(235) Ichiishi, N.; Brooks, A. F.; Topczewski, J. J.; Rodnick, M. E.; Sanford, M. S.; Scott, P. J. H. Copper-Catalyzed [18F]Fluorination of (Mesityl)(aryl)iodonium Salts. *Org. Lett.* **2014**, *16* (12), 3224–3227 DOI: 10.1021/ol501243g.

(236) Ichiishi, N.; Canty, A. J.; Yates, B. F.; Sanford, M. S. Cu-catalyzed fluorination of

diaryliodonium salts with KF. *Org. Lett.* **2013**, *15* (19), 5134–5137 DOI: 10.1021/ol4025716.

(237) Niwa, T.; Ochiai, H.; Watanabe, Y.; Hosoya, T. Ni/Cu-Catalyzed Defluoroborylation of Fluoroarenes for Diverse C-F Bond Functionalizations. *J. Am. Chem. Soc.* **2015**, *137* (45), 14313–14318 DOI: 10.1021/jacs.5b10119.

(238) Liu, X. W.; Echavarren, J.; Zarate, C.; Martin, R. Ni-Catalyzed Borylation of Aryl Fluorides via C-F Cleavage. *J. Am. Chem. Soc.* **2015**, *137* (39), 12470–12473 DOI: 10.1021/jacs.5b08103.

(239) Zhou, J.; Kuntze-Fechner, M. W.; Bertermann, R.; Paul, U. S. D.; Berthel, J. H. J.; Friedrich, A.; Du, Z.; Marder, T. B.; Radius, U. Preparing (Multi)Fluoroarenes as Building Blocks for Synthesis: Nickel-Catalyzed Borylation of Polyfluoroarenes via C-F Bond Cleavage. *J. Am. Chem. Soc.* **2016**, *138* (16), 5250–5253 DOI: 10.1021/jacs.6b02337.

(240) Mfuh, A. M.; Doyle, J. D.; Chhetri, B.; Arman, H. D.; Larionov, O. V. Scalable, Metal- and Additive-Free, Photoinduced Borylation of Haloarenes and Quaternary Arylammonium Salts. *J. Am. Chem. Soc.* **2016**, *138* (9), 2985–2988 DOI: 10.1021/jacs.6b01376.

(241) Rahman, O.; Långström, B.; Halldin, C. Alkyl Iodides and [^{11} C]CO in Nickel-Mediated Cross-Coupling Reactions: Successful Use of Alkyl Electrophiles containing a β Hydrogen Atom in Metal-Mediated [^{11} C]Carbonylation. *ChemistrySelect* **2016**, *1* (10), 2498–2501 DOI: 10.1002/slct.201600643.

(242) Zinelaabidine, C.; Souad, O.; Zoubir, J.; Malika, B.; Nour-Eddine, A. A Simple and

Efficient Green Method for the Deprotection of N-Boc in Various Structurally Diverse Amines under Water-mediated Catalyst-free Conditions. *Int. J. Chem.* **2012**, *4* (3), 73–79 DOI: 10.5539/ijc.v4n3p73.

(243) Wang, J.; Liang, Y.-L.; Qu, J. Boiling water-catalyzed neutral and selective N-Boc deprotection. *Chem. Commun.* **2009**, No. 34, 5144 DOI: 10.1039/b910239f.

(244) Shao, X.; Hoareau, R.; Runkle, A. C.; Tluczek, L. J. M.; Hockley, B. G.; Henderson, B. D.; Scott, P. J. H. Highlighting the versatility of the Tracerlab synthesis modules. Part 2: fully automated production of [11C]-labeled radiopharmaceuticals using a Tracerlab FXC-Pro. *J. Label. Compd. Radiopharm.* **2011**, *54* (14), 819–838 DOI: 10.1002/jlcr.1937.

(245) Balicki, R.; Odrowaz-Sypniewski, M.; Ciesielska, A.; Szelejewski, W.; Zagrodzka, J.; Cieplucha, G. PROCESS FOR THE PREPARATION OF PRAMIPEXOLE BASE AND/OR ITS SALTS. US 20090105483A1, 2009.

(246) Mossine, A. V.; Brooks, A. F.; Makaravage, K. J.; Miller, J. M.; Ichiishi, N.; Sanford, M. S.; Scott, P. J. H. Synthesis of [^{18}F]Arenes via the Copper-Mediated [^{18}F]Fluorination of Boronic Acids. *Org. Lett.* **2015**, acs.orglett.5b02875 DOI: 10.1021/acs.orglett.5b02875.

(247) Mossine, A. V.; Brooks, A. F.; Jackson, I. M.; Quesada, C. A.; Sherman, P.; Cole, E. L.; Donnelly, D. J.; Scott, P. J. H.; Shao, X. Synthesis of Diverse 11C-Labeled PET Radiotracers via Direct Incorporation of [11C]CO2. *Bioconjug. Chem.* **2016**, *27* (5), 1382–1389 DOI: 10.1021/acs.bioconjchem.6b00163.

(248) Slifstein, M.; Rabiner, E. A.; Gunn, R. N. Imaging the Dopamine D3 Receptor In

Vivo. In *Imaging of the Human Brain in Health and Disease*; Seeman, P., Madras, B. K., Eds.; Elsevier: Amsterdam, 2014; pp 265–287.

(249) Mach, R. H.; Jackson, J. R.; Luedtke, R. R.; Ivins, K. J.; Molinoff, P. B.; Ehrenkaufer, R. L. Effect of N-alkylation on the affinities of analogues of spiperone for dopamine D2 and serotonin 5-HT2 receptors. *J. Med. Chem.* **1992**, *35* (3), 423–430.

(250) Bancroft, G. N.; Morgan, K. A.; Flietstra, R. J.; Levant, B. Binding of [3H]PD 128907, a putatively selective ligand for the D3 dopamine receptor, in rat brain: A receptor binding and quantitative autoradiographic study. *Neuropsychopharmacology* **1998**, *18* (4), 305–316 DOI: 10.1016/S0893-133X(97)00162-0.

(251) Bouthenet, M.-L.; Souil, E.; Martres, M.-P.; Sokoloff, P.; Giros, B.; Schwartz, J.-C. Localization of dopamine D3 receptor mRNA in the rat brain using in situ hybridization histochemistry: comparison with dopamine D2 receptor mRNA. *Brain Res.* **1991**, *564* (2), 203–219 DOI: 10.1016/0006-8993(91)91456-B.

(252) Levant, B. Characterization of Dopamine Receptors. In *Current Protocols in Pharmacology*; John Wiley & Sons, Inc.: Hoboken, NJ, USA, 2007; pp 1–16.

(253) Hackling, A.; Ghosh, R.; Perachon, S.; Mann, A.; Höltje, H.-D.; Wermuth, C. G.; Schwartz, J.-C.; Sippl, W.; Sokoloff, P.; Stark, H. *N* -(ω-(4-(2-Methoxyphenyl)piperazin-1-yl)alkyl)carboxamides as Dopamine D_2 and D_3 Receptor Ligands. *J. Med. Chem.* **2003**, *46* (18), 3883–3899 DOI: 10.1021/jm030836n.

(254) *G Protein-Coupled Receptors in Drug Discoery*, Drug Disco.; Lundstrom, K. H., Chiu, M. L., Eds.; CRC Press, Taylor & Franci Group, LLC, 2005.

(255) Lundstrom, K. Present and future approaches to screening of G-protein-coupled receptors. *Future Med. Chem.* **2013**, *5* (5), 523–538 DOI: 10.4155/fmc.13.9.

(256) Love, B. E.; Jones, E. G. The use of salicylaldehyde phenylhydrazone as an indicator for the titration of organometallic reagents. *J. Org. Chem.* **1999**, *64* (10), 3755–3756 DOI: 10.1021/jo982433e.

(257) Beaulieu, J.-M.; Gainetdinov, R. R. The physiology, signaling, and pharmacology of dopamine receptors. *Pharmacol. Rev.* **2011**, *63* (1), 182–217 DOI: 10.1124/pr.110.002642.

(258) Nebel, N.; Maschauer, S.; Kuwert, T.; Hocke, C.; Prante, O. In vitro and in vivo characterization of selected fluorine-18 labeled radioligands for PET imaging of the dopamine D3 receptor. *Molecules* **2016**, *21* (9) DOI: 10.3390/molecules21091144.

(259) Koepp, M. J.; Gunn, R. N.; Lawrence, A. D.; Cunningham, V. J.; Dagher, A.; Jones, T.; Brooks, D. J.; Bench, C. J.; Grasby, P. M. Evidence for striatal dopamine release during a video game. *Nature* **1998**, *393* (6682), 266–268 DOI: 10.1038/30498.

(260) De la Fuente-Fernández, R.; Phillips, A. G.; Zamburlini, M.; Sossi, V.; Calne, D. B.; Ruth, T. J.; Stoessl, A. J. Dopamine release in human ventral striatum and expectation of reward. *Behav. Brain Res.* **2002**, *136* (2), 359–363 DOI: 10.1016/S0166-4328(02)00130-4.

(261) Zald, D. H.; Boileau, I.; El-Dearedy, W.; Gunn, R.; McGlone, F.; Dichter, G. S.; Dagher, A. Dopamine Transmission in the Human Striatum during Monetary Reward Tasks. *J. Neurosci.* **2004**, *24* (17), 4105–4112 DOI: 10.1523/JNEUROSCI.4643-03.2004.

(262) Willeit, M.; Ginovart, N.; Graff, A.; Rusjan, P.; Vitcu, I.; Houle, S.; Seeman, P.; Wilson, A. a; Kapur, S. First human evidence of d-amphetamine induced displacement of a D2/3 agonist radioligand: A [11C]-(+)-PHNO positron emission tomography study. *Neuropsychopharmacology* **2008**, *33* (2), 279–289 DOI: 10.1038/sj.npp.1301400.

(263) Tedroff, J.; Pedersen, M.; Aquilonius, S.; Hartvig, P. Levodopa-induced changes in synaptic dopamine in patients with Parkinson â€TM s disease as measured by [l â€TM C] raclopride displacement and PET. *Neurology* **1996**, No. 8645.

(264) Laruelle, M.; Abi-Dargham, A.; Gil, R.; Kegeles, L.; Innis, R. Increased dopamine transmission in schizophrenia: relationship to illness phases. *Biol. Psychiatry* **1999**, *46* (1), 56–72 DOI: 10.1016/S0006-3223(99)00067-0.

(265) Breier, A.; Su, T. P.; Saunders, R.; Carson, R. E.; Kolachana, B. S.; de Bartolomeis, A.; Weinberger, D. R.; Weisenfeld, N.; Malhotra, A. K.; Eckelman, W. C.; et al. Schizophrenia is associated with elevated amphetamine-induced synaptic dopamine concentrations: evidence from a novel positron emission tomography method. *Proc Natl Acad Sci U S A* **1997**, *94* (6), 2569–2574 DOI: 10.1073/pnas.94.6.2569.

(266) Abi-Dargham, A.; Gil, R.; Krystal, J.; Baldwin, R. M.; Seibyl, J. P.; Bowers, M.; Van Dyck, C. H.; Charney, D. S.; Innis, R. B.; Laruelle, M. Increased striatal dopamine transmission in schizophrenia: Confirmation in a second cohort. *Am. J. Psychiatry* **1998**, *155* (6), 761–767 DOI: 10.1176/ajp.155.6.761.

(267) Gallezot, J. D.; Kloczynski, T.; Weinzimmer, D.; Labaree, D.; Zheng, M. Q.; Lim, K.;

Rabiner, E. a; Ridler, K.; Pittman, B.; Huang, Y.; et al. Imaging Nicotine- and Amphetamine-Induced Dopamine Release in Rhesus Monkeys with [(11)C]PHNO vs [(11)C]raclopride PET. *Neuropsychopharmacology* **2013**, 866–874 DOI: 10.1038/npp.2013.286.